PALEOMAGNETISM, ROCK MAGNETISM AND U-TH DATING OF SPELEOTHEM DEPOSITS

by

ALFRED G. LATHAM, B.Sc., M.Sc.

A Thesis

Submitted to the School of Graduate Studies

in Partial Fulfilment of the Requirements

for the Degree

Doctor of Philosophy

McMaster University

April 1981

PALEOMAGNETISM, ROCK MAGNETISM AND DATING OF SPELEOTHEM DEPOSITS

DOCTOR OF PHILISOPHY (1981)
(Geology)

McMASTER UNIVERSITY
Hamilton, Ontario

TITLE: Paleomagnetism, rock magnetism and U-Th dating of speleothem deposits

AUTHOR: Alfred G. Latham, B.Sc. (Leeds University England)

M.Sc. (Leeds University England)

SUPERVISORS: Professor Henry P. Schwarcz and
Professor Derek C. Ford

NUMBER OF PAGES: xxvi, 507

ABSTRACT

The magnetic field of the Earth undergoes slow changes with time known as the secular variation (SV). The SV apparently arises from changes in both the central main dipole and in the non-dipole sources of the core dynamo. The study of the past field and its SV is contingent upon the reliability of the various paleomagnetic records. Considering SV mainly within the Brunhes chron, however, the available recorders are known to be generally deficient, as follows:

1) The recorded signal is not always directly dateable. The assigned ages often lack accuracy and resolution.
2) The intensity and direction record from lavas and baked materials is fragmentary.
3) The sediment records are often either imperfect or have unknown reliability. Several core records are required in order to establish a dated SV master curve for a given region.

In summary there are very few age-dated combined intensity and direction data so necessary for a full vectorial description of the field.

The calcium carbonate cave deposits known as speleothems are shown here to provide dateable continuous records going some way towards satisfying these problems. Stalagmites and flowstones may be reliably dated by the uranium-thorium disequilibrium method. After allowance has been made for any initial contamination of the sample and precautions taken against analytical chemical errors,

growth rate curves may be fitted by least squares methods.

Some speleothems have too low a magnetic content to have a measurable NRM. Others have shown themselves to possess a measurable and stable NRM which is inferred to be primary. These latter speleothems have yielded reliable paleofield directions and this claim is based upon :

1) In one sample, TS, the directions from known modern deposition was in good agreement with modern field values at the site.
2) Signals were internally consistent. Precision of the direction data was often good, and the directions were serially correlated across the growth layers.
3) In six samples the NRMs were shown to be detectably free of depositional errors.
4) In one sample no magnetic anisotropy was apparent within the experimental error.

The speleothem deposit thus presents a major discovery in the search for a reliable dateable and continuous paleomagnetic recorder.

It was thus found possible to safely make geophysical interpretations from these records as follows:

1) Sample VCCL (Vancouver island) clearly showed clockwise looping of the field from about 6.4 to 2.2 Ka BP. This is interpreted as evidence for westward drift of the field. The virtual geomagnetic poles (VGPs) were mostly far-sided.
2) TS (England) showed clockwise looping though this was not as clear as in the VCCL record. The VGPs were biassed far-sided and right-handed for the period 11.3 to 7.5 Ka BP. It was found possible to correlate

the declination features with those of a Swiss lake sediment record. The lack of a correlation of the coeval inclination features appears to suggest that the sources were assymetrical.

3) A stalagmite SJLS, from Mexico, showed far-sided VGPs but no readily discernable cyclic features, for the period 9.0 to 4.5 Ka BP.
4) Stalagmite SJHS, from Mexico, was found to have ages straddling the Blake event. It showed no evidence for such anomalous field behaviour.
5) By comparing the declinations at latitude 22 ^{o} N around the world with another Mexican record (DAS2), westward drift of the field was shown to have occurred for the last 1.3 Ka, at these latitudes. The record almost covers one cycle of the westward drift of declination features. At the start of this cycle inclinations were shallower than they are today.

These findings suggest that the dated SV records from speleothems may provide excellent magnetostratigraphic master curves for age-dating purposes back to about 350 Ka BP - the limit of the U-Th method.

An attempt was made to recover paleointensity using anhysteretic remanent magnetization (ARM) as an analogue of the NRM. ARM was found to be approximately linear with weak field. and was apparently successful in normalising for the variable magnetic content across the growth layers. Although it was not found possible to make a full assessment of the ARM analogue, the results are encouraging enough to warrant further study.

Many of the more strongly magnetized samples owe their NRM to magnetite-bearing detritus from cave floods. If the bulk of such an NRM is a detrital remanent magnetization (DRM) then it is free from depositional errors. Weaker remanences may have arisen from chemical precipitation, also of magnetite. The evidence for a chemical remanent magnetization (CRM) is largely circumstantial. It may be related to the ubiquitous presence of soluble or insoluble organic material in speleothems. It is suggested that the NRM of most speleothems may be a combined DRM and CRM.

Magnetite (or less likely, maghemite) was shown to be the remanence carrier in most samples. A few titanomagnetite grains were observed in the thin sections from two stalagmites. Oxyhydroxides of iron were shown to be present in samples associated with terra rosa soils. The remanence carrier from a Greek sample is hematite, though this finding awaits confirmation.

ACKNOWLEDGEMENTS

I am grateful to Colin Thomas, formerly of Leeds university Earth Sciences Dept., who first suggested looking at stalagmites for a paleomagnetic signal. We took a couple of broken 'stals' from Gavel Pot, Yorkshire. A couple of days later, he said, " There's a weak signal down the axis, but it's a damn sight more stable than my Welsh green slates!".

Also at Leeds, Prof. Jim Briden gave early encouragement to the possibilities of speleothem paleomagnetism.

Upon making enquiries about speleothem dating, at McMaster university, Henry Schwarcz independently suggested looking at their possible paleomagnetism and was keen to try the project. Some useful communications were made to me by Don Tarling, of the University of Newcastle-upon-Tyne, who had tested Yorkshire and Yugoslav. speleothems.

I especially thank Profs. Derek Ford and Henry Schwarcz of McMaster university, for their interest, support and friendship throughout the project. In particular this thesis has greatly benefitted from Henry's insight and criticism.

Permission to use the excellent paleomagnetic facilities at the Erindale campus, of the university of Toronto, was kindly given by Profs. D.W.Strangway and G.W.Pearce. I thank Bill Pearce for help in the laboratory and for useful discussions on various aspects of paleomagnetism and rock magnetism.

My understanding of the principles of rock magnetism has benefitted from a series of lectures by Prof. D.J.Dunlop and talks with Prof, D. Walton (McMaster university).

The latter imbued me with a necessary healthy scepticism about the ARM technique as an analogue for NRM.
Also at Erindale, expert technical assistance and discussions were given me by Anyl Vyas, Dave Redman, Naoji Suguira, Yeeming Woo, and Charlotte Jackson (Claesson).

At McMaster university the chemical techniques of U-Th dating were taught to me by Ada Dixon and Dr. Mel Gascoyne. I am especially grateful to Mel for many helpful discussion and suggestions on various aspects of the chemistry and geochemistry concerning the U-Th dating method, and for his friendship in cave, pub, canoe trips and parties. Help with early analyses of U and Th was also given by Maryka Russell.

My thanks also go to:

Bob Bowens for assistance with the alpha-counting equipment.

Len Zwicker (Geology) for the preparation of the thin sections.

John Hudak (Engineering-physics) for his permission and guidance in the use of the Zeiss Ultraphot (photography of the thin sections).

Bob Bignell for assistence in the photography of the samples, for carrying a large sample through the hot Mexican jungle, and especially for his friendship in cave, pub, canoe trips and parties.

Prof. Tom Birchall (Chemistry) who kindly ran the Mössbauer spectra and made the interpretation , and to George Dénès.

Judith Johnson for atomic absorption analyses.

Dave Brook (Leeds university) for information on organics in speleothems.

Simcha Stroes-Gascoyne and Prof. J. Kramer (Geology) for

advice on various aspects of water chemistry.

In the collection of samples I was additionally assisted by:
(Canada) Tony Fallick, Pat Shaw, Pete Thompson, Marg Saul, Pete Smart and Chris Smart.
(England) John Thorpe, Paul Everett and Tom Miller.
(Bermuda) George Smith kindly gave permission to enter Crystal and Wonderland caves. My thanks to him also for two excellent fishing trips and hospitality.
(Mexico) Fran Bagenal, Mike Shawcross, John Fish, Chaz Yonge, Pam Burns and my friends in the McMaster Caving and Climbing Club. My thanks also to Chaz and Pam for friendship in cave, pub, canoe trips and parties.
(USA) Geri Sweet and Sandy Margo. Tom Aley kindly gave permission to take broken samples from his underground laboratory.

I finally thank AGL, my excellent secretary for his stirling abilities and performance in drafting all the diagrams and typing the namuscrift. He endured my many mistakes, requests and complaints with a gracious patience, unusual in one so young, and without rancour.

The thesis is dedicated to
mum and dad
and to Joe, my brother, who introduced
me to caving.

AND THERE IS NOTHING NEW UNDER THE SUN

(A very short play in one act)

(The title is taken from Ecclesiastes 1:9)

The action takes place in the court of Queen Elizabeth the first, about the year 1580.

COURTIER: Physician Gilbert, your majesty.

(Enter W. Gilbert, physician to the queen. He is eager and ready to impress her majesty with new-found knowledge. He bows low).

ELIZABETH: Well sirrah, what hast thou been up to? Precious little healing, I'll warrant.

GILBERT: Greeting , most gracious highness (arising from a deep bow). I've been studying the magnetism of the Earth. It is most interesting.

ELIZABETH: Indeed. (Unimpressed),And what have you found?

GILBERT: (Expansively throwing up his arms)."Magnus magnes ipse globum terristris est". The Earth is --

ELIZABETH: (Interrupting). Yes, I know. The Earth is a big magnet. What kind? Bar magnet or horseshoe type?

GILBERT: (Encouraged). Oh, in truth, a bar magnet, your highness. A dipole in fact. I have a most interesting theory --

ELIZABETH: (Interrupting again). Any industrial or military potential?

GILBERT: (Hesitates). Er, one can navigate using the north-pointing force and a small bar magnet on ships, and --

ELIZABETH: (Interrupts). That was already in our ken. Forsooth, have I been granting thee sovereigns these years past just so thou'd regurgitate what the venerable Chinese taught us already.

GILBERT: This theory of mine, your majesty; would'st graciously grant more research money. I'm not to the bottom 'ot mystery yet, I'll wager.

ELIZABETH: Zero probability Doc. I'fact we are cutting you down right now. Thy money's going to the navy.

GILBERT: But gracious majesty! There could be non-dipole parts to the magnetism, and --

ELIZABETH: Forget it Mac. The military needs all the money it can lay its hands on. If Walt Raleigh is correct, we'll not lack in defense spending against possible Spanish aggression.

GILBERT: A few sovereigns only, gracious matron. (Mumbles) This'll put geomagnetism back years.

ELIZABETH: (Turns her back). Enough. I'll have non 'o thy mumblings. Begone before thou lose more than thy research grant.

GILBERT: (Dejectedly walks away and mumbles again), Mayhap I can get money by giving popular lectures, or even teaching, God forbid. (- as curtain falls).

END

TABLE OF CONTENTS

LIST OF FIGURES

LIST OF TABLES

LIST OF PLATES

CHAPTER 1

THE EARTH'S MAGNETIC FIELD AND ITS SECULAR VARIATION

1.1 Introduction

From analyses of world - wide observations it has been shown that most of the Earth's present magnetic field is of internal origin, the remaining few percent being due to crustal sources and weak ionospheric currents. Of this internal field about 80 % has the global shape of a dipole field as Gauss showed in 1839, using sherical harmonic analysis. This part is commonly called the main dipole field as though due to a magnetized geocentric dipole. The remaining internal field is then called the non - dipole field even though smaller dipoles somewhere in the Earth's core are often used to model it. The main dipole, presently inclined 11.5° to the spin axis, is thought to be caused by equatorial electric currents in the core. The generation of the field, the electric currents and how they are linked to the core's fluid motions is studied by the methods of magnetohydrodynamics (MHD). Most geomagnetists and paleomagnetists prefer to adopt the simpler phenomenological approach of ascribing the field features and their changes, as seen on the surface, to combinations of interacting dipoles.

Both the dipole and non - dipole fields change slowly with a time interval spectrum from 10 to 10^4 a. This is known as secular variation* and its historic and

* Secular variation is strictly the changing of the

paleomagnetic characteristics continue to be the subject of much study . It has been supposed that when the dipole and non - dipole variations are averaged over a long period of time they approximate to an axial geocentric dipole field. This assumption has been heavily relied upon in paleomagnetism to construct apparent polar wander (APW) paths, in turn used to reconstruct continental plate motions.

On a time scale of 10^5 to 10^6 a. the field changes polarity between two states - normal and reversed. A polarity time scale has been constructed back to about the middle Jurassic (160 ma.); but its extension through most of the Paleozoic is not as precise. It has also been possible to estimate the paleointensities of the Earth's field. Back to about the Cambrian the field has generally been less than the modern field.

General reading about the Earth's field and paleomagnetism may be found in Irving (1964), Tarling (1971) or McElhinny (1973). A more up-to-date description of secular variation is given by McElhinny and Merrill (1975).

As one looks at the data recorded further back in the past, both the paleomagnetic and the age dating resolution decrease. The records of paleomagnetism are carried by iron oxide particles whose remanence decays or becomes changed with time. The rocks themselves may be deformed , heated or chemically changed through the various processes that

Earth's magnetic field over hundreds and thousands of years. It may also be taken to mean a " snapshot " reading of this changing field at a given place or the extent of this change over some time interval. In this study the context usually indicates which meaning is intended otherwise the former may be assumed.

shape the Earth's surface. The several radioisotope clocks that are used to date the paleomagnetism have inherently less resolution for the longer-lived parents, and they too may become altered or reset by later geological phenomena. The more recent past is therefore the best, though not the only, place to study the shorter-lived fluctuations in the magnetic field.

Can one assume that the last 5 ma., 1 ma. or 1 Ka. was typical for the shorter-term behaviour of the field and if so what do the finer details show ? In particular we may ask:

1) how long a time interval is needed in order for secular variation to give an average which approximates an axial geocentric dipole (AGD) field ?
2) how does the main dipole move and has it always been inclined to the spin axis ?
3) was the main dipole always geocentric ?
4) what is the nature of the non - dipole field ?
5) what are the time scales for the dipole and non - dipole variations, and how long do the large geomagnetic anomalies last ?
6) are the dipole and non - dipole fields interacting or independent of one another ?
7) what happens at a field reversal ?

In order to answer these questions one must turn to experiment and ask :

1) what paleomagnetic field recorders are available and how good are they ?
2) how well can they be dated ?
3) are they continuous or occasional ?
4) which field recorders yield direction and which

intensity ? Are there any that do both ?

5) how well distributed are they globally ?

In the reviews that follow little attempt has been made to relate the models to magnetohydrodynamics even though MHD constraints must apply and are sometimes discussed in the original papers.

1.2 Paleosecular Variation: Introduction

It is convenient to consider secular variation (SV) data as coming from four sources:

1) between-site dispersion of paleomagnetic directions,
2) observatory records,
3) archeomagnetism,
4) sedimentary sequences.

Because the axial geocentric dipole approximation is basic to the construction of APW paths and past continental movements it is incumbent upon paleomagnetists to look at the effects of paleosecular variation on the mean directions of natural remanent magnetization (NRM) or paleopoles.

1.2.1 Paleosecular Variation during the Phanerozoic

Between-site dispersion is essentially the only measure of SV available from times greater than the Quaternary (eg. see Irving , 1964, op cit). Ideally the method consists of computing a mean direction for a set of sites which has a spread of ages long enough for SV to have averaged to the AGD field but not long enough for continental drift to have affected the directions. If the mean direction for a large random sample is the AGD field then the dispersion (eg. the standard angular deviation) is taken to be a measure of the SV.

In detail the analysis is two- or three-tiered. At the lowest level a suite of lavas are sampled at many sites and a mean direction is computed for each site using Fisher statistics (Fisher, 1953). The dispersion of the site mean is due to the measurement and orientation errors, and each site mean is taken to be a "snapshot" recording of the field.

At the next level a Fisherian analysis is made of all the lava sites. The site mean may be taken to represent the AGD field and the inter-site dispersion represents the SV. Apart from the precaution that intermediate directions, due to 'excursions' or reversals are omitted there are two assumptions which must be borne in mind. Firstly the SV may not be Fisherian (ie. random) about the mean, and secondly the site 'spot-readings' may not randomly cover a 'cycle' of SV about the mean.

At the third level the mean for the suite of lavas is now considered as the site and all the sites of the same epoch and same continental region (or of the globe, using paleoinclination data) are combined to yield a grand AGD mean, again using Fisher statistics. Typically the second mean is an AGD approximation over about 10^3 to 10^5 a., while the third level approximation is over about 10^5 to 10^6 a. Correspondingly secular variation of duration 10^3 to 10^5 a. and 10^5 to 10^6 a. are estimated at these two levels.

The criteria for the choice of data are fairly stringent and Irving's (1964) estimate of SV included only 35 values from back to the Precambrian. His estimate of the time interval for which the AGD approximation holds good was "a few thousand years" (Irving, op cit, ch. 6).

His analysis of secular variation is discussed in the next section.

1.2.2 Secular Variations Models

From the historic records several components of SV have been recognised as follows (after Brock, 1971):

1) changes in the strength and direction of the non-dipole field,
2) changes in the strength of the central dipole, known as dipole oscillation,
3) changes in the orientation of the central dipole, such that on the average the dipole axis coincides with the axis of rotation, known as dipole wobble.

Several models have been proposed effectively incorporating one or more of the above components so that the dispersion predicted by them may be compared with the dispersion of the Phanerozoic data.

Model 'A' due to Irving and Ward (1964) has a main axial geocentric dipole, Hd, randomly perturbed by a smaller dipole, Hp, so that the dispersion of the directions at the poles is half the dispersion at the equator. This may readily be seen from the fact that the polar intensity is twice the equatorial intensity, where $H = Ma^{-3}(1 + 3\sin^2\lambda)^{\frac{1}{2}}$, and M is the dipole moment, a the radius of the Earth and λ is the latitude. The equation for the dispersion is $S = Se\,(1 + 3\sin^2\lambda)^{-\frac{1}{2}}$, where Se is the equatorial dispersion. Se is dependent on the relative strength of the perturbing field to the main field and is given by Se = 46.8 Hp/Hd.

The 35 values , mentioned earlier, were selected from igneous and sedimentary rocks and by the single and two-tier analyses. The circular standard deviation was then plotted against paleolatitude determined from $\tan \lambda = 1/2 \tan I$. There was considerable scatter in the data but the dispersion showed a poleward decrease. A best fit model to the data gave $Hp/Hd = 0.38$, and $Se = 17.5^{o}$. It was noted that this best fit model also lay very close to the dispersion-with-latitude of the present field.

Cox's second model (Cox, 1970)(model D after Irving's notation) is more physically complete in that it incorporates variations due to:

1) the oscillation of the main dipole,
2) the relative strength of the non-dipole to the main dipole, (as in model A of Irving and Ward), and
3) dipole wobble..

Brock (1971) used 83 selected values to test model D to give $Se = 18.9^{o}$ and $Sp = 9.4^{o}$, with most of the dispersion being attributable to dipole oscillation and the non-dipole field. Dipole wobble was low.

The scatter was large as in Irving's analysis. To see whether some of this scatter was due to time changes in SV Brock used the best fit curve to normalise the dispersion to equatorial values for all the data and replotted these against the quoted age. This plot also showed scatter but a trend was detectable. In particular the SV was lower in pre-Tertiary than in Tertiary times. This is some comfort to the paleomagnetists in that pre-Tertiary estimates of the AGD approximation may be

at least as good as the more numerous Tertiary estimates, and moreover , Late Tertiary paleopoles group fairly well about the geographic poles (but see section 1.3.3, with regard to offset dipoles).

Brock also used earlier data by Cox (1968), fitted to model D which showed that as the main field decreases, the non-dipole field decreases more and the reversal frequency decreases.

1.2.3 Paleointensities of the Phanerozoic

Smith (1967) plotted virtual dipole moments (VDM) against age. (The virtual dipole moment is that calculated from the paleolatitude, in turn calculated from the paleo-inclination). There was a paucity of data but the following points were noted:

1) There was a general increase of the dipole moment from about 2.3×10^{25} G cm^{-3} at 400 ma. BP to about 5.5×10^{25} G cm^{-3} in the Tertiary.
2) There was uniform agreement among the Tertiary data
3) The present field is 8.0×10^{25} G cm^{-3}, this being 30% higher than the Tertiary mean.

There is scatter in the data for each set of igneous rocks - often up to 50% - part of which is attributed to experimental error and to non-dipole effects. Most scatter, however, must be due to variations in dipole strength over relatively short spans of time. Support for this comes from :

1) the high value of the present dipole moment compared

to the Tertiary mean, and

2) the considerable oscillations found from archeomagnetic studies (see section 1.5.1.3).

If the decreasing field values of the early Phanerozoic were a continuation of a Precambrian trend then this would support Runcorn's hypothesis of a core growing throughout Earth's history. However intensity estimates made from late Precambrian and extending back to Archean rocks are as high or higher than todays value (Carmichael, 1967).

1.3 Late Tertiary and Quaternary Secular Variation

1.3.1 The Use of Spherical Harmonic Analysis

1.3.1.1 Introduction

The spatial form of the Earth's field is a product of the shape and strength of the core's electric currents modified to some extent by the surrounding mantle. The dipolar nature of the main field has led directly to the concept of current loops of core dimensions and this concept has been extended to account for the non-dipole field, for example, by eddy-current loops.

The assignment of the field to sets of dipoles without recourse to basic magnetohydrodynamics is essentially a phenomenological approach. The field data or the field resulting from modelled dipoles have been studied by means of spherical harmonic analysis (SHA) in broadly three ways, as follows:

1) The data from observatory records have been analyzed to find which terms of the harmonic series are the

most dominant and how they change with time. A least squares fit is applied to the X, Y and Z field components up to terms of order 8 or more. Amongst other uses these terms may be used as a guide to the past fields. (For examples see Vestine et al, 1947 and section 1.3.2).

2) SHA has been applied to global paleomagnetic data for the Upper Tertiary and Quaternary. Only the low order terms are reckoned meaningful. This is mainly because the X, Y and Z fields are relative, being solely derived from D and I data; the associated paleointensity data are often lacking. The paleo-NRM directions also have larger associated errors than modern values. The dominant terms suggest the model (eg. see section 1.3.3).

3) SHA has been used on models of sets of dipoles to match the actual field at the Earth's surface. One or more dipole parameters are varied until a best fit is obtained with the real data by a least squares method. The three common parameters are the number, the strength and the positions of the radially-aligned dipoles. It may then be possible to recognise these dipoles, their permanence or transience in the data of the past (eg see section 1.3.3).

1.3.1.2 Spherical Harmonic Analysis

The principles of SHA are given in Chapman and Bartels (1962). A shorter account may be found in Jacobs (1967). The following presentation is largely taken from these two works; the Schmidt-modified Legendre polynomials

are taken from Jeffreys and Jeffreys (1978).

A magnetic potential V bounded externally by a sphere, and satisfying Laplace's equation, may be expressed in terms of a spherical harmonic series thus:

$$V = a\sum_{n=0}^{\infty}\sum_{m=0}^{n}\left(\frac{a}{r}\right)^{n+1} P_n^m(\cos\theta)\left\{a_n^m \cos m\phi + b_n^m \sin m\phi\right\},$$

where r, θ and ϕ are the spherical co-ordinates of V; a_n^m and b_n^m are the potential coefficients where n (degree) and m (order) are positive integers. Thus a Fourier series is fitted to the azimuthal variation, $V(\phi)$, and Legendre polynomials to $V(r,\theta)$.

V cannot be measured directly so harmonic series are fitted to the Earth's field components X, Y and Z, where $X = \frac{1}{r}\frac{\partial V}{\partial \theta}$, $Y = \frac{-1}{r\sin\theta}\cdot\frac{\partial V}{\partial \phi}$ and $Z = \frac{\partial V}{\partial r}$, at r = a, the Earth's radius. The corresponding coefficients, g_n^m and h_n^m, are called the Gauss coefficients and are expressed in field units.

It has been shown by applying SHA to modern data that all but about 1% of the measured field at the surface is of internal origin.

The first few Gauss coefficients, with their corresponding polynomial terms have the following significance (table 1.1):

Table 1.1; The Gauss Coefficients and Their Significance for the Earth's Magnetic Field.

Degree	Order	Polynomial	Gauss Coefficients	Meaning
n	m	$P(\cos\theta)$	g_n^m h_n^m	
0	0	1	$g_0^0 = 0$ 0	Monopole - does not exist.
1	0	$\cos\theta$	g_1^0 0	Geocentric axial dipole.
1	1	$\sin\theta$	g_1^1 h_1^1	Dipole in equatorial plane (or orthogonal components of a tilted geocentric dipole).
2	0	$3/2\cos^2\theta - 1/2$	g_2^0 0	Centred axial quadrupole.
2	1	$3/2\cos\theta \sin\theta$	g_2^1 h_2^1	Next tesseral configuration.
2	2	$3/2\sin^2\theta$	g_2^2 h_2^2	Next sectoral configuration.

In general when $m = 0$, $h_n^m \sin m\phi = 0$ and the configuration with only g_n^0 terms signifies an axial multipole, ie., a configuration of zonal harmonics. The sectoral harmonics occur when $n = m \neq 0$, and the tesseral harmonics when $n > m > 0$.

The following important combinations may be noted. The terms $g_1^0 \cos\theta + (g_1^1 \cos\phi + h_1^1 \sin\phi)\sin\theta$ are dominant in the present day field - this combination represents an inclined dipole. A combination of g_1^0 and g_2^0 terms represents a dipole and a quadrupole both centred and axial. The effect is of a dipole displaced along the axis. This offset dipole is the second approximation to the Upper Tertiary and Quaternary paleomagnetic data as discussed in section 1.3.3 .

When $n = 12$ the series approximation has begun to include the crustal anomalies of dimension 1000 Km. For the best data $n = 8$ is usually taken as the truncation limit of the series for the modern internal field.

1.3.2 The Analysis of Observatory Records

Subsequent analyses have confirmed Gauss's findings of the essentially dipolar nature of the Earth's field but with important refinements. It was soon realised that the field changed with time at each observatory. Not only did the intensity change, decreasing after 1800,

but so also did the declination and inclination; this is the secular variation.

Bullard and others (1950) were the first to analyse in detail the westward drift of the field. By comparing global data from 1907 to 1945 they showed that most geomagnetic (giant) anomalies had moved westward at a mean rate of $0.27^{o}\ a^{-1}$. They also computed the drift of the lower harmonic terms during this period. There was a small longitudinal movement of the poles (akin to precession about the spin axis); the overall secular variation was $0.32^{o}\ a^{-1}$. and the non-dipole field drifted $0.18^{o}\ a^{-1}$ westwards.

A summary of the SV by Nagata (1965) is as follows:

1) A decrease of the moment of the field by 0.05% per year.
2) A westward precession of the dipole at 0.05^{o} of longitude per year.
3) A rotation of the dipole towards the geographic axis at 0.02^{o} of latitude per year.
4) A westward drift of the non-dipole field at 0.2^{o} of longitude per year.
5) Growth and decay of features of the non-dipole field giving changes which average about 10 nT (10^{-4} G) per year.

It was suggested by Bullard et al that westward drift was due to partial decoupling of the outer core motions from the lower mantle; the features (anomalies) themselves may arise from deeper within the core. Nevertheless some features do not move and some even drift eastward. One large anomaly (chiefly in the Z component)

centred on Mongolia, for example, has remained stationary though it has grown considerably in recent years. This prompted Yukutake and Tachinaka (1969) to propose that the non-dipole field consisted of standing and drifting components. Their model consists of a standing and a drifting vector in the equatorial plane and the resulting predictions compared fairly well with the actual time variations of the g_1^1 and h_1^1 coefficients.

Yukutake and Tachinaka also computed the variation in the dipole and quadrupole fields. Since 1600 the g_1^0 and g_2^0 coefficients were negatively correlated, ie, the quadrupole has decreased as the dipole has increased up to about 1800; and vice versa since 1800. Verosub and Cox (1971) likewise proposed that from 1845 energy was being 'exchanged' between the dipole and non-dipole fields. This finding, though intuitively appealing, does not seem to apply for earlier times. Cox himself (1975) and Merrill and McElhinny (1977) showed (for $t \lesssim 5$ ma. ago) that when the dipole field reversed the quadrupole field also reversed suggesting a positive correlation. This is supported by Brock's (op cit) tentative conclusion that for most of the Phanerozoic the ratio of the non-dipole field to the main field was equal to or less than the Tertiary value.

1.3.3 Secular Variation from 5 MA. to Present

In an analysis of 52 marine cores Opdyke and Henry (1964) concluded that the Earth's field approximated to an axial geocentric dipole when averaged over 10^5 to 10^6 a., for the past two million years. Reversals were found to be almost exactly 180^o changes.

However in a series of papers R.L.Wilson and others (see eg. Wilson, 1972) showed that virtual geomagnetic poles (VGPs) from Upper Tertiary to the Present were consistently far-sided of the geographic pole from the observers point of view. In detail his findings were:

1) Inclinations in the northern hemisphere were shallower, and in the southern hemisphere steeper than I_{agd} , so that ,
2) looked at from a common-site longitude, the mean VGP was significantly far-sided (and also right-handed).
3) The reversed VGPs were significantly more far-sided than the normal VGPs.
4) The offset axial dipole was found to have a northerly displacement of about 180 km. for the normal state and about 1000 km. for the reversed state (various estimates have now been made).
5) The offsets may have existed as far as 25 ma BP.

(Most of Opdyke and Henry's cores came from the NW Pacific and appear to be exceptional in giving the inclination of the AGD).

Wilson's intriguing conclusions have been tested and improved upon several times since. Creer et al (1973) used global data of both D and I to find the position and orientation of the best fitting dipole. For the Late Tertiary and Quaternary the dipole displacement was about 150 km. towards the north Pacific; the quadrupole effect was again larger for the reversed than for the normal polarity. By analysing the data in terms of hemispheres they showed that higher order harmonics may also have existed through this interval. For example, the continental

hemisphere gave an anomalously large dipole tilt of 36° compared to 12° for the Pacific hemisphere. Lack of paleointensity data and the usual larger declination errors prevented full confidence being placed in the analyses except for low order harmonic terms.

One of the chief sampling problems is due to the intermittent nature of lava eruptions tending to bias directions otherwise meant to average SV. As an example, Hawaii, with its mostly Brunhes age lavas, has been extensively studied by Cox, Doell and others (eg Doell and Cox, 1971). Now the present field in this area is lacking a non-dipole part, in effect allowing the observer to see only the main dipole. This has been referred to as 'the non-dipole low', or the 'dipole window', and on the basis of their work on the lavas Cox and Doell concluded that this effect had persisted for about 1 ma. Further work by them and others has shown, however, that sampling bias was the cause of the apparently persistent non-dipole low (for a re-analysis, see Cox, 1975). Reappraisal of the new and old data has led to confirmation of the VGP far-sided effect - ie., sequences of flows showed segments of SV of shallow inclination.

Cox (1975, op cit) in combining aspects of Yukutake and Tachinaka's standing / drifting model with a radial dipole model of Alldredge and Hurwitz (1969) proposed that the SV was due to sets of three drifting radial dipoles such that the resulting field lines are shallower at low latitudes ($< 40^{\circ}$) and steeper at high latitudes ($> 60^{\circ}$). This model, averaged zonally around the world, fitted the modern field and the Hawaiian

paleosecular variation data quite well. This zonal model and the offset-dipole model disagree most at high latitudes; the former predicts steepening, the latter predicts shallowing of the inclination. Harrison and Watkins (1979), using the high latitude data from Iceland, showed that the offset dipole model is preferred for the interval 13.5 to 7 ma. ago.

Back on a global scale, the whole matter was re-analysed by Merrill and McElhinny (1977, op cit) using a larger data base ($t < 5$ ma. BP). Their aims were to recompute the offset-dipole effect , reassess the right-handed effect that had puzzled Wilson and see if there were any persistent sectoral coefficients. Using the common-site longitude method they reconfirmed the VGP far-sided effect. To account for the difference between the reversed (more far-sided) and the normal VGP positions they proposed a model in which the main dipole reverses but only 3/4 of the quadrupole reverses.

In order to examine the right-handed effect and the existence of sectoral coefficients the ΔD anomalies were averaged over 30° longitude sectors, where $\tan\Delta D = Y/H$, normalised to the equator. $\tan\Delta D$ then gives the ratio of the equatorial dipole to the g_1^0 coefficient. The indication was that this equatorial dipole was antiparallel to the modern equatorial dipole for $t < 5$ ma. BP.

When ΔD was plotted against longitude the result for the normal data could be fitted, approximately, by a sine curve displaced positively; ie. there was a right-handed effect of about one degree. The reversed data was also quasi-periodic but here the ΔD scale was more than

twice that for the normal data and the positive mean was about two degrees. Merrill and McElhinny state cautiously that where the negative values would be found on the globe the data is mostly missing and so suggest that the right-handed effect is probably a sampling artefact.

A mean VGP offset by as much as 2 or 3° over such a long period, 5 to 25 ma. BP, has obvious implications for paleomagnetism, and Merrill and McElhinny state that "the resolution of paleomagnetic poles (may not be) as good as many paleomagnetists have assumed".

A recent review of attempts to analyse paleomagnetic data by spherical harmonics is given by Coupland and Van der Voo (1980). They preferred a modified zonal Cox-type model , based on finding a large octupole , g_3^0, term in the data.

1.3.4 Summary of the Bi-Stable Behaviour of the Field

In discussing the characteristics of the Earth's magnetic field it is now possible to sketch in a limited way the form of $G_n^m = f(t, \Delta t, \theta, \phi)$ where G_n^m represents the Gauss coefficients and their combinations. The axial geocentric dipole hypothesis requires only the existence of the (averaged) g_1^0 term - but for how long ? Wilson and others have shown that it is only a first order approximation even for t $(\Delta t) \approx 5 \times 10^6$ a. The g_2^0 or g_3^0 terms may have to be considered for this length of time or longer. The right-handed effect, the existence of equatorial dipole terms and the assymetry of results from different hemispheres border on being statistically

significant . Even with the reservation about biassed sampling, common data sets, and errors, it now seems that higher harmonic terms may have persisted in the field for long periods of time. If this becomes confirmed then westward drift of SV was either only partly efficient in averaging sectoral and tesseral coefficients or was simply not always operative.

1.4 Transitional Behaviour During Field Reversals

(Normal, intermediate and reversed fields are those for which the corresponding VGPs occupy the latitudes $0^{\circ} - 40^{\circ}$, $40^{\circ} - 140^{\circ}$ and $140^{\circ} - 180^{\circ}$, (Wilson, et al , 1972). For a reversal and event timescale see for example, McElhinny (1973, op cit). Cox (1975, op cit) has given an analysis of the frequency of reversals as a stochastic phenomenon)*

* The International Subcommission of Stratigraphic Classification (ISSC) of the International Union of Geological Sciences (IUGS), in 1979, set up guidelines for nomenclature in magnetostratigraphy (1979). The subcommission recommended that the word 'epoch' for either a magnetostratigraphic rock unit or, more commonly , a time interval, be abandoned. Instead the magnetostratigraphic polarity rock unit is called a polarity zone , (eg the Matuyama (reversed) polarity zone, the Jaramillo (normal) polarity subzone). The geochronological equivalents are chron and subchron. The chronostratographic equivalents are chronozone and subchronozone.

The word 'event' , as used in for example 'during the Jaramillo event' is replaced by the word 'subchron'. Thus usage of 'event' is discouraged when what is meant is a time unit or polarity unit (zone), or chronozone.

It is evident in reading the literature that 'event' is also taken to mean a field 'happening' (correct), in analogy with , for example, 'a volcanic event' . The same is also true of the word 'excursion' about which the commission made no comments. In this study 'event' and 'excursion' have been retained since the original users were firstly or most often referring to anomalous behaviour of the Earth's magnetic field.

So far the dipole and non-dipole fields have been discussed in terms of the usual 'bi-stable' behaviour of the Earth's field. The question of what happens at a reversal transition or at an excursion (when VGPs occupy the mid-latitudes) is important for two reasons:

1) A knowledge of the VGP paths and field intensity changes would provide insight into the workings of the core dynamo and constraints on MHD models.
2) Sudden or large intensity changes may be directly, or indirectly, related by cause to faunal extinctions (eg, Hays, 1971), to changes in the atmospheric cosmic ray flux (eg, Bucha, 1970; Lingenfelter and Ramaty, 1970) and by cause and effect to climate changes (eg, Kawai, 1972).

The basic questions include:

1) what happens to the dipole and non-dipole fields during a transition ?
2) how do different transitions compare ?
3) how do N to R and R to N transitions compare ?

The main dipole may either maintain its intensity and rotate through 180°, or diminish to zero before reappearing with the opposite polarity. Combinations of both these , without interference from non-dipole components , would show the same VGP path for all sites. The segments of the path would be along great circles. On the other hand if the non-dipole field was comparatively large then VGP paths would be different for different sites for the same transition and for the same site for different transitions. Segments of VGP paths would probably

(not necessarily) be small circle segments.

From seven polarity changes Creer and Ispir (1970) concluded that the non-dipole part diminished but the dipole term had two or three components whose resultants gave similar VGP paths. In an alternative model (see for example, Larson et al 1971) the main dipole diminished and the non-dipole component became dominant giving different VGP paths.

Dagley and Lawley (1974) analysed 23 reported polarity transitions, mostly from lavas. Their analysis showed:

1) east-west swings of field direction before the transition,
2) large east-west swings during the transition with a prominent westward trend in many cases.
3) a decrease in the intensity of the field. This was analysed further to show a decrease to zero for the axial component and an increase to a plateau-maximum for the equatorial component as the transitions reach halfway - and vice versa as the transitions are completed. The total field may show an increase before the transition.
4) there was neither a preferred path nor sector for all VGPs of the same site nor of the same transition for different sites, (however, see Hammond, et al, 1979).

Dagley and Lawley tentatively suggested that the most likely model has three orthogonal components which vary independently. The variation of the (one or two) equatorial components accounts for the east-west swings.

From this and other studies the estimated transition times are from 1500 to 10,000 a.

Sampling problems must again be considered. The lavas were erupted probably sporadically so that:

1) there may not be complete coverage of a given transition ,
2) the transition may not be recorded elsewhere .

The dating may not be precise enough to:

3) estimate the time of the transition, or
4) provide cross-correlation of transitions for different sites.

To obviate some of these problems marine sediments, having the advantage of continuous deposition, have been used (eg, see Hammond, et al, 1979, op cit, for a description of the Jaramillo and Olduvai transitions), with the following observations:

1) The intensity decreases before as well as during a reversal.
2) The east-west swings are not as pronounced as in the lava records; instead the VGP paths are predominantly north-south.

In general marine sediments are deposited too slowly (usually < 1 cm/ka) to permit detailed analysis of a transition. The notable differences between the lava and the sediment records support the suggestion (eg, Løvlie, 1976) that post-depositional movement of fine magnetic grains has occurred. Thus the low intensity and the N-S paths may be partly artefacts of the sediment recorder, (see sections 1.5.2/3/4).

Figure 1.1

Virtual Geomagnetic Pole Positions for England and Japan. (From figure 4.13 of Aitken, 1974)

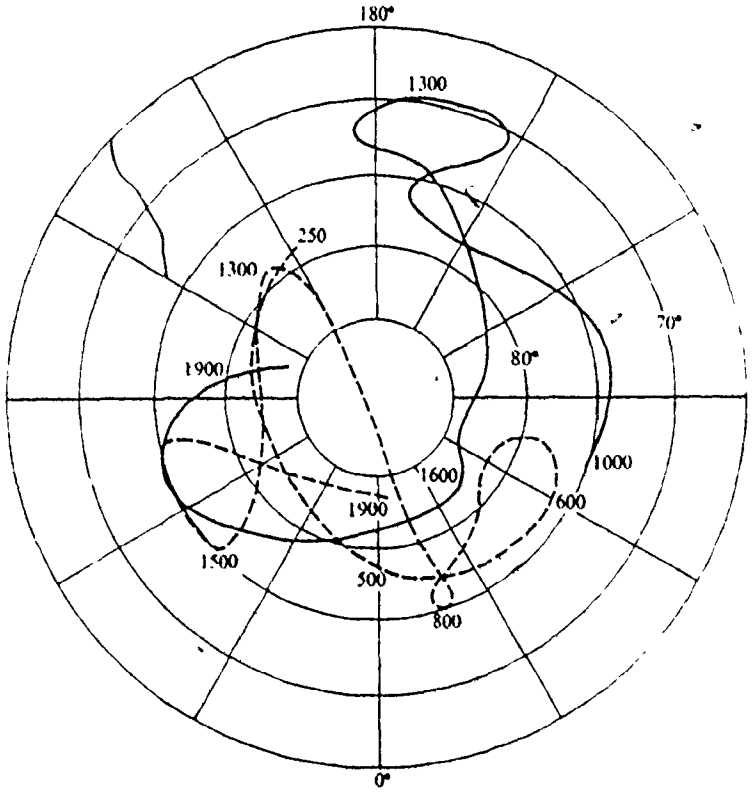

FIG. 4.13. Virtual pole positions derived from archaeomagnetic data for England (solid line) and for Japan (dashed line). The virtual pole for an observing station is the orientation of a dipole at the centre of the earth such that the magnetic field would have the values of *I* and *D* observed at the station. Although the pole positions do not superimpose, it is to be noted that there is a broad similarity in the movement.

1.5 Brunhes Chron Paleomagnetism

1.5.1 Archeomagnetism

1.5.1.1 Introduction

Most of the data about the intensity of the Earth's field in Quaternary times has come from archeomagnetism, the name given to the study of the NRM of baked bricks, pottery, fireplaces and related man-made objects. In situ artefacts also yield D and I as well as the intensity data. The ancient field is estimated , in the laboratory, by comparing an artificial thermoremanent magnetization,(A)TRM acquired in a known field, with the NRM, so that :

$$H_{ancient} = NRM/TRM \times H_{lab.}$$

For a review of the methods see, for example, Thellier (1977) or Aitken (1974). Dating of the material has come from historic records, by thermoluminescence and fission tracks but chiefly by the ^{14}C method.

1.5.1.2 Field Directions

Runcorn (1959) and Skiles (1970) showed that, for normal polarity, when some field feature moves westward it causes clockwise looping, while eastward motion causes anticlockwise looping , of the field direction. In this way archeomagnetic studies from several countries have revealed eastward as well as westward motion of SV over the last several thousand years. In fact SV from England, the Ukraine, and Japan has shown fairly complex looping (eg, see figure 1.1) which may have been due to westward or eastward motion of single features or the resultant motion, growth and decay of two or more features.

1.5.1.3 Field Intensity

For reviews of studies of intensity variations of back to about 10 Ka. see, for example , Aitken (1974, op cit), Smith (1967) and Barton, et al (1979).

From the ancient field intensity H_{anc} the Earth's magnetic moment that produced it, is given by:

$$M_{anc} = H_{anc} . a^3 (4 - 3 \cos^2 \lambda)^{-1/2}$$

where a is the radius and λ the latitude. This ancient moment varies according to the value of λ that is used, giving rise to three models:

1) If λ is the geographic latitude of the site then the moment is assumed to be axial and is called the virtual axial dipole moment (VADM). Besides experimental error, dispersion also arises from both dipole wobble and non-dipole intensity variations.
2) If λ is the present day magnetic latitude then the moment is effectively normalised to the present-day value and is called the reduced dipole moment (RDM). The dispersion excludes that due to dipole wobble so long as the ancient dipole axis coincided with the modern 11.5^{o} tilted axis. It is probably good for a few hundred years only.
3) If λ is that deduced from the paleoinclination by $\tan \lambda = 1/2 \tan I_{anc}$ then this gives the virtual dipole moment (VDM). The poles of the VDM are the VGPs deduced from D and I. The global dispersion always excludes that from dipole wobble but includes that due to non-dipole effects. A knowledge of I_{anc} is necessary but is lacking from many archeomagnetic determinations.

Although a long way in the future of the research,

Figure 1.2; The means of consecutive 500 year intervals for relative virtual axial dipole moments (taken from figure 2b of Barton et al, 1979)

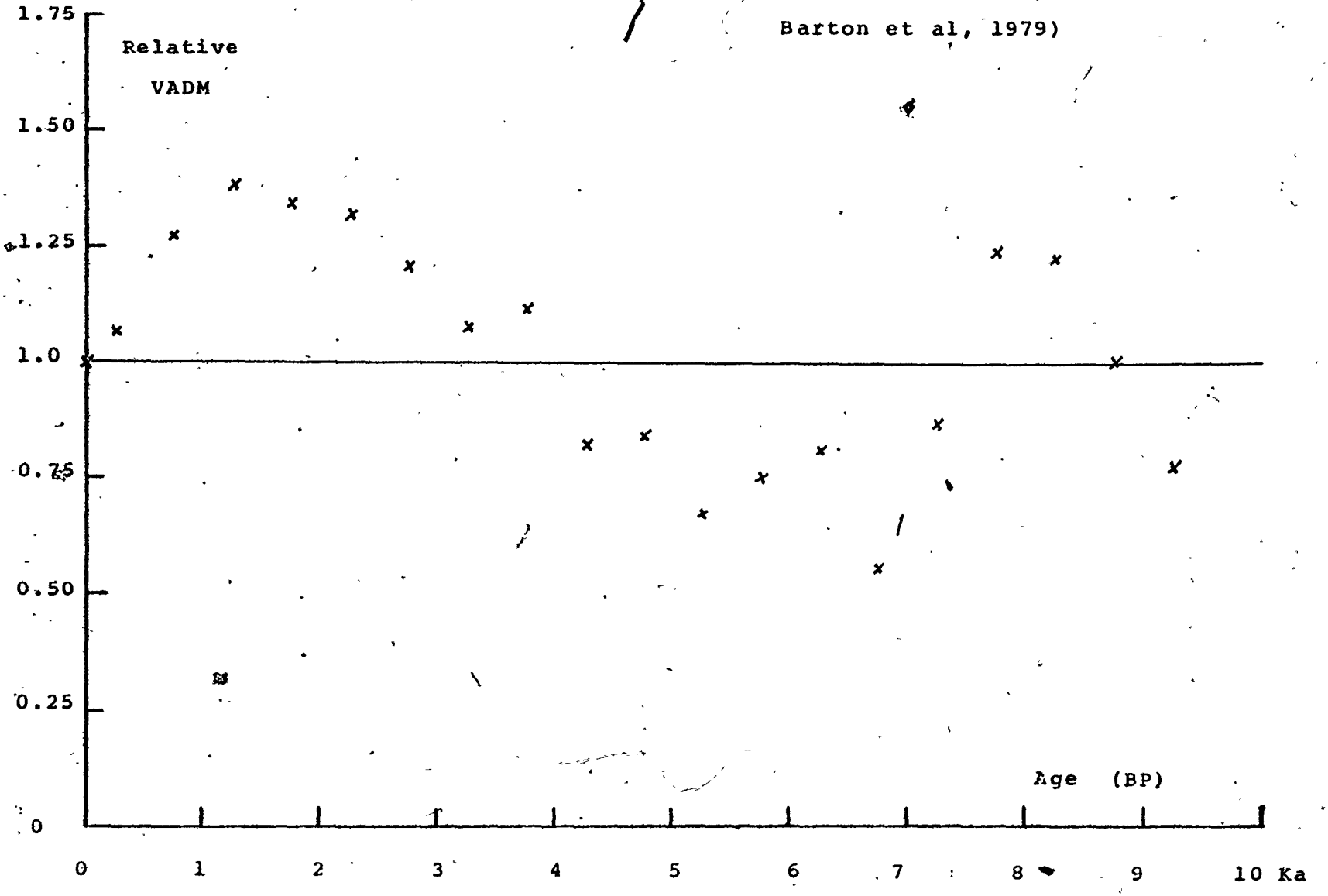

a combination of VDM and VGP global data must be an ultimate aim of archeomagnetism because only then will it be possible to uniquely unravel the relative contributions of dipole oscillation, dipole wobble and non-dipole fields by SHA. From a comparison of the three ways of treating the data Barton et al (op cit) estimated that for $t < 10$ Ka. the contributions to intensity scatter are 10% from dipole wobble, 10% from non-dipole effects and about 15% from experimental error (including dating errors). Thus a first approximation, would be to consider the average of the global data, patchy though it is, to be the main dipole intensity. Reproduced in figure 1.2 is the 500 year interval means of the relative VADMs from Barton et al.

On this time range the variation may be fitted by a sine curve, and to which ^{14}C variations show fair correlation. There are good reasons for supposing that the Earth's field intensity modulates the cosmic ray flux which produces the $^{14}N(n,p)^{14}C$ reaction. (There are other modulating factors to the eventual ^{14}C organic concentrations). Barton et al suggest that pending more data from prior to 5000 a. BP. it would be unwise to rely on any extrapolation of this curve either for accurately dating archeomagnetic samples or, conversely, for correcting ^{14}C dates.

1.5.2 The Sediment Record

Most of the data about the direction of the field during the Brunhes chron has come from the sediments of oceans, lakes and varved sequences. They have the advantage of being continuous, often dateable and of having global coverage. Specimens for NRM measurement are usually taken

at intervals down a split core; at points of interest such as a polarity transition the sampling density is increased. Most sediments show fair to good stability to alternating field (AF) demagnetization. Marine cores are dateable by recognition of the Brunhes-Matuyama polarity transition, by Th, Pa and ^{10}Be methods, assisted by cross-correlation with oxygen isotope and foraminiferal records. Lake sediments have been dated mostly by the ^{14}C method, occasionally by the K/Ar method on intercalated ash layers, and by stratigraphic correlation and pollen analysis.

As discussed below the sediment record is often far from perfect. Together with the limitations of the archeomagnetic record this provides the justification for looking for alternative recorders of the field.

In this study these alternatives are speleothems and hot spring deposits. It may be argued , a priori, that the two possible modes of magnetization of speleothems or hot spring deposits are detrital and chemical remanent magnetizations. Hence a detailed study of the detrital magnetization process is also included here for its possible relevance to the NRMs of these deposits.

1.5.3 The Magnetization of Sediments

When a magnetised grain falls through water it is aligned by the ambient field acting against inertial and viscous torques. Upon settling there is an additional mechanical torque due to the bed itself which tends to misalign the grain moment with the field. The resulting remanence of many grains is proportional to H for low fields ($H \leqslant 2$ Oe)(Johnson et al , 1948), and is called detrital remanent magnetization (DRM).

After settling the particles may continue to move within the pore spaces before eventual dewatering and compaction take place. If total magnetization occurs below the sediment-water interface then the result is termed a post-depositional DRM (pdDRM). All of these torques, and effects such as Brownian motion, are grain size dependant but the field torque is expected to be dominant for magnetite grains of micron and submicron sizes (see, eg Stacey and Banerjee, 1974). A sediment may possess both depositional and post-depositional DRM in some proportion depending on its grain size spectrum (magnetic and non-magnetic) and on its history. In addition some sediment NRMs are known to have a diagenetic chemical 'overprint', which may be as strong or as stable as the DRM.

The DRM of a sediment may have inclination error due either to more elongate particles which rotate upon settling, or to the rolling of more spherical grains into micro-hollows in the surface. The average declination is unaffected but the inclination is decreased. An additional inclination error may occur if the bed is already tilted ; it is called the bedding error. Appreciable currents also exert torques on elongate grains giving rise to errors in both D and I (Griffiths, et al, 1960).

The overall inclination error from deposition and compaction contribute most to the degeneration of the sediment record. In recovering the original field inclination some estimate must be made of the error ΔI. One approach is to assume that the whole core, if long enough, would have had a mean I , but for the error, which satisfies $\tan I = 2 \tan \lambda$ to give the AGD inclination for that latitude. This assumes firstly that the correction factor

is the same for the whole core, and secondly, that the field gave the AGD approximation for that time interval (eg, Creer, et al, 1972). A second approach is to redeposit part of the core in a field of known inclination and see what the DRM errors are. The assumptions are that:

1) the difference between the natural and laboratory deposition times does not cause error, and
2) the intensity of the artificial field is sufficiently close to the original as to make no difference in I (but see Johnson, et al, op cit).

Although there have been several deposition experiments made on synthetic and natural sediments the differences between laboratory and natural conditions are probably too great and unknown for the remanences to be considered equivalent. This approach has been used only as a rough guide to the nature of the errors.

It is thought that burrowing worms cause resetting of magnetization in marine muds. This bioturbation assists in the establishment of post-depositional DRM. Some muds can be shown to exhibit pdDRM from laboratory esperiments (Kent, 1973; Løvlie, 1974), whereas some do not (Verosub, et al, 1979; Barton and McElhinny, 1979). In marine sediments pdDRMs may cause:

1) correction of any depositional error causing a shift towards the ambient field,
2) an apparent increase of the signal age by as much as 30 Ka. or more,
3) a smearing of D and I variations,
4) a lowering of the intensity across a polarity transition (Kobayashi, et al,1971: Løvlie, 1976)
5) the elimination or interference of shorter polarity subzones (Watkins, 1968).

Marine and lake cores are usually recovered by means of piston, gravity or drill cores and possess various undesirable features for paleomagnetic purposes (Opdyke, 1972). Gravity cores are usually too short, may suffer from internal disturbances and may not enter the sediments vertically. Piston cores have provided most of the data on sediments. However the tops of cores may be missing and stretching occasionally happens. They may suffer from internal rotation, are usually discontinuous and generally have no reference to azimuth.

1.5.4 Literature Review of the Sedimentary Record

Early work on the depositional DRM of varves was carried out by Johnson et al (op cit), in which the recorded inclination and field dependence of the DRM were investigated. The inclination, bedding and flow errors were studied in greater detail by Griffiths and coworkers (eg, Griffiths et al, 1960), and the difficulties of using varves for SV studies were discussed in Griffiths et al (1958).

The post-depositional effect was investigated by Irving and Major (1964) on synthetic sediments, and was suggested as a possible factor to account for the low intensity observed at a polarity transition by Kobayashi et al (op cit), and by Kent (op cit). PdDRM of a marine sediment was demonstrated in the laboratory by Løvlie (1974, op cit) and he also showed that pdDRM does indeed lower the intensity at a polarity transition zone (Løvlie, 1976, op cit)

Study of the NRM of marine cores for paleomagnetism was begun by Keen (1963) in which he noted the presence

of bioturbation. The use of 52 marine cores to test the AGD hypothesis by Opdyke and Henry (op cit) has already been noted (section 1.3.3). Watkins and Goodell (1967) in looking for short term subzones within the Matuyama magnetozone proposed a strict method of interpolation upon linear sedimentation rates to eliminate the acceptance of spurious short magnetic 'events'. The possible effects of bioturbation on events were discussed in Watkins (1968, op cit). The first event within the Brunhes chron to be detected in sea cores - the Blake - was proposed by Smith and Foster (1969) from several cores from the N. Atlantic and Caribbean. Subsequently several events or excursions of Brunhes age have been claimed from sedimentary deposits.

Probably because of the depositional errors varves have been little used as paleo-SV recorders. Recently Verosub (1979a and b) resampled the New England varves (as used by Johnson and co-workers) and was fairly successful in separating SV from the variability of the recorder.

Lakes and marginal seas may have sedimentation rates up to several tens of centimetres per Ka. and are high enough to resolve SV. Notable research on British and European lakes has been carried out by Mackereth (1971) and Creer and co-workers(1972). The European SV record has been summarised by Thompson and Turner (1979) and extended to about 13.5 Ka by Creer et al (1980).

SV studies of N American lakes have not been so successful due mainly to the variability of the recorder and the poor dating control (Creer et al, 1976a and b; Dodson et al, 1977; Vitorello and Van der Voo, 1977; Banerjee et al, 1979). Lakes in California have been studied in detail for SV. There is conflicting evidence on the existence

(Denham and Cox, 1971; Liddicoat and Coe, 1979) or non-existence, or age (Verosub, 1977a) of the Mono lake excursion.

Lake Biwa, Japan, with its long history of deposition has been cored for SV studies (eg, Yaskawa, et al, 1973), and has revealed four apparent excursions within the Brunhes chron: the dating controls were not satisfactory.

Dated SV studies of marginal seas include those of Opdyke et al (1972) of the Aegean from 27 Ka. to Present and of Creer (1974) of the Black sea from 25 Ka. to 5 Ka. BP.

With the increase in marine core paleomagnetism in the late sixties came the first cautionary note by Watkins (1968, op cit) on the effects of bioturbation. He included sea cores in a review of the magnetostratigraphic column and its possible refinement (Watkins, 1972), in which he wrote against the uncritical assignment of unexplained curious results to some new (previously described) event, describing it as a psychological trap which he called 'the reinforcement syndrome'.

Sea core paleomagnetism was specifically reviewed by Opdyke (1972) in connection mainly with the polarity stratigraphy and he also cautioned against the too easy acceptance of short events or excursions.

Harrison (1974) in his review of sea-core paleomagnetism applied statistical methods to several hundred cores to pick out the short events within the Brunhes and Matuyama chrons. Of the 216 cores which penetrated the B-M transition 173 showed no reversed events. The two main peaks , of the remainder, in a histogram did occur at about the positions previously claimed for the Laschamps

and Blake events. Likewise peaks in the core sections of the Matuyama magnetozone corresponded to the known events from the established polarity time scale but many cores also showed apparently spurious results. He concluded, "While some of the events may be caused by hitherto undetected reversals of the Earth's field, it is believed that many are caused by spurious effects; therefore short period events (from marine cores) are not reliable stratigraphic markers".

In the 1970's 'excursions', 'flips', 'departures', 'happenings' and 'events' continued to be found within the Brunhes chron, notably from the faster-deposited sea and lake sediments (table 1.2). Verosub (1975a) showed how an undetected slump feature upon maintaining its depositional DRM could easily mimic such anomalous field behaviour.

Cox, et al (1975) in reviewing the literature on polarity transitions, excursions and SV suggested that short reversals like the Laschamps and the Blake may be more localised SV anomalies rather than true global events,

A major review of depositional and post-depositional DRM was made by Verosub (1975b) and the excursion/event record was reviewed critically by Verosub and Banerjee (1977). For a recent review of SV studies of lake sediments see Lund and Banerjee (1979).

The estimation of paleointensities from sediments by ARM, SIRM, susceptibility and Koenigsberger ratios has not been successful except as a first estimate of relative paleointensities. The best approach appears to be by the ARM method (eg, Kent and Opdyke, 1977; Levi and

Banerjee , 1976).

The dating of marine cores has not always been satisfactory. The usual method to locate an event within a Brunhes zone has been to assume a constant sedimentation rate from the B-M polarity transition zone to the core top or to the range of a U-series method. The combined Th and Pa method has an age limit of about 200 Ka, BP. The ^{10}Be method is still being developed but has a limit of about 6 to 7 ma. (see Amin, et al, 1975). The best approach at present appears to be in combining several dating methods to check on the sedimentation rates and on the existence of pdDRM (eg, Dymond, 1969; Ku, et al, 1968). For a critical review of the use of excess radiogenic daughters for dating sea-cores see J.K. Osmond (1979)

The chief method for dating lake sediments has been by the ^{14}C method which is largely uncalibrated before about 7 Ka, BP. Verosub and Banerjee (op cit) point out that there have often not been enough age control points within the published core data.

1.5.5 'Events' and 'Excursions' within the Brunhes Chron

Cox (1975, op cit) reckoned that polarity subchrons (events) may be as short as 3×10^4 a in view of the time (decay) constant estimates of the main core dynamo. If estimates of the polarity transition times are correct ($\approx$2000 a) then global subchrons might be as short as 4 or 5×10^3 a. Thus a knowledge of the transition times of the briefest subchrons has implications for dynamo theory. The importance of transition VGP paths has been mentioned earlier (section 1.4).

Both the marine magnetic anomaly and sea-core data are usually incapable of detecting subchrons less than about 20 Ka., as discussed by Cox, Harrison and others. With the possibility of using chronometric methods with better resolution (shorter half-lives) there has been great interest in characterising anomalous field behaviour within the Brunhes chron, if it occurred. Besides the implications for geomagnetism, the use of SV magnetostratigraphic curves with events or excursions as major markers represents an additional dating tool for the Late Quaternary (see eg, Kukla and Nakagawa, 1977, and volume 7, issue 3 of Quaternary Research devoted to magnetostratigraphy).

Table 1.2 is a brief listing of published claims qualifications and criticisms for events and excursions of the Brunhes chron . This list is not exhaustive of all claims for at least intermediate VGP positions. (see Verosub and Banerjee, op cit). Most of these anomalies are very short - the Gothenburg 'flip', for example, which is claimed as a global phenomenon, was only about 50 a. long !

The Laschamps event is worth further consideration, since firstly, it was the first claim for an event within the Brunhes chron. Secondly it was originally found recorded in lavas and not in sediments. Finally it has been variously used to support claims for other anomalous field behaviour from the NRMs of sediments (eg, Noël and Tarling, 1975).

The Laschamp event was detected in two scoriaceous lava flows of puys Barme and Laschamp, France, (Bonhommet and Babkine, 1967; Bonhommet, 1970), and the NRMs are fully reversed. The first problem was to date the flows.

Table 1.2; Listing of Events and Excursions From 350 Ka. BP. to Present

Starno Event, Sweden, 28 Ka.BP, in post-glacial sed. core, Noël and Tarling , 1957.
critised by Thompson and Berglund, 1976;
reply by Noël, and further discussion by Thompson and Berglund, 1977.

Gothenburg Event, Sweden, 12,350 to 12,400 a. BP, in post-glacial sed. core and sea core. Mörner et al, 1971; Morner and Lanser, 1975, and Mörner, 1977.
criticised by Thompson and Berglund, 1976;
critised by Opdyke and reply by Mörner, 1976;
criticised by Sukroo et al, 1978.

Erieau Excursion, Canada, between 14 to 8 Ka. BP, lake cores, Creer, et al, 1976;
non-confirmation of Erieau and Gothenburg Excursions, Banerjee et al, 1979.

Rubjerg Excursion, Denmark, between 40 to 23 Ka, marine seds., Abrahamsen and Knudsen, 1979.

Linked B and I excursions reported from Gulf of Mexico seds., Clark and Kennett, 1973.

A Lake Biwa Excursion, Japan, 18 Ka. BP.,sed. cores, Nakajima, et al, 1973.

Imuruk Lake Excursion, Alaska, 18 Ka. BP, seds. Noltimier and Colinvaux, 1976;
criticised by Marino and Ellwood, 1978.

Maelifell Event, Iceland, between 40 and 20 Ka. BP, lavas, Peirce and Clark, 1978.

Table 1.2, continued

Mono Lake Excursion, California, 25 or 24 Ka. BP, 850 years long , seds., Denham and Cox, 1971; Denham, 1974; Liddicoat and Coe, 1979.
possible confirmation, Palmer, et al, 1979;
non-confirmation, Verosub, 1977.

Lake Mungo Excursion, Australia, 31 to 28 Ka. BP., baked clays, Barbetti and McElhinny, 1972; 1976,
possible confirmation, Soloyanis and Brown, 1979, Stupavsky, et al, 1979 and Freed and Healy, 1974.

Laschamps Event, see text.

A Lake Biwa Excursion, Japan, 49 Ka. BP.,sed. cores, Yaskawa, et al, 1973;

Blake Event, N Atlantic and Caribbean, 114 to 108 Ka. BP., marine cores, Smith and Foster, 1969; Denham, 1976; Denham et al, 1977;
possible confirmation , eg, Creer et al, 1980;
see section 6.3.4.

Lake Biwa 1 Event, Japan about 186 to 176 Ka. BP, sed. cores, and,

Lake Biwa 2 Event, about 298 to 292 Ka. BP, Kawai, et al, 1972.

A ^{14}C date fixed an upper age limit at about 8 Ka; problems with atmospheric argon contamination rendered tentative the K/Ar lower age limit of 20 Ka. Unlike the events from sediments there seemed little doubt of the reality of the Lashamp reversal. Consequently further attempts were made to determine the age of the lavas as follows:

1) 45.0 ± 2.5 Ka, by K/Ar and $^{40}Ar/^{39}Ar$; Hall and York, 1978
2) 39.0 ± 6.0 Ka, by $^{230}Th/^{238}U$; Condomines, 1978
3) 36.0 ± 4.0 Ka, by TL dating;
4) 42.0 ± 5.0 Ka, by K/Ar;

} Gillot, et al, 1979

More recently Heller (1980) has demonstrated that the flows possess strong self-reversal characteristics and consequently a true field reversal may not have occurred at this time. Perhaps the chief result of these investigations is a positive concordancy test of different dating techniques on Quaternary scoriaceous lavas!

1.6 Summary and Thesis Objectives

This chapter began with a list of questions about the character of the Earth's magnetic field. The sections that followed reviewed some of the answers and indicated where most of the problems lie. In particular it is quite clear that the spatial and temporal variations at the short end of the time spectrum (10^2 - 10^6 a) are inadequately known. Such concepts as standing and drifting fields, vector looping, the right-handed effect, short events, excursions, VGP transition times and paths, SV periodicity, dipole to non-dipole ratios, all lack an adequate data base for a full description.

The paleomagnetist must make the best of what paleofield recorders, from the Brunhes chron, are available.

He then becomes confronted with four broad problems:

1) The recorded signal is generally not directly dateable; there is often loss of accuracy and resolution for various reasons, some of which have already been mentioned (section 1.5.4).
2) The intensity record from lavas and baked materials is fragmentary.
3) The bulk of the paleodirection data, being derived from sediments, is imperfectly recorded.
4) There are very few age-dated, combined intensity and direction data so necessary for a full vectorial description of the field.

The main object of this thesis is to show that there exists a class of dateable continuous deposits which provide an alternative paleomagnetic record going some way towards satisfying the four problems - namely speleothem deposits.

Speleothems are calcium carbonate deposits precipitated inside caves from seepage water (see eg, Ch. 8 of Ford and Cullingford, 1976). Stalactites are formed from the cave roof and usually have a double structure consisting of an inner 'soda-straw' covered by conical or cylindrical layers. The growth layers are not generally accessible to easy sampling.

The falling drips from the stalactites, upon reaching the floor, form stalagmites. These are pillar-like objects in which the growth layers are arranged like stacked, inverted saucers. Their stratigraphy, especially in the central drip area, is simple. The oldest layers are at the base and the youngest layers are at the top.

Often carbonate-rich waters precipitate calcite onto the walls or floors of caves forming sheet-like

deposits called flowstones. The sheets may be flat or curved, horizontal or sloping, rough or smooth, enclose pools (gours to microgours), and in general, grade into other forms of calcite deposits such as stalagmites and stalactites. Nevertheless such sheets are usually simply-ordered from a sampling standpoint.

Because of their simple stratigraphy and greater accessibility stalagmites and flowstones have been studied for age-dating for karst geomorphological purposes (eg, Atkinson, et al, 1978), archeological purposes (eg, Schwarcz, 1980), and as possible recorders of oxygen and carbon isotope variations (Hendy,1970; Thompson, 1973; Gascoyne, 1979), Mg/Sr variations (Johnson, 1979), and herein,of paleomagnetic variations.

Speleothems may be reliably dated by the ^{230}Th-^{234}U method (eg, Thompson, et al, 1974; Thompson, 1973, op cit ; Gascoyne,et al, 1979). For uranium-rich speleothems concordance may be checked by the ^{231}Pa - ^{230}Th dating method (eg, Gascoyne, 1979, op cit). The ^{14}C method has also been used with some success (eg, Hendy, 1970; Spalding and Mathews, 1972). The ^{230}Th - ^{234}U method has been used in this study. The accuracy, precision and limitations of this dating technique are discussed in chapter 3. It has an age-dating limit of about 350Ka.

The mainstream of the research has been to obtain D and I variations across the growth layers of stalagmites and flowstones from various localities. Those speleothems yielding measurable and stable NRMs have then been analysed for U and Th by alpha-particle spectrometry to give dated SV curves. It has then been possible to reconstrust VGP

paths and make some inferences about the Earth's ancient field.

Earlier paleomagnetic studies on unoriented stalagmites from Yorkshire, begun at Leeds university, England, showed either remanences which were stable and weak or no measurable remanence at all. This finding has proved to be generally valid. In consequence not all field and laboratory work in collecting, orienting and preparing samples has paid off. Some environmental preconditions for the occurrence of stable and measurable NRMs have been revealed so it has been possible to suggest where suitable speleothems might be found.

After demonstrating the feasibility of speleothem paleomagnetism (despite the low NRMs) it became necessary to look at their rock magnetic properties. The first consideration was to test for their freedom from depositional errors since it was not known if the remanence was a DRM or a CRM. This has been tackled in two ways. Firstly the NRM directions along variations in growth-layer topography have been examined for various surface influences. Secondly hysteresis loops taken parallel and perpendicular to growth layers have been examined for IRM anisotropy.

The magnetic phases of several samples were identified by their hysteresis and thermomagnetic parameters and the identification was augmented by thin section analysis and by Mössbauer effect spectra in some cases.

An attempt has also been made to recover the relative paleointensity of some samples (one in detail), by ARM and SIRM methods , but with limited success.

CHAPTER 2

FIELD AND LABORATORY METHODS FOR THE MEASUREMENT OF THE NRM OF SPELEOTHEMS

2.1 Introduction

Two alternative recorders of SV, to sediments and baked materials, are speleothems and hot-spring deposits. In 1973, while at Leeds university, Colin Thomas and the author casually tested for NRM using two broken stalagmites from Gavel Pot, Yorkshire, using a PAR spinner magnetometer. A 1 inch core was drilled from the central axis of each sample and with approximate vertical control we showed that there was a positive downwards axial component which was weak. Another sample from Gavel Pot, tested by D. Tarling at Newcastle, was found to have no measurable NRM, but one from a Yugoslavian cave had a measurable NRM which was stable to alternating field demagnetization (D.H. Tarling, pers. comm.). Tarling guessed that the iron , in the latter, was carried in from the terra rosa soils above the cave.

With the adoption and development of the uranium-thorium disequilibrium method for dating speleothems at McMaster university, it became possible to provide dates for NRM variations in speleothems shown to be paleomagnetic recorders. After all magnetic measurements had been made of the sample, selected specimens could be used for dating and a best fit curve of age of SV constructed.

A detailed account of the physico-chemical origins

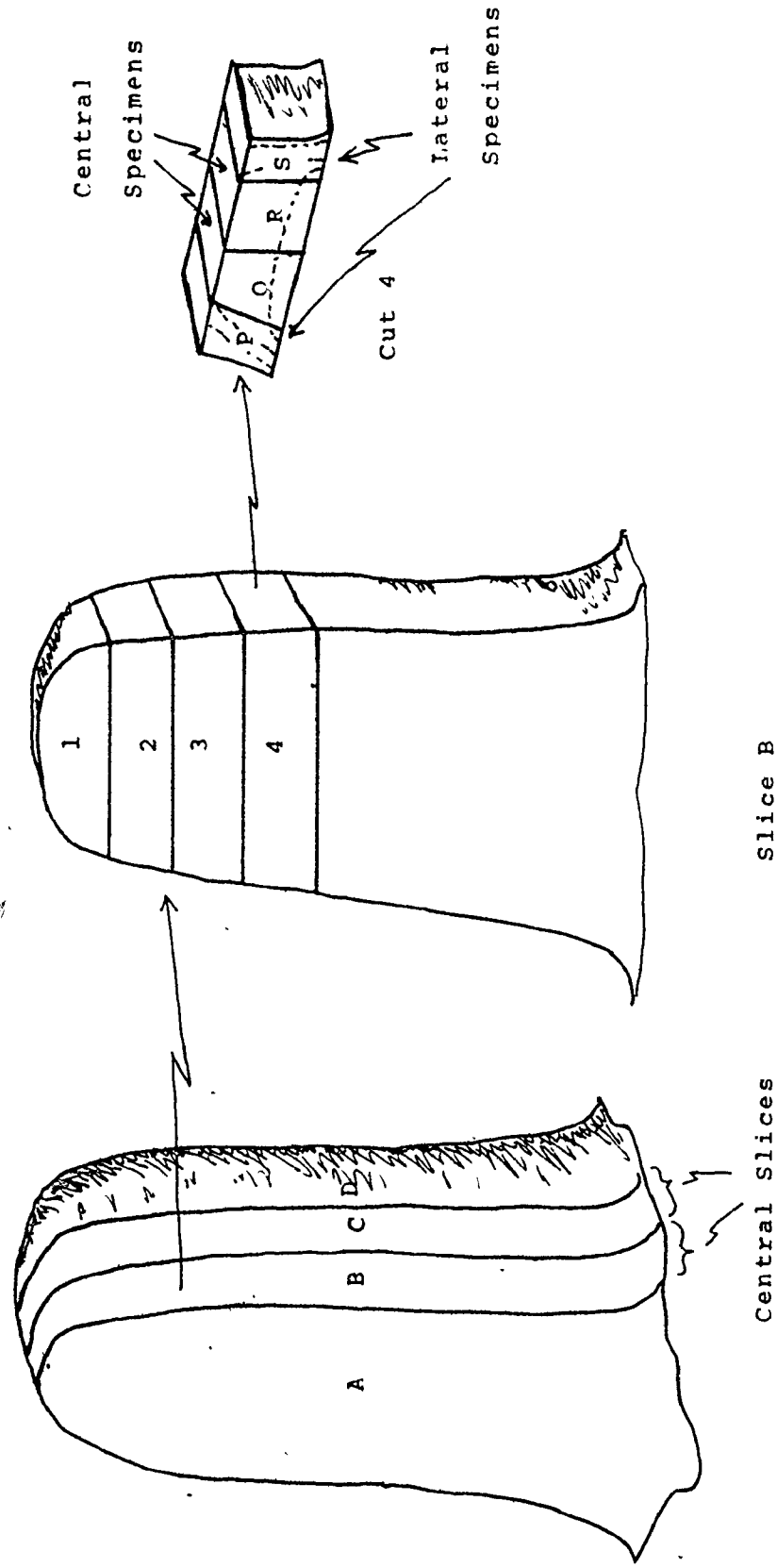

Figure 2.1
Specimen Preparation from Stalagmites

Figure 2.2

The Morphology and Specimen Preparation of Flowstones

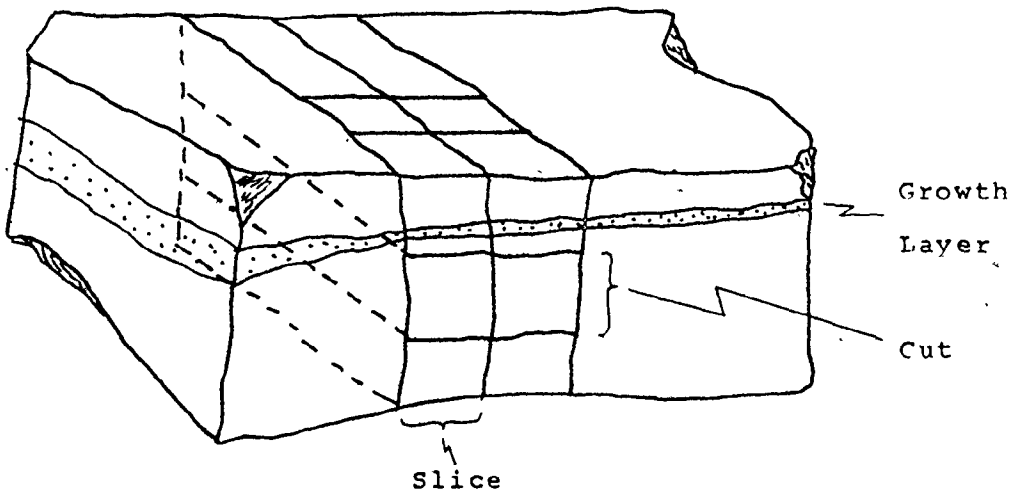

Plate 2.1

Orienting Devices for Stalagmites and Flowtones.

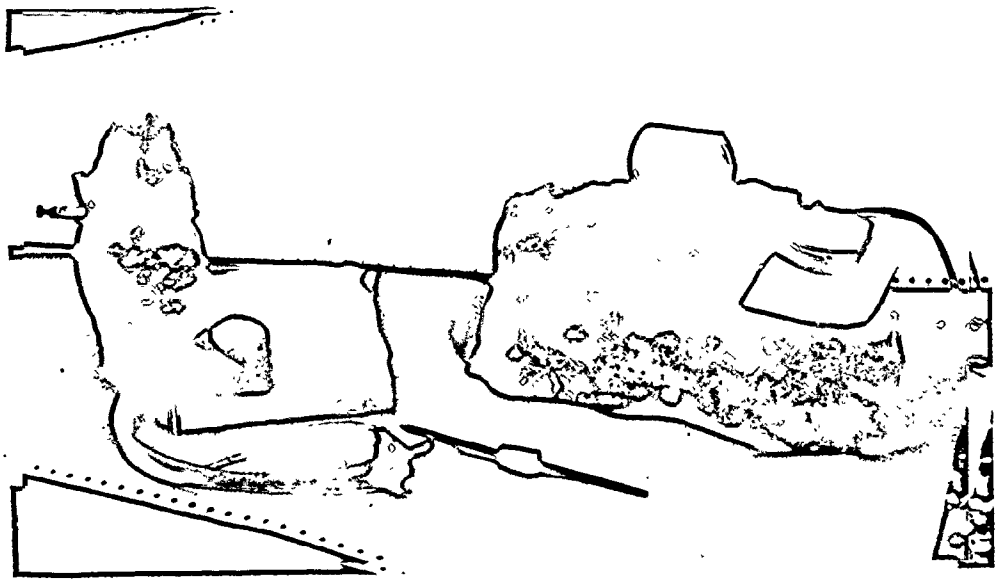

of speleothems is given by White (Ford and Cullingford, ed , Ch. 8, 1976, op cit). For a thin section analysis of speleothems see Kendall and Broughton (1978) or appendix III of this study.

Figures 2.1 and 2.2 represent the usual growth layering of stalagmites and flowstones and the specimen preparation that is appropriate to them. In the case of stalagmites the central portion yields both best paleomagnetic and dating resolution. The number of specimens per growth horizon depends on the width of the (sub)horizontal layering. Stalagmites yielded between one and six specimens using widths of 2 to 4 cms. For flowstones more specimens may usually be extracted from a given horizon unless the layers curve, wedge out or vary in thickness transversely to the water flow.

Oriented speleothems had first to be collected and the first part of the chapter describes the field methods. Laboratory techniques for preparing oriented specimens are then described, followed by NRM measurement and the treatment of the data. Of great value to this work has been the use of a cryogenic SQUID magnetometer having both a low noise level ($\lesssim 2 \times 10^{-7}$ Oe) and a fast response time. NRM measurement and all other magnetic work has been carried out at the university of Toronto.

2.2 The Orientation Devices and Methods in the Field

In order to orient speleothems with respect to the horizontal and to geographic north three lightweight orienting devices were made (plate 2.1). Figure 2.3a shows the stalagmite orientor which carried either a Suunto or Brunton compass to determine azimuth. It is an aluminum

Figures 2 - 3 a, b

Orientation devices for stalagmites and flowstones

(Associated three - arm U - tube for stalagmites not shown)

Figure 2 - 3 a

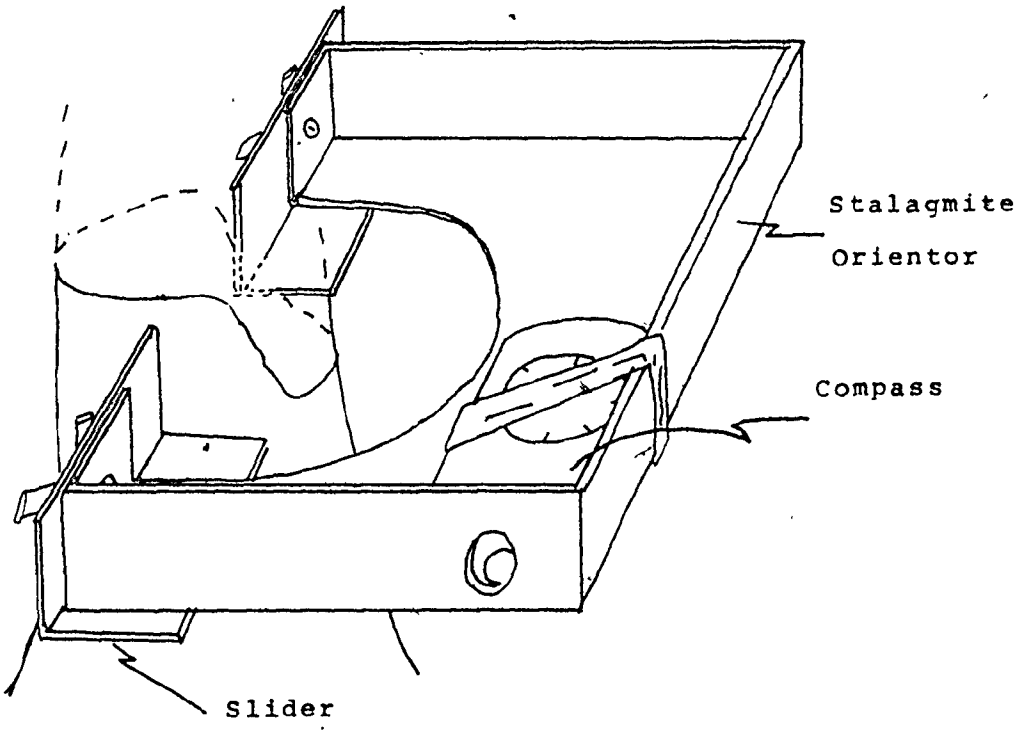

Figure 2 - 3 b

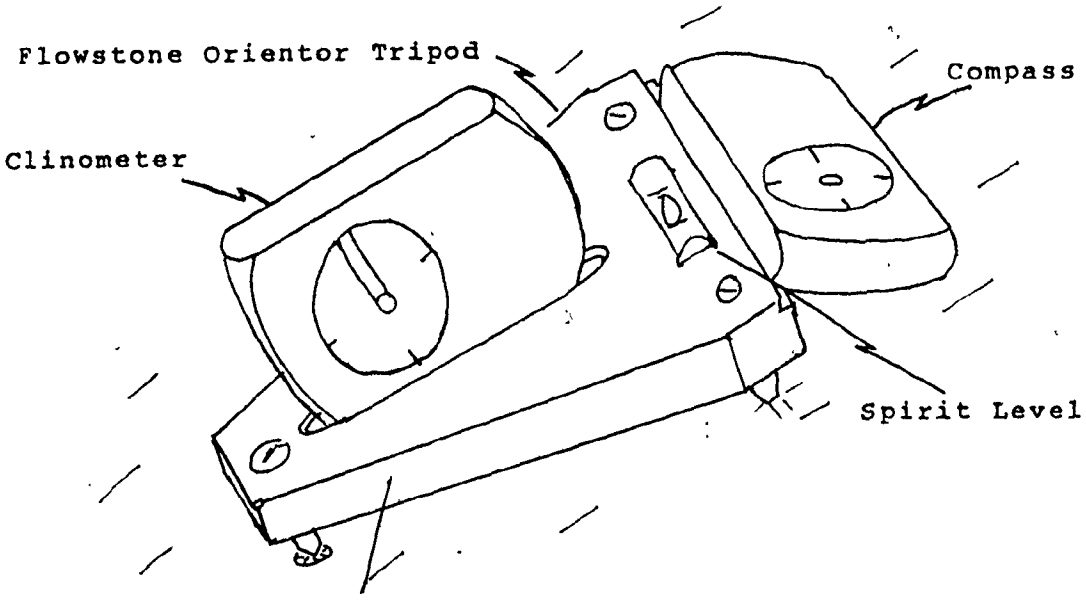

plate in which sliders may be moved parallel to the side holding the compass. Scratch marks were made where the sliders touched the stalagmite on its opposite sides, and a compass reading taken. It was usual to take off the orientor and replace it at the scribe marks whence a second reading was taken. A mark (usually the letter 'A') was placed against one of the scratch marks to indicate the observer's side. A three-arm U-tube of clear polythene was constructed and this was partly filled with water to determine the horizontal. Elastic bands or string were used to fix the U-tube against the sample. Scribe marks were made at the three meniscuses. In the case of long stalagmites two or even three sets of measurements were sometimes taken along the sample.

Figure 2.3b shows the orientor used for flowstones It is a robust lightweight perspex tripod with a slot for a Suunto clinometer and a groove for the compass. A hole was lightly gouged in the flowstone surface for the lower leg. The tripod was then rotated about this leg until a spirit level, set in the top, indicated the strike. The other two leg positions were then scribed and readings taken with the clinometer and compass in position.

Samples were labelled and then removed usually by means of hammer and chisel. Although minor shattering sometimes occurred upon removal and during subsequent preparation this has seldom caused any problems.

Field notes were taken which included a sketch of the site, whether the sample was wet on its upper surface, and the possibility of disturbance having occurred after its formation. There was no easy way to transport large masses of sample, sometimes up to 25 Kg, out of the cave. The

Mexican and Canadian samples, for example, required several cavers to help with portage.

2.3 Declination Correction for Local Variation and Rates of Change

In the Nahanni region of N.W.Canada and again at Crow's Nest Pass the compass was used with a topographic map to obtain local declination in order to convert the compass readings from N_{mag} to N_{true}. For Nahanni the declination, from an average of three readings taken from three identified topographic features, was within 2^{o} of that quoted from the map itself, corrected for annual rates of change. For the Crow's Nest Pass area the average of five readings was within 1^{o} of that quoted from the topographic map. The same compass has been used throughout the study and has subsequently twice been checked to within 0.25^{o} with similar compasses.

The most usual practice for converting N_{mag} to N_{true} has been to use the 1975 World Magnetic charts (1977) corrected for annual rates of change.(See chapter 4 for possible effects of local magnetic anomalies).

2.4 The Preparation of Specimens

In preparing specimens for NRM measurement maximum layer-to-layer definition and least loss of orientation were aimed for. From estimates of growth rates obtained earlier by Thompson (1973) and Harmon (1975) it was decided that a 2 cm. deep specimen would give time resolution of about 500 years or less. This would allow resolution of most secular variation where the time scale was from 10 to 10^{4} years (McElhinny and Merrill, 1975).

Plate 2.2

The Mould used for casting Speleothems
The three-arm U-tube and clinometer are also shown.
The stalagmite is TS (section 4.7).

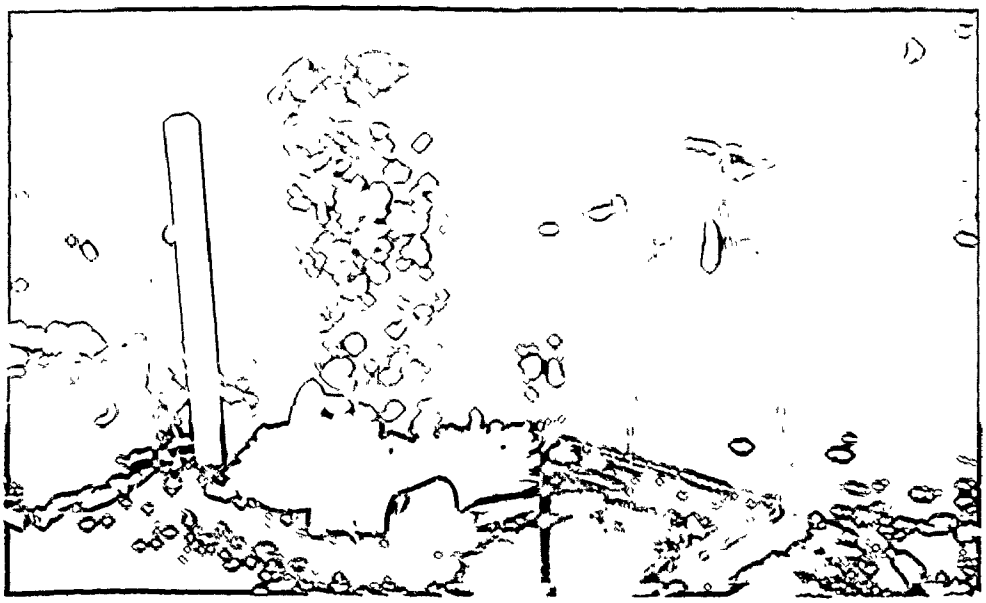

A 30 cm. deep rectangular perspex mould was constructed so that the speleothem could be cast inside it using plaster of Paris. The mould is held together by bolts and wing nuts for easy dissassembly and its floor is levelled by means of three large brass flat-headed screws set into perspex.

The stalagmite to be cast was oriented as follows:

1) It was levelled inside the mould using the three-arm U-tube placed at the original marks, and bits of plaster were used to chock the base. A small amount of fresh plaster was then 'puddled' around the base and allowed to set (plate 2.2).
2) The stalagmite was then rotated about a vertical axis with the attached plaster, until the two azimuth marks were equidistant from one of the sides of the mould. A ruler or a set-square with an attached pointer was used for this operation.

   (For one stalagmite, DBS1, a second set of marks were used to check the first set and they agreed to within 0.5^{o}.)
3) The speleothem was cast in plaster to the top of the mould. The azimuth marks and azimuth value were then transferred to the mould side and to the hardened plaster. The mould was dissassembled.

Since the Geology department rock saw could only accommodate 23 cm. (9 in) deep samples, any stalagmites longer than this had to be sawn in subsidiary sections beforehand. The method for a long stalagmite was as follows:

3a) Marks were made on the stalagmite in order to produce sections 18 to 23 cms. long.
b) The sample was then partly sawn through at these marks

and then broken with hammer and chisel; this was to allow exact repositioning in the mould by matching the broken surfaces.

c) The lowest section was set in the mould with the next section on top, matched at the break.

d) Plaster was poured in up to the break and allowed to harden. Pieces of paper were placed flat on the surface and plastering was continued to the top of the mould.

e) The mould was dissassembled and the two sections were separated at the break, facilitated by the paper.

f) With the mould reassembled the second section was reinserted, if necessary, with the aid of soap on the sides of the mould. Plaster was poured in up to the next break.

g) The third section was added, and so on until the whole stalagmite was cast.

h) Orientation marks were transferred to all sections of the stalagmite.

Examination of the flatness and width of the stalagmite drip area dictated how many specimens could be obtained per growth horizon. Sometimes this area varied down the sample, presumably due to variations in drip rate and other factors.

4) The first saw cuts to be made were vertical ones parallel to one of the sides of the cast. They yielded one, two or three slices from the central area of the sample, each with a constant thickness of about 2 to 2,5 cms. (figure 2.1)

5) The slices were often still attached to their plaster, else the corresponding pieces of plaster were replaced. Dirt and rock saw contamination were washed off

the slices with HCl.

6) The slices were labelled A, B, C etc. , and were laid flat out on a bench. For long stalagmites, corresponding slices of upper or lower sections were also added on by matching at the break and by matching the former vertical sides of the plaster.

7) With a set-square and ruler horizontal lines parallel to the growth layers were marked out with depths around 2 cms. ready for the second set of saw cuts.

The square rod-shaped pieces to be produced are herein referred to as cuts (figure 2.2), and were labelled with numbers from one downwards, ie. from youngest to oldest.

8) The third set of saw cuts were then marked out to allow maximum sampling of each growth layer without incorporating the curved or vertical sides.

9) Each specimen, including the remaining side (lateral) ones, were labelled firstly with the slice, then with the cut and finally with its own position letter, starting with P (left) and continuing to the right with Q, R, S etc.

To give an example of this labelling system, specimen DAS2 B12Q comes from Del Arroyo stalagmite no 2, slice B, the 12 th. cut from thetop and is a central specimen Q. Other specimens of the same growth layers are B12R, B12S, C12Q, C12R and C12S, there being six in all. Lateral specimens from this cut but incorporating side growth are B12P, B12T, C12P and C12T. Front and back pieces A and D were normally left unused.

10) When all the specimens were marked out, colour and / or black and white photographs were made of the

slices. Mylar was placed over the top of each slice and a drawing was made of:

a) the outline of the speleothem and plaster.
b) the most prominent growth layering and any apparent hiatuses.
c) the specimen saw marks and labels.
d) the azimuth.

11) The second and third cuts were made using a smaller rock saw. Each specimen was washed, dried and weighed, and azimuth marks were scribed on the top surface.

Sometimes specimens broke along crystal planes or cracks and some of the earlier samples were glued back together again using epoxy resin. This practice was discontinued after it was found that even small amounts of glue had a high and stable remanence faithful to the ambient field in which it set.

For flowstones the following procedure was adopted:

1) With the mould levelled , the flowstone was placed inside together with the tripod in its original position. The clinometer was inserted into the tripod (plate 2.1).
2) The flowstone was chocked up until the clinometer was levelled. Since the tripod table was often approximately parallel to the growth layers, this procedure later facilitated the cutting of flowstones along their growth horizons. More plaster was 'puddled' around the base and allowed to harden.
3) If necessary the sample was then rotated about a vertical axis until the strike was parallel to one of the sides of the mould. Plaster was poured into complete the cast but leaving the top surface of

the flowstone still uncovered. After the plaster had hardened the mould was dissassembled.

5) The vertical slice marks were made parallel to one of the faces, and the slices were labelled A, B, C etc.

Subsequently the marking, labelling, photography and sawing was as for the stalagmites.

Two flowstones, RCB and GQF1, had to be treated somewhat differently. Their growth layers were curved and so further changes in the orientation of the second set of cut marks had to be made in order to obtain maximum time-resolution between layers.

In general more specimens may be obtained per growth horizon from a flowstone than a stalagmite, but sampling problems such as accessibility and portage have prevented thick sections of flowstones from being obtained. Thus only one flowstone, GQF1 has necessitated the use of a larger rock saw. The kind permission of Mr. A. Rudkin at the Royal Ontario Museum to use a 31 cm rock saw is acknowledged.

2.5 Measurement of Natural Remanent Magnetization (NRM)

2.5.1 The Superconducting Magnetometer

Up until about 1975 most weak NRM measurements were made with astatic or spinner magnetometers having noise levels around 10^{-6} to 10^{-7} Oe. or less. With the spinner type the low signals had to be integrated over many spins, and so the measurements were often time consuming.

The superconducting quantum interference device (SQUID or cryogenic) magnetometer was developed using a

Josephson weak-link sensor to detect persistent direct fields from a superconducting coil. It has proved ideal for measuring the NRMs of weak specimens because of its sensitivity, low noise levels and fast response time. Details of its construction and usage for paleomagnetism is given by Goree and Fuller (1976).

The SQUID magnetometer used in this study has three orthogonal sensing coils with a four inch (10 cm) vertical access tube. The coils have a quoted noise level of less than 2×10^{-7} Oe and a response time of about one second, on the 1 Hz RF scale. The calibrated signal is displayed digitally as well as on a pen-chart recorder. The coils are labelled A, B and C (the vertical axis), but for all work in this study only coils B and C were used. Coil A, the accesory heaters and magnets were no longer used mainly because of instability problems.

The specimen was placed on a sample holder of perspex which was attached to a rotating compass table by means of a perspex tube. A fiducial mark indicated specimen azimuth with respect to coil B. Since the platform holder was level then the vertical component was automatically read out from coil C. There is an adjustment of the perspex tube, fixed by a screw, which allows vertical adjustment within the sensing volume - this is because different workers used different sample holders. The whole magnetometer is shielded from external fields by a superconducting sheath, and by a mu-metal outer sheath.

Any measurements could be affected by the following instrument errors:

1) Noise above 2×10^{-7} Oe due to daytime mains power fluctuations, and following the refilling of the

helium reservoir which was required every seven or eight days. At night noise levels as low as 10^{-8} Oe could be obtained

2) Drift and jump instabilities caused by refilling helium reservoir or other disturbances, or by a detuned RF level. The latter could usually be put right fairly easily using an oscilloscope.

3) Miscalibration of the pen-chart recorder sensitivity. In the last two years of the study its use was discontinued and a microprocessor, with a printer, has been substituted.

4) Cross-talk between sensors has been observed and is pronounced if the specimen is not centred in the sensing volume. Otherwise it is probably less than 1% (Goree and Fuller, op cit).

5) Specimen holder permanent magnetization was kept to about the noise level or less by washing it in dilute HCl in an ultra-sonic cleaning bath, and by AF demagnetization. The holder has been kept wrapped in clean cloth when not in use to prevent dust from settling on it. Occasionally contamination was persistent and required several washings to remove it. In any case all x, y and z signals from the sample holder were eliminated by turning the specimen with respect to the holder and averaging (table 2.3).

The first specimens (from samples BJTL and RCB, chapters 4 and 5) were placed in a small holder and could be fixed by means of a screw. Later a larger holder consisting simply of a tray with parallel sides was constructed. This was used with larger specimens and when specimen stacking was occasionally adopted. The specimens were kept against one

Table 2 - 1

Variations in D , I and total moment of DAS2 - C34Q, AF demagnetized to 50 Oe, for different positions above and below the normal specimen holder position within the sensing volume. (Specimen holder # 2)

Table 2 - 2

Test of faithfulness of laboratory directions when different specimen components were aligned with different sensors using the NRMs of ENF D6P and D6R. z is vertical is the usual orientation. (Specimen holder # 2)

Table 2 - 1

Position	D	I	Total Moment . 10^{-7} G
Normal	352.71	30.19	28.53
½ in above	355.50	30.09	27.37
1 in. above	355.04	27.63	24.36
½ in below	354.11	30.47	29.48
Normal (measured two weeks earlier)	353.05	31.91	28.28

Table 2 - 2

Vertical Component (C Sensor)		D	I	Total Moment . 10^{-7} G
D6P	z	328.06	-55.89	80.92
	x	324.61	-57.48	82.72
	y	333.04	-53.86	84.19
D6R	z	330.66	-55.46	77.39
	x	327.85	-56,59	79.36
	y	333.56	-51.99	80.27

side and the back simply by gravity and this facilitated quicker loading.

2.5.2 Use of the Superconducting Magnetometer

The superconducting magnetometer was used to measure the x, y and z components of the magnetization of each specimen, an in order to minimise the errors mentioned above certain precautions were taken as follows. Early on in the study the position of the specimen holder was moved around in the sensing area to minimise cross-talk and 'sensing anisotropy'. The best holder position was determined firstly by lowering a specimen in successive increments down the access tube until the B and C channel outputs showed least change (table 2.1). Secondly the components of a stable specimen were measured with the z, x and y axes held consecutively vertical to see how well the three directions agreed with each other (table 2.2). Table 2.2 shows that discrepancies were present and that the sensing conditions for specimen holder #2 were barely satisfactory. The data of table 2.1 largely eliminates incorrect positioning as being the cause of these errors. The errors must be due to non-central positioning of the specimen with respect to the horizontal plane, ie. the holder was too big for the 2 cm cubes. The z axis in the vertical position gave values between the other two possible alternatives, and this was always used. Thus any inclination shallowing or steepening observed in the results would probably not be due to systematic measurement error (mentioned a propos sections 1.3.3 & 1.5.3). Since specimens were nearly always placed at the same side of the larger holder the position error contributes to the absolute error

Table 2.3

Procedure for the Measurement of Magnetization using the Superconducting Magnetometer

These are the positions and rotations of the sample holder allowing measurement of the magnetization of a specimen using two sensors.

Sensor	Position 1	Rotate through 180° about vertical axis	Position 2
C	+z + SHz	→	+z + SHz
B	+x + SHx	→	-x - SHx
	Rotate through 90° about the vertical axis		
B	+y + SHy	→	-y - SHy
	Rotate the specimen through 180° about the vertical axis with respect to the specimen holder		
C	+z + SHz	→	+z + SHz
B	+x - SHx	→	-x + SHx
	Rotate through 90° about the vertical axis		
B	+y - SHy	→	-y + SHy
	Rotate the specimen through 180° about the horizontal axis with respect to the specimen holder		
C	-z + SHz	→	-z + SHz

The last C sensor readings were doubled so that by subtracting all x, y and z readings , and dividing by four, the holder contribution to the signal (SHx, SHy and SHz) and most of the instrument drift were eliminated.

and not the relative error.

The routine procedure eventually adopted for measurement of the x, y and z components is shown in table 2.3 .

Jump instabilities were usually easy to detect and simply necessitated a repeat measurement. Replicate measurements of stable specimens were occasionally made and the agreement with first measurements was always good.

The reading of the digital display was tedious though safe. As mentioned earlier a microprocessor was later fitted to the magnetometer and a simple program was used to average and print out the results automatically according to the procedure of table 2.3 .

Specimens of a given sample were measured sequentially, ie, in order of cut number down to the base and alphabetically for a given cut number. This made it easier to detect worker mistakes and to process the results cut by cut.

Some specimens possessed only an upper or a lower surface depending on which side of the break of a stalagmite they occurred. Consequently only the +z or -z component could be read; this has usually been a safe procedure by ensuring that SHz magnetizations were kept low.

2.5.3 Data Processing - The Wang Calculator and Programs

Two programs for a Wang calculator were originally used to process the data. The first, devised by the author, rotated the specimen direction from the laboratory to site

value by means of strike and dip angles. This corresponded to the rotation of two axes of an orthogonal set of three. The output, in hard copy, gave the site values of x, y, z, declination D, inclination I, the total moment and the strike and dip angles. Strike and dip were first entered for the whole sample and then x, y and z values were entered for each specimen.

The second program used Fisher statistics (Fisher, op cit, or see Ch. 4 of Irving, 1964, op cit) on the D and I values on the several specimens of a given cut, to give its mean direction. The output also included:

1) The number of unit vectors and their resultant length R. A comparison can be made between N and R using the tables quoted in Irving (Ch 4), to determine the significance of the mean vector of the cut.
2) The angular standard deviation θ_{63}. The mean direction has a 63% probability of lying within this angle.
3) α_{95} is the semi-angle of the cone within which lie 95% of the N vectors.

The errors in the mean D and I are also quoted in the analyses of directions for several samples. These are denoted by δD and δI and are given by $\alpha_{95} = \cos I \, \delta D = \delta I$.

Fisher statistics are based on a random distribution of directions about their mean. It may be noted that the vectors of any given cut whilst having a random part are also likely to be distributed between the two directions of the cuts above and below. This is because the exact same horizons may not always be included in each specimen, and variation in magnetic content between layers may bias one specimen more than an adjacent one. This does not affect the mean but the small population tends to create

an ellipse of distribution with its long axis lying between the two adjacent directions (for a possible example see DAS2, section 6.5.2; for a possible example of a skewed distribution see,eg. VCCL, section 4.6.2). The vectors have been treated as though they were from a random population about the mean, using Fisher statistics.

2.6 Magnetic Cleaning and the Characterization of the NRM

2.6.1 Introduction

The spectrum of grain sizes and coercive forces of most rocks is such that, subsequent to primary formation , part of the NRM will decay or realign itself by the activation of thermal energy, and under the influence of the changing ambient field (Dunlop, 1973a). This decay or remagnetization is thus a function of time (usually log t) and is known as viscous remanent magnetization, VRM. In rock magnetic studies it is of interest in its own right but in paleomagnetism it is undesirable in that it serves to modify the primary magnetization. If magnetite is the magnetic mineral in speleothems (see chapter 7) then alternating field (AF) demagnetization is usually sufficient to remove or 'clean' away the viscous components. The method is to progressively AF demagnetize a pilot specimen in increasing fields and measure the remaining magnetization at each step. As the field is increased the intensity usually decreases and the direction may change. In order to demagnetize the remaining specimens usually the lowest peak field is sought which satisfies some criterion associated with the magnetization changes, The aim of all such criteria is to isolate a primary stable remanence. They include:

1) the field at which a stable direction is first reached.

Simple examination of consecutive D and I values may suffice or a Zijderveld plot may be used, (Zijderveld, 1967).

2) a stability index which compares successive vectors as the field increases (eg Briden, 1972)

3) the median demagnetization (destructive) field (MDF) may be used as a general guide to stability This is the field required to reduce the magnetization to half of the NRM. High MDFs denote stable magnetization.

In this study the first of these criteria was used. In order to safely remove all VRMs of the remaining specimens it is preferable to use a field higher than the necessary minimum field since it is to be generally expected that some specimens will have higher proportions of VRM than the pilot. This was not always possible in this study because of the weak original NRMs. The optimum field was thus a compromise between removal of most VRM and having a cleaned magnetization sufficient for measurement.

It is known generally that hematite VRM is best removed by thermal demagnetization since it may often be stable to AF demagnetization even in high fields. It was found in this study that VRMs were fairly easy to remove by AF cleaning. Thermal cleaning was carried out on some specimens from sample VCCL (chapter 4) and from sample DAS2 (chapter 6).

2.6.2 The Alternating Field Demagnetizer and Field-Free Room

The apparatus used for progressively demagnetizing specimens was a motor-driven variable transformer giving a range of 0 to 1 KOe peak alternating field,

attached to a 16 cm (I.D.) coil inside which was a large capacity two-axis tumbler. The coil and tumbler were situated in a large doubly-shielded room in which complete annulment of any ambient field was achieved by sets of orthogonal coils around the room and a constant current power supply. Any remaining field could be measured by fluxgate probes and annulment was checked before a demagnetization run. There was no continuous monitoring employing feedback control as is often used with field-free spaces so the probes were sometimes used after a run to see if any field had somehow appeared. The components along any axis were always less than 5γ s.

2.6.3 Demagnetization of the Pilot, and Associated Specimens

The pilot specimen was usually chosen for its high magnetization intensity in order that it could be tested to high field values. Early on in the study demagnetization was stopped at about 500 Oe. Later this was continued to 1 KOe in conjunction with anhysteretic remanent magnetization (ARM) studies.

The specimen was wrapped in tissue and placed, with no particular orientation, inside the tumbler. Since successive placements were probably random any accidental ARM acquired in one step would be mostly concelled in the next step(s). Operation of the demagnetizer was semi-automatic, care being taken to ramp the field down slowly from its peak value. It was observed that the ammeter needle sometimes jumped down slightly from its peak value before smoothly decreasing. This may be due to motor-rheostat backlash, and the effect is thought to be the cause of some anhysteretic 'bumps' in an otherwise smooth

demagnetization curve. It was usual to demagnetize two or more specimens together to check on the acquisition of spurious remanences of this sort. Immediately after demagnetization the specimen was transported in a mu-metal box and its magnetization was remeasured.

The directions were worked out using the Wang calculator and M/M_o was plotted against peak field, M_o being the original NRM and M the intensity remaining after that demagnetization step.

Viscous components were detectable in a number of ways, by:

1) large increases or decreases in magnetization at low alternating fields,
2) low MDFs of about 150 Oe or less,
3) changes of magnetization in the NRM during measurement, indicating relaxation times of the order of minutes,
4) changes of magnetization after storage of several days or weeks.

With the peak cleaning field chosen all specimens from one or more cuts were demagnetized together, their orientation within the spacious tumbler being random so as to randomise any ARM (or, for that matter, any rotational remanent magnetism (RRM)(Wilson and Lomax, 1972). While the first specimen was being measured, the awaiting specimens were stored in a mu-metal box. When attempts were made to separate the stable magnetization from larger viscous components the specimens were also kept in the field-free room immediately prior to measurement. All specimens were measured within 20 minutes of AF cleaning. The orientation and statistics programs were used on the clean directions.

2.7 The Presentation of Results

The tables of D and I values for each sample and their statistics have been listed in the paleomagnetics chapters. They are tabulated against cut number and position reckoned from the centre of the cut.

The common usage of plotting D and I against stratigraphic position has been adhered to. The resulting SV diagrams also include the age data.

Since inclination values have been shown by this study to be free from depositional errors, it has been possible to plot VGP variations from the D and I values , knowing the site latitude and longitude (see eg, Irving , 1964, op cit, pp 43 & 44). This has proved invaluable in making interpretations about the geomagnetic field and in making comparisons with the results from the literature.

CHAPTER 3

DATING SPELEOTHEMS BY THE URANIUM-THORIUM METHOD

3.1 Introduction

When magnetically cleaned NRM values have been obtained for a given speleothem, the specimens may be radioisotopically analyzed to produce dated secular curves. In this chapter the uranium-thorium disequilibrium method used to date these specimens is briefly discussed. More detail is given to attacks on some of the problems involved in its continued refinement. The aim of the studies has been to improve upon accuracy and precision, but some of the experiments were either unsuccessful or incomplete. The experiments were:

1) to determine the radioisotope tracer (spike) ratio,
2) to reduce the background contamination of the alpha-particle detectors,
3) to increase the resolution of the detectors in the signal processing, and
4) to increase the quality of the alpha sources.

3.1.1 A Brief Outline of the Uranium-Thorium Method

Figure 3.1 shows the decay chains, and figure 3.2 the alpha energies of the naturally occurring uranium and thorium isotopes and the artificial ^{232}U isotope.

^{238}U and its daughter ^{234}U are carried along in ground waters probably in the form of carbonate or phosphate complexes of the uranyl ion (UO^{2+}), whereas thorium is

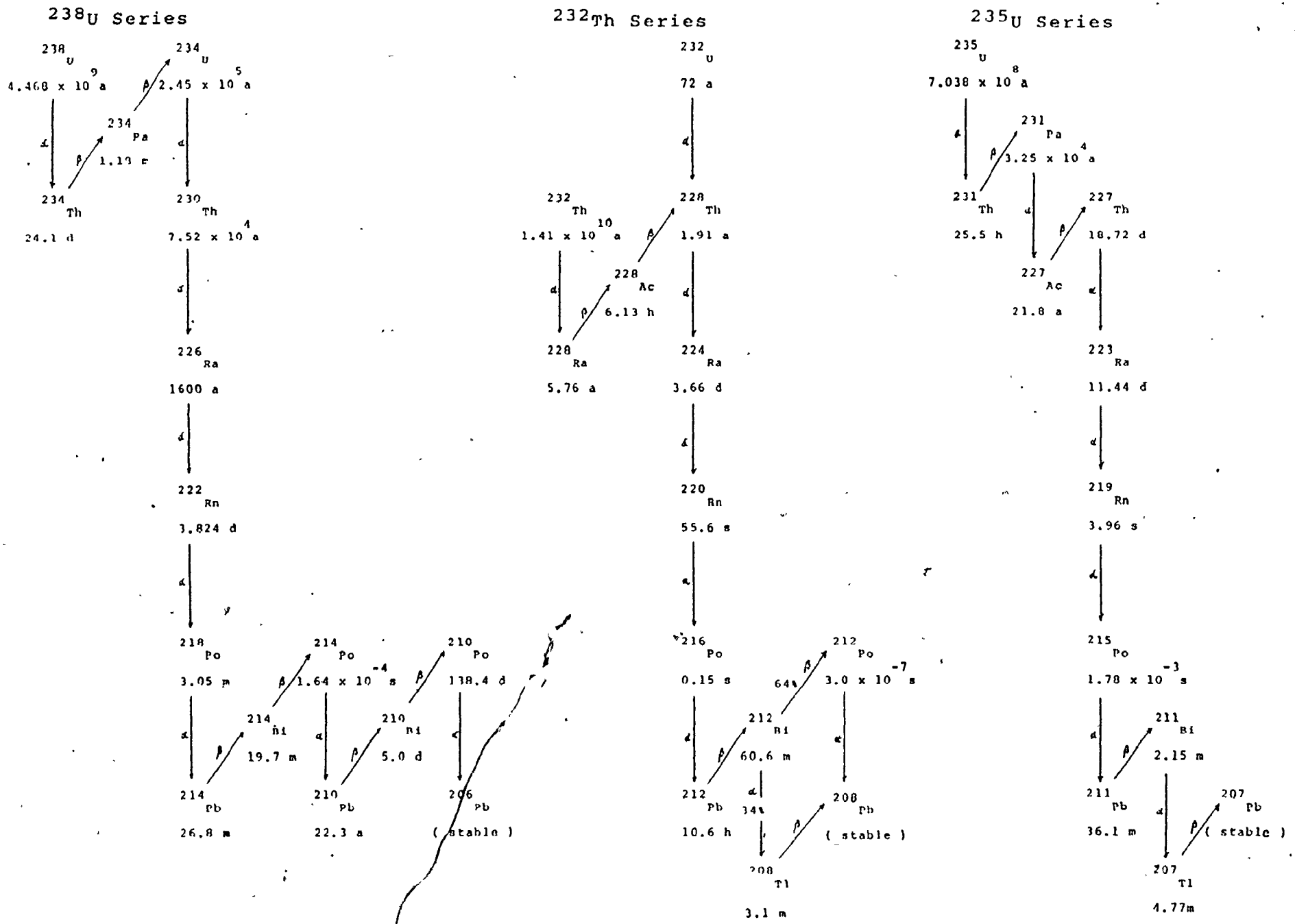

Figure 3 - 1; Decay Chains of the Naturally - Occurring Radioisotopes and Artificial ^{232}U.

Figure 3 - 2 ; Alpha Particle Energies of the three Decay Series.

(from Table of Isotopes, 6th Ed, Lederer, J.M. et al , 1967)

The latter parts of the series have been omitted, and the ^{235}U series has been depressed in activity for comparison with the other two series.

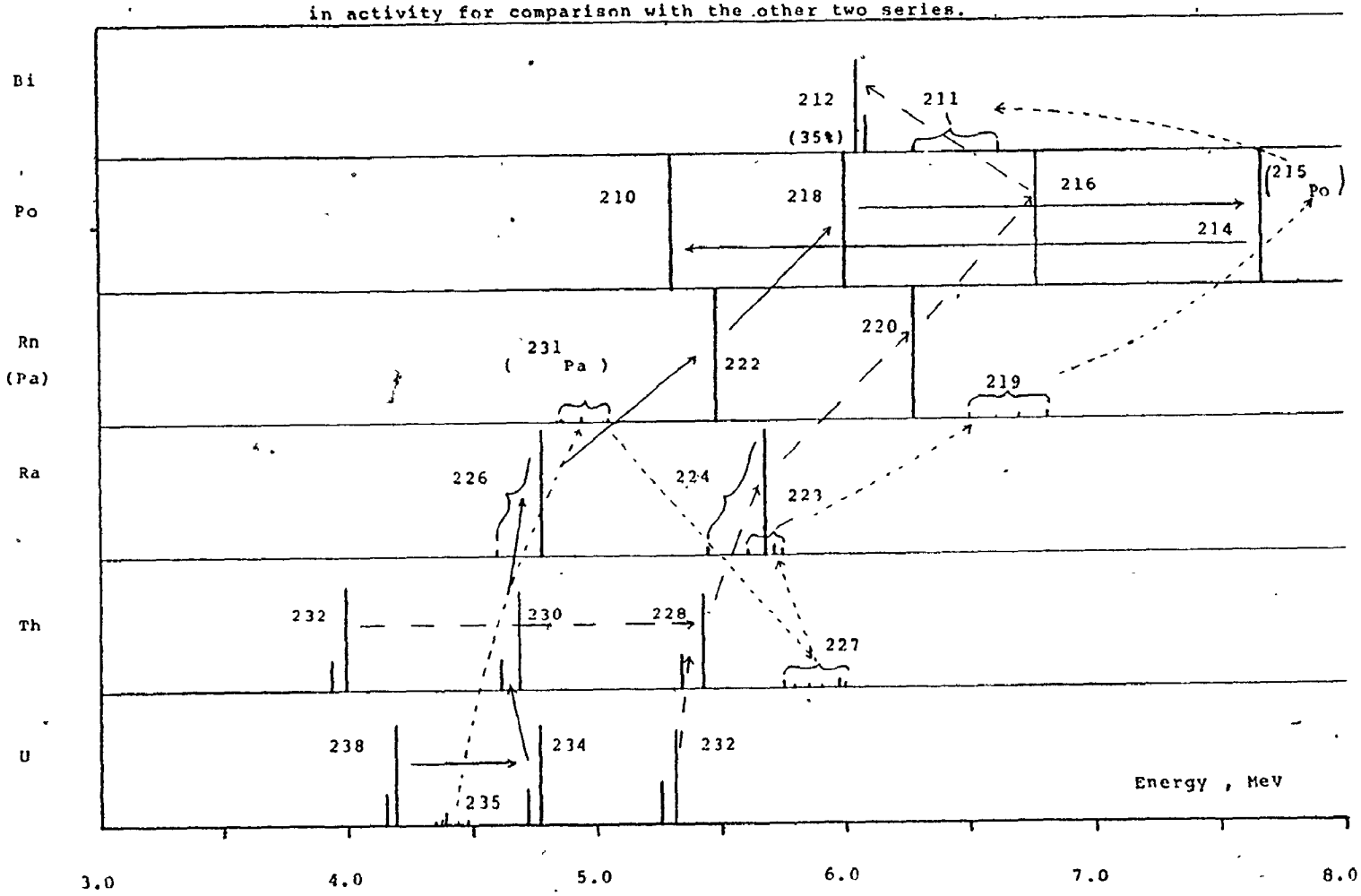

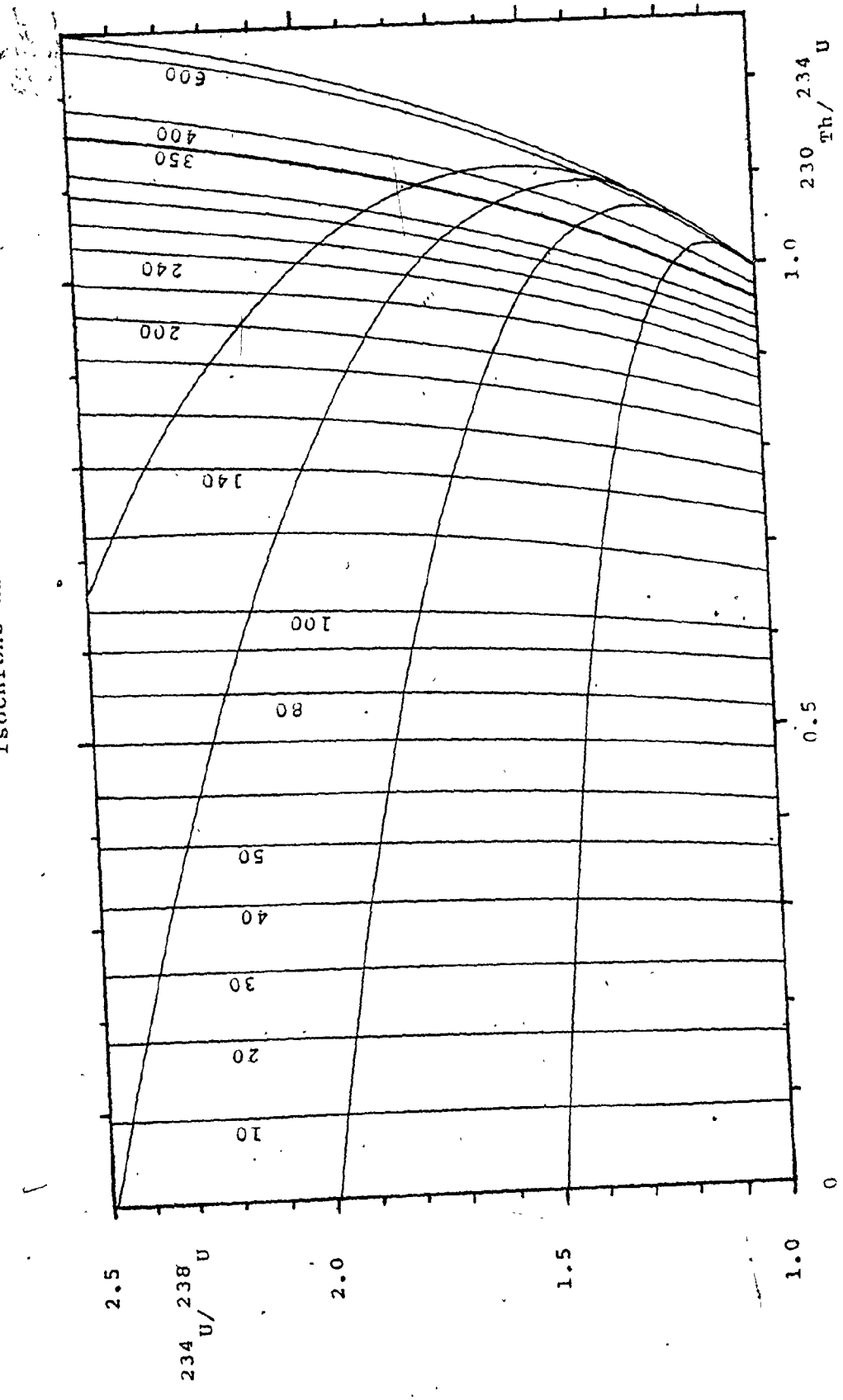

Figure 3 - 3 ; Isochron Diagram for $^{234}U/^{238}U$ and $^{230}Th/^{234}U$ ratios.

Isochrons are in Ka.

hydrated and precipitates out. Thus when calcite is precipitated in a cave ^{238}U and ^{234}U may be incorporated from the groundwater but granddaughter ^{230}Th is not. Subsequently ^{230}Th, with a half-life of 7.52×10^4 a, grows towards secular equilibrium with ^{234}U. The activity ratio of ^{230}Th to ^{234}U is used as a measure of how far equilibrium has been approached and hence of the time elapsed since the calcite was deposited. The age limit of the method is about 350 Ka.

A disequilibrium excess also exists between ^{234}U and ^{238}U, in the groundwater, due to the fact that ^{234}U is preferentially leached from weathering surfaces. The age equation, taking into account this excess, is:

$$\frac{^{230}Th}{^{234}U} = \frac{1 - e^{-\lambda_{230}t}}{^{234}U/^{238}U} + \left\{\frac{\lambda_{230}}{\lambda_{230} - \lambda_{234}}\right\}\left\{1 - \frac{1}{^{234}U/^{238}U}\right\} \times \left\{1 - e^{-\left(\lambda_{230} - \lambda_{234}\right)t}\right\},$$

where λ_{230} and λ_{234} are the decay constants of ^{230}Th and ^{234}U. The corresponding isochrons are shown in figure 3.3 .

A general review of uranium series disequilibrium methods has been given by Ku (1976). The application of the deficient ^{230}Th method to speleothems was first made by Cherdyntsev et al (1965), and subsequently by several others. The method was adopted at McMaster to date speleothems by Thompson (1973) in conjunction with paleoclimate studies. The techniques have been refined by Gascoyne (1979).

Concordancy of the method with protactinium dating

has only been partially successful probably because of the low ^{235}U concentrations present in most speleothems (Thompson, op cit; Gascoyne, op cit). Concordancy with ^{14}C dates was found for submerged speleothems from the Bahamas of about 22 Ka in age (Spalding and Mathews, 1972).

In order that the U-Th disequilibrium method be applicable the following conditions must be met:

1) The system must have remained closed to the movement of the isotopes since the time of deposition.

Occasionally this condition is known to have been violated when thorium is found in excess of its equilibrium activity. The reason is thought to be migration of uranium out of the speleothem through some kind of recrystallization process (Gascoyne, op cit).

2) There should have been no initial ^{230}Th present at the time of speleothem deposition.

^{230}Th may be deposited along with other thorium isotopes such as long-lived ^{232}Th, in clayey detritus on the surface of the speleothem by, for example, cave floods. Therefore if any ^{232}Th is seen in the thorium alpha spectrum it may be expected that some ^{230}Th was also initially present. The question then arises as to whether a correction factor can be applied in order to allow for this initial ^{230}Th. Kaufman and Broecker (1965) deduced an initial $^{232}Th/^{230}Th$ ratio of 1.71 from a study of lacustrine carbonate deposits. Peng , et al (1978) in a similar study found the ratio to be 1.3 . Gascoyne (op cit) in correcting for supposed initial ^{230}Th in speleothems adopted the value of 1.5 and found that dates corrected using this ratio improved the overall precision of the times of onset and termination of glacial and interglacial periods. There is no reason why the ratio should be constant even within a given

speleothem . Largely by convention the value of 1.5 has been adopted in this study and is invoked in the age computations when the present activity of ^{232}Th is greater than 5% of the ^{230}Th activity. As the measured $^{230}Th/^{232}Th$ ratio becomes smaller the correction for detrital thorium becomes more susceptible to the initial correction ratio ($^{230}Th/^{232}Th)_o$ that is used . This problem has frequently arisen in this study where necessarily low ^{230}Th activities were observed in young speleothems, several of which also possessed low initial uranium concentrations. The problem has been compounded in some cases by the unavoidable usage of low resolution, high background detectors, (see, eg, the age dating of DAS1, section 6.4.3).

If the above two conditions hold true then a sequence of dates produced for successively younger layers of a given speleothem should be in stratigraphic order. However non-stratigraphic ordering of dates may be due to instrumental innaccuracies as discussed in section 3.1.2 .

The chemical technique used in this study for separating the uranium and thorium species is given in appendix 1a . It is largely based on that of Thompson (op cit) as modified by Gascoyne (op cit). After dissolution of a specimen the technique involves the introduction of an artificial ^{232}U - ^{228}Th spike which traces the different chemical yields of the U and Th species. At the end of the separation process the U and Th isotopes are plated out separately onto two stainless steel discs by evaporation from TTA in benzene. The alpha-particle activities of the discs are consecutively counted using a surface barrier detector, amplifier and multi-channel analyser. The ratios of the alpha count rates, corrected for background and

Figure 3-4 a, b, and c: Hypothetical Age Data for a Constant Growth Rate Speleothem.

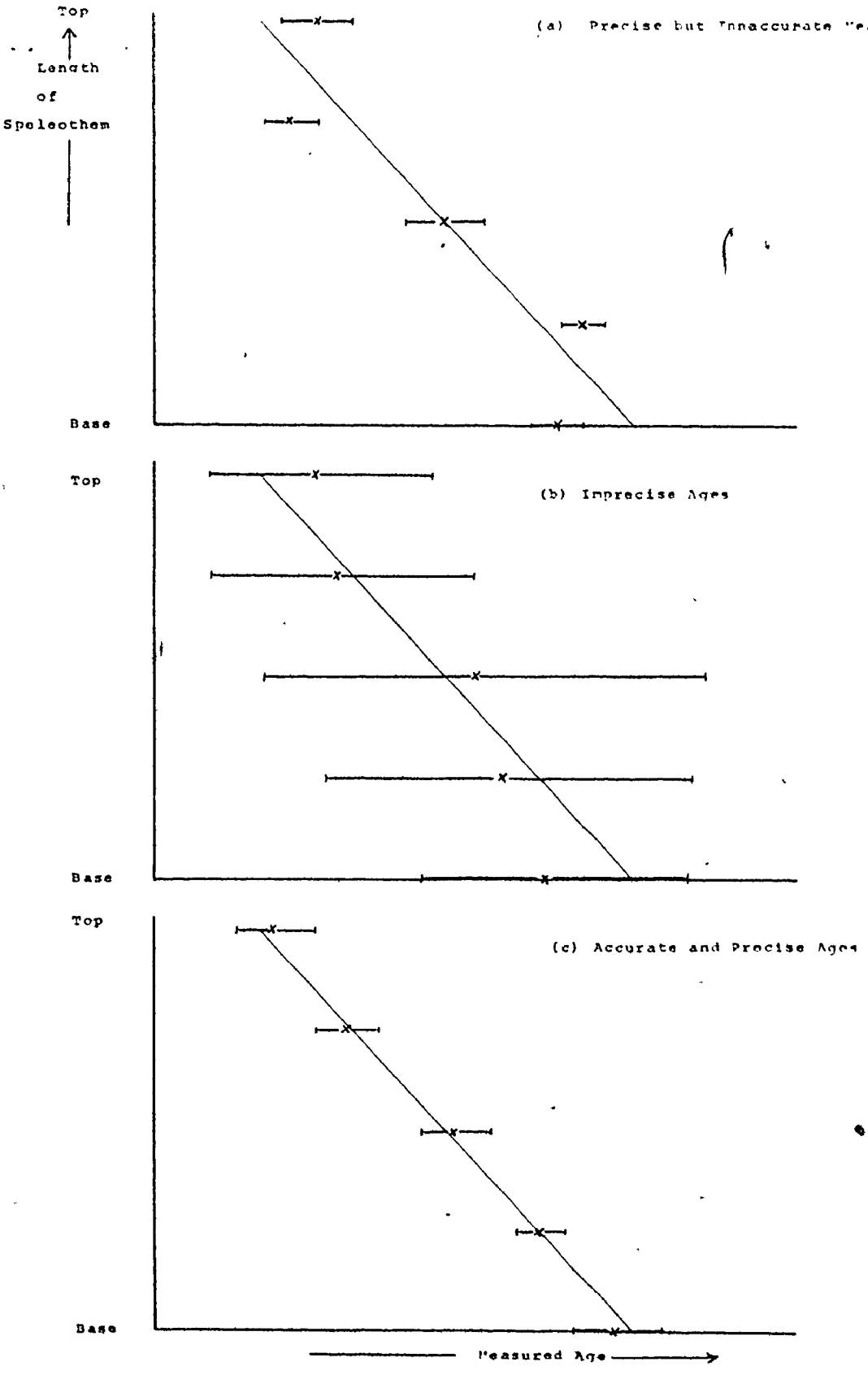

differential yields, are then used to provide the dates by means of the above equation. Details of the presentation of the data from a computer program are given in appendix Ib.

3.1.2 The Derivation of Speleothem Growth Rates

The task of producing dated secular variation curves from speleothems is firstly one of finding precise growth rate curves. It has turned out that several speleothems were both young and fast-growing with the result that a constant growth rate was all that could be justifiably fitted to the data. The meaning of the word 'precise', in the light of the various analytical and sample errors which may be present in the data from a fast growing speleothem, can be illustrated using the following sketches (figures 3.4a, b and c). These are hypothetical age data for a speleothem of a high constant growth rate.

In figure 3.4a the individual ages are precise but the means are innaccurate with respect to each other. The precision arises from a high number of counts and/or young ages. The innaccuracies may have arisen from any or all of:

1) variable and incorrectly monitored background corrections, applied to, for example, low ^{232}Th and ^{230}Th count rates, or problems to do with noise or backscatter.
2) variable resolution of alpha peaks creating 'tail' correction problems.
3) possible contamination by thorium or polonium in the uranium spectrum.
4) memory-effect contamination, especially by thorium, from insufficiently cleaned glassware used in previous runs; or reagent contamination. This is

difficult to monitor, , and is currently assumed to be zero in the McMaster procedures. (For possible memory effect contamination see sections 4.6.3 or 6.2.3)

5) problems to do with correction for detrital ^{230}Th such as a variable initial ($^{230}Th/^{232}Th$) ratio, or the adoption of a wrong correction factor.

Probably the greatest problem here is in deciding upon the number of channels over which to integrate the ^{232}Th and ^{230}Th counts. For young speleothems an integration of just two or three extra channels in the tail may make a difference of several percent in the determined age.

Figure 3.4b shows the effect of instrumental uncertainties about each mean. The reason is a low number of counts in comparison to the high age of the speleothem .

Figure 3.4c shows high relative accuracy and individual dating precision. The resultant line of constant growth rate is then also precise.

Various attempts to increase the precision and accuracy of dates are described in the following sections. In addition, the procedure was adopted of counting pairs of U and Th discs from a given speleothem on the same counter with close monitoring of the background. Despite this some dates are out of stratigraphic order, (eg VCCL, section 4.6.3) probably because of one or more of the problems described above. Therefore linear or polynomial type growth curves were not discernable in the data alone. The statistical treatment of the data in all these cases has been to find a linear least squares fit using the inverse variance in the

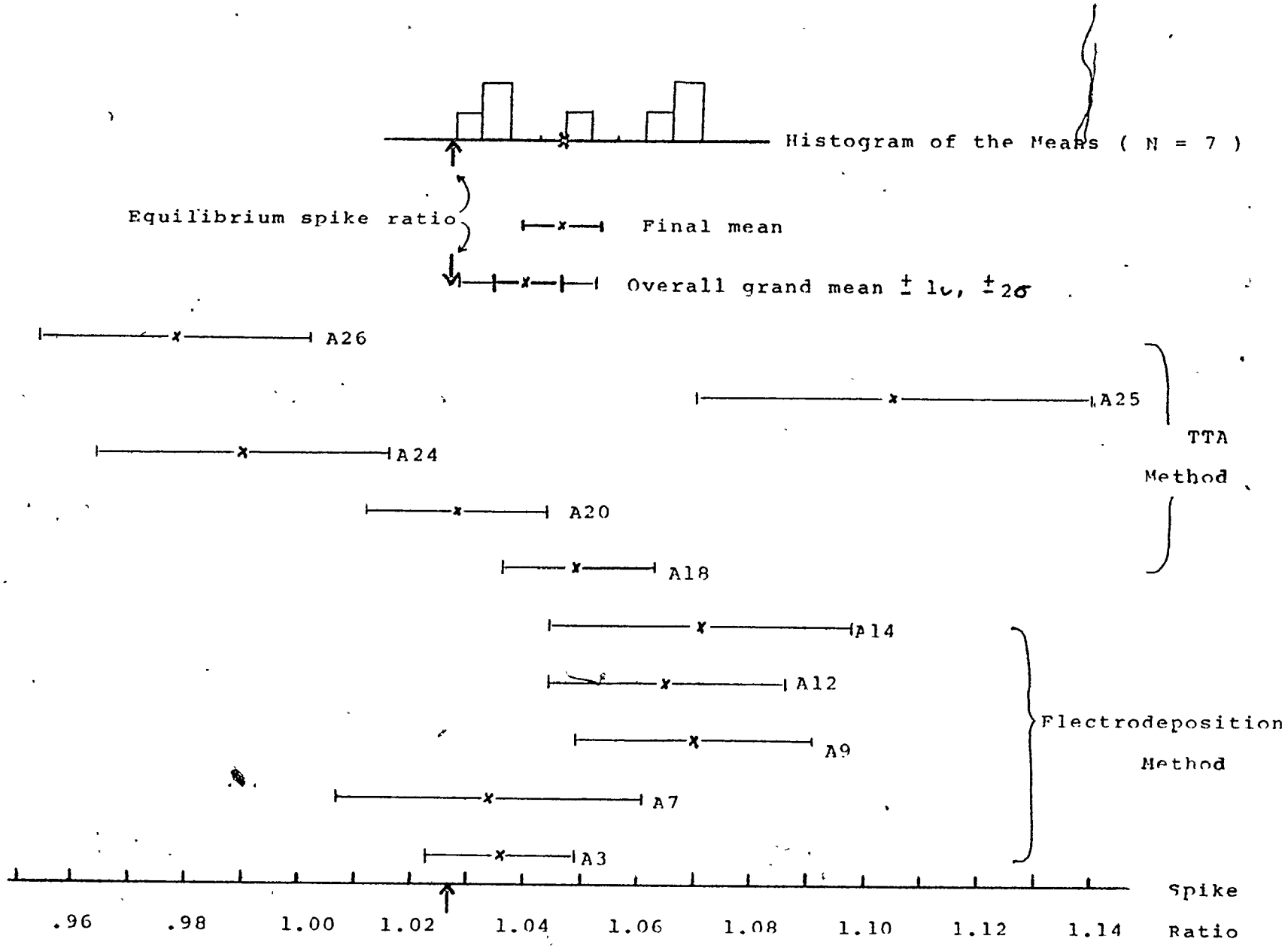

Figure 3 - 5 ; Spike Ratio Determinations and their Means; Comparison with the Equilibrium Ratio.

ages as a weighting factor. The age was considered the dependent variable of the speleotnem length.

3.2 Problems in, and Attempts at Technical Refinement of the U-Th Method

3.2.1 Determination of the Spike Ratio

In order to monitor the chemical yields of the U and Th isotopes an artificial ^{232}U - ^{228}Th tracer was used. The respective half-lives are 72 and 1.91 years. When the tracer was first acquired by Thompson (op cit), the secular equilibrium was accidentally disturbed, the Th being depleted. (The secular equilibrium ratio, $^{228}Th/^{232}U$ is 1.027). Gascoyne (op cit) attempted to remedy this in 1978, by milking off thorium from one spike batch and reintroducing it into the main batch. It was hoped thereby to avoid continuous monitoring of the spike as it grew back towards equilibrium.

Recalibration of the spike was achieved by analysis of an 'infinite-age', ^{232}Th-free uraninite supplied by J.N.Rosholt. Using 7 analyses Gascoyne's final spike ratio was 1.029 ± 0.013. In his subsequent dating work he felt justified in using the equilibrium value of 1.027.

Figure 3.5 summarises the results of ten analyses in this work of which five involved an electroplating method (section 3.2.4.3) and five involved the TTA-evaporation method. The grand mean was 1.040 ± 0.006. It may be noted that twice the standard deviation of the grand mean is 0.012 and this does not overlap with the runs A24, A25 or A26. That is, their means are significantly different from the grand mean at the 95% confidence level. If these three

are excluded then the mean becomes 1.046 ± 0.007 , with the individual means distributed bi-modally.

The variations between these runs are considerable and disturbing. Run A26, for example, had approximately equal peak heights for the spike and standard and the U and Th count rates were about the same (both had a yield of 80%). For the U-aqueous layer the extraction from TTA at pH 1, for possible contaminating thorium, was carried out and the disc was flamed strongly to volatilise any Po. No tail corrections were needed in the alpha-peak integration and the background counts were low. But the resulting spike ratio was significantly different from the mean at the 99% confidence level, The mean was $0,978 \pm 0.024$, (1σ error).

The spike ratio of 1.027 has therefore been adopted in this study as a convention ,and partly by default of a confident determination. The difference between this and 1,046 is about 1.5%. By assuming spike equilibrium there is no error in the value of 1.027. If a spike calibration error applies to the ratio then the relative dating error inferred from this work or Gascoyne's study is less than 1% for young speleothems ($\ll$ 10 Ka). However the age error becomes larger as the speleothem $^{230}Th/^{234}U$ activity ratios approach equilibrium.

3.2.2 The Prevention of Detector Contamination

Contamination of the detector slowly builds up due to alpha-recoiling nuclei from the source, which become embedded in its gold surface. Upon further alpha-decay these contribute background to the alpha-peaks being

measured. Fortunately most of the contaminant peaks have high decay energies and so do not interfere with the alpha-peaks of direct concern. The exceptions are ^{228}Th, the daughter of ^{232}U, and 5% of ^{224}Ra, the recoil daughter of ^{228}Th. It also appears as if undecayed nuclei can find their way to the detector surface being knocked out from the planchet by neighbouring recoiling nuclei. With continued use the contamination builds up on the surface requiring the detector eventually to be retired - a rather expensive proposition! Moreover this increasing background has to be monitored usually at monthly intervals, and the uncertainty in its count rate adds to the overall uncertainty in the computed age.

Detector contamination was investigated by Chetham-Strode et al (1961), and by Sill and Olson (1970). They showed that:

1) it is virtually impossible to clean the detector surfaces to get rid of the imbedded radioisotope; this cleaning procedure may damage the detector surface anyway.
2) a small amount of air may be allowed into the vaccuum housing sufficient to stop the recoiling nuclei without significantly decreasing the resolution of the alpha spectra. In addition a back bias of a few volts must be applied to repel the positive nuclei away from the detector surface.

In this study a housing was made which would allow the admission of a small measured quantity of air. Unfortunately the manometric arrangement and the use of a small battery for the back bias were only introduced late on and could not be tested in time for routine alpha spectrometry.

Plate 3.1

Alpha-Particle Tracks from a TTA-in-Benzene Evaporated Deposit.

The film is cellulose nitrate and the centre of the alpha-particle annulus is to the lower right. The scale is only approximate,

3.2.3 The Cooling of the Detectors and Preamplifiers

Since about July, 1979, an air-conditioning unit has been used to force cold air at about 10 to 20 °C over the detectors and preamplifiers. Before its installation the temperatures in the area of the detectors , in the summer months, rose to 25 °C or higher. The resolution was such that tail corrections from one peak to the next were frequently needed. With much cooler detectors the resolution has improved roughly by a factor of two in some cases.

3.2.4 Electrodeposition Experiments for Uranium and Thorium

An evaporated deposit of U or Th from TTA in benzene (appendix Ia) tends to give sets of annulus-shaped bands of concentration on the surface of the disc. If iron is present in the uranium deposit then these annuli also become thick and the iron acts as a partial absorber of alpha-particle energy, thus degrading the resolution of the alpha-peaks. Plate 3.1 shows the alpha tracks of a uranium sample collected on a cellulose nitrate film which was exposed to one such annulus. The annulus contains an estimated hundred more counts per unit area than adjacent areas. There is no guarantee that the corresponding thorium disc will have the same distribution of deposit. The source-to-detector geometry will be different so that resolution and counting efficiency will change from one disc to another. By comparison an electroplated deposit has the advantages that :

1) it is more uniformly distributed and hence thinner,
2) the areal distribution is repeatable from disc to disc and hence the source-to-detector geometry will be constant.

For these reasons an attempt was made to adapt an electrodeposition procedure for the low concentrations of U and Th ordinarily met with in speleothems.

Electrodeposition methods for U and Th were successfully tried out during and after the Manhattan Project (Casto, 1950), from a variety of acids, ammonium oxalate, ammonium acetate, and other media. The most popular form of anode is a simple platinum spiral or disc. Cathode discs have been made from stainless steel, platinum, gold, nickel and other metals. The appearance of the film has to be smooth and shiny and not spotted. The reduction of hydrogen gas at the cathode may contribute most to the spoiling of the deposit. In order to lessen this effect organic electrolytes such as ethanol or isopropyl alchohol (eg, Kim et al, 1966), or sulphuric acid in a mainly nitric acid medium have been used (Talvitie, 1972). The pH seems to determine the species of the deposit which is usually the metal oxide or the hydrated metal oxide. Temperatures for best deposition are around 60° to 80° C as quoted by several workers. The rate of deposition is strongly dependent on the current density, recommended values varying from 125 mA to 4 A for a 2 cm. diameter disc. Deposition times vary from ten minutes to more than two hours. Increased agitation of the electrolyte also seems to increase the rate of deposition and improves the quality of the film. Yields of greater than 95% for both U and Th for even trace amounts are claimed (eg Kim et al, op cit) for a number of methods.

3.2.4.1 <u>An Electrodeposition Procedure - Introduction</u>

Besides producing a uniform thin film of the U and Th isotopes the deposits must also be free of radiogenic

Figure 3 - 6; The Electrodeposition Cell

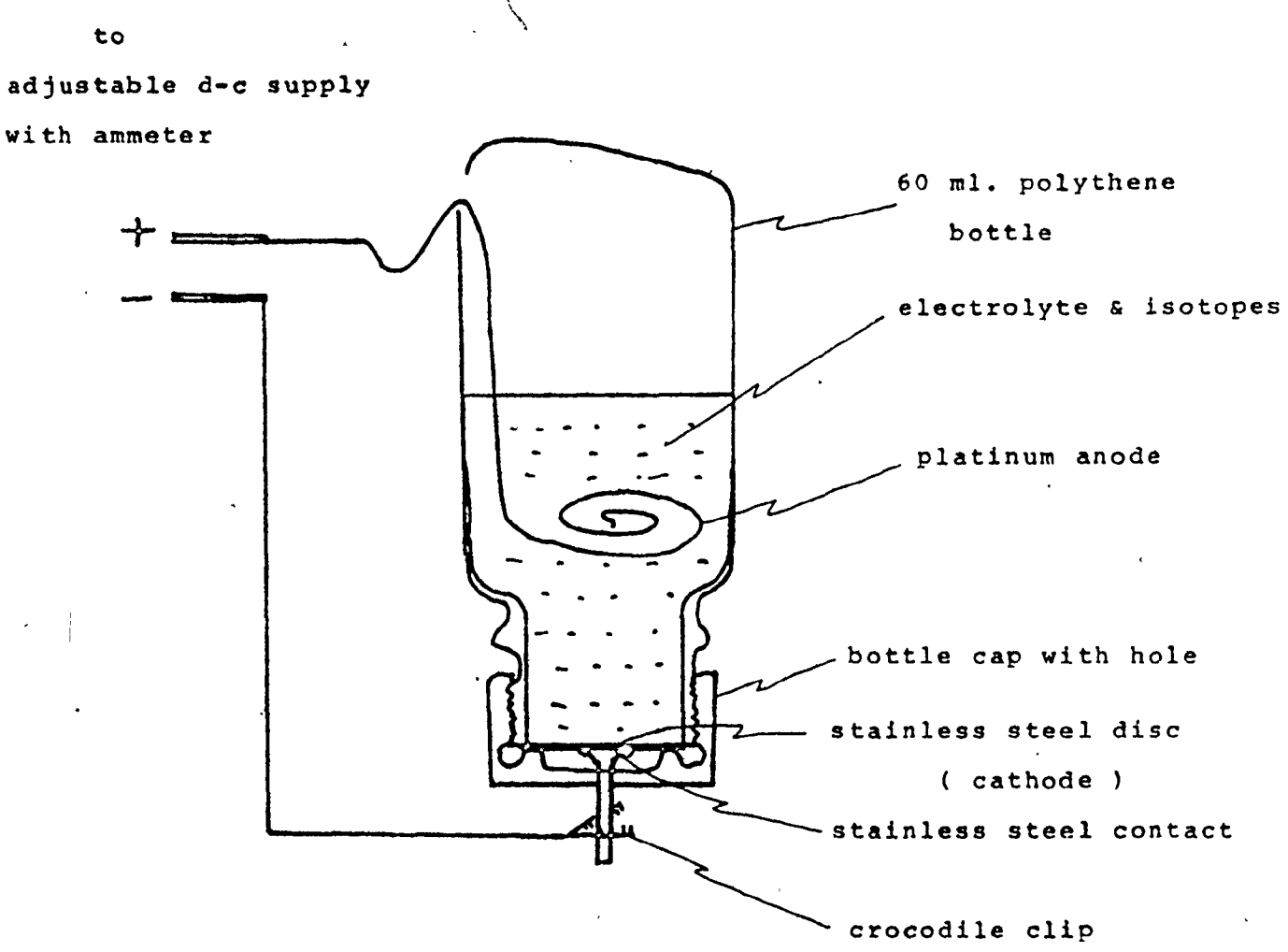

species having interfering alpha-peaks. Considering the eluates from the ion exchange steps (appendix Ia) these include Th, ^{210}Po and ^{226}Ra in the U spectrum, and ^{210}Po, ^{226}Ra and 5% of ^{224}Ra in the Th spectrum. In the evaporation method final purification of these eluates is achieved by extraction into TTA in benzene. (Thompson, op cit, gives a fuller account of these purification steps and how they discriminate against these alpha emitters and beta-decay parents such as Bi).

3.2.4.2 The Apparatus and Methods

A simple electrodeposition cell (figure 3.6) was made from a 60 ml. polythene bottle with the base partly removed. The cathode connection was a stainless steel disc soldered in the centre to a flat-headed screw. A hole was made in the bottle cap to allow the screw to pass through. The disc to be plated was placed on the cathode; the bottle was then firmly screwed into the cap to make a liquid-tight seal and a good electrical contact. The anode was a spiral of platinum wire suspended in the bottle from above. The electroplating current was supplied by a DC source delivering up to 3 A. The electrolyte was HNO_3 and H_2SO_4 in the ratio of 5 : 1, diluted and adjusted to pH 2.4 using dilute ammonia.

The following procedure was adopted and was partly based on a technical memorandum supplied by A. Lalley (Harwell).

Uranium

1) The 0.1N HCl eluate from the anion exchange resin was evaporated to dryness and taken up in 20 mls. of 0.1 N HNO_3 (pH 1).

2) A TTA-in-benzene extraction was carried out in a centrifuge tube to remove any contaminating thorium. The organic layer was discarded.
3) The aqueous layer, in a 100 ml. vycor beaker, was either: a) evaporated to dryness and taken up in 20 mls of the electrolyte, or
   b) converted to electrolyte by adding a few mls. of dilute H_2SO_4 and adjusting the pH to 2.4 with dilute ammonia.

The second alternative is preferred because weak acids are not good solvents of hardened deposits.

4) The electrolyte was poured into the prepared electrodeposition cell. The beaker was rinsed with electrolyte to give a total volume of 50 mls.
5) The current was adjusted to 0.5 to 1 A and deposition carried out for greater than 30 minutes.
6) At the end of the plate-out either:
   a) the cell was quickly inverted with the contents being poured into a beaker. or,
   b) ammonia was added and the current was maintained for one minute before the cell current was stopped and the cell contents poured out.

In both variations the aim is not to loose any plated U by dissolution back into the acid.

7) The disc was squirted with acetone or deionised water and flamed strongly for one minute to volatilise any Po The disc was ready for counting.

Thorium

1) The oxalic acid eluate from the anion column was oxydised either by HNO_3 and HCl or by $HClO_4$ and HNO_3

according to the established procedure (appendix Ia)

2) The deposit was either,
   a) dissolved in the prepared electrolyte, or
   b) dissolved in about 20 mls. of 0.1 N HNO_3 . A few mls. of dilute H_2SO_4 were added and the pH was adjusted to 2.4 with dilute ammonia.

As for uranium the second alternative is preferred.

3) The electrolyte with the thorium was transferred to the deposition cell together with several electrolyte rinses of the beaker to make a total volume of 50 to 60 mls.

4) Electroplating and cleaning of the disc proceeded as for uranium but the cleaned thorium disc did not need to be flamed so strongly.

3.2.4.3 Experiments and Results

The electroplating procedure of the previous section and variations of it were tried out in conjunction with attempts to calibrate the new spike solution (section 3.2.1). The resulting deposits on stainless steel discs were often spotted or uneven but had a metallic shine - blue in the case of uranium and grey in the case of thorium.

The following are some of the variations that were tried:

Experiment,

A4; The thorium was taken from the oxidised eluate, plated out and counted for about 900 minutes. The spectrum appeared to have a higher-than-usual ^{212}Bi peak. The likelihood is that Bi was plated out with the thorium rather than having grown in from preceding parents

such as ^{216}Po. The disc was flamed strongly before recounting and the high Bi peak persisted thus supporting this hypothesis. By implication ^{210}Bi may also have been plated out, which beta-decays to ^{210}Po, the latter occurring under the ^{228}Th peak. Thorium yield was about 12%.

A6; A back extraction of U from TTA in benzene was tried at pH < 1 into HNO_3. The aqueous layer was converted to the composition of the electrolyte for plate-out. The yield was very low ($\approx$1%).

A7; The aqueous layer containing the uranium was squished at pH 1 with TTA in benzene to remove thorium, and then electroplated according to the procedure for uranium.

The oxalic acid eluate for thorium partly sublimed during the oxidation process. It was plated out according to the procedure for thorium. After subtraction of background, correction for ingrowth of ^{224}Ra and decay of ^{228}Th, a spike ratio of 1.032 ± 0.058 was obtained.

A8; The U aqueous layer was squished with TTA at pH 1 to extract any Th. The U was then TTA-extracted at pH 3.5; attempts were made to back extract the U at pH < 1 using 20 mls of the electrolyte and, successively:

1) 1 drop 0.1 N HNO_3 + 1 drop 0.1 N HCl, and plated.
2) 1 drop 0.1 N HNO_3 + 1 drop 3 N HCl, " " "
3) 1 drop 0.1 N HNO_3 + 6 drops 3 N HCl, " " "

All failed to produce appreciable yields. The yield of U at stage 3) was 4%.

A9; As for the procedure. The thorium spectrum showed the high ^{212}Bi peak as in A4. After tail corrections were made the spike ratio was 1.070 ± 0.021.

A10; The thorium was largely lost in the oxidation stage but the peak around ^{212}Bi was anomalously high. Th yield < 1%, U yield ≈81%.

A12; Although a thorium extraction at pH 1 was carried out on the U aqueous layer a low ^{228}Th was observed just above the ^{232}U peak. Significantly a low peak at about the alpha energy of Pa was even more prominent. Evidently the pH 1 extraction was not thorough enough. This observation justifies keeping the pH 1 extraction step - if it is done properly! The spike ratio was 1.065 ± 0.021.

A13; After the oxidation step for oxalic acid, thorium was extracted into the TTA layer at pH 1. The TTA was then oxidised with H_2O_2 and HNO_3 . The plate-out of the resultant amber coloured liquid gave a low thorium yield of 12 %, but the pH of the liquid was not checked.

A14; The thorium was taken directly from the anion column, evaporated to dryness and taken up in 0.1 N HNO_3 . It was then extracted into the TTA layer at pH 1; the TTA in benzene was then oxidised with H_2O_2 and HNO_3 . The amber liquid was electroplated overnight (≈ 7 hrs), before alpha-counting. A usable thorium yield (34%) resulted in a spike ratio of 1.071 ± 0.027.

A16; An attempt to back extract uranium from TTA in benzene using 3 M HNO_3 failed to produce a yield.

A 3 M HNO_3 back-extraction for the thorium from TTA was partially successful (yield not determined).

3.2.4.4 Discussion

The extra purification steps involving TTA in benzene are desirable in removing possible contaminants. Although such contamination may not always be present, (eg. Kaufman, 1964, found that the pH 1 extraction of the U-aqueous layer was not necessary for possible thorium contamination) it is preferable to include it for the sake of reassurance. In any case the spectra from electroplated discs, which did not involve these TTA purification steps, did not always resemble those produced by the usual TTA method. In particular ^{212}Bi may be additionally present in the thorium spectrum. ^{212}Bi does not interfere in the alpha spectrum, but alpha counts from ^{210}Po, the daughter of ^{210}Bi, may be hidden in the tail of ^{228}Th. Some ^{210}Po may be present even after the TTA extraction of U (for a fuller discussion see Thompson, 1973, op cit), and for this reason the U-discs have to be strongly flamed. ^{210}Po electroplates more readily than either U or Th, so electroplated U-discs still need to be flamed. Unfortunately a strong heating may also degrade the U spectrum by oxidising the surface of the steel disc; this effect was observed by repeatedly counting a U-disc after successive strong heatings.

Spike ratios from electroplated discs (figure 3.5) were not significantly different from those produced from the evaporation procedure, which suggest that any contamination was not serious in these experiments.

The thorium and uranium yields were generally lower than those of the evaporation method. This was partly due to the fact that conditions of extraction were being varied

experimentally from run to run.

These experiments were carried out prior to the installation of the air-conditioning unit. Therefore a comparison of alpha-peak resolution between the two types of deposit was not made because the overall resolution was affected more by the temperature changes of the detectors.

3.2.5 Uranium and Thorium Electroseparation Experiments

Electroseparation of minor or trace amounts of metals in a common solution has been successfully carried out by controlled electrode-potential methods on a variety of metals such as Bi, Fe, Cu, Pb and others; sometimes with only a 0.1 V difference in standard potential (Skoog and West, 1971). Although no reference could be found in the literature to electroseparation methods for uranium and thorium it was decided to investigate the possibilities experimentally.

In effect attempts were made to see at what electrode potential U and Th could be separated from one another and from other isotopes of the decay chain. The experiments were carried out on a solution of the uraninite in 9 N HCl, boiled down and taken up in the prepared electrolyte. The electrode potentials were monitored with a saturated calomel electrode and voltmeter having a sensitivity of 0.05 V. The intention was to compare the potentials at which the various species were deposited with quoted electrode potentials, taken from the Handbook of Chemistry and Physics, (1977-78, 58 th.ed). The cell was powered by a , supposedly, constant voltage source, but which in fact had to be closely monitored and adjusted manually; precision was about 0.1 V.

Starting at zero potential the cathode voltage was increased in steps of 0.5 V, with each step taking 30 minutes. The disc was then cleaned, dried under a heat lamp and alpha-counted. A new disc was placed in the cell as the cathode at the next step. This procedure was carried out up to about 3 V.

^{210}Po plated out readily in accordance with its near zero electrode potential. A disc left to plate overnight at a voltage of about 1.5 volts still failed to accumulate all the ^{210}Po, since a second disc plated immediately after also collected some more ^{210}Po.

As the potential was increased both U and Th started to plate out at around 1.8 to 2.0 V and could not be separated under these experimental conditions. The peak heights suggested that the electrodeposition was equally efficient for U and Th. Besides the ^{210}Po peak a more-or-less broad background of alpha energies were observed. The experiments were then abandoned.

3.2.6 Oxalic Acid Conversion Experiments

A. Dixon (pers. com.) has shown in a series of experiments at McMaster university that loss of thorium may often occur in the oxidation step of the oxalic acid eluate. The reason may be as follows. Effective oxidation by aqua regia seems to take place mainly under vigorous boiling with the hotplate thermostat set at temperatures around 250 °C or more. Subsequently complete vaporisation of the mixture may occur if it is not monitored closely. Since oxalic acid sublimes at 150 °C it is soon lost at these higher temperatures taking some or all of the thorium with it.

Ammonium oxalate, as the electrolyte, has been used regularly in the electrodeposition of uranium (eg, see Casto, op cit, or Sebessy and Bakan, 1978 for references). In order to get round the above problem attempts were made to use the oxalic acid as the electrolyte or to convert it to ammonium oxalate, and then plate out thorium from it directly. In detail the experiments were:

B1; A preliminary experiment to plate thorium from the oxalic acid, diluted to a low pH, gave a low yield ($\ll$10%).

B3; The cation (thorium) column was eluted with 3 washes of 0.3 M ammonium oxalate and used directly as the electrolyte (pH $\approx$6). There was essentially no yield.

B4; The thorium wash, in 9 N HCl, from the anion column, (without a cation column separation) was boiled down almost to dryness and ammonium oxalate was added. A current of 0.6 A was used in the electrodeposition for about 2 hrs. The final pH of the solution was about 6, the deposit was not of good quality and the yield was 13%.

B5; In view of the previous experiment it was decided to convert the oxalic acid eluate from the cation column to ammonium oxalate by titration with ammonia (suggested by M. Gascoyne). The eluate also contained some of the tail of the 3 N HCl wash. After dilution with water the resulting pH was about 7. The deposition was carried out at 0.7 A for 2 hrs. to give a yield estimated at about 20 to 30%, but the film was patchy.

Subsequently this kind of thorium yield could not be repeated. The reason was thought to be due to pH changes which occurred during electroplating, following oxidation or reduction reactions at the electrodes. Ie. if the electrolyte solution becomes alkaline too fast the thorium can precipitate out on the walls of the cell; if the solution is too acid the thorium remains in it, being continually stripped from the cathode. Buffer solutions might be used to remedy this type of problem, after the right conditions for deposition have been found. Lack of time has prevented further investigation of the possibilities for an oxalic acid conversion method.

3.3 Discussion on Electroplating Procedured for U and Th

For the reasons stated in section 3.2.4 the electroplating method is preferable to the evaporation method if it can be shown that there is consistent freedom, in the respective U and Th spectra, from interfering alpha emitters. The indications are that without the extra purification steps this may not be the case. Back extraction of U and Th from TTA in benzene was not successful in this study but Mangini and Sonntag (1977) have reported success by back extractions carried out on a regular basis, at $pH < 1$. An additional advantage of back extraction is that iron impurities , which might otherwise produce a thick film, are kept back in the organic phase.

3.4 The Method Adopted for Routine Age Determinations

An internal standard, at McMaster university, was prepared by Gascoyne (1979, op cit) from a crushed homogenised flowstone. Nine age determinations were carried out

by Gascoyne and two by the author using the evaporation technique. The standard deviation of the overall mean was less than the mean of the separate standard deviations (mean age = 47.7 ± 1.7 Ka; mean standard deviation = 2.2 Ka) On this basis therefore the evaporation technique is certainly acceptable. In the absence of a fully satisfactory electroplating procedure it was adopted in this study for finding speleothem growth rates.

CHAPTER 4

THE PALEOMAGNETISM OF SPELEOTHEMS FROM CANADA AND ENGLAND

4.1 General Introduction to Chapters 4, 5 and 6

Several test samples from the McMaster collection showed measurable remanences on a Toronto university PAR spinner magnetometer. Then after the initial encouragement from the BJTL results, described in this chapter, much time was wasted in cutting oriented speleothems which showed little or no remanence. Henceforth test specimens were taken to determine which oriented speleothems could be fully prepared for measurement. All such tests, unless otherwise leading to comprehensive treatment, are listed in appendix II.

In this chapter and chapters 5 and 6 the presentation runs as follows. Firstly a description of the speleothem is given. This is followed by a description of the speleothems morphology with a photograph of its stratigraphic section. Reference is made, when applicable, to a thin section which is described in detail in appendix III. The paleomagnetic results are presented in the form of a table of D and I values against position in the speleothem. The AF cleaned D and I values are plotted with the dates derived from the U/Th method against position in the speleothem. A growth rate curve has been fitted to each speleothem by least squares methods, as appeared warranted. In many cases VGP paths have also been derived. Discussions

of the results include experimental errors, depositional errors, comparisons with other results and implications for the past Earth's field and for rock magnetism.

4.2 Introduction to Chapter 4

This chapter describes the paleomagnetism and U/Th dating of speleothems from Canada and England. A comprehensive account of limestone areas and caves of Canada is in preparation by D.C.Ford. Many of Canada's caves are to be found in the Rocky mountains and on Vancouver island. The U/Th dating of speleothems from these caves was begun by P. Thompson (1973) and has been continued by Harmon (1975), Gascoyne (1979) and by this author.

A number of the dates for Rockies and Nahanni speleothems were greater than 350 Ka. One of the objectives of the paleomagnetic study was to see if any showed reversed magnetization , which would then indicate a probable age greater than 720 Ka. In fact this situation was discovered in flowstones from both Eagle and Castleguard caves in the southern Rockies.

The U/Th dating of British speleothems was begun by Atkinson and others (1978), and was continued by Gascoyne (1979, op cit) and by Gascoyne and Ford (in preparation). The most significant result from these studies has been a more exact definition of the timing of the Late Quaternary glacial and interglacial periods in the northern Pennines.

The first NRM directions from an oriented speleothem were also eagerly conned to see how they compared with the present Earth's field or if they partly reflected the dip of the flowstone surface. These first results came from

Plate 4.1

Flowstone BJTL; the scale is in cms.

Table 4 - 1; NRM of Specimens and Analysis of Directions of BJTL

Cut No.	Distance from top (cms)	NRM N	NRM D	NRM I	NRM α_{95}	NRM K	Alternating Field Demagnetised H (Oe)	Alternating Field Demagnetised D	Alternating Field Demagnetised I	Alternating Field Demagnetised α_{95}	Alternating Field Demagnetised K	Alternating Field Demagnetised δD	Alternating Field Demagnetised δI	VGP (mean) Lat	VGP (mean) Long
1	1.0	9	38.0	77.2	10.6	13	50	42.0	80.5	2.3	410	14	2.3	61.1	-88.5
2	2.9	10	355.7	75.2	12.4	11	100	10.9	78.1	3.1	200	15	3.1	71.7	-101.1
3	4.8	9	357.7	69.7	2.5	347	100	355.8	72.0	1.2	1570	3.8	1.2	82.3	-132.0
4	6.8	8	5.1	65.3	1.5	1072	100	7.3	67.1	1.1	2011	2.8	1.1	85.3	- 28.5

Notes; D is reckoned positive in the clockwise sense.

Latitude is reckoned positive in the northern hemisphere.

Longitude is reckoned positive from 0 to 180° E, negative from 0 to 180° W.

The formulae quoted in Irving ,1964,pp 43-44, have been used to derive the mean VGPs.

FIGURE 4-1 ELEMENT DIRECTIONS OF BEAR JAW CAVE FLOWSTONE, BJTL.

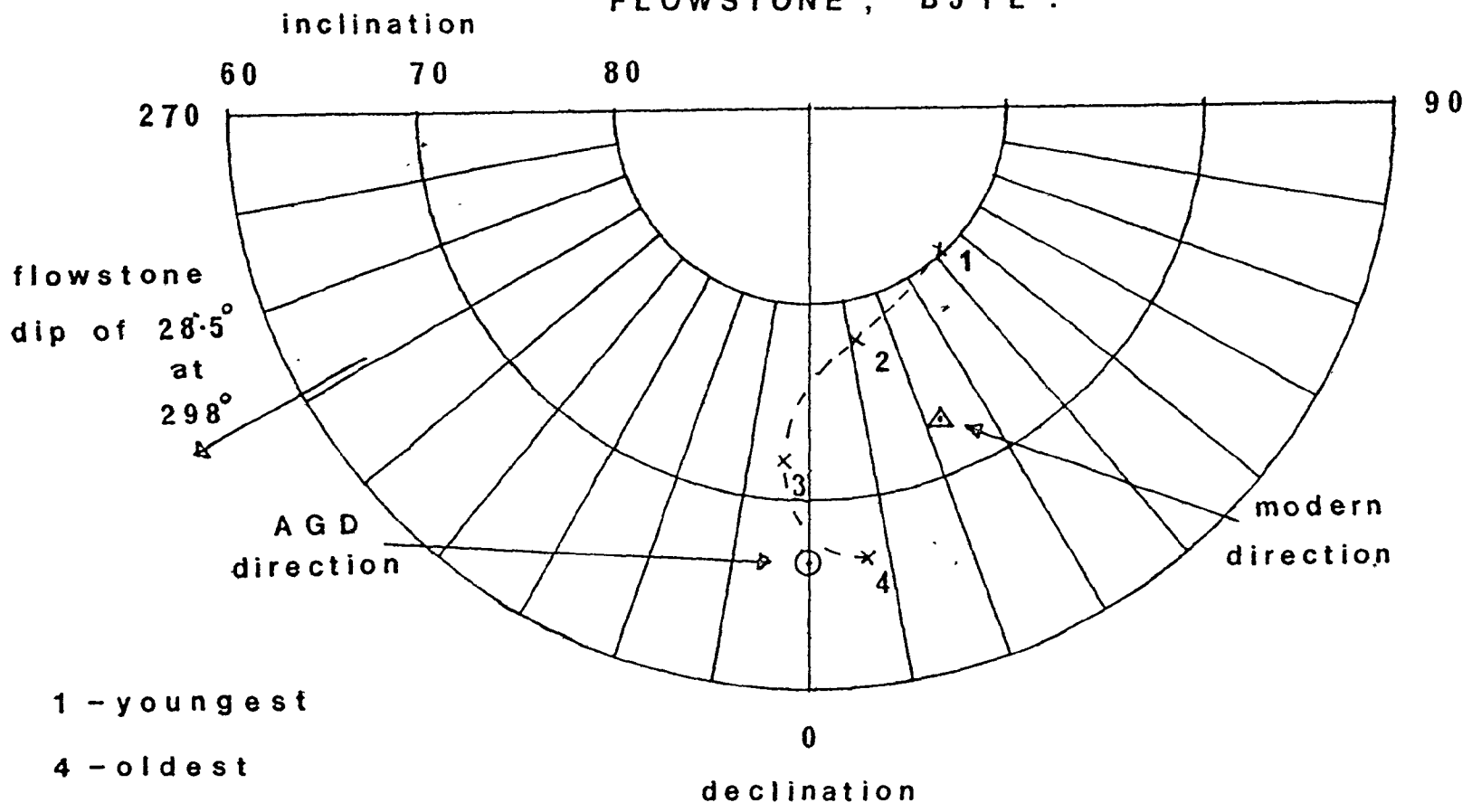

Canadian sample BJTL and they showed that cleaned NRMs corresponded only to the ancient ambient field. Though BJTL proved to be greater than 350 Ka in age the paleomagnetic data was encouraging since it indicated that speleothems could be reliable paleomagnetic recorders.

4.3 BJTL; Description and Results

Plate 4.1. Thin section appendix III.

Rock magnetism; 7.3.1 .

Site; Bear Jaw cave, near Deadman Pass, British Columbia, 49° 43′ N, 114° 39′ W .

This speleothem was the top 7.6 cms of a flowstone sequence situated about 10 m away from, and lower down than the present entrance of Bear Jaw cave. The total sequence, as sampled, was labelled BJB1, BJB2, BJML, BJIL and BJTL in stratigraphic order. BJTL was found to be normally magnetized throughout but two U/Th dates were greater than 350 Ka. A piece of BJB1, the lowest in the sequence, was also normally magnetized.

The layering in all the samples was translucent white to dark brown. The NRM signal of BJTL was markedly stronger in the darker layers. The BJTL layering was approximately parallel throughout and dipped 28.5° in a direction 298°.

Three vertical slices were prepared each of which yielded 4 cuts. Cuts 1 (top), 2, 3 and 4 (base) yielded 9, 10, 9 and 8 specimens respectively. The analysis of the NRMs and the AF cleaned directions of these cuts is presented in table 4.1 . The four cleaned directions have been plotted in figure 4.1 together with the AGD and present day

Table 4 - 2; Specimen Dating and Isotope Activity Ratios.

Sample	Cut no.	U (ppm)	$^{230}Th/^{234}U$	$^{234}U/^{238}U$	$^{230}Th/^{232}Th$	Calculated Age ±1σ (Ka)
BJTL	1	1.1	0.98 ± 0.04	1.00 ± 0.04	609	>350
ENF	1	0.27	1.10 ± 0.05	1.26 ± 0.05	17	>350

directions and the dip of the flowstone layers. The pilot AF demagnetization of several specimens is given in 7.3.1 .

The U/Th isotopic data and date are given in table 4.2, showing that BJTL was older than 350 Ka.

As mentioned, BJTL was the first oriented speleothem to be analyzed in detail for its NRM. Several points stood out which were encouraging to the feasibility of using speleothems for recovering paleofield directions:

1) A stable component of NRM could be isolated. In view of the compactness of the sample and despite exposure to weathering , this stable NRM is probably primary, as indicated by the following points,
2) The precision of directions increased upon AF cleaning . Removal of low coercivity viscous components was not a problem, provided that :
   a) The stable cleaned magnetization was still high enough to measure, and
   b) Cleaning did not introduce ARMs via the magnetically soft grains.
3) The D and I values varied in a regular way and were consistent with what one might expect from a hiatus-free record of a regularly changing field.
4) The cleaned directions lay near the AGD and present day fields. Significantly there appeared to be no bias in the direction of , or at right angles to the flowstone dip.

This last result has been found in all other samples so tested and presents a major advantage of speleothems over many sediments as a paleo-SV recorders. It also supports

Plate 4.2

Flowstone ENF.

Water flow was approximately right to left

Reversed climbing ripples are visible.

Table 4 - 3; NRM of Specimens, Analysis of Directions and VGPs of Sample ENF.

Cut No.	Distance from top (cms)	NRM N	NRM D	NRM I	NRM α_{95}	NRM K	Alternating Field Demagnetised H (Oe)	N	D	I	α_{95}	K	δD	δI	VGP (mean) Lat.	VGP (mean) Long.
1	1.0	4	179.8	-66.4	1.0	5378	80	4	184.7	-67.4	1.1	4303	2.8	1.1	86.9	-36.6
2	2.9	4	196.0	-53.9	2.5	812	80	4	197.2	-57.0	2.4	869	4.4	2.4	72.7	13.0
3	4.7	4	173.2	-54.6	4.3	260	80	4	174.5	-56.4	4.4	254	7.9	4.4	76.7	84.7
4	6.7	4	187.1	-57.8	2.9	567	80	4	186.5	-61.1	1.5	2234	3.1	1.5	81.2	31.8
5	8.5	4	183.9	-69.6	1.4	2564	80	3	186.4	-72.8	1.7	2166	5.9	1.7	80.6	-93.5
6	10.4	4	184.6	-48.8	0.7	8840	80	1	186.2	-52.2	-	-	-	-	72.5	47.9
7	12.4	4	176.0	-66.2	1.0	4869	80	4	179.5	-68.7	0.8	6848	2.3	0.8	87.5	-121.8
8	14.2	4	174.2	-69.4	1.5	2172	80	3	176.4	-72.8	2.0	1669	6.7	2.0	81.1	-126.9
9	16.1	4	177.7	-59.5	1.3	3091	80	3	179.6	-62.5	1.9	1887	4.0	1.9	84.1	62.5
10	18.0	4	181.3	-57.5	1.2	3155	80	4	182.5	-56.3	1.2	3387	2.2	1.2	77.1	56.3

Notes; The distance is measured from the top surface to the centre of the specimen (± 0.1 cm).
Latitude is reckoned positive in the northern hemisphere.
Longitude is reckoned positive from 0 to 180° E, negative from 0 to 180° W.
The reversed south virtual geomagnetic poles around the north geographic pole were found using -
$D' = D - 180$, and $I' = -I.$, and the formulae quoted in Irving, 1964, pp 43-44.

the argument that the stable magnetization of speleothems is probably of chemical rather than of detrital origin. It is otherwise hard to envisage how a dipping surface (in stalagmites, a vertical surface) can not have influenced the average direction of a number of ready magnetized grains.

4.4 ENF; Description and Results

Plate 4.2. Thin section; appendix III

Rock magnetism: 7.3.2.

Site; Eagle cave, Crow's Nest Pass, Alberta, 49° 39′ N, 114° 38′ W.

The cave is situated about 90 to 100 m above the present spring level. A single flowstone lies along a steeply sloping wall, and is more than 25 cms thick. Previous attempts to date this flow showed possible ages between 198 Ka and > 300 Ka, (Thompson, P, 1973, op cit; Harmon, et al, 1975), although there may have been some confusion as to the exact location of samples collected. The U/Th age produced in this study was > 350 Ka; the isotope ratios and age are given in table 4.2 .

The 13 cm thick sample of this work is mostly compact, almost opaque dark-brown, and with fissile 'chocolate' layering about 4 cms from the top. It dipped at 45.5° in a direction of 237° . Two slices were prepared from the sample. A test specimen from one of them showed an easily measurable NRM which was reversed. Slice D was then fully prepared to give four specimens per cut. The whole of the slice was found to be reversely magnetized; the data are presented in table 4.3 . AF demagnetization showed the NRMs to be very stable , and indeed the median demagnetization fields of pilot specimens were the second highest

Figure 4 - 2; Declination and Inclination Changes of ENT

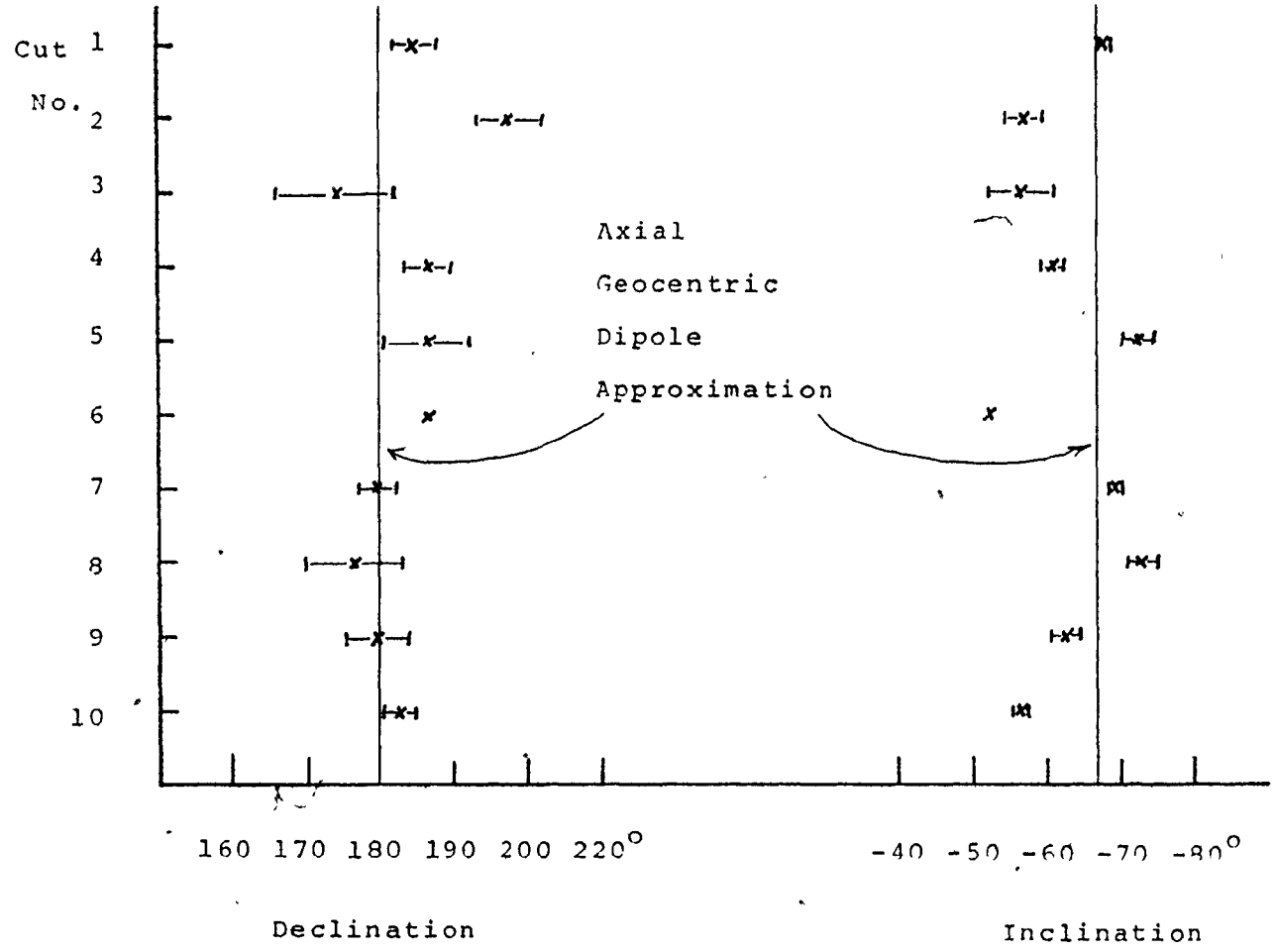

recorded in the whole study.

Figure 4.2 shows the cleaned D and I variations plotted against position. (It is possible that the directions of cuts 2 or 3 have been affected slightly by the magnetization of epoxy glue used to bind fragmented specimens together. The magnetic effects of this glue were only noticed later in much weaker specimens and in a 2 gm test blob which had a remanence in the direction of the Earth's field. Its use was then discontinued).

4.4.1 Discussion

The D and I values vary around the (reversed) AGD values. ENF was the second example of where the NRMs were apparently unaffected by the flowstone slope.

Though it was not possible to date the individual directions of BJTL or ENF, the results showed that the growth rates were fast enough to resolve SV changes. Growth-rate estimates of flowstones (Harmon et.al, 1975, op cit) range from 1 to 4 mm per Ka. The NRMs of 2 cm specimens of BJTL or ENF may therefore represent averages over 20 to 80 Ka. This implies that SV does not average to the AGD direction in less than about 80 Ka.

4.4.2 Discussion of the VGP paths of BJTL and ENF

Figures 4.3a and b represents an attempt to compare the VGP paths of BJTL and ENF. Their sites are proximate; viz, for BJTL, 49.72° N, 114.65° W, and for ENF, 49.65° N, and 114.63° W. Unfortunately BJTL does not have a long enough record for a thorough comparison. The path segment of BJTL is near-sided to the sampling site.

Figures 4 - 3a and b; The Virtual Geomagnetic Pole Paths for BJTL and ENF.

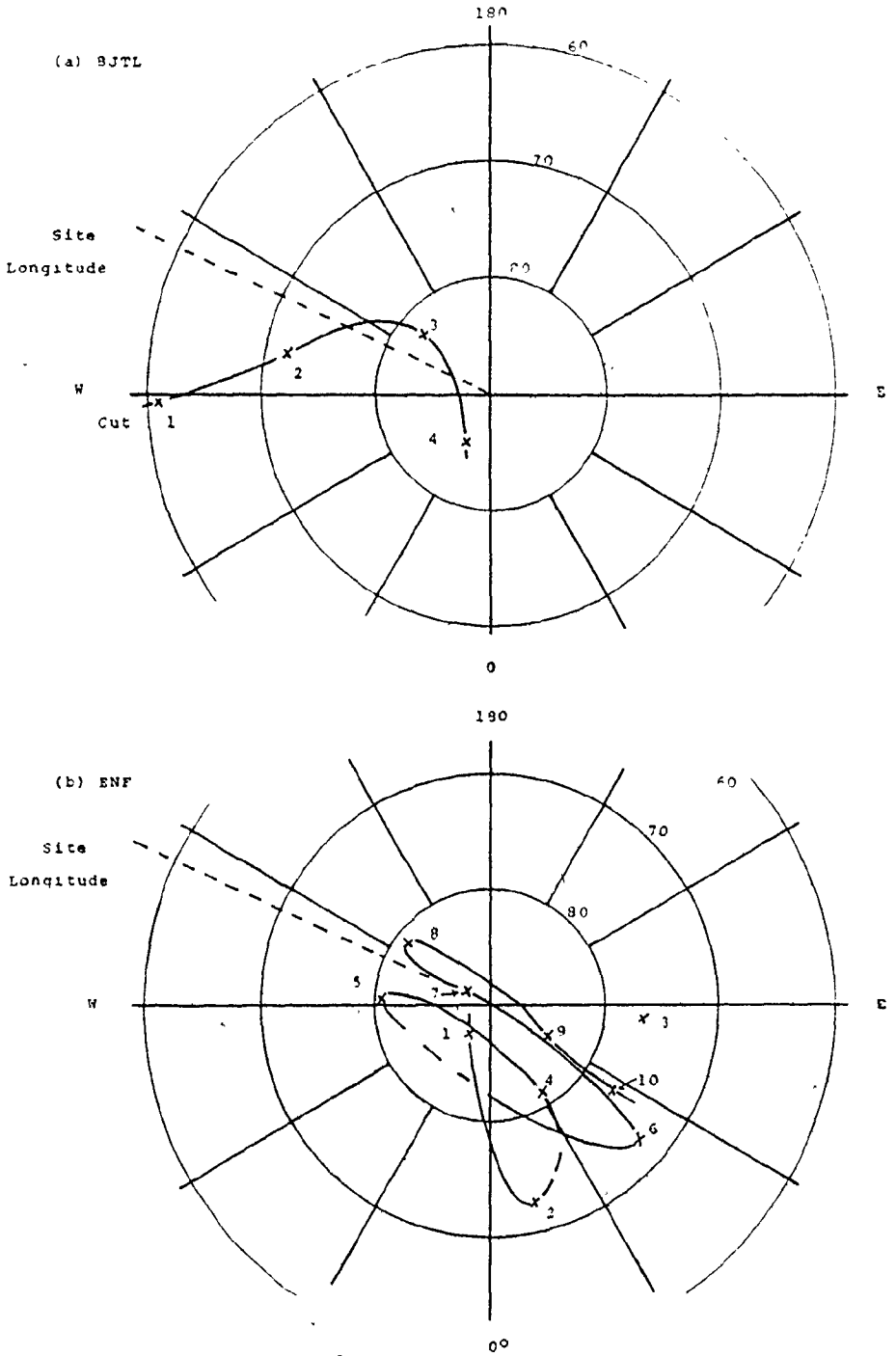

For ENF the south VGP has been mapped onto the N geographic pole. In the southern hemisphere, the path of the reversed N. VGP is exactly the same but out of phase by 180° of longitude.

Figures 4.2 and 4.3b show either that secular variation was quiet, for ENF, most of the change being recorded in the inclination, or that the flowstone did not grow very fast in comparison with the secular variation.

4.5 CGF1; Description and Results

Site; Castleguard cave, Castleguard mountain, Alberta.

Three pieces of flowstone were taken from Castleguard cave by P. Smart in 1980 with approximate orientation data. Two came from the supposed base and top of an eroded flowstone in the Waterfall Room (Thompson, P, 1976), and gave equivocal results from the point of view of whether they had reversed or normal magnetization. M. Gascoyne (1979) had previously determined U/Th ages for the Waterfall Room flowstone to be greater than 350 Ka. The third piece, CGF1, came from beneath a prominent stalagmite in the Grottoes and was distinctly reversed according to the orientation data given. No stability tests were tried other than to allow the specimen to stay in the ScT magnetometer for a minute or so; no changes in magnetization were noticed. All three samples had prominent yellow and white layering and in some layers black particles could be seen using a hand lens. The signals were strong - on the order of 10^{-5} G for 40 gms of the first pieces, and 10^{-4} G for a 40 gm mass of CGF1.

Plate 4.3

Stalagmite VCCL (on the right).

Also shown is GYS1, described in appendix II.

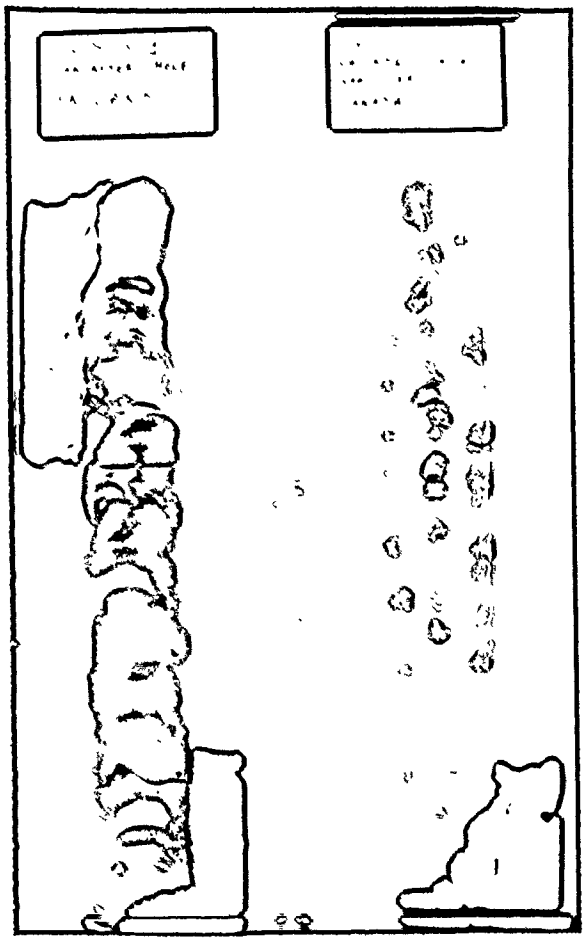

4.5.1 Geomorphological Implications from the Data of BJTL, ENF AND CGF1.

Bear Jaw cave, Eagle cave and the Grottoes area of Castleguard cave were either springs or phreatic passage sections. The flowstones contained in them may be the oldest following dewatering of the passages (they were sought and picked as such). It is probable that the dewatering is a consequence of a lowering of spring level following on the lowering of the valley floor by erosion. From considerations of the elevations of the old cave from the new spring, and using the U/Th ages and age limits suggested by the normal or reversely magnetized flowstones, Ford et al (1981, in press) have been able to estimate erosion rate limits for the southern Canadian Rockies. These estimates are in the range 0.04 to 0.52 m per Ka.

4.6 VCCL

Plate 4.3, Thin section; appendix III,
Rock magnetism; 7.3.3
Site; Cascade cave, Vancouver Island, BC, Canada, 49° 31′ N, 124° 45′ W.

4.6.1 Description

Cascade cave is described in Thompson (1976, op cit). VCCL was the largest of three stalagmites collected from a small alcove in Hare's Breadth Passage. It is known that the passage acts as a flood bypass route (P. Shaw, pers. com.) The alcove itself appears to act as a temporary repository for sediments from sand up to about cobble size.

The stalagmite is 50 cms long, a fairly consistent 8 cms wide, and the top 3 to 5 cms contain the parent soda-

straw stalactite. The speleothem shows marked sediment bands which provide a record of the flood events. From the base to about halfway, the sand grains are so dense that they have caused holes to form by interruption or deflection of the calcite growth; they are often poorly cemented. The upper half of the sample also showed strong banding but the calcite is more compact.

The distribution of the detritus, as revealed by sectioning the sample, appears to have come about as follows;

1) Floods have deposited coarse sediment up to 0.5 cm in diameter on the speleothem surface. It has adhered best to the top and curved edges rather than the sides.
2) After each flood has subsided the drip water has splashed most of the detritus towards the curved edges and vertical sides. This mechanism appears to be common in many speleothems and is referred to hereafter as the 'wash-off' effect or feature.*
3) Calcite precipitation has continued in the centre and the sides, but the curved edges have not been cemented quite so well. Further precipitation on the vertical sides may nave continued after the straw was joined to the stalagmite.

* A formal definition might be; "The 'wash-off' effect is the mechanism whereby detrital material, on the upper surface of a stalagmite becomes wholly or partially removed by the splash and flow of water from an overhanging feed-source, to be redeposited further down."

Table 4 - 4 ; NRMs, Analysis of Directions and VGPs of Simple VCGI:

Cut No	Distance from top (cms)	NRM		Alternating Field or Thermally Demagnetised				VGPs	
		D	I	H (Oe)	(T) (^{o}C)	D	I	Lat.	Long.
2	1.0	12.2	63.0	100		7.8	60.4	80.4	17.0
3	3.0	6.5	61.5	100		1.1	58.6	77.6	41.0
4	5.0	348.7	63.5	100		339.4	65.8	76.4	-212.6
5	7.0	356.8	68.6	100		351.1	71.2	81.6	-161.4
6	9.0	20.0	66.0	100		14.2	68.8	80.6	-57.9
7	11.0	23.6	46.0	100		26.8	47.6	61.0	0.6
8	12.9	7.9	44.0	100		1.0	43.2	65.8	53.1
9	15.0	359.0	51.4	100		357.0	51.3	72.4	63.7
10	16.9	14.0	57.5	100		359.0	57.0	78.0	59.4
11	18.6	6.8	49.0		210	351.9	45.3	66.6	73.8
12	20.5	359.8	57.5	125		349.3	54.7	73.0	88.3
13	22.5	3.0	62.6	200		333.1	55.5	72.7	-202.2
14	24.5	4.0	65.9	100		346.8	67.3	81.5	-205.1
15	26.5	45.5	62.3	100		17.0	67.9	79.0	-49.7
16	28.5	17.1	69.3	100		353.9	69.0	85.8	-188.6
17	30.6	31.6	69.9	100		355.6	67.4	87.0	-196.8
18	32.7	2.5	66.0	100		347.1	66.3	81.6	-213.9
19	34.5	29.3	65.4	100		5.1	65.0	85.9	-1.1
20	36.4	24.4	53.9	100		11.8	59.4	77.6	8.6
21	37.9	357.3	63.2	100		343.0	62.5	77.1	126.2
22	39.7	0.3	71.2	100		349.0	69.3	82.3	-183.1
23	41.7	19.0	73.9	200		9.2	72.9	79.5	-97.3
24	43.8	21.3	69.9		100	7.3	71.5	81.8	-94.9
25	45.9	18.7	76.4	100		5.9	74.8	77.4	-111.8

Notes: VGPs were found using the formulae quoted in Irving,1964, pp 43 - 44.

Latitude is reckoned positive in the northern hemisphere.

Longitude is positive eastwards, negative westwards.

The present day direction of the field is 23^{o} E, inclination 71^{o}.

In addition there is the possibility that the stalagmite, in its early growth, was temporarily buried by sediment from some floods. There is no evidence for any hiatus. The basal layers up to a height of about 6 cms (cut 23) are not coaxial to the rest of the stalagmite and this suggests there has been a small shift in the original drip location.

Upon dissolving specimens for dating the insoluble residue contained unidentified organic material, quartz, black magnetic grains and other detrital minerals. Opaque grains were fairly abundant in thin section and some were titanomagnetite grains showing exsolution and oxidation features.

4.6.2 The Paleomagnetism of VCCL

The stalagmite was cast in three parts and sawn according to the procedure of section 2.4 . It yielded one central vertical slice, having a width of about 2 cms; and then 25 specimens. Specimen #1 comprised the soda-straw and outer stalactite and was not analyzed for its NPM . The analysis of the NRMs and the cleaned magnetizations is presented in table 4.4 and the AF and thermally cleaned directions are plotted against distance from the top in figure 4.4 .The corresponding VGPs are plotted in figure 4.5 .

The intensities of specimens ranged from about 3×10^{-6} G cm^{-3}, near the base to 2×10^{-7} G cm^{-3} near the top.

The two thermally demagnetized specimens show that viscous components were removed at temperatures below about

Figure 4 - 4 ; Declination, Inclination and Dates of VCCL.

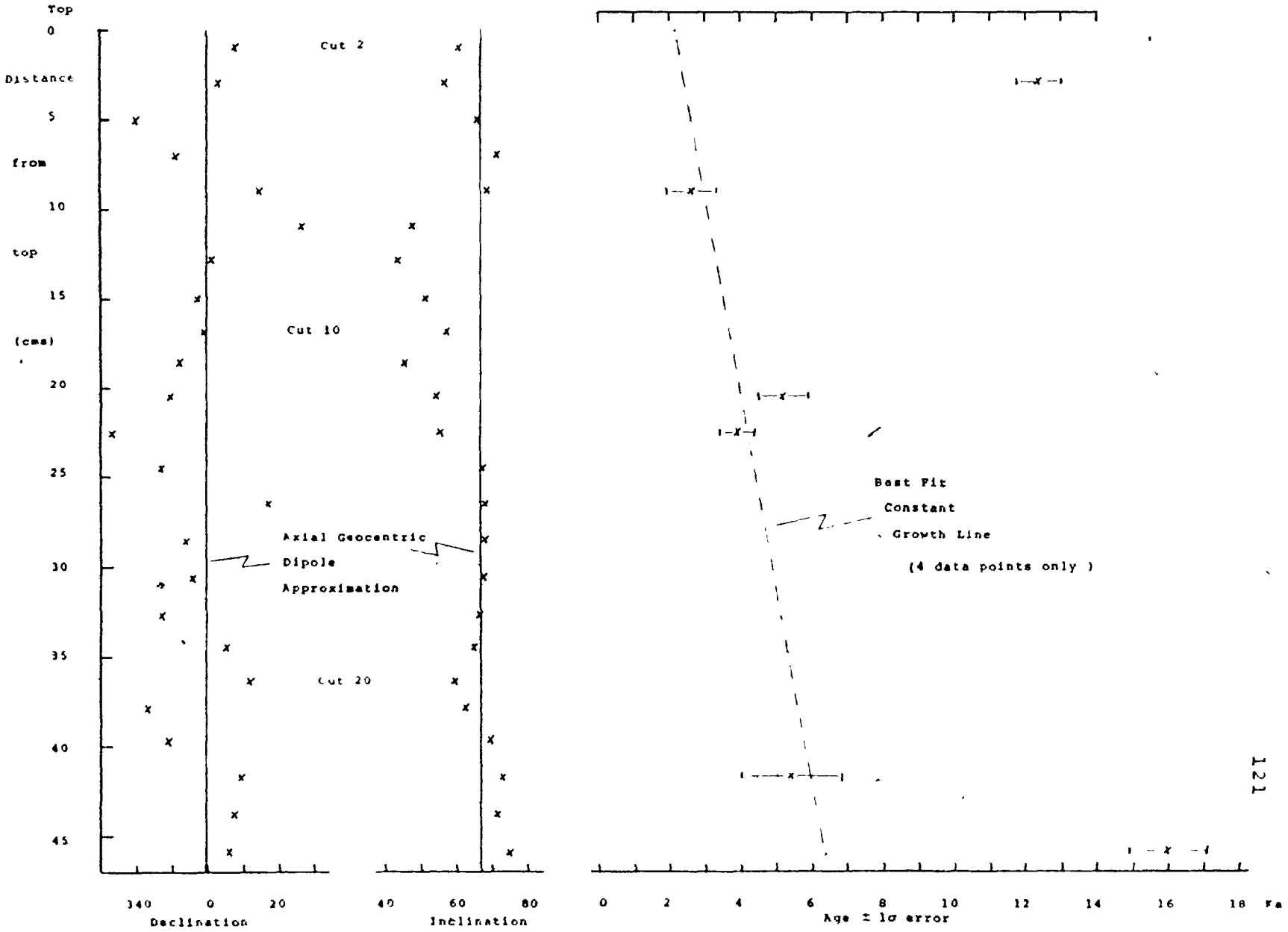

210 °C. Four specimens were AF demagnetized and the Zijderveld plots show that consistent stable directions are attained in fields from 100 to 200 Oe. The field used for routine AF demagnetization, chosen originally without recourse to these plots (see section 9.3.3), was 100 Oe and in retrospect this was probably too low for most specimens.

The viscous component has been acquired mostly in the present-day field as shown by all the Zijderveld plots. Most of the vector displacement upon cleaning took place in the horizontal plane.

Since all the data points are reckoned to be of about the same quality there is no reason to suspect such directions as those from cuts 7 or 15, for example, which appear to be non-sequential. The point was made in section 2.5.3 that the cut vector is the resultant of the directions of all the horizons which recorded the instantaneous field. It is clear that in the case of cuts such as 7, 15 or 18 the actual field must have been even more distant from the flanking directions than is indicated by the median resultant. In other words, the actual extreme field probably lay some way along the normal to the direction path, or the VGP path, at the resultant . Except for experimental limitations, this field could be more closely approximated by taking finer cuts of the recorder around the point.

4.6.3 The U-Th Dating of VCCL

The isotope activity ratios and dates of VCCL are given in table 4.5 and the dates are plotted against length in figure 4.6 .

Table 4 - 5; Isotope Activity Ratios and Dates of VCCL.

Cut No.	Distance from top (cms)	U (ppm)	Yields (%) U	Yields (%) Th	$^{230}Th/^{234}U$	$^{234}U/^{238}U$	$^{230}Th/^{232}Th$	Calculated Age (Ka) Uncorrected	Calculated Age (Ka) Corrected
3	3.0	0.43	55	64	0.108 ± 0.005	1.42 ± 0.03	34 ± 20	12.4 ± 0.6	12.4 ± 0.6
6	9.0	0.36	77	85	0.027 ± 0.003	1.53 ± 0.04	11 ± 8	3.0 ± 0.3	2.6 ± 0.7
12	20.5	0.48	57	24	0.055 ± 0.004	1.47 ± 0.03	10 ± 3	6.2 ± 0.5	5.2 ± 0.7
13	22.5	0.44	52	68	0.041 ± 0.003	1.47 ± 0.035	11 ± 4	4.5 ± 0.3	3.9 ± 0.5
23	41.7	0.28	45	69	0.072 ± 0.006	1.46 ± 0.06	4 ± 1	8.1 ± 0.7	5.4 ± 1.4
25	45.9	0.36	55	51	0.149 ± 0.006	1.47 ± 0.04	17 ± 4	17.3 ± 0.8	16.0 ± 1.1

Note; The detrital thorium corrections were made assuming a $\left(^{230}Th/^{232}Th\right)_0$ ratio of 1.5.

A new detector, free from contamination by alpha-recoil nuclei, was used for this speleothem. The background was therefore zero or very low.

A linear growth rate was fitted to the four middle dates using the inverse variance as a weighting factor to each date, (Bevington, 1969). The top of cut two, the junction of the stalagmite and stalactite was 2.15 ± 0.95 Ka, and the speleothem possessed an overall growth rate of 1 cm = 0.092 ± 0.044 Ka. Cut 25, the lowest, corresponds to an age of about 6.4 Ka; the paleomagnetic record has a time span of 4.14 ± 1.98 Ka.

Dates on two of the cuts at 3 and 25, are anomalous having ages of 12.4 ± 0.6 and 16.0 ± 1.1 Ka respectively. The date for cut 25 is physically reasonable. It could indicate an initial slow growth or an otherwise undetected hiatus somewhere between it and cut 23. Either of these interpretations appears to be ruled out by the paleomagnetic data (figures 4.4 & 4.5), which show a slowly varying sequence from cut 25 to 23. The most likely explanation for the older dates for both these cuts is the presence of thorium contamination from improperly cleaned glasware (see section 9.4.1).

4.6.4 Geophysical Interpretations of the VCCL Record

Despite the low cleaning field used on some specimens it is probably safe to assume that the declination and inclination changes of figure 4.4 and the VGP path of figure 4.5 are a satisfactory record of the ancient field.

Figure 4 - 5; Virtual Geomagnetic Pole Positions for VCCL, The numbers denote the cut and arrows denote direction of VG polar movement with time.

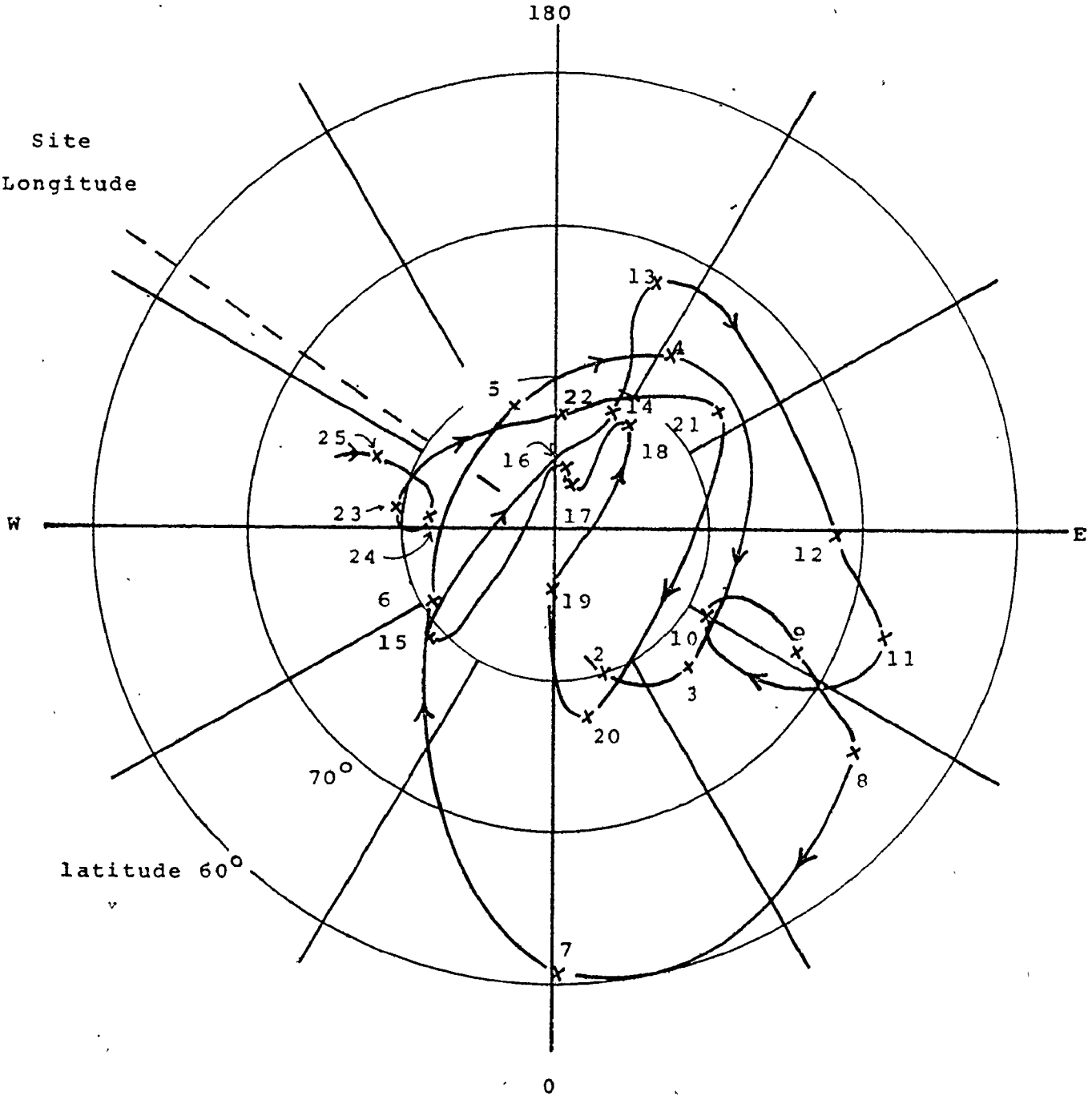

The declination repeatedly made rapid changes over a period of about 100 years, and encompassed large swings. The major swings are 43°, east to west, between cuts 15 and 13, and 46°, east to west between cuts 7 and 4. There are several other swings of about 25° eastwards and westwards. If these represent cyclic changes then either the cycle frequency decreased or the speleothem growth rate increased, the latter being undetected in the dating.

There does not appear to be any corresponding cyclicity in the inclination changes. The inclinations are at first slightly steeper than I_{agd}. From cuts 19 to 14 they change very little and approximated I_{agd} almost exactly. From there to the top the changes are quite marked.

The overall cyclicity of the secular variation is best seen in the VGP path, figure 4.5 . About 2½ clockwise rotations of the path are traceable, with an overall far-sidedness. Imposed on these rotations are minor loops. From the considerations of Runcorn (1959, op cit) or Skiles (1970, op cit) this is clear evidence for mainly westward-drifting secular variation for the interval 6 to 2 Ka.

The 2½ cycles may be reckoned to span cuts 23 to 3 and this implies a time interval of 3500 a. The best estimate of an average period is thus about 1.45 ± 0.7 Ka. This is not significantly different from estimates of periods of declination cycles of 2.0 Ka from Lake Erie (Creer et al, 1976a), of 2.1 Ka from lake Michigan (Creer, et al, 1976b), but is smaller than the 2.8 Ka estimate from lake Windermere (Thompson, 1975) and the Black Sea (Creer, 1974). These are all at about the same latitude as

the VCCL site. Second generation estimates of periodicity of the total directions from British lake records show that the changes were not periodic; the duration of declination cycles steadily decreased from 4.0 to 1.7 Ka during the period 7 Ka to present (Turner and Thompson, 1979; Thompson and Turner, 1979). The converse is seen in the VCCL record; that is, two short duration cycles are observed between 6 and 4.5 Ka and one long period between 4.5 and 2.6 Ka.

The inclinations are significantly shallower than the AGD inclination throughout the record and this supports Wilson's more general observations about far-sided VGPs (Wilson, 1972, op cit, and section 1.3.3). In order to test for the right-handed bias, which Wilson had also observed, the declination record was separated into easterly and westerly segments over the two cycles begining at 41.0 cms and ending at 8.0 cms - the lower and upper crossover points (ie at $D = 0^{o}$)*. In terms of stalagmite length and hence of time (for the assumed uniform growth rate) the declination is biassed 2 : 1 in favour of westerly declination. This is despite the contrary visual appearance of the VGP path. Thus a deposit which had averaged out these two cycles would have a left-handed mean VGP. It was Merrill and McElhinny's contention (1977, op cit; see section 1.3.3) that where left-handed (more westerly) declinations should be observed in the global analysis , the data was partly missing in some areas; one such area was the N.W. Pacific.

* More exact estimates of overall westerly or easterly bias should be calculated as the integral $\int D.\ dt$ over as many complete cycles as are available from the record, where D is the declination and t is the time. Similarly, overall left- or right-handed bias is the integral $\int L.\ dt$ over completed cycles where L is the VGP longitude reckoned from the observer's longitude.

Plate 4.4

Stalagmite TS.

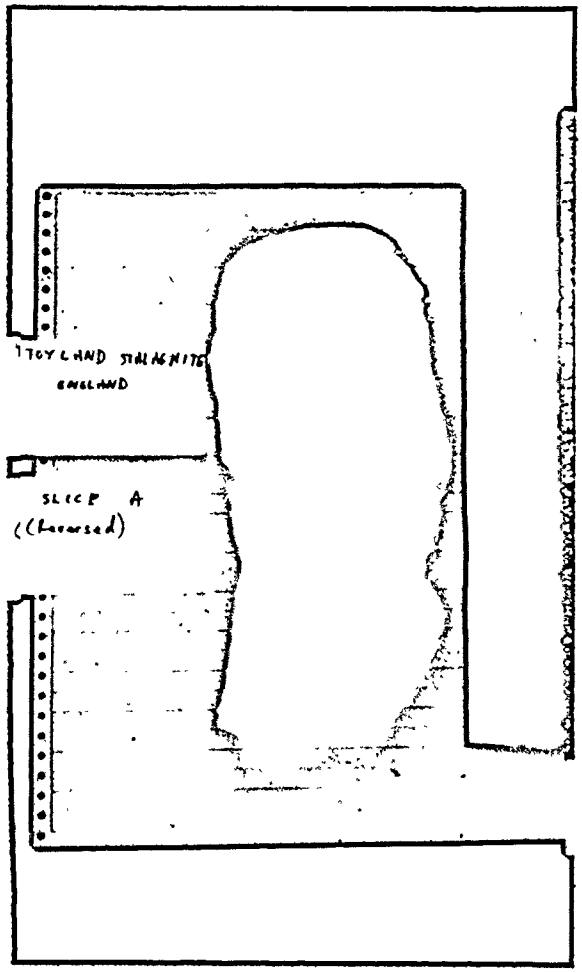

The VCCL results, though covering just a few thousand years lend some support to their suggestion of westerly declination bias for the N.W.Pacific.

4.7 TS

Plate 4.4. Thin section; appendix III.
Rock magnetism; section 7.3.5.
Site; West Kingsdale System, Yorkshire, England, 54° 11.4′ N, 2° 27′ W.

4.7.1 Description

The West Kingsdale System is described in Brook and Crabtree (1969). Toyland is a small cavern in the system and is a junction of three passages, one of which is mostly blocked by flowstone. The cavern is floored by block-fall, gravel, sand and mud. Stalagmite TS was partially hidden by and cemented to angular limestone blocks. Its upper surface was wet when sampled and this is taken to indicate some modern deposition. It is 37 cms high with a uniform diameter of 13 to 14 cms.

Before TS was cast it was split into three pieces using a bolster chisel and lump hammer. The sample revealed a compact and macrocrystalline fabric such that the breaks followed prominent cleavage planes across the interior. Three slices were made after the sample had been cast. Growth appears to have been continuous from the base to within about 1 - 2 cms from the top. Here there are concave layers and an irregular crystal fabric which may indicate that part of the sample has been redissolved. Subsequently the modern cap was formed. Near the base are dark layers containing quartz grains showing that detritus has been

washed onto the sample; the same information is revealed by the thin section.

The three parts of each slice were glued back together again in order to make the cuts and specimens. It was shown with this and other samples that the epoxy glue that was used, has an appreciable remanence (appendix II). The glue therefore had to be scraped off again and as a result the extensively shattered specimens from cuts 10 and 14 could not be measured for their NRM. It is probable that the anomalous direction of B11Q is attributable to the effects of this glue (table 4.6).

The slices revealed that the central cap area was quite wide throughout the stalagmite length. Therefore rod-shaped specimens were made up to 6 cms long - the width of the cap. Long specimens are normally avoided in paleomagnetic measurements since they may exhibit self-demagnetization effects such that the overall magnetization prefers to lie in the long dimension. These specimens are, however, too weakly magnetized to show this kind of specimen shape-anisotropy.

The weakest specimens of the stalagmite occupied cuts 3 to 13 and had to be stacked for NRM measurement. For cut 3 there were 6 specimens and these were stacked in twos to give 6 vectors. Specimens for cuts 4, 7, 9, 11, 12, and 13 were stacked in twos and then all three together for a total of four vectors. Cuts 5, 6 and 8 had two specimens each, because of shatter, and gave only one vector. Elsewhere NRM measurement was as usual.

Table 4.6

NRMs, Analysis of Directions and VGPs of Sample TS.

Notes; # Two specimens stacked to give one vector.

@ Three specimens stacked in twos, and then all three togetner to give four vectors.

* Specimens B11Q possessed an anomalous cleaned direction of 353° and -32°, after vector subtraction, and has tnerefore been excluded from the mean. The reason may be due to remanence-bearing epoxy glue used in the original cast.

Specimens from cuts 10 and 14 were shattered during preparation.

Table 4 - 6 ; NRMs, Analysis of Directions and VGPs of Sample TS

Cut No.	Distance from top (cms)	NRM					Alternating Field Demagnetised							VGP	
		N	D	I	α_{95}	K	H (Oe)	D	I	α_{95}	K	δI	δD	lat.	long.
1	0.5	3	3.5	64.0	7.3	121	100	354.0	67.2	3.5	529	3.5	9.0	84.4	220.7
2	1.9	3	11.3	58.0	32	6.5	100	21.0	44.3	20.2	16	20.2	28.2	57.8	140.1
3	3.7	6	355.2	49.7	5.3	120	50	10.8	49.0	8.3	47	8.3	12.6	64.5	155.5
4 @	5.65	4	12.3	44.1	11	37	50	11.1	51.5	7.4	90	7.4	11.9	66.6	153.4
5 @	7.55	1	14.8	47.5	-	-	50	11.2	55.5	-	-	-	-	70.3	149.9
6 @	9.55	1	14.8	53.4	-	-	50	12.1	61.8	-	-	-	-	76.3	137.1
7 @	11.4	4	355.6	63.0	1.6	2010	50	354.5	66.9	1.7	1670	1.7	4.3	84.2	216.0
8 @	13.45	1	11.5	63.4	-	-	50	6.4	70.6	-	-	-	-	86.2	75.5
9 @	15.2	4	357.7	70.5	1.5	2156	50	359.7	71.2	1.7	1737	1.7	5.3	88.4	-8.4
10	17.2	Missing													
11 @	19.15	4	356.5	40.6	16.6	18	50	3.7	66.9	3.4	850	3.4	8.7	84.9	149.9
12 @	21.15	4	3.1	56.2	2.5	779	50	5.1	56.5	2.9	583	2.9	5.3	72.5	164.0
13 @	23.0	4	10.1	46.0	8.9	62	50	8.8	47.0	8.1	76	8.1	11.9	63.3	160.2
14	24.85	Missing													
15	26.85	3	6.0	55.7	4.9	271	100	0.7	58.3	3.2	626	3.2	6.1	74.7	175.5
16	28.7	3	5.2	55.3	9.0	80	100	1.1	59.0	7.9	104	7.9	15.3	75.5	174.1
17	30.5	3	3.3	61.5	6.4	158	100	355.4	63.3	3.6	496	3.6	8.0	80.2	196.9
18	32.4	4	10.0	65.7	3.6	380	100	9.3	67.7	2.7	661	2.7	7.1	83.3	115.9
19	34.2	3	20.8	67.2	2.4	1090	100	21.0	69.4	2.7	925	2.7	7.7	77.5	84.2
20	35.85	3	35.2	64.3	5.0	263	100	34.7	65.0	6.7	148	6.7	15.9	67.1	91.6
		Lateral Specimens													
8 Left	13.45	4	0.0	62.9	2.7	678	50	0.7	63.7	1.5	2227	1.5	3.4		
9 Left	15.2	4	335.7	39.4	22.5	9.7	50	3.5	55.6	5.4	168	5.4	9.6		
9 Right	15.2	4	12.0	59.6	1.5	2053	50	1.3	61.9	2.6	709	2.6	5.5		
18 Right	32.4	3	0.9	58.3	3.3	618	80	358.6	57.4	2.2	1317	2.2	4.1		

Table 4 - 7 ; The AF demagnetization of B1Q and B18Q, Sample TS.

	Peak Field (Oe)	D	I	M (x 10^{-7} G)	M/M_o
	NRM	2.26	67.63	45.3	1.00
	30	358.24	67.20	43.4	0.96
	50	353.65	66.53	40.5	0.89
	100	351.06	65.81	35.08	0.77
	185	351.31	66.59	27.24	0.60
	200	354.02	65.96	25.18	0.56
B1Q	250	349.53	66.66	21.78	0.48
	300	357.04	66.62	19.61	0.43
	350	348.62	63.20	16.80	0.37
	400	341.51	61.55	17.06	0.38
	500	347.02	57.80	15.95	0.35
	NRM	6.42	59.93	123.31	1.00
	30	6.45	61.14	119.89	0.97
	50	7.08	62.71	115.53	0.94
	75	9.98	62.99	111.12	0.90
	100	8.78	64.06	105.08	0.85
	185	12.31	63.57	87.10	0.71
	200	8.27	63.88	85.75	0.70
B18Q	250	9.36	64.48	77.01	0.63
	300	10.59	60.50	71.23	0.58
	350	8.84	63.48	64.82	0.53
	400	9.68	62.94	61.76	0.50
	500	11.71	66.14	53.58	0.44

The present field is in a direction D = 352°, I = 67°.

4.7.2 The Paleomagnetism of TS

The analysis of the NRM directions is given in table 4.6 together with the VGPs. The AF cleaned inclinations and declinations are plotted against length in figure 4.6 .

As noted above the specific magnetizations are low except for cuts 19 to 17 which contain the detrital layers. Detritus in several of the stalagmites of this study has generally resulted in higher magnetizations.

Two pilot specimens showed fairly high stability to AF demagnetization, having MDFs of 235 and 400 Oe. Table 4.7 shows the movement of their directions upon cleaning . The lowest field for general cleaning, as indicated by these pilots was about 100 Oe, but the weaker specimens could only be cleaned to 50 Oe. The precision of the directions , as indicated by Fisher's precision factor K, or the α_{95}s, generally show an improvement upon cleaning. The low precision of cut 2 may be partly a reflection of the calcite dissolution at this horizon, but its mean appears to be approximately sequential with earlier directions as shown by either the plot of the direction versus length, or by the VGP path (figures 4.6 & 4.7).

The inclinations are about 10^{o} shallower than the inclination of the AGD field ($I = 70.2^{o}$). Knowing that detritus was deposited near the base of the stalagmite it was thought possible that depositional effects were the cause of the shallow inclinations. These effects may include slope or roughness of the surface, water flow or crystal growth habit. Thus it was supposed that the vertical sides may have influenced the magnetized grains in a direction different than had the horizontal cap , since

Figure 4 - 6 ; The Paleomagnetism and Dating of Sample TS.

(The direction errors of the lateral specimens have been omitted for clarity.)

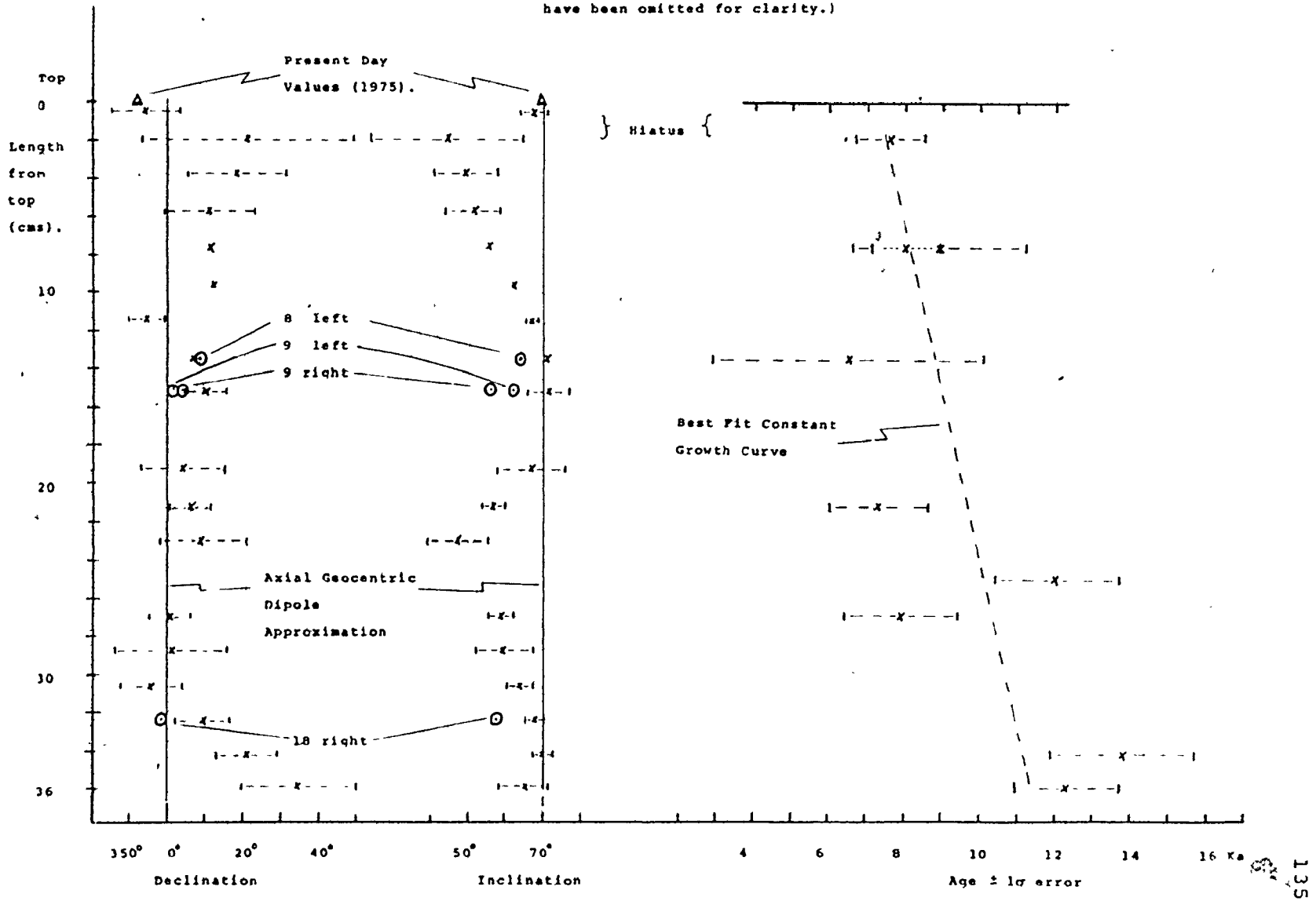

it was hard to see that such extremes of topography could have produced the same directional error. So to test for this the NRM of some lateral specimens were also measured. They were taken from cuts 8 left-, 9 left-, 9 right- and 18 right-facing sides. They contain, more or less, horizons spanning cuts 1 to 7, 8, 8 and 17 respectively. The directions (table 4.6 and figure 4.6) are well in accord with the values from the central cap area. Depositional effects were therefore dismissed as a possible cause of the low inclinations.

Another possible cause of these shallow inclinations is the presence of local magnetic anomalies. A broad positive magnetic anomaly of about 300 γs maximum lies just to the south-east of the cave, near Ingleton. It is thought to be associated with Ordovician- Silurian basement rocks which underlie the Carboniferous limestone (Bott, 1967). However the anomaly is an induced magnetization in the direction of the ambient field . Even as an anomaly of magnetic remanence it would still not be great enough to have influenced the magnetization direction of TS (M.H.P.Bott, pers, com).

The fact that the top cap is modern provides a test of whether the primary magnetization is syngenetic with the host growth horizon. The modern field direction is $D = 8^{o}$ W, $I = 69^{o}$, while the 1 cm thick cut 1 has a mean direction of $D = 6^{o}$ W, $I = 67^{o}$, with an α_{95} of 3.5^{o}, (figures 4.6 & 4.7). This mean direction is probably an average of 50 years or more.

The direction of cut 1 is distinctly offset from the serially-correlated directions ending at cut 2. This

Table 4 - 8 ; Isotope Activity Ratios and Dates for Sample TS

Specimen	Distance from top (cm)	U conc. (ppm)	Yield (%) U	Yield (%) Th	$^{230}Th/^{234}U$	$^{234}U/^{238}U$	$^{230}Th/^{232}Th$	Ages ± 1σ, (Ka) uncorrected	Ages ± 1σ, (Ka) corrected
B2Q,new	2.9	0.16	37	37	0.082 ± 0.005	1.61 ± 0.05	8 ± 2	9.3 ± 0.5	7.6 ± 0.9
C5Q,new	7.6	0.17	34	45	0.083 ± 0.005	1.70 ± 0.05	10 ± 3	9.3 ± 0.6	8.0 ± 0.9
B5Q,old	7.6	0.15	30	36	0.092 ± 0.010	1.70 ± 0.08	10 ± 7	10.4 ± 1.2	8.9 ± 2.3
B8Q,old	13.5	0.13	40	31	0.097 ± 0.015	1.70 ± 0.08	3.5 ± 1.5	11.0 ± 1.8	6.5 ± 3.6
C12Q,new	21.2	0.14	34	38	0.089 ± 0.006	1.67 ± 0.06	5 ± 1	10.1 ± 0.7	7.3 ± 1.3
B14Q,old*	24.9	0.12	86	43	0.14 ± 0.02	1.70 ± 0.08	> 1000	16.3 ± 2.35	16.3 ± 2.35
D14Q,old	24.9	0.16	63	29	0.106 ± 0.014	1.77 ± 0.06	> 1000	12.0 ± 1.65	12.0 ± 1.65
B15Q,new	26.8	0.13	30	34	0.092 ± 0.007	1.72 ± 0.06	6 ± 1	10.5 ± 0.9	7.9 ± 1.5
D19R,new	34.2	0.19	29	26	0.171 ± 0.009	1.49 ± 0.05	4.5 ± 0.5	20.1 ± 1.2	13.8 ± 1.9
D20Q,old	35.9	0.18	58	24	0.108 ± 0.011	1.61 ± 0.06	41 ± 133	12.3 ± 1.4	12.3 ± 1.4
D20R,old*	35.9	0.16	44	11	0.095 ± 0.02	1.61 ± 0.06	15 ± 34	10.7 ± 2.25	9.7 ± 4.75

Notes. * A detector with poor resolution was used. The dates have been omitted from figure 4 - 6 and were not used in the growth rate determinations.

" Old " refers to analyses made prior to Sept. 1979 , mostly using detectors with a high background contamination. " New " refers to analyses made in 1980 with a high resolution detector and low background.

is the only such discontinuity and is consistent with the macroscopic appearance of these layers (section 4.7.1).

The stable directions of TS are thus inferred to be primary and to have accurately recorded the ancient geomagnetic field. The lack of depositional errors in the presence of the detrital magnetic grains, and the origins of speleothem remanence, are discussed in detail at the end of chapter 7.

4.7.3 The U-Th Dating of TS

The uranium and thorium ratios and the dates for TS are presented in table 4.8 . Six analyses, labelled "old", were produced for an earlier publication (Latham et al, 1979), and two of these, B14Q and D20R, were obtained by means of a low resolution counter. In figure 4.6 the old dates, with the omission of B14Q and D20R, have been replotted using a detrital thorium correction , where $(^{230}Th/^{232}Th)_0 = 1.5$. Also plotted are five new determinations from a high resolution, low background detector.

The following points may be noted:

1) The dates of B5Q and C5Q ("old" and "new" dates respectively) are in good agreement; their means are within the 1 σ error of each other. Their $^{230}Th/^{232}Th$ ratios are also the same.
2) The date from D14Q would seem to be too old by comparison with the overall growth trend. This older date is probably due to incorrect allowance for background thorium.
3) The growth rate from about cut 15 to cut 2 seems to have been quite high. The dates from D19R and

D20Q appear to indicate an early start ≈13 Ka, and therefore a slower growth for the first basal layers.

4) The corrected date for D19R, of 13.8 Ka, entailed a considerable shift from the uncorrected age of 20.1 Ka. The cuts 19 to 17 included the detrital layering, and this has probably resulted in a significant amount of initial ^{230}Th. The corrected date in comparison with the overall growth trend then suggests that the correction factor of 1.5 is about right, or a bit too low for this speleothem (see sections 6.5.3 and 9.4.2.2).

If D14Q is included in a growth rate analysis then the data only warrants an overall linear fit. The 9 data points then give the following least squares fit to a constant growth rate:

a) The top of the stalagmite corresponds to an age of 7.25 ± 0.74 Ka. (However this is not its true age, since the top 1 cm is almost certainly modern, from the earlier considerations of section 4.7.1)

b) The growth rate is 0.114 ± 0.04 Ka per cm, or 8.8 ± 3.1 cm per Ka.

c) Cut 2 is at 7.47 Ka; cut 20, the base, corresponds to a date of 11.3 Ka.

4.7.4 Geophysical Interpretations of the TS Record

As a reflection of the changes of the ancient field, the record from TS shows:

1) Both declination and inclination exhibit rapid and large changes from the base to cut 4 (6 cms).

2) Near the base the declination swings east to west

Figure 4 - 7; Virtual Geomagnetic Pole Positions for TS.

The numbers denote the cut and arrows denote direction of VG polar movement with time.

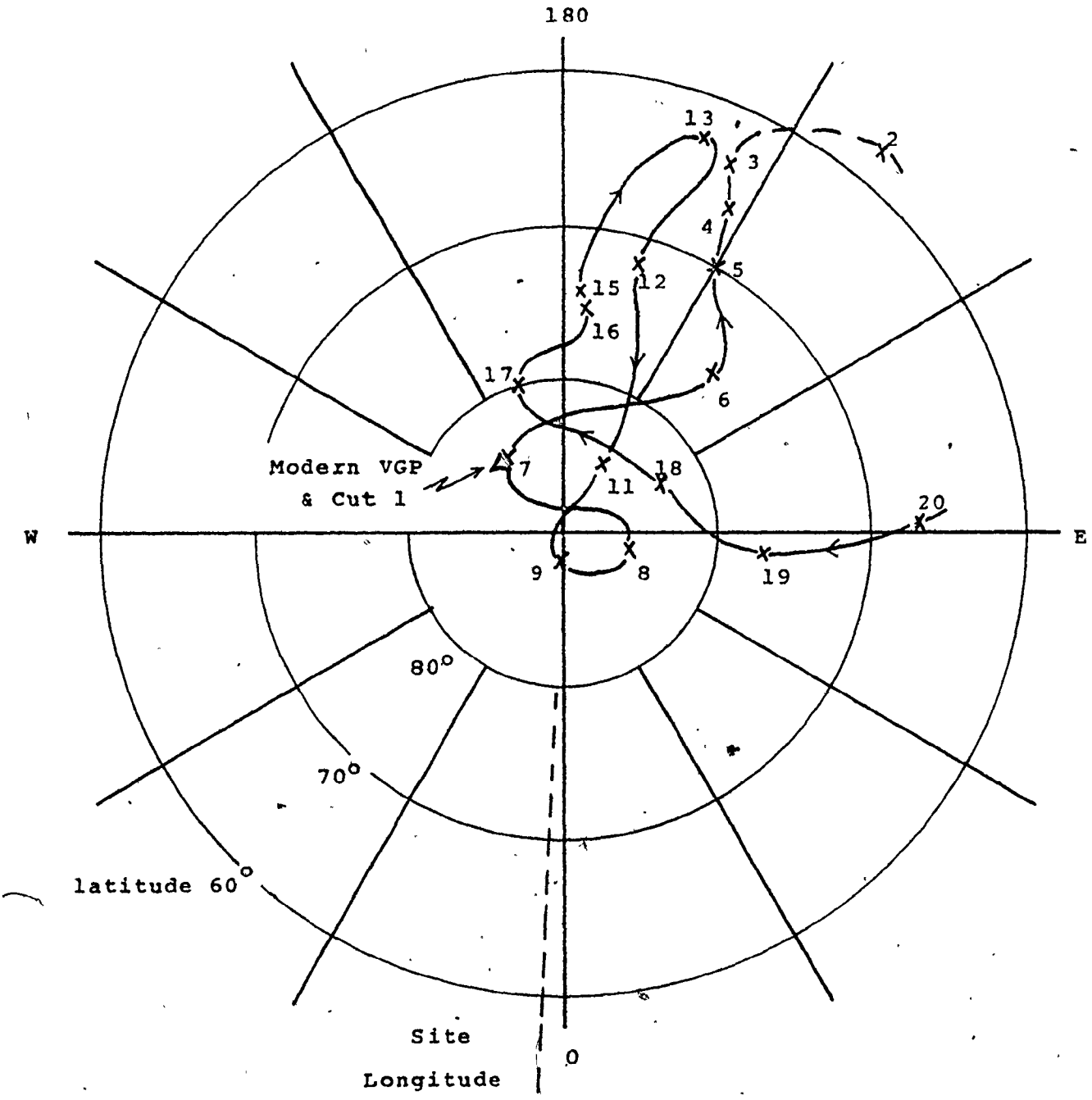

by 40^{o}. Here and elsewhere it shows a mainly easterly bias.

3) The average inclination is shallower than I_{agd} by $8 - 10^{o}$.

4) The corresponding VGP path is mostly far-sided and right-handed for this short period of about 4 Ka. The motion is mainly clockwise but a distinct cyclic pattern is not readily discernable.

Further interpretation of the TS record is made in the next section and in section 9.8.3 .

4.7.5 Comparison of the Lake Windermere, Lac de Joux and TS Records

Figure 4.8 is a reproduction of figures 8a and b from Creer et al (1980, op cit) of the Lake Windermere and Lac de Joux records together with the TS record.

Lac de Joux is at 46^{o} 37 N, 6^{o} 16 E, with I_{agd} of 64.7^{o}. The lake Windermere and TS sites are at $\approx 54^{o}$ N and 2^{o} W, with an I_{agd} of 70.2^{o}. Lac de Joux is about 1600 Km to the SE of the Windermere and TS sites.

A comparison of the TS and the lake records shows the following:

1) The lake records are more complete and cover a longer time span.

2) The Lac de Joux record shows up better early cusp-shaped changes in inclination.

3) Features of declination L to H correlate exactly with the TS declination features.

4) The Windermere record at the base is younger than the Lac de Joux record by $\approx$500 a. The TS record, in

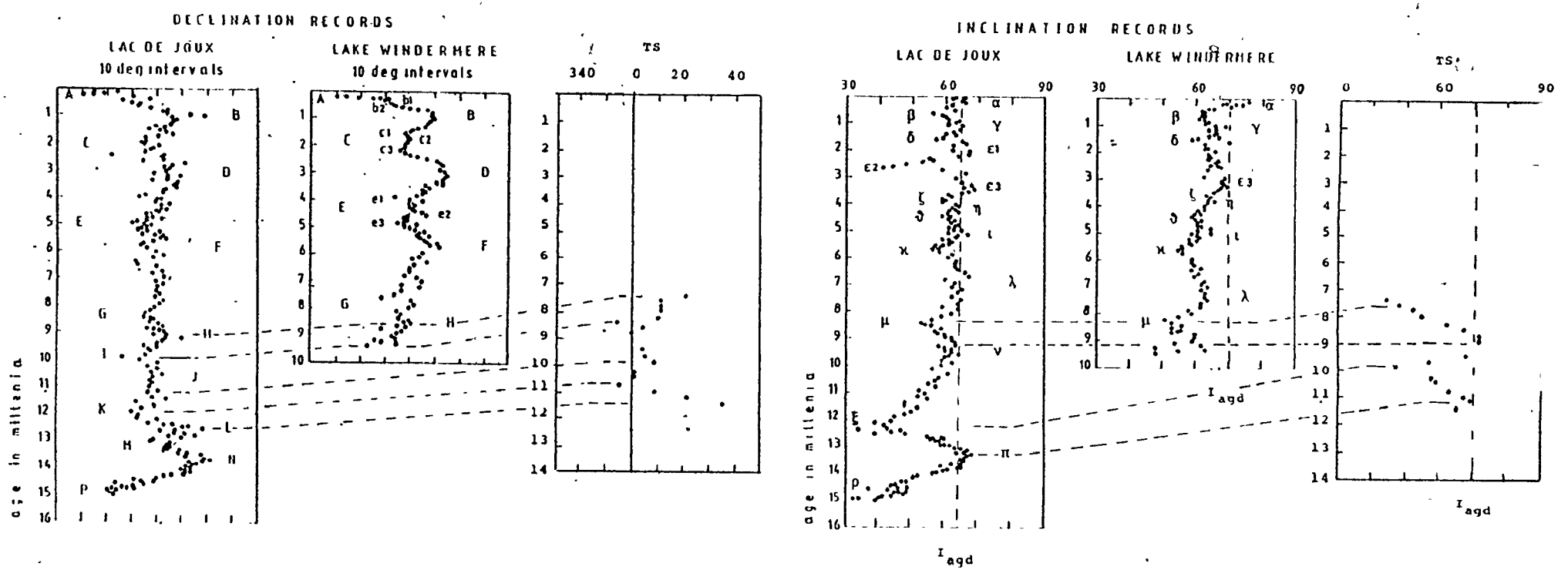

Figure 4.8: Correlation of Directions from Lac de Joux, Lake Windermere (Creer, et al, 1980) and Stalagmite TS.

Notes: 1) Lake sediment dates assigned by ^{14}C and pollen analysis.

2) I_{agd}s of the lake records added by this author.

3) The lettering of features in the lake records differs from that of Thompson and Turner (1979).

declination is younger by about 1.5 Ka (feature H).

5) The inclination features of TS do not correlate quite so well as did the declination features. In particular feature μ of the top of the TS record is shallower , but ξ is not as shallow as in the Lac de Joux record.

If one chooses to correlate either the declination or inclination variations of two separate but nearby sites, it may be expected that:

a) There will be an average age difference between the two sets of D (or I) variations, (the causes; inexact dating, the presence of pdDRM and drift of the field).

b) Insufficient age allowance may have been made for 'stretching' (or ' compression') of one record or the other, (the causes; assuming a constant deposition rate, when in fact it was variable, and variable pdDRM).

If now both D and I are paired together then their average age differences and their feature-to-feature age differences should be the same. In other words the D phase lag in age of one record with respect to the other, should be the same, point-to-point, as the I phase lag. This is clearly not the case with the Lac de Joux and TS records. The two sets of phase lags are quite different overall and point-to-point. Obviously neither sample nor experimental errors in either the paleomagnetism or the dating are tenable as causal explanations. One is therefore forced to conclude that the two different phase lags resulted from actual changes of the drifting geomagnetic field between the two sites.

Further comparison between the TS and Lac de Joux records shows that:

6) The field decreased more slowly between features π to ξ, and ν to μ, and

7) increased faster between ξ to ν.

The comparison of the fields between the two records may be summarised as:

a) The declination features remained about constant in amplitude and rate of change,

but b) the inclinations suffered both a change in the shape of their features and in their drift rate.

The cusp-shaped inclination changes are what one would observe as a result of a radial dipole source passing a given site. (for further discussion on radial dipoles, see section 9.8.3). However it is clear that during the period from about 13 to 9 Ka, the geomagnetic source or combination of sources were asymmetrical and, apparently, decaying in western Europe.

CHAPTER 5

THE PALEOMAGNETISM OF SPELEOTHEMS FROM BERMUDA, THE USA AND GREECE

5.1 Introduction

The area between Harrington Sound and Castle Harbour, Bermuda, contains caves mostly in the older Walsingham eolianite limestone (Bretz,1960). Parts of these caves may have formed during glacial periods when sea level was much lower. This is certainly true for their presently submerged speleothems. In order to unravel the Pleistocene sea-level changes and their timing Harmon and co-workers have attempted to date several such speleothems (Harmon, 1975; Harmon et al, 1978).

Being partway across the Atlantic also makes Bermuda a desirable site for possible SV studies from its speleothems. The speleothems may, for example, record features in common with European , N. American or Mexican records, or the extent of westward-drifting features of the field. Two visits were made to Bermuda in 1977 to collect oriented speleothems. Three samples have been analyzed in some detail but unfortunately none of them has yielded dated magnetization variations. The flowstone OULF from the Ozarks, USA, is included here because of its similar appearance to the Bermudan samples, similar association with terra rosa-like soil and similar magnetic properties.

Three samples from the Petralona cave, in Greece,

Plate 5.1

Flowstone RCB.

In this photograph, the flowstone has been tilted back towards the horizontal. The deep red layers are at the base. Also noticeable are reversed climbing ripples and microgour remnants.

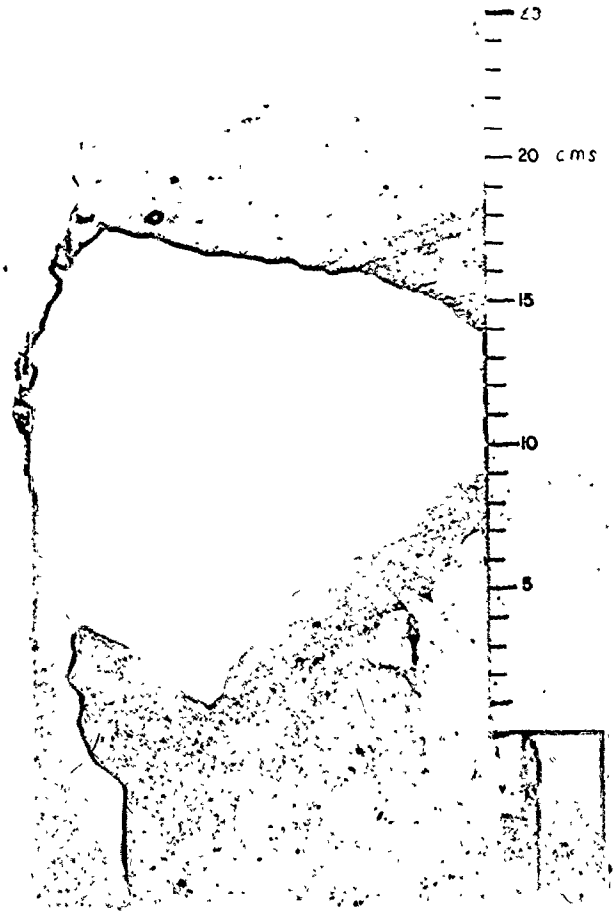

have been tested. They too have red-brown layering within them and have a stably reversed magnetization. Petralona is a site of considerable archeological importance and the age constraints suggested by these reversely magnetized travertines have much significance to the history of the evolution of man.

5.2 RCB

Plate 5.1. Thin section; appendix III.

Rock magnetism 7.3.6

Site; railway cutting, Hamilton parish (west) 32° 21′ N, 64° 43′ W.

5.2.1 Description

A railway cutting has intersected a small cave most of which is now destroyed. A widened crack containing soil and vegetation connects the old surface, 3 m above, to a steeply dipping and curved flowstone. The flowstone is more than 40 cms thick and is cracked into several pieces. Lying immediately above the flowstone is some red soil - one of the red paloesols of the island - incorporating pieces of detached limestone. It is not difficult to imagine some of the soil being washed or leached onto the flowstone surface as water came down the crack. The same process is in operation, at present, in Muddy cave and Admirals cave on Blue Hole Hill.

A large piece of this flowstone of 16 cms stratigraphic thickness was cast in plaster of Paris. Specimen preparation was not straightforward because of the layer curvature and the lensing out of some layers. The layers were coloured opaque red-brown, translucent light brown,

Table 5-1.

The AF Cleaning of Specimen RCB D7R

Field (Oe.)	Comments	Declination	Inclination	M $\times 10^{-5}$ G	M/M_o
NRM		358.2	54.5	93.3	
NRM	remeasured after a few days.	350.3	62.5	83.3	1
50	unprotected in lab. fields	345.1	57.4	73.3	0.88
100	" "	341.3	57.8	36.8	0.44
150	" "	317.9	62.7	18.5	0.22
200	" "	223.4	71.5	11.2	0.13
250	protected from lab. fields	352.5	47.2	5.2	0.06
250	unprotected from lab. fields	58.4	51.7	16.4	0.20

The M/M_o versus AF field graph is presented in section 7-3-6.

Table 5-2

RCB ; Analysis of directions for cuts 2 and 3 of slice C

Cut No.	Distance from top (Cms.)	N	NRM			AF Cleaned				
			D	I	α_{95}	H (Oe)	D	I	α_{95}	K
C2	2	4	358.3	64.7	3.1	50	2.6	47.3	1.4	2644
C3	4	4	347.3	65.9	1.6	50	357.7	49.6	2.1	1121

Flowstone surface dip 50° - 60° in a direction of 140°

Present Field , changing slowly. 345 62

AGD Field 0 51.6

and opaque or translucent white with gradations between. The sample consisted of small cemented crystals and was compact except for many remnant microgours. The pronounced banding in many layers may be associated with events of some kind such as the renewal of soil inwash through flooding.

The flowstone dipped from 50° to 65°. in a direction of 140°.

Several slices were prepared perpendicularly to the growth layers. The preparation of the cuts necessitated changes of angle both within and between slices. The matching of specimens of the same growth horizons proved difficult in some cases.

5.2.2 The Paleomagnetism and U-Th Dating

The NRMs and AF cleaned magnetizations of specimens lay in the general direction of the AGD field. It was soon obvious, however, that viscous components were present especially in the upper layers. Care was needed during AF cleaning and in remeasuring the cleaned magnetizations, since:

1) It proved easy to introduce spurious ARMs if the AF was ramped down too fast,
2) Specimens soon acquired VRMs in the laboratory field.

The effect of soft components is seen in the movement of the direction of specimen D7R (table 5.1), upon AF demagnetization. This is discussed further in section 7.3.6. Despite these problems, cleaned directions could generally be obtained with reasonable precision (table 5.2). The project was abandoned when the U/Th ratios produced ages

Table 5-3

Specimen Dating and Isotope Activity Ratios

Sample & Specimen	U conc (ppm)	Yields (%) U	Yields (%) Th	$\frac{230\text{Th}}{234\text{U}}$	$\frac{234\text{U}}{238\text{U}}$	$\frac{230\text{Th}}{232\text{Th}}$	Calc. Age (Ka)	Distance from top (cms)
RCB C3	0.14	24	29	1.0 ± 0.2	1.05 ± 0.23	6.3 ± 4.3	>350	6
RCB C4	0.11	22	48	1.1 ± 0.3	0.8 ± 0.2	3.4 ± 0.9	>350	8
RCB C5	0.15	27	45	0.8 ± 0.2	0.7 ± 0.2	2.8 ± 0.9	241^{+276}_{-131}	9
GQF1 top	0.9	17	3	0.2 ± 0.1	1.13 ± 0.09	2.3 ± 2.5	23^{+14}_{-12}	1
OULF base	0.58	55	37	0.93±0.04	2.60 ± 0.07	26.4±2.2	184^{+16}_{-14}	21

in excess of 350 Ka (table 5.3).

5.2.3 Discussion

It is shown in the rock magnetism chapter, section 7.3.6, that magnetite and a superparamagnetic mineral are present in the red soil and in RCB. The proximity of the loose red soil, the superparamagnetic component, the flood-like events of the rich red-brown layers, the unidentified organic material seen in thin section and the clumping of uranium nuclei (see below), all combine to show that detrital material has been incorporated into the fabric of RCB; iron in some form(s) is undoubtedly one of these materials. Yet the stable remanence due to the magnetite lies fairly close to the AGD field; there appears to be no effect on the cleaned directions from the dip of the layers. It is argued in chapter 7 that reprecipitation of magnetite from detrital sources may be a common process whereby speleothems acquire their NRMs. RCB may be a good example of this.

A specimen from the distinctly banded layers of cuts 7 and 8 was given to Marilyn Truscott, at McMaster university, for fission-track analysis of the uranium. She recognised three distinct U concentration bands, giving 2.3, 3 and 4.3 ppm. It is interesting that she also recognised oblique en echelon banding, because the sample does show climbing ripples. (Ripples in flowstones tend to climb against the flow, unlike sediments in which they climb with the flow). She also adds, "Some of the U appears to occur in detrital grains, as there are some U starbursts which do not seem due to (laboratory) contamination". She also analysed a filter paper containing red residue

Plate 5.2

Flowstone GQF1.

This is a good example of lensing-out and changes of direction of the layering. The lighter coloured part, at the base, is a piece of eolianite wall rock. The scale to the right is in inches.

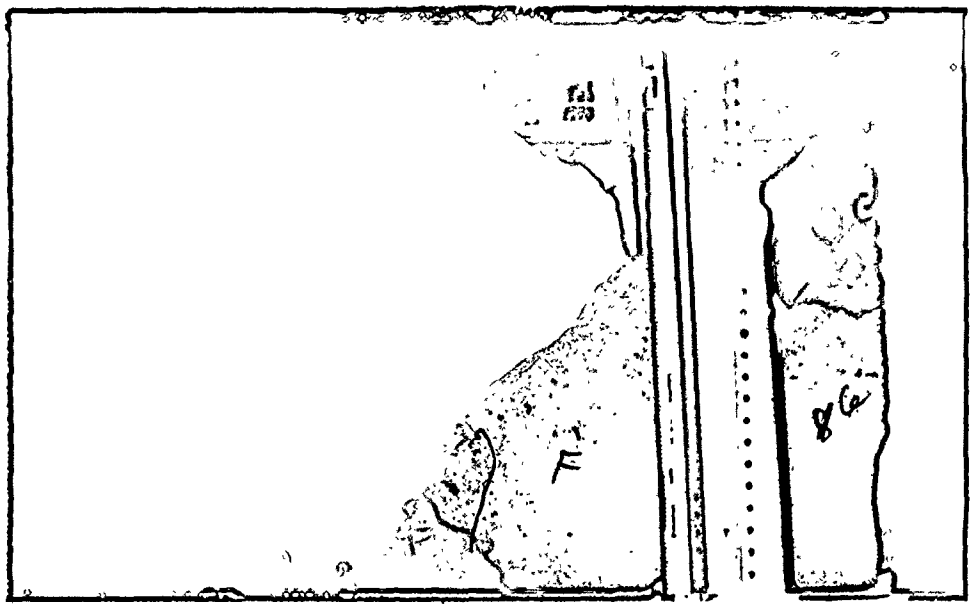

from the dissolution of one of the specimens used for dating. The lexan was backed against the filter paper for irradiation and starbursts were observed associated with the red residue. It is known that U is readily co-precipitated by Fe_2O_3 and ferric oxyhydroxides (Langmuir, 1978). Advantage is taken of this fact in the dating experiments when U and Th are scavenged on an $Fe(OH)_3$ precipitate (appendix I). M. Truscott's final observation therefore may mean that the red residue has leached uranium , either during acid dissolution or during diagenesis and transport. This may be linked to the fact that the fission-track determination of the total U concentration was over an order of magnitude greater than the alpha-particle determination from the dissolved calcite.

5.3 GQF1; Description, Paleomagnetism and U-Th Dating

Plate 5.2

Rock magnetism 7.3.8

Site; Government Quarry cave, Hamilton parish

32° 20´ N, 64° 42´ W

Government Quarry cave is in the Walsingham formation, and consists of a large chamber with adjoining smaller ones. Like most of Bermuda's caves the lower reaches are water-filled, and connected to the sea. It is heavily adorned with flowstone deposits. The upper floor of the cave is covered with a thick compact straw-coloured, or amber-pink flowstone that may be several metres thick in some areas. It is cracked and parts have fallen away, probably due to the quarrying which is still in operation. A 26 cm thick piece of this flowstone was

oriented and sampled. It dipped 2^{o} in a direction 285^{o} and this is thought to be its original orientation. Three slices of it were cut with a 30-inch rock saw, made available by Mr. Alan Rudkin at the Royal Ontario Museum, Toronto.

The top 2 cm cut showed a measurable magnetization of about 0.3×10^{-7} G cm^{-3}, using stacked specimens. The NRM was normal with D = 50^{o} W and I = 24^{o} ($I_{agd} = 51.6^{o}$). Lower cuts were much weaker and the signal was comparable to the noise level of the magnetometer, even for stacked specimens up to about 90 gms mass.

An attempt was made to date the top of the sample but the thorium yield was unacceptably low (table 5.3).

5.4 WCS1; Description and Paleomagnetism

Thin section; appendix III

Rock magnetism 7.3.7

Site; Wonderland cave, Hamilton parish, 32° 20′ N, 64° 42′ W

The stalagmite was 15.5 cms high and about 6.5 cms in diameter. Its appearance was a translucent amber colour with indistinct growth layering. The amber colouring may be due to organic substances originally dissolved in the drip water. It is possible, judging from thin section evidence, that the sample has been recrystallised. The sample was cut into two 2 cm thick slices from which 2 cm cubes were prepared. Thus there were four specimens per cut, but stacking of any set of four failed to produce a measurable NRM. Only rock magnetic work was continued on this speleothem.

Plate 5.3

Flowstone OULF

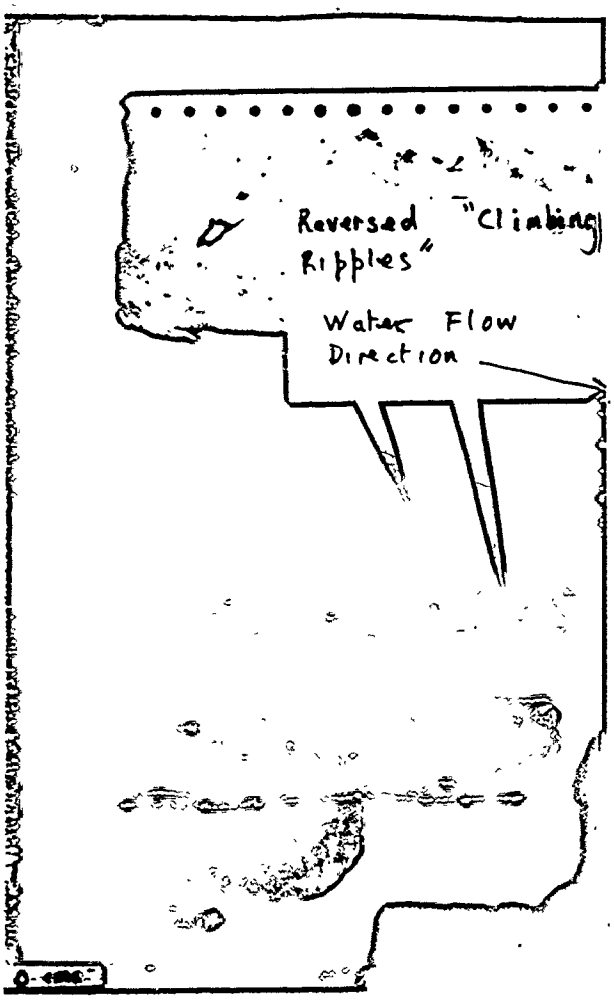

5.5 OULF; Description, Paleomagnetism and U-Th Dating

Plate 5.3

Rock magnetism 7.3.9

Site; Tumbling Creek cave, Taney Co., Missouri, USA. 36° 32′ N, 92° 48′ W

The area around Tumbling Creek cave (also called the Ozarks Underground Laboratory, proprietor T. Aley) has a red-brown clayey soil. A red clay, probably derived from this soil, is the principal fine sediment of the caves. Speleothems from this cave have been found to have ages ranging from 236 to 25 Ka BP (Harmon et al, 1977).

OULF is a 22 cm thick fragment of an extensive flowstone sheet which had been blasted for a walkway. It was underlain by red clays on a limestone floor. At the base of the sample (0 to 3 cms) are gently dipping parallel layers of white transparent and translucent calcite with occasional opaque red bands. Some small holes contain red clay and pieces of clay up to 2 cms in length which have somehow been transported onto the surface. Calcite has continued to grow round and over these clay blobs. At about 3½ cms there seems to be a hiatus marked by a 1 mm thick red clay layer. This is followed by 5½ cms of less compact, parallel layering which is rich in fluid inclusions. It seems to be be porous and some layers show 'coconut meat' texture (Folk and Assereto, 1976). There is a slight red tinge to these layers which distinguishes them from whiter layers above. Here the milky appearance, due to fluid inclusions, is even more pronounced. Each succeeding layer becomes less milky until, within 3 cms from the top, the calcite is compact, transparent and darker. It is by then a straw colour. Only a few microgours have developed.

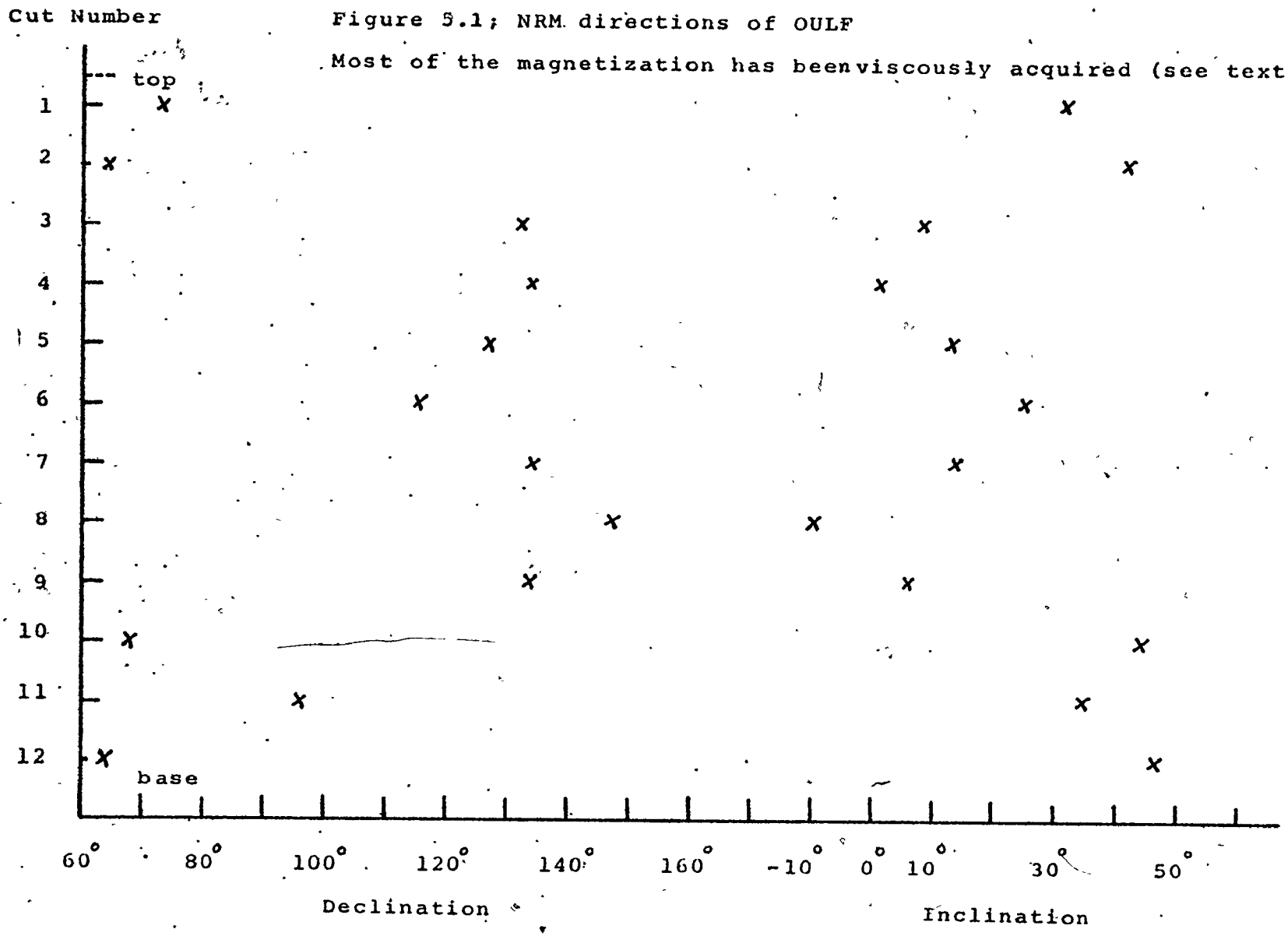

Figure 5.1; NRM directions of OULF

Most of the magnetization has beenviscously acquired (see text).

Table 5.4

The AF Demagnetization of OULF C12Q

Field (Oe)	D	I	M(total moment) $\times 10^{-7}$ G	M/M_o
NRM	69.3	36.8	22.1	1.0
20	47.1	9.6	15.3	0.7
50	19.2	15.4	9.6	0.4
75	41.2	23.3	4.2	0.2
100	337.2	46.9	1.5	0.06
150	256.4	47.0	2.8	0.12

Instead the flowstone shows sets of reversed climbing ripples in its upper 11 cms. The flowstone dipped at 17° in a direction of 253°.

Two slices were prepared and a signal was just measurable for doubly stacked specimens whose total mass was between 40 and 100 gms. The measurement of the NRMs was continued to completion (table 5.4) and the D and I values are plotted against position in figure 5.2 .

The AF demagnetization of C12Q shows that nearly all the remanence is soft and viscous (table 5.4, and section 7.3.9). Thus the anomalous directions of figure 5.1 are all due to VRMs picked up since removal from the cave. All specimens were prepared at the same time and , until measurement, all maintained the same relative orientation in a folder. The D and I values seem correlated, ie, the more easterly declinations correspond to shallower inclinations. The reason, apparently, is that each new D and I is the extent to which the magnetization has shifted from its old position acquired in the cave towards a new direction in the laboratory. The precision on 2 to 4 vectors is good enough in some cases to show that the variation in VRM is lower within cuts than between cuts as might be expected. In other words, the charecteristics of the grains are more or less the same along the layers but differ to some extent between the layers.

The base of the flowstone was dated at 184 Ka (table 5.3).

75- and 76GR; Paleomagnetism

Site; Petralona cave, N. Greece.

Petralona cave is on the Khalkidiki peninsular of northern Greece and it was the site of hominid remains. The skull that was found is of either Neanderthal or Homo Erectus type (Poulianos , 1973; Stringer, 1974). The McMaster speleothem collection contains pieces of travertines associated with the skull (sample 75GR-4). Also collected was sample 76 GR3-1 from a pit dug into the sediment of a hall adjoining the site from where the skull was found. The pit contained vertebrate bones and have been assigned to the Cromerian stage by Kurtén and Poulianos (1977).

The samples are compact with distinct reddish layering, and although none of them was oriented their appearance leaves little doubt as to their geopetal orientation. Sample 76GR3-1 has been dated at McMaster by the U/Th method but the U concentration was very low (Schwarcz, et al, 1980). The date was 211, +118, -58 Ka. Two pieces of the sample were tested in the cryogenic magnetometer and specimens of 40 to 60 gms showed a negative component of 10^{-5} G. The specimens were then AF demagnetized to 100 Oe and still gave negative inclinations with little decrease in the vertical component. A hysteresis experiment, performed too late to include details in chapter 7, showed it to have the highest stability of all specimens examined so far in this study. The remanence carrier is probably hematite.

Sample 75GR4 is thought to be coeval with the calcite that had encrusted the skull itself. From the

U/Th ratios and other considerations Schwarcz and others (Anthropos, 7, 1980), suggested a "very crude age estimate" of 600 ± 250 Ka for this sample. The sample was subdivided into three pieces for NRM measurement. Inclinations were positive. Unfortunately the AF demagnetization characteristics suggest that most, if not all, of the remanence of each of the subsamples was acquired viscously.

CHAPTER 6

THE PALEOMAGNETISM OF SPELEOTHEMS FROM MEXICO

6.1 Introduction

Mexico lies between latitudes 15° and 33° north. Any Mexican speleothems carrying an NRM might therefore be expected to reveal the effect on these lower latitudes on the dispersion of directions, or VGPs, as predicted by several models of secular variation (eg, Irving, 1964, op cit). The Mexican region may also be favourable for sampling because it is generally asserted, though without direct proof, that speleothem growth is rapid in more tropical regions; the finest details of SV might be revealed in some cases.

This chapter deals with four stalagmites from Mexico, three of which have furnished excellent records of secular variation. One of them, sample SJHS, grew around the time of the proposed Blake event (Smith and Foster, 1969, op cit), but has provided no evidence for such anomalous behaviour.

6.2 SJLS

Plate 6.1. Thin section, appendix III.

Rock magnetism 7.3.11

Site; State of Chiapas, Mexico , 17.1° N, 92.88° W.

Plate 6.1

Stalagmite SJLS.

The hiatus at the top (section 6.2.1) is hardly visible here.

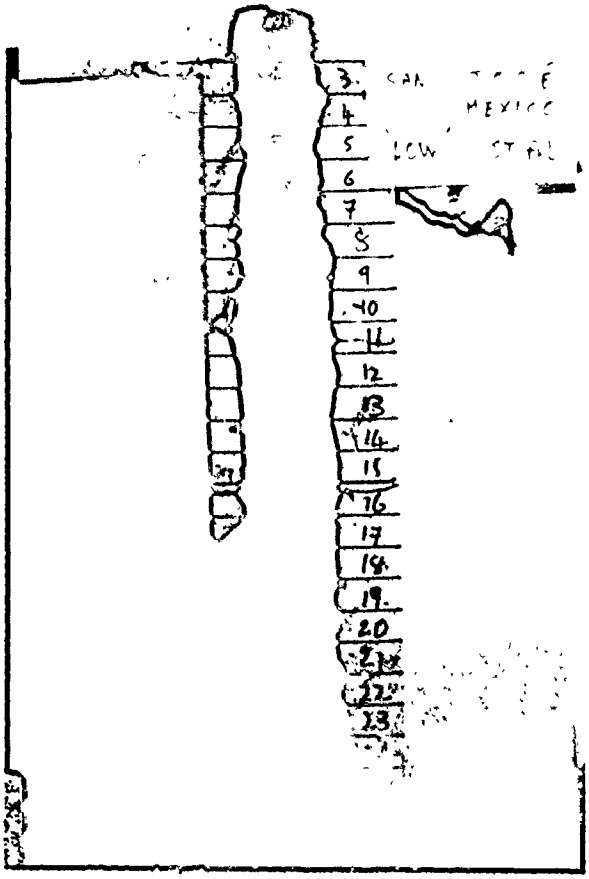

6.2.1 Description

SJLS was the first of two stalagmites taken from Sima de San José in Chiapas, Mexico. The cave is described in two expedition reports of the Canadian Caver (1976, 1977). At the bottom of the entrance pitch is a large passage, one part of which contains abundant quantities of mud and some stalagmites. SJLS was taken from an alcove off to one side of this passage. The speleothem is 46.5 cm long and is a uniform 6 cms in diameter up to about 33 cms from the base, after which it has a uniform diameter of 5 cms to its top.

The sample broke in five pieces during transport but this presented no problems either in the preparation of the specimens or in the measurement of their NRMs. The sample was cast in three sections according to the procedure outlined in section 2.4 . One vertical slice was obtained having a thickness of 2 cms. The calcite was an overall white or light brown colour in which the growth layers were marked by many bands. These bands showed fine dark particles and appeared to be due to flood events. Within about 0.5 cms of the top, the growth layers may have been modified by a short solutional hiatus. Dissolution of specimens for dating purposes resulted in an insoluble residue of quartz and black magnetic grains adding further evidence for the flood events. The thin section further showed that some of the opaque grains are titanomagnetites. It seems likely therefore that some, if not all, of the NRM is of detrital origin (for further discussion see chapter 7).

Table 6 - 1 ; NRMs , Analysis of Directions and VGPs of Sample SJLS.

Cut No.	Distance from top (Cms)	NRMs		AF Demagnetized		VGPs	
		D	I	D	I	Lat.	Long.
1	0.7	354.81	12.46	352.49	28.81	82.5°	164.74
2	2.2	347.47	32.00	353.47	22.29	81.61	136.88
3	4.1	357.79	30.48	0.80	27.37	87.30	70.44
4	6.0	0.07	27.82	359.94	27.92	87.74	88.59
5	7.9	0.39	22.26	9.09	23.43	79.95	24.91
6	9.9	354.54	18.78	4.82	22.89	83.01	44.47
7	11.9	4.96	26.17	3.83	26.10	85.02	38.70
8	13.8	1.02	23.36	4.15	20.61	82.40	54.61
9	15.6	346.63	28.34	357.65	23.05	84.40	111.51
10	17.5	352.13	33.67	353.71	31.89	83.99	-180.23
11	19.3	355.03	27.27	358.30	27.65	87.08	121.39
12	21.3	347.67	28.06	350.96	24.61	80.31	152.66
13	23.2	348.25	33.12	353.76	32.51	84.02	-176.44
14	25.1	353.61	36.68	353.17	35.15	83.12	-162.35
15	27.0	357.69	40.25	356.56	38.13	84.59	-129.20
16	28.9	348.56	40.76	357.78	37.37	85.66	-121.44
17	30.8	350.97	33.01	354.52	27.06	84.04	150.16
18	32.7	351.00	26.61	355.85	17.80	81.06	114.48
19	34.6	352.75	18.08	355.34	10.90	77.54	109.12
20	36.5	2.19	21.19	4.32	21.48	82.71	51.50
21	38.4	342.75	39.39	350.04	36.00	80.13	-164.46
22	40.3	352.05	33.89	2.58	28.94	87.03	30.35
23	42.3	324.75	60.56	325.94	22.73	56.65	172.69
24	44.1	327.01	45.31	353.38	27.79	83.22	157.89
25	45.7	358.16	43.89	348.09	43.51	76.02	-143.28

All specimens were AF demagnetized to 120 Oe. except pilot specimen B15Q which in this table was demagnetized to 100 Oe.

Figure 6 - 1; Paleomagnetic Directions and Dating of SJLS.

Note; The date from cut 25 (base) has been omitted in finding the best fit constant growth line.

Figure 6.1

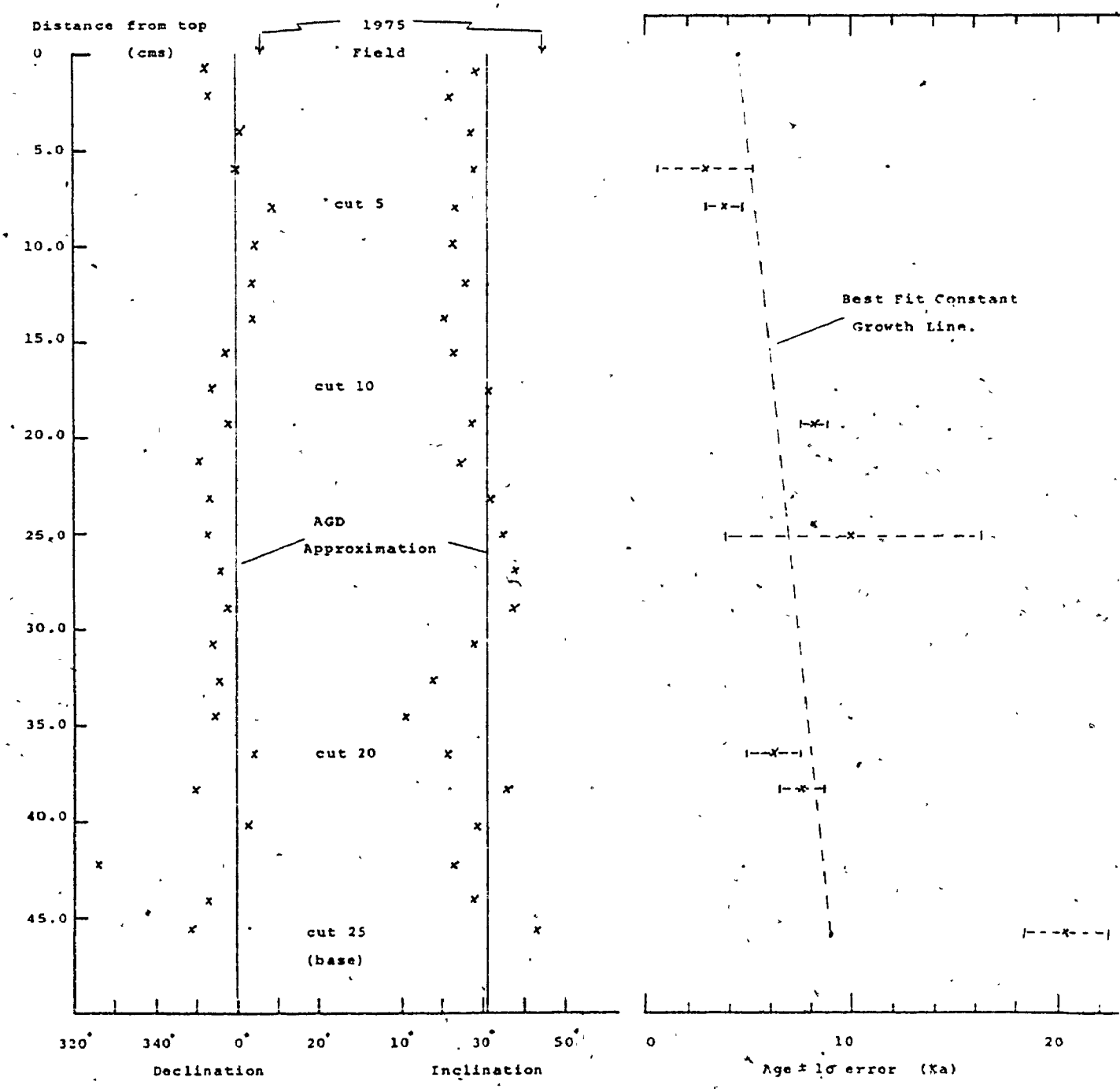
Distance from top
(cms)
1975
Field
0
5.0
10.0
15.0
20.0
25.0
30.0
35.0
40.0
45.0
cut 5
cut 10
cut 20
cut 25
(base)
AGD
Approximation
320°
340°
0°
20°
10°
30°
50°
Declination
Inclination
Best Fit Constant
Growth Line.
0
10
20
Age ± 1σ error (Ka)

Table 6 - 2; The AF demagnetization of B15Q, Sample SJLS.

Peak Field (Oe)	D	I	M (x 10^{-5} G)	M/M_o
NRM	358.34	38.53	6.82	1.00
21	358.73	38.92	6.57	0.96
50	358.47	38.93	5.97	0.88
100	356.55	38.13	4.66	0.68
150	356.92	39.05	3.25	0.48
200	357.09	40.42	2.47	0.36
250	353.19	39.55	1.96	0.29
300	358.51	37.07	1.49	0.22
350	1.09	37.48	1.38	0.20
400	356.67	37.05	1.06	0.16
500	355.04	34.20	0.81	0.12

The present day declination is 6° E, and the inclination is 45°.

The small diameter of the sample only allowed one specimen to be obtained from each cut. Due to the fracturing on transport, some specimens possessed only one oriented basal plane for NRM measurement. This does not seem to have affected the measurement of the directions significantly. The cuts concerned are 6, 7, 8, 9, 10 (in two pieces), 16 and 17.

6.2.2 The Paleomagnetism of SJLS

The NRMs, AF cleaned directions and VGPs of SJLS are given in table 6.1 . The cleaned directions are plotted against length in figure 6.1 . The pilot specimen was B15Q (section 7.3.11) and its behaviour upon AF demagnetization is given in table 6.2 . The direction changed very little in 300 Oe. Those changes which occurred in higher fields are most certainly due to small ARMs. Intensities of most specimens were up around 10^{-5} G, total moment. This permitted a higher general cleaning field than usual. The value chosen was 120 Oe.

The following points are noted from the data:

1) Taken along the length of the sample the cleaned directions are more smoothly varying than the NRMs (see section 9.3.3)
2) Movement of the directions upon cleaning was mostly away from the present field, which is at $D = 6^{o}$ E, and $I = 45^{o}$. Thus it is inferred that the VRMs were acquired largely in the present field in this region.
3) Specimens near the base at cuts 23 and 24 had directions some tens of degrees away from the AGD direction and adjacent directions. Upon AF cleaning

Table 6 - 3; Isotope Activity Ratios and Dates for SJLS

Cut No.	Distance from top (cms)	U (ppm)	Yields (%) U	Yields (%) Th	$^{230}Th/^{234}U$	$^{234}U/^{238}U$	$^{230}Th/^{232}Th$	Age ±1σ (Ka) Uncorrected	Age ±1σ (Ka) Corrected
4	6.0	0.37	29	33	0.043 ± 0.009	1.56 ± 0.06	4 ± 3	4.8 ± 1.0	2.9 ± 2.3
5	7.9	0.25	50	44	0.050 ± 0.004	1.50 ± 0.05	5 ± 1	5.5 ± 0.5	3.8 ± 0.9
11	19.3	0.54	41	45	0.084 ± 0.004	1.72 ± 0.05	11 ± 2	9.5 ± 0.5	8.2 ± 0.7
14	25.1	0.24	36	20	0.100 ± 0.023	1.43 ± 0.07	12 ± 31	11.4 ± 2.65	10.0 ± 6.3
20	36.5	0.17	41	50	0.073 ± 0.006	1.45 ± 0.06	6 ± 2	8.2 ± 0.7	6.2 ± 1.3
21	38.4	0.38	59	64	0.080 ± 0.005	1.67 ± 0.04	11 ± 5	9.0 ± 0.5	7.8 ± 1.1
25	45.7	0.72	41	25	0.184 ± 0.009	1.81 ± 0.04	21 ± 14	21.8 ± 1.2	20.4 ± 2.1

the direction of cut 24 moved more into pattern with other cuts, but the declination of cut 23 remained well to the west at 326°. The directions near the base are rapidly changing so it is not certain if the direction of cut 23 is a real record of the ancient field, or if it represents a VRM, ARM or a measurement error. Cut 23 has been omitted from the VGP diagram (figure 6.2)

6.2.3 The U-Th Dating of SJLS

The isotope activity ratios and dates of SJLS are presented in table 6.3, and the dates are plotted in figure 6.1 . The uranium concentrations are between 0.2 and 0.7 ppm. The detrital thorium correction is quite large in some cases and in age terms represents a shift of up to 40% in the case of cut 4. The data points of figure 6.1 do not allow anything other than the simple assumption of a constant growth rate. It is not known if the date for cut 25 is real or is due to, for example, thorium contamination from unclean glassware. This date has been omitted from the final best fit constant growth line.

If the date of cut 25 is included, a linear least squares fit to the data gives:

1) that growth finished at 3.3 ± 0.9 Ka (ignoring the hiatus at the top),
2) the speleothem grew in a period of 8.0 Ka,
3) the base of the speleothem was started at about 11.3 Ka .

The error bars of the date of cut 25 do not intersect this constant growth line at the 2 σ (95%) level.

Figure 6 - 2; Virtual Geomagnetic Poles of SJLS.

Numbers denote the cut and the arrows denote the direction of VP polar movement with time.
Cut 23 with VGP at 56.65 and 172.69 has been omitted (see text).

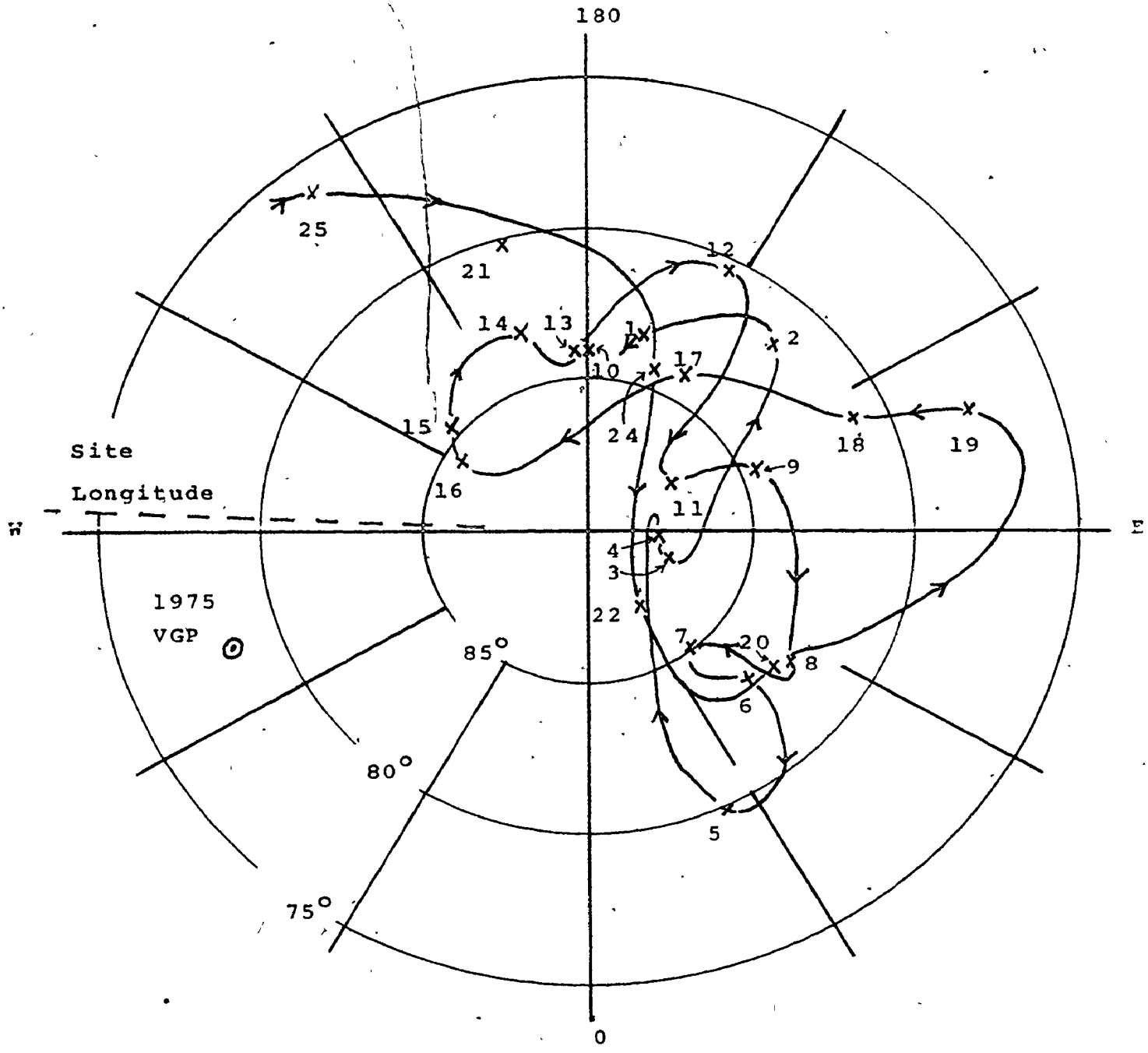

If it is omitted then a linear least squares fit to six points gives;

1) that growth finished at 4.5 ± 0.9 Ka,
2) the speleothem grew in the period of 4.5 Ka, and,
3) started to grow at about 9.0 Ka.

These data highlight the necessity of obtaining at least six data points for accurate and precise growth rate estimates, when the speleothem is shown to have grown fast and with a low uranium concentration.

6.2.4 Geophysical Interpretations of the SJLS Record.

The paleomagnetic direction swings and changes from the lower half of SJLS are the largest throughout the record. The most likely interpretation of the data is of a rapidly changing field with large swings in between. The problem of cut 23 and of the apparently old date of cut 25 necessitates looking at a second record for confirmation of these findings. The period concerned is from about 9 to 7 Ka.

In constructing the VGP path cut 23 has been omitted from the diagram and cuts 10 and 21 have also been ignored although all three may represent real directions of the field. Cut 10 was originally glued with epoxy resin; it was subsequently taken apart, cleaned free from the resin, and magnetically measured as a composite of the two pieces. Its AF-cleaned direction is not far from the path segments defined by cuts 11 and 9.

The direction of cut 1 with its hiatus, is mostly due to the remanence of the lower part of the specimen

since, from visual examination, it alone carried the black magnetic grains. If we discount the growth above the hiatus, then cut 1 is probably not modern, though the age data at the 2-sigma level does allow this. The directions of cut 1 are some angular distance away from the 1975 field direction.

The declinations of SJLS are mostly westerly and the inclinations mostly shallower than I_{agd} . Overall this has produced a left-handed and far-sided VGP path.

The VGP path shows no overall cyclicity. A large anticlockwise loop from cut 25 to 17 is followed by a small clockwise loop to cut 11. A clockwise half-loop to cut 8 is followed by little change to cut 6, another clockwise loop to cuts 4 and 3, and then part of an anticlockwise loop to cut 1. Ignoring cut 23, the path lies between the 75° latitude and the north geographic pole.

6.3 SJHS

Plate 6.2. Thin section, appendix III.

Rock magnetism 7.3.10

Site; State of Chiapas, Mexico, 17.1° N, 92.88° W.

6.3.1 Description

SJHS was the second stalagmite collected from near the large passage in Sima de San José, Chiapas. It possessed a height of 29.5 cms. Its shape was irregular - narrow at the base (7 cms) increasing irregularly to about 11 cms in diameter at a point 7 cms from the top. The cross-section was roughly oval. It had a dark brown coloured

Plate 6.2

Stalagmite SJHS

The first prominent hiatus is marked out.

The black inner dirt rind is also clearly visible.

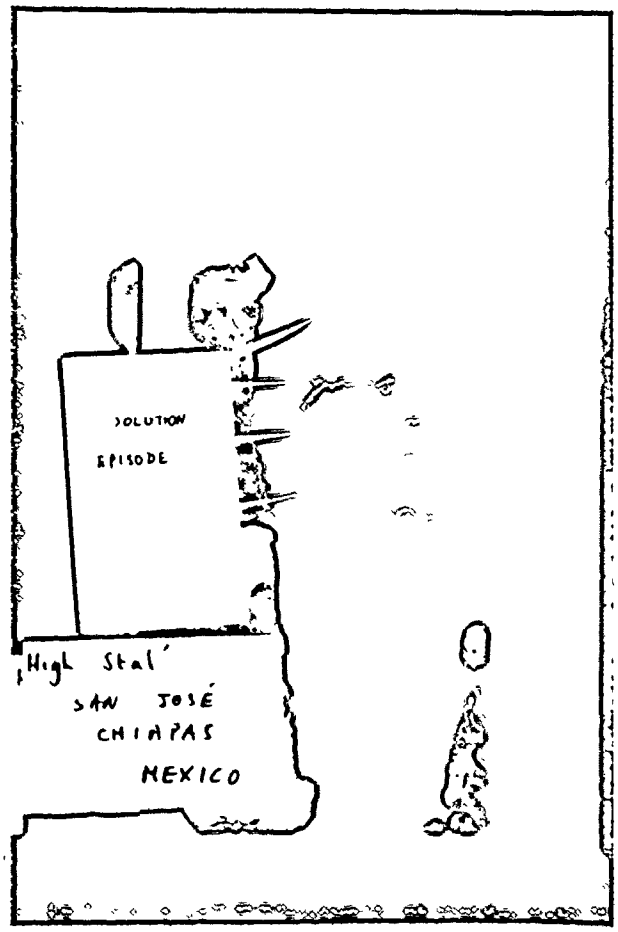

rough surface which tended to crumble away in places. The sample broke in the centre upon transport, but after gluing together with epoxy resin, it was cast and sliced as one. Subsequently, the resin was cleaned off the surfaces concerned prior to magnetic measurement. Two vertical slices labelled B and C were made from the centre. They revealed that:

1) An early stalagmite grew from base having a clear, slightly tan-coloured, compact crystalline core and regular growth layering.
2) There is a solutional hiatus about 6.5 cms from the top and this was followed by 6 cms of alternate depositional and solutional phases and perhaps by flood events. (organic detritus is present). There is at least one other clear solutional hiatus present at about 5 cms from the top. Examination of the slices and thin sections show that the original stalagmite was wider than the resultant by a few centimetres.
3) Covering the whole speleothem is a thick 0.5 cm rind of calcited dirt. The rind is layered indicating that it has arisen from multiple coatings of mud-laden flood water. Upon acid dissolution it yielded quartz, a few black magnetic grains and lots of froth. The froth is probably indicative of organic material.

Specimens were prepared from both slices though at the time of NRM measurement it was not certain that a good horizon match could be achieved from one slice to the other. Both slices yielded 15 cuts.

An early attempt to date calcite chippings from the base gave an age of 226 Ka. The detector had a high

Table 6 - 4: NRMs. Analysis of Directions and VGPs of Sample SJHS

Slice & Cut	Distance from top (cms)	NRM N	NRM D	NRM I	NRM α_{95}	AF Demagnetised N	AF Demagnetised D	AF Demagnetised I	AF Demagnetised α_{95}	K	δD	δI	VGP Lat	VGP Long
B1	0.25	1	347.83	19.71		3	351.66	19.12	0.8	10324	0.8	0.8	79.12	136.31
C1		2	351.01	20.38	1.6									
B2	2.7	1	348.19	32.69		2	348.32	32.89	2.3	1907	2.7	2.3	78.83	-176.92
C2		1	341.95	28.64										
B3	4.6	2	343.82	38.89	4.6	4	354.43	33.35	10.1	48	12.1	10.1	84.57	-170.13
C3		2	354.10	30.77	5.6									
B4	6.5	2	356.94	31.49	6.2	4	359.69	28.31	5.5	163	6.2	5.5	87.95	95.5
C4		2	355.87	31.81	5.4									
B5	8.3	1	357.34	31.27		2	356.21	30.63	4.1	584	4.8	4.1	86.32	168.16
C5		1	341.09	35.35										
B6	10.2	1	356.75	29.67		2	356.61	29.76	5.9	284	6.8	5.9	86.55	158.18
C6		1	356.32	42.45										
B7	12.1	1	352.97	25.99		2	355.54	32.11	13.3	55	15.8	13.3	85.73	-177.92
C7		1	341.54	35.72										
B8	14.1	1	351.16	30.62		2	357.44	29.56	4.6	464	5.3	4.6	87.24	150.22
C8		1	356.12	26.47										
B9	16.2	1	337.36	41.77		2	340.72	40.13	12.2	65	14.0	12.2	71.01	-162.10
C9		1	344.94	41.53										
B10	17.4	1	338.60	35.02		2	343.77	36.56	6.4	242	7.9	6.4	74.30	-168.42
C10		1	346.40	37.93										
B11	19.8	1	343.89	37.03		2	349.63	35.27	2.7	1366	3.3	2.7	79.87	-167.72
C11		1	348.17	32.86										
B12	21.7	1	352.30	37.26		2	357.33	35.08	5.6	315	6.8	5.6	86.61	-140.87
C12		1	353.86	35.95										

Table 6 - 4 continued : Sample SJHS

Slice & Cut	Distance from top (cms)	NRM N	NRM D	NRM I	NRM α_{95}	AF Demagnetized N	AF Demagnetized D	AF Demagnetized I	AF Demagnetized α_{95}	K	δD	δI	VGP Lat	VGP Long
B13	23.6	1	350.81	40.83		2	358.09	39.70	4.8	418	6.3	4.8	84.27	-110.87
C13		1	357.40	37.47										
B14	25.5	1	355.88	42.52		2	359.80	44.40	5.2	365	7.3	5.2	81.02	-94.02
C14		1	1.48	38.71										
B15	27.5	1	6.51	38.02		2	10.40	32.52	9.4	111	11.1	9.4	80.06	-7.80
C15		1	12.53	27.62										
Lateral Specimens														
B5P	8.3	1	352.59	22.62		1	355.63	20.95						
B7S	12.1	1	351.70	19.07		1	354.87	17.86						
All 5 specimens containing the dirt rind.														
		5	350.81	20.43		5	351.85	19.81	1.3	2235	1.4	1.3		

Note; The general AF demagnetization field was 100 Oe.

Table 6 - 5; Pilot AF Demagnetizations of SJHS.

Specimen C1Q

Peak AF (Oe)	D	I	M (x 10^{-3} G)	M/M_o
NRM	350.22	20.92	3.85	1.00
20	351.99	20.23	3.90	1.01
50	352.78	19.77	3.61	0.94
75	351.96	18.64	3.22	0.84
108	351.83	18.26	2.73	0.71
150	351.43	18.46	2.12	0.55
200	352.10	19.23	1.60	0.51
308	348.60	21.40	1.04	0.27
400	355.78	20.32	0.78	0.20
500	349.54	18.62	0.52	0.14

Specimen C14Q

Peak AF (Oe)	D	I	M (x 10^{-6} G)	M/M_o
NRM	1.48	38.71	11.59	1.00
20	3.06	32.78	12.45	1.07
50	4.58	38.26	11.95	1.03
75	3.65	36.83	10.67	0.92
108	358.71	47.29	8.71	0.75
150	6.34	39.09	7.29	0.63
200	9.80	40.58	6.30	0.54
308	4.30	45.20	3.95	0.34
400	5.13	38.65	3.20	0.28
500	1.39	47.32	2.72	0.24

M/M_o is the ratio of the cleaned remanence to the NRM.

The present day field (1975) is D = 6^{o} E, I = 45^{o}.

background. Later isotope activity analysis of the rest of the sample showed this to be too old by almost 100 Ka!

6.3.2 The Paleomagnetism of SJHS

Because it was not certain that horizons could be matched from slice B to slice C, the respective specimens were at first measured and analyzed separately for their NRMs. Later AF-cleaned directions of corresponding specimens agreed fairly well and the directions were combined by treating them as though they were from a random distribution of vectors. This treatment probably fails in the case of cuts 14 and 15 where it is known from visual examination and from the directions that the specimens do not quite correspond. In detail, the stratigraphic order of the specimens is C15Q, B15Q, C14Q and then B14Q.

The NRMs, AF-cleaned directions and VGPs are given in table 6.4, and the cleaned directions are plotted against length in figure 6.3 . The AF-cleaned direction changes of pilot specimens C1Q and C14Q are given in table 6.5. For C1Q the direction change is very small. The direction change is greater in C14Q - it evidently has a larger fraction of grains carrying the softer magnetization. The 108 Oe step, for example, appears to show the acquisition of a small ARM in C14Q. C1Q was treated under the same conditions and at the same time but shows no evidence of any spurious ARM. A field of 100 Oe was reckoned adequate to magnetically clean the rest of the specimens.

Apart from the specimens of cut 1, the total moments of most specimens were around 10^{-5} G. Specimens of cut 1 were dominated in intensity by the dirt rind.

Figure 6 - 3; The Paleomagnetism and Dating of SJH5.

(Cuts 1, 3 (7) and 4 each straddle a hiatus)

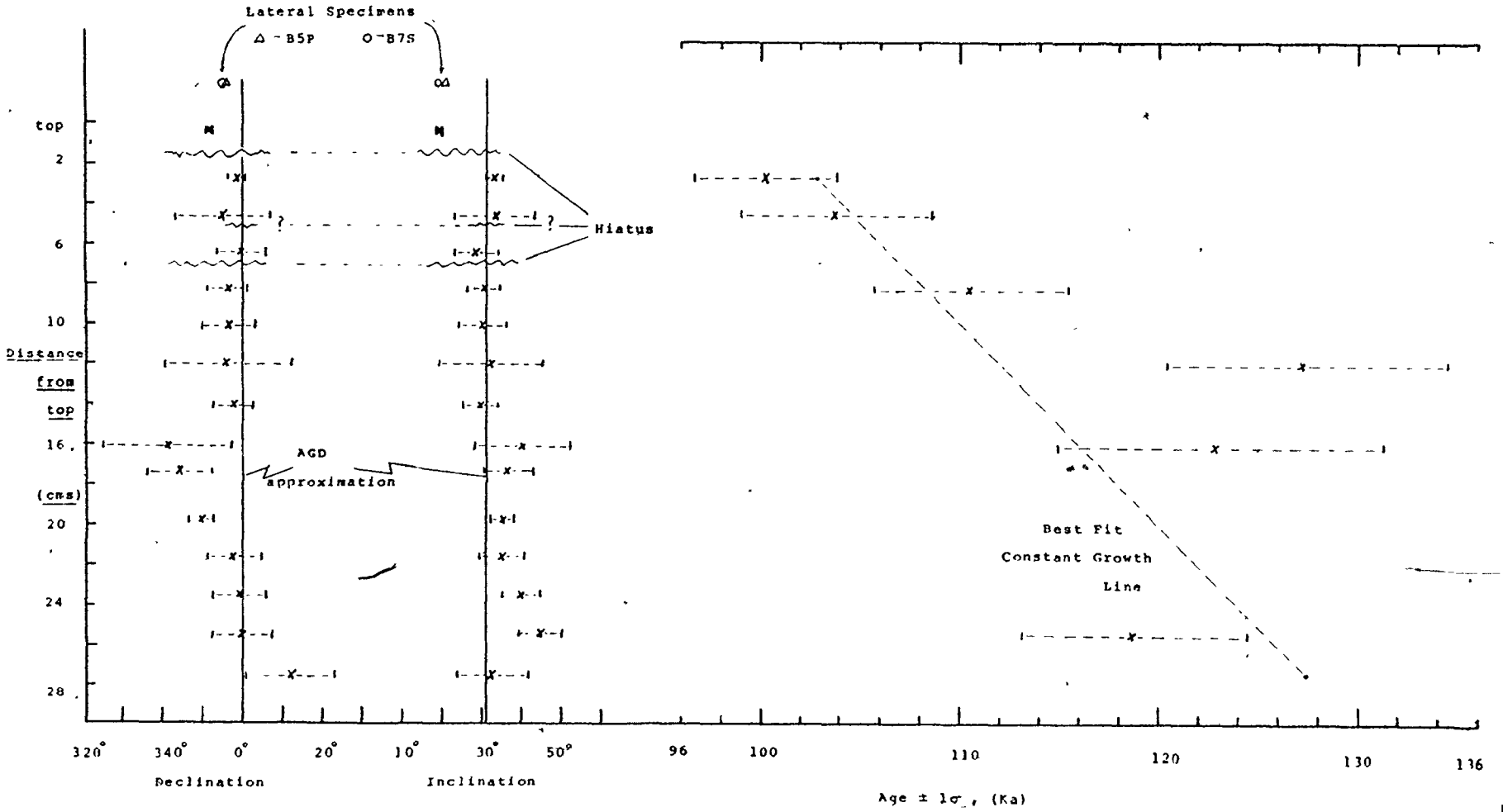

Their total moments were up around 10^{-4} to 10^{-3} G. This was also true of the lateral specimens which incorporated the dirt rind such as B5P or B7S. Their directions are also given in table 6.4 . A combination of the three specimens of cut 1 and the two lateral specimens gave a direction whose precision estimate, K, was 2235, and whose α_{95} was 1.3^{o}. The conclusion is that though magnetic grains were initially laid down by flood waters, this has not led to any depositional errors. Otherwise the directions of the lateral specimens would have been different from each other and from the directions of the top specimens (for further discussion, see section 9.3.1.2)

Cuts 3 and 4 each straddle a hiatus. This makes it difficult to estimate the jump in the direction, or in the VGP path (figure 6.4), or the length of the hiatus (see the next section). The appearance of the directions, the VGPs, and the dates lead one to believe that the hiatuses were not long in terms of secular variation (unless it was changing very slowly) or of time. This may not be true of the dirt rind which has not been dated, and which may be significantly younger than the rest of the sample. For this reason the unknown VGP path between cuts 2 and 1 has been drawn dashed.

6.3.3 The U-Th Dating of SJHS

The isotope activity ratios and dates are presented in table 6.6, and the dates are plotted against length in figure 6.3 . The analyses were performed on a new detector having a low background. No corrections were needed for detrital thorium.

Table 6 - 6; Isotope Activity Ratios and Dates for SJHS

Cut No.	Distance from top (cms)	U (ppm)	Yields (%) U	Yields (%) Th	$^{230}Th/^{234}U$	$^{234}U/^{238}U$	$^{230}Th/^{232}Th$	Age ± 1σ (Ka)
2	2.7	0.63	59	66	0.624 ± 0.014	1.36 ± 0.03	154 ± 46	$100.2^{+3.6}_{-3.5}$
3	4.6	0.66	67	66	0.640 ± 0.019	1.41 ± 0.03	380 ± 300	$103.7^{+4.9}_{-4.7}$
5	8.3	0.40	69	72	0.663 ± 0.018	1.37 ± 0.03	41 ± 6	$110.5^{+5.0}_{-4.8}$
7	12.1	0.28	60	80	0.716 ± 0.022	1.30 ± 0.04	52 ± 10	$127.2^{+7.3}_{-6.8}$
9	16.9	0.41	32	35	0.699 ± 0.026	1.24 ± 0.04	86 ± 29	$122.9^{+8.4}_{-7.9}$
14	25.5	0.50	63	56	0.693 ± 0.019	1.39 ± 0.03	168 ± 67	$118.7^{+5.8}_{-5.5}$

The two analyses corresponding to cuts 7 and 9 are out of stratigraphic order. As an explanation it seems unlikely that the calcite could have been leached of uranium in a later solutional event since this would also apply to cut 5 whose age is in accord with those of cuts 3 and 2. Apart from bands of fluid inclusions the calcite was compact and showed long palisade type crystals - which is evidence against recrystallization. Alternatively unclean glassware may have contributed contaminating thorium which has given these apparently older dates. Further dating analyses will be necessary to help resolve this problem.

A least-squares best fit to a constant growth rate from the six data points gives;

1) The top of the speleothem (but for the uppermost hiatus and dirt rind) corresponds to about 100 ± 3 Ka. Cut 2 corresponds to about 103 Ka,
2) The growth rate was 1.0 ± 0.3 Ka per cm (1 cm = 1 Ka),
3) The record up to cut 2 spans 24 - 25 Ka,

and 4) Growth began at about 127 - 128 Ka.

A comparison of the dates of cuts 5, 3 and 2 show that the hiatuses were probably less than a few thousands of years duration. This is a long time in terms of secular variation which can occur in periods of only 50 years or less. Clearly from the age data other interpretations are possible about the growth of SJHS. It is reasonable to state that most of the stalagmite grew somewhere between 130 and 96 Ka BP, and that the dirt rind is younger than this.

Figure 6 - 4; Virtual Geomagnetic Pole Positions for SJHS.

The numbers denote the cut and arrows denote direction of VG polar movement with time.

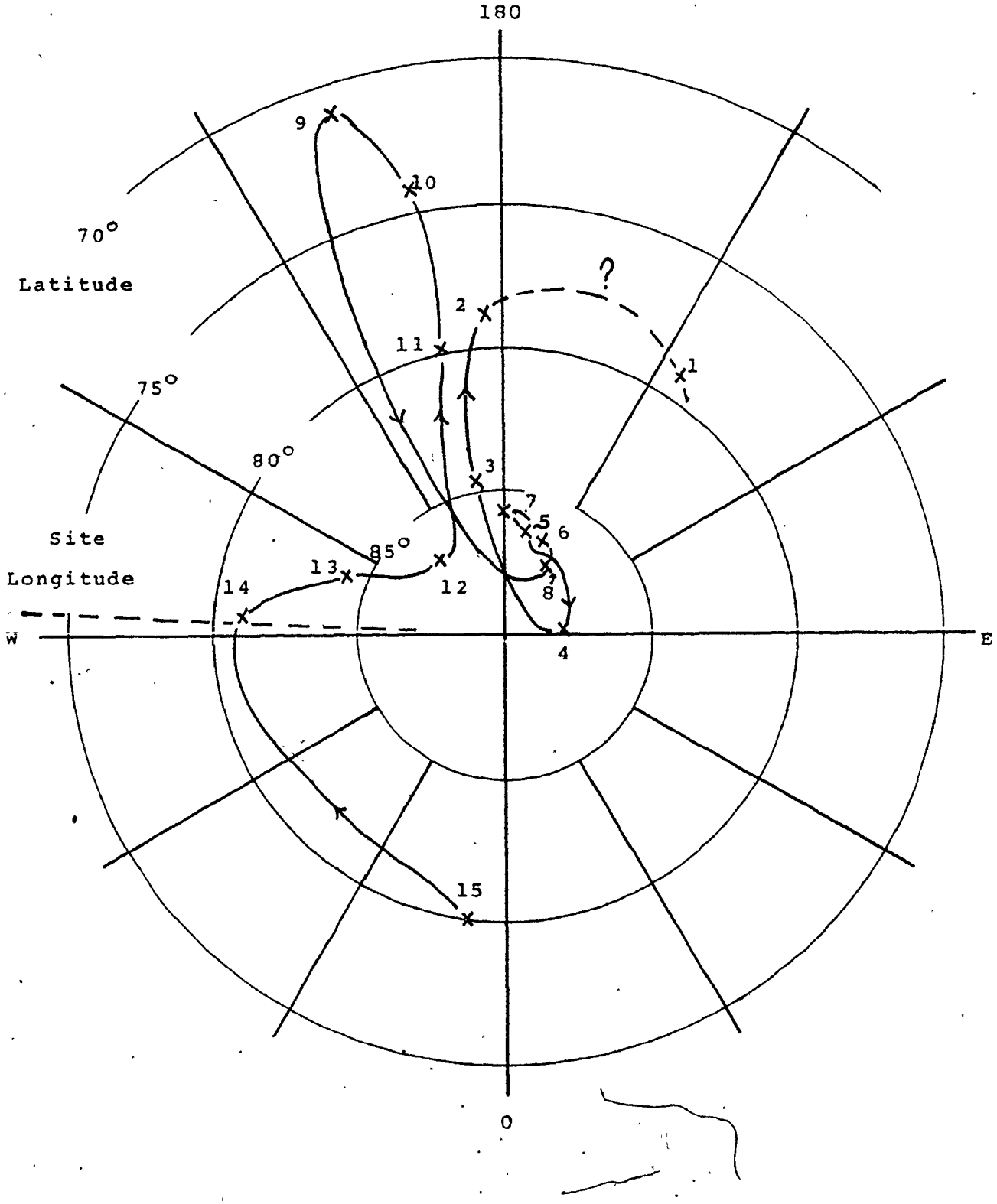

6.3.4 Geophysical Interpretation of the SJHS Record

The SJHS paleomagnetic record (figure 6.3) shows westerly declinations so that up to cut 2 the VGP path (figure 6.4) is predominantly left-handed. In contrast to the Holocene speleothems of this study the inclinations of SJHS are mostly steeper than I_{agd} giving near-sided VGPs. The most far-sided VGP is from the dirt rind and this is the youngest.

No overall cyclicity is readily discernable from the VGP path. From cut 15 a clockwise loop segment is fairly well defined to cut 12 and is followed by a long swing, chiefly in declination , westwards to cut 9. Cut 9 marks a sharp change of direction followed by rapid movement to cut 8 and little change to cut 5. Despite the hiatuses a near-sided path segment seems fairly well defined from cut 4 to cut 2. However it must be borne in mind that both 4 and 3 are the resultants of directions of adjacent sides of their respective hiatuses. The hiatus between the clear calcite and the dirt rind may be a major one.

Further interpretation of the SJHS record is limited by the inadequate dating control and uncertainty as to the duration of the hiatuses. From the base up to cut 5 (below the first hiatus) there are about 2 loops of the VGP path. In comparing the complexity of this path with that of TS, VCCL, SJLS, DAS1 or DAS2 (this chapter), one might estimate that the two loops span no more than about 5 Ka. This is allowed by the dates of cuts 14 and 5 if the dates of cuts 7 and 9 are ignored. One would expect that if the speleothem was as slowly growing as all four dates indicate, then it would have averaged out the SV more than it appears to have done.

If, on the other hand, the growth rate estimate from the six points is reasonably accurate, so that cuts 15 to 5 span 10 Ka (say, 125 to 115 Ka), then SJHS was a slow recorder of a slow but widely varying field (ie. as widely varying as in the other records).

6.3.5 The SJHS Record and the Blake Event

The age assignment of the SJHS record is of some importance since it covers or adjoins the time of the Blake event (Smith and Foster, op cit; Denham , 1976, op cit; Denham, et al, 1977, op cit). Also if the event was regionally restricted, then judging by the distribution of the sampling sites from which the claim has arisen, Chiapas could easily be considered to be part of this region.

The Blake event has been best defined in cores from the W. Atlantic and Caribbean sea, and stratigraphnically is contained within the X biozone of Ericson, et al (1961). The event is fully reversed and age estimates place it just before or at 100 Ka. BP. Smith and Foster's estimate of the duration and time of the event was from 114 to 108 Ka ± 10%, and was based on sedimentation rates within the X biozone. The lower boundary of this biozone is placed at 126 Ka (Broecker et al, 1968), and the upper boundary is placed at 88 Ka ± 10% by Smith and Foster. A radiochemical estimate of the age of the event by Denham et al, was not entirely succesful. Their duration estimate of 30 Ka was from cores KN25-3 and KN25-4, but they found this period unacceptably long. The event has not been convincingly seen and dated in cores elsewhere and in many cores of this age it is absent. So Denham suggested that the 'event' was localised to the Caribbean

and W. Atlantic area and covered , perhaps, only 9% of the globe. Denham suggests a duration of 5 to 7 Ka.

More recently Creer et al (1980) have claimed to recognise the event from a long unoriented core of marine clays from Italy. They were able to identify the Brunhes - Matuyama boundary and the established events within the Matuyama chron. As in KN25-4, the Blake event appeared as two reversals split by short normal polarity. Extrapolation from sedimentation rates gave a total duration estimate of 50 Ka. However as stated earlier by Denham, such a long period for the event presents problems since it ought then to have been recognised globally in all but the slowest-deposited sediments.

Of about the same age as the Blake event, speleothem SJHS shows no evidence for anomalous field behaviour. Despite the poor age data, they are still good enough to preclude a speleothem basal age of greater than about 130 Ka or a top age of less than 96 Ka, unless migration of uranium or thorium radioisotopes has occurred. In addition core KN25-4, which has provided the best record of the Blake event, shows inclinations much lower than I_{agd} before, during and after the event, whereas SJHS shows steeper inclinations than I_{agd} for the presumed same period. It is hardly likely that characteristic signatures of the event such as shallow or steep inclination, would vary so much when the two sets of records were regionally so close.

These conflicting results may eventually be resolved in a number of ways. If the SJHS paleomagnetic and age data are correct then either:

1) The reversed record from the Caribbean and

W. Atlantic area is an artefact of sedimentation processes due to erosion, slumping, turbidity currents or other processes; and the assignment of other sediment-recorded anomalous features to the proposed event are, perhaps, examples of the 'reinforcement' syndrome (Watkins, 1972, op cit; and see section 1.5.4),

or 2) the identification of, or the age assignment of the X biozone is incorrect (the latter is unlikely).

If the reversal occurred then as far as the SJHS record is concerned:

3) The age data of SJHS is grossly in error. One possibility, already mentioned, is that uranium has leached out during the known later phase of dissolution associated with the hiatus at cut 4. However the earlier speleothem core does not show such recrystallization features as interlocking equant calcite crystals, for example. Moreover the newer growth of cuts 3 and 3 date from 100 to 104 Ka, which is still at, or close to the time of the proposed event.

Pending further work on SJHS, other speleothems, sediment cores or any other records of this age this conflict remains.

6.4 DAS1

Plate 6.3

Rock magnetism 7.3.12

Site; El Sótano del Arroyo, El Abra, Mexico, 22.09° N, 99.0° W

Plate 6.3

Stalagmite DAS1

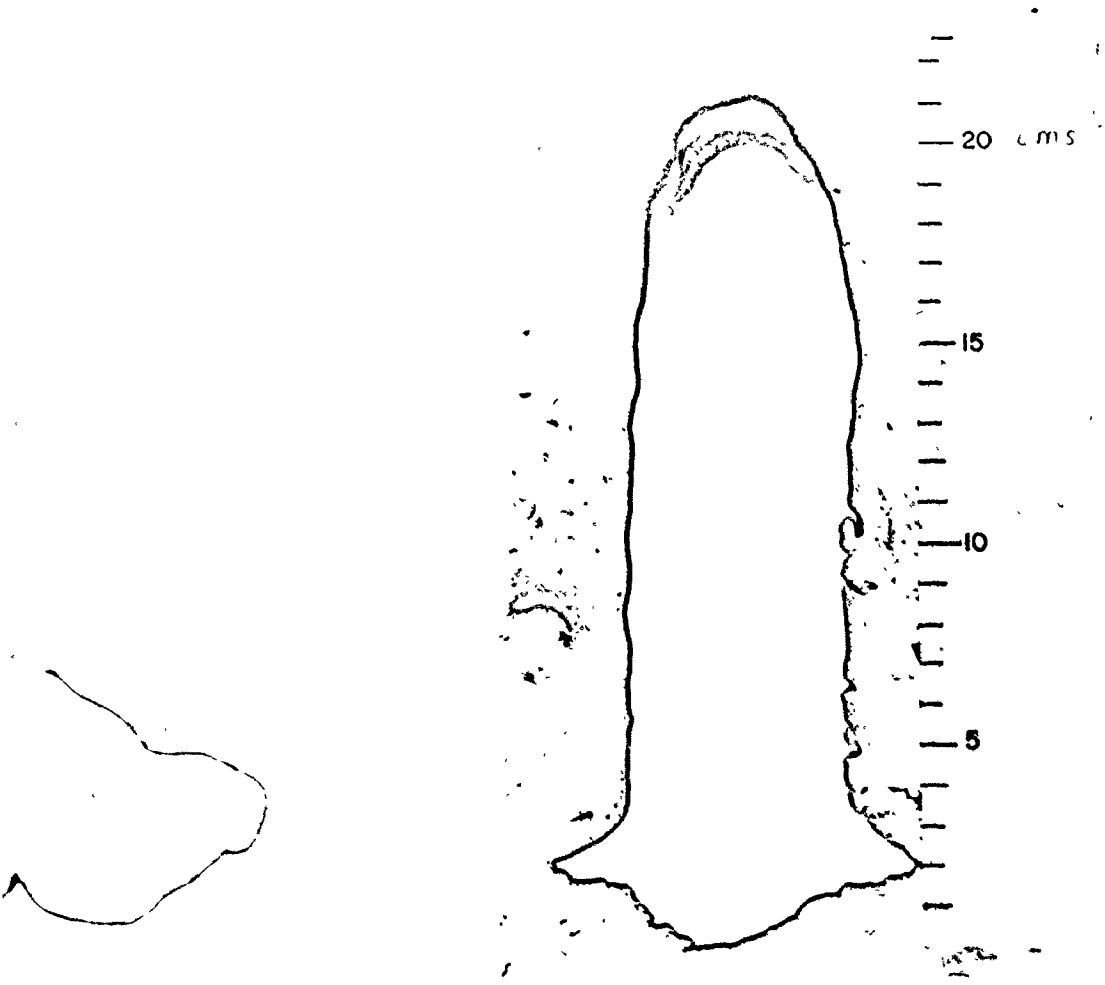

6.4.1 Description

The cave El Sótano del Arroyo is described by Fish (1977). Stalagmite DAS1 was found near the highest point of a rising passage, called Left Hand Passage, that behaves as a flood overflow route from a main passage. Fish states that modern flood water probably rarely uses this Left Hand Passage. When it does DAS1 would be inundated by several feet of water. That flooding does occur in modern times is testified to by mud deposits and vegetal debris in the vicinity.

The stalagmite is 21.5 cms high with a uniform diameter of 5.5 cms. It was cast in one piece and one 2 cm thick slice was obtained from its centre. The section revealed uniform deep amber colouring of the calcite which is probably due to organic matter of unknown type. Growth layers are marked by fine dark bands of material that laterally coalesce and dominate the colouring of the vertical sides. The base of the stalagmite was begun as a drip pit in unconsolidated mud. Some of the lower layers contain abundant quantities of this mud. It seems likely that the calcite and the mud alternated in depositional frequency before regular calcite growth was established. When the speleothem was sampled it showed no evidence of having been disturbed after formation. Though dry the top of the sample appeared to be fresh.

Eleven cuts were prepared from the slice with one specimen per slice. Specimens 6 and 7 broke partway through preparation with the result that each lacked one oriented horizontal plane. This meant that only one estimate of the vertical component could be made, ie either +z or -z. In addition specimen 6 was small and 7

Table 6 - 7; NRMs, Analysis of Directions and VGPs of Sample DAS1.

Cut No.	Distance from top (cms)	NRM		AF Demagnetized			
		D	I	D	I	VGP Lat.	VGP Long.
1.	0.8	1.98	46.42	6.54	42.00	83.62	-29.92
2	2.6	359.34	44.89	354.65	37.28	84.87	157.87
3	4.5	14.48	33.76	10.33	35.08	79.96	4.97
4	6.5	14.05	27.88	8.56	25.61	78.25	36.18
5	8.4	23.77	29.55	12.98	30.06	76.38	14.64
6	10.1	22.73	38.01	41.01	36.47	51.83	-14.11
7	11.9	28.23	45.76	10.98	42.68	79.58	-25.95
8	14.0	355.08	41.80	355.32	29.76	82.44	117.59
9	15.9	351.78	46.65	345.34	38.28	76.38	-188.59
10	17.9	343.92	36.53	344.19	31.30	74.23	154.61
11	19.6	356.78	35.81	352.00	28.47	79.74	129.96

Notes: All specimens were AF cleaned to 50 Oe except cut 10 (specimen B10Q) which was cleaned to 450 Oe.

Table 6 - 8; Pilot AF Demagnetization of DAS1 B10Q.

Peak AF (Oe)	D	I	M ($\times 10^{-7}$ G)	M/M_o
NRM	340.75	38.60	18.23	1.00
100	341.55	30.24	13.65	0.75
150	340.55	30.30	11.15	0.61
200	431.21	30.46	9.62	0.53
250	342.70	31.79	7.59	0.42
307	341.65	31.60	6.68	0.37
350	342.65	28.72	6.37	0.35
400	335.68	32.03	5.54	0.30
450	338.08	29.65	5.05	0.28

Notes;1) M/M_o is the ratio of the cleaned remanence to the NRM.

2) Magnetometer noise level was around $2. 10^{-7}$ G. Due to the lower intensity of most specimens , 50 Oe had to be chosen as the optimum cleaning field.

3) The 1975 field is at $D = 8^{o}$ E, and $I = 50^{o}$.

Figure 6 - 5; The Paleomagnetic Directions and Dating of DAS1.

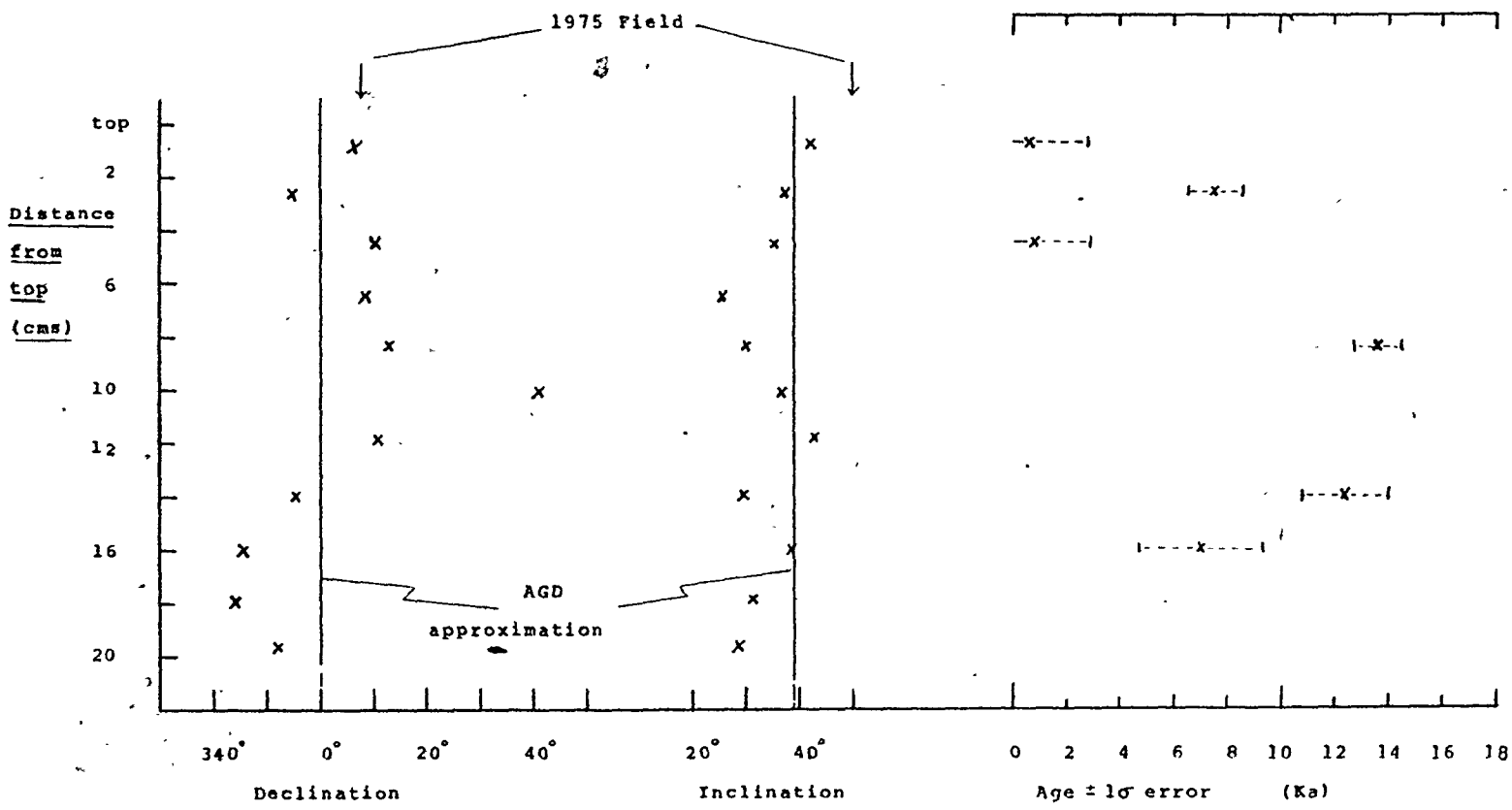

was large. Specimen 11 also lacked an oriented basal plane.

6.4.2 The Paleomagnetism of DAS1

The NRMs, AF-cleaned directions and VGPs of DAS1 are presented in table 6.7 . The AF-cleaned directions are plotted against length in figure 6.5 . Total intensities ranged from 2×10^{-7} G (cut 6) to 28×10^{-7} G (cut 11).

The behaviour of the pilot specimen B10Q to AF demagnetization is given in table 6.8 . Most of the movement of the vector took place within the 100 Oe step . This movement was away from the direction of the modern field in this region , so this part of the NRM probably represents a VRM acquired in the modern field.

Unfortunately most of the other specimens had much lower intensities than B10Q. A compromise had to be made between adequately cleaning the specimens and retaining sufficient magnetization above the noise level of the magnetometer. The NRM of B6Q was already low (2.1×10^{-7} G, total moment), and its AF-cleaned magnetization (1.9×10^{-7} G) and direction probably reflects some of this noise. All other AF cleaned magnetizations were above 3×10^{-7} G.

6.4.3 The U-Th Dating of DAS1

The U/Th isotope activity ratios and dates of DAS1 are presented in table 6.9, and the dates, with correction for detrital thorium, have been plotted against length in figure 6.5 .

Two sets of analyses were obtained and are labelled "old" and "new". The old set was obtained in 1979 using

Table 6 - 9; Isotope Activity Ratios and Dates of DAS1

Cut No.	Distance from top (cms)	U (ppm)	Yields (%) U	Yields (%) Th	$^{230}Th/^{234}U$	$^{234}U/^{238}U$	$^{230}Th/^{232}Th$	Calculated Age, ±1σ (Ka) Uncorrected	Corrected
1 (old)	0.8	0.38	43	45	0.014 ± 0.005	1.17 ± 0.04	2 ± 2	1.6 ± 0.5	0.6 ± 1.2
2 (new)	2.6	0.41	37	67	0.077 ± 0.005	1.15 ± 0.03	11 ± 4	8.6 ± 0.6	7.5 ± 1.0
3 (old)	4.5	0.42	31	42	0.025 ± 0.008	1.11 ± 0.04	2 ± 1	2.8 ± 0.9	0.8 ± 2.1
5 (new)	8.4	0.37	11	55	0.118 ± 0.007	1.17 ± 0.04	28 ± 15	13.6 ± 0.9	13.6 ± 0.9
7 (old)*	11.9	0.65	29	21	0.015 ± 0.005	1.05 ± 0.03	1.0 ± 0.4	1.7 ± 0.6	-0.4 ± 1.2
8 (new)	14.0	0.42	46	15	0.117 ± 0.010	1.16 ± 0.03	16 ± 6	13.4 ± 1.2	12.2 ± 1.6
9 (old)	15.9	0.36	44	26	0.085 ± 0.009	1.15 ± 0.03	5 ± 2	9.6 ± 1.1	7.0 ± 2.3

Notes; 1) " Old " data was obtained from a low resolution counter. ^{230}Th background ≈ 1/3 total ^{230}Th.

2) " New " data was obtained from a high resolution counter. ^{230}Th background was nearly zero.

3) * A. $^{230}Th/^{232}Th$ ratio of 1.3, rather than the usual 1.5, was used to produce this corrected ' negative ' age.

a low resolution detector with a high background, whereas the new set was obtained in 1980 with a high resolution detector in which the background was nearly zero. The following points are noted:

1) The $^{230}Th/^{232}Th$ ratios are quite low in the old data despite having chosen specimens which appeared to have a low detrital content. Therefore the final dates are susceptible to the chosen value for the initial $^{230}Th/^{232}Th$ ratio (normally 1.5) which is used to correct the initial dates. The shifts in ages for the old data are 62.5% for cut 1, 71.4% for cut 3, 76.5% for cut 7 (producing a negative age for a correction ratio of 1.3) and 27% for cut 9.

2) In producing the new dates specimens were also chosen having little apparent detrital content. The detrital thorium corrections are low and the ages are high by comparison with the old data. This leads to the supposition that in the old data too much background has been subtracted from the ^{230}Th raw count rates, and/or insufficient background has been subtracted from the ^{232}Th raw count rates. It is possible that some noise in the ^{232}Th region of the alpha spectrum of the old detector has contributed to the observed counts (this has been observed in other detectors and may be due to incorrect bias settings).

   The corrections in age terms for the new data are 12,8% for cut 2, 0% for cut 5, and 8.6% for cut 8.

3) In the corrected dates, the ages of cuts 8 and 5 are well out of stratigraphic order.

4) If the top is modern then the speleothem grew fast

Figure 6 - 6; Virtual Geomagnetic Pole Positions for DAS1.

The numbers denote the cut and arrows denote the direction of VG polar movement with time.

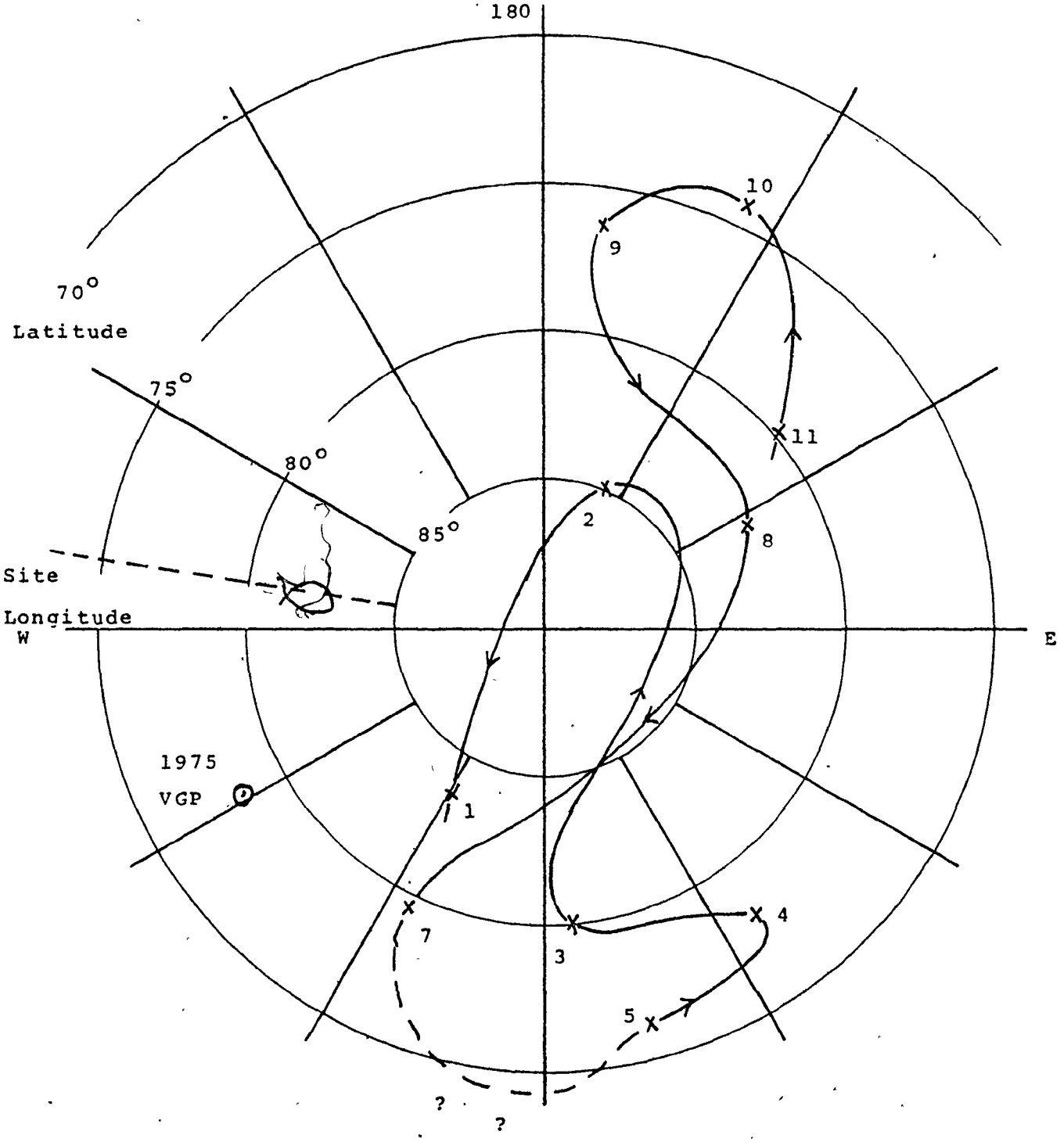

Note; The VGP of cut 6 (B6Q), at Lat. 51.83, and Long. -14.11 has been omitted (see text).

to about cut 2 and then growth slowed up considerably to the top.

5) There is some resemblance in the paleomagnetic records of DAS1 and DAS2 (cf figures 6.6 and 6.8). If DAS1 was contemporaneous with DAS2 then it grew from about 1.5 Ka to present and not from about 14 Ka as implied by the above "new" data!

6.4.4 Geophysical Interpretations of the DAS1 record

Sections of the direction data appear to be sequential . Correspondingly segments of the VGP path are reasonably well defined. These are from cuts 11, 10 and 9, and from cuts 5, 4 and 3. Between these segments there is much freedom of choice as to where to draw the VGP path! Even so the following points may be noted:

1) The inclinations are mostly shallower than I_{agd} resulting in far-sided VGPs.
2) Most of the change in direction is in declination with the result that the VGP path is approximately orthogonal to the site longitude.
3) The VGP path is contained within latitude 75^{o} and the north geographic pole.
4) The direction (or the VGP) of the top cut is not far from the modern direction (or modern VGP)(see DAS2 for comparison).

Further interpretation of the DAS1 record is rendered somewhat tenuous by the uncertain age control.

Plates 6.4 & 6.5

DAS2; The lower plate shows the work-hole, cusps and growth layering in greater detail.

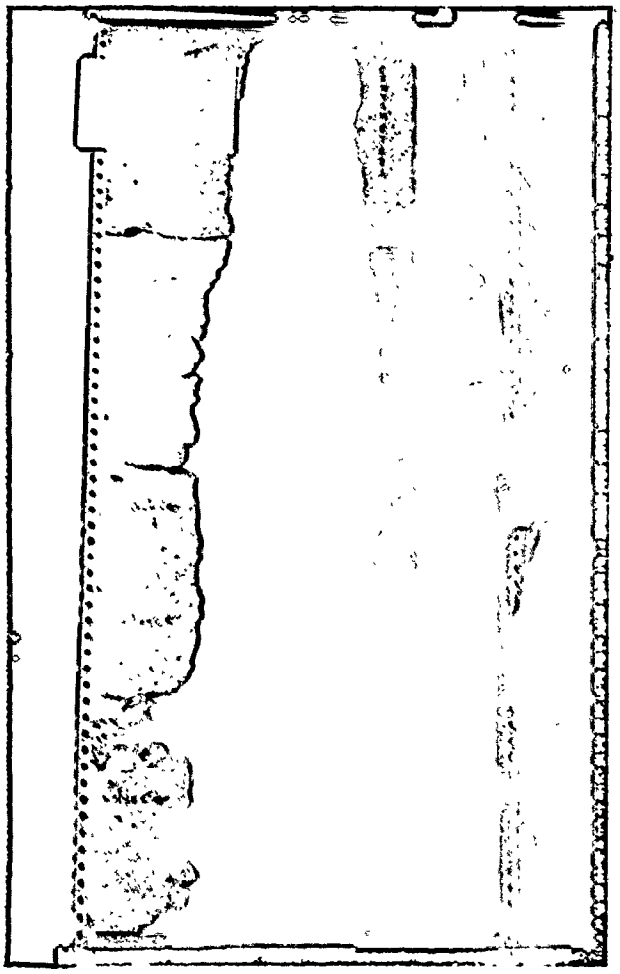

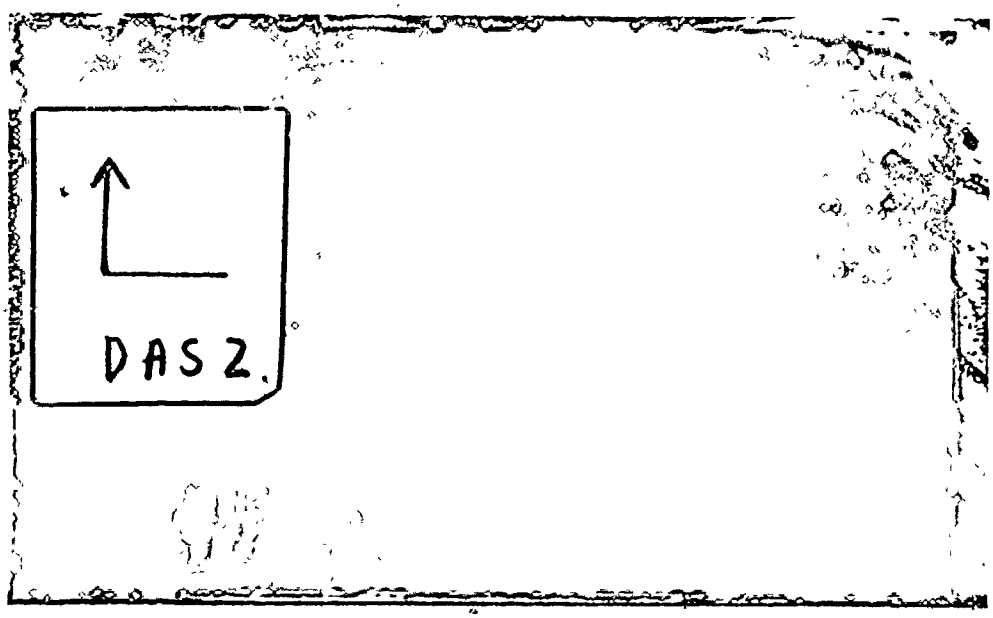

6.5 DAS2

Plates 6.4 & 6.5 . Thin section appendix III

Rock magnetism 7.3.13

ARM studies chapter 8

Site; Sótano del Arroyo, El Abra, Mexico

22.09° N, 99.0° W

6.5.1 Description

Stalagmite DAS2 was taken from a grotto off the main passage of the cave Sótano del Arroyo, near the El Abra range of mountains, As described by Fish (1977, op cit) this passage (called Main Passage) takes most of the river water in flood and frequently fills to the roof, depositing various grades of sediment up to boulder size, in various places. In the grotto where DAS2 was found the sediment ranged in size from mud up to sand and small pebbles. When sampled the stalagmite was firmly attached to a wide calcite canopy at its base. Though dry the top appeared to be fresh.

The sample was 72 cms high but with a variable diameter, as follows. The basal section up to about 55 cms from the top had a diameter of 17 to 15 cms, and the internal growth layering (as revealed by later sectioning) appeared to contain some detritus from flood events. The lower middle section is from about 55 cms to about 37 cms from the top and the diameter decreased to about 13.5 cms. The inner growth was an amber colour and was less influenced by the dark detrital bands. The diameter increased again to about 14.5 cms up to a point 23 cms from the top , where detrital bands were again more evident. From about 20 cms to the top the diameter decreased steadily from 11 cms to

9.5 cms and the amber colouring was mostly clear of detrital bands. Finally a few detrital bands were incorporated along growth layers near the top.

The exterior surface of the stalagmite was a medium grey colour except for the white-amber drip area at the top. The surface was rough in places because of calcite ripples and microgours.

The stalagmite was cast in four parts according to the procedure of section 2.4 . Two 2 cm thick slices were obtained from the centre of the stalagmite and the cuts from these slices yielded 4, 5 and 6 specimens according to the flatness of the drip areas.

The centre slices also revealed the following;

1) Where the calcite was clearest it was a translucent amber colour. It is probable that the amber colour was due to an unknown organic constituent carried with the drip water. The uniformity of the colouring suggests that a specific size or type of organic molecule is responsible. The amber colour is made to appear lighter than in DAS1 by the greater abundance of fluid inclusions.
2) As the speleothem grew, floods coated the surface principally with mud. Most of it was usually washed off the cap area by the splash of the drip. It is probable that where the detritus is less dense within the drip area either the drip frequency increased, or the flood frequency decreased. Also these regions occur where the diameter has decreased and the average distance between growth bands has increased, so the first explanation is preferred.
3) Some parts of the centre slices, eg the lower

Table 6 - 10; NPMs, Analysis of Directions and VGPs of Sample DA52.

Cut No	Distance from top (cms)	NRM					AF Demagnetized							VGP	
		N	D	I	α_{95}	K	N	D	I	α_{95}	F	δD	δI	Lat.	Long.
1	1.2	4	10.57	32.43	4.0	312	4	12.87	38.76	3.2	493	4.0	3.2	78.07	-10.38
2	3.1	4	7.39	39.18	11	41	4	10.38	37.94	6.5	115	8.3	6.5	80.32	-6.23
3	5.2	4	24.17	40.88	18	16	4	43.20	39.89	19	14	25	19	50.20	-18.38
4	7.1	4	22.99	15.05	44	2.5(NS)	4	15.90	30.26	6.0	138	7.0	6.0	73.90	9.45
5	9.1	4	337.34	33.86	41	2.9(NS)	4	338.11	49.81	33.2	4	52	33	68.66	-160.85
							(2)	20.41	39.61	12.7	61	16	13	71.12	-3.76
6	11.1	4	20.65	31.89	23	9.5	4	14.80	30.32	13	31	15	13	74.88	10.93
7	13.1	4	10.55	25.12	17	17	4	6.49	29.58	8.7	65	10.0	8.7	81.25	35.40
8	15.1	4	11.05	29.50	12	34	4	6.08	28.12	15.1	22	17	15	80.83	41.03
							(3)	13.34	33.65	5.4	227	6.4	5.4	76.96	5.01
9	17.1	4	40.88	3.69	23	9.2	4	22.33	21.42	8.8	64	9.4	8.8	65.99	14.62
10	19.1	4	23.35	38.73	9.2	58	4	18.76	34.16	8.1	75	9.8	8.1	72.12	-1.61
							(3)	13.84	34.84	5.7	203	6.9	5.7	76.73	1.19
11	21.1	4	7.62	31.85	5.7	153	4	6.28	31.63	3.2	487	3.7	3.2	82.27	29.96
12	23.1	6	7.44	31.81	4.5	161	6	2.99	30.10	4.2	386	4.8	4.2	83.44	55.01
13	25.1	6	3.16	29.11	2.1	735	6	359.83	28.54	2.1	726	2.4	2.1	83.12	82.17
14	27.1	6	2.21	27.58	2.3	609	6	1.03	26.76	2.2	646	2.5	2.2	82.00	73.80
15	29.1	6	7.77	30.03	7.9	52	6	3.40	25.99	7.4	60	8.2	7.4	81.01	59.37
							(5)	359.94	28.41	3.4	333	3.9	3.4	83.04	99.48
16	31.0	6	6.69	31.82	3.6	248	6	2.74	29.36	4.3	173	5.0	4.3	83.11	58.43
							(5)	0.81	30.00	3.7	293	4.2	3.7	83.96	73.58
17	33.0	6	3.21	32.90	6.3	82	6	358.19	31.37	5.5	107	6.5	5.5	84.59	99.68
							(5)	355.73	33.43	2.7	539	3.2	2.7	84.46	128.09
18	35.2	6	2.94	29.52	2.3	612	6	1.39	30.05	2.7	454	3.1	2.7	83.90	68.33
19	37.4	4	358.27	36.35	6.2	126	4	354.67	36.31	5.1	189	6.3	5.1	84.67	150.90
20	39.1	6	9.08	39.86	8.8	42	6	359.30	36.32	10.5	30	13.0	10.5	87.98	100.01
							(5)	356.51	31.20	4.1	232	4.8	4.1	83.81	113.71
21	41.0	6	8.10	28.83	24	5.9	6	356.76	24.43	27	4.6	29	27	80.21	99.91
							(5)	0.73	35.54	7.1	78	8.7	7.1	87.48	80.99

Table 6 - 10, continued.

Cut No.	Distance from top (cms)	NRM N	NRM D	NRM I	NRM α_{95}	NRM K	AF Demagnetized N	AF Demagnetized D	AF Demagnetized I	AF Demagnetized α_{95}	AF Demagnetized K	AF Demagnetized δD	AF Demagnetized δI	VGP Lat.	VGP Long.
22	43.1	5	0.36	30.20	5.1	151	5	356.54	32.94	5.6	127	6.6	5.6	84.74	119.75
23	45.1	4	5.74	29.84	7.1	98	4	357.72	31.94	7.1	98	8.3	7.1	84.76	105.59
24	47.1	4	355.77	30.63	6.9	102	4	350.25	29.74	9.7	52	11.2	9.7	78.93	138.97
							(3)	349.29	33.91	9.1	79	10.9	9.1	74.37	153.73
25	49.1	4	6.83	38.06	7.3	91	4	356.74	31.01	8.2	72	9.6	8.2	83.82	111.39
26	51.1	4	28.18	50.26	23	9.6	4	355.44	36.90	19	13	24.2	19.4	85.49	152.23
27	53.1	4	353.08	30.67	5.4	166	4	351.80	33.87	3.5	408	4.2	3.5	81.54	147.76
28	55.1	6	350.44	35.65	2.8	415	6	346.64	33.13	2.3	623	2.7	2.3	76.83	155.63
29	57.1	6	347.84	35.37	3.3	298	6	344.20	33.08	2.8	403	3.4	2.8	74.63	158.56
30	59.1	6	347.52	36.76	3.6	248	6	342.81	34.21	2.5	534	3.0	2.5	73.56	162.48
31	61.1	6	344.13	34.94	2.4	550	6	340.55	33.45	2.4	547	2.9	2.4	71.37	162.71
32	63.1	6	343.34	33.53	2.1	706	6	341.94	32.87	1.0	3068	1.2	1.0	72.53	160.37
33	65.1	6	351.47	30.25	2.8	431	6	349.31	30.59	1.8	1036	2.1	1.8	78.45	143.72
34	67.1	4	0.15	33.34	6.5	115	4	353.23	32.88	3.4	423	4.1	3.4	82.39	138.90
35	69.1	4	3.33	24.34	7.4	88	4	356.34	24.59	3.8	333	4.2	3.8	80.16	102.35
36	70.8	2	7.74	29.47	11	76	2	356.38	22.37	6.6	223	7.2	6.6	78.98	99.89
Lateral Specimens															
CJOP	59.1		346.55	53.12				348.30	35.81					Thermally Demagnetized at 200°C	
CJOT	59.1		346.36	56.63				346.38	32.11						

Notes: 1) All specimens were demagnetized to 55 Oe. 2) (NS) signifies that the mean is not significant at the 95 % confidence level.

3) N is quoted in parentheses where one or more specimen directions have been omitted from the computation of the AF mean for that cut.

4) * The VGP has not been considered in plotting out the VGP path or has been omitted entirely from the VGP plot.

Table 6 -11 a; AF Demagnetization of Pilot Specimen C32S.

Peak AF (Oe)	D	I	M (10^{-6} G) Total Moment	M/M_o
NRM	342.94	33.83	8.98	1.00
25	342.74	32.59	8.72	0.97
50	341.54	32.08	8.28	0.92
100	338.83	31.65	7.15	0.80
200	339.75	31.46	5.27	0.59
300	339.30	31.69	3.95	0.44
400	341.89	30.04	3.20	0.36
500	340.06	25.38	2.62	0.29
1000	347.10	22.17	1.26	0.14

Note to table 6 -11a & b; M/M_o is the ratio of the cleaned remanence to the NRM

Table 6 -11b; Thermal Demagnetization of Lateral Specimens .

	Degrees C	D	I	M (x 10^{-6} G) total moment	M/M_o
	NRM	346.55	35.12	12.08	1.00
	100	347.09	32.74	12.11	1.00
	200	348.30	35.81	9.65	0.80
	300	352.03	36.69	6.15	0.51
C30P	400	338.47	32.58	3.71	0.31
	450	348.40	37.39	2.47	0.20
	518	340.67	56.14	1.14	0.09
	550	347.67	42.86	0.96	0.08
	600	19.89	-34.25	0.67	0.06
	NRM	346.36	36.63	14.58	1.00
	100	351.03	33.50	13.50	0.93
	200	346.38	32.11	10.81	0.74
	300	349.99	32.44	6.99	0.48
C30T	400	0.07	32.84	4.06	0.28
	450	333.17	44.17	2.94	0.20
	518	316.60	10.87	2.12	0.15
	550	308.72	36.25	1.78	0.12
	600	160.36	43.63	0.98	0.07

Table 6 -12; Isotope Activity Ratios and Dates of DAS2.

Cut No;	Distance from top (cms)	U (ppm)	Yields (%) U	Yields (%) Th	$^{230}Th/^{234}U$	$^{234}U/^{238}U$	$^{230}Th/^{232}Th$	Age ± 1σ error (Ka) Uncorrected	Age ± 1σ error (Ka) Corrected
1	1.2	0.70	34	38	0.007 ± 0.001	1.08 ± 0.02	1.8 ± 0.6	0.8 ± 0.1	0.1 ± 0.3
11	21.1	0.57	30	40	0.006 ± 0.001	1.11 ± 0.02	1.5 ± 0.5	0.7 ± 0.1	0.0 ± 0.3
18	35.2	0.65	16	34	0.015 ± 0.002	1.08 ± 0.03	1.2 ± 0.6	1.6 ± 0.2	0.5 ± 0.5
26	51.1	0.42	66	74	0.013 ± 0.002	1.06 ± 0.02	3.6 ± 1.4	1.5 ± 0.2	0.9 ± 0.4
34	67.1	0.54	63	78	0.030 ± 0.003	1.09 ± 0.03	3.1 ± 0.8	3.3 ± 0.8	1.7 ± 0.7
base (old)	72	0.43	76	73	0.058 ± 0.004	1.07 ± 0.02	2.2 ± 0.3	6.5 ± 0.4	2.1 ± 0.9

Notes; " Old " refers to data obtained from a low resolution , high background detector. The remainder were obtained with a high resolution, low background detector.

centre slice, show a hole up the middle together with cusp-shaped growth layering (plate 6.5). At various points along the hole are quartz grains either loose or cemented into the calcite. What appears to have happened is that the drip splash has failed to dislodge sand grains from the cap area, while the stalagmite has continued to grow. Instead the splash has merely agitated the grains in such a way as to leave behind a more or less vertical work-hole. At several points the grains have become cemented by the calcite but the process has been repeated higher up. Once the work-hole was established it was possible for successive floods to replenish the abrasive grains.

Due to the sectioning procedure some cuts had only one basal plane for measurement of the vertical component of magnetization. These are 1, 9, 10, 18, 19, 27, 28 and 36.

6.5.2 The Paleomagnetism of DAS2

The NRMs, AF-cleaned directions and VGPs of the DAS2 record are presented in table 6.10. The AF-cleaned directions are plotted against their position in the stalagmite in figure 6.7, and figure 6.8 is the plot of the VGPs.

Table 6.11a shows the behaviour of pilot specimen C32S to AF demagnetization. Up to the 100 Oe step there is movement of the vector away from the modern field direction, after which the cleaned direction stays approximately constant to the 400 Oe step. The low

coercive force part of the NRM is probably a VRM acquired in the modern field. It is probable that any movement after this latter step is due to the introduction of small ARMs.

Unfortunately many specimens had low intensity NRMs. For example, specimens from cuts 3, 4 and 5 had total moments of about 12×10^{-7} G down to 1.2×10^{-7} G. The NRMs of one or two of these specimens were anomalous when compared with others of the same cut. For example specimen B4Q had an NRM direction of $D = 24.6^{o}$, $I = -15.2^{o}$ which is contrasted with a direction of $D = 23^{o}$, $I = 31^{o}$ of the other 3 specimens. This may be to do with loose black speckly material which was seen to coat holes within these specimens.

For specimens of those cuts which show detrital banding the total moments had intensities ranging from 16×10^{-7} to 10^{-5} G. Specimens of cuts 23 to 25 had low intensity and specimens of cut 26 were especially low (from 1.4×10^{-7} to 6.1×10^{-7} G). The intensities of cut 33 were high and range from 1 to 2×10^{-5} G.

Because of the low intensities of quite a number of specimens a general AF cleaning field of 50 to 55 Oe was chosen. This was a compromise between adequately removing the low coercivity VRMs and at the same time leaving a sufficiently measurable magnetization above the noise level of the magnetometer. It was also intended to carry out ARM experiments involving AF demagnetization of this speleothem (see chapter 8), using AF steps from 100 Oe upwards. Therefore a lower cleaning field was adopted so as not to influence the higher coercive force magnetizations. In view of the

apparently anomalous directions in some cases the low intensity specimens were not stacked for the measurement of their cleaned directions.

There was a positive correlation between the density of the detrital banding and the total magnetic moment. In addition the thin section showed that opaque grains and organic muck were closely associated along growth layers. The inference is that the magnetization of those specimens having a higher intensity was undoubtedly due to the detritus deposited by the floods. In order to test whether the detrital magnetization was the cause of possible depositional errors, two lateral specimens were measured using the magnetometer. If depositional errors existed then it might be expected that the magnetization directions would be different from those of specimens from the central drip areas. The specimens were chosen for their high detrital content. They were C30P and C30T, taken from opposite sides of slice C of cut 30. The NRMs and thermally cleaned directions (table 6.11b) were in accord with each other and with the directions from the central specimens, (Changes of direction after about 300°C are likely due to artificial TRMs imposed by the apparatus - see section 7.2.2). It is therefore concluded that there are no directional errors due to the deposition of ready magnetized grains from the flood laid detritus.

The specimen directions for each cut have been statistically combined as though they came from a random distribution. This is obviously not true in some cases where it can be seen that directions from specimens near

the curved edges of the cut lay between the very central directions and the directions of the succeeding cut*. This has probably not affected the cut mean significantly but the distribution about the mean is probably an ellipse rather then a circle (see section 2.5.3).

Where an AF-cleaned direction of a specimen has not fallen within the α_{95} of the cut mean it has been omitted in order to obtain a second mean. The first mean and the error bars are shown in figure 6.7 . The second mean is drawn as ⊗ , but the error bars have been omitted from figure 6.7 for clarity. The precision of the mean has improved considerably for most cuts treated this way. The original α_{95} s of cut 3 and 5, AF-cleaned, were large though still significant at the 95% confidence level.

In plotting the VGPs (figure 6.8) the second improved means have been used, but the VGPs of cuts 3, 9 and 24 have been omitted. Further, in constructing the VGP path the VGPs of cuts 5, 7, 15, 17 and 19 have been either lightly considered or not considered at all. This subjective approach was made in order to produce what was thought to be a more realistic path in the light of better defined path segments seen in this and other records.

The fresh appearance of the top and the age data (see next section) suggests that the top is modern , (the direction of cut 1 would, of course, be somewhat older).

* Individual specimen directions of DAS2 have not been presented in the thesis for the sake of brevity.

Figure 6 - 7; Paleomagnetic Directions and Dating of Sample DAS2.

Notes; 1) The specimen directions lying outside the α_{95} of the first mean have been omitted in order to obtain the second mean denoted by ⊗ : the error bars of the second mean have been omitted from the figure for the sake of clarity.

2) The large error bars for cuts 3 and 5 have been omitted from the figure for clarity.

3) The best fit constant growth line was obtained from the 6 data points with the additional constraint that the top is modern, ie. age of top = 0.0 Ka.

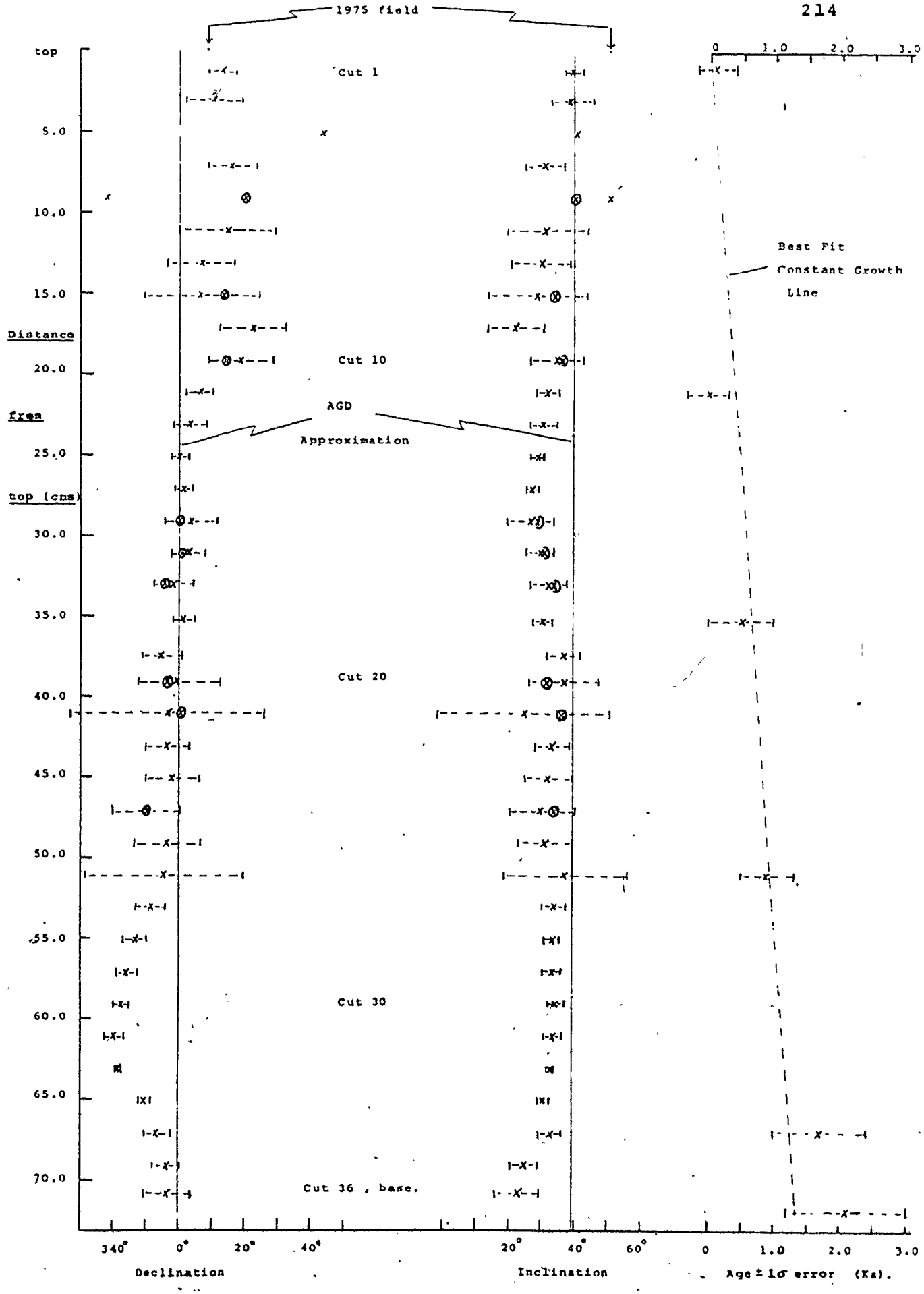
1975 field
top
5.0
10.0
15.0
Distance
20.0
from
25.0
top (cms)
30.0
35.0
40.0
45.0
50.0
55.0
60.0
65.0
70.0
Cut 1
Cut 10
AGD
Approximation
Cut 20
Cut 30
Cut 36 , base.
Best Fit
Constant Growth
Line
0
1.0
2.0
3.0
340°
0°
20°
40°
20°
40°
60°
0
1.0
2.0
3.0
Declination
Inclination
Age ± 1σ error (Ka).

In figure 6.9 the path segment from cut 1 to the 1975 VGP has been completed with a dashed line.

In considering the precision of the means, the best defined segments of the VGP path are from cut 36 to 27, from cut 16 to 11 and cut 2 to 1.

6.5.3 The U-Th Dating of DAS2

The U/Th activity ratios and dates are plotted against position in figure 6.7 .

An initial test date was carried out on the base of DAS2 in 1979 using a detector of high background and low resolution. The data, corrected for detrital thorium is about in accordance with the newer more reliable data. It has been included in the derivation of the growth rate estimate.

Uranium concentrations ranged from 0.4 to 0.7 ppm, - about the same range as for DAS1 (table 6.9).

Because of the low age of the sample the $^{230}Th/^{232}Th$ activity ratios are necessarily low. Inevitably this has meant fairly large shifts in the corrected ages, and such large shifts are more susceptible to error if the value that is chosen for the $(^{230}Th/^{232}Th)_0$ correction is wrong (it is normally fixed at 1.5 in the McMaster procedures). In particular cut 34 was shifted from 3.3 to 1.7 Ka and the data for the base was shifted from 6.5 to 2.1 Ka. The corrected dates are in agreement with the growth trend from the remaining four dates alone, though slightly older than is predicted by the constant growth curve. This is not unexpected since many stalagmites must

necessarily have a slow early growth rate considering that feedwater drip rates must start from zero before they become established at some higher value. In addition to these two corrected dates the correction shifts for cut 1 (0.8 to 0.1 Ka) and cut 11 (0.7 to 0.0 Ka) indicate that 1.5 is a realistic estimate of the correction factor. (See sections 4.7.3 & 9.4.2.2 for further discussion).

Only the simplest assumption of a constant growth rate is warranted by the corrected age data. In obtaining a linear least squares fit it has been assumed, in addition, that the top is modern; ie, the least squares fit utilized 7 data points including a zero intercept on the age versus length plot.

Cut 11 is out of stratigraphic order with the other six data points. The error bars of cut 11 fall on the constant growth line at about the 75% confidence level; it has been retained in the constant growth rate estimate. The linear least squares fit to the seven data points gave:

1) A growth rate of 0.019 ± 0.005 Ka per cm (19 years per cm),
2) The growth interval and the age at cut 36 is about 1.3 Ka.

As mentioned earlier, the two dates of cuts 36 and 34 suggest that perhaps growth started earlier at about 2 Ka. This possibility may be open to test with further radiometric analyses. Elsewhere variations in diameter may represent variable growth rates but a test of this may not be amenable to U/Th radiometric age analysis in view of the precision that would be required.

Figure 6 - 8 ; VGPs of DAS2.

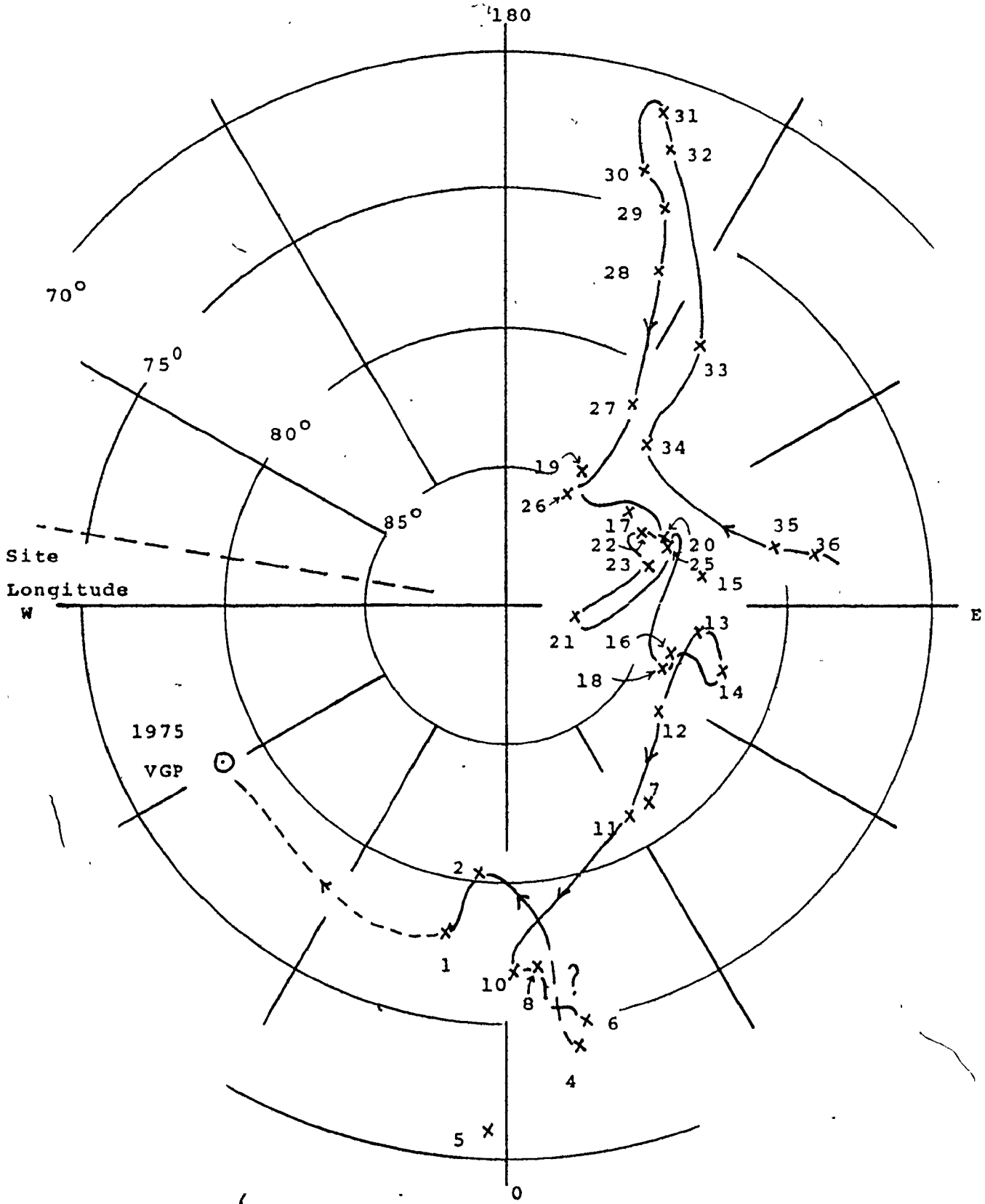

The numbers denote the cut and the arrows denote the direction of VG polar movement with time. ---completes the path from cut 1 to the present day field VGP.

6.5.4 Geophysical Interpretation of the DAS2 Record

6.5.4.1 Introduction

From figures 6.7 and 6.8 the following features stand out:

1) The inclinations are consistently shallower than I_{agd}, mostly within a range of values around 32° ($I_{agd} = 39.1^{\circ}$).
2) Most of the field change is in declination.

In detail the field changes are:

3) Far-sided VGPs describe a left-handed path
4) This is followed by abrupt change and long swing back to a pole position opposite the site longitude thus producing a hairpin loop.
5) There appears to be at least one, and possibly two, pauses in SV, followed by
6) A resumption of right-handed movement and slowly steepening inclinations (more near-sided VGPs).
7) Near the top of the record there may be another pause in SV.
8) Completion of the path to the modern day VGP involves near-sided movement and steepening inclinations.

(From earlier considerations, section 6.5.1, there are no reasons for believing that the shallow inclinations are due to systematic errors of the recorder).

The overall appearance of the record, as with DAS1, is of a VGP path which is far-sided and approximately orthogonal to the site longitude.

Table 6 - 13; Field Directions and VGPs at Latitude 22° N.

Direction at longitude	D	I	VGP No.	VGP at longitude -100° (W) Lat.	Long.
-100 (W)	8.5	50.0	1	78.4	-60.9
-120	11.0	45.0	2	79.0	-36.7
-140	11.5	42.0	3	79.2	-24.2
-160	11.5	39.5	4	79.4	-14.3
180	10.0	34.0	5	80.0	7.9
+160 (E)	4.0	27.0	6	81.4	53.1
+140	-1.5	26.0	7	81.6	90.0
+120	-2.0	27.0	8	82.2	94.4
+100	-0.5	27.5	9	82.6	83.8
+80	-1.0	28.0	10	82.8	87.8
+60	0.0	30.0	11	84.1	80.0
+40	+1.5	29.0	12	83.3	67.4
+20	0.5	26.0	13	81.7	76.6
0	-5.5	25.0	14	79.7	111.5
-20 (W)	-13.0	30.0	15	76.4	146.6
-40	-18.5	41.0	16	72.9	-181.5
-60	-14.0	51.5	17	74.0	-147.8
-80	-0.5	52.5	18	78.9	-102.2
-100 (repeat)	+8.5	50.0	(1)19	78.4	-60.9

The field directions are taken from round the world at latitude 22°, and the VGPs are reckoned at longitude -100° assuming constant westward drift. (Directions are taken from World Magnetic Charts, (1975 ,1976)

Figure 6 - 9; Earth's Field Directions at Latitude 22° N, a Westward Drift Construction.

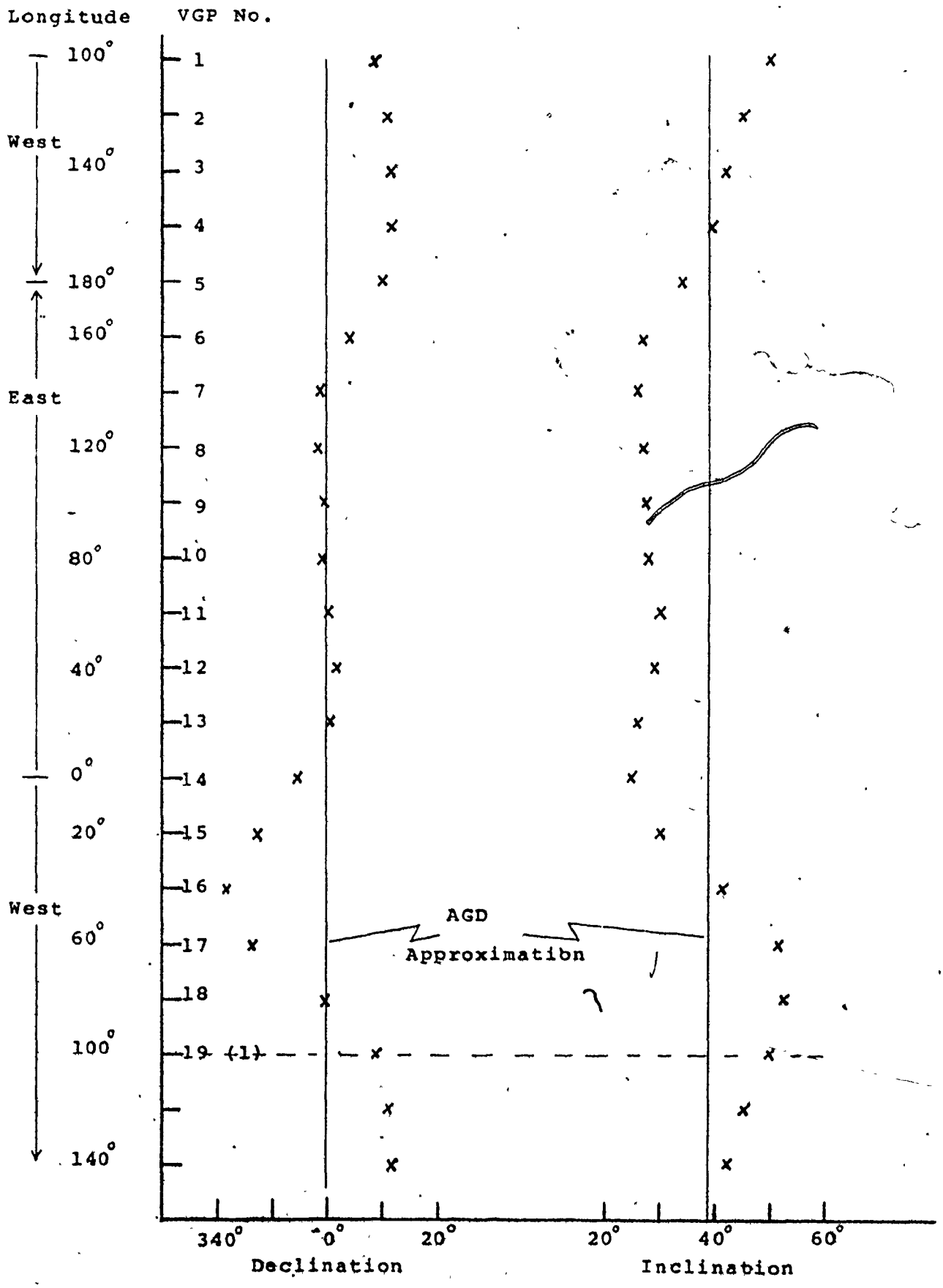

Figure 6 - 10; VGPs from the present field drifting past longitude -100°.

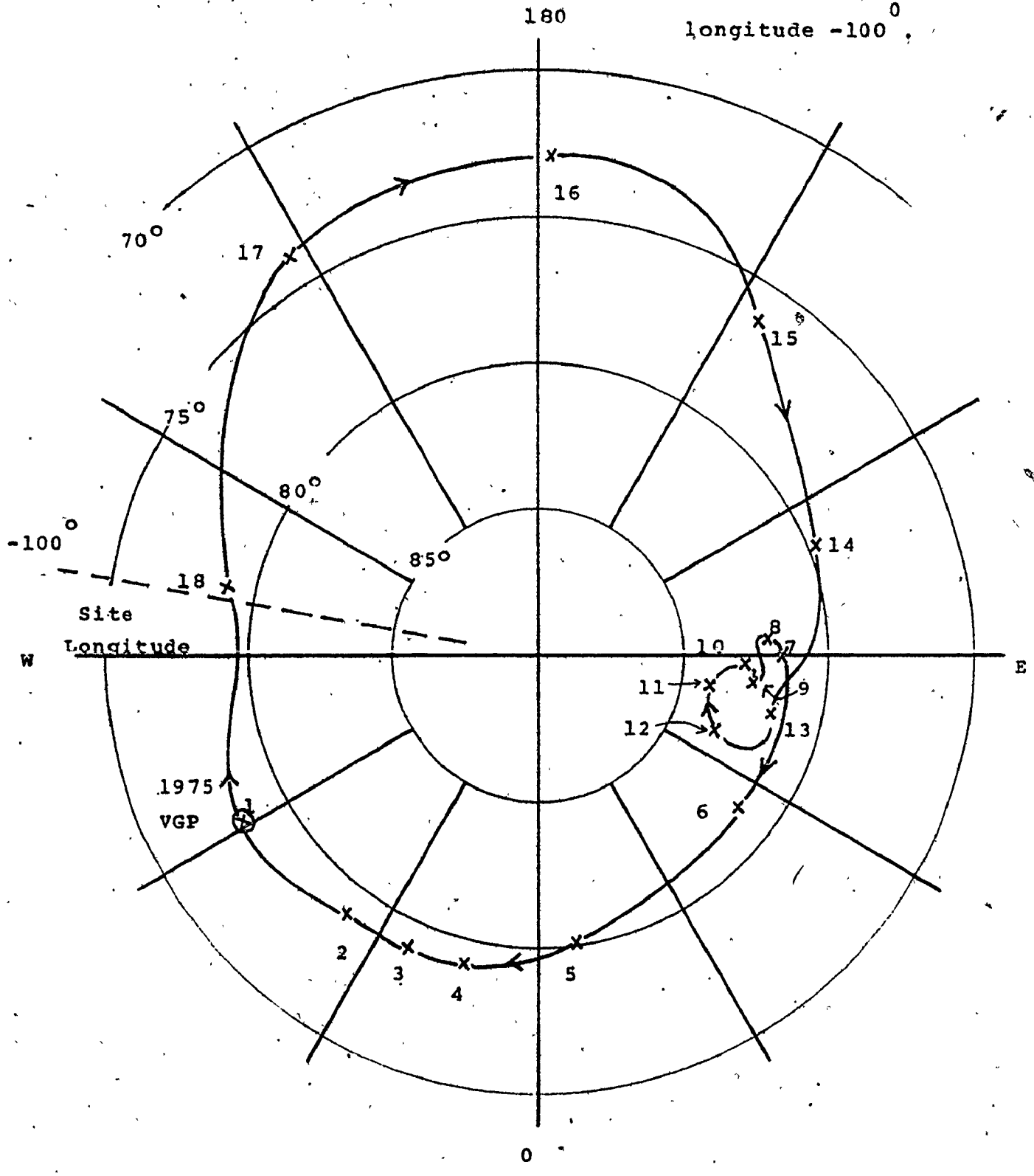

VGP numbers correspond to table 6 - 12. Arrows denote VG polar movement with time for a " 1975 " field which has drifted constantly westwards past -100°, and at latitude 22° N.

6.5.4.2 Comparison of the DAS2 Record with a Westward Drift Construction

Bullard et al (1950, op cit) estimated that present day geomagnetic field elements Y (east) and Z (vertical), at latitude 20^{o} N were drifting westwards at a rate of about $0.24^{o}\ a^{-1}$; the X (north) component had a westerly drift rate, somewhat less, of $0.11^{o}\ a^{-1}$. Similarly the large westerly declinations observed in the Atlantic region at these latitudes are drifting westwards at about $0.24^{o}\ a^{-1}$. A global cycle in declination would therefore be completed in about 1500 a, if this rate was maintained.

In order to compare westward drifted declination or inclination with the DAS2 record, modern values of D and I were tabulated longitudinally as though they had drifted westwards past the DAS2 site at 100^{o} W and latitude 22^{o} N. The D and I values, estimated to 1^{o}, were taken from the 1975 world magnetic charts (1976, op cit). They are numbered and plotted against their original longitude in figure 6.9, and their VGPs have been plotted in figure 6.10 . This construction corresponds to a drift of the non-dipole field and a precession of the dipole axis, both at the same angular velocity. Although this is not the case even for the modern field (see sections 1.3.2 & 9.8.5) it is used here for ease of comparison.

A comparison of the DAS2 record with the westward drift construction shows that:

1) The declination changes are remarkably similar in that:
   a) there is a westward swing out to about 340^{o}, which is followed by,
   b) a long period of little change at around 0^{o}, which

is followed by,

c) an eastward swing for a long period.

2) Differences in the two sets of declination values are:

a) the declination at the very base of DAS2 is more westerly. This is probably a real difference rather than being due to a more frequent sampling of the field by fast calcite deposition.

b) in the DAS2 record the first pause in SV is in two stages rather than in a single stage, (cut 26 to about cut 20 and cut 18 to cut 12). It is probable that the earlier apparent pause merely represent an increased growth rate for the stalagmite, (see section 6.5).

c) the pause in easterly declination in the DAS2 record is a bit longer than in the construction of figures 6.9 or 6.10 . Again there is some evidence to suggest that this may be due to an increased growth rate for the stalagmite.

3) The match in inclination variations between the two sets of results is not as close as for the declinations. In particular, at the base of DAS2 the inclinations are far shallower than in the construction. Only after the westward declination feature has passed do the I values begin to match up.

4) If the geomagnetic field features grow or decay, then one would expect that, going back into the past, the DAS2 record and the westward drift construction should match closely and then, perhaps, match less and less. It is obvious , in comparing the two VGP paths that there is an imperfect match at the

young end of the record (in the DAS2 record this corresponds to cuts 1 to 10, or back to about 300 or 400 a BP.) One reason is that cut 1 does no record just the latest field, but effectively a somewhat earlier one. At the present westward drift rate of $\approx 0.24^{o}\ a^{-1}$ VGP number 2 of the construction would have occurred about 83 a BP, and corresponds more to cuts 1 to 4. Secondly the region of cuts 10 to 3 may have been faster growing as discussed earlier, and combined with the poorer quality signal, has caused poofer match.

From longitude 0^{o} to 180^{o} on the VGP diagrams the match is good including the pause in SV between 60^{o} and 90^{o} east. But earlier than this the two sets of VGPs are less matched mainly because of the inclination differences mentioned earlier (see section 9.8.5 for further discussion).

5) If the present westward drift continues for about 350 years then the large westerly declinations, now seen in the Atlantic region, will pass the DAS2 site once again. In fact the zero of declination will be due in only 80 to 90 years time, and by about 100 to 150 years from now the whole DAS2 declination cycle will have been completed. The overall period from the DAS2 radiometric data plus the 100 years needed for completion is thus 1.3 + 0.1 = 1.4 Ka. This is well in accord with the declination cycle period deduced from the drift estimates of Bullard,et al. From the DAS2

radiometric data or from the rate estimates, the range in period is probably between 1.1 and 1.7 Ka. (The average drift rate for Y and Z components of all latitudes, from Bullard, et al, was 0.19 ^{o} a $^{-1}$, giving an overall cycle time of about 1850 years).

In summary, a combination of the DAS2 record and the westward drift construction, as observed at latitude 22 ^{o} N, show that a geomagnetic field feature, chiefly in declination, has circled the Earth in a period of about 1.4 Ka. The associated inclinations were considerably shallower when this feature made its earlier pass of the Central American region.

A unique explanation of these observations must await the constraints supplied by contemporaneous records from other regions. An explanation may lie between the following extreme possibilities:

1) A westward drifting non-dipole feature has shifted latitude in circling the earth; the main dipole was essentially fixed in magnitude and direction,

or 2) a zonally-constrained non-dipole field was superimposed upon a changing main dipole field. The changes may include southward shift, tilting, or decreases in intensity.

Comparison of the DAS2 record with other records and further discussion of implications to the study of the paleomagnetic field may be found in chapter 9.

CHAPTER 7

THE ROCK MAGNETISM OF SPELEOTHEMS

7.1 Introduction

The paleomagnetic measurement of the NRM of speleothems , its precision and its stability form a self-consistent study which is sufficient for declination and inclination estimates of the ancient field. The main objective of this thesis is achieved when corresponding dates by the U/Th method, have been assigned to these directions.

By themselves these measurements are insufficient to determine the nature and origin of the magnetization of speleothems. Various rock magnetic and other studies were therefore undertaken to ascertain the nature of the carriers of remanence and are described in this chapter. These studies were expedient rather than exhaustive, and the discussion is further limited in that only the briefest excursion into the principles of rock magnetism is possible and most of the apparatus used is not fully described.

For theory of rock magnetism see, for example Nagata (1961) or Stacey and Banerjee (1973). For descriptions of apparatus and the techniques in rock magnetism see, for example, Collinson (1975).

Detailed descriptions of the samples from which the specimens in this chapter were taken are given in chapters 4, 5 and 6. Some duplication in the description of specimens and their AF demagnetization characteristics

was unavoidable.

The use of anhysteretic remanent magnetization, ARM, to recover the ancient field intensity is discussed in chapter 8, but certain aspects of that study have implications for rock magnetism and are referred to here.

The paleomagnetic studies reported in chapters 4, 5 and 6 demonstrated that the NRM directions of speleothems did not show any influence from surface effects. The matter is also discussed in this chapter with further evidence being presented from the hysteresis experiments on the Eagle cave flowstone ENF.

Discussion of the origins of the NRM in speleothems, particular to some samples, follows the description of their rock magnetism. The overall discussion of the origins of NRM is left to the end of the chapter.

7.1.1 The Magnetic Mineralogy of Terrestrial Rocks

The minerals capable of carrying a magnetization in terrestrial rocks are;

Magnetite, and members of the solid - solution series, magnetite - ulvöspinel (Fe_3O_4 - Fe_2TiO_4).

Maghemite, a cation-deficient magnetite (γFe_2O_3).

Hematite, and members of the solid-solution series hematite - ilmenite (αFe_2O_3 - $FeTiO_3$).

Pyrrhotite, $Fe_{1-x}S$.

Oxyhydroxides of iron, such as goethite and lepidocrocite.

For a description of the oxide minerals and their magnetic properties see Rumble (1976).

Magnetite has an inverse spinel structure with

a spontaneous (ferri-)magnetization of 480 G cm^{-3}. The Curie point is 578 °C, which decreases with increasing Ti content. Maghemite also has spinel structure with about one ninth of the Fe positions vacant. Its spontaneous magnetization is 450 G cm^{-3} - nearly the same as magnetite. Its magnetic properties are therefore similar to those of magnetite. It converts to hematite at about 300 °C to 350 °C in an oxydising atmosphere and to magnetite when heated in a reducing atmosphere.

Hematite is canted antiferromagnetic with a spontaneous magnetization of 2.2 G cm^{-3}, which is much weaker than magnetite. The Curie point is 675 °C, decreasing with Ti content.

Goethite is imperfectly antiferromagnetic and is either superparamagnetic or weakly magnetic at room temperatures, depending on grain size and crystalline order. The same may be true of lepidocrocite, although little is known of the magnetic properites of either of these minerals. They occur in sedimentary rocks as weathering products and dehydrate to hematite upon heating above 350 °C.

7.2.1 Rock Magnetism and its Experimental Characterization

The magnetic properties of the grains of a particular mineral, such as stability (coercive force, H_c, field on ; coercivity of remanence, H_{cr}, field off), saturation magnetization ($J_{sat(s)}$, field on) and remanent magnetization after saturation (J_{rs}, with field off) are size dependent. Figure 7.1 illustrates this dependence.

Variation of Remanent Magnetization and Coercive Force with Grain Size for Magnetite.

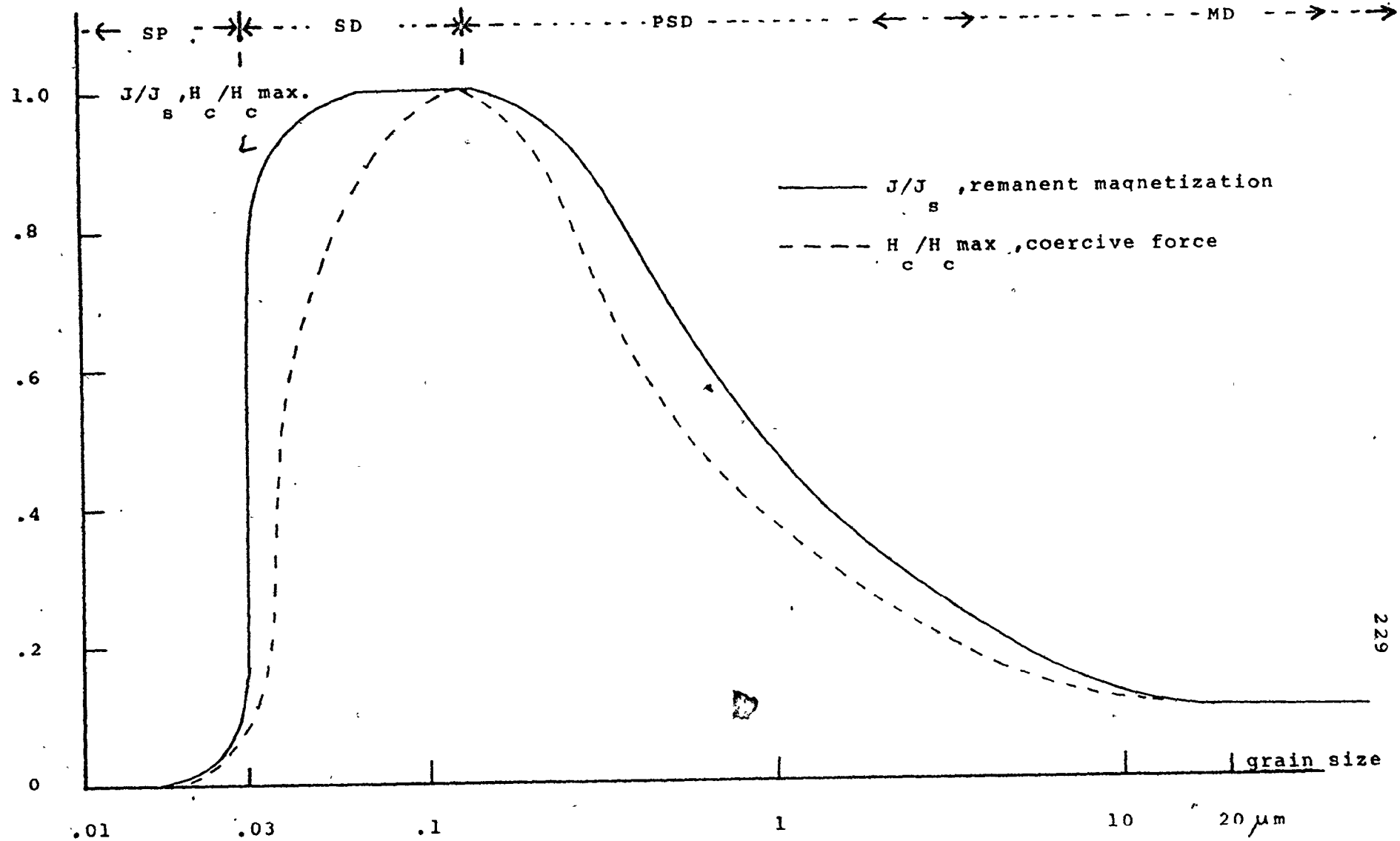

Figure 7 - 1.

There are three regions of stability and magnetization according to the grain size. When the grains are very small, at room temperature and with no external field, thermal activation is sufficient to randomise the small grain moments, and this is described as the superparamagnetic (SP) state. As the grains continue to grow the long range ordering of spins renders the thermal activation insufficient to rotate the spins of the domains en masse. The grains have now reached the stable single domain (SD) state. The energy barrier to a 180° flip of the spins from one easy direction to the other is often controlled by grain shape for magnetite. The domain spins may be flipped over by applying a high enough field (coercive force) or by raising the temperature above the blocking temperature, T_B.

As the grains continue to grow the self-demagnetizing field increases. The grain splits into two or more domains - the multi-domained (MD) state - so as to minimise the total energy.

The stability and remanence decrease as the grain size, and hence the number of domains, increase - up to about 17 μm for magnetite. Above this region stability and J_{rs} are constant. Many rock magnetists also recognise a region, from < 1 μm to about 10 μm, in magnetite, in which grains exhibit both SD- and MD- like properties, called the pseudo-single domain (PSD) state. The SD and PSD states are believed responsible for most primary stable remanences (eg, Evans, 1977). In magnetite the SD range is from about 0.03 to 0.5 μm (various estimates - see Day, 1977), and is therefore beyond the range of optical microscopy. Most rocks exhibit a spectrum of grain size,

and many rocks may also contain two or more magnetic minerals. Therefore there is often a spectrum of stabilities and other properties.

Various criteria have evolved to identify the mineral responsible for the NRM and to measure its stability as follows:

1) In routine magnetometry unstable components are present if the output changes during measurement or before and after long period storage of the specimen.
2) In AF demagnetization experiments:
   a) An unstable component is mainly present if the MDF of the NRM is < 150 Oe (this study), or is additionally present if M/M_o changes rapidly with low fields.
   b) The shape of the demagnetization curve for a single mineral is, in effect, a coercive force spectrum (CFS), which points to the domain state of the ensemble; MD grains are magnetically soft and have low coercivities, whereas SD grains are randomised mainly at higher fields (Dunlop, 1973). An estimate of the CFS may be made by plotting $\Delta(M/M_o)$ against field (Zijderveld, 1967). M_o in this case is the saturation isothermal remanent magnetization (SIRM; per cm or per gm).
   c) An appreciable remanence after 150 Oe indicates a stable component which is probably primary (There are two exceptions possible; one is 'hard' VRM in fine-grained hematite (eg, see Dunlop and Stirling, 1977), and the other is a pdDRM carried by fine-grained magnetite in sediments Neither of these are primary.)

Indices have been devized, with related criteria, to test for the AF or temperature stability of the NRM vector (eg, Briden, 1972). Zijderveld (1967) diagrams are commonly used to observe the movement of the vector upon demagnetization.

3) In hysteresis experiments (using large magnet and ScT magnetometer, vibration magnetometer):
   a) Magnetization M_s , M_{rs}, are obtained in fields of 2 - 3 KOe for magnetite, in $\geq$ 30 KOe for hematite.
   b) Coercivity of remanence H_{cr} for magnetite-bearing rocks usually ranges up to 500 Oe or less; for hematite it ranges up to several KOe.
   c) Kinks in the M - H curve may indicate that more than one mineral is present
   d) An ensemble of magnetic grains is considered stable of $H_{cr}/H_c < 5$ (Parry's rule; see Stacey and Banerjee, op cit, pp80 - 83), but as for demagnetization experiments, a rock with low overall stability may still posses a stable component useful for paleomagnetism.
   e) For an ensemble of entirely SD particles M_{rs}/M_s is equal to 0.5 . For MD particles $M_{rs}/M_s < 0.5$ and is typically < 0.3 . A ratio less than 0.5 usually results from a mixture of grain sizes.
4) In thermomagnetic and thermal demagnetization experiments:
   a) The Curie point, and to some extent the shape of the M - T (J_s - T; J_s= M/V) curve indicate the magnetic phase present. For example the Curie point for magnetite is 580 ^{o}C, for hematite 675 ^{o}C.
   b) Kinks in the M - T curve may indicate the

presence of more than one mineral or that a phase change has occurred. Repeating the expiment may help to decide between these two, since phase changes are usually irreversible.

c) Low stability components are lost at low temperatures. The thermal demagnetization curve is essentially a blocking temperature spectrum.

d) If the specimen is cooled in the Earth's field and acquires a substantially different magnetizion, then part or all of the magnetic mineral may have been converted to a new mineral upon heating.

7.2.2 The Experiments

1) AF demagnetization was carried out routinely on the NRMs of pilot specimens to an end point which varied from 250 to 1000 Oe, the limit of the apparatus. It reveals through the median demagnetizing field (MDF) the overall stability, and often the presence of low coercivity components. A more accurate estimate of the stability of the grain ensemble was obtained in four specimens, by AF demagnetizing their SIRMs. A coercive force spectrum up to 1 KOe was produced by plotting the differences in M/M_o ($\Delta M/M_o$) as a function of the field, $\tilde{H}$.

2) The first hysteresis experiments were carried out with a large electromagnet and the ScT magnetometer. The field was calibrated with a Schonstedt gaussmeter.

3) Later hysteresis experiments utilized a PAR vibration magnetometer. The rod leading from the vibrating head was screwed directly into each specimen to hold it in the field. This minimised the contribution from

the specimen holder to the total moment. The magnet was run with the field on and field off to obtain total isothermal and remanent moments. In order to obtain the total ferromagnetic moment the field was increased well beyond saturation (no hematite present; see section 7.4.1), so that the ensuing linear negative moment was due only to the perspex and calcite matrix. The diamagnetic moment of the perspex and calcite at every field setting could then be subtracted from the total moment to give the ferromagnetic moment. The negative half-cycles were obtained by rotating the specimen through 180^{o} to the field. Quoted values of H_c, H_{cr} and M_{rs}/M_s were averages from the two half-cycles.

4) Thermal demagnetization experiments were carried out in a field-free room using an inductionless electrical furnace. The field was nulled with trimming coils and tested with a low field gaussmeter. The temperature was calibrated by a thermocouple, which in turn, was used to regulate the current-temperature setting by a feedback circuit. Two or more specimens having different orientations were demagnetized together.

The apparatus was not entirely trustworthy, for the following reasons:

a) Appreciable gradients, of order 10γ over a few cms. were observed and could not be eliminated.

b) Checking the furnace after a heating cycle sometimes showed that fields of over 20γs had arisen.

c) There was some doubt, in the author's mind at any rate, about the faithfulness of the thermocouple-preset temperature device.

e) An attempt was made to impart an artificial TRM using windings on the furnace, and powered by a

Table 7-1 Summary of Rock magnetic and other tests

Sample and specimen	Origin	AF cleaned	Thermally cleaned	IRM Magnet and SCT	IRM Vib. Mag.	Mössbauer	Other
BJTL	Canada	A2T A3T B4R	C4U	B4X			cut 4 (AA) C4W, A3T (ARM) thin section
ENF	Canada	D2P D5R D6Q	C6R		D6R		D9R (ARM) thin section
VCCL	Canada	B12Q,B3Q B13Q,B23Q	B11Q B24Q				thin section
TS	England	B1Q B18Q		D7Q		(Yorks. cave soil)	B2P,B11P (ARM) thin section
DBS1	England			C4Q			
RCB	Bermuda	C2Q,C8R F3Q,D7R			B8Q soil	cut 8 (failed) soil	cut 2s8(AA) thin section
WCS1	Bermuda			C5P			(AA) & thin section
GQF1	Bermuda			C10S			
OULF	USA	C12Q			cut 1 soil	soil	
SJHS	Mexico	C1Q C14Q					B2Q,C4S,B11P (ARM)
SJLS	Mexico	B15Q				insoluble residue	B2Q (ARM) thin section
DAS1	Mexico	B10Q		B4Q			
DAS2	Mexico	C32S	C30P C30T		C17T		thin section (ARM see Ch. 8)
76GR3	Greece				3-1	3-1 soil	

Table 7.2

Summary of Magnetic Properties

The following notation and notes apply;

1) The NRMs are in units of 10^{-7} G cm^{-3}
2) MDFs, in Oe, are quoted for the NRMs. When quoted for the SIRMs they are in parentheses ( ). Using Danker's data it has been possible to estimate an average or range of grain sizes (G.S.) for magnetite from the MDF of the SIRM. The unit is the micron , μm.
3) H_{sat} is in KOe, whereas H_c and H_{cr} are in Oe.
4) Mte. is magnetite. Goethite (or lepidocrocite) is the most probable contender for the SP or the viscous components of OULF or RCB.
5) ENF has two sets of vibration magnetometer results. The first is for layers perpendicular (perpr) and the second is for layers parallel (parll) to the inducing field.

Table 7-2 Summary of Magnetic Properties

Sample	NRM	ppm Fe	MDF of NRM (of SIRM & GS)	Magnet & ScT H(KG) sat	H cr (G.S.)	Vibration Magnetometer H(KG) sat	H cr	H c	H cr /H c	J rs /J s	(G.S.)	Curie point	Minerals
BJTL	25-50	120	180-200 (95,20μm)	2	230 (10μm)							550-600	Mte
ENF	≈20		385-775 (190,<5μm)		perpr.	2-3	550	290	1.9	0.45)	(<5μm)	550-600	Mte
					parll. (see text)		590	390	1.5	0.44)			
VCCL	50-500		260-400									500-600	Mte
TS	0.4-2.5		235-400	3	350(<5μm)								Mte
DBS1	<0.2			2.5-3	350(<5μm)								Mte
RCB	14-200	50-700	90-140 (140,10μm?)			2-3	300	60	5	0.19	(<5μm?)		Mte
						(+ SP & fast decaying compts.)							(Goethite?)
RCB soil						2-3	150	22	6.7	0.15			Mte
						(+ SP & fast decaying compts.)							(Goethite?)
WCS1	<0.2	42?		2-3	280(5-10μm)								Mte
GQF1	1-5	6?		2-3	350(<5μm)								Mte
OULF	<0.2		60			2-3	50	SP compts?					Mte
													(Goethite?)
OULF soil						2	150	SP compts					Mte
													(Goethite?)
SJHS	20-760		165-200										Mte
SJLS	6-70		145										Mte
DAS1	0.4-3		210	2.5-3	295(5-10μm)								Mte
DAS2	0.4-18		255 (105,15μm)			2	210	35	6	0.18	(15μm)	550-600	Mte
76GR3	>50					14	1400	400	3.5	0.3			

constant current supply. The field, initially fixed at 0.50 Oe in the vertical direction, had dropped to 0.39 Oe after 700°C had been reached.

5) Atomic absorption (AA) analyses were carried out on a few specimens using iron standards made up in calcium carbonate solutions. Several of the early determinations were carried out on a Perkin Elmer 403 AA unit by Judith Johnson. She professed not to trust the results too much because of the low concentrations of iron being analyzed. Three determinations were carried out by the author using a Perkin Elmer 603 unit.

6) Several specimens were made up for Mössbauer spectroscopy, mostly from soils associated with the samples. They were prepared in their own soil matrix or in an inert BN_3 matrix and set in copper rings. Spectra were run at room temperature and at liquid nitrogen temperature by prof. Tom Birchall, and he also did the curve fitting and interpretation (appendix IV).

7) Several thin sections were prepared and studied by transmission and reflection optical microscopy (appendix III).

7.3 Rock Magnetic Properties of the Samples in Detail

7.3.1 BJTL

Paleomagnetism, 4.3

The NRM intensities ranged from 25 to 50 x 10^{-7} G cm^{-3}. The highest intensities corresponded to the opaque brown layers.

Figure 7 - 2

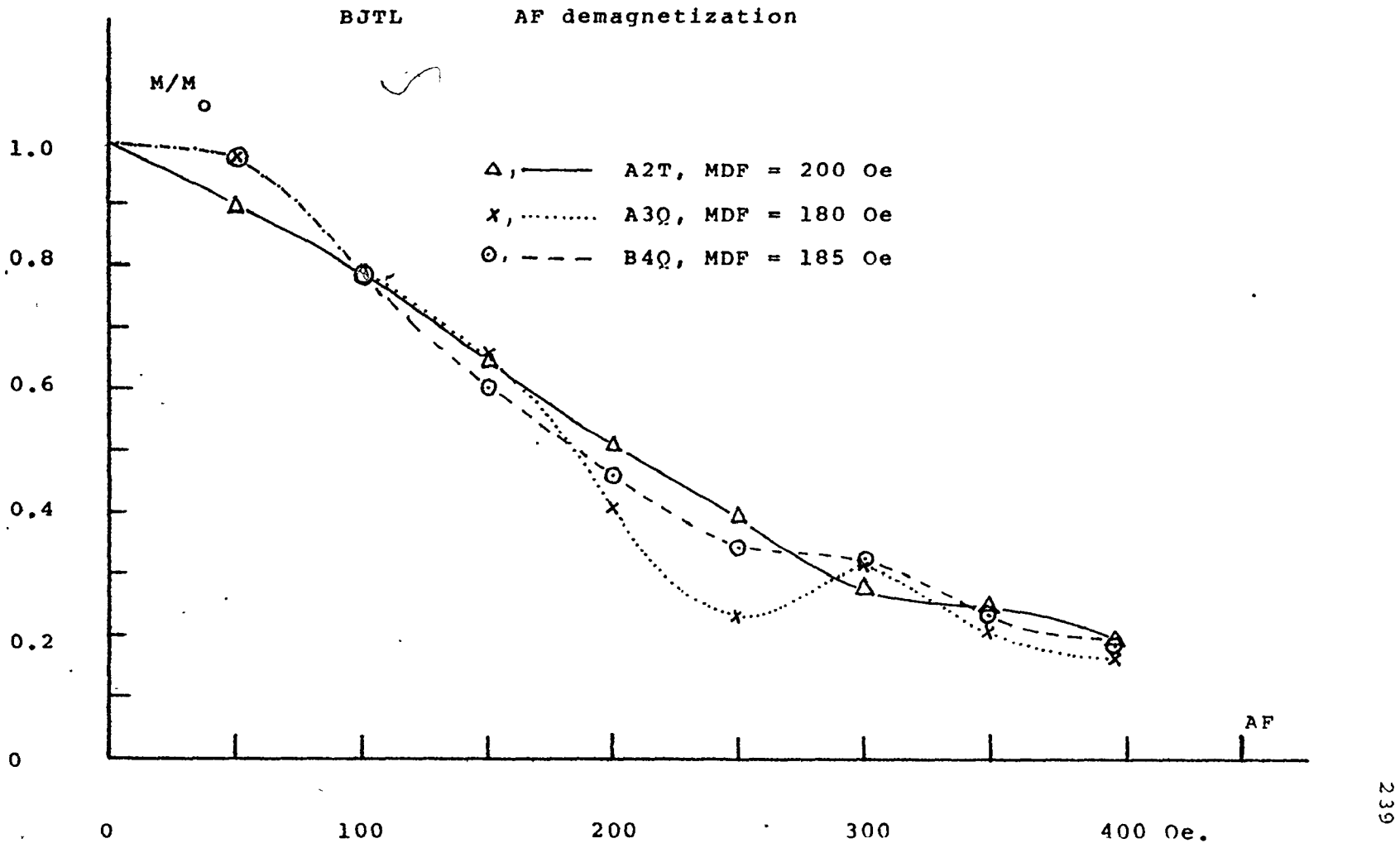
BJTL AF demagnetization
M/M o
1.0
0.8
0.6
0.4
0.2
0
Δ, —— A2T, MDF = 200 Oe
x, ... A3Ω, MDF = 180 Oe
⊙, - - - B4Ω, MDF = 185 Oe
AF
0
100
200
300
400 Oe.

Figure 7 - 3 ,

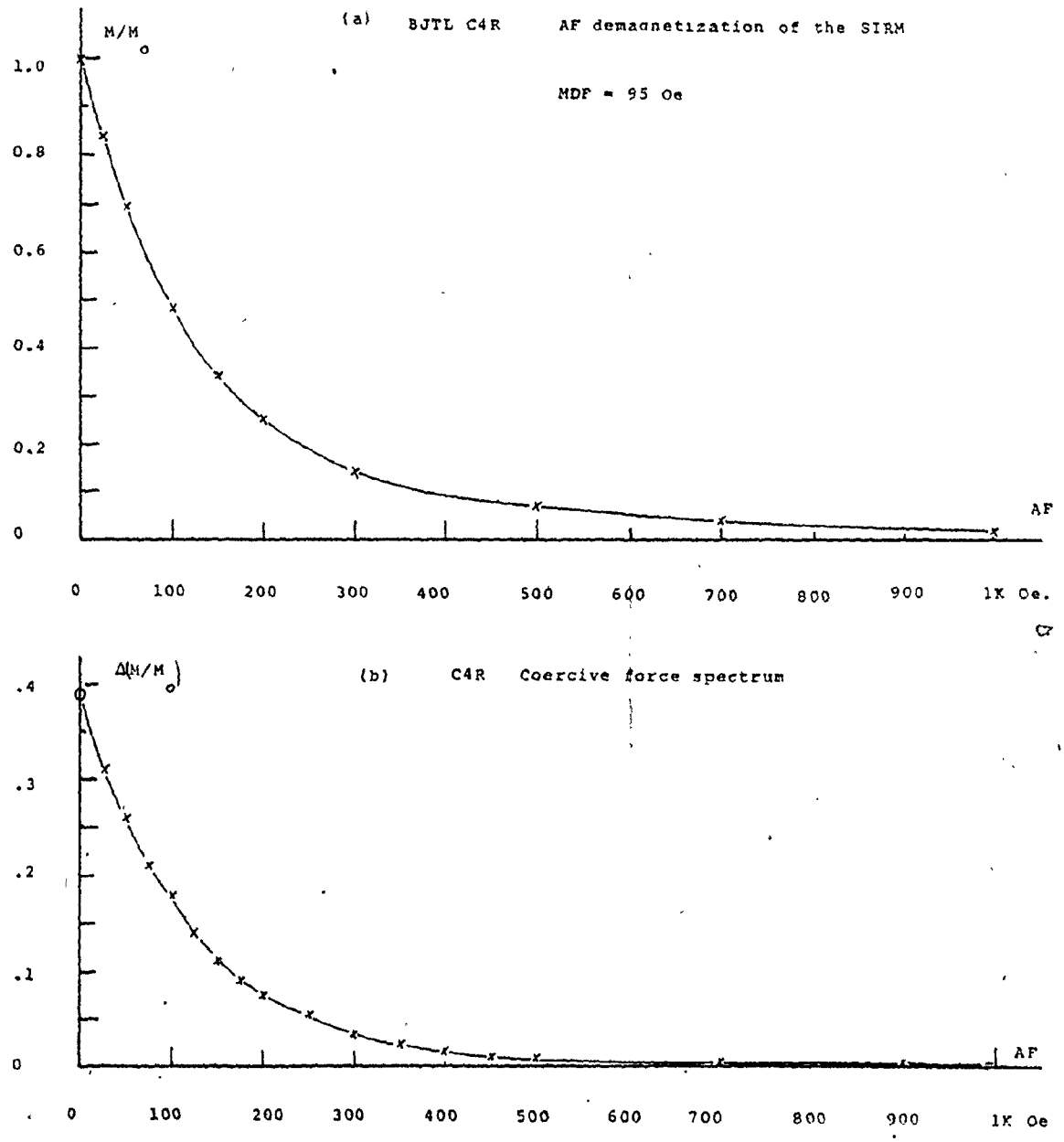
(a) BJTL C4R AF demagnetization of the SIRM
MDF = 95 Oe
M/M o
1.0
0.8
0.6
0.4
0.2
0
AF
0
100
200
300
400
500
600
700
800
900
1K Oe.
(b) C4R Coercive force spectrum
Δ(M/M o)
.4
.3
.2
.1
0
AF
0
100
200
300
400
500
600
700
800
900
1K Oe

Figure 7 - 4

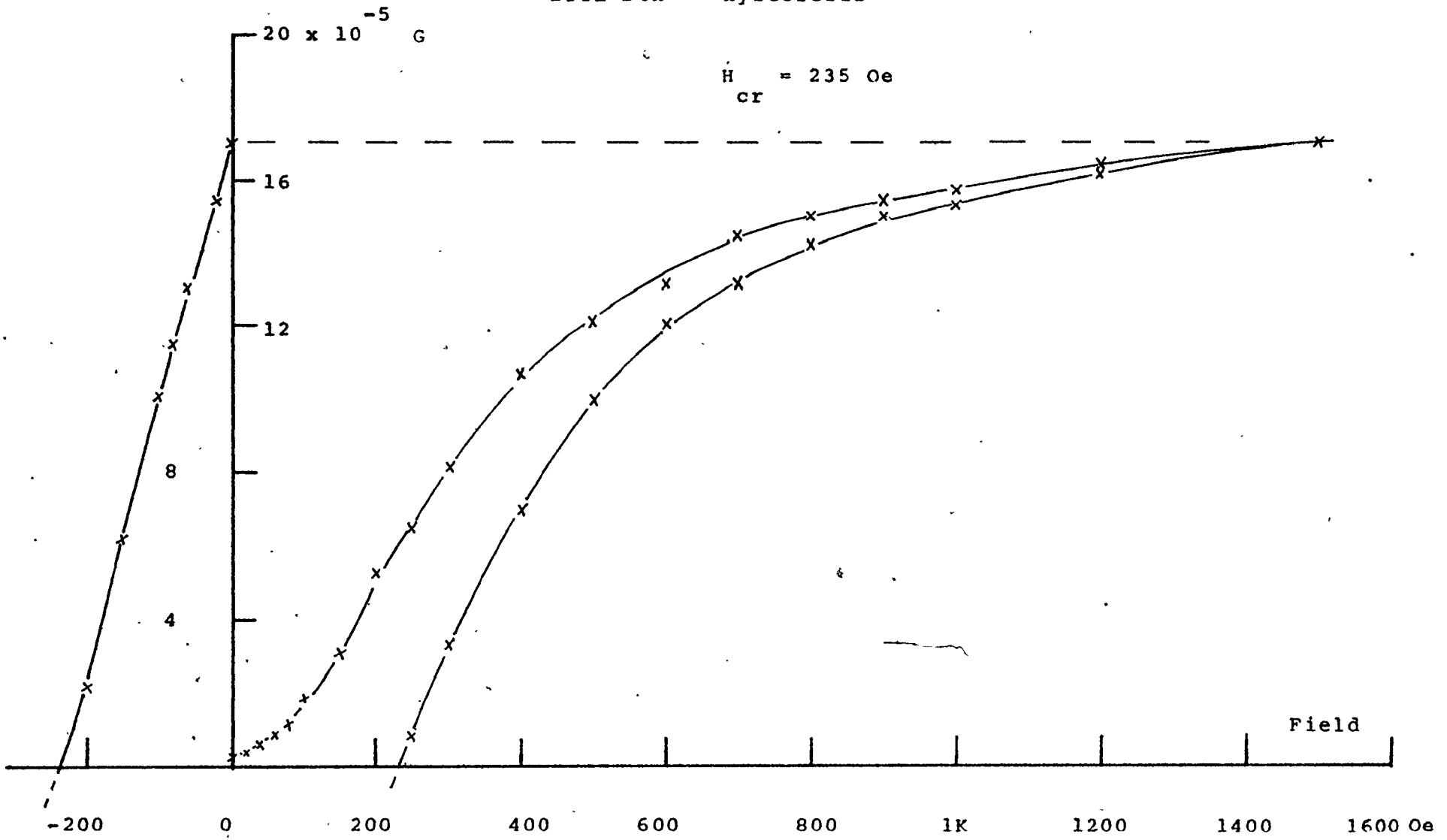
BJTL B4X Hysteresis
20 x 10 -5 G
H cr = 235 Oe
16
12
8
4
Field
-200
0
200
400
600
800
1K
1200
1400
1600 Oe

Figure 7 - 5.

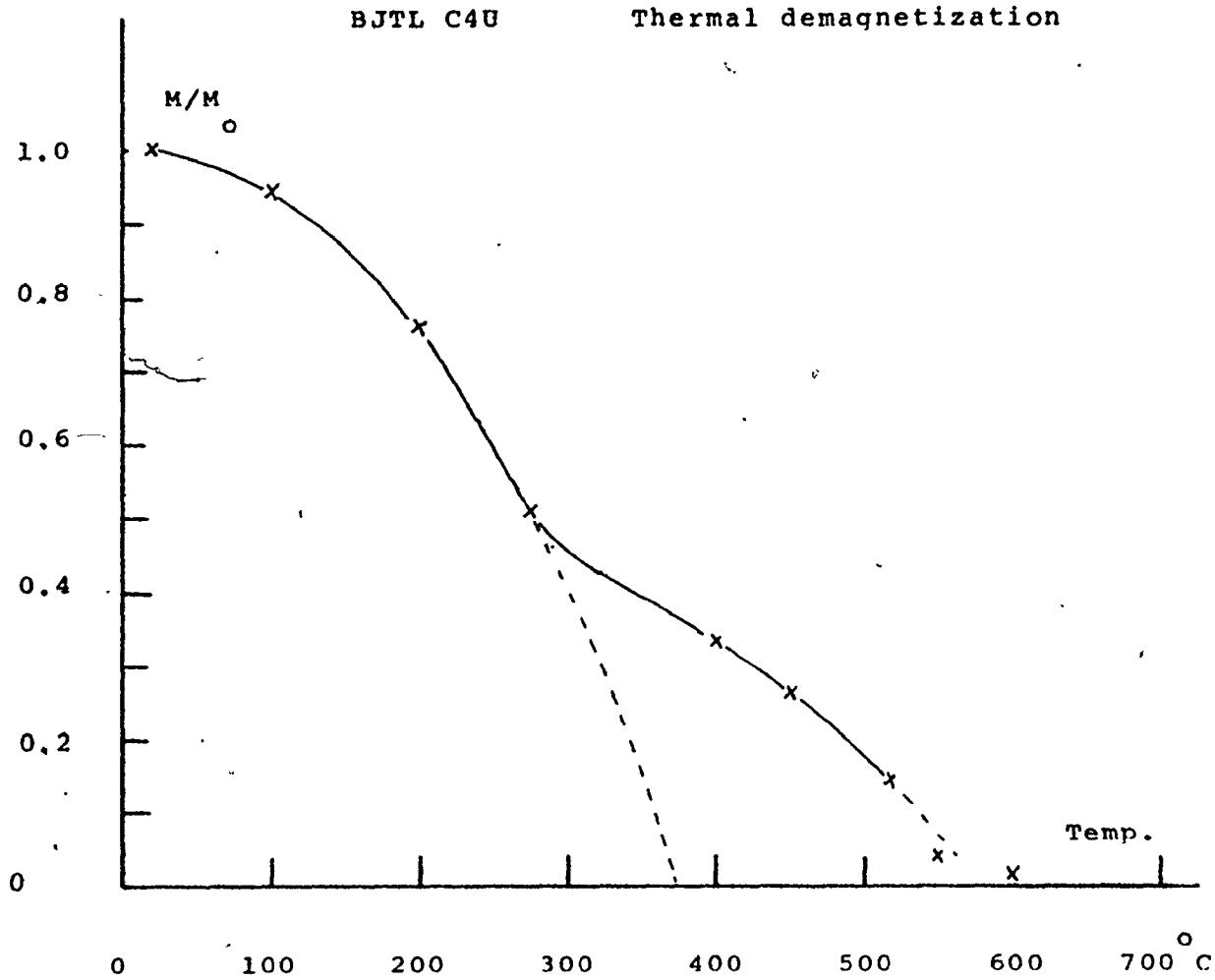
BJTL C4U
Thermal demagnetization
M/M
o
1.0
0.8
0.6
0.4
0.2
0
Temp.
0
100
200
300
400
500
600
700
o
C

Figure 7.2 shows the AF demagnetization of specimens from cuts 2, 3 and 4. The kinks in the curves around 200 to 300 Oe are almost certainly due to ARMs imparted to the softer grains by the apparatus. The MDFs of the NRMs ranged from 180 to 200 Oe.

It seems that one effect of giving an SIRM to these specimens was to reactivate (realign) low coercive force grains which had viscously decayed in the NRM. An example, shown in figures 7.3a and b, is the SIRM AF demagnetization and coercive force spectrum of a specimen from cut four. The MDF is now 95 Oe and the bulk of the spectrum (to about 10% of 'maximum') lies between 0 and 275 Oe. Thus the low components have been enhanced with respect to the high components and the MDF is only half of its NRM value. Furthermore the lack of any initial peak or shoulder in the coercive force spectrum indicates the predominance of MD over SD grains (D.J.Dunlop, pers com). However no opaque grains were large enough to be observed in the thin section.

Figure 7.4 shows the remanent hysteresis curve of another specimen from cut 4. Saturation was not quite obtained in a field of 1.5 KOe. The coercivity of remanence was 230 Oe, and the ratio of the NRM to the SIRM was about 0.02 or less.

Figure 7.5 shows the thermal demagnetization of C4U. The abrupt change in gradient at about 260 ^{o}C is thought to be an artefact of the experiment, as with other specimens so demagnetized. This is unfortunate because these results possibly hide a phase change from maghemite to magnetite, or the creation of new magnetic material (section 7.3.2.2). The best estimate of the Curie

point is 560°C to 570°C.

7.3.2 ENF

Paleomagnetism, 4.4

The NRM intensities of this compact uniformly opaque brown flowstone were around 20×10^{-7} G cm^{-3}, and it was reversely magnetized.

MDFs ranged from 385 Oe (eq, figure 7.6) to 775 Oe (single axis demagnetization).

Figures 7.7a and b show the demagnetization of the SIRM and the coercive force spectrum of D6R. The MDF was 190 Oe and the bulk of the CFS lay between 0 and 600 Oe. There is a peak in the spectrum at about 50 Oe; most of the magnetization is probably carried by PSD and SD grains. This sample showed the second greatest stability to AF demagnetization of the 12 speleothems tested in this study (see section 9.7.1, for the most stable sample!)

A comparison of the demagnetization of the NRM of D6Q (figure 7.6) with the SIRM of D6R (figure 7.7a) shows that the SIRM appears to have reactivated the low coercivity grains as was the case with BJTL. Using the data of Dankers (1978), these values of MDF and H_{cr} correspond to magnetite grain sizes of less than 5 μm.

7.3.2.1 Magnetic Anisotropy and Hysteresis Experiment

It is possible that the depositional fabric of speleothems is reflected in anisotropy of magnetic properties such as susceptibility. Elongated or platy magnetized

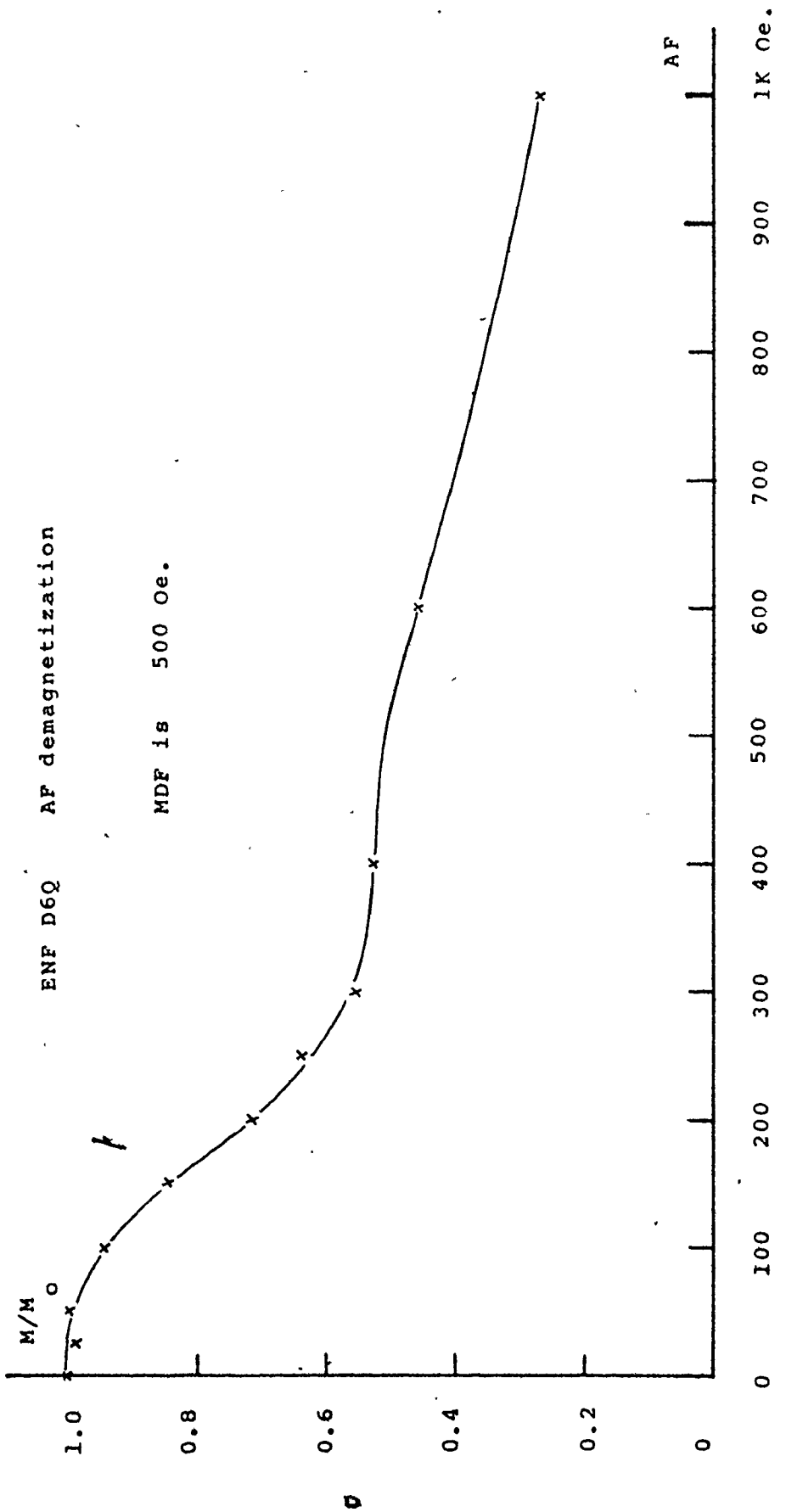
ENF D6Q AF demagnetization
MDF is 500 Oe.
M/M o
1.0
0.8
0.6
0.4
0.2
0
0
100
200
300
400
500
600
700
800
900
1K Oe.
AF

Figure 7 - 6.

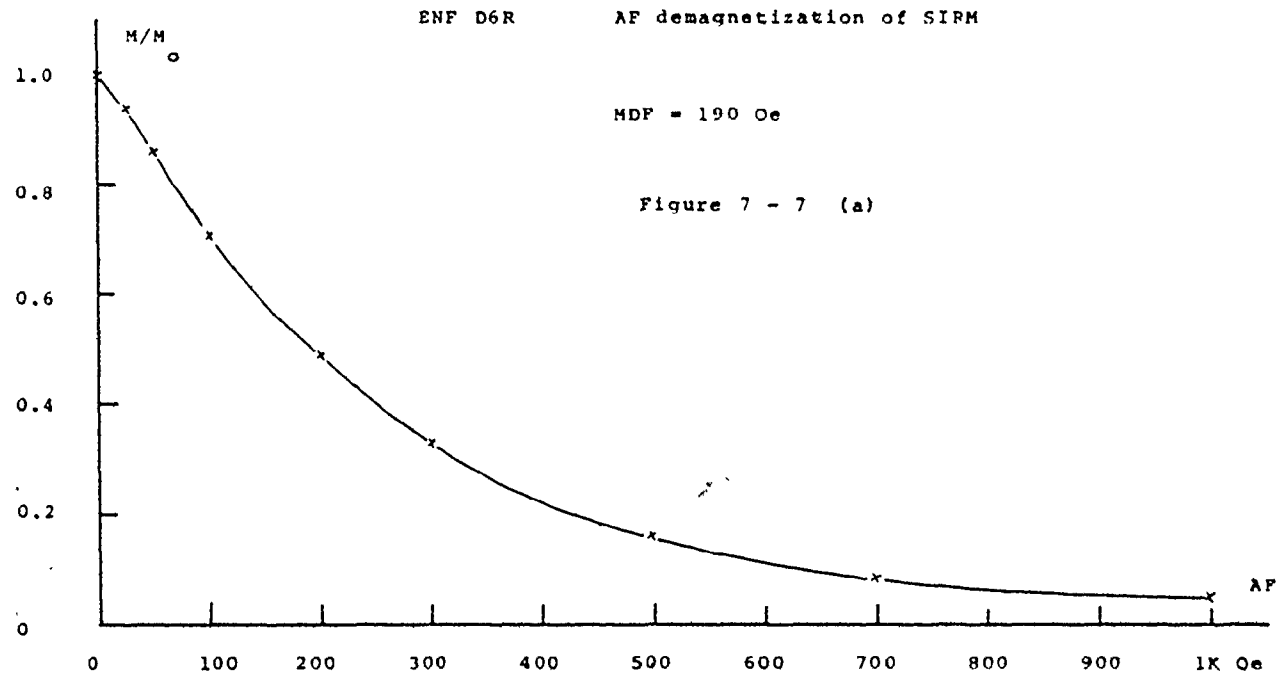
ENF D6R
AF demagnetization of SIRM
M/M
o
1.0
0.8
0.6
0.4
0.2
0
MDF = 190 Oe
AF
0
100
200
300
400
500
600
700
800
900
1K Oe

Figure 7 - 7 (a)

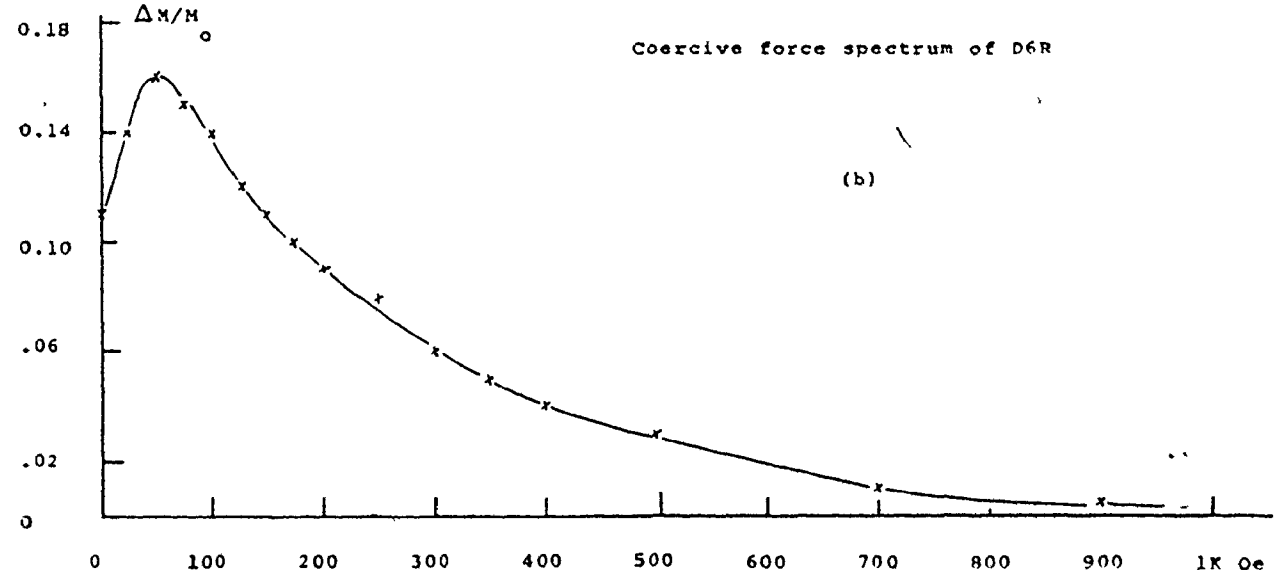
ΔM/M
o
0.18
0.14
0.10
.06
.02
0
Coercive force spectrum of D6R
(b)
0
100
200
300
400
500
600
700
800
900
1K Oe

Figures 7 - 8a and b;

Hysteresis curves of total induction and remanent magnetization of ENF D6R.
The upper curves are for growth layers held parallel to the field and the lower curves are for layers perpendicular to the field

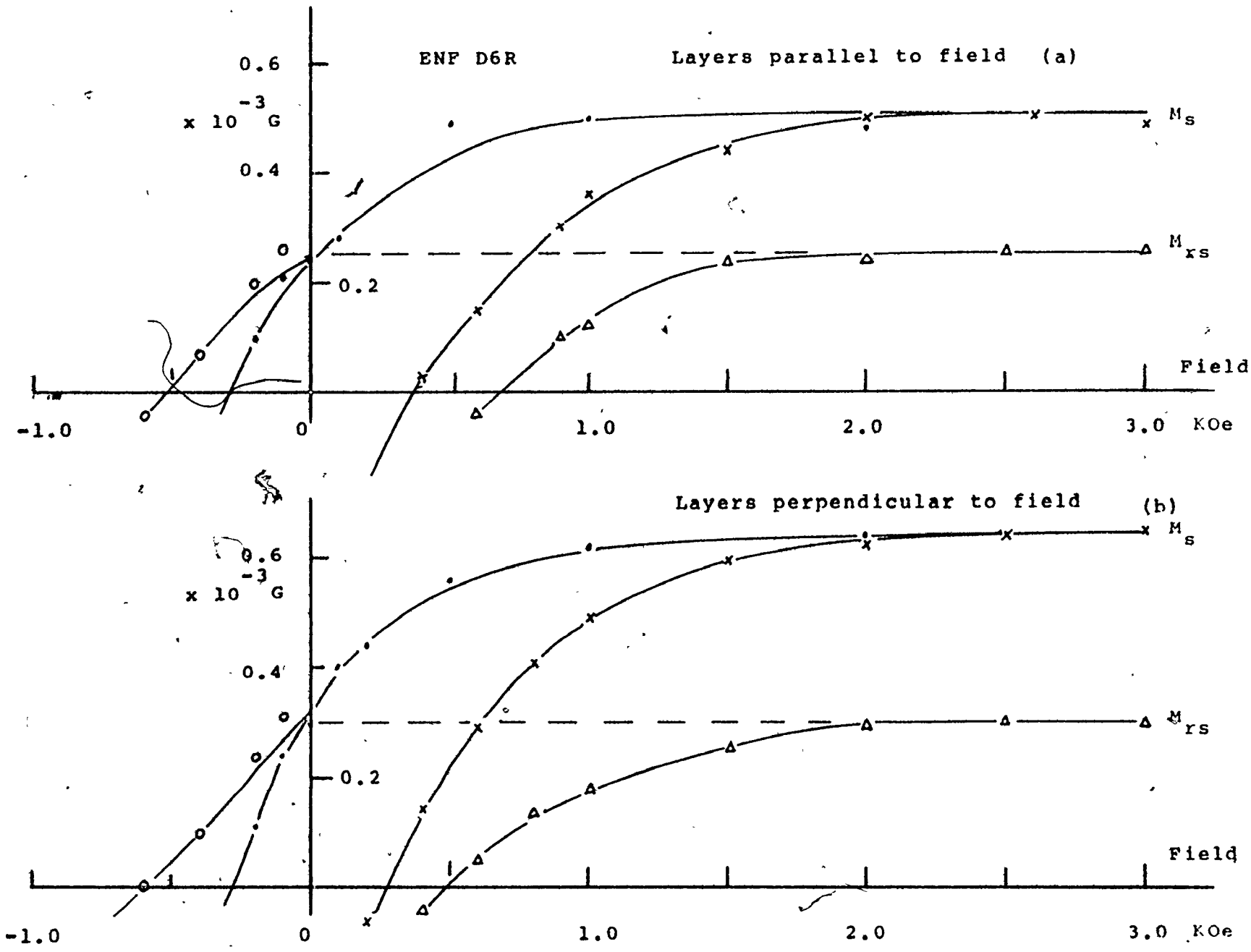
ENF D6R
Layers parallel to field (a)
0.6
x 10 -3 G
0.4
0
0.2
Ms
Mrs
Field
-1.0
0
1.0
2.0
3.0 KOe
Layers perpendicular to field (b)
0.6
x 10 -3 G
0.4
0
0.2
Ms
Mrs
Field
-1.0
0
1.0
2.0
3.0 KOe

grains, for example, may lie along the surface of deposition. Since the easy direction of magnetization is along the long axes of an ellipsoidal grain, the susceptibility is greater in the direction of grain alignment than in a perpendicular direction. (For susceptibility anisotropy and fabric studies in sediments, see, for example, Taira and Lienert, 1979). In view of the low intensities of most speleothem samples it was felt that weak field susceptibility measurements would not have been accurate enough for grain anisotropy studies. Instead hysteresis loops for fields parallel and perpendicular to the growth layers of ENF specimen D6R were obtained using the vibration magnetometer. The results are given in figures 7.8a and b.

The values of M_s from the parallel to the perpendicular orientation should be the same. Therefore the difference between the parallel value, 75×10^{-4} G (total moment) and the perpendicular value, 65×10^{-4} is a measure of the experimental error. It is about 15% . The corresponding values of M_{rs} are 3.4 and 3.0×10^{-4} G, and are not significantly different considering the 15% error in M_s . Any anisotropy of $\approx$15% would have a maximum deflection from the field direction of about 4^{o} (from a formula given in McElhinny, 1973, op cit, pp 66 - 67). Although this experiment is not proof it does give support to the findings discussed in chapters 4, 5 and 6 that depositional processes have not affected NRM directions.

The cause of the moment error was probably incongruent positioning of the specimen between the two sets of measurements.

The two values of M_{rs}/M_s of 0.44 and 0.45 is further evidence for a considerable SD and PSD component

Figure 7 - 9

ENF C6R Thermal demagnetization

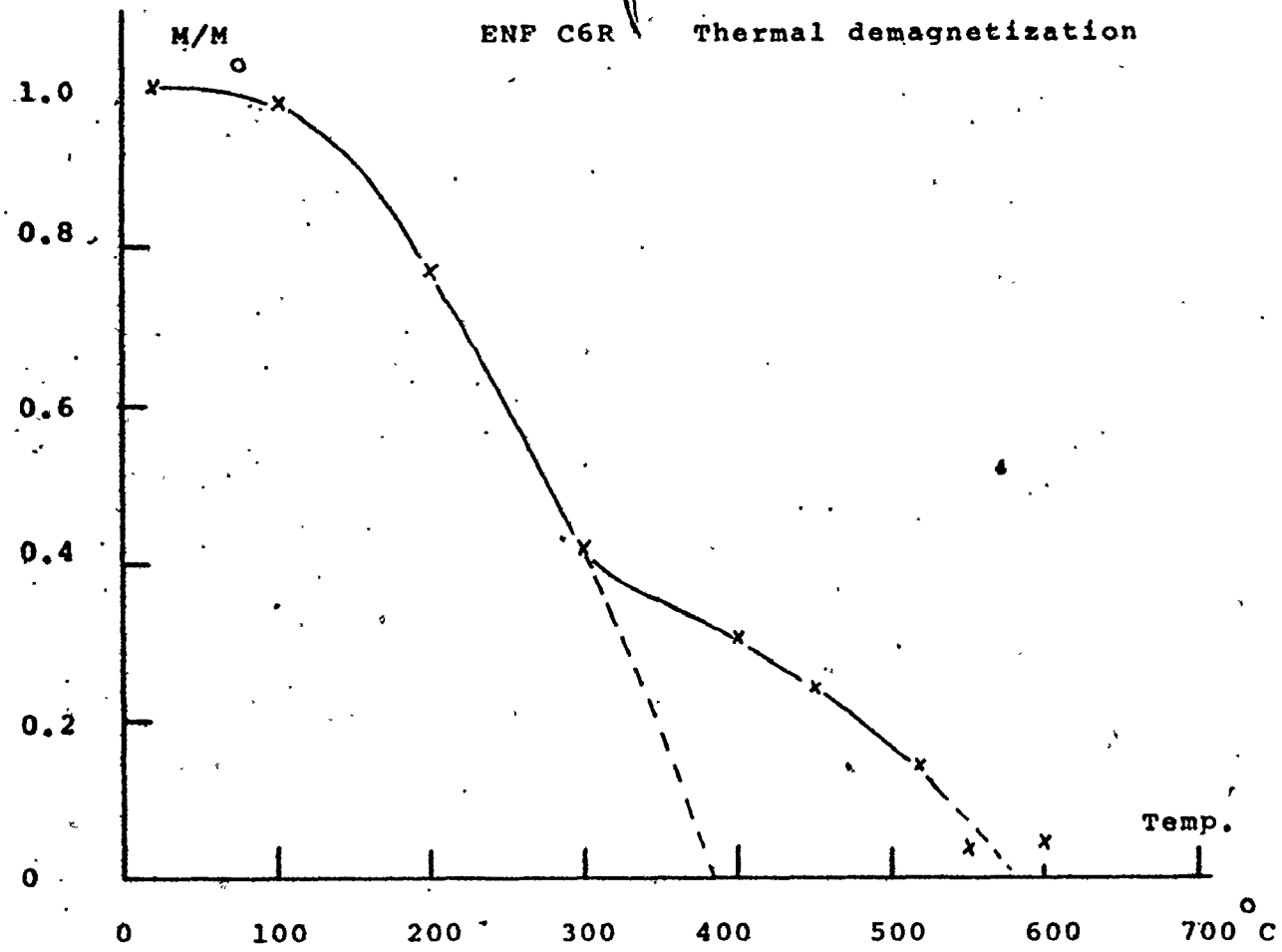

to the grain assemblage. This finding is further reinforced by the high values of H_{cr} and H_c .

The thermal demagnetization curve, figure 7.9 possesses a break in gradient at about 300 °C. As before the uncertainties in the experimental arrangement prevent interpretations being made about phase changes or the blocking temperature spectrum. The best estimate of the Curie point is 560 - 575 °C.

7.3.2.2 The TRM Experiment

Specimen D9R was given the following treatment along one axis and measured at each AF demagnetization step:

1) demagnetization of the NRM to 1 KOe,
2) demagnetization of ARM(1), acquired in a 0.5 Oe direct field with an AF of 1 KOe.
3) demagnetization of a TRM acquired in a nominal field of 0.5 Oe, (but which,in fact, dropped to 0.39 Oe at the onset of cooling).
4) demagnetization of ARM(2), which was produced under the same conditions as ARM(1),
5) measurement of a nominal SIRM produced by a field of 10 KG.

This specimen was treated together with DAS2 B30T (see section 7.3.13.1). A detailed discussion of the ARMs is given in section 8.4.5 . Apart from minor changes in their external appearance - a 'burnt' look - both specimens remained compact and intact after heating.

The TRM was much higher than the NRM by a factor ofabout 150 (or NRM/TRM $\approx$ 0.007). If, for the sake of arguement, the original Earth's field along this axis had also been 0.5 Oe , rather than, say, 0.1 Oe, then the ratio

Figure 7 - 10a; The AF demagnetization of the NRM, (X) and TPM (Δ) of ENF D9R

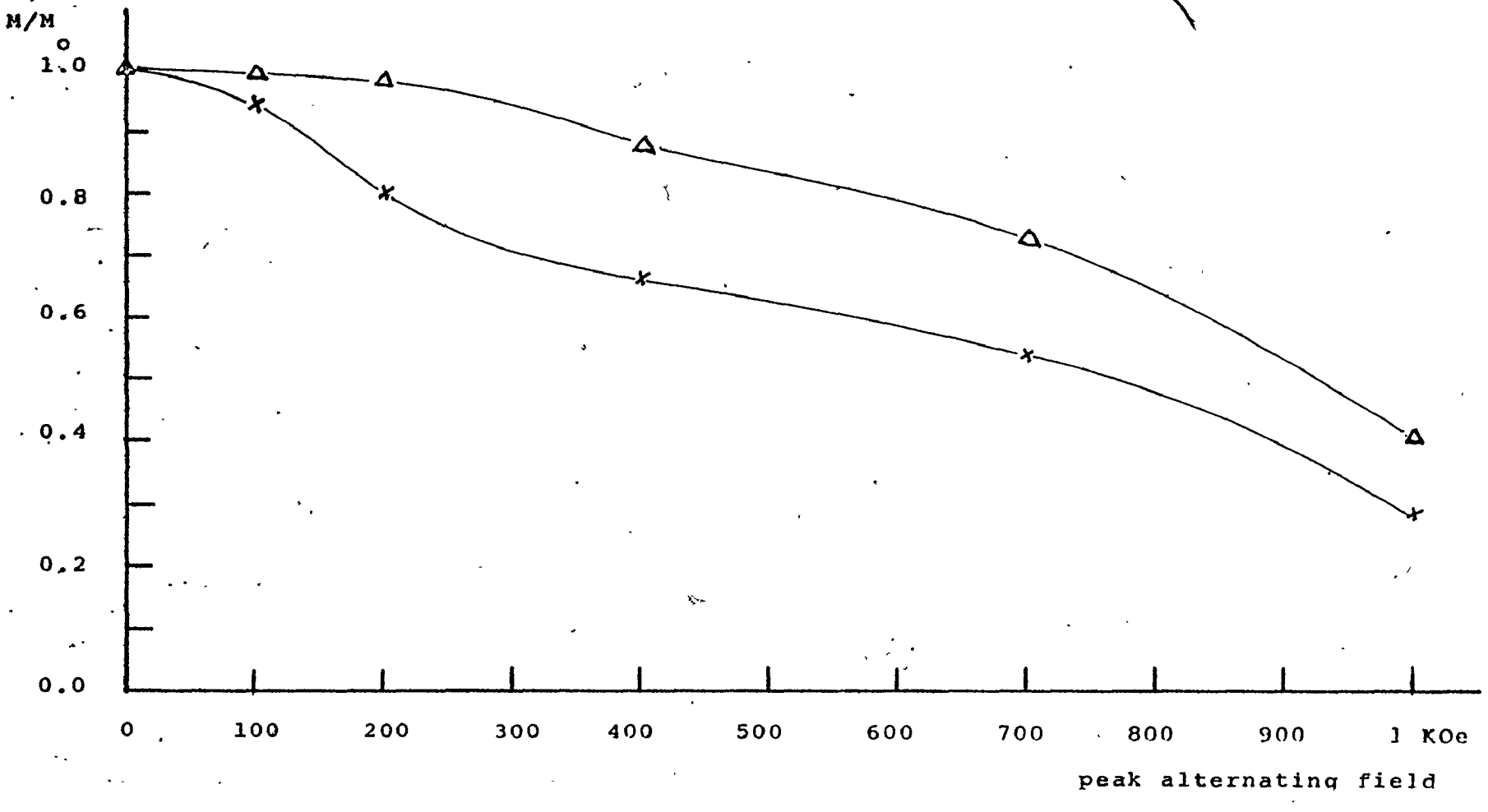

Figure 7 - 10 (b)

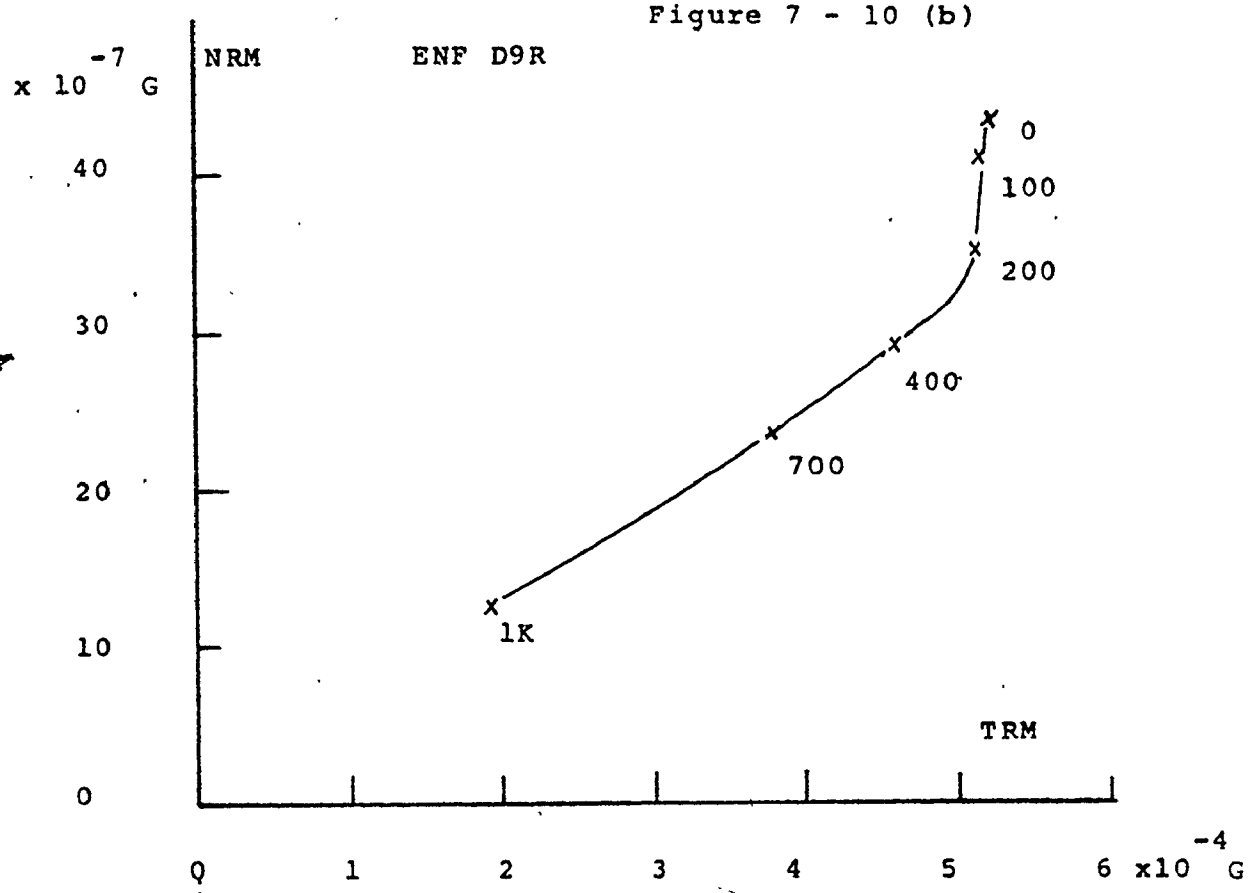
NRM
ENF D9R
x 10 -7 G
40
30
20
10
0
0
100
200
400
700
1K
TRM
0
1
2
3
4
5
6 x10 -4 G

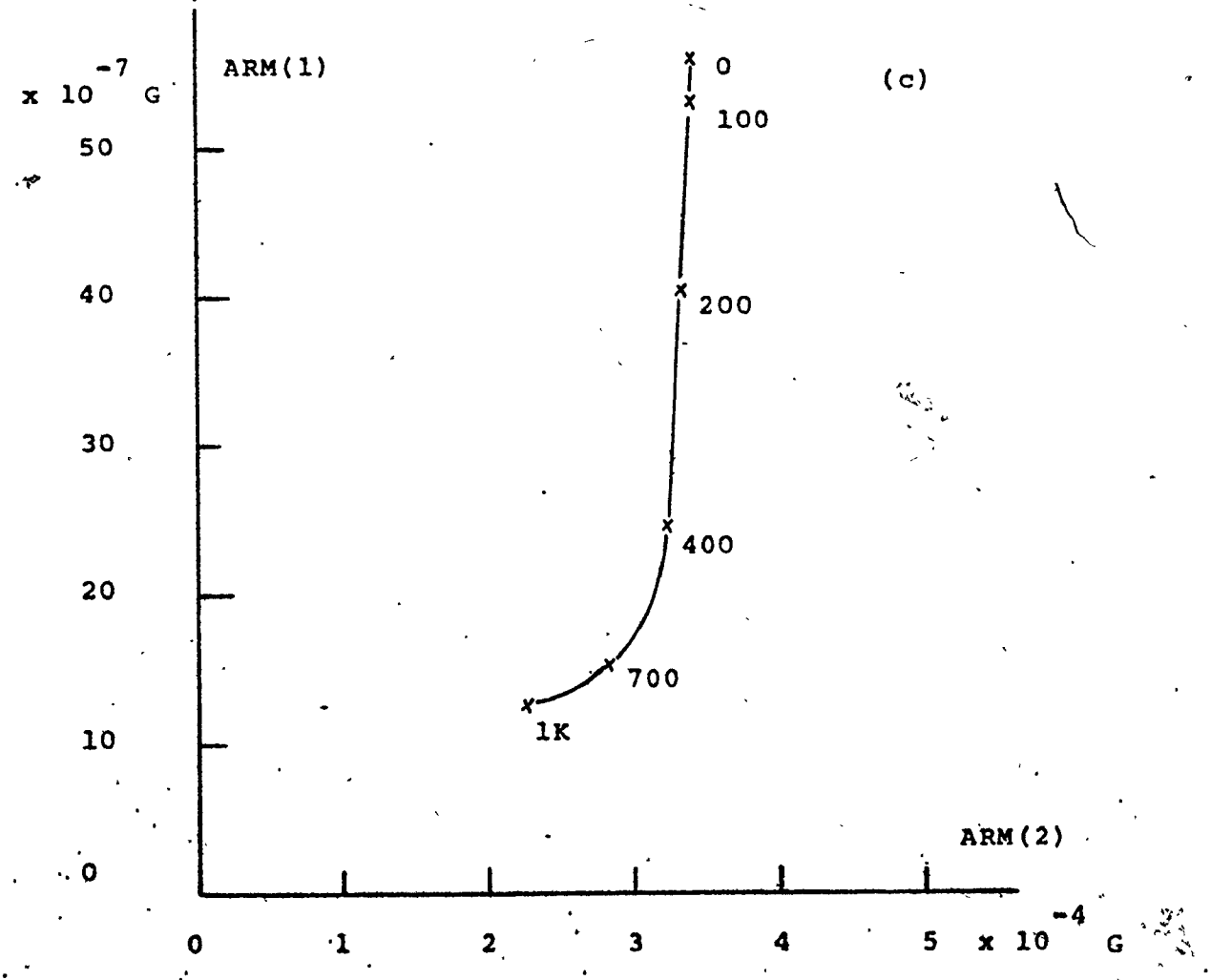
ARM(1)
(c)
x 10 -7 G
50
40
30
20
10
0
0
100
200
400
700
1K
ARM(2)
0
1
2
3
4
5 x 10 -4 G

becomes 0.035. Assuming the NRM to be principally a CRM this ratio is still much lower than the experimental ratio of 0.1 for magnetite by Kobayashi (1962) or of 0.17 by Pucher (1969).

After demagnetization to 1 KOe, the specimen was given an SIRM. To judge by the SIRM of D6R an estimate of D9R,s saturation remanence, M_{rs}, should have been about 4.6×10^{-4} G, which is actually less than the TRM of 5.2×10^{-4} G. In fact the SIRM saturated the ScT magnetometer at over 33.3×10^{-4} G (ie, the first quantum flux jump). Heating the specimen had apparently created more than seven times as much new magnetic material.

This TRM is even more intriguing when the stability is considered (figures 7.10a and b). Unlike the SIRM of D6R and its own NRM, the TRM has hardly any soft component and the MDF has increased from 775 Oe (NRM) to 930 Oe. In addition the TRM possessed about the same AF demagnetization characteristics as the NRM after about 300 Oe. It thus appears that each grain size fraction has been increased by a constant factor except those with coercive forces below about 300 Oe (the larger grains ?); and the TRM has then been imposed on the total assemblage.

Essentially the same information is given by the plot of ARM(1) against ARM(2), figure 7.10c. The comparison of the two ARMs is more valid than for the NRM - TRM plot, because ARM(1) will have realigned those softer grains which had viscously changed in the NRM. The curve has two parts because the TRM, monitored by ARM(2) (but see section 8.4.5) has not produced lower coercive force grains to the same extent as higher coercive

force grains. Put another way, if the same production factor had applied throughout the whole spectrum then the AF demagnetization curves of ARM(1) and ARM(2) would have matched from the low end upwards, producing a single straight line.

Comparison with DAS2 B30T may be found in section 7.3.13.1, and the question is taken up again in sections 7.4.2 and 9.7.4.

There were no opaque grains large enough to be visible in the thin section which covered cuts 4, 5 and 6. This therefore agrees with the evidence from the rock magnetism that there are proportionately few soft magnetic grains.

7.3.3 VCCL

Paleomagnetism, 4.6

This stalagmite contained both loose and cemented detrital material including quartz grains, organic debris and even small pebbles in the base. Some of the acid insoluble black grains could be picked up by a magnet. In the thin section most opaque grains were a uniform gray colour to reflected light and are thought to be magnetite. A few opaque grains showed exsolution features indicative of titanomagnetite.

The MDFs of several specimens range from 260 to 400 Oe.(figures 7.11a and b). Despite the fairly high MDFs most specimens had significant low coercive force components possessing a VRM in the direction of the present Earth's field. This is revealed by their Zijderveld plots (figures 7.12a and b; 7.13a and b).

VCCL B3Q and B13Q

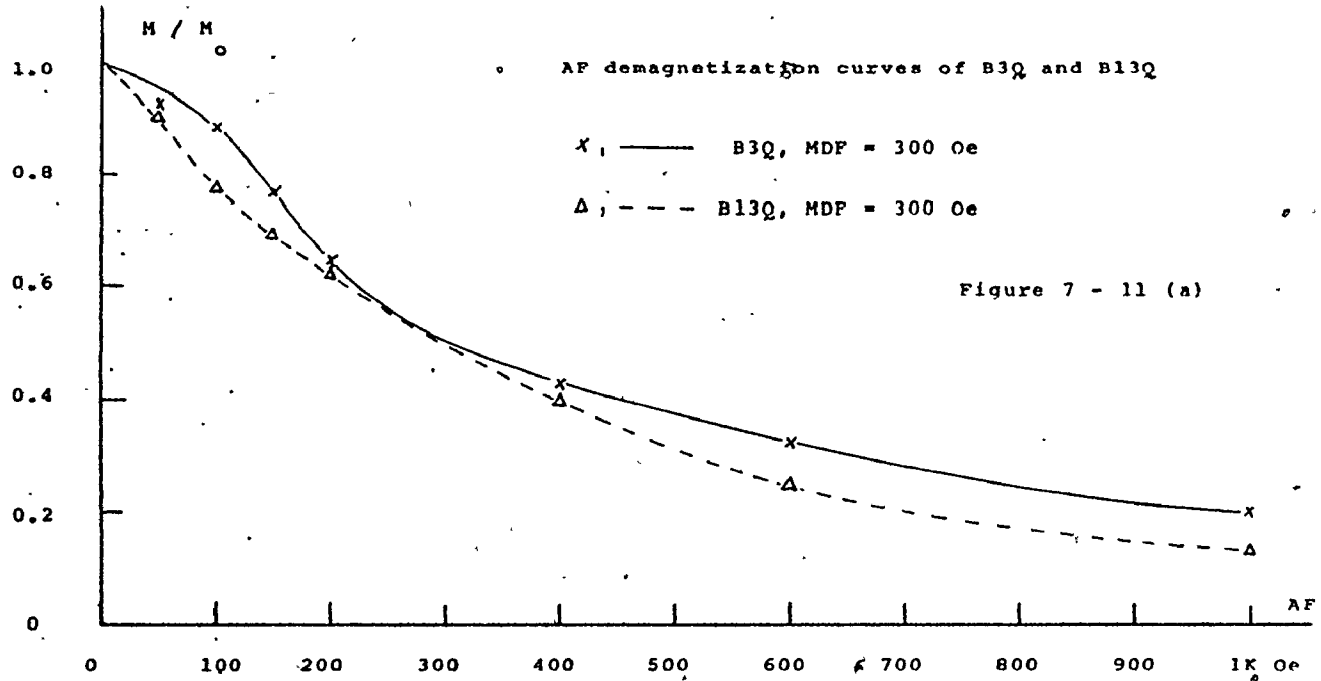

Figure 7 - 11 (a)

VCCL B12Q and B23Q

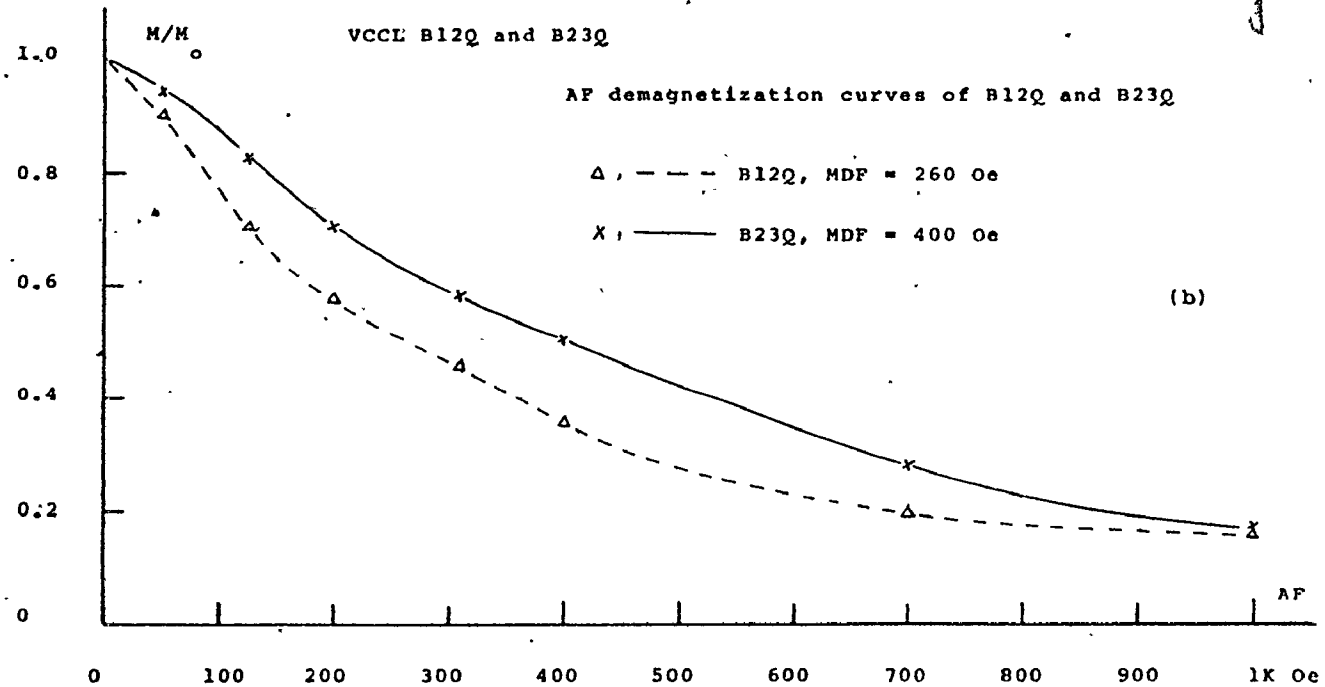

(b)

Figures 12a, b and c.

Zijderveld plots of AF and thermally demagnetized specimens of VCCL.

A short dashed line (vector) joins the NRM to the magnetization at the first demagnetization step. For comparison a longer dashed line towards the origin represents the 1975 declination for the site.

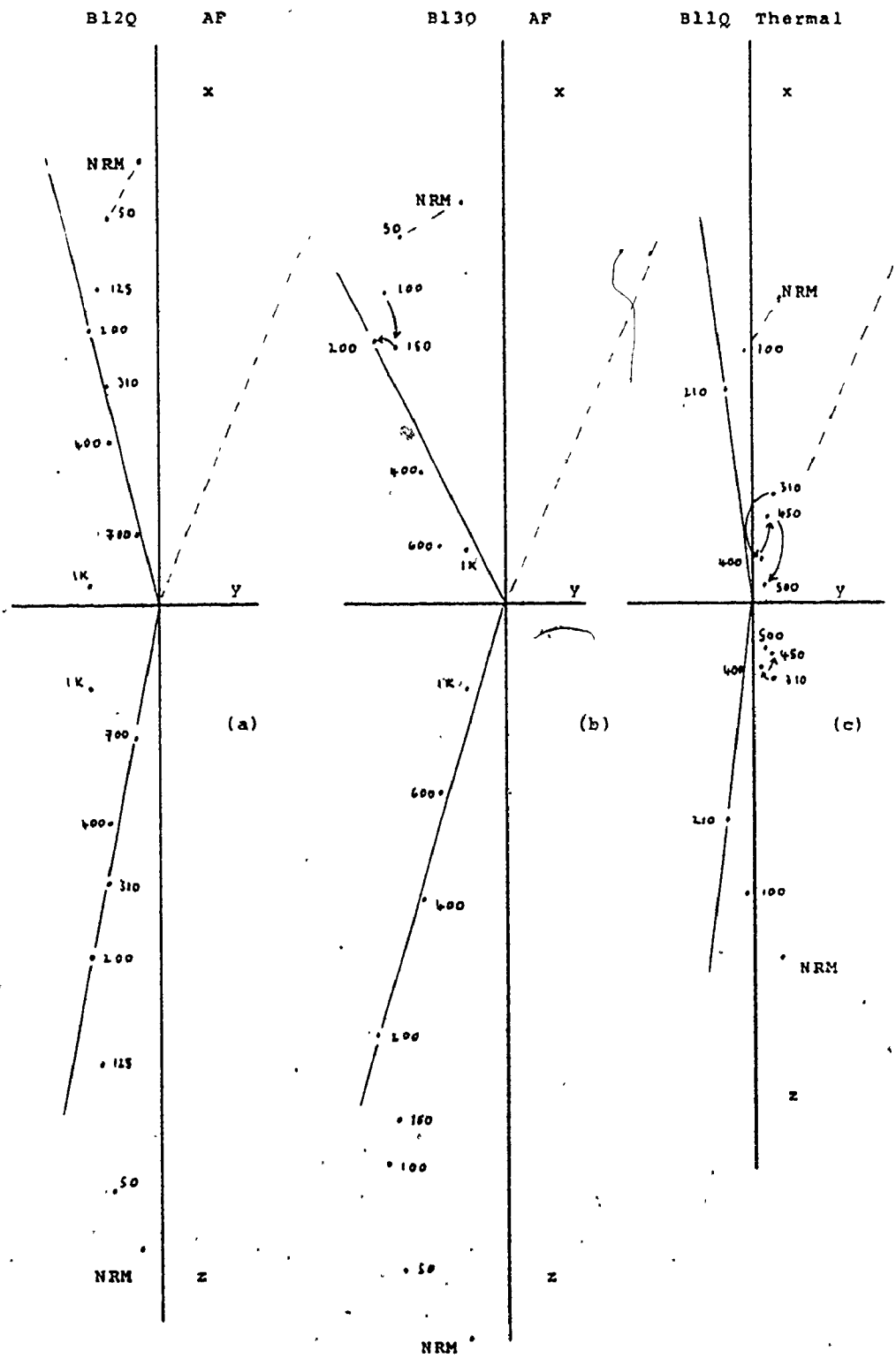
B12Q AF
x
NRM
50
125
200
310
400
500
1K
y
1K
700
600
310
200
125
50
NRM
z
(a)
B13Q AF
x
NRM
50
100
200
150
400
600
1K
y
1K
600
400
200
150
100
50
z
NRM
(b)
B11Q Thermal
x
NRM
100
210
310
450
400
500
y
500
450
400
310
210
100
NRM
z
(c)

Figures 13a, b and c.

Zijderveld plots of AF and thermally demagnetized specimens of VCCL.

A short dashed line (vector) joins the NRM to the magnetization at the first demagnetization step. For comparison a longer dashed line towards the origin represents the 1975 declination for the site.

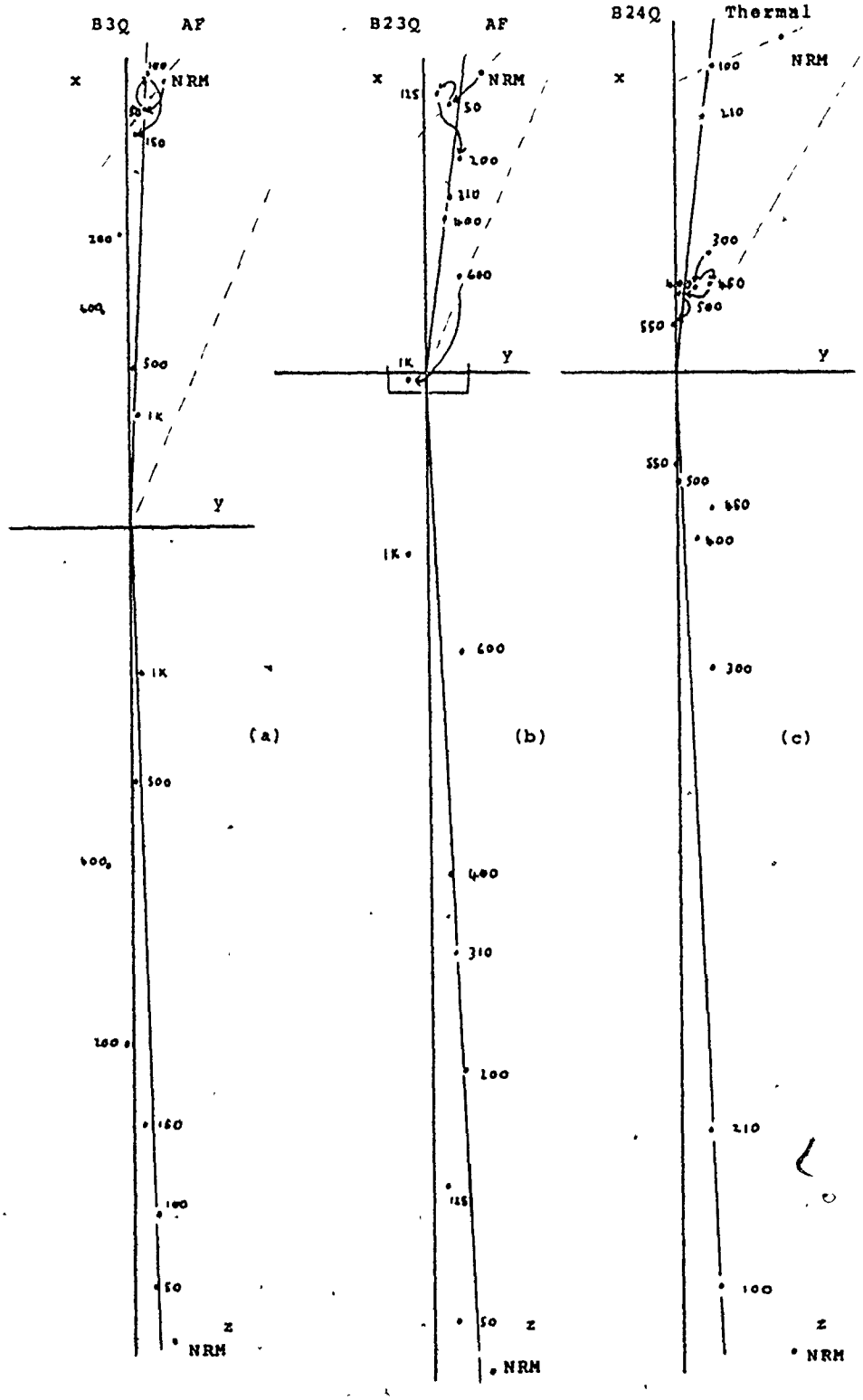
B3Q AF
NRM
100
150
200
400
500
1K
x
y
z
NRM
(a)
B23Q AF
NRM
115
50
200
310
400
600
1K
x
y
z
NRM
(b)
B24Q Thermal
NRM
100
210
300
450
500
550
x
y
z
NRM
(c)

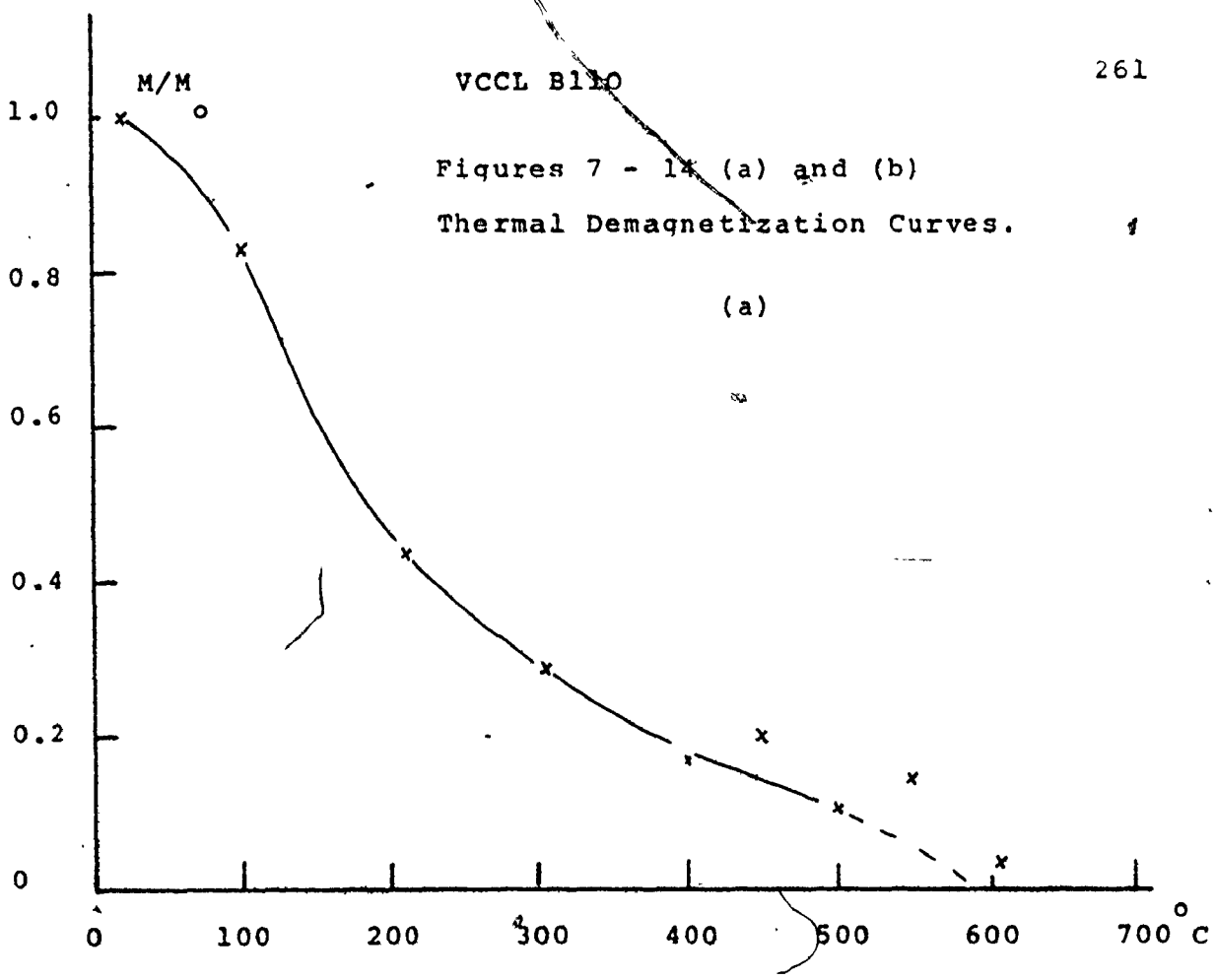

Figures 7 - 14 (a) and (b)
Thermal Demagnetization Curves.

(a)

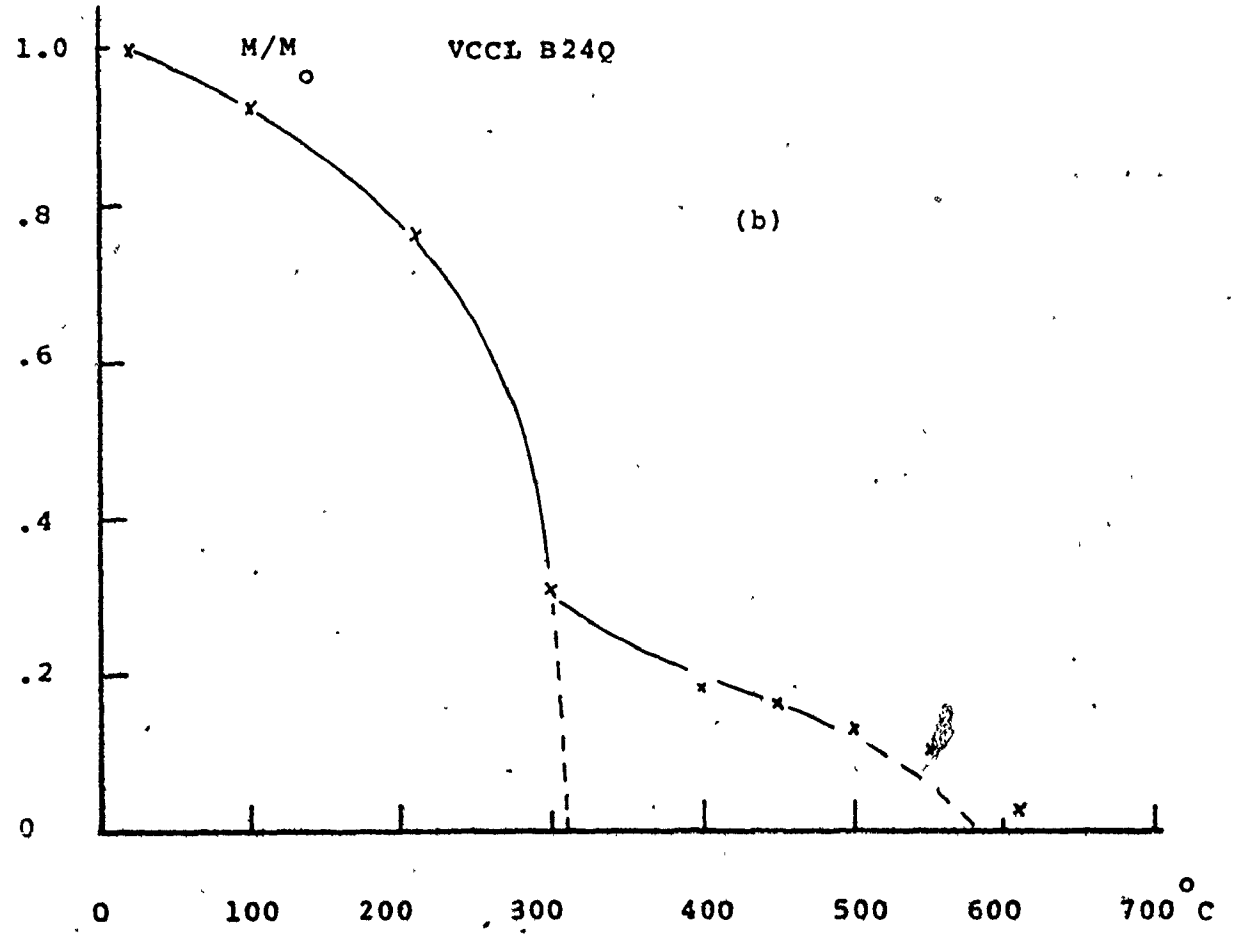

(b)

Specimens B11Q and B24Q were thermally demagnetized and their Zijderveld plots (figures 7.12c and 7.13c) also show the low coercive force viscous components. The demagnetization is not as clean as the AF method. There is the 'usual' kink around 250 to 315 °C (figures 7.14a and b), and there appear to be spurious TRMs introduced above this temperature. Estimates of the Curie temperature(s) for B11Q and B24Q are in the range 550 to 600 °C

7.3.4 DBS1

This Yorkshire stalagmite showed no measurable NRM above the magnetometer noise level of $\approx 10^{-7}$ Oe, for specimens of 12 to 14 gm mass. Magnetite did show up in the hysteresis experiment , however, with an SIRM of 15×10^{-6} G (figure 7.15). This corresponds to a volume fraction of about 14 ppb of magnetite in calcite. (This was worked out from ; volume fraction = $\frac{SIRM/V}{0.5\ I}$, where V is the volume of the specimen, I represents the spontaneous magnetization of magnetite (480 G cm^{-3}), and 0.5 assumes that the grains are all SD type).

The H_{cr} of 300 - 350 Oe , according to Dankers (op cit) corresponds to grain sizes of $< 5 \mu m$.

7.3.5 TS

Paleomagnetism, 4.2

The base of this stalagmite showed evidence of flooding with its dark banding and quartz grains. The remainder of the sample is devoid of such material and appeared 'clean' even along the washed-off sides.

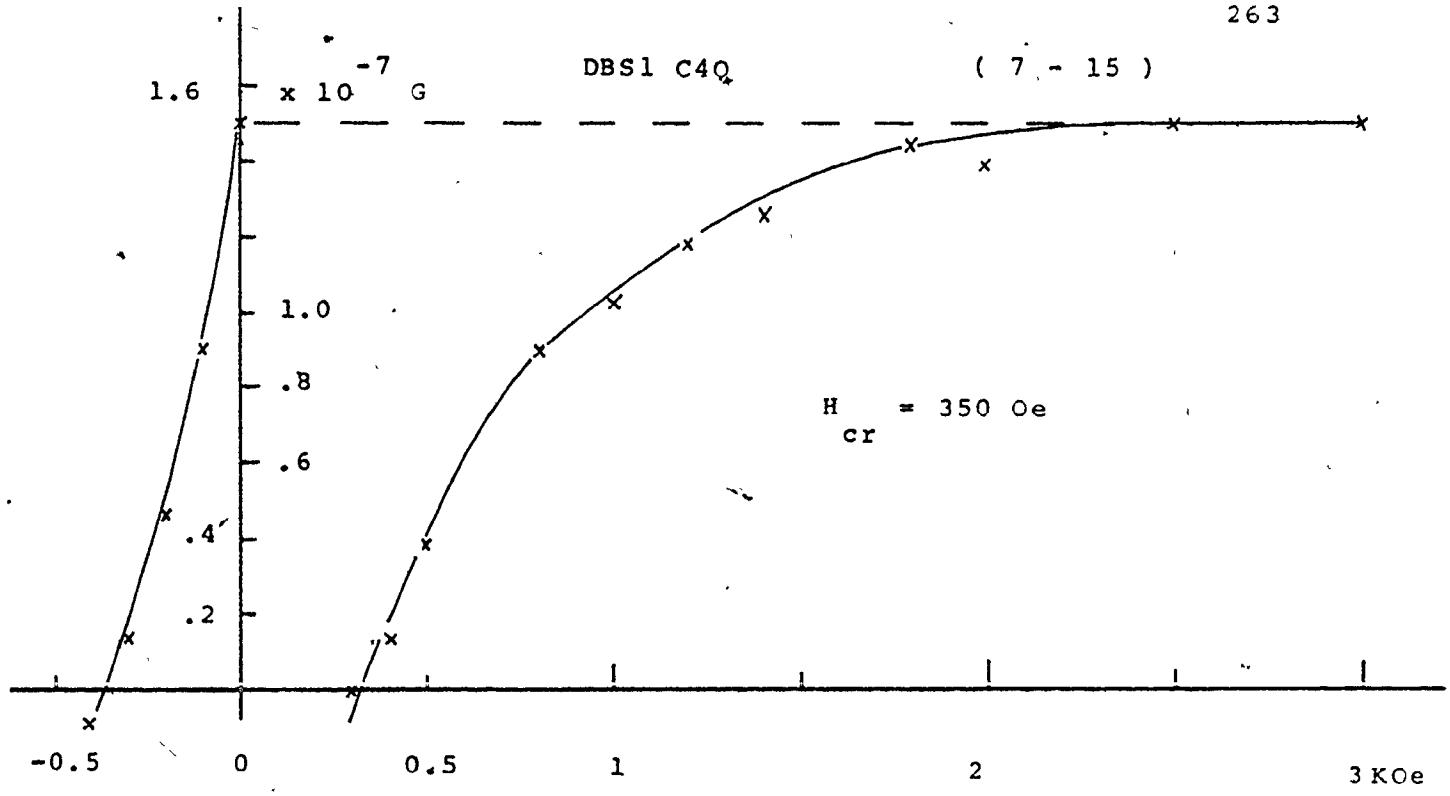

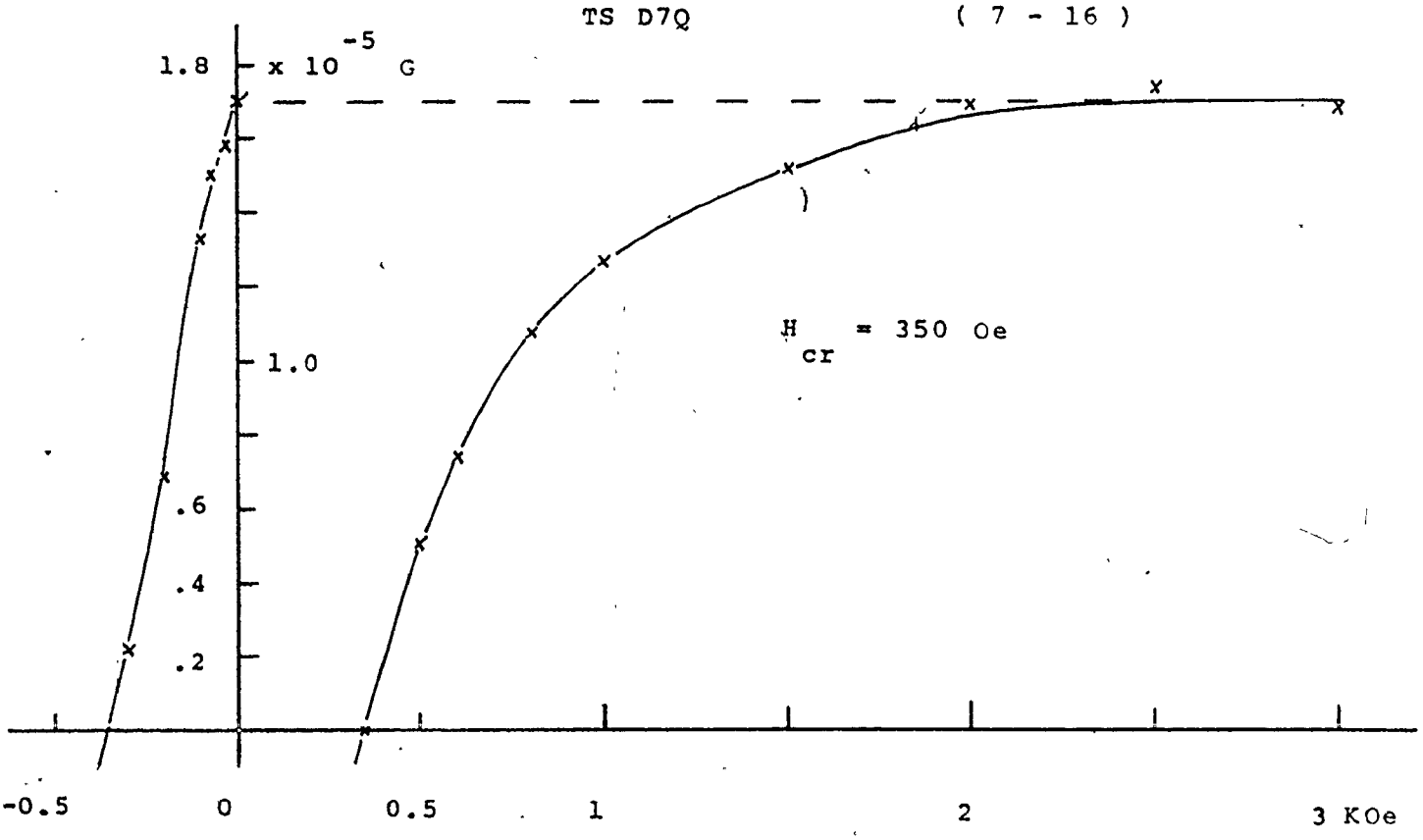

Figures 7.15 & 7.16; Hysteresis curves of remanent magnetization

Figure 7 - 17

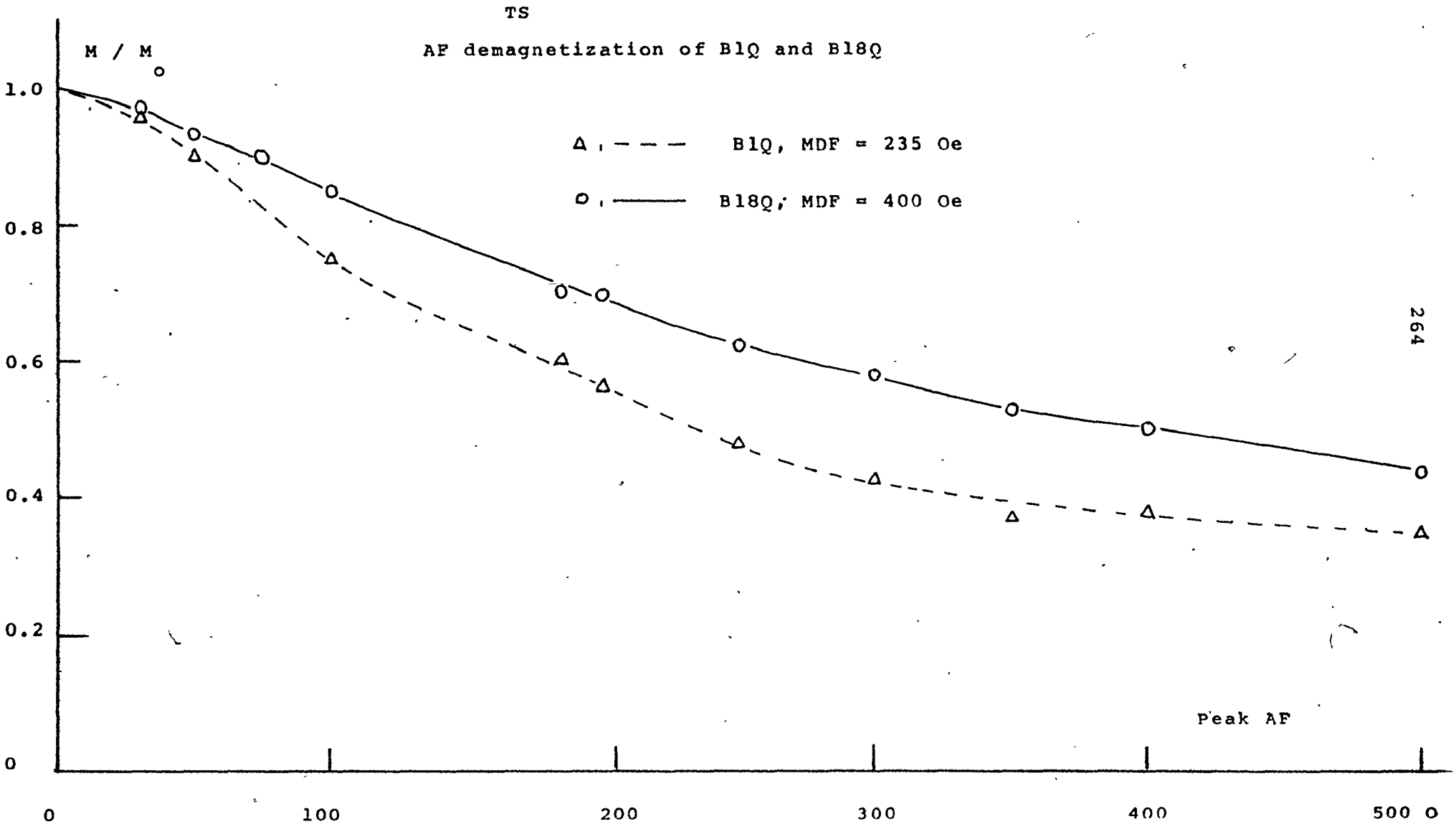
TS
AF demagnetization of B1Q and B18Q
M / M o
1.0
0.8
0.6
0.4
0.2
0
Δ , - - - B1Q, MDF = 235 Oe
o , —— B18Q, MDF = 400 Oe
Peak AF
0
100
200
300
400
500 O

Specimen D7Q weighing 30.2 gms was taken round a hysteresis loop of remanence (figure 7.16), The loop characterises a high coercive forcemagnetite; the H_{cr} of 350 Oe corresponds to < 5μm grains of PSD/SD states. This is in accord with the AF demagnetization of the two specimens B1Q and B18Q which showed high stability (figure 7.17).

It is interesting to compare the 6 ppb volume fraction derived from the SIRM of D7Q, which was one of the weakest of TS, with the 14 ppb of the DBS1 specimen. D7Q had a barely measurable NRM of about 6×10^{-7} G. Thus it would appear that 6 - 10 ppb of magnetite is about the detection limit (assuming moderate field intensities), and that such specimens have to be stacked for reasonable NRM measurement.

7.3.6 RCB and its Associated Soil

Paleomagnetism, 5.2

Mössbauer spectra, appendix V

The light and dark red-brown layering of the flowstone corresponded to remanent intensities of 14×10^{-7} to 200×10^{-7} G cm^{-3} respectively. From atomic absorption analyses the corresponding iron concentrations were 50 and 700 ppm.

Most specimens showed viscous effects especially those from the top of the sample. Decay time constants from seconds to minutes were observed and there may even be superparamagnetic components. Figure 7.18 shows specimen demagnetization curves. Specimen D2Q has evidently picked up a component which is antiparallel to the stable

RCB

AF demagnetization of NRMs

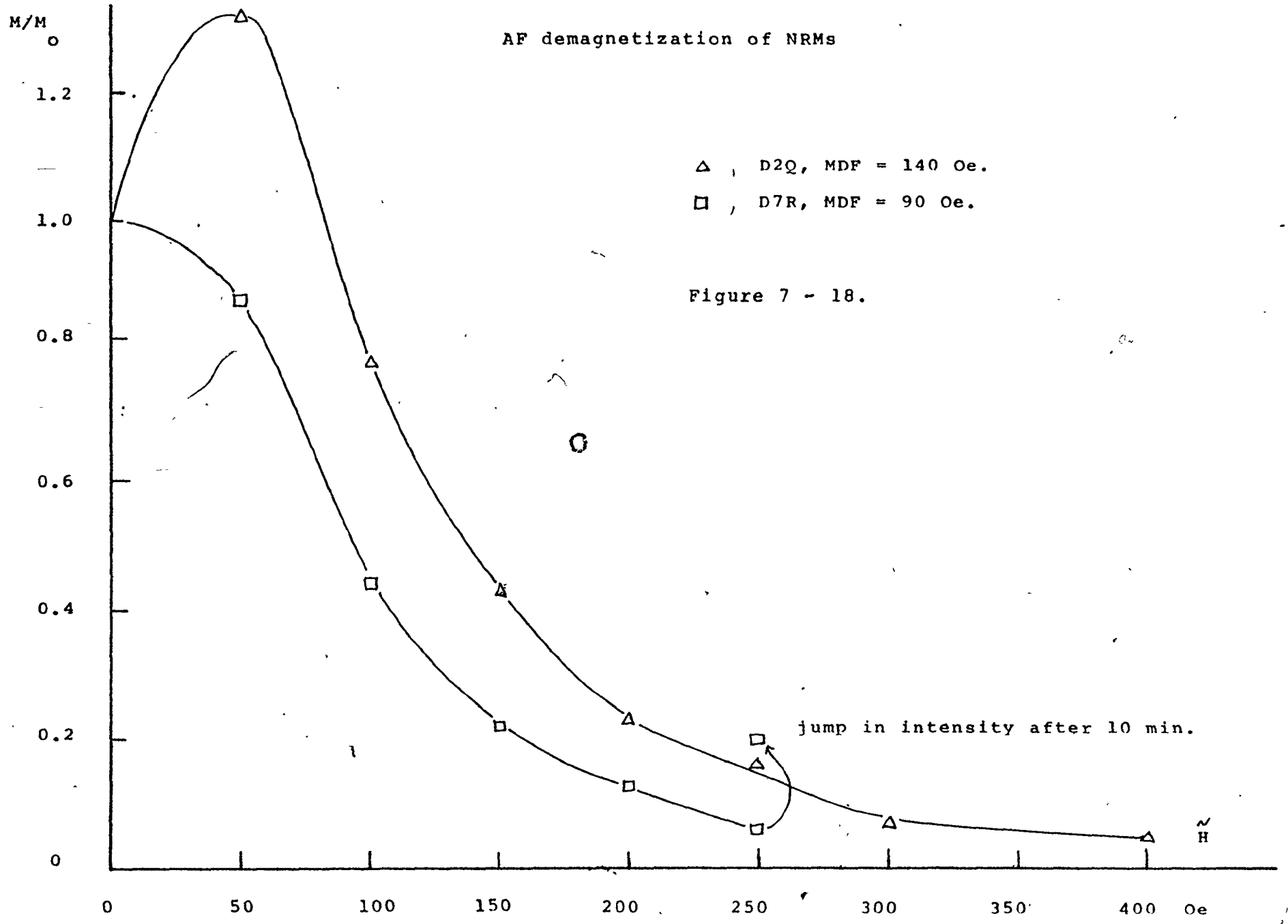

Figure 7 - 18.

RCB B3T

AF demagnetization of the SIRM of B3T and coercive force spectrum. MDF = 140 Oe.

Figure 7 - 19 (a)

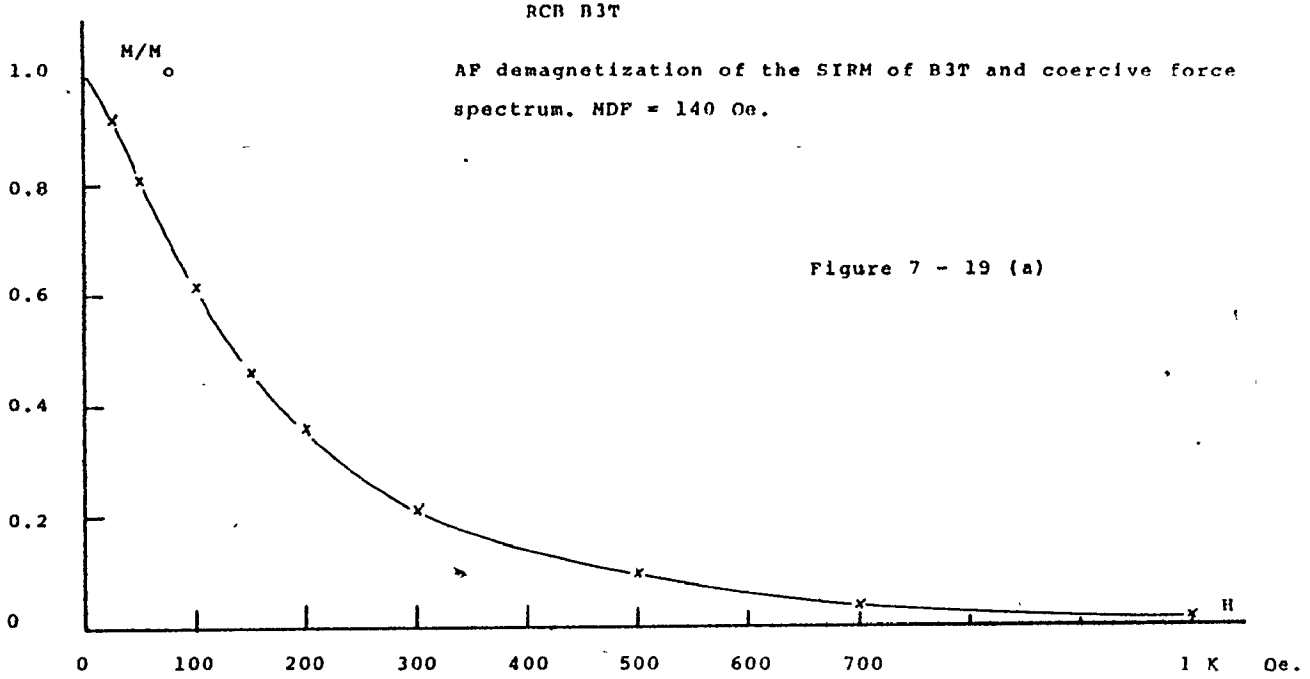

(b)

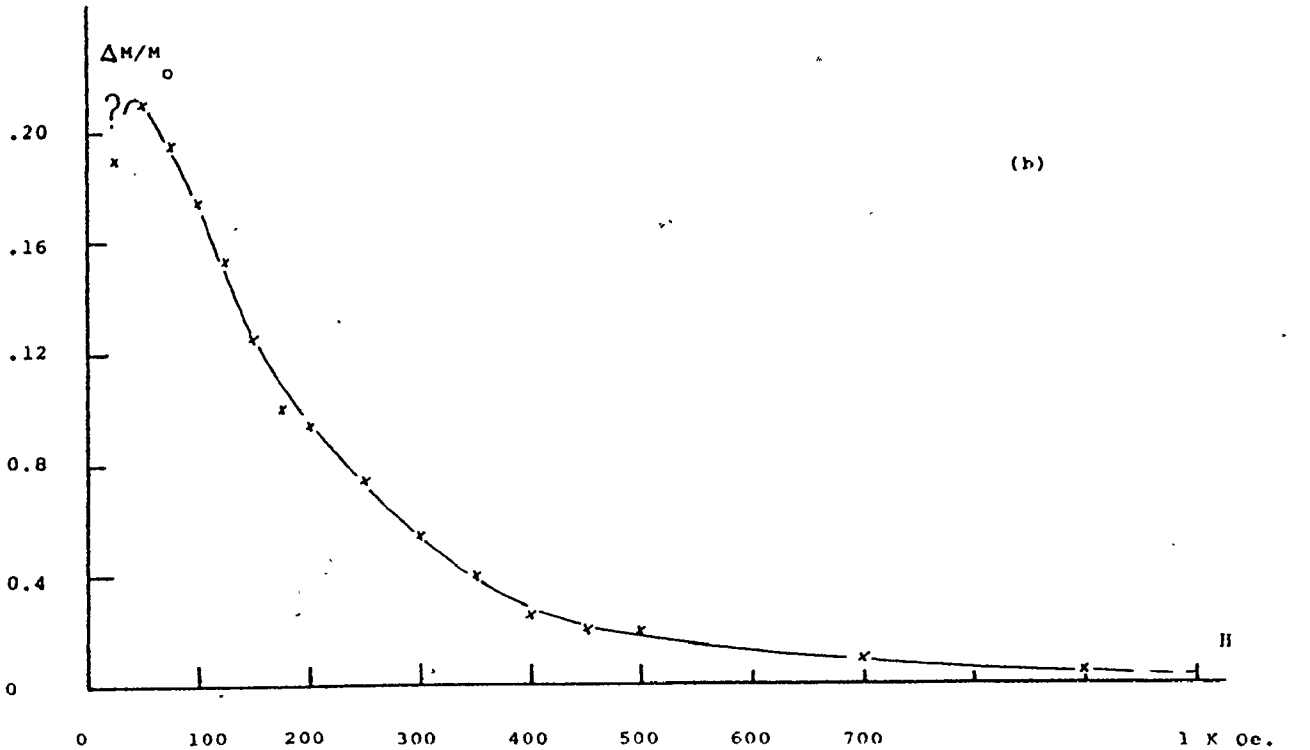

Table 7.3

Estimates of the Diamagnetic Susceptibility of Calcite from Various Specimens

Specimen	$\chi_c \times 10^{-7}$ G Oe^{-1} gm^{-1}
ENF D6R	-2.8
OULF-cut 9	-3.0
DAS2 C17T	-3.65
Calcite (Weast, 1978)	-3.82

Note ; The diamagnetic susceptibility of these specimens also includes some contribution from the perspex specimen holder. The average χ_c used to correct RCB B8Q (see text) was -3.2×10^{-7} G Oe^{-1} gm^{-1} .

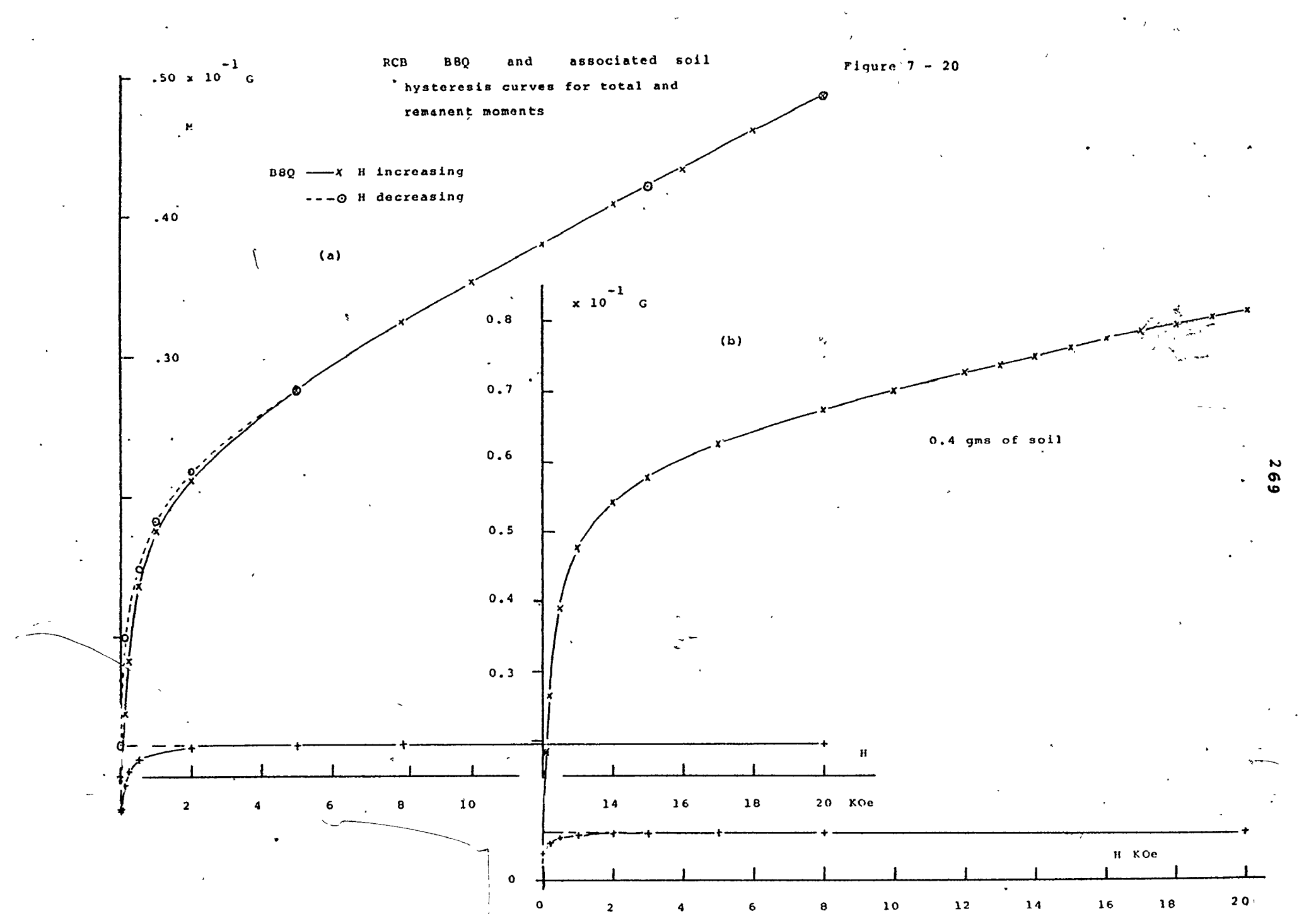
RCB B8Q and associated soil hysteresis curves for total and remanent moments
Figure 7 - 20
B8Q ——x H increasing
---⊙ H decreasing
(a)
(b)
0.4 gms of soil
H KOe

part of the NRM. D7R after demagnetization to 250 Oe subsequently picked up a viscous component after 10 minutes in the laboratory field. NRM MDFs ranged from 90 to 140 Oe. If specimens were protected from stray fields and measured immediately after cleaning , then primary directions could be recovered. This was not attempted, except for a few specimens, because as discussed earlier, radiometric dates could not be assigned to the directions.

Figures 7.19a and b show the SIRM demagnetization and coercive force spectrum of B3T. The MDF has been pushed artificially high by fast-decaying components. The bulk of the spectrum lies below 450 Oe.

Figures 7.20a and b show the hysteresis loops of a specimen from cut 8 and of the calcareous red-brown soil, found above the flowstone. Dissolution of the soil sample showed that the soluble organics and carbonate (both diamagnetic) contributed less than 5% by weight. Thus the positive susceptibility for the high field part of figure 7.20b is probably a reasonable estimate of a superparamagnetic component of the soil.

For specimen B8Q the total moment is plotted against field in figure 36 appendix IV. Beyond 2KOe the overall susceptibility is diamagnetic and continues to go more negative. The specific susceptibility, at 18 to 20 KOe is significantly more positive than for OULF, DAS2 or ENF (table 7.3), all of which compare with the accepted value for pure calcite. The likely explanation is that the flowstone also contains a superparamagnetic component. The curve of (ferromagnetic plus superparamagnetic) moment versus H, of figure 7.20a, was constructed by subtracting

$\chi_c H$ from the observed moment, where χ_c is the average calcite diamagnetic susceptibility from OULF, DAS2 and ENF.

Because of the fast decaying components in B8Q there are uncertainties in M_r which was measured about ½ minute after switching off the field. Thus low τ components are included in the total induction curve, M_s and H_c but not in the remanence curve, M_{rs} and H_{cr}.

In their analysis of the red-brown paloeosols of Bermuda, Blackburn and Taylor (1969) reported various iron-bearing minerals including ilmenite and 'iron oxide'. Goethite was found in the black-banded limestone of Whalebone Bay not far from the RCB site. The RCB soil , under hand lens, contains yellow to yellow-brown grains indicative of limonite.

Goethite is either weakly magnetic or is SP for fine grain sizes (Strangway, et al, 1968; Vlasov, et al, 1967a and b). According to Vlasov, et al, goethite does not saturate until about 18 K0e. In figure 7.19b there is a slight tendency towards saturation at around 17 K0e, but the subsequent trend is still SP (or paramagnetic ?).

Appendix V, figures1-3show the Mössbauer spectra of the soils at room,and liquid nitrogen temperatures. The low temperature magnetic field of 492 K0e indicates βFeOOH, rather than αFeOOH or fine αFe_2O_3 ; but in any case the magnetic components are not well ordered (T. Birchall, pers, com). Evidently the spinel component from the hysteresis experiment is not intense enough to be seen in the room temperature spectrum. Unfortunately targets prepared from the high iron layering of the flowstone, using a finely crushed matrix of the host calcite, did

not give definitive spectra.

The thin section reveals the fine particulate form of the red iron oxide minerals. It is closely associated with what appears to be detrital organic matter.

7.3.6.1 Discussion on RCB

The red-brown soil was certainly the source of the iron content of RCB, and a similar relationship may hold for Bermudan speleothems generally. In the soil and the speleothem there are three magnetic components, these being SP, unstable (viscous, soft) and stable. If the SP component is due to αFe_2O_3 it is not accompanied by a coarse fraction of high enough concentration to show in the remanence curve. Rather the SP component is due to iron oxyhydroxides of variable grain size and crystalline order. Some goethite samples are also known to be magnetic at ordinary temperatures (Govaert, et al, 1976), so part of this range in size and order may also account for the unstable remanence. Alternatively the unstable component is due to fine magnetite (or maghemite).

The stable component as indicated by the hysteresis remanence curve is either magnetite or maghemite.

Soil wash undoubtedly accounts for the presence of FeOOH in the flowstone. For one thing there are enough microgours and irregularities in the growth layers to trap any insoluble detrital matter carried by the surface water. Magnetite may also arise from the soil wash, or may have been chemically precipitated. The cleaned directions of chapter 5, table 5.2, are not far from the present or

AGD directions. They have not been affected by the steep dip of the flowstone surface.

7.3.7 WCS1

Paleomagnetism, 5.4

WCS1 was a 15 cm high stalagmite from Wonderland cave. It was a translucent amber colour which, in thin section, showed almost equant crystals of order 0.25 cm on a side.

Stacked specimens up to about 40 gms failed to produce any measurable NRM. The atomic absorption analysis for iron, of a basal specimen, showed it to have less than the detection limit of 10 ppm.

Figure 7.21 shows the IRM hysteresis loop for specimen C5P. No short term viscous components were observed. Saturation occurred between 2.3 and 3 KOe and the coercivity of remanence was about 280 Oe.

It is probable that the amber colouring is due to organic material which was soluble in the dripwater.

7.3.8 GQF1

Paleomagnetism, 5.3

This 23 cm thick flowstone, from Government Quarry cave, was the top part of a flow which was locally over one metre thick. In this sample the translucent amber-pink layers lens out near the middle. Some layers are compact, some contain vugs partly filled with calcite needles, these being remnant microgours, whereas other are more milky due to fluid inclusions.

Figure 7 - 21.

WCS1 C5P

hysteresis of remanence

H_{cr} = 280 Oe

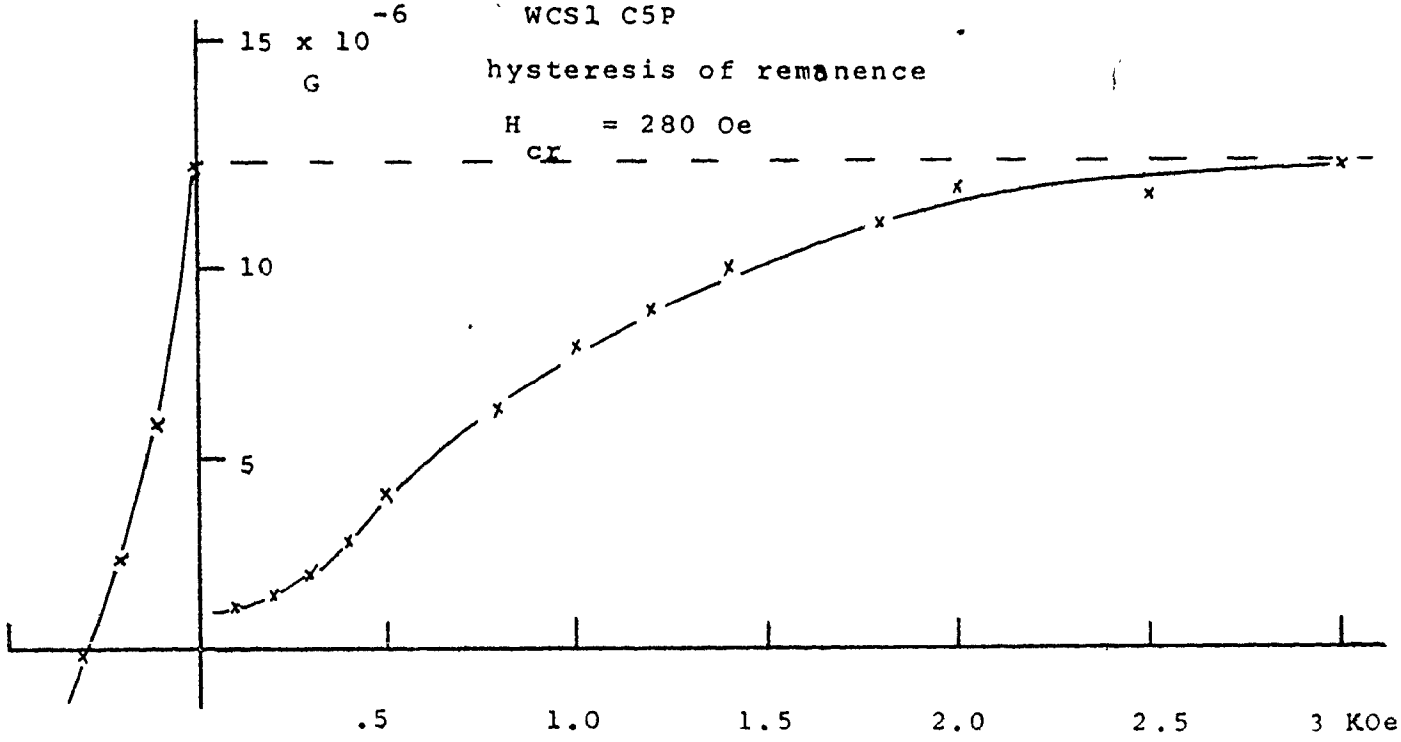

Figure 7 - 22.

GQF1 C10S

hysteresis of remanence

H_{cr} = 350 Oe.

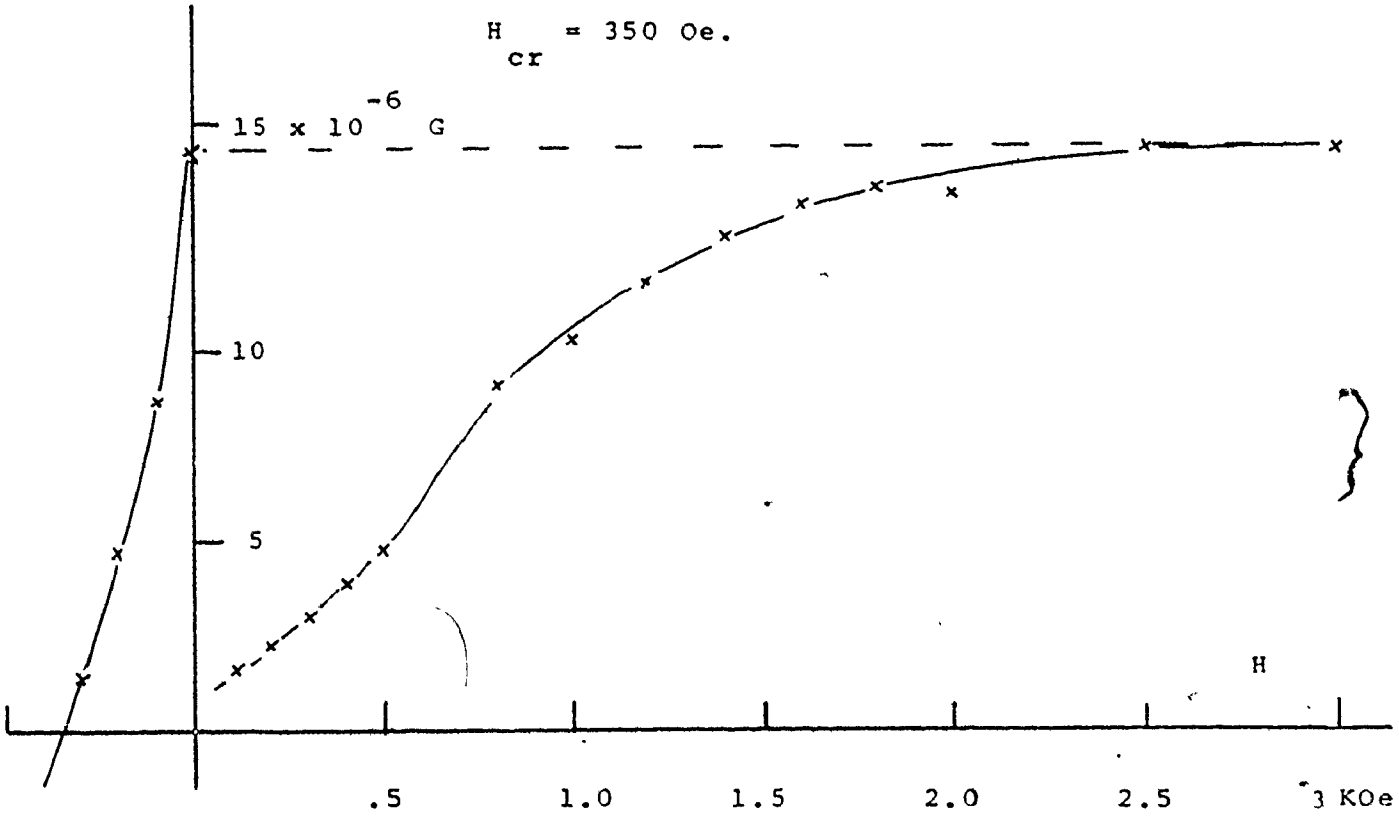

Figure 7 - 23.

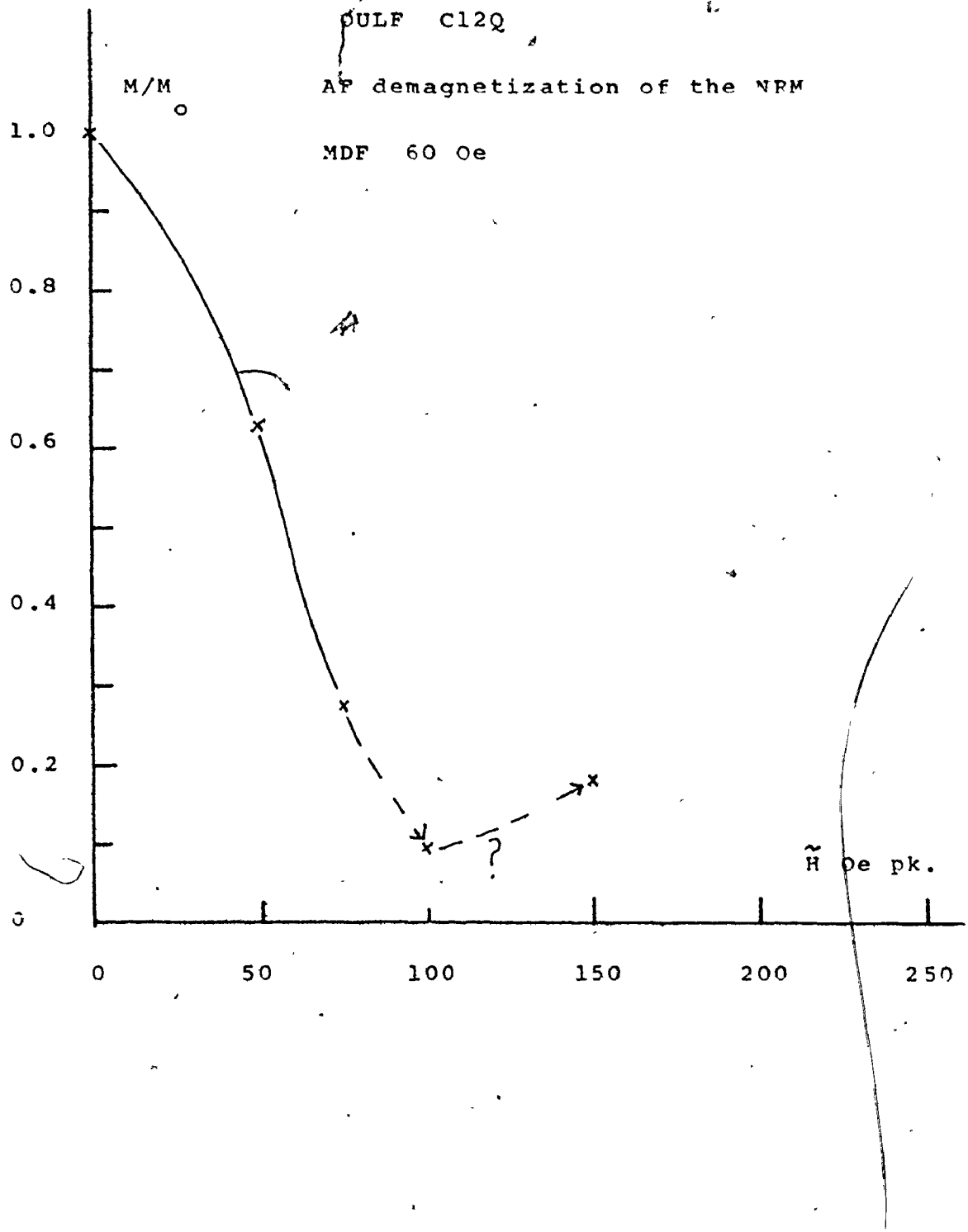
GULF C12Q
M/M
o
AF demagnetization of the NRM
MDF 60 Oe
1.0
0.8
0.6
0.4
0.2
0
?
H Oe pk.
0
50
100
150
200
250

A low remanence 10^{-6} G, total moment, for stacked specimens was found in the top layers. Elsewhere the NRM was barely measurable.

Figure 7.22 shows the IRM loop for specimen C10S. Saturation was probably obtained by 3 KOe and the coercivity of remanence was about 350 Oe. No short term viscous components were detected.

As with WCS1 it seems likely that the colouring was partly due to water soluble organic material. From the U/Th radiometric analyses, a very light-coloured $Fe(OH)_3$ precipitate probably indicates the presence of aluminum (M. Gascoyne, pers. com).

7.3.9 OULF and its Associated Soil

Paleomagnetism, 5.5

This sample was a 22 cm thick compact flowstone with pink-brown and opaque white layering. Towards the base occur thin partings of red soil along growth layers. Occasionally blobs of red clay up to 1 cm diameter are included over which the calcite has continued to grow. The blobs may have been emplaced by floods.

Stacked specimens of mass $\approx$50 gms gave low intensities of order 10^{-7} G, total moment. The directions showed considerable dispersion about the mean. Specimen C12Q (fig. 7.23) showed almost complete instability to AF demagnetization. It had an MDF of 60 Oe and was completely demagnetized in about 112 Oe. It was evident from remeasuring specimens that almost the full intensity could be acquired viscously.

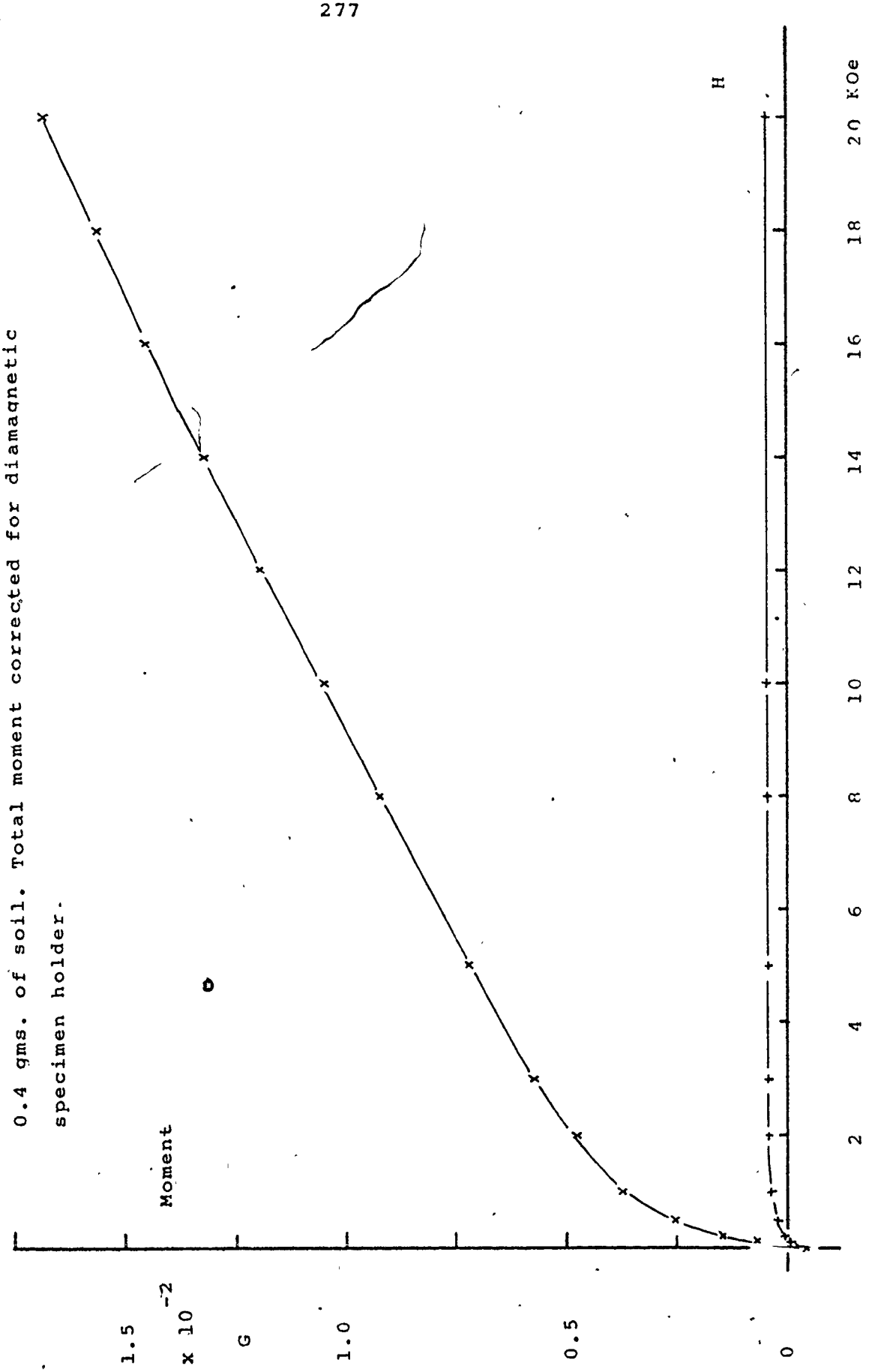

Figure 7 - 24; OULF associated soil . Induced and remanent hysteresis curves. 0.4 gms. of soil. Total moment corrected for diamagnetic specimen holder.

Hysteresis experiments on a specimen from cut 9 (figure not shown) showed a low and unstable magnetic content. H_{cr} was about 50 Oe. Because of uncertainties in the large diamagnetic correction to the total induced moment, it is not known whether a superparamagnetic component is present in the speleothem.

Figure 7.24 shows the hysteresis of the red clay extracted from the sample. Low remanence and high SP components are present. Thus the OULF soil resembles the RCB soil in possessing stable, unstable and SP components.

Appendix V, figures 4-6 showed the FeII and FeIII fits to the room and liquid nitrogen temperature Mössbauer spectra for the soil. The FeIII ordering at 77 ^{o}K appears to indicate the presence of an iron oxyhydroxide. Though magnetite (or maghemite) is evident in the hysteresis experiment (the remanence has saturated by 2 KOe), it is not concentrated enough to appear in the room temperature Mössbauer spectrum.

7.3.10 SJHS

Paleomagnetism, 6.3

Notable features of this stalagmite were the presence of several hiatuses near the top, and a ½ cm thick brown-black rind which had become cemented to the outer surface. Specimens incorporating the outer rind possessed intensities of around 760×10^{-7} G cm^{-3}; the inner layers were around 20×10^{-7} G cm^{-3}. The interior was a translucent light-brown, banded with light red-brown layers.

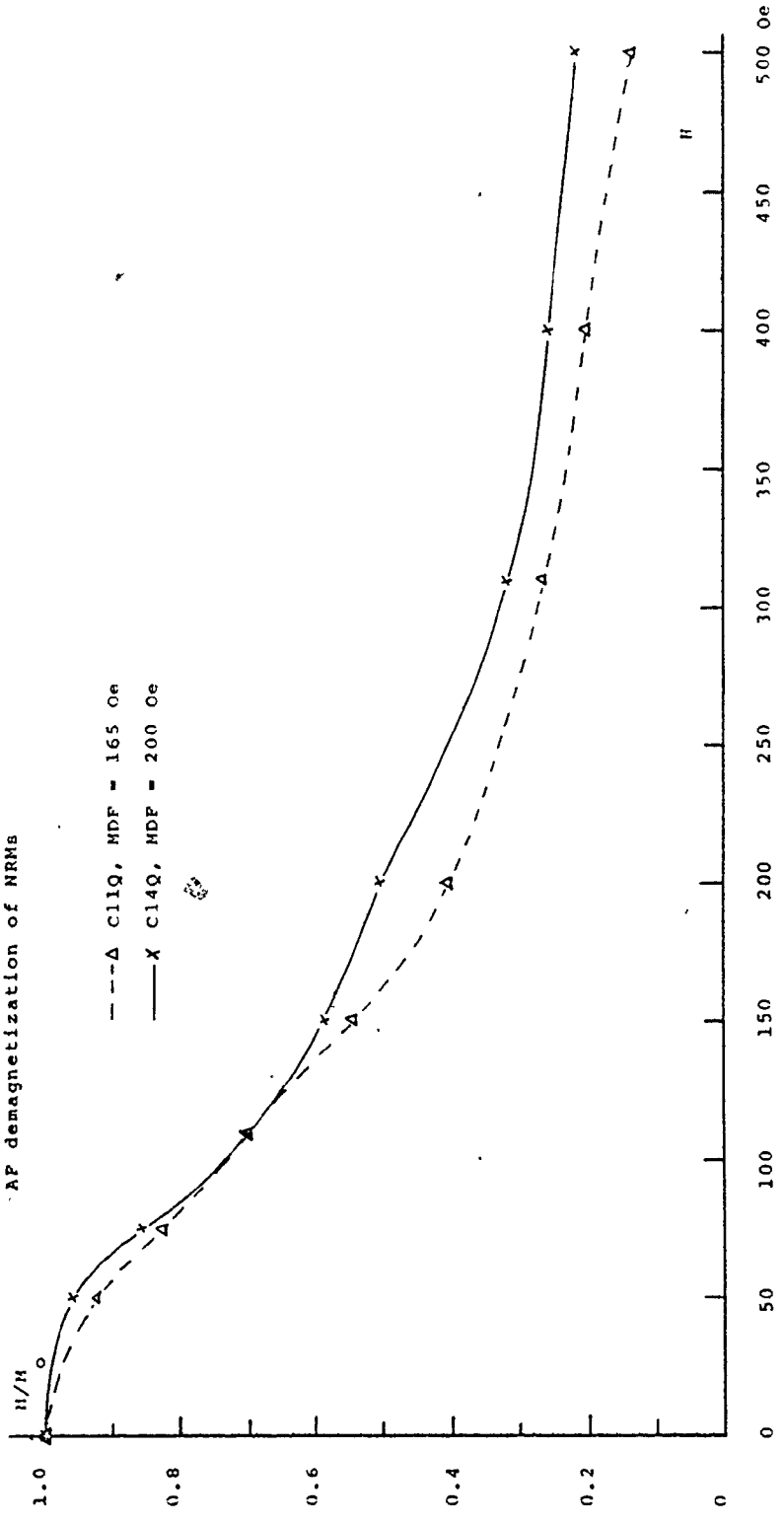
Figure 7 - 25.
SJHS
AP demagnetization of NRMs
---Δ C11Q, MDF = 165 Oe
——X C14Q, MDF = 200 Oe
H/H o
1.0
0.8
0.6
0.4
0.2
0
0
50
100
150
200
250
300
350
400
450
500 Oe
H

Dissolution of specimens, by nitric acid, revealed black insoluble particles which could be picked up by a magnet.

The MDFs of the NRMs of two specimens (figure 7.25) were 165 and 200 Oe.

7.3.11 SJLS

Paleomagnetism 6.2

Mössbauer spectra, appendix V

SJLS was a 46 cm high stalagmite with distinct speckled layering in opaque white and translucent white calcite. Intensities of central specimens ranged from 6 to 70 x 10^{-7} G cm^{-3}.

Specimen B15Q, figure 7.26, had an MDF of 145 Oe upon AF demagnetization of its NRM.

Dissolution of central and lateral specimens produced copious frothing, leaving behind quartz and black magnetic grains as chief constituents of the insoluble residue.

The thin section showed opaque grains arranged along growth layers with quartz grains and other non-calcite material, undoubtedly of flood-deposited , detrital origin. The opaque grains ranged up to about 0.5 mm in size; they were rounded to angular, frequently being tabular. In reflected light the surfaces of the opaques were mostly a uniform gray colour , identified as magnetite; a few were identified as exsolved titanomagnetites. The sides showed bays, pits and reentrant

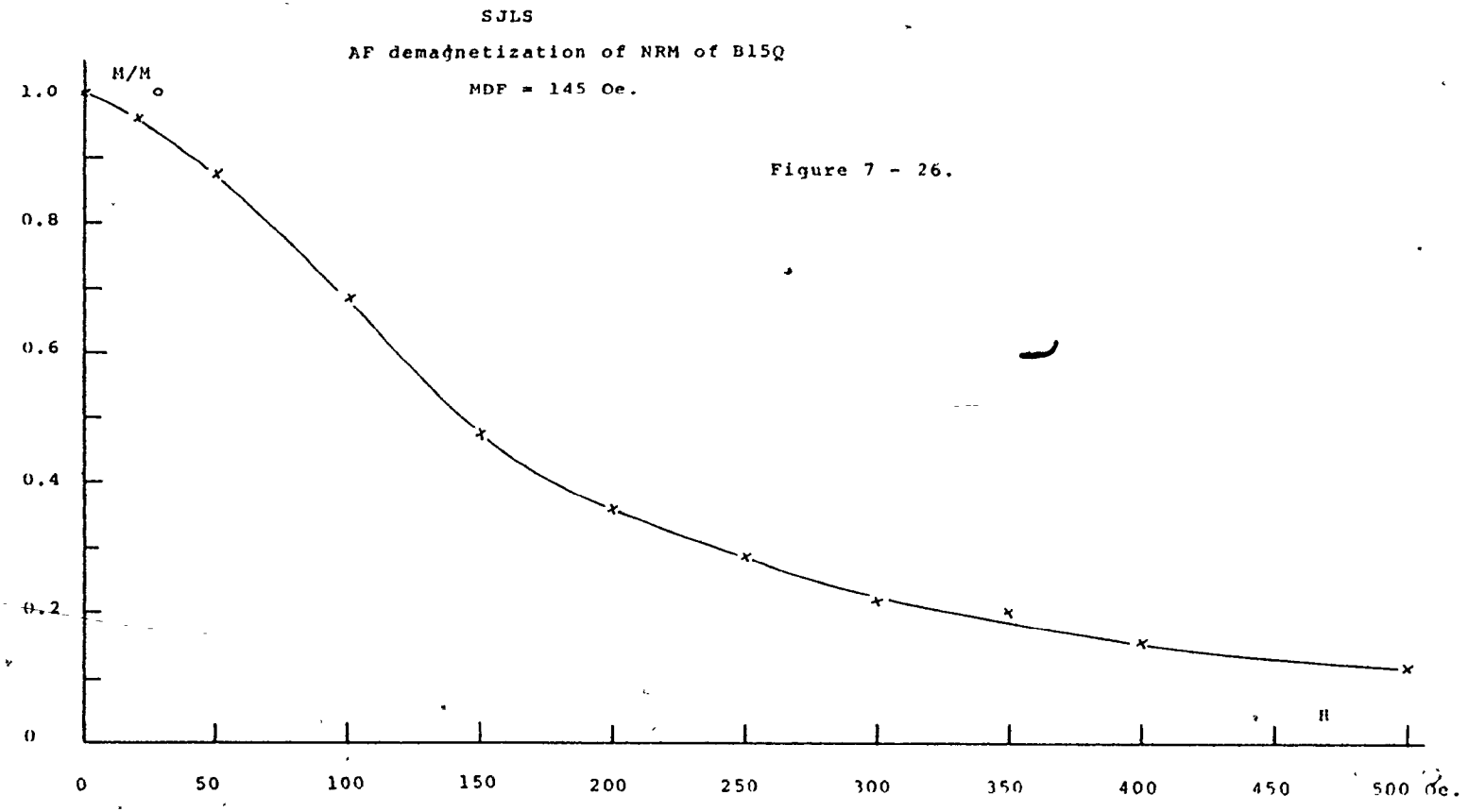
SJLS
AF demagnetization of NRM of B15Q
MDF = 145 Oe.
M/M
o
1.0
0.8
0.6
0.4
0.2
0
0
50
100
150
200
250
300
350
400
450
500 Oe.
H

Figure 7 - 26.

cavities as though due to solutional attack. The cavities were often filled with calcite or fine detrital material. There did not seem to be any associated alteration products or rims although this possibility was not ruled out.

Clearly the opaque mineral and the insoluble black magnetic mineral are the same. It was possible to separate magnetic grains from the insoluble material, using a small magnet inside a test tube, in preparation for Mössbauer spectroscopy. Dilute HCl was used to minimise oxydation effects of the finer particles. After withdrawing the magnet the particles were washed off the test tube into a mortar using acetone. A few hundred mgrams were mixed with inert BN_3 paste and set inside a copper ring for the absorber. The spectra and best fits are shown in appendix V, figures10-11. The sample is magnetically ordered at room temperature with an internal field of 470 KOe, which corresponds to magnetite (eg Sprenkel-Segel, 1976). The separate hyperfine fields appear smaller, perhaps due to partial cation substitution, or to cation deficiency (Weber and Hafner, 1971). The first explanation is preferred because of the few titanomagnetite grains observed in the polished thin section.

7.3.12 DAS1

Paleomagnetism, 6.4

This 21 cm high stalagmite possessed a translucent amber centre and gray-black sides. The amber colour is probably due to water soluble organic material in the calcite, whereas the gray-black sides are due to insoluble organics and other detritus.

Figure 7 - 27.

DAS1 B10Q

AF demagnetization of the NRM

MDF = 210 Oe.

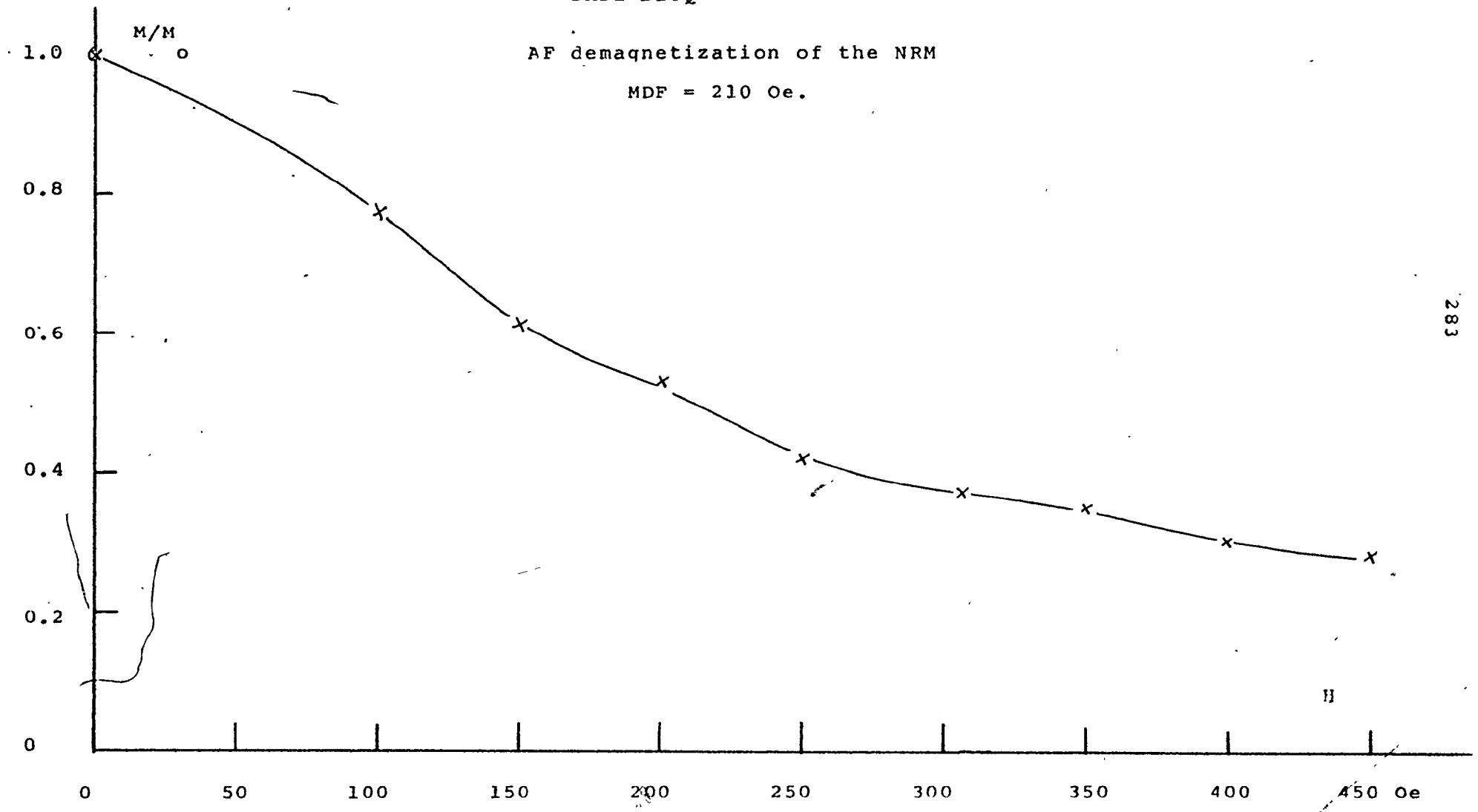

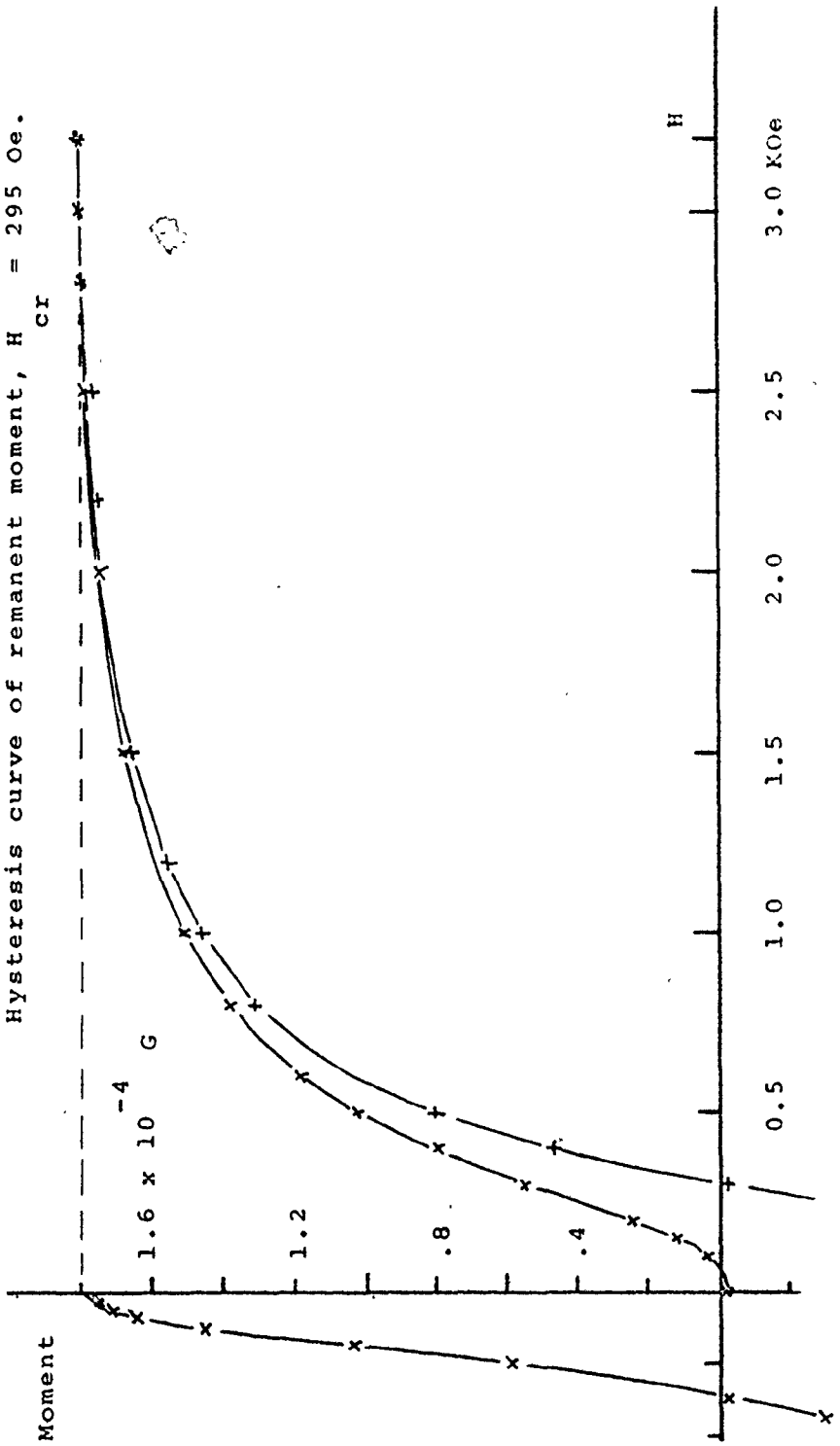
Hysteresis curve of remanent moment, H = 295 Oe.
cr
DÂS1 B4Q
Moment
1.6 x 10 -4 G
1.2
.8
.4
0.5
1.0
1.5
2.0
2.5
3.0 KOe
H

Figure 7 - 28.

Figure 7.27 shows the demagnetization of the NRM of B10Q. The MDF was about 210 Oe. Figure 7.28 shows the hysteresis of specimen B4Q. Small viscous effects were noticed in the magnetometer output. Even so the coercivity of remanence was a respectable 295 Oe. Fields high enough to convincingly produce saturation could not be obtained in this experiment.

NRM intensities of central specimens ranged from 0.4×10^{-7} to 3×10^{-7} G cm^{-3}.

7.3.13 DAS2

Paleomagnetism, 6.5

DAS2 was a 71 cm high stalagmite having a variable diameter from 10 to 17 cms. From the same cave as DAS1, it showed the same kind of translucent amber centre and opaque gray-black sides.

The thin section showed growth layers marked by detrital material. Dissolution of specimens in HCl or HNO_3 always produced copious amounts of froth. This is interpreted as being due to the decomposition of organic material. A few large opaque grains up to about 0.2 mm were observed. They were tabular with a uniform gray colour in reflected light. Their sides showed indentations and reentrant cavities as though altered from euhedral shapes; but rims of some kind of alteration product were not detected. These large opaque grains were associated with detrital material along the growth layers.

DAS2 C32S

AF demagnetization of the NRM Figure 7 - 29

MDF = 255 Oe

(a)

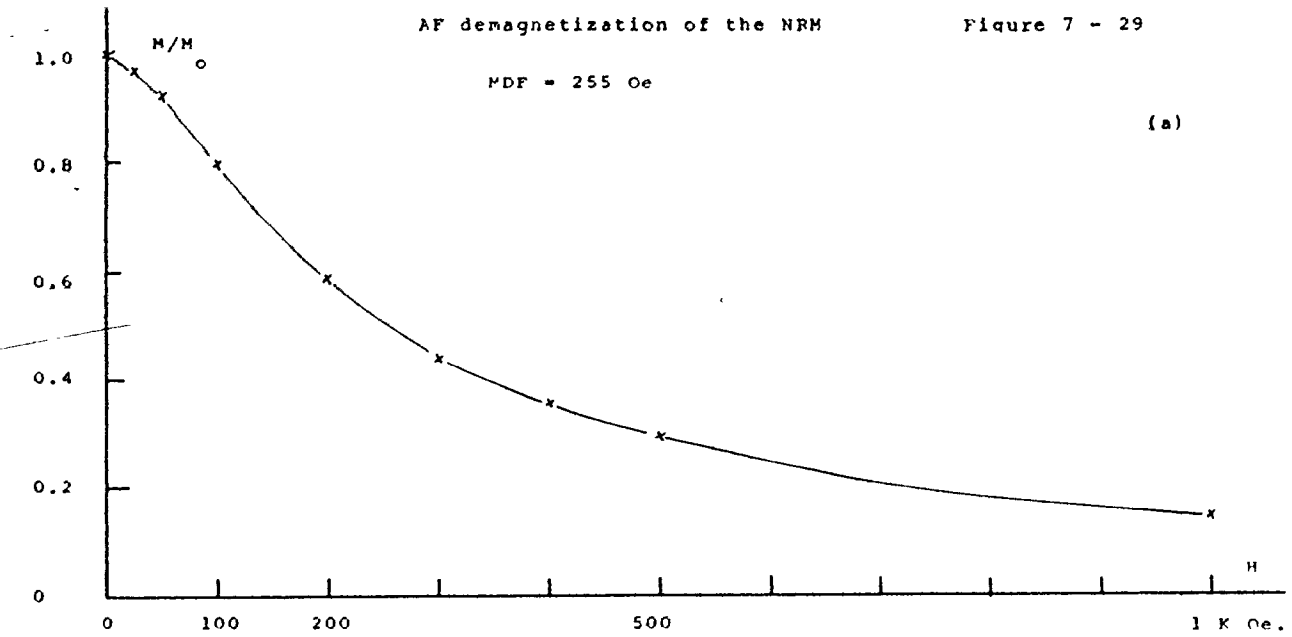

Zijderveld diagram from the AF demagnetization of C32S

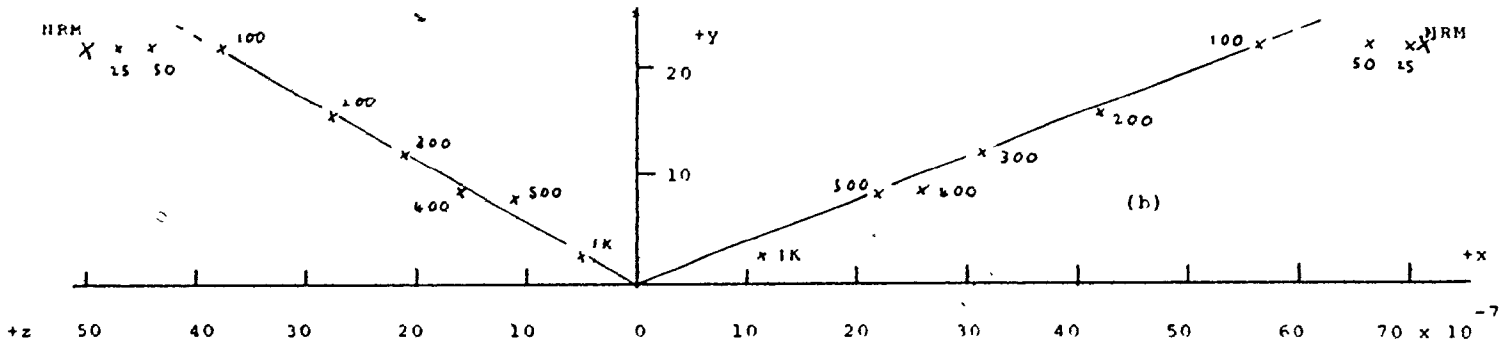

DAS2 Figure 7 - 30 (a)

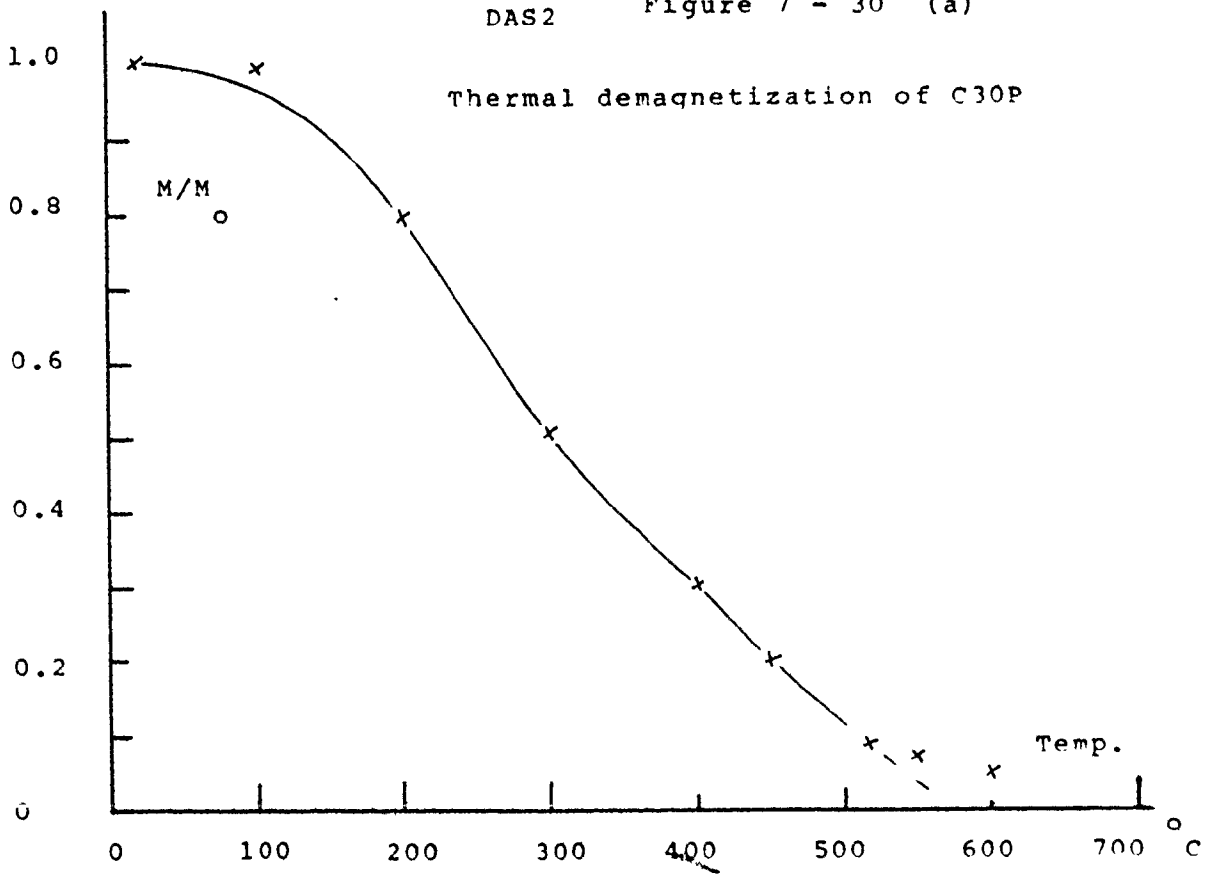

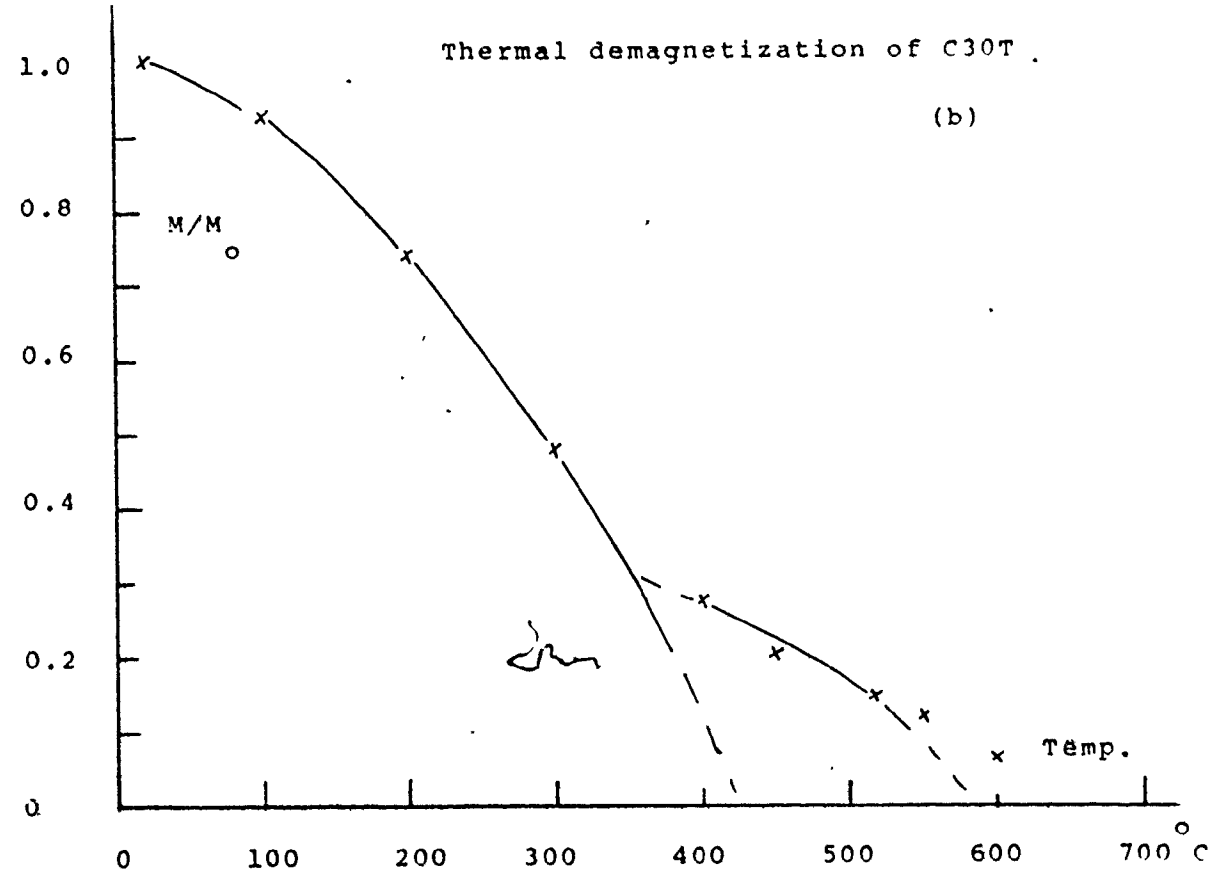

DAS2 C17T

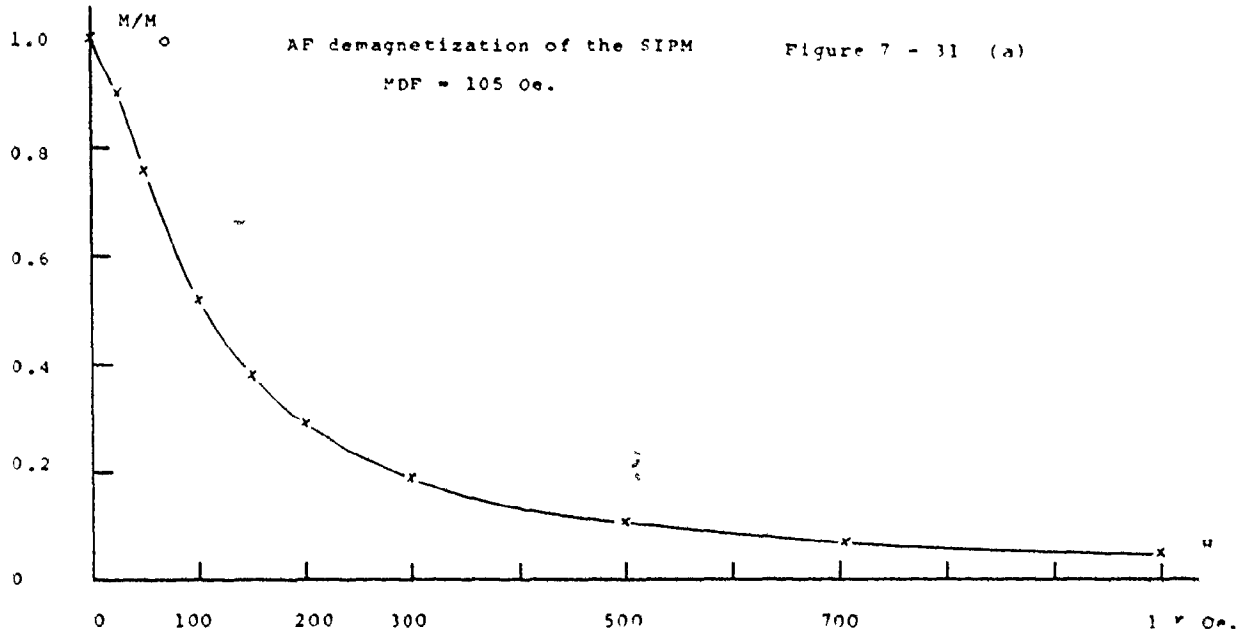

AF demagnetization of the SIPM

MDF = 105 Oe.

Figure 7 - 31 (a)

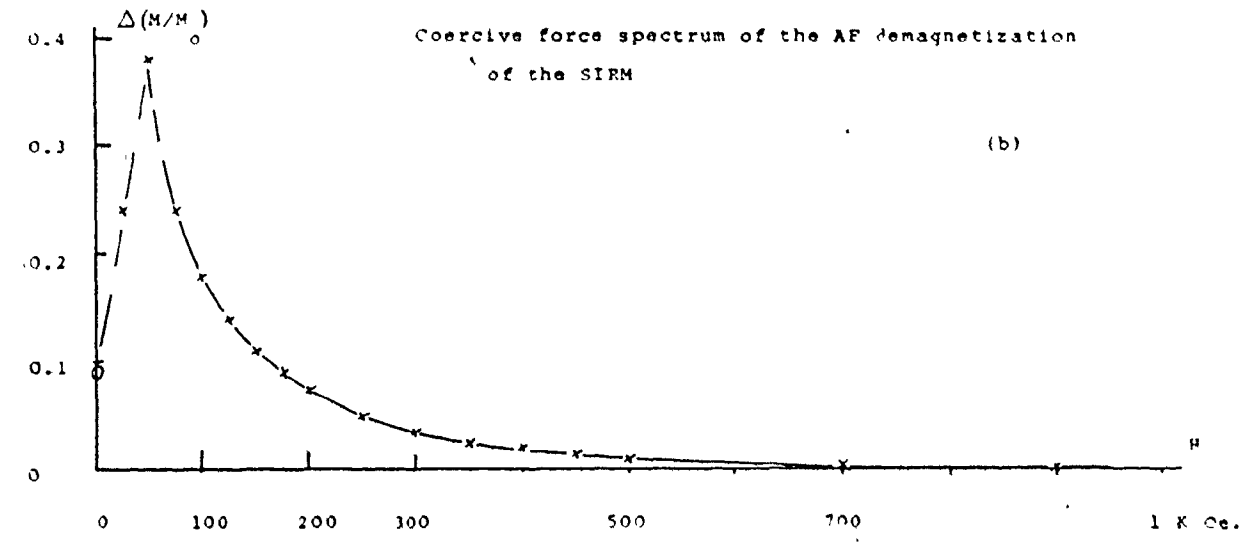

Coercive force spectrum of the AF demagnetization of the SIRM

(b)

Figure 7 - 32.

DAS2 C17T. Induced and remanent hysteresis curves

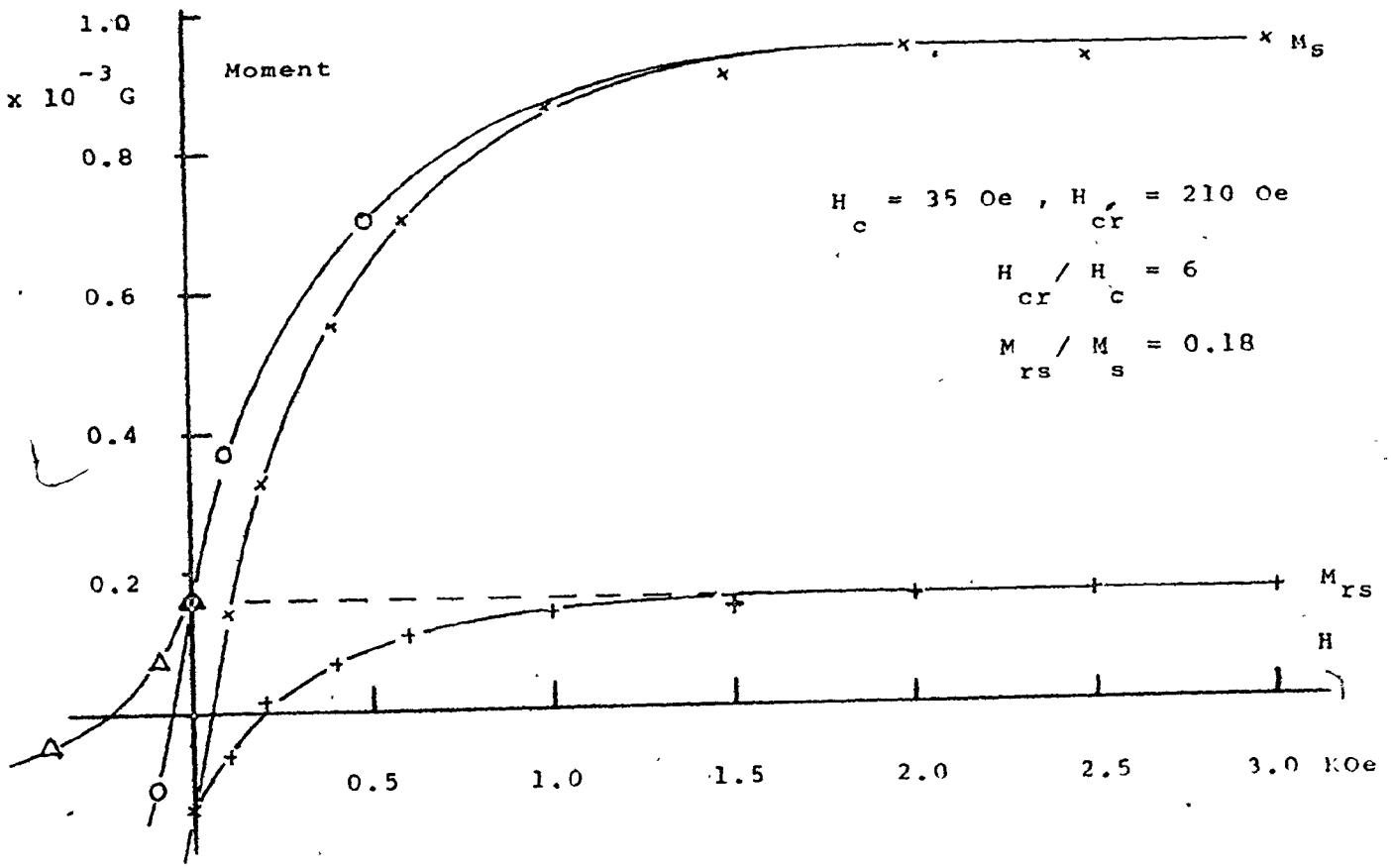

NRM intensities of central specimens ranged from about 0.4×10^{-7} to 18×10^{-7} G cm^{-3}.

Figures 7.29a and b show the AF demagnetization and Zijderveld plots of pilot specimen C32S. The MDF was about 250 Oe.

The best estimate of Curie point temperatures from the thermal demagnetization of C30P and C30T was 560 to 600 ^{o}C (figures 7.30a and b).

Lateral specimen C17T was given an SIRM and AF demagnetized to 1 KOe (figures 7.13a and b). The MDF was 105 Oe and the bulk of the CFS was below about 300 Oe.

Figure 7.32 shows the hysteresis of this specimen using the vibration magnetometer. The ratio M_{rs}/M_s was 0.18 and H_{cr}/H_c was 6. By Parry's rule and the low pilot MDF this sample possessed soft components. They are probably due to large MD magnetite grains as seen in the thin section. The clean NRMs were still adequate for paleofield direction estimates, and where the remanence was high enough, the precisions of the cuts were often good.

7.3.13.1 The TRM Experiment

Specimen B30T was given the following treatment along one axis and was remeasured at each demagnetization step (see also section 7.3.2.2):

1) demagnetization of the NRM to 1 KOe,
2) demagnetization of ARM(1) acquired in a 0.5 Oe direct field, with an AF of 1 KOe.
3) demagnetization of a TRM acquired in a nominal field of 0.5 Oe, (but which in fact had fallen to

Figure 7 - 33a; The AF demagnetization of the NRM(X) and the TRM(Δ) of DAS2 B30T

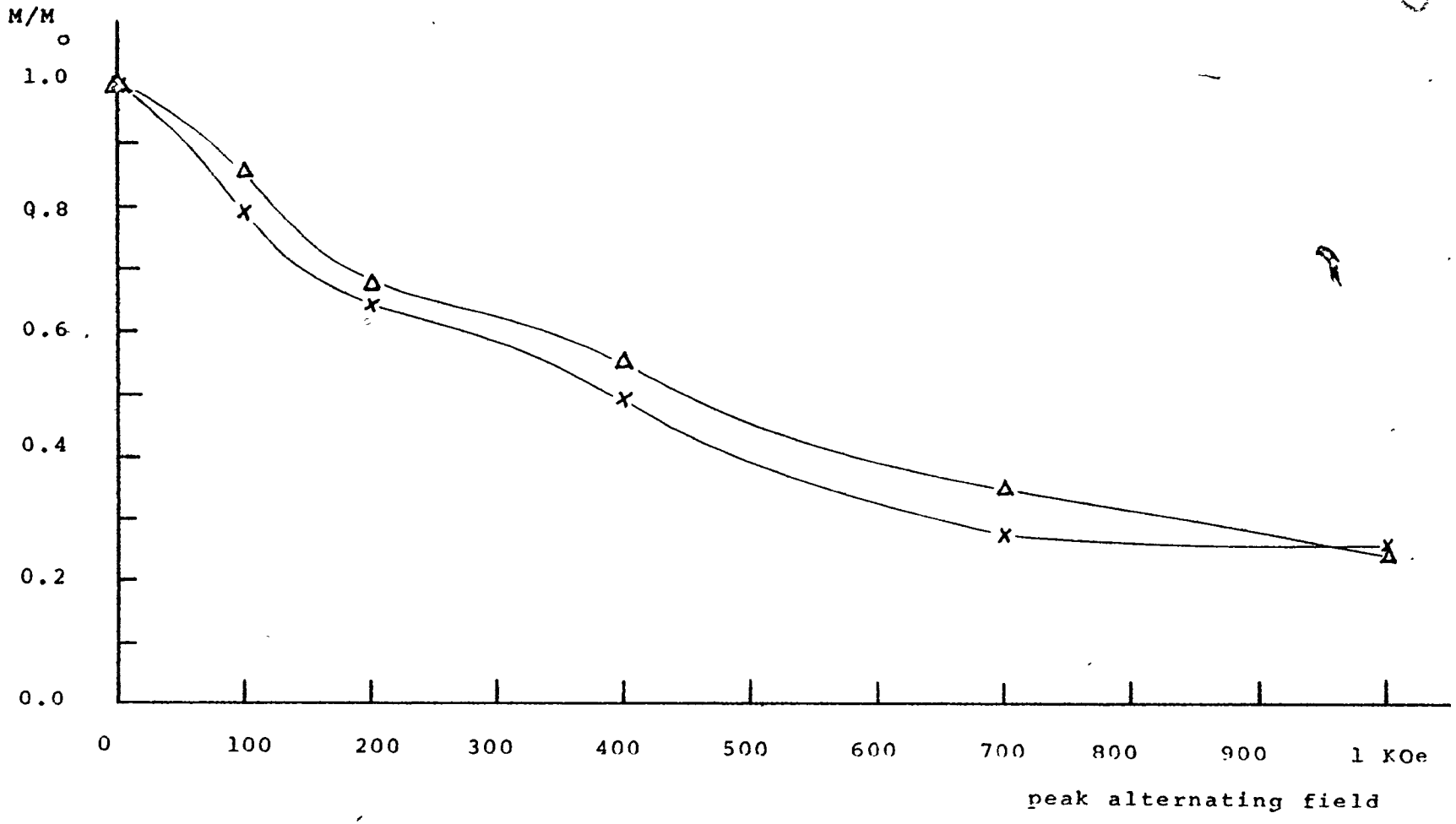

Figure 7 - 33 (b) DAS2 B30T

NRM against TRM after stepwise AF demagnetization

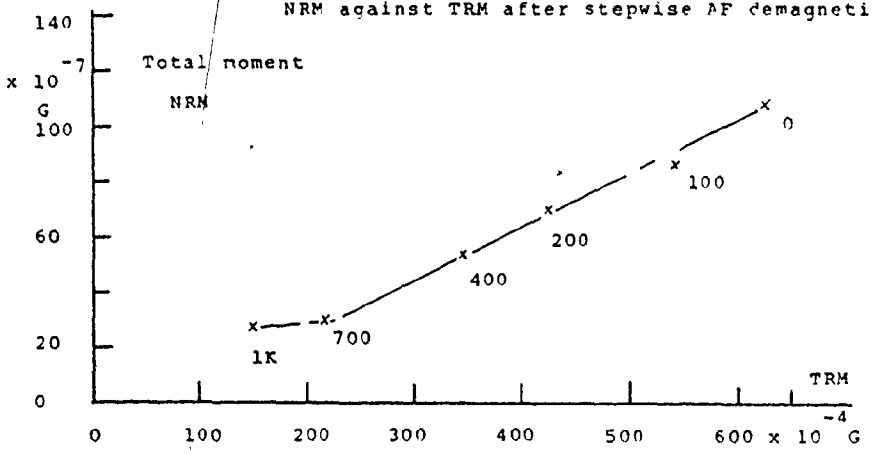

(c)

ARM(1) against ARM(2)

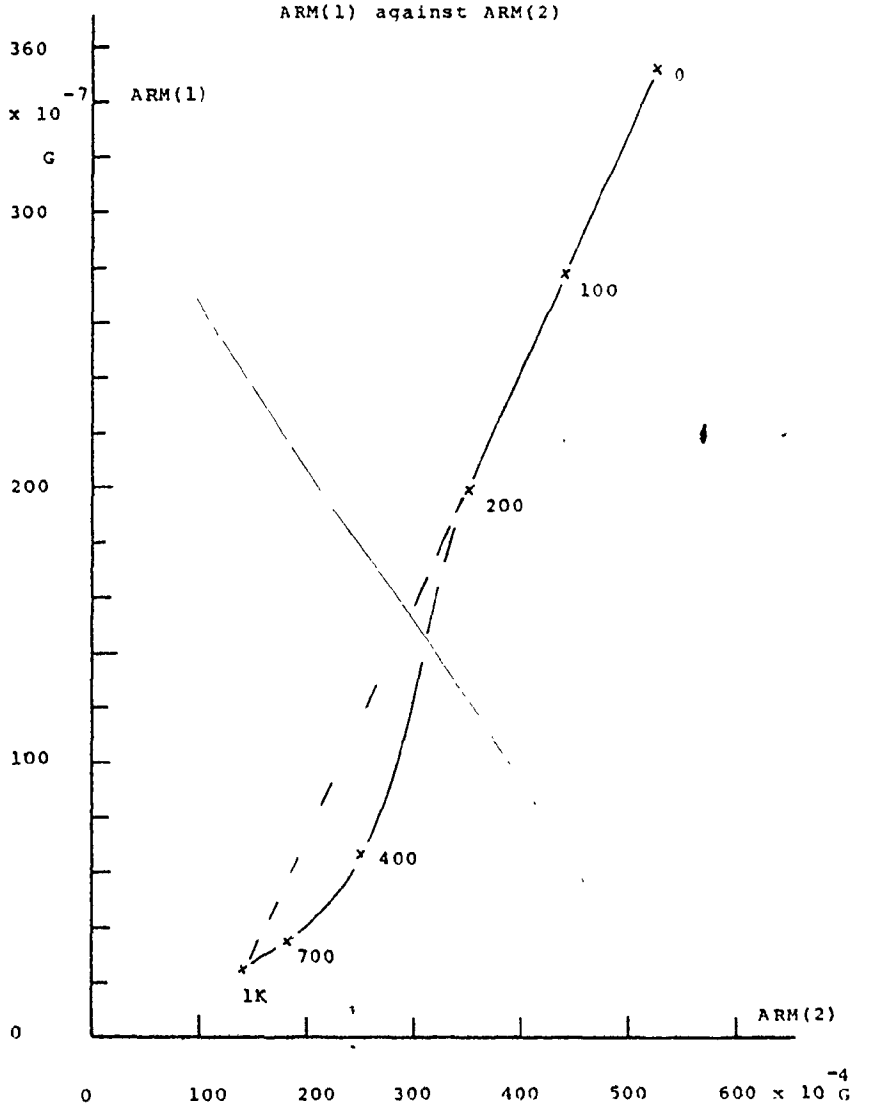

0.39 Oe at the start of cooling).

4) demagnetization of an ARM(2), acquired under the same conditions as ARM(1).

5) demagnetization of a nominal SIRM acquired in a field of 10 KOe.

After heating, the specimen had a 'burnt' look, but was otherwise intact. A detailed discussion of the ARMs is given in section 8.4.5 .

Figure 7.33a shows the AF demagnetization of the NRM and TRM, and in figure 7.33b the NRM and TRM are plotted against each other. The ratio of the NRM to the TRM was 0.17 . Assuming that the original paleofield along this axis was lower than the laboratory field by a factor of 2, then the ratio would have been 0.34. If also the NRM was a CRM, then this CRM/TRM ratio may be compared with Kobayashi's value of 0.1 or with Pucher's value of 0.17.

The SIRM of C17T was 3.9×10^{-4} G cm^{-3}, (or for 43 gms - the mass of B30T - this corresponds to 6×10^{-4} G cm^{-3}). As measured on the ScT magnetometer the SIRM of B30T, following the TRM, was $> 3.3 \times 10^{-3}$ G, this being the flux jump point of the channel used. Because of the probable inhomogeneity of magnetic material throughout DAS2, this comparison of SIRMs is not strictly valid. Even so it does indicate that magnetizable material has been created by the heating process, as in the case of ENF D9R.

The TRM parallelled the NRM except at the low and high field ends of the spectrum. The latter mismatch may be due to a spurious ARM imposed on the NRM at the 1 KOe demagnetization step. The TRM spectrum possessed a trimodal distribution.

The ARM(1) - ARM(2) plot (figure 7.33c) is not so easy to interpret in comparing the NRM with the TRM. For one thing the ARM(1), at the 400 Oe step, is anomalous. A spurious ARM would have to be quite large to account for it.

7.4 Discussion

7.4.1 The Magnetic Mineralogy of Speleothems

Diverse evidence points to either magnetite or maghemite as the carrier of the magnetic remanence of speleothems. This evidence comes from:

1) In hysteresis experiments all the specimens saturated before 3 KG, and had coercivities of remanence H_{cr}, up to a few hundreds of Oersteds.
2) The Curie temperatures of five specimens lay between 550 and 600 °C, the precise points being obscured by artificial TRMs.
3) Polished thin sections containing opaque grains showed them to have a uniform gray colour; they are probably magnetite grains. In three samples, VCCL, SJLS and SJHS were found a few (< 10%) grains of titanomagnetite in various states of exsolution and oxydation.
4) A Mössbauer spectrum of the insoluble magnetic black particles of a piece of SJLS showed the strong field-splitting characteristic of magnetite (or titanomagnetite).
5) The AA analysis of RCB gave Fe concentrations of 50 and 700 ppm. The magnitudes of the associated NRMs can be accounted for if the remanence carrier is magnetite or maghemite, but not hematite because of its much lower spontaneous magnetization.

If hematite was present in any of the specimens as the remanence carrier then it would have shown up in the high fields necessary to produce saturation and in the coercivities, H_c, or coercivities of remanence, H_{cr}. If we consider the saturation segment of the hysteresis curves for example, the percentage hematite remanence to be observable would have to be greater than the 2% error in the RCB magnetization between 5 and 20 KOe, or greater than the 2% error in the ENF magnetization between 2 and 3 KOe. The corresponding concentration ratio, Fe_2O_3 to Fe_3O_4, (as estimated from their spontaneous magnetizations) would have to be about 400 to 1. Such a proportionately high concentration as this would have been detected by the Mössbauer analyses of SJLS, or of the RCB and OULF soils. (A late discovery of hematite was found in the Petralona flowstone; see section 9.7.1)

There remains the possibility that maghemite, rather then magnetite is the the chief carrier of the remanence. It is difficult to distinguish between these two from hysteresis experiments since their spontaneous magnetizations and concomitant properties are so similar. Unfortunately it has not been possible to use the thermal demagnetization experiments to confirm a maghemite to magnetite phase change, because of doubts about the fidelity of the apparatus. It may be possible that speleothems contain mixed maghemite/magnetite grain assemblages. (see also section 8.5.1 and 9.7.1)

The RCB sample shows that fine grained iron oxyhydroxides may be incorporated in the fabric of speleothems from the detritus of nearby soils. By implication hematite may be similarly transported if present in the original soil

and if it withstands hydration. Fe_2O_3 and the oxyhydroxides of iron can be transported quite long distances in the form of sols ('Iron', Handbook of Geochemistry). The oxyhydroxides evident in the Mössbauer spectra of the calcareous soils account for the superparamagnetism of both soil and sample. They may also account for the VRM of RCB and OULF. They do not account for the bulk of the remanence since saturation occurs at about 3 KOe in all the Bermudan samples and in OULF. The oxyhydroxides probably require much higher fields to produce saturation (eg, as for goethite; Strangway, et al, op cit).

The coercivity spectra from the SIRMS of the magnetite-bearing specimens ranged from low ($H < 40$ Oe) to high ($H > 1$ KOe). This indicates the full range of coercivities as met with in other terrestrial rocks. Of those samples carrying a measurable remanence OULF was the only one possessing a VRM larger than the stable component, and hence, unusable for paleomagnetism.

This study has nothing to say about the presence or evolution in speleothems of non-magnetic iron minerals such as siderite, $FeCO_3$.

7.4.2 The Origins of Speleothem NRM

Evidence is now discussed to show that the natural remanence of speleothems is of both detrital and chemical origin. The speleothem DRM may have significant differences from the classical case, the CRM is probably complex and these two modes of magnetization may often be intimately linked.

7.4.2.1. The DRM of Speleothems

In the canonical case of DRM (section 1.5.3) magnetized particles settle in still water onto a sedimentary bed having been aligned by the field torque against viscous drag, thermal agitation and bed surface effects. In the case of speleothems, magnetite-bearing detritus may be considered to have been deposited in three ways:

1) Cave floodwater has swept past the speleothem coating its surface with magnetite along with other sediment. The water flow was fairly fast and the floods probably subsided quickly. Examples are:
   a) Near the base of TS are coarse quartz grains included in a black layer which has a higher remanent intensity than the rest of the speleothem.
   b) VCCL carries visible magnetite grains along with quartz and other grains of sand size. Near the base there are even some small pebbles up to 0.5 cm in diameter. The sample came from a passage which acts as a flood route at the present time.
   c) DAS2 lay in a sandy alcove of a large passage which takes a flood current fast enough to move boulders. Magnetite grains are seen in thin section associated with detrital organic and other material along growth layers. Their distribution is inhomogeneous.

2) Several speleothems came from passages which were not such fast flow conduits , but suffered backflooding due to obstruction further downstream.

The magnetic particles may then have settled from muddy water onto the speleothem surface. This more nearly resembles the classical DRM. Examples are:

a) SJHS was on the side of a large semi-abandoned flood passage, and possessed a thick multilayered outer dirt rind which had become calcified. The passage itself contained abundant quantities of mud.

b) DAS1 was situated at the top of a long upward-sloping passage having thick mud deposits. It is known that the passage back-flooded in modern times, over a lip to another passage. DAS1 would then be under several feet of water.

3) From personal observations the feedwater from which flowstones grow is often quite substantial following rainy weather. So although flowstones may lie well away from floodable parts of the cave, the feedwater may itself be enough to bring in iron-bearing detritus. Examples are:

a) RCB contains insoluble iron oxyhydroxides and perhaps insoluble organic materials from nearby soils. There are vugs and microgours to trap the water-borne matter. OULF may be included here. Other examples may be ENF and BJTL which appear to contain insoluble organic matter.

All of these detrital coatings are subsequently amenable to physico-chemical changes by the speleothem feedwater (dripwater). It is a simple observation that mud smeared on the top of a modern stalagmite tends to become redistributed down the sides from the action of the dripwater. This has been referred to earlier (section 4.6.1)

as the 'wash-off' effect. It also applies to dust particles which have settled from the cave atmosphere, which could include submicron-sized magnetite grains.

7.4.2.2 The CRM of Speleothems

In igneous rocks CRMs are associated with such alteration products as intergrowths and relict pseudomorphs which may be observed in thin section. It is often an oxidation process and by definition, occurs below the blocking temperature of the original grain (see, for example, Rumble, 1976, or Johnson and Merrill, 1974).

CRMs are often invoked to account for some or all of the NRM of red beds (for a review, see Turner, 1979). The magnetic mineral is hematite. Black specular grains carry a primary DRM, because they possess the direction appropriate for the age of the bed, whereas the red coatings on quartz grains are evidence for a secondary CRM carrying directions of post-depositional age. This is probably the best situation in which to use the technique of chemical demagnetization to separate the two directions, (Collinson, 1966).

Magnetite and titanomagnetite in limestones are considered to carry primary DRMs because they reflect the depositional fabric (Turner, 1975). However the reducing conditions which often prevail during the diagenesis of pelagic limestones may also be the cause as well as the preserver of minerals like magnetite, pyrite and pyrrhotite. Similar conditions may apply to modern lacustrine sediments, whence it may become difficult , if not impossible, to distinguish between a post-depositional DRM

and a CRM (the so called chemical overprint, Creer et al,1972).

Research into the transport, dissolution or crystallization of sub-micron sized remanence carriers, such as magnetite, has hardly been attempted under the conditions which approximate natural environments. In chemical studies of surface and subsurface waters, for example, the lowest size of millipore filter used is commonly 0.5 μm. Metal or metal oxide grains, etc, which may be in colloidal suspension or adsorbed onto fine clay particles of less than this size are often assumed to be in solution ('Iron', Handbook of Geochemistry, 1970). Large magnetite or titanomagnetite MD grains can safely be ascribed to a DRM. In contrast, the history of the submicron SD grains or their type of remanence in a sediment may often be uncertain.

It is emphasized at the outset that the evidence for the nucleation and growth of remanence-bearing magnetite grains in speleothems is largely circumstantial. Indeed it is difficult to see how the presence of speleothem CRM can be directly proved or disproved since it is the finished product that is observed rather then the process itself. A complete CRM, carried by fine grains, has no rock magnetic properties which will distinguish it from a DRM or (artificial) TRM, with the possible exception of its generally lower intensity. The best evidence for speleothem CRM could only come from a controlled laboratory experiment in which the crystallization process itself is observed.

In speleothems the indirect evidence for CRMs is as follows:

1) Low intensity NRMs are present in the upper part of

TS, in GOF1, the early core of SJHS and in various test samples, in the apparent absence of other detrital material . SIRMs could be produced in pure-looking samples like DBS1 and WCS1. The mineral is magnetite.

2) In these and all other cases where AF cleaning was carried out there were apparently no inclination or declination errors, here taken to indicate the absence of depositional effects. This was true, however even where detrital material was known to be present, for example, in the outer dirt rind of SJHS.

This last observation is somewhat surprising in view of the large amounts of detrital material present in SJHS and others like it. There are two possibilities. Either there exists a DRM always free of surface effects, or a secondary CRM considerably modifies the primary detrital grains as the drip water continues to flow. For the first possibility it may be noted that the larger grains are more likely to be affected by the surface than the micron and submicron grains. However, the larger grains are magnetically softer and are also likely to acquire VRMs in thedirection of the present field. In summary, the larger grains though being most subject to surface effects, will contribute least to the stable part of the NRM.

3) It is probable that Eh - pH conditions in drip-waters are favourable for the transport of FeII and the precipitation of Fe_3O_4. Edmunds (1973) has shown that in a confined limestone aquifer Eh decreased and pH increased to a point where dissolved oxygen was undetectable, nitrate and sulphate were successively reduced and ferrous iron increased.

Specific reducing bacteria may also be present to assist these processes.

4) Much of the colouring seen in speleothems is probably due to organic material , rather than to trace elements (Gascoyne, 1977). Such coloured speleothems always produce copious quantities of scummy froth upon acid dissolution of the calcite and is taken to indicate the presence of organics. By contrast "pure" white speleothems seldom produce froth (M.Gascoyne, op cit; and this study). The speleothem colours are - black (eg GVF1), brown (ENF, BJTL), red-brown (RCB , but most of the colour is due to iron), yellow or amber (DAS1, DAS2, & WCS1), yellow-brown (TS), red (the so-called carrot speleothems) and brown-pink (GQF1). Laverty and Crabtree (1978), using I-R spectroscopy showed that in a red 'carrot' speleothem iron was present complexed with humic substances.

It is well known that organic materials (humic and fulvic acids) in water, are capable of absorbing or complexing iron in both valency states, and of stabilizing soluble iron in the ferrous state (Theis and Singer, 1974). Organic acids in natural waters are strongly adsorbed onto calcium carbonate particles and are effectively co-precipitated (for a review of organic - metal interactions see Jackson et al, 1978). Ca^{2+} ions can displace some of the iron from the organics as precipitation occurs (Boyle, et al, 1977). The exact mechanisms may not be fully understood, but the ubiquitous presence or organics in speleothem is indication that iron might have been transported and precipitated by the organic complexes.

5) Additional magnetite was apparently created upon heating ENF D9R and DAS2 B30T. The effect is not uncommon in other areas of rock magnetism where, for example, magnetite may be produced from the thermal decomposition and oxidation of titanomagnetite, pyrite or pyrrhotite (Turner, 1975, op cit Kono, M, 1978). In these speleothems the source is likely to be iron bound by organic material. The match of coercivity spectra of ENF D9R (and to a limited extent of DAS2 B30T) before and after heating is strong indication of a common source for NRM and TRM. It could then be argued that this favours an original crystallization process for most of the NRM.

7.4.3 Models of the NRM of Speleothems

Figures 7.34a, b and c are cartoons, with descriptions, to illustrate possible models for the origins of the NRMs of speleothems. The three styles may not just be alternatives to one another but may operate concurrently in some cases.

Briefly, speleothem NRM may be a primary DRM, a secondary CRM following the DRM, or a primary CRM. If the primary DRM exists without chemical modification it must be free of surface-effect errors in order to be consistent with the experimental findings. Some NRMs may be combinations of these three styles and perhaps SJHS, SJLS, DAS1, DAS2, RCB and the base of TS provide examples. VCCL might be an example of style 1. The upper part of TS and the early core of SJHS might be examples of style 3.

Figure 7 - 34a

Models of speleothem NRM Style 1. Flood prone stalagmites with relatively high remanent intensities.

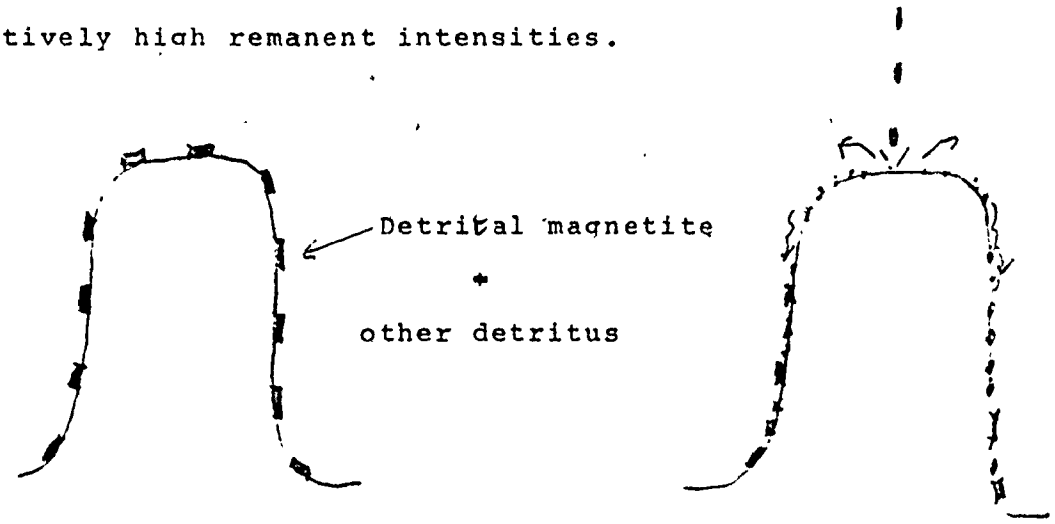

Flood deposition of magnetized grains on surface of speleothems,

↓

flood subsides,

↓

Dripwater pummels grains ('wash-off' effect and dissolution),

↓

recrystallization of grains with origin of NRM. Average grain size decreases. Calcite cementation.

This is a secondary CRM following on a primary DRM.

Figure 7 - 34b

Style 2. ' Pure ' speleothems of low or non-measurable remanent intensity.

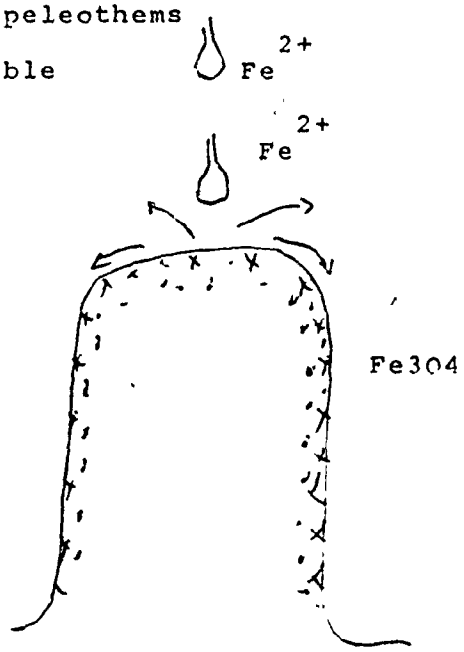

Feedwater contains Fe^{2+} in solution, low or zero dissolved oxygen, buffered by organ or microorganisms.

↓

Water reemerges from closed system into cave air CO_2 released from carbonate waters. Drip water splash, for example, reintroduces oxygen at the depositional surface.

↓

$3Fe^{2+} + 2O_2 \longrightarrow Fe_3O_4$ at alkaline pH and low Eh. Origin of the NRM and cementation.

This is a primary CRM

Figure 7 - 34c

Style 3 Organic rich speleothems of variable remanent intensity

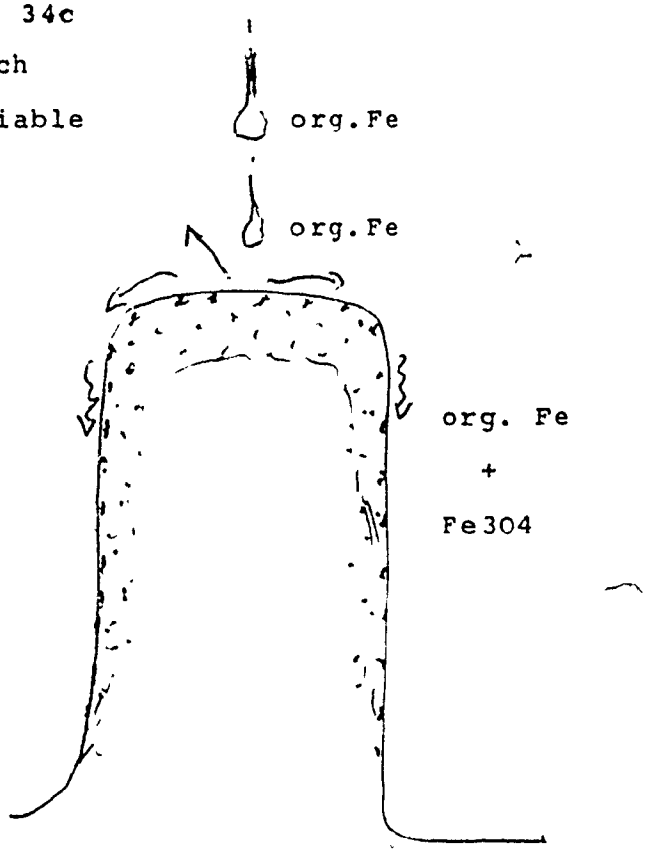

Either flood detritus or feedwater contain soluble and insoluble organic compounds with complexed or absorbed iron,

↓

At the depositional surface precipitation or colloidal flocculation of organics causes some or all iron to be released,

↓

Either Ca^{2+} + Fe org. → Ca org + Fe^{2+}

or $CaCO_3$ + Fe org → $CaCO_3$ org + Fe^{2+} / Fe^{3+}

then $3Fe^{2+}$ + $2O_2$ → Fe_3O_4

↓

Precipitation traps soluble and insoluble organics and Fe_3O_4. Origin of NRM.

This is a primary CRM.

In recovering the ancient field directions the important finding is that the directions appear to have been faithful to the field whatever the origin of the NRM. Where the intensity has been high enough viscous components are easy to remove and the statistical precision of the directions of coeval specimens has increased upon AF cleaning.

The study of the origins of speleothem remanence is important firstly for its own sake. It is also important where paleointensities are to be estimated by the analogue methods, because some kind of regularity in the original magnetization process is a necessary condition for such a method to be valid.For example, if the lower part of a given stalagmite has a secondary CRM of style 1 different from the upper primary CRM of style 2, then variable $(ARM/NRM)_{h\,const}$ ratios could result. One can envisage a secondary CRM whose magnetization was influenced by an earlier magnetization, either by direct exchange, in the case of overgrowth contact, or by close grain-grain interactions. Such a CRM would thus be different from a primary CRM.

The testing of these models and their relevence to paleointensity analogue techniques point to the desirability of trying to reproduce speleothem remanences in the laboratory. Such experiments might take rather a long time. It is suggested they include a set of drip sources at controlled pH, into a controlled atmosphere, with and without organics, with and without detritus and in a magnetic field which could be reversed.

7.5 Conclusions

The following are the general conclusions from this chapter and, to some extent, from the paleomagnetics chapters 4, 5 and 6:

1) The remanence carrier in speleothems is magnetite. or maghemite. This applies whether detritus is present or not.
2) Detrital magnetite is detected by its presence in hand sample and thin section where it occurs in association with quartz grains, insoluble organics and other non-calcite minerals all arranged along growth layers. Cave floods are largely responsible for the detritus. The magnetite grains are accompanied by a few titanomagnetite grains in some cases.
3) Organics and observed detrital magnetite contribute to a darker layering in speleothems and the NRM intensities are usually higher. From the point of view of a usable signal level therefore, the 'detrital' speleothems will tend to be preferred over the 'purer' speleothems.
4) Fortunately there do not appear to be any depositional errors even where detrital magnetite is known to be present.
5) Stabilities and coercive force spectra show that a range of grain sizes are met with, existing in the SD, PSD and MD states. Viscous components are often easily removable by AF or thermal means to recover a stable direction.
6) Some speleothems additionally can carry large viscous and superparamagnetic components of magnetization. The minerals responsible are oxyhydroxides of iron derived from nearby terra rosa soils.

7) The mode of origin of speleothem magnetization is believed to be a CRM even where there is considerable detritus. The evidence is indirect but includes the fact that magnetizations can exist without detritus, and that there are no surface depositional errors in the NRM of any of the speleothems studied so far. In most cases the crystallization of magnetite grains may have followed quite complex routes.

8) It is not likely that stable magnetic grains will continue to evolve or be reset to another magnetization once they have become cemented into the calcite matrix. Most speleothems are compact whether micro- or macrocrystalline. The contemporary top of TS has an NRM direction well in accord with the present field direction. There are no reasons for believing that cleaned NRMs of speleothems reflect anything other than the ambient paleofield.

CHAPTER 8

THE USE OF ANALOGUE MAGNETIZATIONS IN THE ESTIMATION OF PALEOINTENSITY

8.1 Introduction

The following study and discussion address the question of whether it is possible to estimate paleofield intensities from the NRM of speleothems. The method has been to impose an ARM, in a known field, or an SIRM, as a so-called analogue magnetization, and to compare its magnitude and stability with the NRM.

The NRM of any rock is a function of the magnetic material, the grain size assemblage, the external field and the conditions (mode) of origin of the magnetization. In rocks which have been cooled through the Curie point the usual method of finding paleointensity is to reheat and then cool the sample in a known field, thus giving it an artificial (A)TRM. Since TRMs are proportional to the applied field, the ancient field is then given by:

$$H_{anc} = H_{lab} \quad NRM/TRM$$

There are certain conditions to be met which are testable. If a sample does not meet these tests, due to mineral alteration during heating, for example, it is rejected. Alternatively analogue methods may be used (for discussions on TRM and analogue methods, see volume 13 of Physics of the Earth and Planetary Interiors, 1977).

The experiments of Johnson et al (1948) have shown

that DRMs of some sediments were not linear with field up to 10 Oe. Their graph does show however, that for fields of about Earth's intensity the linearity of DRM with H was a fair approximation. The few experiments on CRMs of synthetic specimens (Kobayashi, 1962) have shown that CRM is proportional to the applied field, is as hard as a TRM for the same field, but is about one tenth as intense.

Even if it can be assumed that the original DRM or CRM was proportional to the field, there is little likelihood of repeating the various unknown but determinant conditions under which the magnetizations were acquired. As examples, for a DRM the depositional rate may be important but not known; for a CRM the same grain size assemblage may not be reproducible.

For a DRM or a CRM the next best approach to the estimation of paleointensity is to use an analogue magnetization, the most favoured of which is ARM. For SD grains, at least, it has been shown theoretically that for $\tilde{H} \geqslant H_{sat}$ the same coercive forces are activated by ARM as for TRM (eg Jaep, 1971, Banerjee and Mellama, 1974). We then have;

$$H_{anc} = H_{lab} \cdot f. \text{ TRM/ARM, f to be determined.}$$

The same approach could be applied to a CRM using a different f factor. Unfortunately most rocks possess a range of SD, PSD and MD grain sizes. This and other factors make f variable as Bailey and Dunlop (1977) and Levi and Merrill (1976) have shown.

Finally the paleomagnetist may be reduced to looking at relative paleointensities by using ARM, SIRM or other parameters such as saturation magnetization, M_s, or

susceptibility χ . For lake sediments, for example, Levi and Banerjee (1976) have compared the AF stabilities of SIRM and ARM to see which of these activated the coercive force spectrum nearest to that of the NRM; they favoured ARM.

Use of M_s or χ is supposed to normalize for the magnetic content of the NRM. However both these parameters bring out induction as well as remanence magnetizations. The normalization is false if the sample contains proportionately large numbers of soft MD grains.

The matching of the AF stability curve of a proposed analogue with that of the NRM is a first criterion for acceptibility as Levi and Banerjee pointed out. In any case SIRM and ARM ought to have congruent stability (M/M_o - H) trends since they both activate the same CFS (but see section 8.4.4). Thus ARM is more favoured because its intensity is similar to most NRMs and like them it is a probabilistic process.

8.2 The Experiments

8.2.1 Introduction

If magnetite-bearing calcite could be deposited in a known field then it would be possible to test the dependence of the speleothem magnetization on H(spel), the dependence of ARM on H_{arm} , and to compare the intensities and stabilities of the speleothem magnetization with ARM. This would directly lead to a test of;

$$H(spel) = f. H_{arm} .M(spel)/ARM, \text{ and the}$$

evaluation of f.

The feasibility of producing a remanence in artificial speleothem has not been tried here mainly through lack of time. The alternative is to study the tops of modern speleothems for which the field intensity over the past 50 or 100 years is known fairly well. This has yet to be tried with any thoroughness.(see section 8.4.6).

The experiments were limited to comparing SIRMs and ARMs with NRMs of speleothems for intensity and stability, and to testing the dependence of ARM on H_{arm}. Unfortunately though ARM was used extensively in the following studies $\tilde{H}$ was limited, by the apparatus, to 1 KOe. Therefore coercive forces from 1 KOe to saturation (2 to 3 KOe) could not be accessed.

8.2.2 The Apparatus and its Application

The NRMs of the specimens were AF demagnetized along one axis and remeasured at each step. ARMs or SIRMs were applied along the same axis, stepwise demagnetized and remeasured. Direct fields were applied by a constant current supply attached to Helmoltz coils and were measured and checked with a sensitive fluxgate probe. No attempt was made to annul other direct fields (eg, Earth's field components) transverse to the specimen axis. AFs were applied parallel to the DFs by a solenoid powered by a Schonstedt 1 KOe demagnetizer. Remanence measurements were made using one channel of the ScT magnetometer. A mean was taken from four measurements and this also excludes any sample holder contribution. In every run two or three specimens were treated sumultaneously as a check on instr-

instrumental or measurement errors.

8.2.3 Treatment of the Data

If due to the limitations of the apparatus the maximum demagnetization of the NRM is 1 KOe and this is followed by an ARM for which $\tilde{H}$ is also 1 KOe, then the subsequent remanence at any demagnetization step will include the NRM remanence from 1 KOe to saturation, if it existed originally. In other words, before demagnetization of the nominal ARM:

$$M_0 = ARM_0 - 1K + NRM_{1K - sat.},$$

and for any subsequent demagnetization step,

$$M_H = ARM_H - 1K + NRM_{1K - sat}.$$

It is not strictly valid therefore to compare the M/M_0 v H, $(J/J_0$ v H) stability curves of the ARM with the NRM to test for congruency as, for example, Levi and Banerjee((op cit) have done. Instead it is better to plot NRM against ARM (or SIRM) for each demagnetization step, or to plot NRM/ARM against field as McElhinny and Evans (1968) have done. In both cases a straight line will result if the analogue activates the same coercive forces as in the NRM, whatever the shape of the spectrum. Departures in linearity at low $\tilde{H}$ may be interpreted , for example, as being due to the viscous changes in the NRM. The two 1 KOe endpoints should be the same for the ARM as for the NRM - it is simply $NRM_{1KOe - sat}$, as we have seen. Any difference between the two endpoints is most likely an indication of instrument and measurement errors.

From the NRM - ARM straight line graph we may estimate;

$$H_{app.anc} = H_{arm} \cdot NRM/ARM ,$$

where $H_{app.anc}$ (hereafter shortened to H_{a-a}) is understood to be an apparent ancient field, with f put equal to unity. NRM and ARM are considered to be partial remanences between two demagnetization steps.

With sample DAS2 some attempt was made to find the H_{a-a} variations along the length. The procedure was adopted of using the 100 to 1 KOe steps, even though departures from a straight line, through this range, sometimes existed. Thus;

$$H_{a-a} = H_{arm} (NRM_{100} - NRM_{1K})/(ARM_{100} - NRM_{1K}) ,$$

As before $f = 1$, and this assumes in addition that f is the same from layer to layer.

In a few cases ARM_{100} was also plotted against H_{arm} to test for linearity . Because the final demagnetization step NRM_{1K} is almost the same whether H_{arm} is a few Oersteds or zero (except for small differences), and if NRM_{100} is read off the ARM ordinate, the same equation results. We have:

$$(ARM_{100} - NRM_{1K})/H_{arm} = \text{gradient} = (NRM_{100} - NRM_{1K})/H_{a-a},$$

from which,

$$H_{a-a} = H_{arm}(NRM_{100} - NRM_{1K})/(ARM_{100} - NRM_{1K}),$$

as before.

All NRM - ARM plots are for total moment of that specimen, and the units are in Gauss, or G x 10^{-7} . The exception is the graph of figure 8.9 of $H_{a-a,x}$ against

$NRM_{100,x}$ where the latter is in G cm^{-3} x 10^{-7}, ie it is the specific magnetization.

Where there is uncertainty in the line of any graph the probable trend is indicated by "- - -", and greater uncertainty is expressed by a "?" .

8.3 Specimens BJTL A3U and SJHS B11P

The samples BJTL and SJHS were known to have low or zero remanences after the 1 KOe demagnetization point. Therefore the ARMs and NRMs could be compared within this range using a M/M_0 - $\tilde{H}$ plot. The specimens were treated together with demagnetization of the NRMs taken to 1 KOe. The ARMs were imposed in an AF of 1 KOe.

Figures 8.1a and b. For A3U the ARMs were all of the same hardness but were significantly softer than the NRM to almost 350 Oe. For B11P the ARMs were only slightly softer than the NRM and the curves were parallel after about 100 Oe. Figures 8.2a and b also show these trends despite the poorer data at the higher AF levels.

Figures 8.3a and b are the plots of ARM versus DF, normalized to unity at 2.0 Oe in order to compare shapes. Neither plot shows ARM proportional to field , and A3U is more curved than B11P. For fields of Earth's intensity, ie. $H < 10$ Oe, the approximation of ARM linear to H is only fair; the change in the ARM - H gradient in this region being over 20%.

The specimens were chosen for their low coercivities and these are almost certainly due to MD type grains. Indeed SJHS is known to have large magnetic grains visible

General Note

For all NRM - ARM figures in this chapter and in appendix IV, the magnetizations are; x 10^{-7} G, total moment, unless otherwise stated.

Figures 8.1a and b

Alternating field demagnetization curves for the NRM and two ARMs of BJTL A3U and SJHS B11P.

Figure 8 - 1a

BJTL-A3U

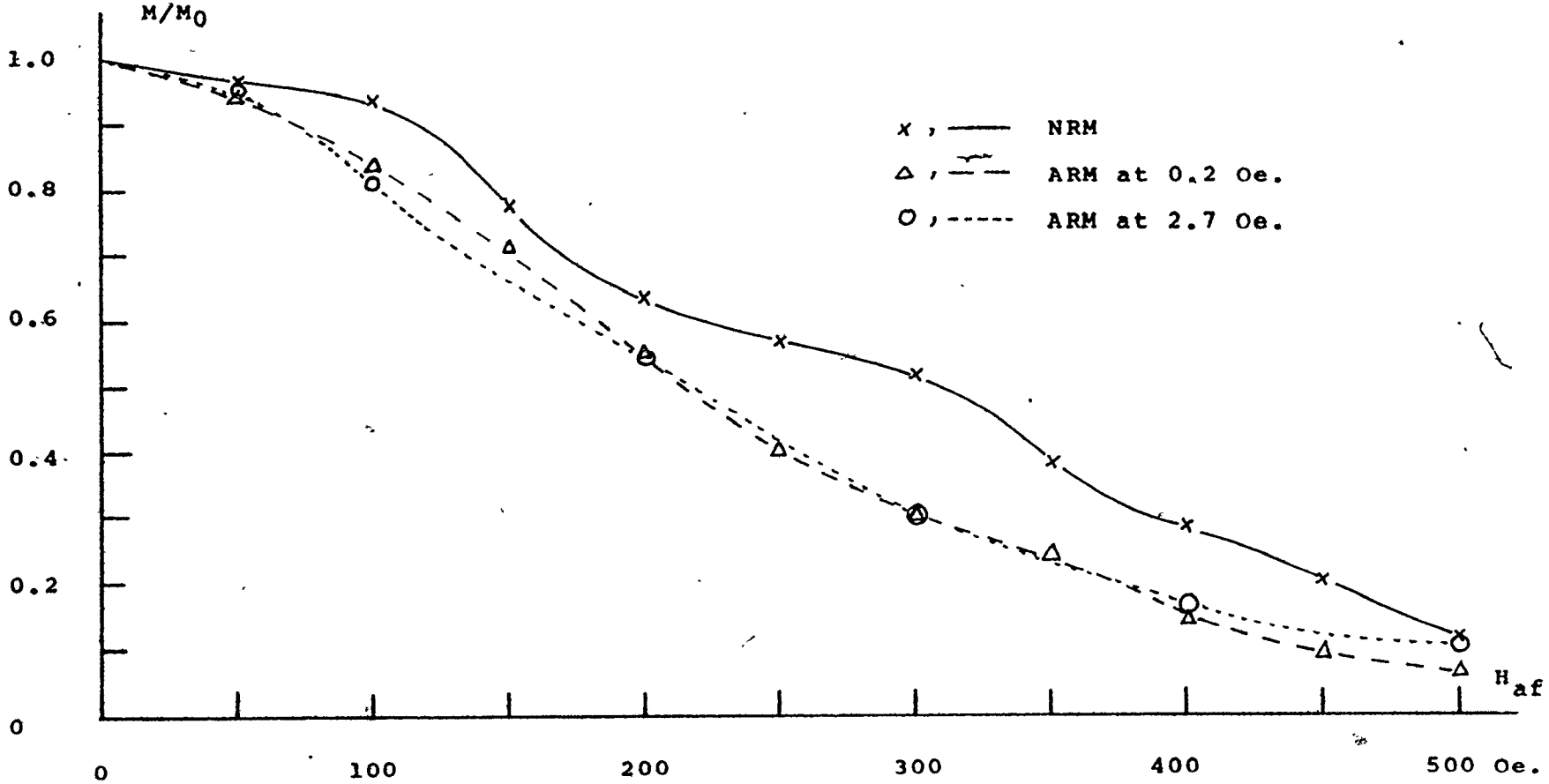

Figure 8 - 1b

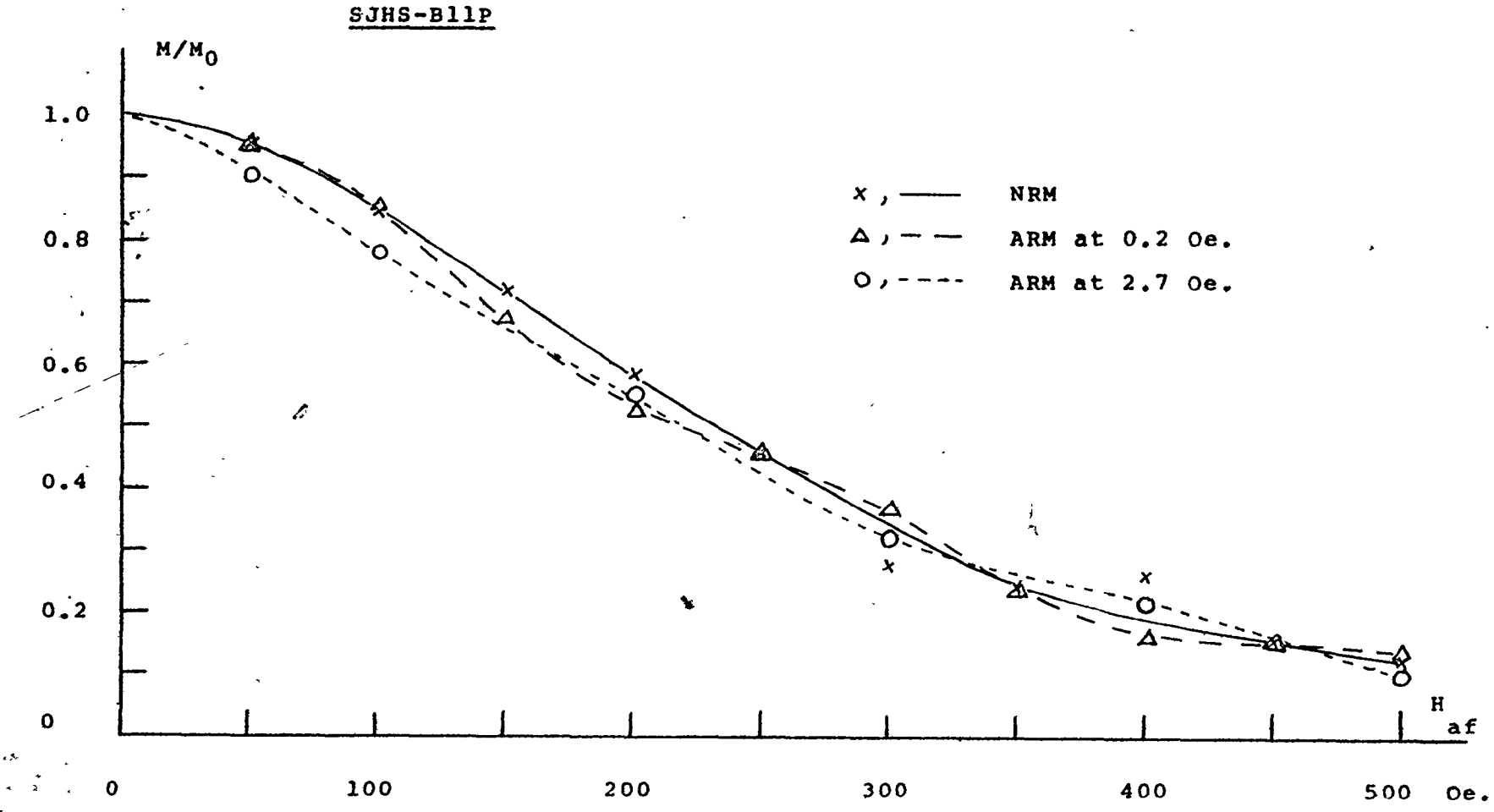
SJHS-B11P
M/M0
1.0
0.8
0.6
0.4
0.2
0
x , —— NRM
Δ , — — ARM at 0.2 Oe.
O , ---- ARM at 2.7 Oe.
H af
0
100
200
300
400
500 Oe.

Figures 8.2a and b

The NRM - ARM plots of BJTL A3U and SJHS B11P The AF demagnetization steps, in Oe, are shown adjacent to each point.

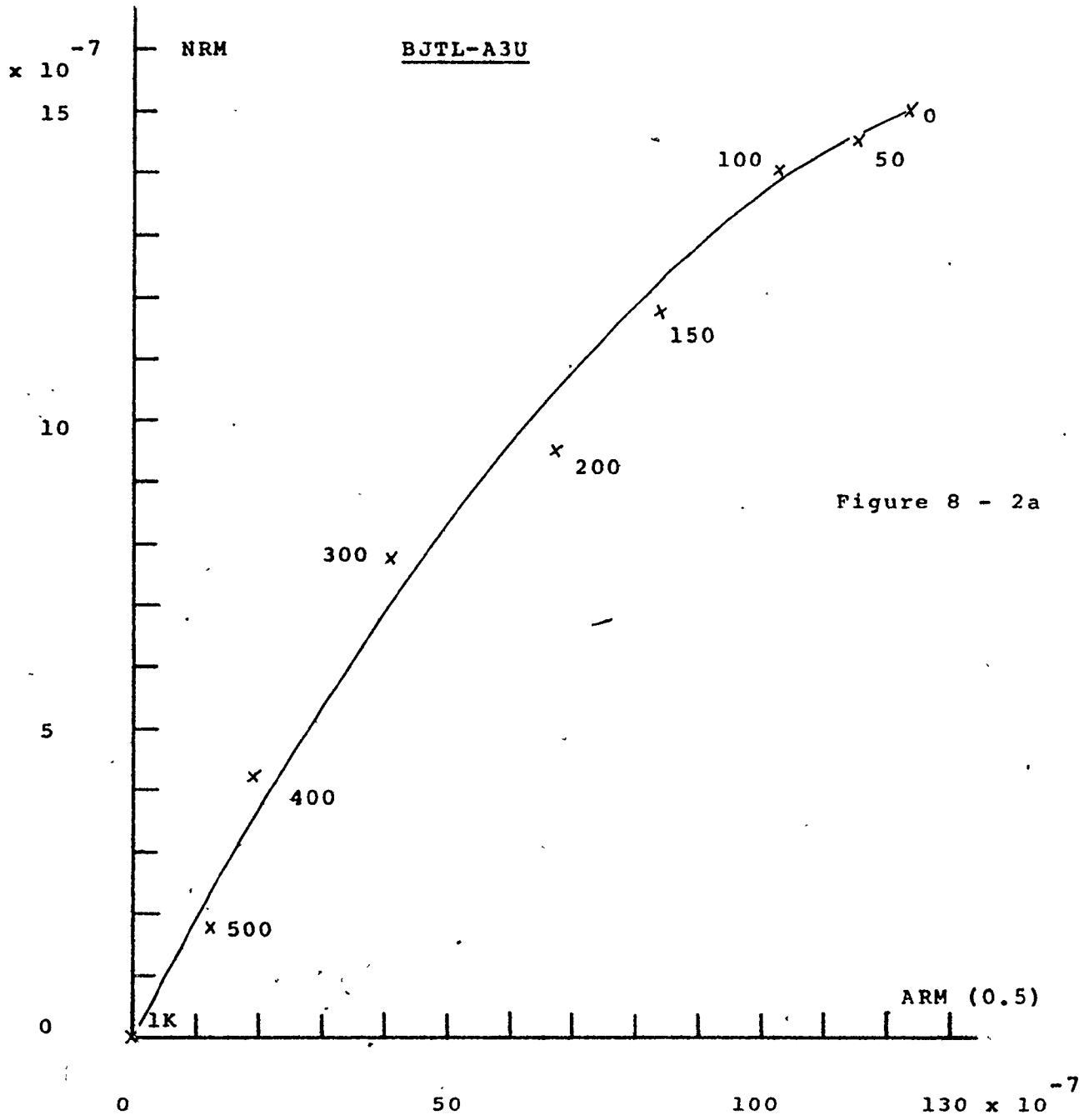
NRM
BJTL-A3U
x 10 -7
15
10
5
0
0
50
100
130 x 10 -7
ARM (0.5)
0
50
100
150
200
300
400
500
1K

Figure 8 - 2a

Figure 8 - 2b

SJHS-B11P

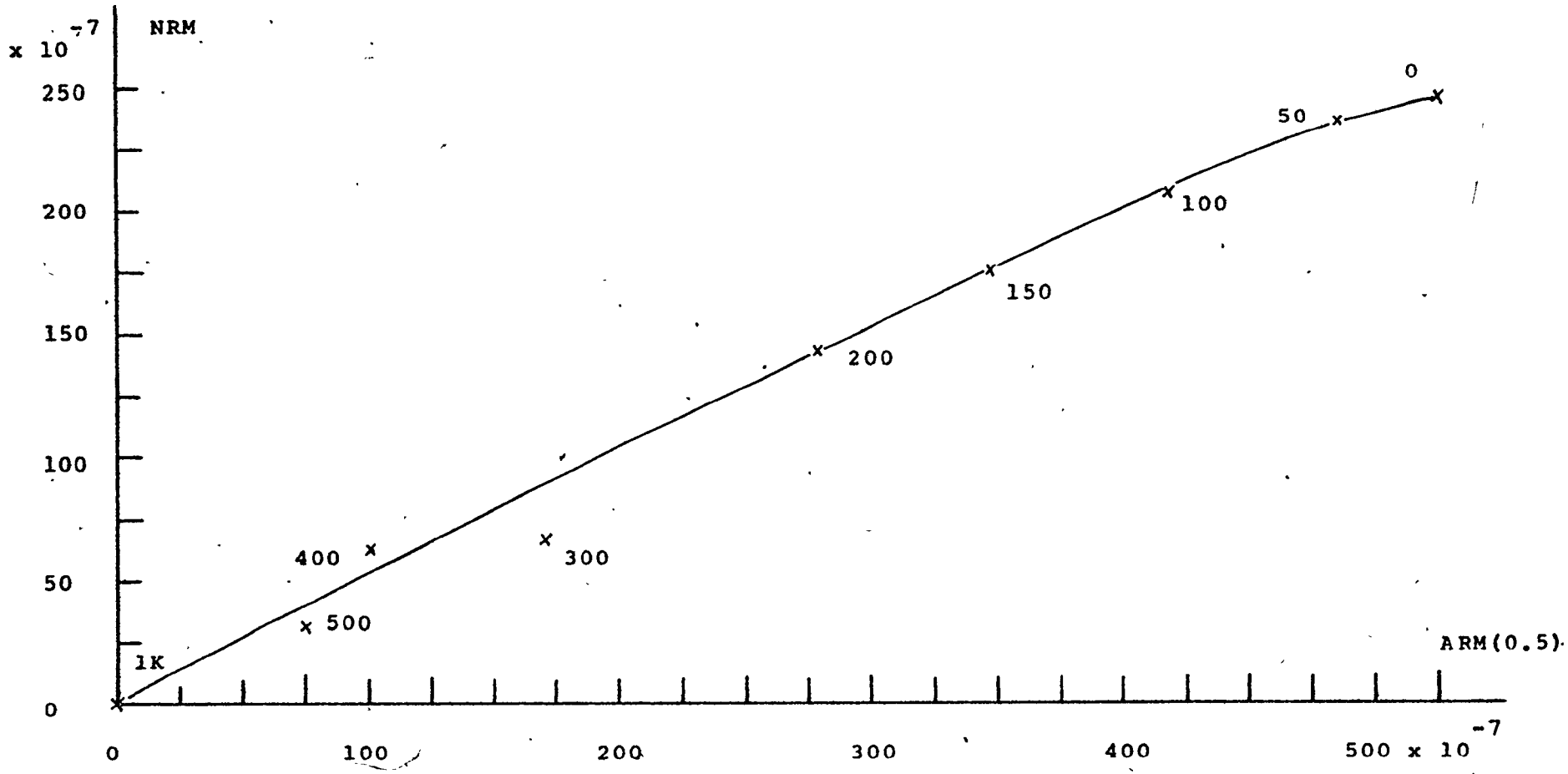

Figures 8 - 3a, and b; Comparative shapes of the curves of the ARM versus direct field, normalised at 2.0 Oe, for A3U and B11P.

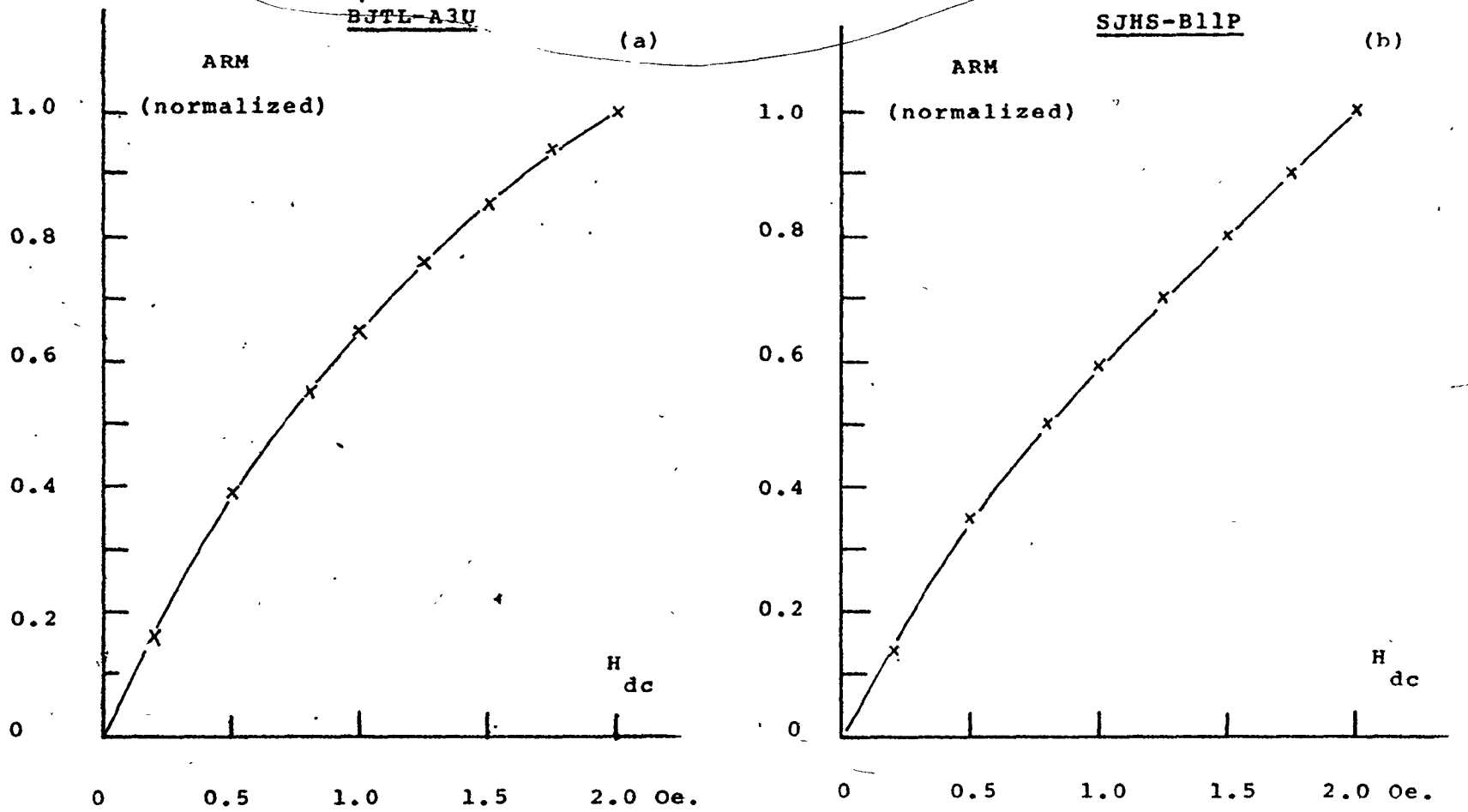

to the naked eye, and the hysteresis properties of BJTL (table 7.2), using the data of Dankers (1978), suggest a predominantly MD grain assemblage. The strict ARM analogue for an MD assemblage is therefore seen to fail here in two ways. Firstly ARM is not as stable as NRM at low demagnetizations and secondly ARM is not linear with field.

By using the 100 to 500 Oe range, the NRM/ARM ratios are 0.14 for A3U, and 0.51 for B11P, corresponding to the H_{arm} of 0.50 Oe. The estimates of H_{a-a} in the direction of the total NRMs are about 0.2 and 0.3 Oe respectively, assuming linearity of NRM and ARM with external field and that f = 1.

8.4.1 The ARM and SIRM Experiments on DAS2

Various ARM and SIRM experiments were carried out on many specimens from DAS2 and the results from these will be described first. This is followed by the presentation of H_{a-a} using a field of 0.5 Oe. The values are estimated from;

$$H_{a-a} = 0.5.(NRM_{100} - NRM_{1K})/(ARM_{100} - NRM_{1K})$$

plotted against their position in the speleothem.

The chapter closes with a discussion of the SIRM and ARM results, their implications for rock magnetism, and an assessment of the analogue approach to paleofield intensity estimates.

The demagnetization of both NRMs and SIRMs (section 7.3.13) showed that there remained a considerable proportion of magnetization at the 1 KOe level. This suggests that SD and PSD grains were also present in the assemblages

Figures 8.4a, b, c and d

The NRM - ARM(0.5 Oe) plots of DAS2 B13Q, C12Q B12R and C19Q/R.

The lines are based on NRM versus a first ARM, ad and the points are denoted by X. NRMs versus repeat ARMs are denoted by Δ .

The probable trend is shown by a dashed line, here and in appendix IV. Greater uncertainty is shown by ?. The 1 KOe endpoint mean and error is shown by a +.

Figure 8 - 4a.

B130

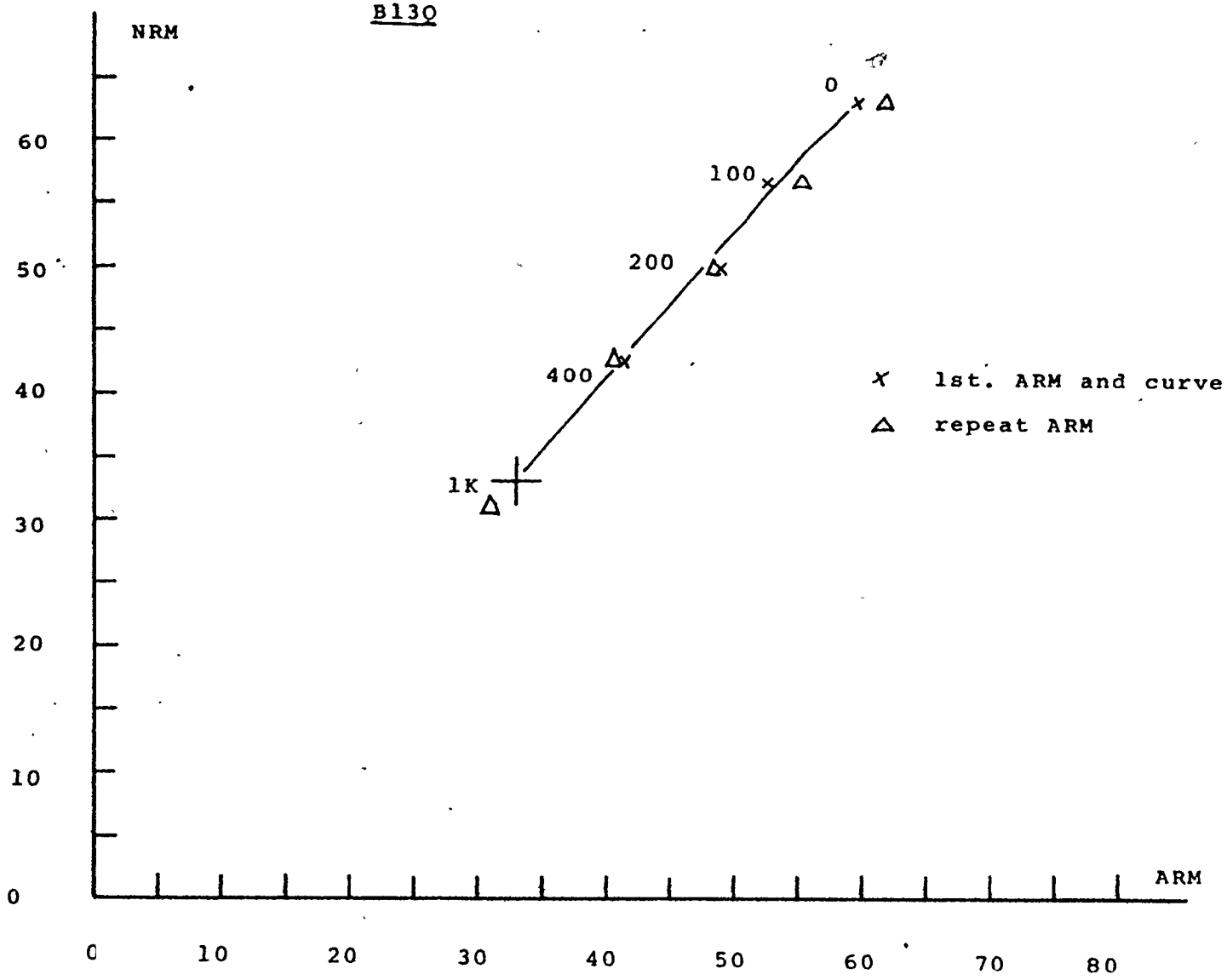

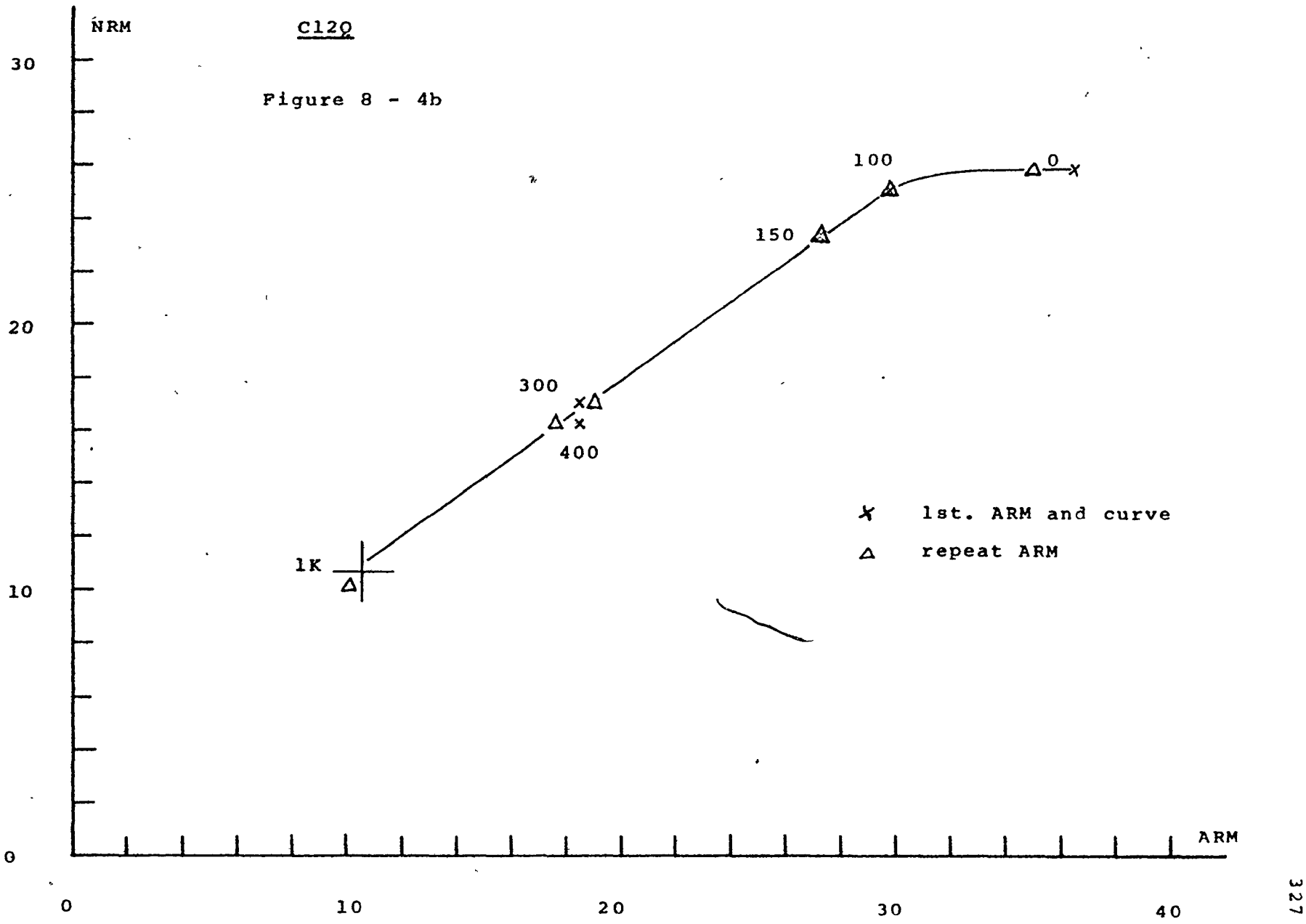
NRM
C120
30
20
10
0
0
10
20
30
40
ARM
100
0
150
300
400
1K
1st. ARM and curve
repeat ARM

Figure 8 - 4b

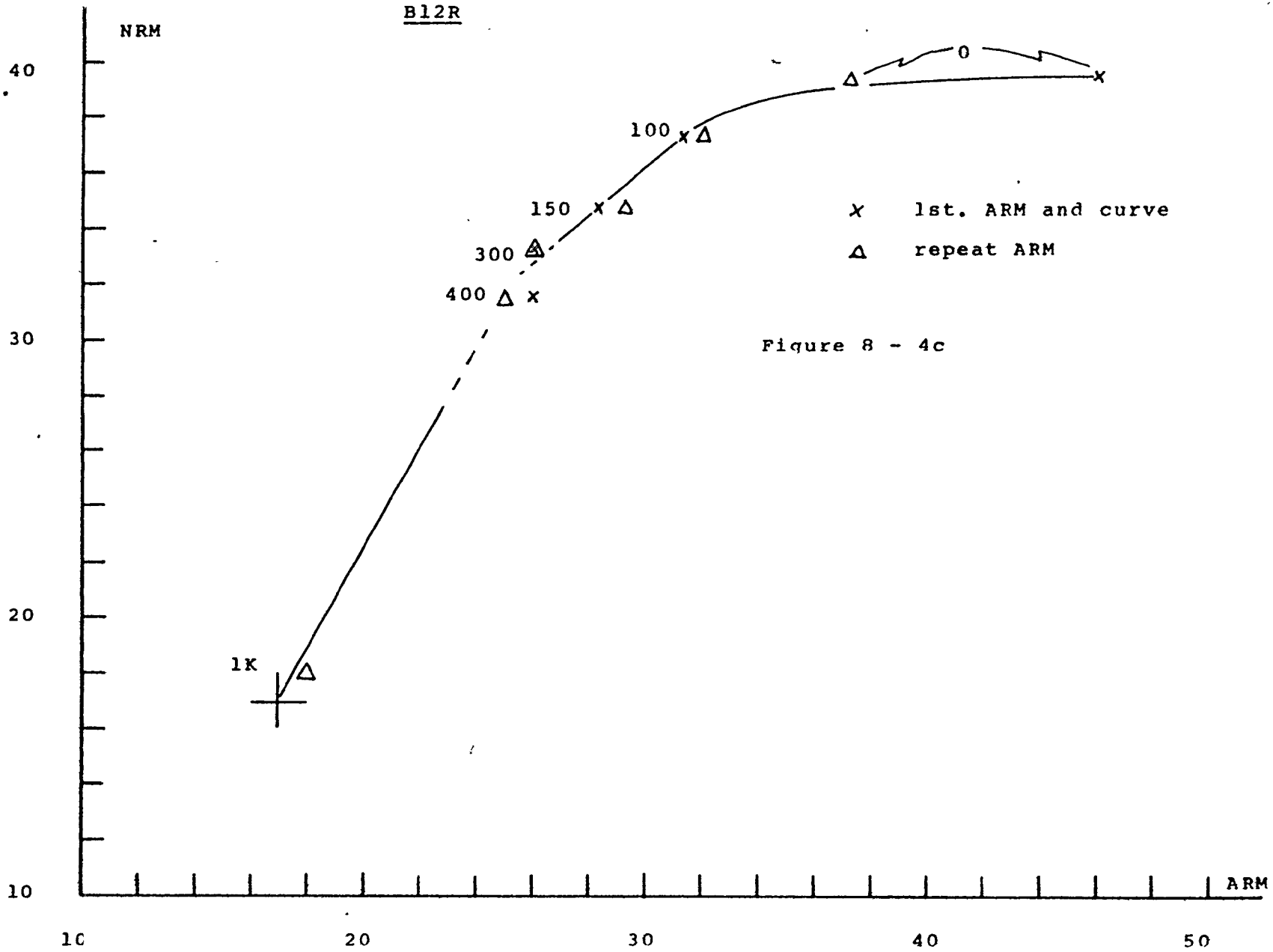
B12R
NRM
40
30
20
10
0
100
150
300
400
1K
x 1st. ARM and curve
Δ repeat ARM
10
20
30
40
50
ARM

Figure 8 - 4c

C190/R

Figure 8 - 4d

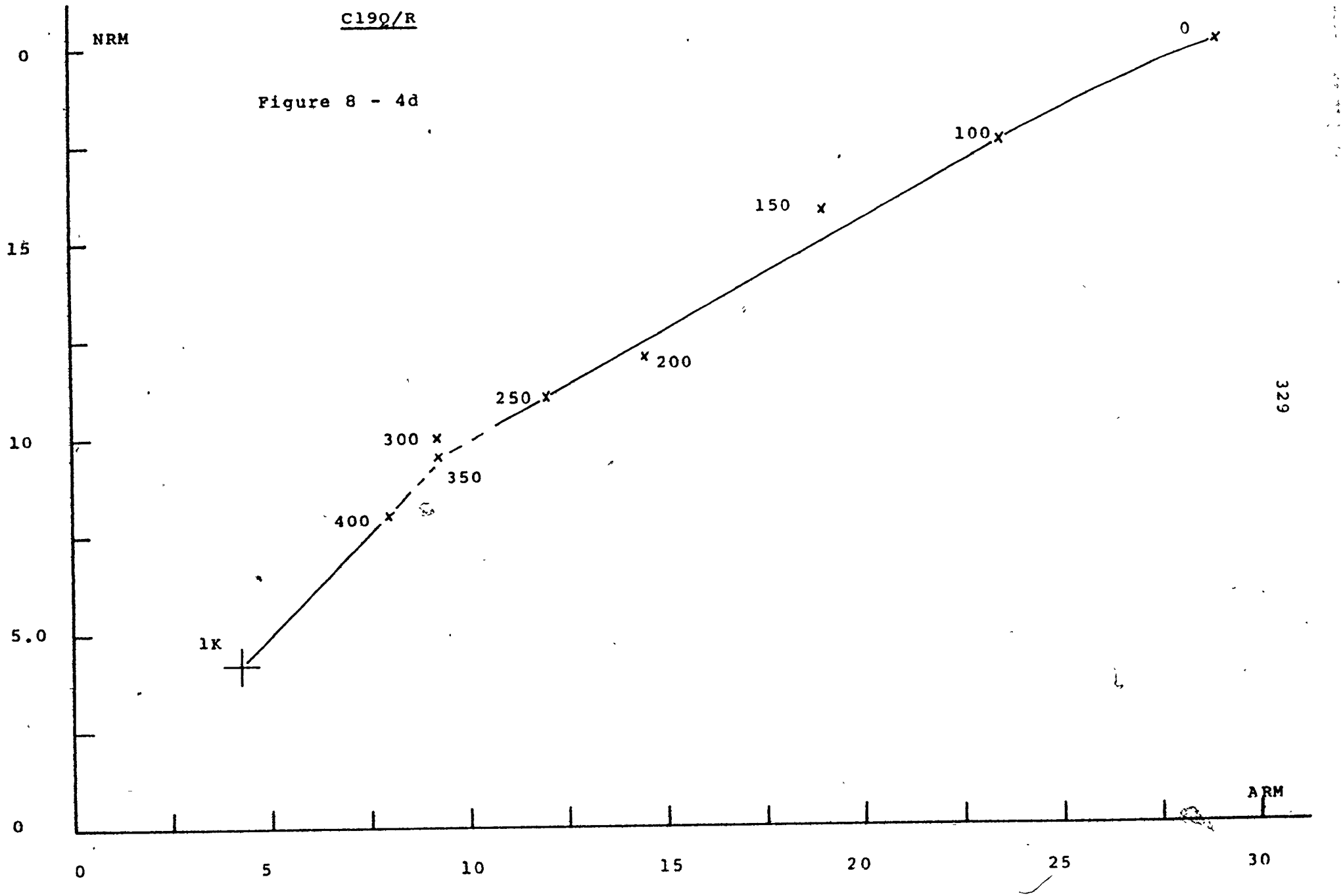

along with MD grains. Therefore by the argument outlined earlier M/M_0 - H plots could not be used to compare the stability of ARM with NRM; the NRM versus ARM (or SIRM) plots were more meaningful. The experiments would have greatly benefitted from having AFs which could reach saturation of the grains , but were limited by the fact that the maximum AF was only 1 KOe.

8.4.2 The NRM - ARM Diagrams

There are two types of NRM - ARM diagrams. Full AF demagnetization plots are discussed in detail , though most are presented in appendix IV, figures 1 to 12. The H_{a-a} values were derived from the diagrams showing only the 0, 100 and 1 KOe steps; all of these are in appendix IV, figures 18 to 35.

Figures 8.4a, b, c and d. These four plots were chosen to be representative of NRM/ARM behaviour generally. B13Q (figure 8.4a) showed NRM - ARM to be linear from almost 0 all the way to 1 KOe. C12Q (figure 8.4b) was typical of several. The plot was linear from the 100 Oe step onwards, the NRM from 0 - 100 Oe being softer than the ARM.

B12R (figure 8.4c) of the same growth horizon as C12Q, on the other hand, was mostly non-linear.

C19Q/R (figure 8.4d) showed linearity from 100 to at least 400 Oe. Thereafter the NRM/ARM ratio was quite different from the lower end of the spectrum. Also the the spectrum was distinctly bimodal with comparatively few grains having coercivities, as measured by $\tilde{H}$, between 300 and 350 Oe. This specimen was typical of several,

especially those having a bimodal spectrum such as B19Q/R, B34R and B34Q.

8.4.3 ARM Dependence on Weak Field

Figures 8.5a and b, and appendix IV, figures 13 to 16. These graphs are for ARMs which were AF demagnetized to 100 Oe. (The graphs for non-demagnetized ARMs were not basically different, except of course, they had steeper gradients; the data are not presented for the sake of brevity).

The ARMs were linear with field up to 2 Oe, to a good approximation. Some specimens tended to show either a discontinuity in gradient around 0.8 to 1.0 Oe (eg C1R, B12Q) or consistent curvature (eg, C13Q), both of which may be instrument error. Any errors in H_{a-a} from assuming ARM - H linearity are probably less than 10%.

8.4.4 Comparisons of SIRM with ARM and NRM

Figures 8.6a, b, c and d for B12R and B13Q are the plots of ARM and NRM against SIRMs imposed in a DF of 3 KOe. Similar plots for C12Q are shown in appendix IV, figures 17a and b.

The three ARM - SIRM plots show an SIRM as hard as, or slightly softer than, the ARM at the lower AF, levels. In the case of B13Q this relative change in stability has reached 400 Oe or more. It may be that the relatively softer SIRM is linked to greater demagnetization fields within MD grains.

In the case of B12R where SIRM and ARM were linear from 0 to 1 KOe, there was in increase in the NRM/SIRM

Figures 8.5a and b

Graphs of linearity of ARM, demagnetized to 100 Oe, with direct field H_d .

ARM is x 10^{-7} G, total moment.

Uncertainty in the curves is expressed by , and by ? . The H = 0 endpoint is the mean of all 1 KOe endpoints. See also appendix IV, figures 13 to 16.

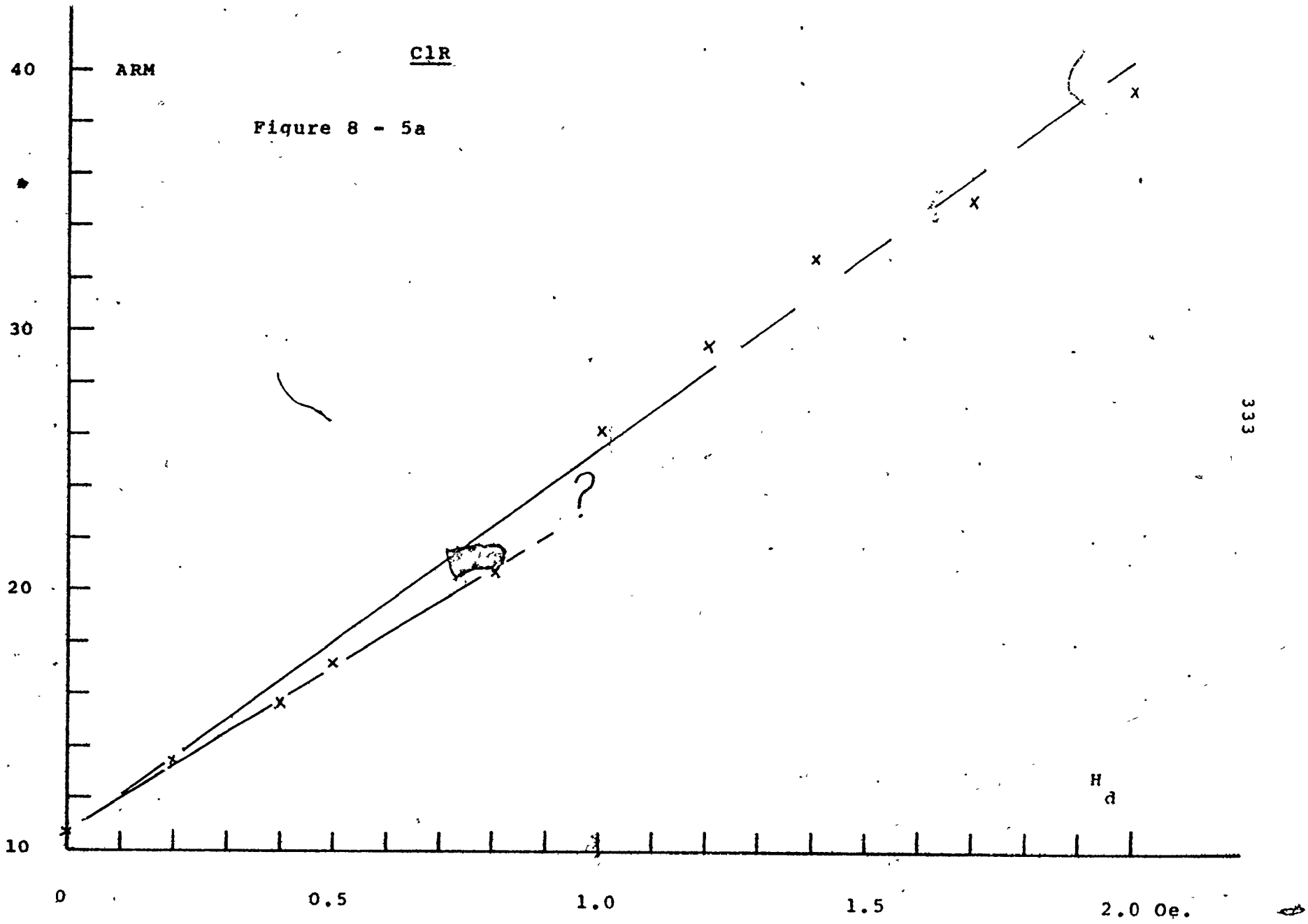

Figure 8 - 5a

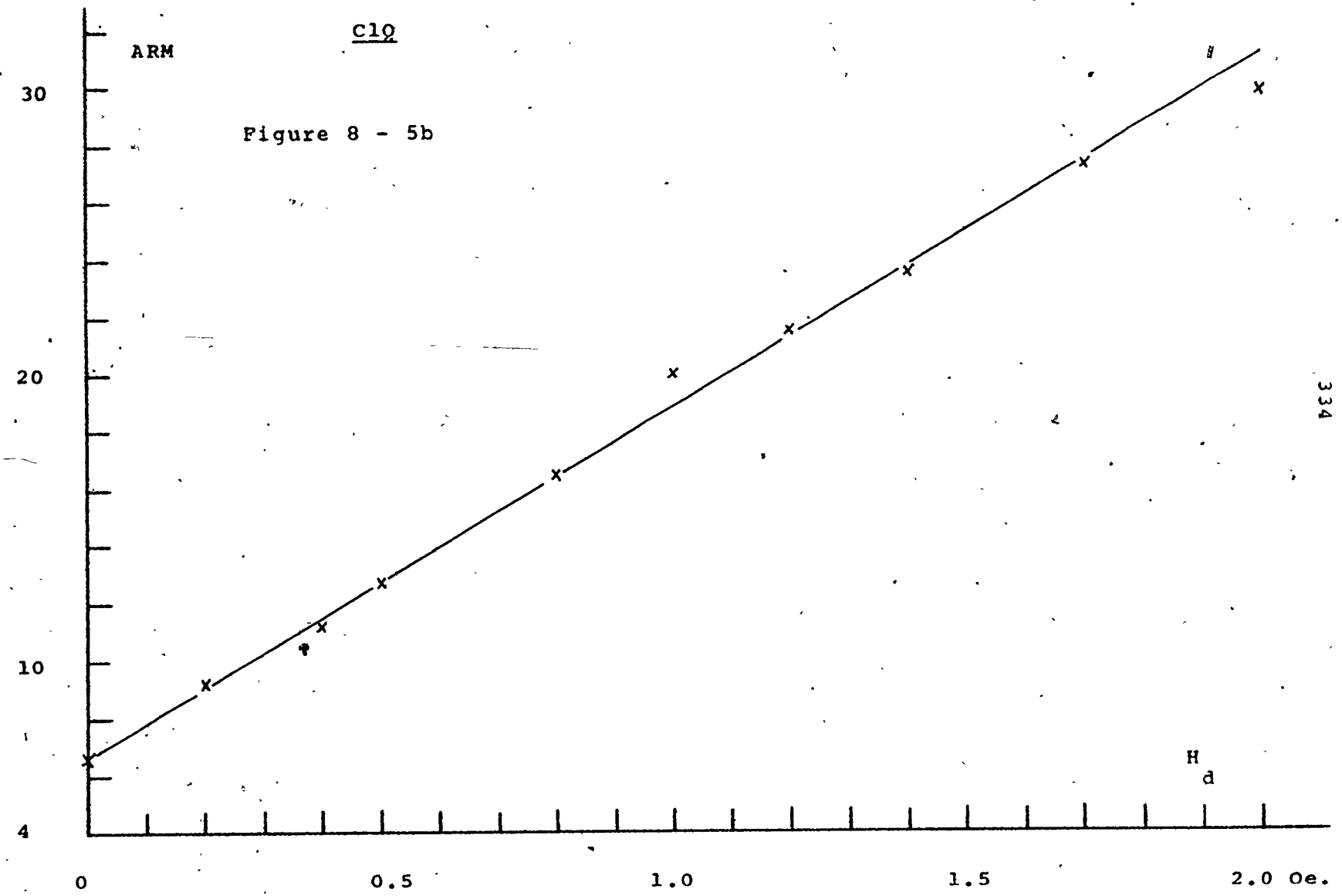

Figure 8 - 5b

Figures 8.6a, b, c and d

Graphs of NRM and ARM(0.5 Oe), versus SIRM, for DAS2 B13Q and B12R.

See also appendix IV, figures 17a and b.

The repeat ARM was made before the SIRM.

B130

Figure 8 - 6b

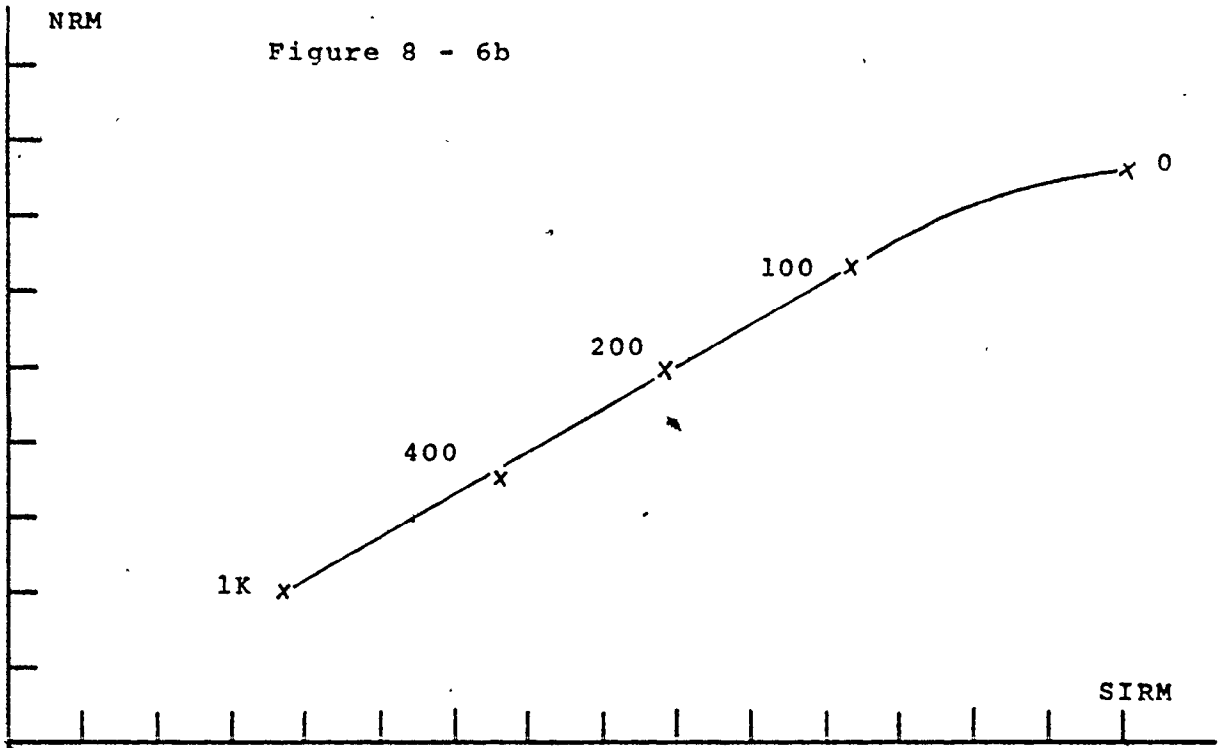

Figure 8 - 6a

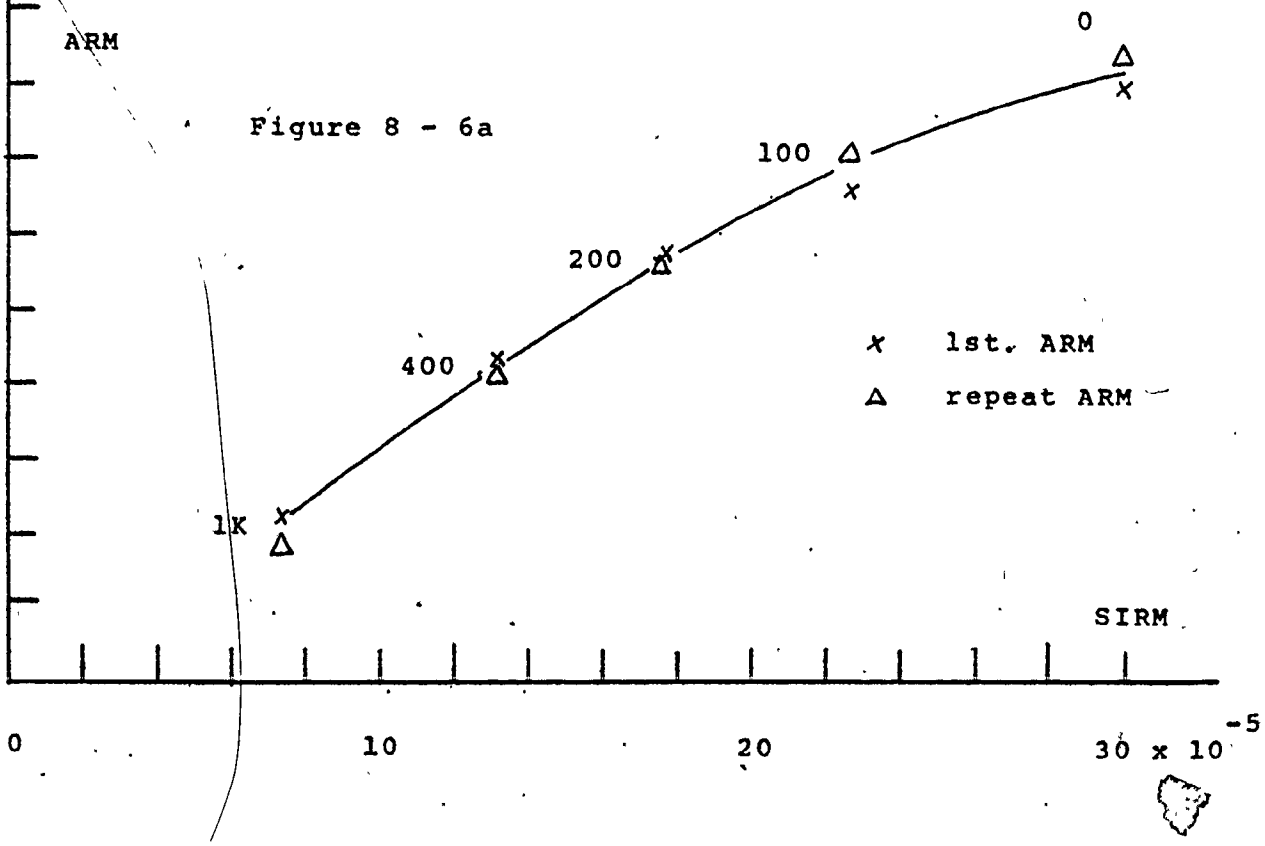

B12R

Figure 8 - 6d

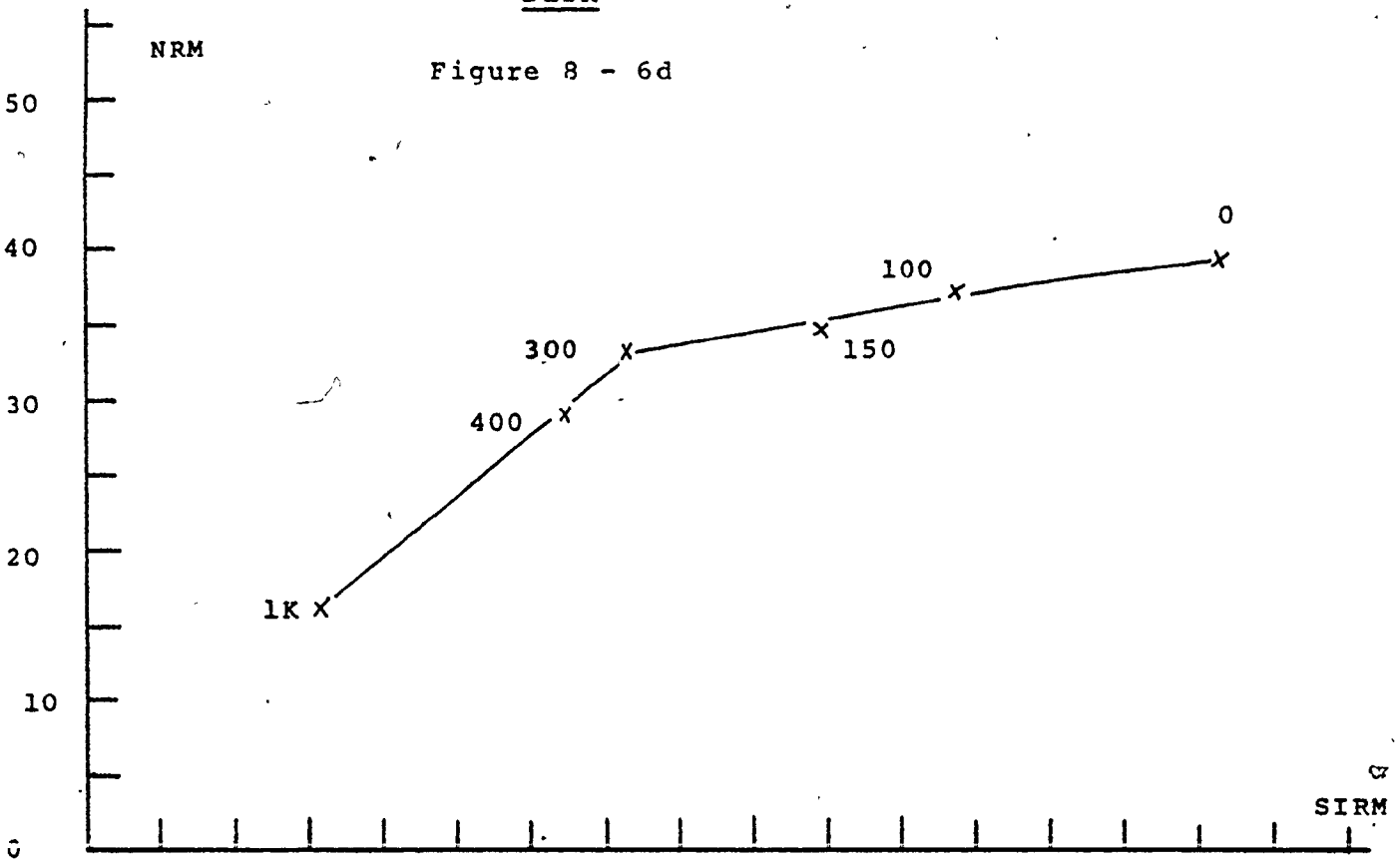

Figure 8 - 6c

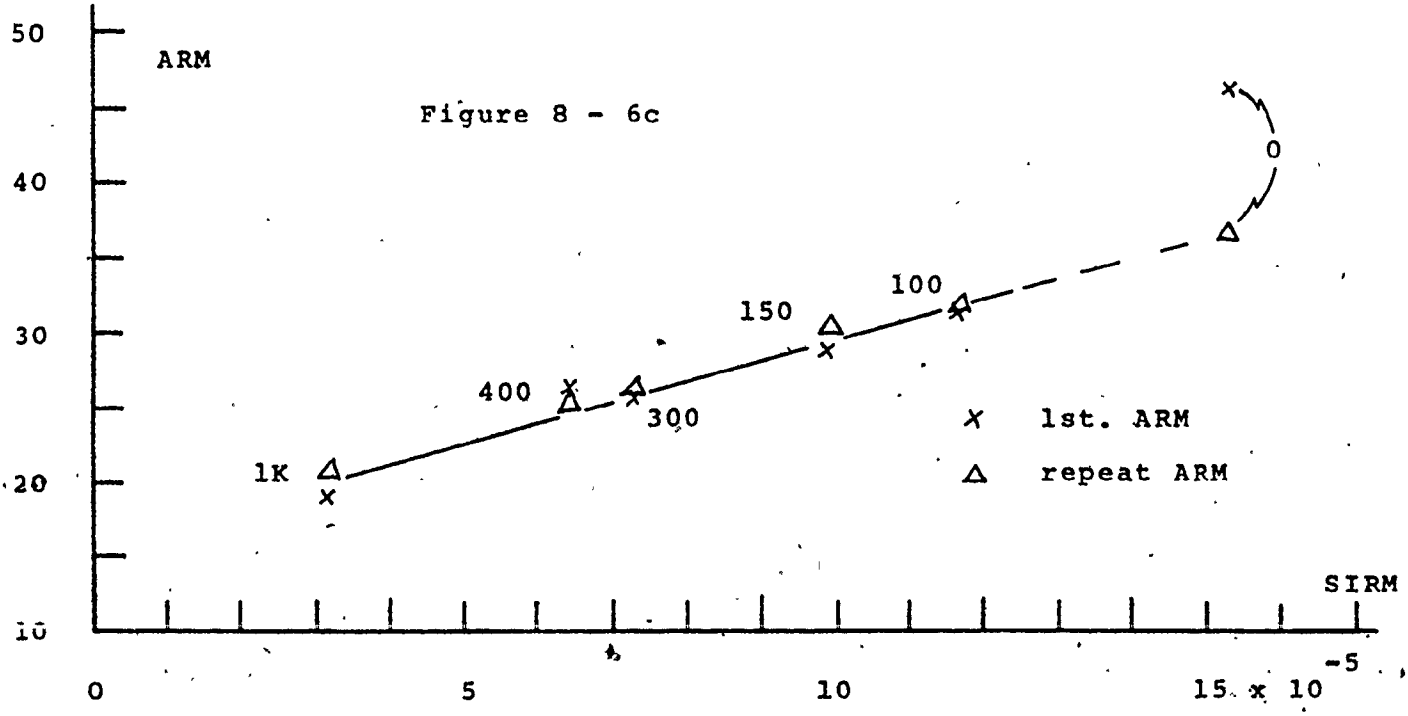

ratio after 200 Oe, just as there was for the NRM/ARM ratio (figure 8.4c). A similar behaviour was apparent in C12Q (appendix IV, figure 17a and b), except that the gradient change occurred between 100 and 150 Oe.

8.4.5 The TRM and ARM Experiments of DAS2 B30T and ENF D9R

The experiments on these two specimens have already been described in sections 7.3.2.2 and 7.3.13.1. It was noted there that new magnetic material seems to have been created by the heating process and that most of this material occupied the higher end of the coercivity spectrum.

Figures 8.7a and b are for the NRM versus ARM(1) and TRM versus ARM(2), for B30T. In figure 8.7a the 400 Oe point is probably not significantly in error and therefore the plot is either curved or a composite of two straight lines with a knee at about 400 Oe.

Similar behaviour is seen with D9R. In the NRM - ARM(1) plot (figure 8.8a) the gradient knee is at or greater than 700 Oe, but in the TRM - ARM(2) plot (figure 8.8b) this point has moved back to about 200 Oe. The second higher coercive force gradient therefore corresponds to the newly created material.

The TRM field changed during the experiment from a room temperature setting of 0.50 to 0.39 Oe, but both specimens will have experienced the same field(s). Therefore it was possible to compare the TRM fields from these two specimens by treating the ARMs as though they were analogues.

Figures 8.7a and b; 8.8a and b

Graphs of NRM versus ARM(1), and of TRM versus ARM(2).
Uncertainty is expressed by - - -, and greater uncertainty by a ?.

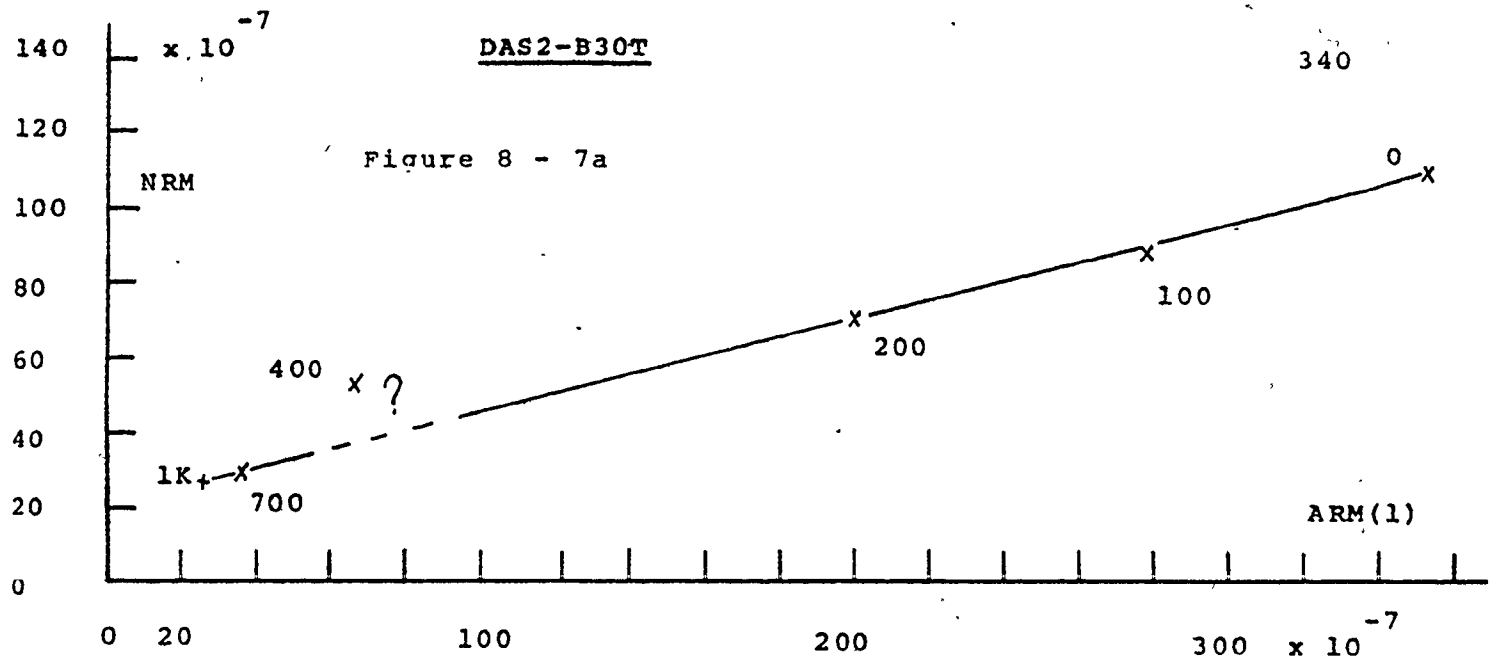

Figure 8 - 7a

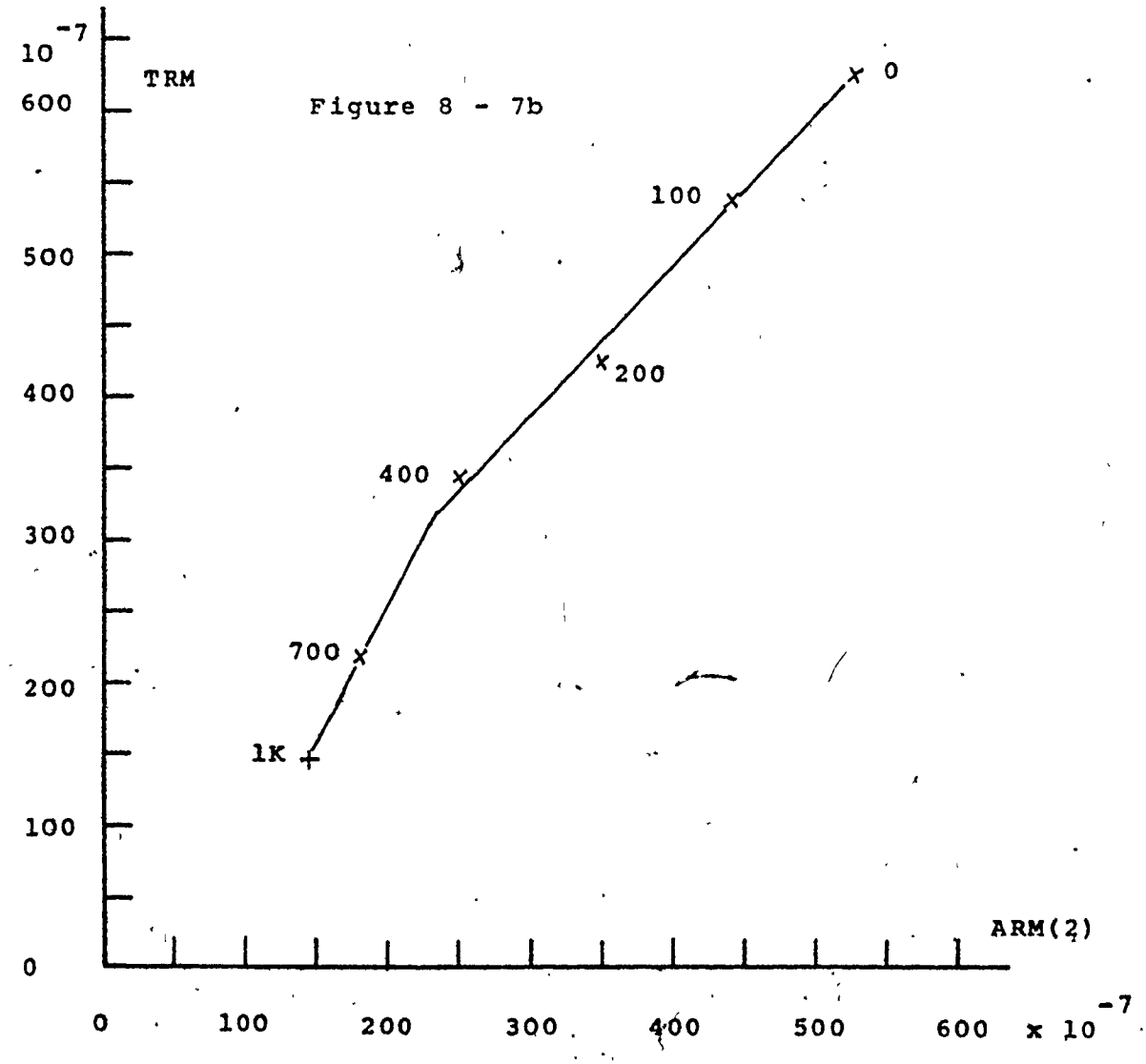

Figure 8 - 7b

Figure 8 - 8a

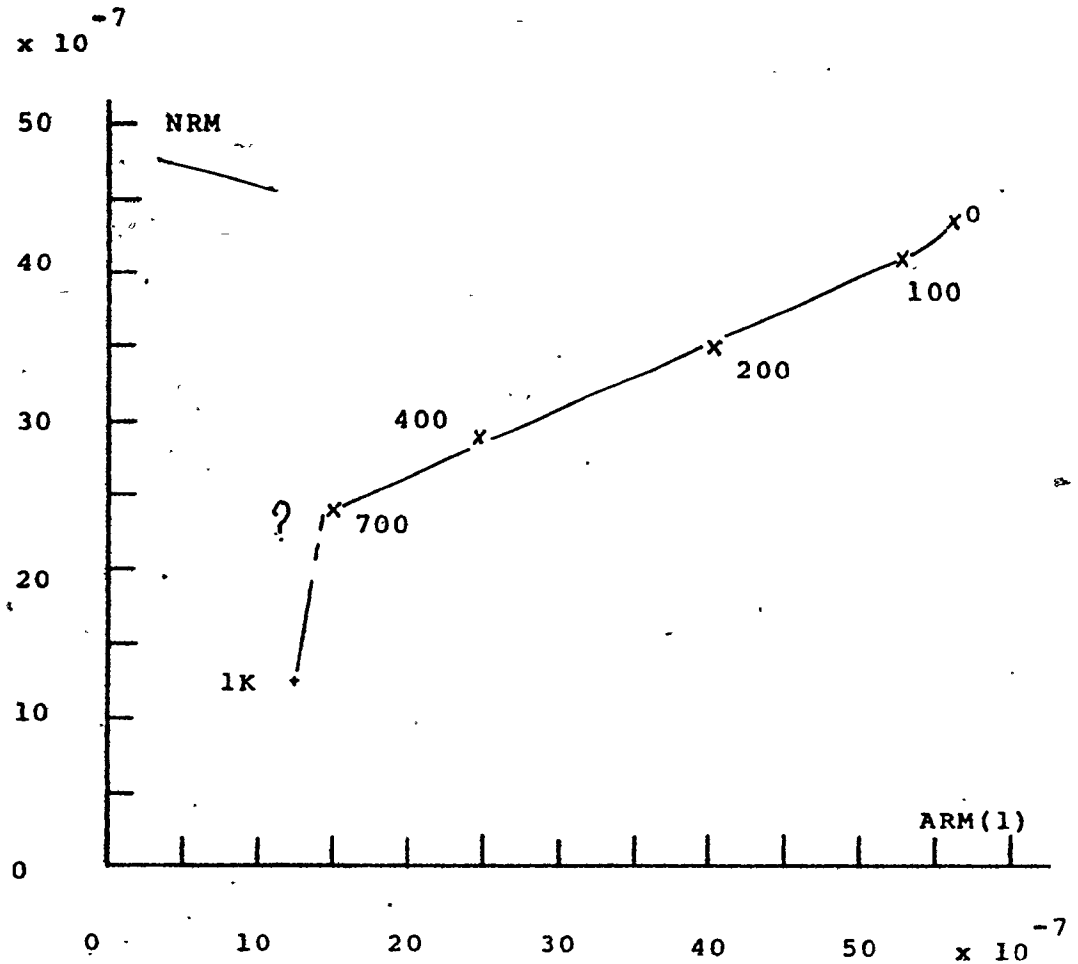

Figure 8 - 8b

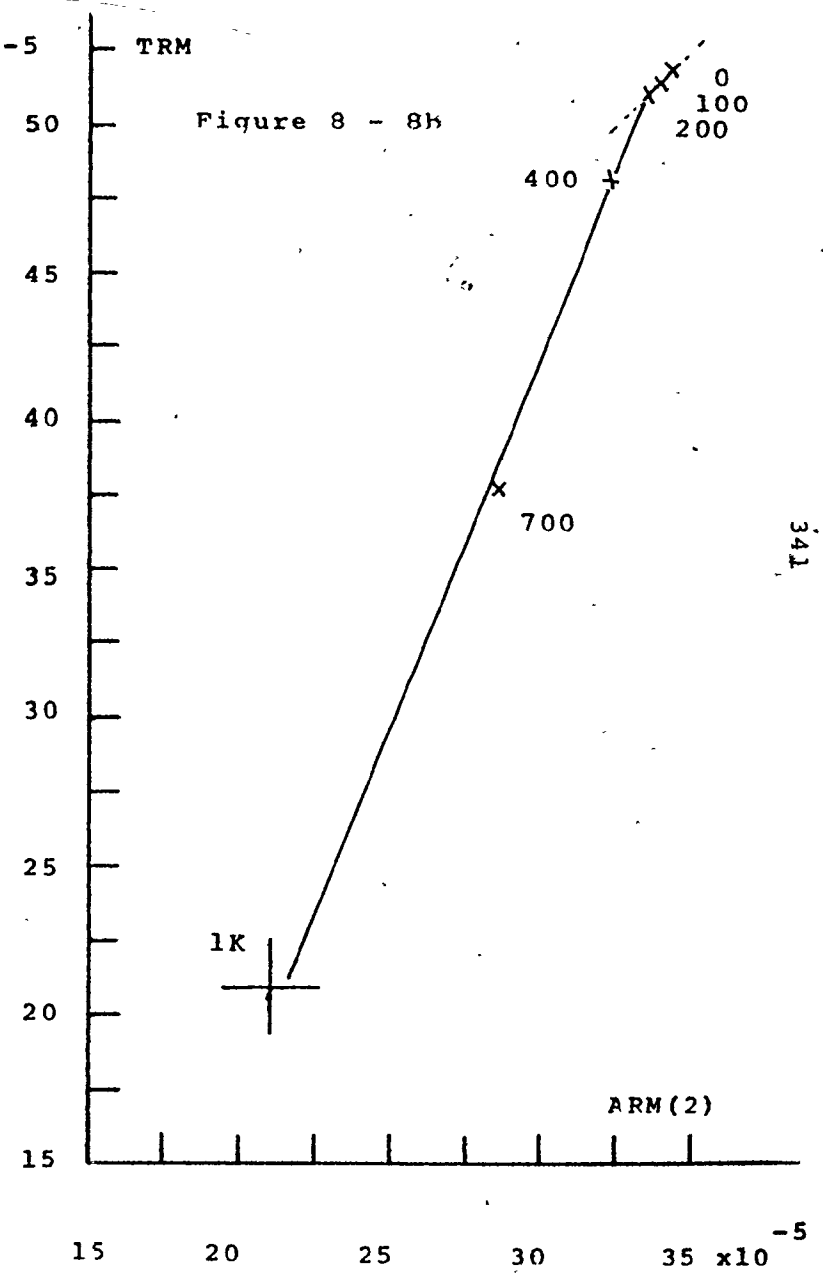

Putting f = 1, and using;

$$H_{trm} = 0.50 \cdot TRM/ARM ,$$

the field estimates are;

	Low-coercivity gradient	High-coercivity gradient
B30T	0.50	0.95
D9R	0.54	1.17

These results are discussed in section 8.5.1 .

Although the comparison of ARM(1) with ARM(2) in figure 7.10 brings to mind Shaw's method for determining paleointensities (Shaw, 1974), there is no question of using it here because:

1) The ratios between CRM (DRM) and TRM for the same field has still not been confidently ascertained, and in any case may be grain-size dependent.
2) New magnetic material was created which carried only the TRM,
3) The ARM(1) - ARM(2) graphs appear to show quite different coercivity spectra.

8.4.6 Apparent Ancient Field, H_{a-a} , Variations in DAS2

As already noted the gradients of several NRM - ARM plots were quite variable through their stability range. Estimates of H_{a-a} for B12R, for example, were 0.48 and 0.79 Oe from the two gradients shown in figure 8.6c . The next step in finding out the meaningfulness of H_{a-a} was to compare values from specimens having the same growth horizons (cuts). In order to do this a standard demagnetization interval between 100 and 1 KOe was chosen for each specimen in order to produce H_{a-a}. These comparisons are shown in figures 18 to 35, appendix IV. and are discussed again below.

Figure 8.9

$H_{a-a,x}$ versus $NRM_{100,x}$.

The intensity of magnetization, $NRM_{100,x}$ is in G cm^{-3}, x 10^{-7}.

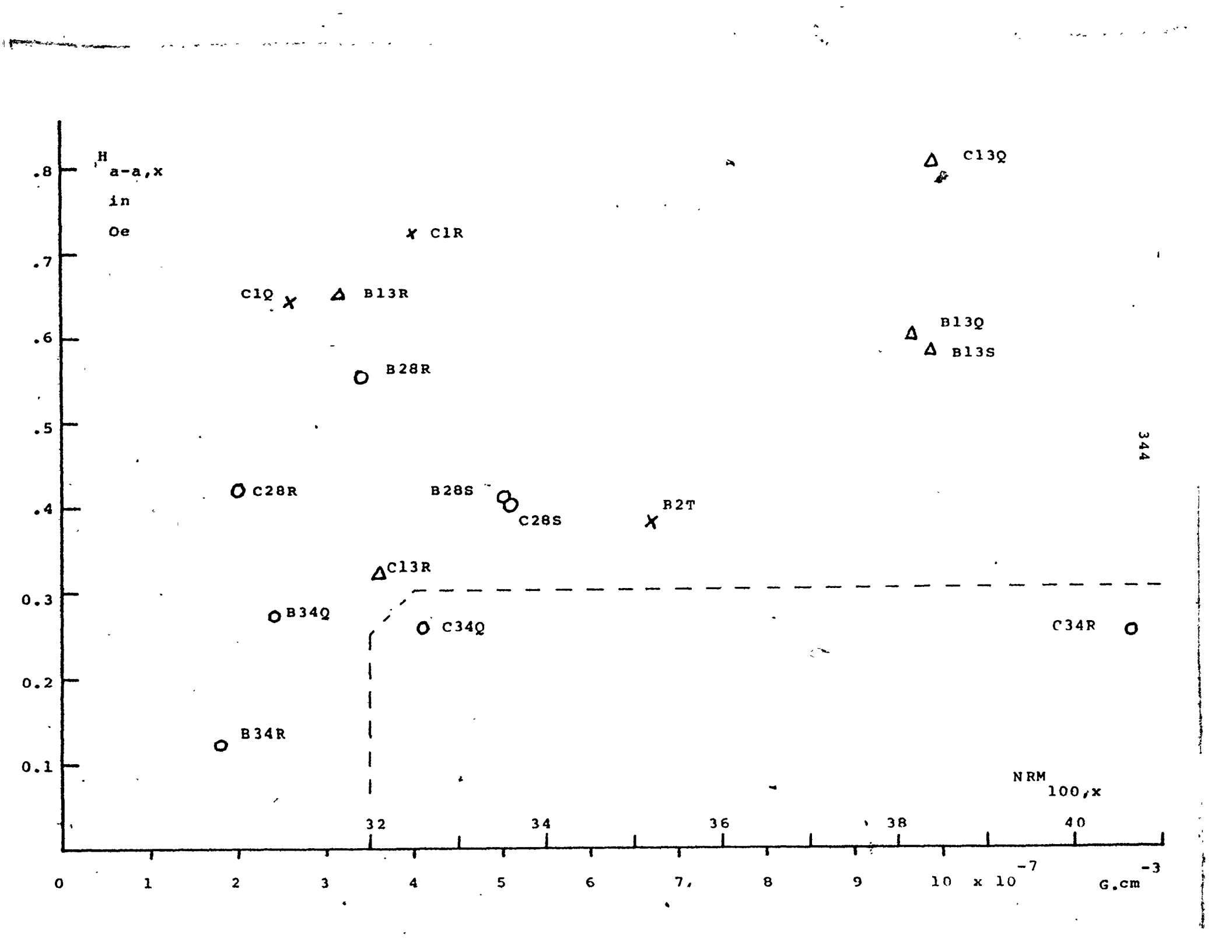
H
a-a,x
in
Oe
.8
.7
.6
.5
.4
0.3
0.2
0.1
C13Q
C1R
C1Q
B13R
B13Q
B13S
B28R
C28R
B28S
C28S
B2T
C13R
B34Q
C34Q
C34R
B34R
NRM
100,x
32
34
36
38
40
0
1
2
3
4
5
6
7
8
9
10 x 10
-7
-3
G.cm

Figure 8.10

Variations of Apparent Field Intensity, H_{a-a}, against Cut Number.

The H_{a-a} means, (x), are taken from 2, 3 or 4 specimens (except specimen B2T which is plotted on its own - see text), and the errors are standard deviations.

From chapter 6 it is shown that the speleothem grew in a period of about 1.3 Ka., and that the declination variations have nearly completed one cycle of westward drift around the world.

The line ---------- is a construction (± 0.05 Oe) of one complete cycle of westward drift of intensity at latitude 22° N past the site (from World Magnetic Intensity Chart, (1976)).

The line — — — represents intensity trends of worldwide archeomagnetic data estimated from figure 2 of Barton et al (1980). The same trend is evident in figure 4.14 Of Aitken (1974), except that the values are a bit higher.

The line - — - — - represents intensity variations from archeomagnetic data as estimated from figure 2(b) of Bucha (1970), for the Mexico region.

The line ———— - represents intensity variations from Peruvian archeomagnetic data estimated from figure 8 of Gunn and Murray (1980), but made to correspond to latitude 22° N using a VADM model.

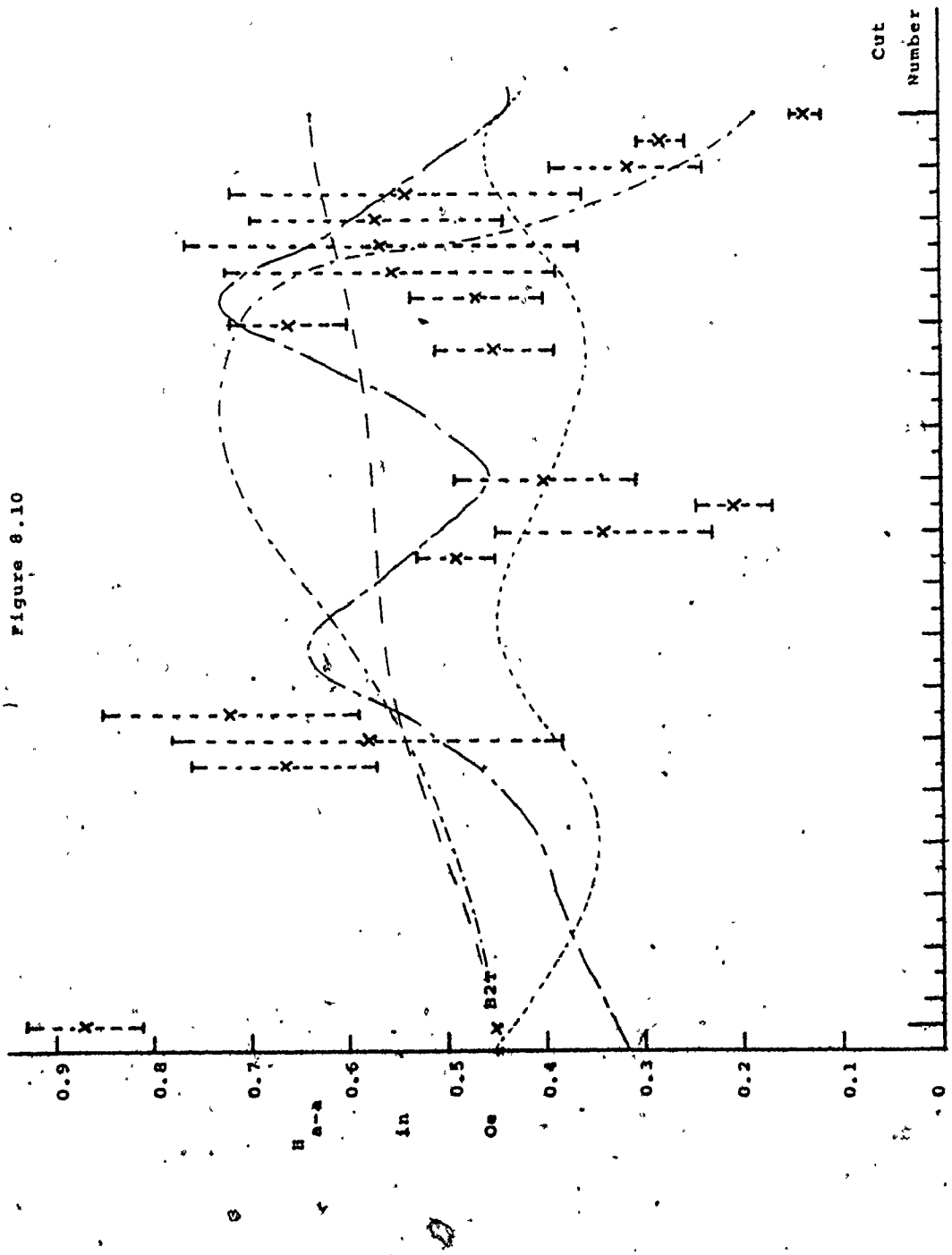
Cut Number
top 1
10
20
30
base 16
0.9
0.8
0.7
0.6
0.5
0.4
0.3
0.2
0.1
0
B2t
Oe
In
a-a

Figure 8.10

Another test of the meaning of H_{a-a} is to plot it against NRM intensity, to see if there is any correlation between them. In figure 8.9 the x-axis magnetizations values of H_{a-a} and NRM have been plotted against each other for a few cuts, with the understanding that specimens of the same cut must have experienced the same ambient field. Some cuts such as 13 appear to show a positive correlation between apparent field and magnetic intensity, whereas others like 34 do not. Thus the amount of magnetic material as represented by $NRM_{100,x}$ does not appear to have affected H_{a-a} in this speleothem. On the face of it the ARM analogue has been fairly successful in normalising for the magnetic content - an essential requirement for any such analogue.

The total analogue intensities were worked out from;

$H_{a-a} = H_{a-a,x} \cdot M(55)/X(55)$, where $H_{a-a,x}$ was the ancient field intensity deduced from the x-axis magnetization. M(55) and X(55) were the total and x-axis magnetizations taken from the 55 Oe-cleaned NRMs.

Cut 1 has been separated from B2T, a lateral specimen, showing the same growth horizons. Otherwise cut 12 (N = 3) showed the greatest scatter of about 30%. The least scatter was shown by cut 36 (N = 2) of 8%, and by cut 35 (N = 4) of 9%.

These H_{a-a} values versus cut number are shown in figure 8.10. The apparatus was dismantled for use by other workers, so the completion of these ARM and SIRM experiments had to be postponed.

Despite large deviations about the mean, the H_{a-a}s of adjacent cuts tend to agree fairly well, and in the early part of the record, cuts 36 to 27, the variations appear serially correlated (excepting cut 28).

Although the value of B2T agrees well with the modern value, the mean of the two specimens of cut 1 do not agree with the modern value - they are higher by a factor of 2!

8.5 The ARM Analogue

8.5.1 Discussions and Conclusions

As argued in the concluding part of chapter 7, section 7.4.2, the most likely origin of the NRMs of most speleothems is:

1) a component from the deposition of already magnetized grains - a kind of DRM, and
2) a CRM formed either from the primary precipitation of magnetite or from the (partial) dissolution of detrital grains.

The probable complex origins of most NRMs is subsequently compounded with the viscous acquisition or decay of part of the NRM.

In the ARM experiments VRM was seen in the initial ($\tilde{H} < 100$ Oe) non-linearity of the NRM - ARM plots. For example, a VRM component acquired in the general direction of the stable NRM made the latter appear softer compared to the ARM. Conversely the NRM appeared more stable if its soft components had decayed, or if VRM components were opposed or perpendicular to the rest of the NRM.

The puzzling feature in several NRM - ARM and NRM - SIRM plots was the increase in gradient seen well beyond the recognizable VRM. When it was most distinct it tended to occur between 300 and 400 Oe, but in other cases, eg, ENF D9R, figure 8.8a, it occurred at 700 Oe, or more. Where the gradient segments were based on three or more points they appeared to be linear or nearly so.

In order to discuss this effect further, the following observation is first made. Since CRM and TRM have the same stability to AF demagnetization, though differing in magnitude, then CRM and ARM should likewise have the same stability.

That TRM and ARM have the same stability , to AF demagnetization, whether carried by SD or MD grains, was shown experimentally by Dunlop and West (1969), Dunlop et al (1973) and by Johnson et al (1975). Bailey and Dunlop (op cit) and Levi and Merrill (op cit) have shown further that the TRM/ARM ratio (R = 1/f) varies with grain size. The ratio increased as the grain diameter decreased (Levi and Merrill) but the data were insufficient to distinguish ratios of particles within the submicron range.

It was noted earlier that the linear segments were most evident where the CFS was bimodal. C19Q/R, for example (figure 8.4d) has few coercive forces between 300 and 350 Oe; the gradients on either side are approximately linear. This is compatible with the possibility that there are two sets of coercive forces each with a different CRM/ARM ratio . The higher-CF grains possess the higher ratio and this agrees with the sense of Levi and Merrill's

data for tne TRMs. Where there is no coercive force gap the gradient change is more gradual - for example, C34Q appendix IV, figure 10.

One objection to this that can be raised is that the gradient knee occurred at different $\tilde{H}$ for different specimens. It was at 700 Oe for C1Q, C1R and ENF D9R, but in others it was as low as 300 Oe, for example C34Q. In some specimens it did not appear at all or may have been innaccessible to observation above the 1 KOe step. In one case, C34R, the high-CF gradient is lower from 400 to 1 KOe; however the 1 KOe magnetization had an anomalously high ARM value. It was treated the same as C19Q/R and B34R both of which showed the usual gradient increase.

These gradient changes were also noted in the TRM - ARM(2) plots of B30T (figure 8.7a) and of ENF D9R (figure 8.8b). The gradient changes are at 400 and 200 Oe respectively. An assumed laboratory field of 0.4 to 0.5 Oe produces the following f ratios; (f = 1/R = ARM/TRM)

	Low-CF gradient	High-CF gradient
B30T	0.79 - 0.99	0.42 - 0.52
D9R	0.74 - 0.92	0.34 - 0.43

The two sets of ratios are approximately the same, specimen to specimen. From Levi and Merrill's data they correspond to grain sizes of about 5 - 10 μm from the low-CF gradients, and to submicron-sized grains from the high-CF gradients. Contrary to the graph produced by Levi and Merrill, the two ARM/TRM ratios were each constant over its associated CF interval. They were not continuously varying functions of coercive force, and by implication, of grain size.

Another possibility is that the gradients correspond to a coarse-grained DRM and a fine-grained CRM in accordance with the arguments of section 7.4.2 . This might explain the shift of the gradient knee from specimen to specimen, and the absence of a knee in other specimens. It does not explain, however, the double gradient of the ATRMs of B30T and D9R which were imposed on all the grains.

Finally the tendency to bimodal distribution together with the different ARM/TRM (NRM) ratios might be due to the presence of two magnetic phases.

The reason for the curved ARM - H graphs of BJTL A3U and SJHS B11P is not known. By comparison DAS2 specimens repeatedly showed linear plots. A3U and B11P were magnetically softer than the DAS2 specimens suggesting that ARM - H curvature is due to a dominantly MD-grain assemblage. The data of Johnson et al (op cit), and of Sugiura (1979) indicate that ARM - H plots thus curved are characteristic of harder SD/PSD grains.

Although the derived ancient field intensities of DAS2 bare some comparison with archeomagnetic work , little credence should be attached to the H_{a-a} variations along the speleothem as an accurate reflection of, even relative, paleointensity variations. H_{a-a} is probably strongly dependent upon weak field and this dependence is most likely linear or nearly so. But H_{a-a} is also a strong function of magnetization processes which are different for different grain sizes, or modes of magnetization (DRM or CRM) or mineralogy (γFe_2O_3, or Fe_3O_4).

Lack of time has prevented the full use of SIRM as a means of obtaining relative paleointensities. It was seen to have about the same stability as ARM to AF demagnetization and exhibited the same kind of gradient changes as ARM to the NRM

8.5.2 Problems and Criteria for the Acceptance of the ARM Analogue

As pointed out by Bailey and Dunlop no theoretical relationship has yet been found between ARM and TRM which predicts the grain size dependence as seen from experiment. Although the sense of the ARM/TRM ratio dependence with grain size was established by Levi and Merrill, their results would benefit from being refined and extended . For one thing Bailey and Dunlop's more limited grain size range showed the opposite sense of dependence, as incidentally, do the theories of Dunlop and West (op cit) and of Banerjee and Mellama (op cit) based on Jaep (op cit). Moreover the experiments from this study suggest that the CRM/ARM or TRM/ARM ratio is fixed over a range of coercivities, with the next range having a different fixed ratio.

If ARM is to be used as an analogue of speleothem NRM (here considered chiefly as a CRM) then the following steps must be taken:

1) The NRM dependence upon field should be investigated in the laboratory by calcite deposition which approximates the Eh - pH conditions under which the magnetic phase formed in the cave. ARM in weak fields may then be compared directly with the NRMs to find R or f.
2) Then any CRM/ARM ratio(s) thus deduced , must predict

the modern field intensity from the modern tops of young speleothems.

3) Further confidence in the analogue would follow if the dated paleofield variations matched those from archeomagnetism for the same global region and time range.

CHAPTER 9

SUMMARY AND CONCLUSIONS

9.1 Introduction

The chapter begins with broad guidelines for the selection of speleothems likely to carry a measurable NRM. From an aesthetic point of view, it is of some comfort to know that they are mostly of the mud-covered, less pretty variety; the nice clean, white ones may be left untouched!

Most of the chapter concerns the analysis of various sources of error in the resulting paleomagnetic and U - Th data. The errors, for the five SY records that have been produced, are reckoned to be small. A full assessment of the errors will only be finalised with the production of other overlapping or contemporaneous records.

Only a brief summary of the results of the rock magnetism and ARM experiments is made. As mentioned at the begining of the chapter on rock magnetism, the experiments were not much more than a serious 'dabble' into what speleothems could reveal. This work was complemented by thin section analysis (appendix III) and Mössbauer spectroscopy, (by T. Birchall; appendix V).

The ARM experiments and their results were found to hold promise in two directions. Firstly for their general implications for rock magnetism, and secondly as a means of estimating paleointensity.

The chapter ends with further discussions on what the dated SV records have revealed about the Earth's magnetic field, for the time spans and the regions which they cover. It has been found possible, mainly for Holocene times, to compare and contrast features of the field as seen in Europe, W. Canada and Mexico.

9.2 Speleothems with Measurable NRM; Guidelines for Location

Most limestones contain little iron, mostly in the form of hematite (Iron; Handbook of Geochemistry). Their magnetic content is one of the lowest among sedimentary rocks (Dobrin, M, 1952). These facts may partly account for the observation that many speleothems of pure white appearance lack iron (Gascoyne, 1977, op cit), and a measurable NRM (this study, appendix II).

Firm evidence from samples VCCL, TS, SJLS, SJHS, DAS1 and DAS2 show that detrital magnetite is a source of the magnetization of some speleothems. Largely circumstantial evidence shows that significant amounts of iron are also carried through the limestone in the feedwater by organic materials (eg as found in TS, GQF1,SJHS and others). The source of iron is probably the soil derived from an allochthonous sediment such as a till, as in Yorkshire. The iron in the soil may be mobilised by strong organic acids as in the process of podzol formation, which occurs in the cool humid parts of the world (Bridges, 1970),

As a general rule the speleothem most likely to have a measurable NRM is one that has been subject to frequent inundation by sediment-laden flood waters. The pure white speleothem is the least likely to carry a

measurable NRM. Unfortunately, along with the detritus that carries the magnetite resistate, travels the spectre of detrital ^{230}Th to spoil the dating of the magnetic record. In practice it has been found, however, that either detrital ^{230}Th was low (SJLS, VCCL, and most of DAS2 and TS, or it could be realistically allowed for (eg TS, DAS2, - but not RCB).

In order to maximise the accuracy and precision of both the paleomagnetic and the U/Th data and of the ARM paleointensity work, it is desirable to choose samples yielding several specimens per growth horizon, such as stalagmites of large diameter or flowstones.

9.3 Errors of the Paleomagnetic Record.

Given that a speleothem has a measurable NRM and provides an estimate of the secular variation of the past, what are the errors in the record? Putting aside, for the moment, the question of paleointensity estimation (see section 9.7.4), the three sources of error are the recorder (sample) errors, measurement errors, and errors associated with VRM and low intensity NRM.

9.3.1 Recorder Errors

There are two principal types of recorder error - recorder lag and depositional error. A third type - post-depositional disturbance - is usually easy to recognise (eg, stalagmite AGS1, appendix II, had been knocked over and replaced at an angle of about 10° to the vertical). The question of VRM and low intensity NRM is dealt with in section 9.3.3 .

9.3.1.1 Recorder Lag

The question is whether grain moments can continue to move under the influence of a later field after the enclosing calcite has formed? Is there a speleothem analogue of pdDRM or the chemical 'overprint'? In sediments the essential requirement for either of these two is the presence of pore water so that either tiny grains may rotate within the pore spaces, or that the water may act as a medium for recrystallization. Entrapped water is present in many speleothems as fluid inclusions, but in such small amounts (0.1 to 0.01%, Schwarcz, et al, 1976) that it could not have exercised the role of pore water. Thus, once the newest calcite has cemented the detrital or recrystallized grains of the magnetic mineral, then the grain moments must remain fixed (except those capable of viscous changes).

The fastest growing sample was DAS2 with an average growth rate of about 38 yrs per cm. The rapidly changing field around cuts 32 to 27 were resolved by this growth rate. Had there been a record lag, say over ≈100 years, then perhaps one might expect these hairpin variations to have been smoothed out.

Overall these considerations rule out post-depositional realignment or recrystallization of magnetic grains fixed in compact crystalline speleothems.

9.3.1.2 Depositional Error

A DRM contribution to the total NRM of several speleothems appears certain. Overwhelming evidence is presented in appendix III from the analysis of the thin

sections. Also specimens of VCCL, TS (cuts 17 and 18), SJLS and SJHS, when dissolved in acid yielded quartz and magnetic grains together. These are resistates of weathering and were emplaced from sediment-laden flood water.

It has been suggested in this study (section 7.4.2 and 9.7.3) that the DRM is carried principally by the larger MD grains whereas a primary or secondary CRM is carried by the smaller SD or PSD grains. Therefore if any kind of depositional error, associated with the DRM, was caused by surface dip or roughness, or calcite growth habit, or water flow then it might be observable in the remanence of these low coercive force MD grains. However these same grains are also magnetically the softest, and so would probably acquire VRM, perhaps masking any possible depositional errors. The initial direction shifts for low AF, of pilot specimens could indeed be solely accounted for by VRM (see section 9.3.3). Possible errors from depositional effects carried by low coercive force remanences, have not been detected.

There is substantial evidence to show that the cleaned magnetizations were free of depositional errors as follows:

1) The NRM directions of flowstones BJTL and RCB lay in the region of the AGD field. Flowstone ENF had NRM directions about a reversed AGD. All these three samples possessed substantial layer dips in directions oblique to the meridian. No errors from the dip or water flow were evident.
2) Lateral specimens of TS clearly agree in D and I with the horizontal growth horizons which they span. The same is true of lateral specimens of DAS2. In

the case of SJHS lateral specimens were dominated in intensity by the outer dirt rind. Their directions were exactly the same as those of specimens from the top where the surface was horizontal.

3) Within the errors of the hysteresis experiment, the magnetization of flowstone ENF showed no preferred alignment in direction parallel to the growth layers when compared to a direction transverse to these layers (section 7.3.2.1).

The conclusion is that the NRM, whether a DRM, CRM or a combination of both, was detectable free of depositional errors.

9.3.2 Measurement Errors

These are the direction errors acquired by sets of specimens from a sample or part of the sample, incurred during the course of orientation, specimen preparation and measurement.

9.3.2.1 Field (Orientation) Errors

Stalagmites are oriented by an aluminum tray and Suunto compass and a three-arm U-tube carrying water. The practice was adhered to of retaking measurements to within 0.5°. The error in vertical orientation is estimated to be no more than 1° using the U-tube. Both of these errors decrease for the wider stalagmites.

Errors in measuring flowstones are estimated to be no more than 0.5° in strike, and 0.5° in inclination. It is important that a small hole is gouged in the surface for the lower leg and that the surface under the other

two legs is hard and free of any loose material.

9.3.2.2 Errors in Correcting from N_{mag} to N_{true}.

The world Magnetic Variation charts (1977) do not take into account small regional magnetic anomalies of dimension less than about 1000 Kms. Otherwise the use of the chart involves errors of less than 0.3^{o}. Regional anomalies were considered in the interpretation of the TS record but these were found to be insignificant. Limestones themselves have no associated regional magnetic effect because of their low iron content.

9.3.2.3 Errors Incurred in the Preparation of Specimens

1) The base of the mould was levelled using the clinometer and errors were not more than 0.25^{o}. A check for level was sometimes made when one compartment of the mould was weighed down with the speleothem and plaster. No significant shifts were detected.

2) Azimuth of stalagmites or flowstones with respect to the sides of the mould was reckoned to be better than 0.25^{o}. The errors in the vertical orientation from using the U-tube is no more than 1^{o} for a thin short stalagmite. It was found possible, incidentally, to vertically orient long stalagmites by eye to within 1^{o} of that shown by the U-tube meniscuses.

3) The errors involved in splitting long stalagmites into 2, 3 or 4 sections is about zero in azimuth and less than 0.25^{o} in the vertical.

4) Errors incurred by slicing using the large rock saw can be detected by referring the saw cuts to the original marks, and suitable allowance can be made. For example, ENF was found to have an azimuth error of 1.5°.

5) The small rock saw was within 0.5° of being at right angles to its wooden base upon which the slices were placed.

In summary, errors in the orientation and preparation of the specimens may be up to 2 or 3°, exceptionally 5°, but are probably less than about 1.5° in most cases.

9.3.2.4 NRM Measurement Errors

Systematic errors in measurement of NRM involve:

1) Misalignment of the x, y and z axes of the specimens with respect to the sensors. Sample holder positioning was always checked in both the vertical and horizontal planes. Errors are reckoned to be less than 0.25°.

2) 'Sensing volume' errors (section 2.5.2) may be the largest source of systematic error. They may be as much as 2 to 4° for small 2 cm cubes, using the large specimen holder. The error was less for larger specimens and least for stacked specimens. Larger specimens came from VCCL, TS, SJLS, SJHS, DAS1 and DAS2; stacked specimens from TS.

9.3.3 Errors Associated with VRM and Low NRM

Figure 9.1 gives a rough idea of the range of MDFs met with in samples of this study, and hence of the presence of soft or viscous remanences.

Figure 9.1; Histogram of MDFs

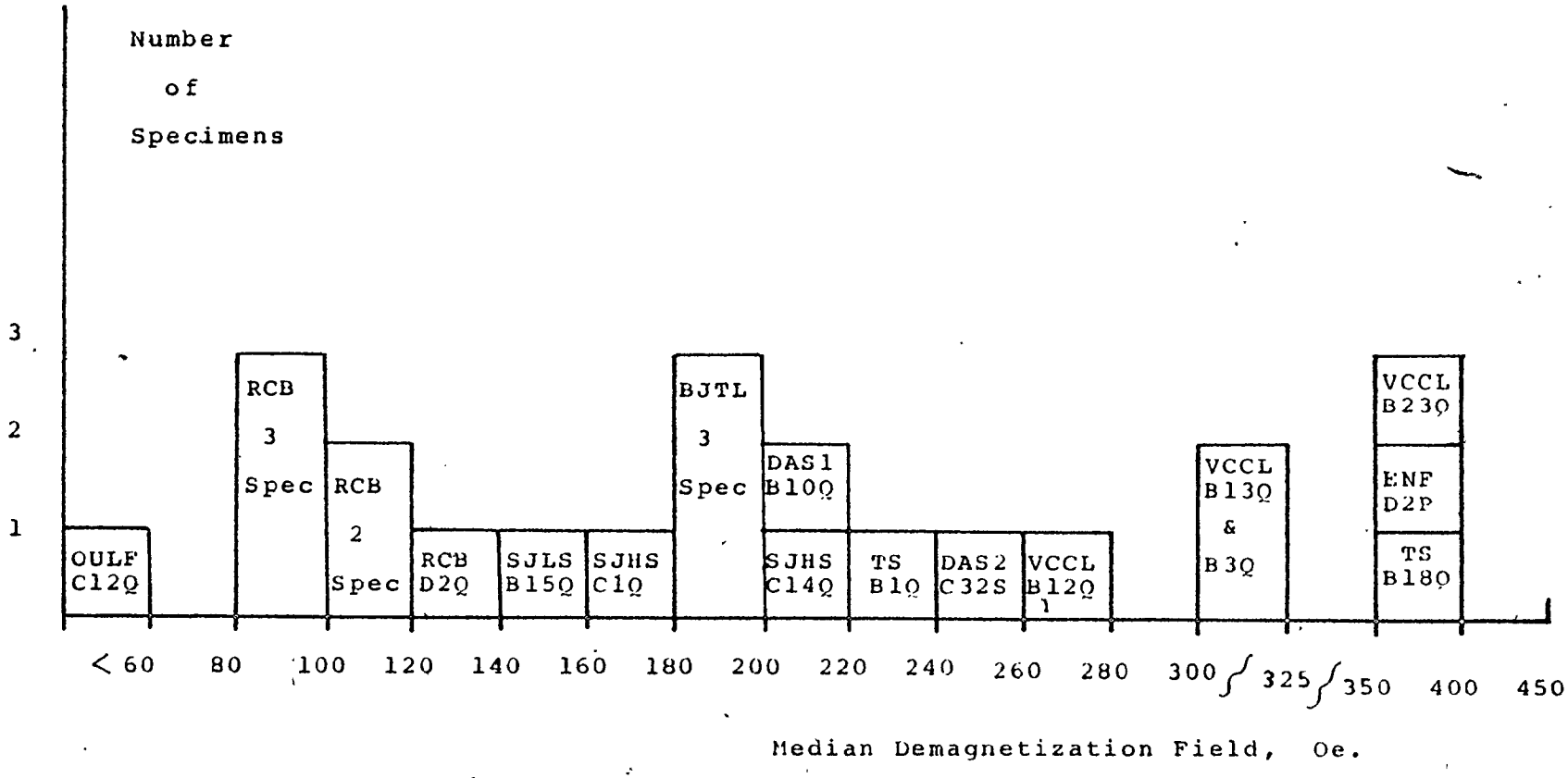

OULF had no stable remanence after about 110 Oe (section 7.3.9). Specimens of RCB possessed stable remances which could be isolated from the VRMs to give meaningful direction data. Only low viscous components were observed in SJLS, SJHS and other samples with high MDFs. These speleothems with higher MDFs have been used in the production of paleomagnetic records; they are now considered in more detail.

One of the chief problems encountered with the low intensity speleothems such as TS, DAS1 and DAS2 has been the inability to insure that all VRM has been removed. Pilot specimens from a given sample were chosen for their high intensity. However the minimum AF cleaning field which they indicated could not always be used for associated specimens, without diminishing the total moment to below the noise level of the magnetometer. Indeed the biggest problem with the accuracy and precision of part of the TS, DAS1 and DAS2 records was not the VRM but the very low magnetic intensities.

In general direction changes upon AF cleaning were small and usually away from the present field for that area. Good examples are SJLS and VCCL. It was noted that the SV curves of SJLS (section 6.2.2) and other samples became less spiky after AF cleaning. This is opposite to what one might expect in that VRMs of the present field when added to stable components would tend to have a smoothing effect thoughout the sample. There are probably two reasons for this:

1) The ratio of VRM to stable magnetization is probably variable throughout most samples. This is to be expected with such samples as SJLS which, during

its growth history, was subject to variable grain size contributions from the detritus.

2) Little attempt was made to keep specimens of a given sample in the same relative orientation from preparation to measurement. It is possible that some VRMs were acquired, effectively, in various field directions other than the field for the site (in contrast, see OULF, section 5.5)

By way of criticism of the use of the AF cleaning procedures in this study it is regretted that:

a) Not enough use was made of Zijderveld plots to more fully assess the VRM contributions to the NRM.

b) With SJLS and DAS2 two or three more pilot specimens should have been used to test for variability of VRM down these samples.

c) Where the specimen intensity permitted, higher cleaning fields should have been considered since it may be argued that the higher magnetization is likely to be characterized by a higher proportion of larger, softer, MD grains.

Changes of direction, as the VRM is removed upon cleaning, should become progressively less with equal increments of AF. For example, it it takes 100 Oe to remove all the VRM then the first 50 Oe step should remove more than 50% of the VRM (depending on the exact coercivity spectrum). There is therefore some comfort from being forced to use an AF a little less than the ideal cleaning field for these low intensity specimens. (Perversely enough, this effect is not shown by the Zijderveld plots of either VCCL, figures 7.12, 7,13, nor by DAS2 C32S, figure 7.29 ! Ie, equal increments in AF produced equal

increments in the direction up to the stable direction).

The errors due to insufficient treatment of VRM in most cases are probably small, $<3^{o}$, and precision of combined directions has generally improved upon cleaning. The exceptions have been noted in the relevant sections on the paleomagnetism. For example, the possibility that specimens of the base of SJLS may have been insufficiently cleaned was discussed in section 6.2.2 . With the exception of VCCL, section 4.6.2, most NRM directions were close to their AF cleaned directions.

9.4 Age Dating Errors

The useful lower age limit of the U/Th method has been quoted as 5 Ka BP (Schwarcz, 1980, op cit). Cascoyne (1979, op cit) concluded that a lower age limit of 200 years was attainable for high uranium speleothems. It has been a pleasant surprise to find from this study that the method can be used on speleothems of the more usual concentrations (0.2 - 1 ppm) to find ages almost up to the present. The proviso is that the samples must have grown over a sufficient span of time so that growth rate curves may be fitted. The production of such ages and growth rates has entailed:

1) The use of high resolution, low background counters.
2) Careful monitoring of the slowly increasing background contamination.

In the correction for background, it was usual in the McMaster procedures to consider common background energy regions for ^{238}U and ^{232}Th, ^{234}U and ^{230}Th, and ^{232}U with ^{228}Th. Because of the alpha-recoil contamination, as discussed in section 3.2.2, the ^{228}Th background (which

is enhanced by 5% of ^{224}Ra background) becomes considerably higher than all other background count rates, as the detector ages. With the higher resolution detectors used in this study, it has been possible to resolve the ^{232}U and ^{228}Th backgrounds, thus providing separate corrections to the corresponding U and Th spectra.

3) Comparison of spectra from specimen to specimen in order that the integration of counts should cover the same ranges of alpha-particle energy in corresponding peaks. This at least ensures that errors in relative ages are minimised between specimens from the same sample.

4) Dating of at least six specimens from a given speleothem, so that:

   a) An estimate can be made of variations in, and corrections for detrital thorium.

   b) Growth rates (all taken to be constant in this study) could be fitted by least squares methods.

   c) Specimen ages could be eliminated if they occurred more than 2 σ away from the fitted curve. A new more precise curve could then be constructed.

The systematic dating errors are now detailed in terms of their chemical and sample contributions.

9.4.1 Chemical Errors

From samples VCCL, SJLS and perhaps SJHS, significant errors in a few specimens appear to be due to thorium contamination from insufficiently cleaned glassware. Substantial apparent age shifts on the order of 10 Ka may have been induced. Uranium contamination is thought to be less likely because unlike thorium, it is not adsorbed onto

glassware. Because of the precautionary TTA - pH 1 extraction step, Th will not appear in the uranium spectrum; and apropos of the remarks of section 3.3.4.4, this is a good reason for keeping this step. At the time that the dating of these mostly young samples was in progress, the same glassware was concurrently being used to date older samples. Therefore the Th contamination may account for the apparently greater ages. Similar problems were encountered by M. Gascoyne (1979, op cit) in his attempts to assess reagent blank corrections; the 'memory' effects from the glassware, were found to be variable and occasionally substantial. From the time the effect was confirmed in this study the glassware has been cleaned a second time prior to usage.

The adoption of the TTA method for the plating of U and Th has presented few problems. A second set of ether extractions for the uranium eluate was occasionally required to extract more iron. The resulting thin deposits together with the use of small area detectors has meant that no low-energy tail corrections were needed between the well-resolved adjacent alpha peaks.

Chemical yields of both thorium and uranium were satisfactory (30%) to good (70%). ^{230}Th count rates were always at least several times greater than background. For example, for DAS2 B1QR (the top cut) the ^{230}Th count rate (less background) was 0.016 cpm and the background was 0.003 cpm. This satisfies the criterion of Komura and Sakanoue (1964) in which they fixed a limit of detection at four times the standard deviation of the background count rate. The limit is therefore $4\,(b/T)^{\frac{1}{2}}$, where b is the background count rate and T is the blank

disc count time. With b = 0.003 cpm and T = 1487 mins, this gives a detection limit of 0.006 cpm in the above case, which is safely exceeded by the ^{230}Th count rate.

9.4.2 Sample Errors

There are three possible violations of the closed-system assumptions leading to age error; they have all appeared from time to time in the analysis of speleothems of the McMaster collection. These are leaching of uranium, the presence of unsupported ^{228}Th in young samples, and detrital thorium contamination. The last is the most common.

9.4.2.1 Leaching of Uranium and the Presence of Unsupported ^{228}Th

If natural leaching of uranium has occurred in a sample it would be observable as an apparent increase in the calculated age. In low U samples even a 'mild' leaching at a significantly later time after formation would produce ^{230}Th/^{234}U ratios well in excess of unity , and this is how the effect has usually been recognised. Leaching of uranium was discussed, but dismissed, as a possibility in sample SJHS (section 6.3.3).

^{228}Th has a half-life of 9.91 years and is the decay product (via ^{228}Ac) of ^{228}Ra (half-life = 5.76 a; see figure 3.1). ^{228}Ra, the daughter of ^{232}Th, has the same group II chemical properties as Ca. A porous speleothem, or an actively growing calcite layer such as DAS2 - cut 1, may therefore incorporate ^{228}Th (from ^{228}Ra) unsupported by ^{232}Th. It would have the effect of enhancing the spike ^{228}Th peak, and would therefore produce anomalously younger ages.

P.Thompson (1973, op cit) observed this effect in the top 1.9 cms of a speleothem from West Virginia, and confirmed the presence of ^{228}Th from unspiked analyses. The speleothems of this study were all compactly crystalline and not porous, and were therefore unlikely to favour easy migration of Ra. The calculated age of DAS2 - cut 1 , when compared with the overall growth rate rules out any significant influence from unsupported ^{228}Th. However no unspiked analyses of young speleothems (the effect is insignificant after ≈40 yrs) were made to test for unsupported ^{228}Th.

9.4.2.2 Errors from Detrital Contamination

Flood lain detritus was clearly visible in VCCL, the base of TS, RCB, SJLS, the upper part of SJHS, DAS1 and DAS2. Either U or Th from the detritus may be leached into the solutions of dissolved specimens intended for analysis. The separate effects on the calculated ages are:

1) ^{234}U (with ^{238}U) will cause a decrease.
2) ^{230}Th will cause an increase.
3) ^{228}Th supported by ^{232}Th can be directly allowed for (^{228}Th/^{232}Th = 1) in all but the youngest layers. Preferential leaching of ^{228}Th (it sits in an alpha-recoil damaged site in the detrital grains) will cause a decrease.

Most sediment in transport will not have loosely bonded U because it is readily carried in solution, whereas Th is adsorbed onto clays as a hydrolysate*. Therefore the

* The exception, in this study , is RCB (section 5.2.3) where detrital U may have been carried by FeIII (in the form of FeOOH or Fe_2O_3?)

expected overall effect of acid attack on detritus is for Th to be predominantly incorporated into the solution. This is usually what is observed. In this study and that of M. Gascoyne layers richer in detritus always gave ages older than adjacent clearer layers (eg TS, section 4.7.3).

In correcting for detrital Th in the present McMaster procedures, $^{228}Th/^{230}Th$ is assumed to be in secular equilibrium in the detrital leachate, and $(^{230}Th/^{232}Th)_o$ is fixed at 1.5, as discussed in section 3.1.1. A more thorough analytical approach to a similar problem was carried out by Ku, et al (1979) on pedogenic carbonates from California. In addition to radiometrically analysing the carbonate rinds, whose age they sought, they also analysed the incorporated silicates in order to correct for its leachate contribution to the former. They also found it possible to analyze the sample as a whole in order to produce a second age estimate which was independent of the assumptions of their first method. The overall agreement was fairly good. (incidentally, using the results of their table 3 gives an average initial $^{230}Th/^{232}Th$ ratio of 1.54, for the silicate detritus). It may be possible to use the methods of Ku, et al, on future analyses of speleothems known to have detrital content. In this study the more empirical approach was adopted of comparing the corrected ages of detrital and clear layers using the growth rate trends for reference (eg TS and DAS2). The conclusion was that the ratio of 1.5 was realistic, but perhaps, a bit too low. The corrections , when applied to DAS2 - cut 1, gave a modern age which is in accord with the field evidence.

Such modern stalagmites suggest another variation

on this kind of approach . This is to compare the age of the top (nominally ≈0 yrs BP) with that of coeval layers of the sides which contain washed-off detritus. Such a comparison would automatically give a correction factor which is specific to that stalagmite. To a first approximation the factor could be assumed constant for the remainder of the sample.

If the ages were left uncorrected for detrital Th this would generally give growth rates and growth spans which are about the same as those derived from the corrected ages; but the average age for the whole sample would be shifted to somewhat older values.

In summary, the sample errors in the ages arising from the breakdown of the closed-system assumptions, and in particular, from insufficient allowance for detrital Th, are probably less than 10 or 15% for DAS2. This claim is based on:

1) The radiometrically derived age from cut 1 of the top, when corrected for detrital thorium is 100 ± 300 years, which is in good agreement with the zero age from field evidence.
2) Without the constraint of, age = 0, when length = 0, the best fit constant growth curve still predicts a near zero age for the top.
3) As mentioned in section 6.5.3, the large correction shifts for the basal dates are in close agreement with the overall dating growth trend deduced without them.

In the case of SJLS and VCCL the age errors are probably less than 10%. Further radiometric analyses of

Table 9.1

Analysis of Growth Rates

Sample	Growth Rate $cm\ Ka^{-1}$	Time spanned by 2 cm cuts (years)
VCCL	10.87	184
TS	8.77	228
SJLS	10.0	200
SJHS	1.0	2000
DAS2	52.6	38

specimens of VCCL, produced too late for inclusion in this work, have confirmed the original age and constant growth rate estimates.

9.5 Resolution of the Paleomagnetic Record

Table 9.1 summarises the growth rates of five speleothems of this study which have provided dated records. Growth rates varied between 1.0 and 52.6 cms per thousand years. Correspondingly, the two-cm. thick cuts represented, on the average, from 2000 to 38 yrs. It is therefore clear that speleothems, especially stalagmites, are capable of resolving the fine detail in secular variation. The NB10 stalagmite analysed by P. Thompson (1973, op cit), from West Virginia, grew at an average rate of 2.5 cms per Ka, from 200 Ka BP almost to the present. It may be possible therefore, to obtain quite long records of fairly well-resolved SV.

9.6 Reliability of the Speleothem Paleomagnetic Record

The reliability of any paleomagnetic record is assessed in the context in which it may be used. For example, the generalised record from lake Tlapacoya, Mexico (Liddicoat, et al, 1979) for the interval 25 Ka to about 4 Ka BP is adequate for revealing overall westerly declinations, but not much else. The authors were unable to say for certain whether inclinations were shallower or as steep as I_{agd}, and produced conflicting evidence about a possible Tlapacoya excursion at 14.5 Ka BP.

By contrast the European lake record, back to about 13.5 Ka, is now well defined, and may be relied upon:

1) For magnetostratigraphic use (with some reservation about the dating of the older part of the record).
2) For detailing the changes in the field including the geomagnetic features of this time.
3) For pointing out easterly or westerly trends in declination (the upper part may be fixed in azimuth by comparison with archeomagnetic data and historic records).

Without the considerable effort that was required in examining multiple cores, it is evident from reading the literature that one is seldom sure that a given sediment core is free of recorder errors, such as inclination shallowing or pdDRM. For example, in referring to the Lac de Joux record, Creer et al:

1) Discuss the possibility of core disturbance to explain mismatch between cores,
2) Leave unspoken the problem of whether part of the shallow inclinations which they see was due to compaction or settling errors.

From the (partially) contemporary TS record it is clear that the shallow Lac de Joux inclinations (see section 4.7.5) were recording a real feature of the geomagnetic field. Similarly Liddicoat, et al, observed shallow inclinations in the Tlapacoya record. Having already retracted on claims about the excursion, they continued to play safe and say that either a structural correction of 10^{o} - 15^{o} could bring average inclinations towards I_{agd} (there is no choice about a structural correction - it must be applied!), or inclination error was the cause. The SJLS record shows that mostly shallow inclinations between 9 and 4 Ka BP were a real feature of the geomagnetic field in Mexico.

The reliability of the individual speleothem records is discussed in the relevant sections of the palaeomagnetics chapters. From these chapters and from the preceeding sections it may, in general, be concluded that for speleothems with stable, measurable NRM well-resolved D and I variations closely match those of the ambient field. With suitable precautions they may be dated with reliable accuracy. They may be put to a full range of use, such as:

1) Revealing SV, via D and I and the VGPs, and its timescales.
2) Constructing VGP paths for comparison with other records.
3) Magnetostratigraphy. The resolution of master curves is as good as or may be better than many sediment records.

From 1) the SV measurements lead to knowledge and understanding about:

4) Westward/eastward drift, far-sided and left-handed VGPs and cyclicity of field features.

Via comparison with records from other regions this leads to:

5) An estimate of the relative contribution of non-dipole and dipole variations to the whole field.

No claims are made at this stage about paleointensity estimates from speleothems. The possibilities of this work are discussed in sections 8.5.1/2 and 9.7.5 .

9.7 Conclusions from the Rock Magnetism and ARM Experiments on Speleothems

9.7.1 Mineralogy

Magnetite, or possibly maghemite, is the dominant carrier of the natural remanence in speleothems. Summarising the evidence from chapters 7 and 8 and appendices III and V:

1) Coercivity H_c and coercivity of remanence H_{cr} were in the range usually quoted for magnetite.
2) Saturation fields were ≤ 3 KOe.
3) Curie point estimates from thermal demagnetization were in the range 570 to 580 °C.
4) Opaque grains from specimens dissolved from samples VCCL, SJLS and SJHS could easily be picked up by a magnet.
5) These same opaque grains could also be seen in thin section and most were a uniform gray colour in reflected light.
6) These same grains, from the Mössbauer spectra, showed the strong field splitting characteristic of magnetite.

The thermal demagnetization experiments seemed to indicate a phase change around 300 to 350 °C. If the apparatus was reliable (see section 7.2.2) this could be evidence for maghemite which then converts either to magnetite by reduction or to hematite. Maghemite may account for the high susceptibility of many organic soils (Le Borgne, 1955), including those from weathered limestone. It may therefore be present in the detritus of some speleothems.

The kind of detrital material found in speleothems depends on the original material, its sorting and

transport, and on the newly evolved material. Thus in TS, VCCL, SJLS, SJHS, DAS1 and DAS2 were found the resistate minerals quartz, magnetite and titanomagnetite, with occasional feldspar and other unidentified minerals often in association with fibrous organic material. In sample RCB red particulate matter, which is almost certainly a hydrated iron oxide, and organic material were found. In OULF the chief detrital constituent was a fine red clay containing goethite or lepidocrocite.

If hematite was present it was not in sufficient quantities to show up in the hysteresis experiments: (-with the possible exception of the Petralona samples! , section 5.6 . In accordance with Murphy's Law a late experiment on the hysteresis of a Petralona specimen showed it to have H_c = 400 Oe, H_{cr} = 3.5 KOe and H_{cr}/H_c=3.5 . The remanent and total induced moments increased smoothly to saturate in a field of about 15 KOe. These characteristics are more indicative of hematite, except that the saturation field is a bit low).

9.7.2 Grain Size and Coercivity; Range and Distribution

From the various samples, the hysteresis parameters indicated the usual range of magnetite grain sizes ordinarily met with in most other rocks, excepting grains greater than $\approx$0.1 mm. ENF, (and perhaps a few other samples) may be fairly unique in that it was dominated by single domain grains, judging by the M_{rs}/M_s ratio of $\approx$0.45 . The heating of a specimen from ENF appeared to produce a large increase of these SD grains. A similar effect, to a lesser extent, was observed in a specimen from

DAS2. Organics may be responsible for somehow giving rise to these SD grains but as yet there is no satisfactory explanation for this thermally enhanced magnetization.

In the samples RCB and OULF, whose detritus is more akin to terra rosa soils, the grain sizes are too fine for observation by optical microscopy; the coercivities are distinguished by low and superparamagnetic components.

9.7.3 The Origins of the NRM of Speleothems

A complete explanation of the origins of the NRM of speleothems is not yet possible. DRM is undoubtedly part of the total remanence of several speleothems in this study. The evidence is summarised in section 9.3.1.2 . However there appears to be, either in addition or on its own, a fine-grained CRM. Low remanences exist in some samples, or parts of samples which lack evidence of a detrital content, for example, the upper part of TS. In samples with no measurable NRM, SIRMs indicative of magnetite may be induced (eg DBS1 or WCS1). It is probable that magnetite grains of micron and submicron size could be transported in cave seepage water. However they are unlikely to survive intact as the hydro-chemical conditions change from the soil zone to the deposition of the calcite. Thus a fine-grained (SD or PSD?) DRM is likely to be a small fraction of, or absent from the total magnetite grain assemblage. The transport of iron (as Fe^{2+} and Fe^{3+}) and the crystallization of Fe_3O_4 at the growth horizon appears intimately linked with the presence of (soluble or insoluble) organic material. Anaerobic bacteria may also play a role in crystallizing magnetite at the growth horizon.

9.7.4 The ARM Experiments

The ARM of specimens from several samples showed approximate linearity with weak field. This finding is one of the requirements for using ARM as an analogue of NRM in estimating either relative or absolute intensities of the ancient field.

ARM ($\tilde{H}$ = 1 KOe) and SIRM ($H \geq 3$ KOe) showed similar AF demagnetization characteristics, that is, SIRM/ARM = constant, when demagnetized through the same AF. As expected, they thus have about the same coercivity spectra as revealed by the AF demagnetization.

By contrast to the above, ΔNRM/ΔARM ratios were (approximately) constant over only limited AF intervals. Specimens were taken mainly from DAS2 but they also included one from ENF. Several NRM - ARM plots showed two segments and it was noticeable that where these two segments joined there was a gap in the coercivity spectrum. This gap was not the same for all such specimens; but it did tend to occur around 300 - 400 Oe as measured by AF demagnetization. Therefore either:

1) assuming all the grains of the original NRM experienced the same field, then

$$\frac{NRM}{ARM} = \text{function(coercive force)}, \text{ with } H_{nrm}, H_{arm}$$

both constant. Coercive force is in turn a function of grain size, shape and mineralogy. In other words, the variable NRM/ ARM ratio may be due to either:

a) the presence of both MD and SD grains, or

b) mixtures of titanomagnetites, maghemite or magnetite grains.

Alternatively,

2) if the NRM is composed of a DRM and a CRM, then we may write,

$$\frac{NRM}{ARM} = f(DRM_{H_{drm}}, CRM_{H_{crm}}),$$ ie we make the distinction that the ambient field on the same grain assemblage produces a different magnetization depending on whether it was detrital or chemical. If, as appears likely, the DRM is carried in the coarse grains and the CRM is carried in the fine grains, then perhaps the 'normalization' by ARM has effectively separated the two magnetizations.

One clue to the choice between these alternatives may be offered by the heating experiments (ATRMs) on DAS2 - B30T and ENF D9R - especially the latter. There it was shown that, (section 8.4.5)

$$\frac{ATRM}{ARM} = f(\text{coercive force range}),$$ in which it is almost certain, for ENF, that the mineralogy is the same throughout. Thus possibilities 1b) and 2) are ruled out, at least for the ATRMs.

Similar findings to these ARM experiments have been reported by Kono (1978), from igneous rocks, in a test of Shaw's method for finding paleointensity from TRMs (Shaw, 1974). Kono observed that:

1) In some samples NRM - TRM, or ARM(1) - ARM(2) diagrams showed linear segments over coercivity intervals,
2) In some samples, heating produced increases, or decreases in the ATRM, when compared with the original NRM (TRM), without changing the shape of the coercivity spectrum.
3) between the samples f (= ATRM/ARM) varied between 1 and 5.

The ATRM - ARM experiments may be of some general importance to rock magnetism. Thus the linear segments over ranges of coercive force confirms the interchangeability of ARM for TRM for SD particles (Dunlop and West, 1969, op cit; Dunlop et al, 1973, op cit; Johnson et al, 1975, op cit), and perhaps for MD particles (Johnson, et al, 1975 op cit). It would be of considerable advantage to this type of work if alternating fields of order 2.5 to 3 KOe were accessible.

9.7.5 The ARM Analogue as used in the Estimation of Paleointensity

Section 8.4.6 detailed an attempt to recover (relative) intensity of the ancient field from DAS2 via an equation,

$$H_{a-a} = \frac{NRM_{100} - NRM_{1\ KOe}}{ARM_{100} - ARM_{1\ KOe}} \times H_{lab}$$

where H_{a-a} is understood to mean 'apparent ancient' field. There was considerable variability in H_{a-a} of specimens from the same cut, but it was tentatively suggested that H_{a-a} was more a function of the ancient field than of other possible factors such as magnetic content. In view of the variability of $\Delta NRM/\Delta ARM$ with AF (previous section) it was encouraging to see that, (figure 8.10)

1) The mean H_{a-a} values were of about the same magnitude as modern and archeomagnetically derived field estimates, for example, those from Peru.
2) The mean H_{a-a} of adjacent cuts agreed fairly well with each other.
3) The magnitude changes and rates of change were about the same as observed in the archeomagnetic data.

It would nowever be unwise at this stage to place faith in H_{a-a} until further studies have been made into its exact meaning. It is suggested tnat this could most easily be done by deriving H_{a-a} from the latest growth horizons of modern speleothems, and comparing it with the modern field. In this respect the result from the top of DAS2 was not a good match.

9.8 Further Discussions on the Geophysical Interpretation of the Paleomagnetic Records

9.8.1 Persistent Bias in Direction or VGP Path

Several of the paleomagnetic records of this study are notable for their consistently shallow inclinations giving far-sided VGPs. They are:

1) VCCL (Vancouver, 6.4 to 2.2 Ka); average $I \approx 57^{\circ}$, compared to $I_{agd} = 66.8^{\circ}$.
2) TS (England), 11.3 to 7.5 Ka); average $I \approx 61^{\circ}$, compared to $I_{agd} = 70.2^{\circ}$.
3) SJLS (Mexico , 9 to 4,5 Ka); average $I \approx 27.5^{\circ}$, compared $I_{agd} = 31.6^{\circ}$.
4) DAS2 (Mexico, 1.3 Ka to present): average $I \approx 33^{\circ}$, compared to $I_{agd} = 39^{\circ}$.

The directions of the reversely magnetized flowstone ENF (Canada, >720 Ka) change closely about an axial geocentric dipole position. The Mexican stalagmite SJHS (about 127 to 100 Ka) had consistently steeper inclinations than I_{agd} (average $I \approx 34^{\circ}$, $I_{agd} = 31.6^{\circ}$).

The average declinations of these speleothems showed some slight bias, eg VCCL and SJHS had westerly declinations , giving left-handed VGPs and TS gave markedly right-handed VGPs.

9.8.2 Looping of Directions (or VGPs); Cyclicity; Westward Drift.

VCCL gave a clear record of 2½ loops of direction (or VGPs) from 6.4 to 2.2 Ka. This is firm evidence for westward drifting features of the field. Clockwise looping is also evident, though less clear, in the record of TS from 11.3 to 7.5 Ka.

Such predominant clockwise looping is not evident in the record of SJLS (9 to 4,5 Ka), nor is it evident in the older record of SJHS (127 to 100 Ka). This is not incompatible with what is known generally about the ancient field or even the modern field. For example, all x, y and z components in Alaska are presently moving eastwards, and significant westward drift is absent in most of Canada (Skiles, 1970, quoting other sources).

Except for ENF (BJTL is probably too short a record to judge by), all the records show that, whether cyclicity is present or not, the field for that region has a bias in direction over several thousands of years. In the case of TS the bias is strongly far-sided and right-handed. This again serves as a reminder that (substantially thick?) lava sequences of the past may give average paleopoles which are still not good estimates of the paleo-geographic pole.

Figures 9.2a and b

Declination and Inclination Variations due to a Radial Eccentric Dipole

(a) (Figure 4(b), from Skiles, 1970): Combined declination and inclination variations as observed at London (51.2° N, 0° E) when an eccentric radial dipole located in the earth's core, at a fixed radius, rotates about the earth at a given latitude. The sense of each curve is clockwise (anticlockwise) for a westward (eastward) drifting dipole. The arrow indicates when the dipole lies in the zero meridianal plane (0° E). The + indicates the AGD direction for London.

(b) Illustrates the D and I variations from a hypothetical well resolved record, assuming the solid curve of 20° N from 9.2(a).

Note: 1) The inclinations are shallower than I_{agd}.

2) The large declination swings are about twice those of inclination in this case.

Figure 9.2 (a)

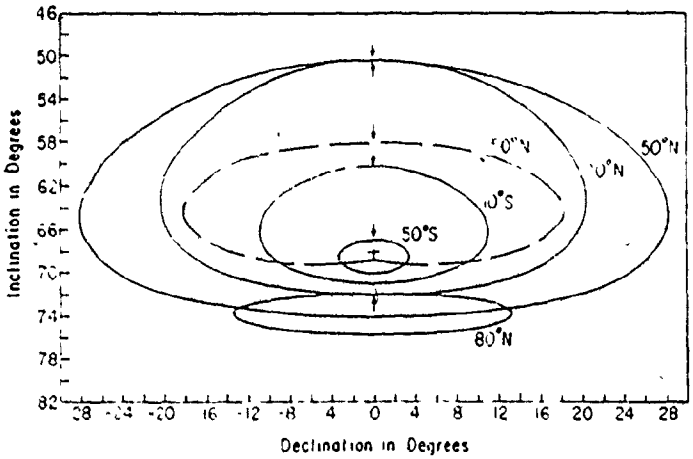

Fig. 4(b) Dipoles of the same magnitude drifting at different latitudes. For the solid curves $M_r/r_e^3=0.1144$ gauss, and for the dashed curve $M_r/r_e^3=0.0078$ gauss.

From Skiles (1970)

(b)

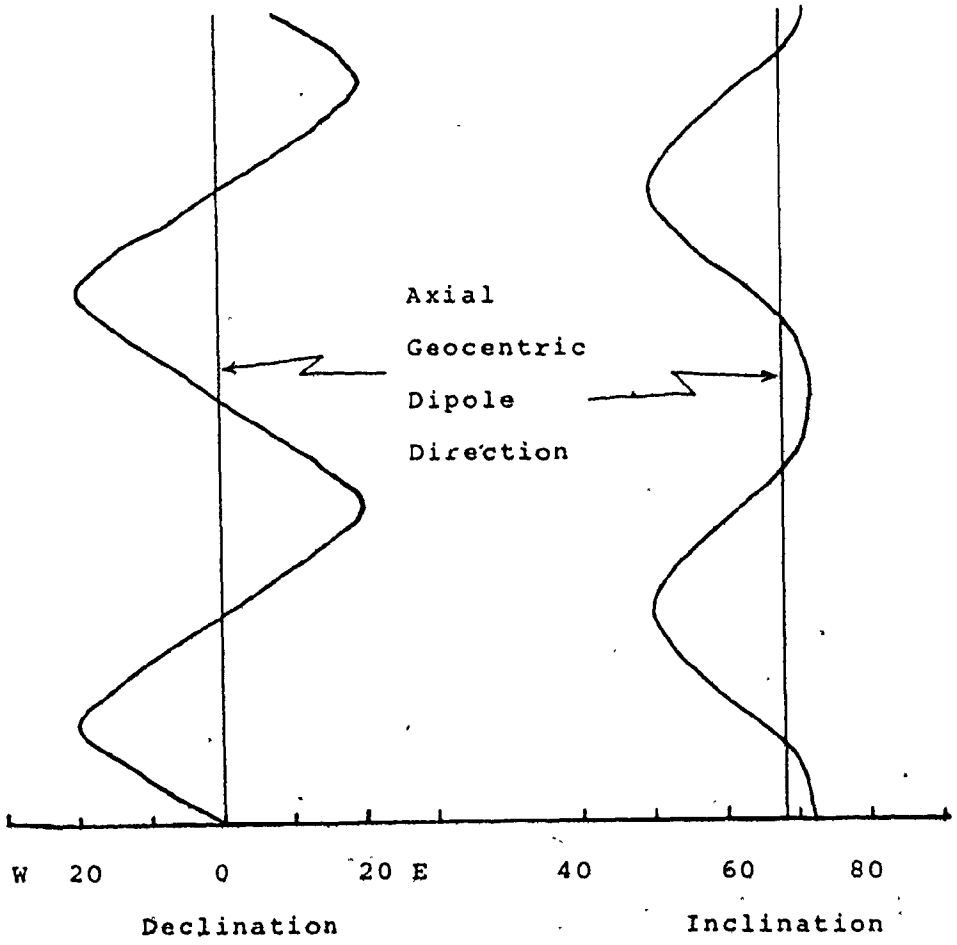

9.8.3 The Magnetic Field Features of the TS and Lac de Joux Records

Section 4.7.5 .

Creer, et al (1980, op cit) noted the cusp-shaped features in the Lac de Joux inclination record. Earlier Creer, Gross and Lineback (1976, op cit), and Creer (1977) had attempted to explain the Windermere and Michigan lake records in terms of stationary but oscillating radial dipoles. Indeed, various workers have frequently attempted to explain present or past anomalies or features of the field in terms of sets of radial dipoles (eg, Alldredge and Hurwitz, 1964, op cit)

The declination features of either the TS or Lac de Joux records are only partly coherent with the corresponding inclination features (eg D is not as regularly varying as I). Nevertheless the inclination cusps are what one might observe if a radial dipole were to move repeatedly past the longitude of the site. In addition to the cusp features, the shallow inclinations and large east-west-east swings can all be explained if the hypothetical drifting dipole was positive, and at a latitude somewhat to the south of the site latitudes. Figure 9.2a is a clockwise loop in direction, taken from figure 4 of Skiles (op cit), which would result from the circulation of such a radial dipole. Figure 9.2b is a sketch of the resulting inclination and declination features, as they would be observed from a resolved paleomagnetic record. Comparisons of figure 9.2b and the TS and Lac de Joux records show:

1) The inclination cusps are considerably sharper than

Table 9.2

Lowest Latitudes of VGPs, (as an approximate measure of dispersion).

Record	Latitude (degrees)	VGP latitude from geographical north.
BJTL	49.7	61.1
ENF	49.7	72.5
VCCL	49.5	61.0
TS	54.2	63.3
SJLS	17.1	75
SJHS	17.1	71
DAS2	17.1	71

is expected from radial dipoles.

2) The TS declinations are not symmetrical about the meridian; they are biased to the east.

3) There appear to be rapid changes in I between the two sites.

As with the modern field, it is very likely that the paleofield at any given site was influenced by more than just one (radial dipole) source.

9.8.4 Angular Dispersion of the VGPs

A full analysis of the dispersion of each record in terms of directions or VGPs has not yet been made. As a rough guide, the latitudinal extremes of VGPs are presented in table 9.2 . In accordance with the discussion of, for example, Irving, ch 3, 1964, or Harrison (1980) there is a tendency for VGPs from more southerly records to show less dispersion. As a cautionary remark to this kind of analysis, Cox (1975, op cit) has noted sequences of lavas from Hawaii having apparently quiet and noisy records, which in turn would give low and high dispersion from the same latitude.

9.8.5 Further Discussion of the DAS2 Record

A westward drift construction was used to compare the present world geomagnetic features at latitude 22°N with the DAS2 record, which spanned about 1.3 Ka to the present (section 6.5.4.2). The match of the declination features was particularly good. It was pointed out however, that the construction assumes that the main dipole precesses at the same rate as the westward drift rate of the non-dipole

field and with a tilt to the spin axis equal to its present tilt. This is probably not a good assumption. It is known from modern data that the main dipole is spiralling towards the spin axis with a westward rotation of $\approx 0.05^{o}\ a^{-1}$ and a northerly tilt velocity of $\approx 0.02^{o}\ a^{-1}$; the non-dipole field average velocity is about $0.2^{o}\ a^{-1}$, (Nagata, 1965; see section 1.3.2).

The DAS2 record matches the westward drift construction least over the interval 1.3 to 1 Ka; in particular the DAS2 inclinations are much shallower. In the dim light of the H_{a-a} variations and the archeomagnetic data (section 8.4.6) it might be instructive to attempt an explanation of these shallow inclinations. H_{a-a}, and the data of Bucha et al (1970) show low intensity from about 1.3 to 1 Ka, BP. A tilt of the main dipole away from the site might explain the shallow inclination and part of the low intensity of these data - especially if the geomagnetic equator moved across the Mexican region at the time. However, intensity changes in the contemporaneous Peruvian record of Gunn and Murray (1980) ought then to be negatively correlated with the Mexican records, which is not the case. As an alternative explanation, an overall diminished main field would appear to be ruled out by the worldwide (European and Japanese!) archeomagnetic data. If these paleo- and archeomagnetic data are confirmed it would strongly suggest that a considerable contribution to the field came from non-dipole sources at this time. The data reinforce an increasing feeling amongst archeomagnetists that ancient field intensity may have been more regionally variable than was originally thought.

9.9 Magnetostratigraphy

The development of magnetostratigraphy from Brunhes chron SV records is partly stalled at present because of the considerable effort that has been required to prove the reliability of the sediment master curves. The problems are concerned not only with the faithfulness of the sediment recorder but also with the dating of the sediments, usually by ^{14}C methods. As a result there has been, so far, little application of SV magnetostratigraphy for dating purposes. Early attempts were those of Ellwood (1974), to date cave sediments from Georgia, USA, Creer and Kopper (1974) to date Spanish cave paintings, and Creer and Kopper (1976) to date and correlate cave sediment records from the Mediterranean region. In dating Finnish lake sediments, Stober and Thompson (1977) preferred to use the dated British lake declination master curves to their own ^{14}C dates.

From this study the SV records from speleothems were shown to be free of depositional errors and may be reliably dated by the U/Th method. The 350 Ka dating limit of the method, implies a considerable extension for magnetostratigraphy from SV. In the long term it is expected that the SV records from sediments, archeomagnetism and speleothems will complement each another.

In this study the magnetic polarity of very old speleothems were referred to the Brunhes-Matuyama boundary in order to provide age limits. Thus the reversely magnetized samples ENF and CGF1, and the normally magnetized sample BJTL have been used to estimate erosion rates in the southern Canadian Rockies (section 4.5.1).

REFERENCES

ABRAHAMSEN, N. & Knudsen, K.L., 1979, Indication of a geomagnetic low-inclination excursion in supposed Middle Weichselian marine clay at Rubjerg, Denmark. Phys. Earth Plan. Int., 18, 238-246.

AITKEN, M.J., 1974, Physics and Archaeology, Oxford U. P., 2 nd. ed.

ALLDREDGE, L.R., 1977, Geomagnetic variations with periods from 13 to 30 years, J. Geomag. Geoelec., 29, 123-135.

ALLDREDGE, L.R. & Hurwitz, L., 1964, Radial dipoles as the sources of the Earth's main magnetic field, J. Geophys. Res., 69, 2631-2640.

AMIN, B.S., Lal, D. & Somayajulu, B.L.K., 1975, Chronology of marine sediments using the ^{10}Be method: intercomparison with other methods , Geochim. Cosmochim. Acta, 39, 1187-1192.

BAILEY, M.E. & Dunlop, D.J., 1977, On the use of anhysteretic remanent magnetization in paleointensity determination, Phys. Earth Plan. Int., 13, 360-362.

BANERJEE, S.K. & Mellama, J.P., 1974, A new method for the determination of paleointensity from the ARM properties of rocks, Earth Plan. Sci. Lett. 23, 177-184.

BANERJEE, S.K., Lund, S.P. & Levi, S., 1979, Geomagnetic record in Minnesota lake sediments - Absence of the Gothenburg and Erieau excursions, Geology, 7, 588-591.

BARBETTI, M. & McElhinny, M.W. 1972, Evidence of a geomagnetic excursion, 30,000 yr BP. Nature, 239, 327-330.

BARBETTI, M.F. & McElhinny, M.W. 1976, The Lake Mungo geomagnetic excursion, Phil. Trans. Roy. Soc. Lond. A281, 515-542.

BARTON, C.E. & McElhinny, M.W. 1979, Detrital remanent magnetization in five slowly redeposited long cores of sediment, Geophys. Res. Lett. 6, 229-232.

BARTON, C.C., Merrill, R.T. & Barbetti, M. 1979, Intensity of the Earth's magnetic field over the last 10,000 years, Phys. Earth Plan. Int. 20, 96-110.

BLACKBURN, G & Taylor, R.M. 1969, Limestones and red soils of Bermuda. Geol. Soc. Amer. Bull. 80, 1595-1598.

BEVINGTON, P.R. 1969, Data reduction and error analysis for the physical sciences. McGraw-Hill.

BONHOMMET, N. 1970, Discovery of a new event in the Brunhes period at Laschamp (France). in Palaeogeophysics, ed. S.K. Runcorn, Academic Press, 159-163.

BONHOMMET, N. & Babkine, J. 1967, Sur la présence d'aimantation inversées dans la Chaîne des Puys. Comptes R. Acad. des Sci. Paris, 264B, 92-94.

BONMOMMET, N & Zähringer, J. 1969, Paleomagnetism and potassium argon age determinations of the Laschamp geomagnetic polarity event. Earth Plan. Sci. Lett. 6, 43-46.

BOTT, M.H.P. 1967, Geophysical investigations of the Northern Pennine basement rocks, Proc. Yorks. Geol. Soc. 36, 139-168.

BOYLE, E.A., Edmond, J.M. & Sholkovitz, E.R. 1977, The mechanism of iron removal in estuaries, Geochim. Cosmochim. Acta, 41, 1313-1324.

BRETZ, J.H. 1960, Bermuda; a partially drowned late mature Pleistocene karst, Geol, Soc. Amer. Bull, 71, 1729-1754.

BRIDEN, J.C. 1972, A stability index of remanent magnetism, J. Geophys. Res. 77, 1401-1405.

BRIDGES, E.M. 1970, World Soils, Cambridge U.P.

BROCK, A. 1971, An experimental study of paleosecular variation, Geophys. J. Roy. Astr. Soc. 24, 303-317.

BROECKER, W.S., Thurber, D.L., Goddard, J., Ku, T-L. , Mathews, R.K. & Mesolella, K.J. 1968, Milankovich hypothesis supported by precise dating of coral reefs and deep-sea sediments, Science, 159, 297-300.

BROOK, D. & Crabtree, H.C. 1969, Explorations Journal of U.L.S.A. University of Leeds, England, (amateur caving publication).

BUCHA, V. 1970, Influence of the Earth's magnetic field on radiocarbon dating. in Radiocarbon Variations and Absolute Chronology, 12 th Nobel Symp. Wiley Intersci. p 501.

BUCHA, V., Taylor, R.E., Berger, R. & Haury, E.W. 1970, Geomagnetic intensity; changes during the past 3000 years in the Western hemisphere, Science, 168, 111-114.

BULLARD, E.C., Freedman, C., Gellman, H. & Nixon, J. 1950 The westward drift of the Earth's magnetic field. Phil. Trans. Roy. Soc. Lond. A243, 67-92.

CANADIAN CAVERs, 1976, 8(2) & 1977, 9(1). Amateur caving publications of McMaster University, Hamilton, Ontario, L8S4M1.

CARMICHAEL, C.M. 1967, An outline of the intensity of the paleomagnetic field of the Earth. Earth Plan. Sci.Lett. 3, 351-354.

CASTO, C.C. 1950, Electrolytic separation methods, ch 23 of Analytical Chemistry of the Manhattan Project. NNES. Div. VIII, v 1. McGraw-Hill.

CHAPMAN, S & Bartels, J. 1962, Geomagnetism, Oxford U.P. Vol I & II, 3 rd,edn.

CHERDYNTSEV, V.V., Kozachevsky, I.V. & Kuz'mina, E.A. 1965, Dating of Pleistocene carbonate formations by the thorium and uranium isotopes. Geochim. Int. 2, 794-801.

CHETHAM-STRODE, A., Tarrant, J.R. & Silva, R.J. 1961, The application of silicon detectors to alpha particle spectroscopy. I.R.E. Trans. Nuc. Sci. 18, 59-63.

CLARK, H.C. & Kennett, J.P. 1973, Paleomagnetic excursion recorded in latest Pleistocene deep-sea sediments. Gulf of Mexico, Earth Plan. Sci. Lett. 19, 267-274.

COLLINSON, D.W. 1966, Carrier of remanent magnetization in certain red sandstones, Nature, 210, 516-517.

COLLINSON, D.W. 1975, Instruments and techniques in paleomagnetism and rock magnetism, Rev. Geophys. Sp. Phys. 13, 659-686.

CONDOMINES, M. 1978, Datation de la coulée à aimantation inverse d'Olby (Chaîne des Puys) par le déséquilibre radioactif $^{230}Th - ^{238}U$. Comptes R. Géol.Soc. Fr. 5, 254-257.

COUPLAND, D.H. & Van der Voo, R. 1980, Long term non-dipole components in the geomagnetic field during the last 130 MY, J. Geophys. Res. 85, 3529-3548.

COX, A. 1968, Lengths of geomagnetic polarity intervals, J. Geophys. Res. 73, 3247-3260.

COX, A. 1970, Latitude dependence of the angular dispersion of the geomagnetic field, Geophys. J. Roy. Astr. Soc. 20, 253-269.

COX, A. 1975, The frequency of geomagnetic reversals and the symmetry of the non-dipole field. Rev. Geophys. Sp. Phys. 13, 35-51.

COX, A., Hillhouse, J. & Fuller, M.D. 1975, Paleomagnetic records of polarity transitions, excursions and secular variation, Rev. Geophys. Sp. Phys. 13, 185-189.

CREER, K.M. 1974, Geomagnetic variations for the interval 7000 - 25,000 yr BP, as recorded in a core of sediment from station 1474 of the Black Sea cruise of Atlantis II, Earth Plan, Sci, Lett. 23, 34-42.

CREER, K.M. 1977, Geomagnetic secular variations during the last 25,000 years; an interpretation of data obtained from rapidly deposited sediment. Geophys. J.Roy Astr. Soc, 48, 91-109.

CREER, K.M. & Ispir, Y. 1970, An interpretation of the behaviour of the geomagnetic field during polarity transitions. Phys. Earth Plan. Int. 2, 283-293.

CREER, K.M., Thompson, R., Molyneux, L. & Mackereth, F.J.H. 1972, Geomagnetic secular variation recorded in the stable magnetic remanence of recent sediments. Earth Plan. Sci. Lett. 14, 115-127.

CREER, K.M., Georgi, D.T. & Lowrie, W. 1973, On the representation of the Quaternary and Late Tertiary geomagnetic fields in terms of dipoles and quadrupoles, Geophys. J. Roy. Astr. Soc. 33, 323-345.

CREER, K.M. & Kopper, J.S. 1974, Paleomagnetic dating of cave paintings in Tito Bustillo cave, Asturias, Spain. Science, 186, 348-350.

CREER, K.M. Anderson, T.W. & Lewis, C.F.M. 1976a, Late Quaternary geomagnetic stratigraphy recorded in lake Erie sediments, Earth Plan. Sci. Lett. 31, 37-47.

CREER, K.M., Gross, D.L. & Lineback, J.A. 1976b, Origin of regional magnetic variations recorded by Wisconsinan and Holocene sediments from Lake Michigan, USA and Lake Windermere, England, Geol, Soc. Amer. Bull. 87, 531-540.

CREER, K.M. & Kopper, J.S. 1976, Secular oscillations of the geomagnetic field recorded by sediments deposited in caves in the Mediterranean region. Geophys. J. Roy. Astr. Soc. 45, 35-58.

CREER, K.M., Readman, P.W. & Jacobs, A.M. 1980a, Palaeomagnetic and palaeontological dating of a section at Gioia Tauro, Italy; identification of the Blake event. Earth Plan. Sci. Lett. 50, 289-300.

CREER, K.M., Hogg, T.E., Readman, P.W. & Reynaud, C, 1980b Palaeomagnetic secular variation curves extending back to 13,400 yr BP recorded by sediments deposited in Lac de Joux, Switzerland. J. Geophys, 48, 139-147.

DAGLEY,P. & Lawley, E. 1974, Palaeomagnetic evidence for the transitional behaviour of the geomagnetic field. Geophys. J. Roy. Astr. Soc. 36, 577-598.

DANKERS, P.H.M. 1978, Magnetic properties of dispersed natural iron oxides of known grain-size. Unpubd. PhD Thesis, University of Utrecht.

DAY, R. 1977, TRM and its variation with grain size, Adv. Earth Plan. Sci. 1, 1-33.

DENHAM,C.R. 1974, Counter clockwise motion of paleomagnetic directions 24 ,000 yrs, ago at Mono Lake, California. J. Geomag. Geoelec. 26, 487-498.

DENHAM, C.R. 1976, Blake polarity episode in two cores from the Greater Antilles outer ridge, Earth Plan. Sci. Lett. 29, 422-434.

DENHAM, C.R. & Cox, A. 1974, Evidence that the Lascnamp polarity event did not occur 13,300 - 30,400 years ago. Earth Plan.Sci.Lett. 13, 181-190.

DENHAM, C.R. Anderson, R.F. & Bacon, M.P. 1977, Paleomagnetism and radiochemical age estimates for Late Brunhes polarity episodes. Earth Plan. Sci. Lett. 35, 384-397.

DICKSON, J.A.D. 1978, Length-slow and length-fast calcite: a tale of two elongations, Geology, 6, 560-561.

DOBRIN, M. 1952, Introduction to Geophysical Prospecting, New York.

DOELL, R.R. and Cox, A, 1971, Pacific geomagnetic secular variation, Science, 171, 248-254.

DODSON, R.E.,Fuller, M.D. & Kean, W.F. 1977, Paleomagnetic records of secular variation from Lake Michigan sediment cores, Earth Plan. Sci. Lett. 34, 387-395.

DUNLOP, D.J. 1973a, Theory of the magnetic viscosity of lunar and terrestrial rocks. Rev. Geophys. Sp. Phys. 11, 855-901.

DUNLOP, D.J. 1973b, Thermoremanent magnetization in sub-microscopic magnetite. J. Geophys. Res. 78, 7602-7613.

DUNLOP, D.J. &.West, G.F. 1969, An experimental evaluation of single domain theories. Rev. Geophys. Sp. Phys. 7, 709-757.

DUNLOP, D.J., Hanes, J.A. & Buchan, K.L. 1973, Indices of multidomain magnetic behaviour in basic igneous rocks: Alternating field demagnetization, hysteresis, and oxide petrology, J. Geophys. Res. 78, 1387-1393.

DUNLOP, D.J. & Stirling, J.M. 1977, 'Hard' viscous remanent magnetization(VRM) in fine-grained hematite. Geophys. Res. Lett. 4, 163-166.

DYMOND, J. 1969, Age determination of deep sea sediments: a comparison of three metnods, Earth Plan. Sci. Lett. 6, 9-14.

EDMUNDS, W.M. 1973, Trace element variations across an oxidation-reduction barrier in a limestone aquifer, in Proc. of Symp. on Hydro-geochem. and Bio-geochem. Tokyo.

ELLWOOD, B.B. 1971, An archeomagnetic measurement of the age and sedimentation rate of Climax Cave sediments, south west Georgia, Amer. J. Sci. 271, 301-310.

ERICSON, D.B. Ewing, M., Wollin, G. & Heezen, B.C. 1961, Atlantic deep-sea sedimentary cores, Geol. Soc. Amer. Bull. 72, 193-286.

EVANS, M.E. 1977, Single domain oxide particles as a source of thermoremanent magnetization. Adv. Earth Plan. Sci. 1, 35-43.

FISH, J.E. 1977, Karst hydrogeology and geomorphology of the Sierra de el Abra and the Valles - San Luis Potosi region, Mexico. Unpubd. PhD Thesis, McMaster University. Ontario, Canada, L8S4M1.

FISHER, R.A. 1953, Dispersion on a sphere. Proc. Roy. Soc. Lond. A217, 295-305.

FOLK, R.L. & Assereto R. 1976, Comparitive fabrics of length-slow and length-fast calcite and calcitized aragonite in a Holocene speleothem, Carlsbad Caverns, New Mexico. J. Sed. Pet. 46, 486-496.

FORD, D.C., Schwarcz, H.P., Drake, J.J., Gascoyne, M., Harmon, R.S. & Latham, A.G. 1981, Estimates of the age of the existing relief with the Southern Rocky mountains of Canada. Arctic and Alpine Res. 13, 1-10.

FORD, T.D. & Cullingford, C.H.D. 1976, The Science of Speleology, Academic Press.

FREED, W.K. & Healy, N. 1974, Excursions of the Pleistocene geomagnetic field recorded in Gulf of Mexico sediments. Earth Plan. Sci. Lett. 24, 99-104.

GASCOYNE, M. 1977, Trace element geochemistry of speleothems, Proc. 7 th. Int. Spel. Congr. Sheffield. England. 205-208.

GASCOYNE, M. 1979, Pleistocene climates determined from stable isotope and geochronologic studies of speleothem. Unpubl. PhD Thesis, McMaster, Univ. Hamilton, Ontario, L8S4M1.

GASCOYNE, M. Benjamin, G.J., Schwarcz, H.P. & Ford, D.C. 1979, Sea level lowering during the Illinoian glaciation: Evidence from a Bahama Blue Hole. Science, 205, 806-808.

GILLOT, P.Y., Labeyrie, J., Laj, C., Valladas, G., Guerin, G., Poupeau, G. & Delibrias, G. 1979, Age of the Lascnamp paleomagnetic excursion revisited. Earth Plan. Sci. Lett. 42, 444-450.

GOREE, W.S. & Fuller, M. 1976, Magnetometers using RF-driven squids , and their applications in rock magnetism and paleomagnetism. Rev. Geophys. Sp. Phys. 14, 591-608.

GOVAERT, A,, Dauwe, C., Plinke, P., De Grave, E. & De Sitter, J. 1976, A classification of goethite minerals based on the Mössbauer behaviour. J. de Phys. 37, supp. 12, C6, 825-827.

GRIFFITHS, D.H., King, R.F. & Wright, A.E. 1958, An assessment of the difficulties involved in using Quaternary varved sediments for palaeomagnetic studies of the secular variation. Ann. de Géophys. 14, 515-518.

GRIFFITHS, D.H., King, R.F., Rees, A.I. & Wright, A.E. 1960, The remanent magnetism of some recent varved sediments. Proc. Roy. Soc. A256, 359-383.

GUNN, N.M. &.Murray, A.S. 1980, Geomagnetic field magnitude variations in Peru derived from archaeological ceramics dated by thermoluminescence. Geophys. J. Roy. Astr. Soc. 62, 345-366.

HALL, C.M. & York D. 1978, K-Ar and $^{40}Ar/^{39}Ar$ age of the Lascnamp geomagnetic polarity reversal. Nature, 274, 462-464.

HAMMOND, S.R., Seyb, S.M. & Theyer, F. 1979, Geomagnetic polarity transitions in two oriented sediment cores from the north west Pacific. Earth Plan. Sci. Lett. 44, 167-175.

HARMON, R.S. 1975, Late Pleistocene paleoclimates in north America as inferred from isotopic variations in speleothems. Unpubd. PhD Thesis, McMaster Univ. Hamilton, Ontario, L8S4M1.

HARMON, R.S., Ford, D.C. & Schwarcz, H.P. 1977, Interglacial chronology of the Rocky and Mackenzie mountains, base upon $^{230}Th - ^{234}U$ dating of calcite speleothems. Can. J. Earth Sci. 14, 2543-2552.

HARMON, R.S. Thompson, P. Schwarcz, H.P.& Ford, D.C. 1978, Late Pleistocene paleoclimates of North America as inferred from stable isotope studies of speleothems. Quat.Res. 9, 54-70.

HARRISON, C.G.A. 1974, The paleomagnetic record from deep-sea sediment cores. Earth Sci. Rev. 10, 1-36.

HARRISON, C.G.A. 1980, Secular variation and excursions of the Earth's magnetic field. J. Geophys. Res. 85, 3511-3522.

HARRISON, C.G.A. & Watkins, N.D. 1979, Comparison of the offset dipole and zonal non-dipole geomagnetic field models using Icelandic paleomagnetic data. J, Geophys. Res. 84, 627-635.

HAYS, J.D. 1971, Faunal extinctions and reversals of the Earth's magnetic field. Geol. Soc. Amer. Bull. 82, 2433-2447.

HELLER, F. 1980, Self reversal of natural remanent magnetization in the Olby - Laschamp lavas, Nature, 284, 334-335.

HENDY, C.H. 1970, The use of C14 in the study of cave processes., in Radiocarbon Variations and Absolute Chronology. Ed. I.U.Olsson. 12 th. Nobel Symp. 419-443.

HOLLAND, H.D. Holland, H,J, & Munoz, J.L. 1964, The coprecipitation of cations with $CaCO_3$. II The coprecipitation of Sr^{2+} with calcite between 90 ^{o} and 100 ^{o} C. Geochim. Cosmochim. Acta. 28, 1287-1301.

Iron; Ch 26 of Handbook of Geochemistry, 1970, Springer-Verlag.

IRVING, E. 1964, Paleomagnetism,and its application to geological and geophysical problems. Wiley.

IRVING, E & Major, A. 1964, Post depositional detrital remanent magnetization in a synthetic sediment. Sedimentology, 3, 135-143.

IRVING, E & Ward, M.A. 1964, A statistical model of the geomagnetic field. Pure Appl. Geophys. 57. 25-30.

I.U.G.S. International Subcommission on Stratigraphic Classification, 1979, Magnetostratigraphic polarity units - A supplementary chapter of the I.S.S.C. international atratigraphic guide. Geology, 7, 578-583.

JACKSON, K.S., Jonasson, I.R. & Skippen, G.B. 1978, The nature of metals - sediment - water interactions in fresh water bodies, with emphasis on the role of organic matter. Earth Sci. Rev. 14, 97-146.

JAEP, W.F. 1971, Role of interactions in magnetic tapes. J. Appl. Phys. 42, 2790-2794.

JACOBS, J.A. 1963, The Earth's core and geomagnetism, Pergamon.

JEFFREYS, H. & Jeffreys, B.S. 1978, Methods of Mathematical Physics, 3 rd. Edn. Cambridge U.P.

JOHNSON, E.A., Murphy, T. & Torreson, O.W. 1948, Prehistory of the Earth's magnetic field. J. Terr. Mag. Atmos. Elec. 53, 349-372.

JOHNSON, H.P. & Merrill, R.T. 1973, Low temperature oxidation of a titanomagnetite and the implications for paleomagnetism. J. Geophys. Res. 78, 4938-4949.

JOHNSON, H.P., Lowrie, W. & Kent, D.V. 1975, Stability of anhysteretic remanent magnetization in fine and coarse magnetite and maghemite particles. Geophys. J. Roy. Astr. Soc. 41, 1-10.

JOHNSON, J.A. 1979, Investigation of Mg and Sr distribution in speleothem. BSc Thesis, Geology Dept. McMaster, Univ. Hamilton, Ontario, Canada, L8S4M1.

KAUFMAN A. 1964, Th^{230}/U^{234} dating of carbonates from Lakes Lahontan and Bonneville. PhD dissertation, Columbia Univ.

KAUFMAN, A. & Broecker, W.S. 1965, Comparison of Th^{230} and C^{14} ages for carbonate materials from Lakes Lahontan and Bonneville. J. Geophys. Res. 70, 4039-4054.

KAWAI, N. 1972, The magnetic control on the climate in geological time. Proc. Japan Acad. 48, 687-689.

KAWAI, N., Yaskawa, K., Nakajima, T., Torii, M. & Horie, S. 1972, Oscillating geomagnetic field with a recurring reversal discovered from Lake Biwa, Proc. Jap. Acad. 48, 186-190.

KEEN, M.J. 1963, The magnetization of sediment cores from the eastern basin of the North Atlantic Ocean. Deep-sea Res. 10, 607-622.

KENDALL, A.C. & Broughton, P.L. 1978, Origin of fabrics in speleothems composed of columnar calcite crystals. J. Sed. Pet. 48, 519-538.

KENT, D.V. 1973, Post depositional remanent magnetization in deep-sea sediment. Nature, 246, 32-34.

KENT, D.V. & Opdyke, N.D. 1977, Paleomagnetic field intensity variation recorded in a Brunhes epoch deep-sea sediment core. Nature, 266, 156-159.

KIM, S.M., Noakes, J.E. & Miller, W.W. 1966, Electrodeposition method for counting alpha and beta emitters, Nucleonics 24, 66-67.

KOBAYASHI, K. 1962, Magnetization blocking process by volume development of ferromagnetic fine particles. J. Phys. Soc. Japan, 17, suppl. B1, 695

KOBAYASHI, K., Kitazawa, K. Kanaya, T. & Sakai, T. 1971, Magnetic and micropaleontological study of deep-sea sediments from the west central equatorial Pacific. Deep-sea Res. 18, 1045-1062.

KOMURA, K. & Sakanoue, M. 1964, Studies on the dating methods for Quaternary samples by natural alpha-radioactive nuclides. Sci. Rep. Kanazawa Univ. 12(1) p21.

KU, T-L. 1976, The uranium - series methods of age determination. Ann. Rev. Earth Sci. Lett. 4, 347-379.

KU, T-L., Broecker, W.S. & Opdyke, N.D. 1968, Comparison of sedimentation rates measured by paleomagnetic and ionium methods of age determination. Earth Plan. Sci. Lett. 4, 1-16.

KU, T-L., Bull, W.B., Freeman, S.T. & Knauss, K.G. 1979, ^{230}Th - ^{234}U dating of pedogenic carbonates in gravelly desert soils of Vidal Valley, southeastern California. Geol.Soc. Amer. Bull. 90, 1063-1073.

KUKLA, G. & Nakagawa, H. 1977, Late Cenozoic magnetostratigraphy. Quat. Res. 7, 283-293.

KURTÉN, B. & Poulianos, A.N. 1977, New stratigraphic and faunal material from Petralona, with special reference to the carnivora. Anthropos, 4, 47-130.

LANGMUIR, D. 1978, Uranium solution - mineral equilibria at low temperatures with applications to sedimentary ore deposits. Geochim. Cosmochim. Acta, 42, 547-569.

LARSON, E.E., Watson, D. & Jennings, W. 1971, Regional comparison of a Miocene geomagnetic transition of Oregon and Nevada, Earth Plan. Sci. Lett. 11, 391-400.

LATHAM, A.G., Schwarcz, H.P., Ford, D.C. & Pearce, G.W. 1979, Palaeomagnetism of stalagmite deposits, Nature, 280, 383-385.

LAVERTY, M. & Crabtree, S. 1978, Rancéite and mirabilite: some preliminary results on cave mineralogy. Trans. Brit. Cave Res. Assoc. 5, 135-142.

LE BORGNE, E. 1955, Susceptibilité magnétique anormale du sol superficiel. Ann. de Géophys. 11, 399-419.

LEVI, S. & Banerjee, S.K. 1976, On the possibility of obtaining relative paleointensities from lake sediments. Earth Plan. Sci. Lett. 29, 219-226.

LEVI, S. & Merrill, R.T. 1976, A comparison of ARM and TRM in magnetite. Earth Plan.Sci. Lett. 32, 171-184.

LIDDICOAT, J.C., Coe, R.S., Lambert, P.W., & Valastro, S. Jr. 1979, Paleomagnetic record in late Pleistocene and Holocene dry lake deposits at Tlapacoya, Mexico. Geophys. J. Roy. Astr. Soc. 59, 367-377.

LIDDICOAT, J.C. & Coe, R.S. 1979. Mono Lake geomagnetic excursion. J. Geophys. Res. 84, 261-271.

LINGENFELTER, R.E. & Ramaty, R. 1970, Astrophysical and geophysical variations in C14 production. Radiocarbon Variations and Absolute Chronology. 12 th. Nobel Symp. Wiley, 513

LØVLIE, R. 1974, Post depositional remanent magnetization in a re-deposited deep-sea sediment. Earth Plan. Sci. Lett. 21, 315-320.

LØVLIE, R. 1976, The intensity pattern of post-depositional remanence acquired in some marine sediments during a reversal of the external magnetic field. Earth Plan. Sci. Lett. 30, 209-214.

LOWRIE, W. & Fuller, M. 1971, Onthe alternating field demagnetization characteristics of multi-domain thermoremanent magnetization in magnetite. J. Geophys. Res. 76, 6339-6349.

LUND, S.P. & Banerjee, S.K. 1979, Paleosecular variations from lake sediments. Rev. Geophys. Sp. Phys. 17, 244-249.

MACKERETH, F.J.H. 1971, On the variation in direction of the horizontal component of remanent magnetization in lake sediments. Earth Plan. Sci. Lett. 12, 332-338.

MANGINI, A. & Sontag, C. 1977, ^{231}Pa dating of deep-sea cores via ^{227}Th counting. Earth Plan. Sci. Lett. 37, 251-256.

MARINO, R.J. & Ellwood, B.B. 1978, Anomalous magnetic fabric in sediments which record an apparent geomagnetic field excursion, Nature, 274, 581-582.

MCELHINNY, M.W. 1973, Palaeomagnetism and Plate Tectonics. Cambridge U. P.

MCELHINNY, M.W. & Evans, M.E. 1968, An investigation of the strength of the geomagnetic field in the early Precambrian. Phys. Earth Plan. Int. 1, 485-497.

MCELHINNY, M.W. & Merrill, R.T. 1975, Geomagnetic secular variation over the past 5 my. Rev. Geophys. Sp. Phys. 13, 687-708.

MERRILL, R.T. &.McElhinny, M.W. 1977, Anomalies in the time-averaged paleomagnetic field and their implications for the lower mantle. Rev. Geophys. Sp. Phys. 15, 309-323.

MÖRNER, N-A. 1977, The Gothenburg magnetic excursion. Quat. Res. 7, 413-427.

MÖRNER, N-A.. Lanser, J.P. & Hospers, J. 1971, Late Weichselian paleomagnetic reversal. Nature Phys. Sci. 234, 173-174.

MÖRNER, N-A. & Lanser, J. 1975, Paleomagnetism in deep-sea core A179-15, Earth Plan. Sci. Lett. 26, 121-124.

NAGATA, T. 1961, Rock Magnetism. Maruzen, Japan.

NAGATA, T. 1965, Main characteristics of recent geomagnetic secular variation. J. Geomag. Geoelec. 17, 263-276.

NAKAJIMA, T., Yaskawa, K., Natsuhara, N., Kawai, N. & Horie, S. 1973, Very short period geomagnetic excursion 18,000 yr BP. Nature Phys. Sci. 244, 8-10.

NOEL, M. & Tarling, D.H. 1975, The Laschamp geomagnetic 'event'. Nature, 253, 705-706.

NOEL, M. reply, & Thompson, R. & Berglund, B. further discussion 1977, The late Weichselian geomagnetic event. Nature, 267, 181-182.

NOLTIMIER, H.C. & Colinvaux, P.A. 1976, Geomagnetic excursion from Imuruk Lake, Alaska, Nature, 259, 197-200.

OPDYKE, N.D. 1972, Paleomagnetism of deep-sea cores. Rev. Geophys. Sp. Phys. 10, 213-249.

OPDYKE, N.D., Ninkovich, D. Lowrie, W. & Hays, J.D. 1972, The paleomagnetism of two Aegean deep-sea cores. Earth Plan. Sci. Lett. 14, 145-159.

OPDYKE, N.D. 1976, Discussion of paper by Mörner and Lanser concerning the paleomagnetism of deep-sea core A179-15. Earth Plan. Sci. Lett. 29, 238-239, and Mörner, N-A. reply 240-241.

OSMOND, J.K. 1979, Accumulation models of ^{230}Th and ^{231}Pa in deep-sea sediments. Earth Sci. Rev. 15, 95-150.

PALMER, D.F., Henyey, T.L. & Dodson, R.E. 1979, Paleomagnetism and sedimentological studies at Lake Tahoe, California - Nevada, Earth Plan. Sci. Lett. 46, 125-137.

PEIRCE, J.W. & Clark, M.J. 1978, Evidence from Iceland on geomagnetic reversal during the Wisconsinan ice age. Nature, 273, 456-458.

PENG, T-H. Goddard, J.G. & Broecker, W.S. 1978. A direct comparison of ^{14}C and ^{230}Th ages at Searles lake, California. Quat. Res. 9, 319-329.

POULIANOS, A.N. 1978, Stratigraphy and age of the Petralonian Archanthropus; Correction to English text. Anthropos, 5, 264-266.

PUCHER, R. 1969, Relative stability of chemical and thermal remanence in synthetic ferrites. Earth Plan. Sci. Lett. 6, 107-111.

RUMBLE, D, Ed, 1976, Oxide Minerals, short course notes, vol 3, Min.Soc. Amer.

RUNCORN, S.K. 1959, On the theory of the geomagnetic secular variation, Ann. Geophys. 15, 87-92.

SCHWARCZ, H.P., Harmon, R.S., Thompson, P. & Ford, D.C. 1976, Stable isotope studies of fluid inclusions in speleothems and their paleoclimatic significance. Geochim. Cosmochim. Acta. 40. 657-665.

SCHWARCZ, H.P., Liritzis, Y. & Dixon, A. 1980, Absolute dating of travertines from Petralona cave Khalkidiki peninsular, Greece. Anthropos, 7, 152-173.

SCHWARCZ, H.P. 1980, Absolute age determination of archeological sites by uranium-series dating of travertines, Archaeometry, 22, 3-24.

SEBESSY, L. & Bakan, J. 1978, Electrolytic precipitation of natural uranium on stainless steel cathode. J. Radioan. Chem. 47, 83-91.

SHAW, J. 1974, A new method of determining the magnitude of the palaeomagnetic field. Application to five historic lavas and five archaeological samples. Geophys. J. Roy. Astr. Soc. 39, 133-141.

SILL, C.W. and Olson, D.G. 1970, Sources and prevention of recoil contamination of solid state alpha detectors, Analyt. Chem. 42, 1596-1607.

SKILES, D.D. 1970, A method of inferring the direction of drift of the geomagnetic field from paleomagnetic data. J. Geomagn. Geoelec. 22, 441-462.

SKOOG, D.A. & West, D.M. 1971, Principles of Instrumental Analysis. Holt, Rinehart and Winston.

SMITH, J.D. & Foster, J.H. 1969, Geomagnetic reversal in Brunhes normal polarity epoch. Science, 163, 565-567.

SMITH, P.J. 1967, The intensity of the ancient geomagnetic field; a review and analysis. Geophys. J. Roy. Astr. Soc. 12, 321-362.

SOLOYANIS S.C. & Brown, L.L. 1979, Late Pleistocene magnetic stratigraphy recorded in some New England tills. Geophys. Res. Lett. 6, 265-268.

SPALDING, F. & Mathews T.D. 1972, Stalagmites in caves in the Bahamas; indications of low sea level stand. Quat Res. 2, 470-472.

SPRENKEL-SEGEL, E.L. 1970, Recoilless Resonance spectroscopy of meteoritic iron oxides. Geophys. Res. 75, 6618-6630.

STACEY, F.D. & Banerjee, S.K. 1974, The Physical Principles of Rock Magnetism. Elsevier.

STOBER, J.C. & Thompson, R. 1977, Palaeomagnetic secular variation studies of Finnish lake sediments and the carriers of remanence. Earth Plan. Sci. Lett. 37, 139-149.

STRANGWAY, D.W., Honea, R.M., McMahon, B.E. & Larson, E.E. 1968, The magnetic properties of naturally occurring goethite. Geophys. J. Roy. Astr. Soc. 15, 345-359.

STRINGER, C.B. 1974, A multivariate study of the Petralona skull, J. Human Evoln. 3, 397-404.

STUPAVSKY ,M., Gravenor, C.P. & Symons, D.T.A. 1979, Paleomagnetic stratigraphy of the Meadowcliffe till, Scarborough Bluffs, Ontario; a late Pleistocene excursion ? Geophys. Res. Lett. 6, 269-272.

SUGUIRA, N. 1979, ARM, TRM and magnetic interactions; concentration dependence, Earth Plan. Sci. Lett. 42, 451-455.

SUKROO, J.C., Christoffel, D.A., Vella, P. & Topping, W.W.1978, Rejecting evidence of Gothenburg geomagnetic reversal in New Zealand. Nature, 271, 650.

TAIRA, A. & Lienert, B.R. 1979, The comparitive reliability of magnetic, photometric and microscopic methods of determining the orientations of sedimentary grains. J. Sed. Pet. 49, 759-772.

TALVITIE, A.N. 1972, Electrodeposition of actinides for alpha-spectrometric determination. Anal. Chem. 44, 280-283.

TARLING, D.H. 1971, Principles and Applications of Palaeomagnetism. Chapman and Hall.

THEIS, T.L. & Singer, P.C. 1974, The stabilization of ferrous iron by organic compounds in natural waters, in Trace Metal - Organic Interactions in Natural Waters, Ed. P.C. Singer, Ann Arbor.

THELLIER, E. 1977, Early research on the intensity of the ancient geomagnetic field. Phys. Earth Plan. Int. 13, 241-244.

THOMPSON, P. 1973, Speleochronology and Late Pleistocene climates, Unpubd, PhD Thesis, McMaster Univ. Hamilton, Ontario, L8S4M1.

THOMPSON, P., Schwarcz, H.P. & Ford, D.C. 1974, Continental Pleistocene climatic variations from speleothem age and isotopic data, Science, 184, 893-895.

THOMPSON, R. 1975, Long period European geomagnetic secular variation confirmed. Geophys. J. Roy. Astr. Soc. 43, 847-859.

THOMPSON, R. & Berglund, B. 1976, Late Weichselian geomagnetic 'reversal' as a possible example of the reinforcement syndrome, Nature, 1976, 490-491.

THOMPSON, R. & Turner, G.M. 1979, British geomagnetic master curve 10,000 - 0 yr BP for dating European sediments, Geophys, Res. Lett. 6, 249-252.

TURNER, G.M. & Thompson, R. 1979, Behaviour of the Earth's magnetic field as recorded in the sediment of Loch Lomond. Earth Plan. Sci. Lett. 42, 412-426.

TURNER, P. 1979, Depositional magnetization of Carboniferous limestones from the Craven basin of northern England. Sedimentology, 22, 563-581.

TURNER, P. 1979, The paleomagnetic evolution of continental red beds, Geol. Mag. 114, 289-301.

VEROSUB, K.L. 1975, Paleomagnetic excursions as magnetostratigraphic horizons; a cautionary note. Science, 190, 48-50.

VEROSUB, K.L. 1977a, The absence of the Mono Lake geomagnetic excursion from the paleomagnetic record of Clear Lake, California, Earth Plan, Sci. Lett. 36, 219-230.

VEROSUB, K.L. 1977b, Depositional and post depositional processes in the magnetization of sediments. Rev. Geophys. Sp. Phys. 15, 129-143.

VEROSUB, K.L. 1979a, Paloemagnetism of varved sediments from western New England; variability of the paleomagnetic recorder. Geophys. Res. Lett. 6, 241-244.

VEROSUB, K.L. 1979b, Paleomagnetism of varved sediments from western New England; secular variation. Geophys. Res. Lett. 6, 245-248.

VEROSUB, K.L. & Cox, A. 1971, Changes in the total magnetic energy external to the Earth's core. J. Geomag. Geoelec. 23, 235-242.

VEROSUB, K.L. & Banerjee, S.K. 1977, Geomagnetic excursions and their paleomagnetic record. Rev. Geophys. Sp. Phys. 15, 145-155.

VEROSUB, K.L., Ensley, R.A. & Ulrick, J.S. 1979. The role of water content in the magnetization of sediments. Geophys. Res. Lett. 6, 226-228.

VESTINE, E.H., Laporte, L., Lange, I. & Scott, W.E. 1947, The geomagnetic field, its description and analysis. Washington: Carnegie Inst. Pubn. No 580.

VITORELLO, I. & Van der Voo, R. 1977, Magnetic stratigraphy of Lake Michigan sediments obtained from cores of lacustrine clay. Quat. Res. 7, 398-412.

VLASOV, A.Ya., Kovalenko, G.V. & Chichachev, V.A. 1967a. The superparamagnetism of αFeOOH. Izv. Earth Phys. 7, 64-69.

VLASOV, A. Ya., Kovalenko, G.V. & Chichachev, V.A. 1967b, Temperature induced phase and magnetic transitions of iron hydroxide. Izv. Earth Phys. 10, 63-70.

WATKINS, N.D. 1968, Short period geomagnetic polarity events in deep-sea sedimentary cores. Earth Plan. Sci. Lett. 4, 341-349.

WATKINS, N.D. 1972, Review of the development of the geomagnetic polarity time scale and discussion of prospects for its finer definition. Geol. Soc. Amer. Bull. 83, 551-574.

WATKINS, N.D. & Goodell, H.G. 1967, Confirmation of the reality of the Gilsa geomagnetic polarity event, Earth Plan. Sci. Lett. 2, 123-129.

WEAST, R.C. Ed. 1978, Handbook of Chemistry and Physics. 58 th. Edn.

WEBER, H.P. & Hafner, S.S. 1971, Vacancy distribution in nonstoichiometric magnetites. Zeit. für Kristall. 133. 341-363.

WILSON, R.L. 1972, Palaeomagnetic differences between normal and reversed field sources, and the problem of far-sided and right-handed pole positions. Geophys. J. Roy. Astr. Soc. 28, 295-304.

WILSON, R.L. Dagley, P. & McCormack, A.G. 1972. Palaeomagnetic evidence about the source of the geomagnetic field. Geophys. J. Roy. Astr. Soc. 28, 213-224.

WILSON, R.L. & Lomax, R. 1972, Magnetic remanence related to slow rotation of ferromagnetic material in alternating magnetic field. Geophys. J. Roy. Astr. Soc. 30, 295-303.

The World - Total Magnetic Intensity, epoch 1975, and Annual Rates of Change, pubd. 1976, sheet, 5382.
The World - Magnetic Variation, epoch 1975, and Annual Rates of Change, pubd. 1977, sheet 5375.
The World - Magnetic Dip, for epoch 1974, and Annual Rates of Change, pubd. 1976, sheet 5383. by the Hydrographer to the Navy, pubd. at Taunton, England.

YASKAWA , K., Nakajima, T. Kawai, N., Torii, M. Natsuhara, N. & Horie, S. 1973, Palaeomagnetism of a core from Lake Biwa (1). J. Geomag. Geoelec. 25, 447-474.

YUKUTAKE, T. & Tachinaka, H. 1969, Separation of the Earth's magnetic field into the drifting and the standing parts. Bull. Earthquake Res. Inst. Tokyo, Univ. 47, 65-97.

ZIJDERVELD, J.D.A. 1967, AC demagnetization of rocks; Analysis of results, in Methods in Palaeomagnetism, Eds. Collinson, Creer and Runcorn. Elsevier, 254-286.

APPENDIX Ia

Separation techniques for U and Th by the TTA evaporation method, and notes to the method.

APPENDIX Ib

An example of the computer printout.

APPENDIX Ia

Separation Techniques for U and Th by the TTA Evaporation Method

1) Place weigned specimen in a 1 L beaker, label, and cover with deionised water (DD H_2O). Add conc. HNO_3 to dissolve, and cover beaker with watch glass. Note date.

2) After dissolution add 3-5 mls of $FeCl_3$ with Pasteur pipette and add 1 ml (or as appropriate) of spike using an Eppendorf pipette with disposable tip.

3) Filter into 500 ml beaker using Whatman 50 (acid hardened) paper. Rinse litre beaker with 3 M HCl. Wash paper with 3 M HCl.

4) Transfer 500 ml beaker to tripod, lower in magnetic bar, and boil for 1-2 minutes.

5) Transfer beaker to magnetic stirrer and turn on motor. Using the same filter funnel slowly add ammonia until red-brown precipitate becomes permanent. Add a few drops of ammonia.

6) Remove beaker from stand and remove bar. Rinse bar and the retriever magnet into the beaker with DD H_2O. Allow beaker and contents to cool with watch glass as cover.

7) Decant precipitate-free supernate to waste. Label 2 x 1" (2.5 cm) diameter polytnene centrifuge tubes and pour in supernate with precipitate. Centrifuge to obtain a compacted precipitate. Decant supernate to waste and add more from the beaker. Continue until all the precipitate has been compacted and include the water wash from the beaker.

Notes to the steps

1) and 2) The mass of calcite dissolved and the volume of spike added depends on the U conc. Otherwise 20 to 40 gms and 1 ml of new spike.

4) Boiling drives off CO_2 which might otherwise form a soluble complex with U.
Longer boiling times may result in a light coloured gel-like precipitate at step 5) and is thought to be the cause of some U loss. The reason may be due to an unflocculated colloidal suspension of $Fe(OH)_3$ (M. Gascoyne, pers com) Otherwise this is a convenient place to oxidise suspected natural organics. Treat with aqua regia, boil to near dryness redissolve in HNO_3 and water, and reprecipitate as for step 5).

5) U and Th are coprecipitated on $Fe(OH)_3$ .Ca and Ra remain in the supernate. Precipitate colour should be deep red-brown. Appearance of supernate should be light amber to colourless. Deeper brown colour may be due to organics. If iron is suspected in supernate, collect in clean vessel, evaporate to near dryness, add HNO_3 + DD H_2O, heat and reprecipitate. Add precipitates.

8) After decanting the last of the supernate to waste, squirt a jet of DD H_2O to wash the precipitate. Decant the water and repeat the step at least once.

9) Transfer the two polythene tubes with wet precipitate to a stand under a heat lamp. Dry precipitates until they begin to crack.

10) Add 9 N HCl to 1/3 fill the tubes. Add an equal volume of isopropyl ether and squish with a Pasteur pipette for more than one minute to remove iron colour. Allow ether layer to separate from aqueous layer. Use a second pipette to remove ether layer and eject it into waste bottle.Add a few mls of conc. HCl to restore molarity and repeat above extraction twice. Transfer aqueous layer and washings to a cleaned labelled 250 ml Vycor beaker.

11) If iron colour has persisted either (a) boil to dryness in the beaker and take up in 9 N HCl and repeat ether extraction, or, (b) go on to the next step and remove iron later at step 16).

12) Place beaker on heater and gently evaporate off ether and leave it to cool. Replace watch glass cover.

13) Place and tamp glass wool plug at the bottom of the anion exchange column. Squirt in a few mls of 9 N HCl. Transfer enough resin to fill the column so that there are no air bubbles in the column (a cleaned glass rod may be used for puddling the resin). Allow the 0.1 N HCl of the resin to drain into a waste beaker. Wash the reservoir and condition the column with 50 mls of 9 N HCl and allow to drain to waste.

9) Very dry precipitates may take some time to dissolve in 9 N HCl, but the concentration at the extraction is likely to be nearer 9 N.

10) and 11) The Fe scavenger is separated into the isopropyl ether in 9 N HCl. A few drops of conc. HCl are added to offset the excess water. Good iron extractions are needed to prevent thick U deposits in the final step.
Ether appears to be partly miscible in the (strong) acid; it thus has the effect of holding back the iron. Gentle heating will separate out this ether layer which may then be drawn off. Thus more of the iron may be extracted into new ether from a heated aqueous layer.

13) and 14) The anion column is 1/2 cm bore by 20 cms with tap and 100 ml reservoir.
The anion resin is AG1 - X8 (chloride form), analytical grade stored in 0.1 N HCl.
At this stage the U stays in the resin but Th passes through in the 9 N HCl.

14) Replace waste beaker with a 250 ml Vycor beaker and label with the name and "Th"; cover with watch glass so as to allow in column wash containing thorium. Pour the sample from step 12) into reservoir and rinse beaker at least twice with 9 N HCl. Note the date. After the sample has passed through wash the reservoir and column with 4 x 20 mls of 9 N HCl, allowing each aliquot to drain through separately.

URANIUM

15) Replace the 250 ml beaker containing the thorium, with a 50 ml Vycor beaker and watch glass cover. Label it and add "U". Elute anion column with 2 x 20 ml of 0.1 N HCl.

16) Evaporate eluate to dryness. If iron colour is present take up in 10 - 20 mls of 9 N HCl and extract iron with isopropyl ether as for step 10). Repeat if necessary. Gently evaporate off ether and evaporate dry.

17) Evaporate deposit down in a beaker wash of 20 mls of 0.1 N HNO_3 and store with watch glass cover ready for plate out.

URANIUM PLATE-OUT

18) Wash beaker with a few ml's of 0.1 N HNO_3 (pH 1) and warm gently to dissolve the deposit. Transfer the solution to a glass centrifuge tube using a Pasteur pipette, #1. Repeat the washing and dissolution until the tube is 1/4 to 1/3 full.

19) With pipette #2 add, volume-for-volume, TTA in benzene and squish for at least 2 minutes with pipette #1, to extract any thorium. Centrifuge and eject TTA to waste using pipette #1.

15) The U and Fe are eluted with 0.1 N HCl.

16) The iron colour is seen in the deposit on the bottom of the beaker. If ether derived organics (eg, polymers) are present in the next evaporation they show up mainly as a black (carbonised) deposit. A small amount may be tolerated in the TTA extraction. A larger amount may cause U loss; it must be oxidised before the next step using aqua regia.

17) and 18) It is an advantage to keep some liquid in the bottom of the beaker before plate-out since later dissolution of hardened deposits may be difficult.

19) The recipe is 25 gms of TTA in 500 mls of benzene. The pH 1 step also discriminates against Pa contamination.

20) With pipette #3 add dil. NH_4OH dropwise. Mix using pipette #1 until pH paper indicates 3.5 .

21) Add 3 pipettes of TTA and squish with pipette #1 to extract U for about 1 min. and centrifuge.

22) With pipette #4 transfer TTA layer and U into a 10 ml beaker and begin to gently evaporate off the organic layer on an electric heater.

23) Repeat step 21) twice, transferring organic layer to the same beaker to be evaporated down to less than 1/4 ml.

24) Using pipette #4 dropwise transfer organic layer to heated disc to form concentric rings. Twice rinse beaker with TTA and evaporate almost to dryness and each time transfer washings to the disc as before.

25) With TTA now evaporated flame the disc strongly and allow to cool. After attaching a label to the reverse side the disc is ready to count.

THORIUM

26) Place and tamp a glass wool plug in the bottom of the cation column and fill the column with cation resin. Allow the 0.1 N HCl to drain through and wash the reservoir and condition the resin with one 20 ml wash of 3 N HCl.

27) Mark the level of the 9 N HCl wash, which contains the thorium, on the side of the beaker and add twice this volume of DD H_2O to make a 3 N HCl solution. Pour this into the cation column reservoir and allow to drain through. Wash reservoir with 4 x 20 mls of 3 N HCl.

20) The appearance of the red iron colouring also indicates that the correct pH has been reached.

22) Care is needed not to include any of the aqueous layer in the 10 ml beaker, firstly because it may hold contaminants, but chiefly because it causes violent spitting upon evaporation.

24) The stand for the discs is an aluminum tube which creates a temperature gradient hotter on the outside than the centre, thus causing the drops to evaporate near the centre. The disc may be moved about on this stand to distribute the deposit.

25) Strong flaming volatilises Po (in particular ^{210}Po is undesirable). Too strong a flaming may cause oxidation of the surface and degrade the resolution of the spectrum.

26) The resin is AG 50 - X8 (hydrogen form), analytical grade, stored in 0.1 N HCl.
The column is 1/2 cm bore by 20 cms, with a tap and a 250 ml reservoir.

28) Elute the thorium with 2 x 20 mls of 0.75 M oxalic acid.

29) The oxalic acid may be oxidised in either of two ways:

a) add an equal volume of conc. HNO_3 and 3 volumes of conc. HCl in the beaker and heat strongly using the watch glass to reflux the acids. Repeat if oxalic acid crystals begin to appear as the acids evaporate.

b) add three Pasteur pipettes of $HClO_4$ and about 50 mls of HNO_3 and replace the watch glass to reflux the acids. Set heater to 200°C, then before liquids uncover the bottom of the beaker reduce temperature to about 130°C. Remove watch glass and add more HNO_3 to assist in the dispersal of the dense $HClO_4$ fumes.

30) Wash the watch glass, beaker rim and insides copiously with 0.1 N HNO_3 and evaporate to dryness (or near dryness). The beaker with watch glass cover may be stored ready for plate out.

THORIUM PLATE-OUT

31) Dissolve the deposit by adding a few mls of 0.1 N HNO_3 and warming gently. Transfer this to a centrifuge tube with Pasteur pipette #1. Continue to transfer beaker wash to the tube until it is about 1/4 to 1/3 full./

32) With pipette #2 add 3 fills of TTA in benzene giving volume-for-volume amounts of aqueous and organic layers. Squish for at least 2 minutes. Note time at end of squishing to the nearest minute.

33) Centrifuge and with pipette #1 transfer the upper organic layer to a 10 ml beaker. The TTA is then evaporated gently to near dryness while two more TTA extractions are made and added to it.

34) As for the uranium step 24).

35) The thorium disc does not have to be heated as strongly as the U desc. Allow to cool and attach label to reverse side. Count as soon as possible.

29) Oxalic acid is oxidised in order to free Th for the TTA extraction step. Oxalic acid sublimes at 150°C and may take thorium or thorium oxalate with it if sublimation is too rapid. This step has been known to be the principal source of Th loss. Therefore the aqua regia must cover the bottom of the beaker at all times during the oxidation-reflux process. This step may take about 1 day or more.
The usual precautions and conditions apply to the use of $HClO_4$.
A small quantity of $HClO_4$ can be tolerated with the 0.1 N HNO_3 in the TTA extraction so long as the pH remains between 1 and 1.2 .

31) and 32) The optimum pH is reckoned to lie between 1 and 1.2, but it may be that the partition factor is less than 80% with the prepared solution; therefore the extraction for thorium , by squishing, takes longer than it does for uranium. U is discriminated against at this step.

Appendix 1b ; Example of Computer Printout.

SAMPLE NO. = SJLS85Q DATE RUN 27OCT/80

SAMPLE WT. = 24.6 G

BLANK DISC COUNT TIME ON U COUNTER = 2614. MIN

BLANK DISC COUNT TIME ON TH COUNTER = 2614. MIN

DELAY IN COUNTING THORIUM = 16. DAYS

DELAY BETWEEN COUNTING AND PLATING THORIUM = 32. MIN

SPIKE USED = 1.00 ML

ACTIVITY OF 1 ML 232 SPIKE ON U COUNTER = 5.90 CPM

ACTIVITY OF 1 ML 232 SPIKE ON TH COUNTER = 5.90 CPM

238-U OF EQUIVALENT ACTIVITY TO SPIKE = 22.7 MICROGRAMS

RAW DATA

U COUNT TIME = 3042. MIN TH COUNT TIME = 4187. MIN

U-238 =	.800	CPM	TH-232 =	.012	CPM
U-234 =	1.210	CPM	TH-230 =	.054	CPM
U-232 =	2.959	CPM	TH-228 =	2.690	CPM

****

BACKGROUND

U-238 =	.001	CPM	TH-232 =	.001	CPM
U-234 =	.002	CPM	TH-230 =	.002	CPM
U-232 =	.002	CPM	TH-228 =	.002	CPM

****

CORRECTED DATA

		ERROR			ERROR
U-238 =	.791	.017 CPM	TH-232 =	.011	.003 CPM
U-234 =	1.183	.029 CPM	TH-230 =	.052	.004 CPM
U-232 =	2.957	.031 CPM	TH-228 =	2.685	.025 CPM

****

URANIUM CONCENTRATION	= .25	P.P.M.
THORIUM-232 CONCENTRATION	= .01	P.P.M.
CHEMICAL YIELD OF URANIUM	= 50.12	PERCENT
CHEMICAL YIELD OF THORIUM	= 44.30	PERCENT
SPIKE RATIO	= 1.027	

****

		ERROR
U-234/U-238 =	1.496	.048
(U-234/U-238)0 =	1.501	.050
TH-230/U-234 =	.050	.004
TH-230/TH-232 =	4.727	1.3

THORIUM AGE = 3800. + 900. - 900. YEARS

AGE CALCULATED USING THORIUM CORRECTION

CORRECTED AT INITIAL THORIUM RATIO, R = 1.50000

UNCORRECTED = 5500. + 500. - 500. YEARS

APPENDIX II

Test Specimens for Paleomagnetism

Notes

* Samples taken from the McMaster collection of P. Thompson (1973),(P.T.) or of R.S.Harmon (1975),(P.S.H.)

\$ English samples collected by M.Gascoyne (1979),(M.G.), and dates by him.

1) The intensity of 2.10^{-7} G is the quoted sensitivity of the SCT magnetometer. The usual noise level was about this value.

2) Specimens of mass 15 gms and of moment 2.10^{-7} G must await a more sensitive SQUID magnetometer ! Specimens of mass 15 gms and of moment $2\text{-}10.10^{-7}$ G may be stacked for NRM measurement.

S = stalagmite, F = flowstone

Sample	Origin	Description	Oriented	Mass (gms)	Intensity x 10^{-7} G	Comments
Plaster of Paris,Fisher Sci. Can. High gde.			no	~10	easily measurable !	
Epoxy glue Lepages			yes	0.5	easily measurable and faithful to the ambient field !	
Canadian Speleothems						
BJDL	Bear Jaw cave	brown and white F	yes	35	2-5	>350 Ka (this study)
BJML	Bear Jaw cave	mostly white F	yes	30-50	<2	"
IPUG	Gargantua	brown/green S translucent	yes	100 ?	<2	(P.T.)
PMB, PMUM, PMTL	Plateau Mountain Ice cave	mostly white F or brown F translucent F	yes	42.5, 55.6, 95.1	≤2	probably >350 Ka (P.T.)
Middle Sentry *		brown/amber F translucent	no	86	10-50	102-197 Ka (P.T.)
Coulthard *		brown translucent F	no	19	10-20	235-296 Ka (P.T.)
Boon's Glittering Ice Palace *		brown translucent F	no	55	≤2	
Middle caves *		dark brown transl. and opaque F	no	104	>50	>350 Ka (P.S.H.)
76A4	Grotte Valerie	green/brown transl.F	yes	115	<2	>350 Ka (P.T.) (P.S.H.)
Grotte Louise *		brown opaque F	no	30	2-6	
73051	Igloo cave *	dark brown transl.F.	no	25	≤2	>350 Ka (P.S.H.)

English Speleothems

GYS1	Lancaster Hole	white S	yes	30	≤2	MPM measurement abandoned
GYS2	Lancaster Hole	brown and white translucent S	yes	30	2-10	MPM measurement temporarily abandoned ; low signal.
CF	Lancaster Hole	white F	yes	40	2-6	Colonades area; 114-109 Ka (this study)
KWP	Lancaster Hole	white F	yes	30	≈2	corresponds approx with 76135 of M.G. 85-86 Ka.
76131*	Lancaster Hole	white S	yes	96	5-10	9 Ka (M.G.)
AGS	Aygill cave	brown transl.S	probably not in situ	20	2-10	sat on loose seds. MPMs showed S not in original orientation.
76209*	Gaping Gill	mostly white S	yes	39	≈2	base is 0.8 Ka (M.G.)
76163*	Lost John's system	amber brown S	yes	52	2-6	
Victoria cave		brown F	no	43	2-4	150 to>350 Ka (M.G.)
71178	G.B. cave (Mendip)	'coconut meat' white F	approx.	50	<2	collected P.Smart reported age >350 Ka.

Bermudan Speleothems

AC2S	Admiral's cave	white, amber transl. S	yes	31	5-10	
GO2S	Gov't Quarry cave.	red opaque amber transl. S	yes	12.7	>50	
GO1S	Gov't Quarry cave.	amber transl. S	yes	25	2-4	

Mexican Speleothems

RSM	Roadside cave,Chiapas.	pure transl. S	yes	53	4-6	91 Ka (this study)

U.S.A. Samples

76503*	Tumbling Creek cave, Missouri	amber transl. milky white S	no	41	≈2	140-25 Ka (Harmon et al 1979)
Coldwater cave,Iowa*		opaque gray S	no	30	>100	48 Ka (P.S.H.)
R77-14	Warm Springs Creek,Wyoming	pale brown, opaque hot spring travertines	no	65	>100	290 Ka (H.P.Schwarcz,p.com.)
R77-17				86	>100	95 Ka collected by
R77-18				119	>100	undated G.M.Richmond

APPENDIX III

NOTES ON THIN SECTIONS OF THE SPELEOTHEMS

Introduction

Thin sections were prepared having known orientation to each speleothem and its growth layers. This short study was undertaken to look at the fabric of speleothems, to look into the nature and effects of detritus on the fabric and to examine the size and type of any opaque grains present. The appearance of the hand specimens is described in chapters 4, 5 and 6. Some of these characteristics are repeated here when they are especially pertinent to the thin section.

Columnar or palisade calcite crystals are common in speleothems and are stacked approximately normal to the growth surfaces (Kendall and Broughton, 1978). This may readily be seen in stalagmites sliced down the middle and acid polished to bring out reflections from different face orientations (plate III.1). Stacked crystals near the centre have their long axes vertical. As they approach the side they appear to curve in 'jumps', ie. they give way to new, generally shorter, crystals having a more favourable orientation to the growth surface. The fast growth axis is usually the axis of symmetry of the crystal. Evidently a c-axis orientation that is at a more acute angle to the growth surface does not compete as well. This length-fast direction to the growth surface (calcite is uniaxially negative) is referred to by Folk and Assereto (1976), Kendall and Broughton and others as the 'normal' situation.

Plate III.1

Crystal growth habit of a stalagmite.

An example of discontinuous curvature of palisade crystals in relation (normal) to the growth layering of a stalagmite.

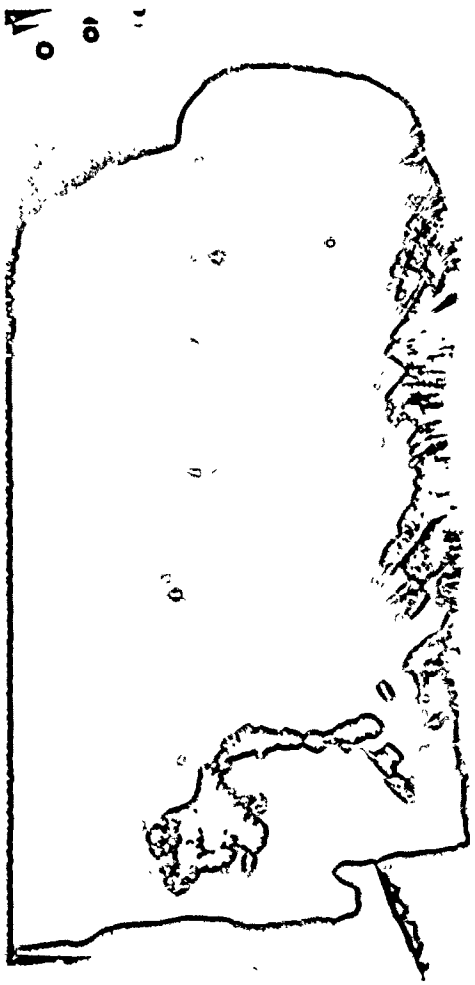

Length-slow calcite is abnormal. This point was contended recently by Dickson (1978) who argued that the shape of anhedral crystals is dependent only on the orientation of the greatest growth vector and is independent of the optic axis orientation. All but one of the speleothems examined here were of the length-fast type.

Aragonite may be recognised by its small 2V angle, perhaps by acicular or columnar growth habit or when in euhedral tabular form, by 6-sided basal sections. The flowstones BJTL and ENF showed long fans of crystals with a fairly moderate 2V. However this is thought due to a brush form of calcite rather than to aragonite. Aragonite is not common in speleothems (Holland et al, 1964; Folk and Assereto, op cit; M.Gascoyne, pers.com.; the latter used X-ray crystallography). Its presence in these speleothems was not ruled out.

Gascoyne (1977) argued for the presence of organic materials in speleothems (fulvic and humic acids) to account for much of their colour). In the thin sections examined here hazy, hard-to-focus, fibrous material, often in the form of mats, occurred along growth planes and frequently caused the nucleation of microcrystalline calcite. The optically continuous crystals of amber translucent sample WCS1 showed a fine mottling which may be due to organic acids. Many speleothems, though translucent, show a variety of colours which are thought to be due to organic materials rather than to trace elements (see section 7.4.2.2). Perhaps the best method of detecting organic materials in speleothems is to use IR spectra to compare functional groups of known organic acids with those from speleothems (D. Brook, pers. com.)

Kendall and Broughton (op cit) and Beck (1978) showed that the outer milky white appearance of stalagmites, especially of the 'fried egg' type is due to smaller crystals, to infillings and to a greater density of fluid inclusions. This finding is also confirmed in this study as a general case. Fluid inclusions of the 'thorn' type were common both within and between crystals. Smaller fluid inclusions were often arranged in bands along growth layers.

Growth layers were commonly marked by detrital material in the form of :

1) unidentified fine aggregated 'muck' material,
2) quartz, feldspar and opaque grains, and
3) fluid inclusions partly filled with foreign material.

The magnetization of some speleothems must possess some contribution from opaque grains that are detrital. From the thin sections the evidence is two-fold:

1) Opaque grains were associated with other detrital material, as discussed above,
2) some of these grains showed 'exsolution' and oxidation features typical of titanomagnetites of igneous provenance. These grains could not have formed in situ.

Many of these opaque grains showed pits, bays or reentrant cavities as though due to solutional attack (etching). The question arises as to whether any of this etching occurred just prior to cementation of the growth surface, or whether they were chemically inert to the feed water. The question arises in consideration of the possibility of forming a secondary CRM from a primary DRM (see section 7.4.3). It has not so far been possible to answer this question.

Plate III.2

Flowstone BJTL

In transmitted light; the section shows growth layering as 'tree rings', and brush extinction in fans.

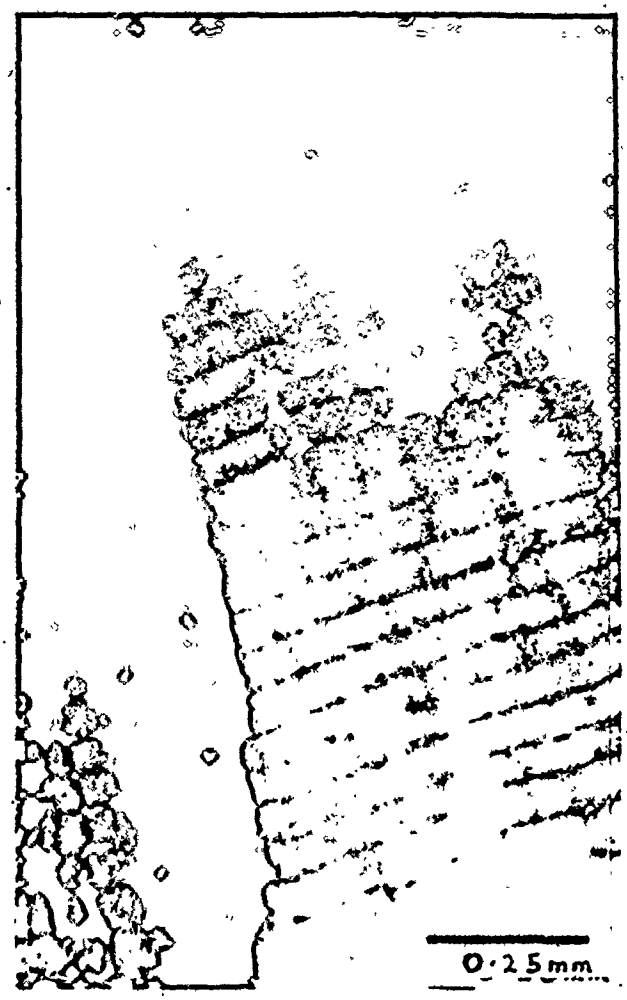

Thin Section Details

BJTL The section covers cuts 4 to 2.

Much of the thin section texture is marked by fine brush crystals arranged in sets of fans. There are many fine parallel growth layers like tree-rings which Vee at the intersection of the fans. In and above each layer are a few microcrystals which have failed to interrupt the vertical continuity of the fans.

Continuing up the section, the brushes become gradually broken up following an increase in impurities which tend to clump together. The fine brushes end at a prominent layer of fine (fibrous?) material. The microcrystals compete for space with larger equant crystals whose optic axes are oriented perpendicular to the section. These are succeeded by new sets of brush crystals which again become broken up by detrital material along the growth layers, and which in turn has nucleated microcrystals. The microcrystals and detrital material correspond to the opaque brown layering seen in hand specimen.

The 'tree-ring' horizons become more coherent across the section. Some optical continuity is achieved where the fine detritus is less concentrated -eg. in the middle sections of the brush fans. At the top of the section the horizon thickness is about twice what it was at the bottom. The number of horizons is estimated to be from 50 to 100 per cm. It is possible that such remarkable regularity in these rings is annual . Unfortunately it was not possible to resolve this question from the U/Th isotope data.

There were no opaque minerals visible in either transmitted or reflected light.

Plate III.3

Flowstone ENF.

Palisade crystals are observable by their vertical continuity. Arranged horizontally across the section are 'sagging' mats of organic matter.

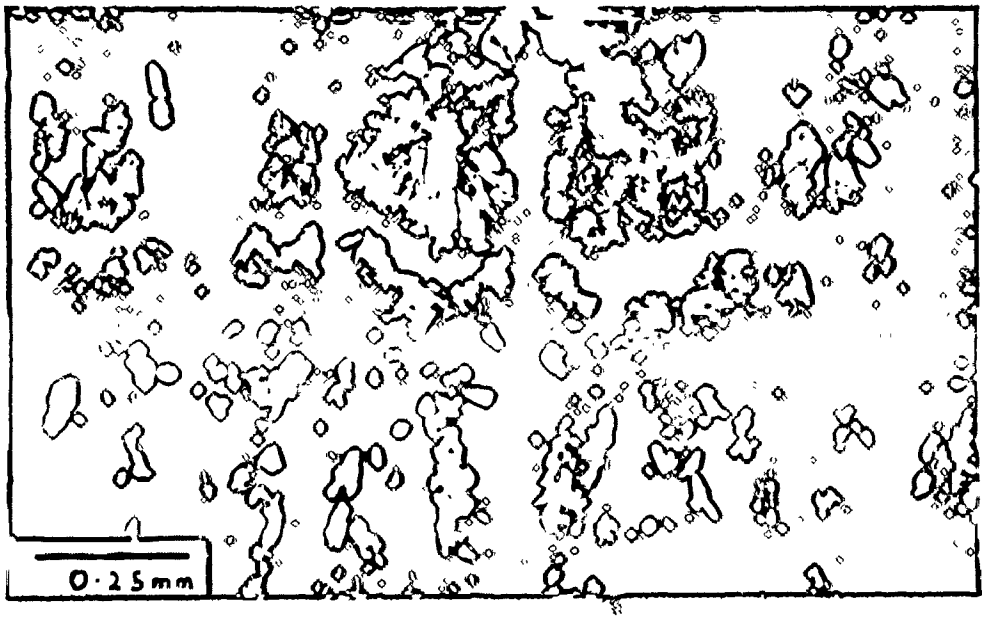

ENF The thin section covers cuts 6 to 4.

The section is characterized throughout by long palisade crystals whose boundaries are marked by sub-vertical curved edges or by multiple interlocking microcrystals giving a fir-tree appearance. Some tabular crystals show interference effects part of which is probably due to reflections from boundaries oblique to the section; but broader interference bands may be due to strain.

Undulating coarse brush extinction is common and appears to mimic a biaxial figure. The length-fast direction is perpendicular to the substrate growth horizons.

Growth norizons are marked by fine and coarse impurities which terminate the long crystals and nucleate microcrystals. The impurities are occasionally dense and appear fibrous. It is common for small horizontal mats (blobs) of impurities to occur inside an optically continuous columnar crystal. Fluid inclusions are not common.

Opaque minerals were not detected and there was no other detrital mineral present such as quartz.

A second thin section, taken from a piece of ENF heated to 700 °C, showed a marked increase in these impurities.

VCCL The section covers the top and lateral parts of growth horizons and is taken from near the base

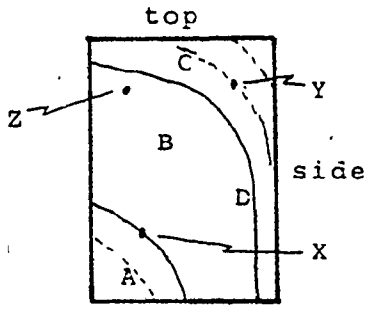

In area A the columnar crystals have grown perpendicular to the growth horizons. They are anhedral and interlocking and, apart from coarse brush extinction, are optically continuous. Between the columnar crystals, but less common are anhedral equant crystals which appear to show strain and oriented with their c-axes approximately normal to the section.

Fluid inclusions along growth layers are common and are thorn-shaped pointing outwards. They occur inside crystals and along boundaries.

Growth layers are marked by heterogeneous unidentified mats, microcrystalline calcite, quartz, opaque grains and by red-brown colouring.

Area B is marked by more equant interlocking crystals whose fast directions are only approximately perpendicular to the growth horizons. There is little detrital material to mark the growth horizons. Instead there are thin milky layers of very small fluid inclusions.

Area C is the cap area of the stalagmite. Growth layers are distinct and are marked by foreign material including several opaque grains up to 0.1 mm, and angular quartz grains. Calcite grains are equant , anhedral and interlocking. Their fast direction is perpendicular to the growth horizon.

Plates III.4 & III.5

Opaque grains of stalagmite VCCL;
in reflected light.

Plate III.4; grain Y in air.

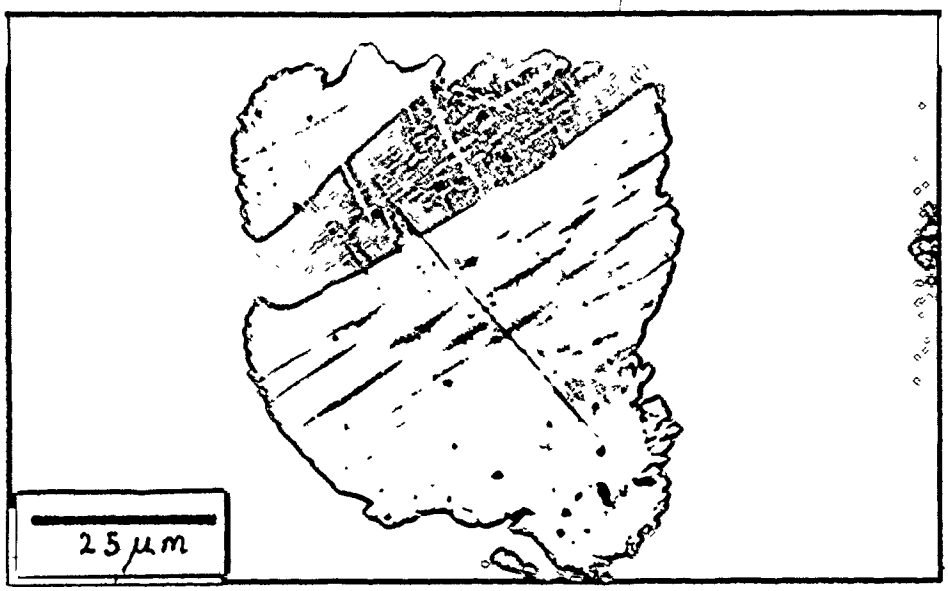

Plate III.5; grain Z in oil.

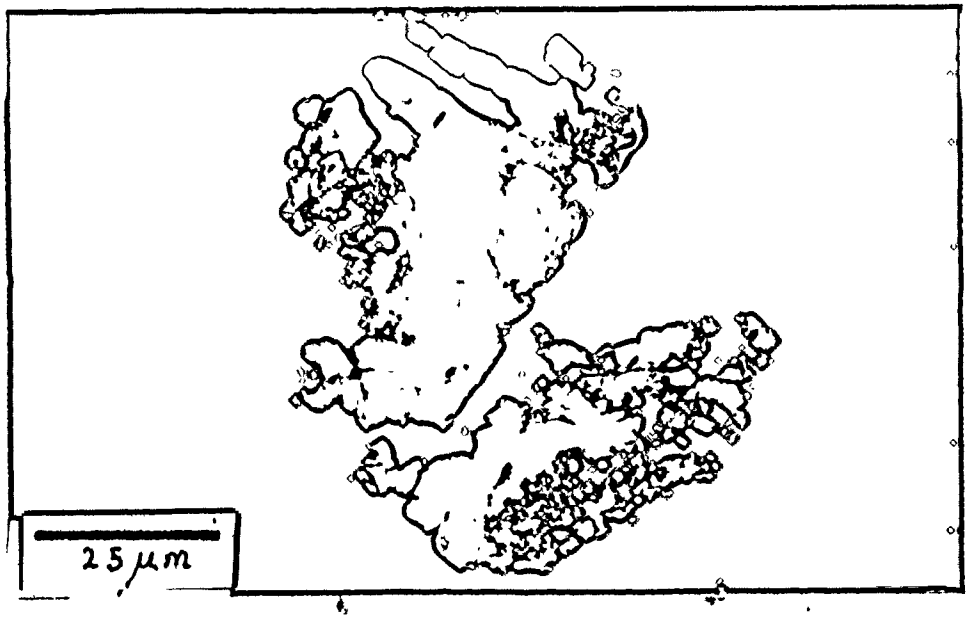

The area D is similar to C except that the growth layers are, of course, much closer.

The Opaque Grains

Opaque grains are abundant along the horizons of areas A, C and B. They are commonly rounded, subrounded, or subangular with indistinct edges as though due to etching. Etching may also have produced pits, bays, and reentrant cavities. The subangular grains reveal former cubic or hexagonal shapes.

A few grains show the textures of 'exsolved' titanomagnetites.* The grain at X is about 0.1 mm. long having two sides of a hexagon. In reflected light, and in air, one side of the grain appears white and shiny. The bulk of the grain is a duller gray colour with small vermicular 'intergrowths' of the whiter phase. It appears to be a composite ilmenite-titanomagnetite grain.

Grain Y (plate III.4) has a cubic shape, subrounded and with etch pits. It is chiefly a composite of (in air) a brown-gray phase and a light gray phase in which the latter contains lenses of the former, and vice versa. It is possible that another light gray phase is present in one corner. The grain may be partially oxidised ilmenite.

*Haggerty (in Rumble, 1976, ch4) distinguishes between composite ilmenite-titanomagnetite grains and true oxidised (exsolved) trellis titanomagnetites. In the former the ilmenite formed first and the titanomagnetite formed epitaxially or from ilmenite nuclei. In the second the ilmenite lamellae 'oxyexsolved' from the titanomagnetite host.

Plate III.6

Stalagmite TS.

In transmitted light; the growth layering slants from lower left to upper right. Quartz and opaque grains are visible.

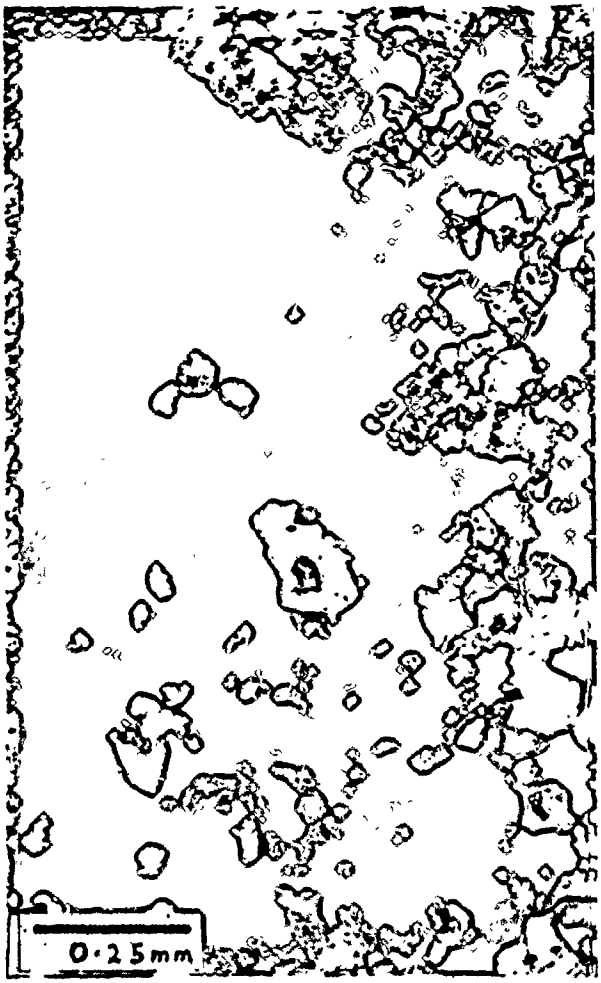

Grain Z (plate III.5) has a hexagonal, subrounded shape. Fine cracks give it a partly clastic appearance. Three phases appear to be present but with little intergrowth. The overall shape suggests it is a titanomagnetite grain, perhaps with considerable alteration.

TS The section covers cuts 18 and 17, from near the base.

Area A consists of large (≈1 cm long) columnar anhedral interlocking crystals which are length-fast perpendicular to the growth horizons.

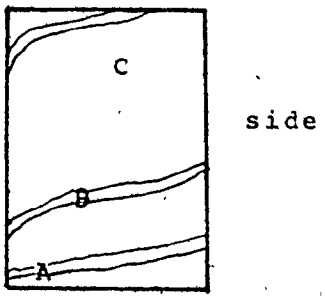

Growth surfaces are marked by multiple banding of sets of small fluid inclusions having the appearance of tree rings. Fluid inclusions are both large, ≈0.1 mm and small and are rounded and thorn shaped. Some of the fluid inclusion bands are accompanied by dirt material often following the rhombic crystal growth surfaces, and give a saw-tooth appearance.

Area B is a dark 0.5 cm thick band rich in quartz grains. They range in size up to ≈0.1 mm and are mostly angular and subangular. Other grains include tabular euhedral subangular feldspar grains some of which are twinned, and other transparent grains of about the same size.

Plate III.7

Flowstone RCB

Shown here is the effect of the dense reddish muck layer ; viz. the termination of the underlying crystals, the creation of drusy cavities and the nucleation of micro-crystals. Transmitted light and crossed Nichols.

Fine amorphous (?) dirt material is also present in area B and may be organic material.

Opaque grains are abundant and range in size up to about 0.1 mm. Some are in part a translucent red colour to transmitted light, and a few appear to be composite with quartz. Their shapes varied from angular to rounded and many showed pits and etch-like features. It is possible that opaque grains are of more than one type but each grain appeared to be of only one composition.

The upper part of the thin section (area C) is characterized by large almost equant calcite crystals. Some of these show glide-twinning which may be either part of the original fabric or an artefact of section preparation. The fast direction is perpendicular to the growth horizons except for the more equant grains whose optic axes are perpendicular to the section. Growth horizons are marked by fine dirt material and by bands of fluid inclusions.

RCB The section was cut to cross the red bands of cut 8 up to the white milky bands of cut 6.

Palisade calcite occurs below cut 9. The columnar crystals are 8 mm long but less than 1 mm wide and show undulating coarse brush extinction parallel to their length. Smaller included crystals show interference colours which may be due to strain. Holes and fluid inclusions occur mostly along the grain boundaries.

Proceeding upwards, growth of the columnar crystals is partly interrupted by a 1 mm thick reddish layer of fine muck material with microcrystals.

The crystals are finally terminated by a dense, almost opaque layer of muck which has created some large drusy cavities between it and the crystals beneath. The crystal terminations give an irregular saw tooth effect. Microcrystals have then nucleated out in aggregates normal to the undulating substrate. The crystals become larger and those that grew in tne direction of the overall average normal competed most successfully for space. Interference colours are common and appear to indicate original strain effects.

Cut 8 is characterized by a series of red layers wnich are about 2-4 mm thick. The red colouring gives a zoning effect which marks out the triangular growth surfaces.

The last of the prominent red growth horizons (there are five) is followed by an increase in large fluid inclusions of the thorn type within and between crystals. The crystals become larger, up to 2 mm across , and more than 1 cm long.

Towards the top of the section the fluid inclusions are very abundant indeed and together with unidentified very fine material accounts for the milky white appearance of these layers. The inclusions account for between 5 and 10% of the surface area. A few large cavities occur near the top. In hand specimen these are identified as remnant microgours.

The red colouring is generally very fine but some of it is particulate. No quartz, opaque or other non-calcite grains were detected.

Plate III.8

Stalagmite SJLS

In reflected light; opaque grain X, in oil.

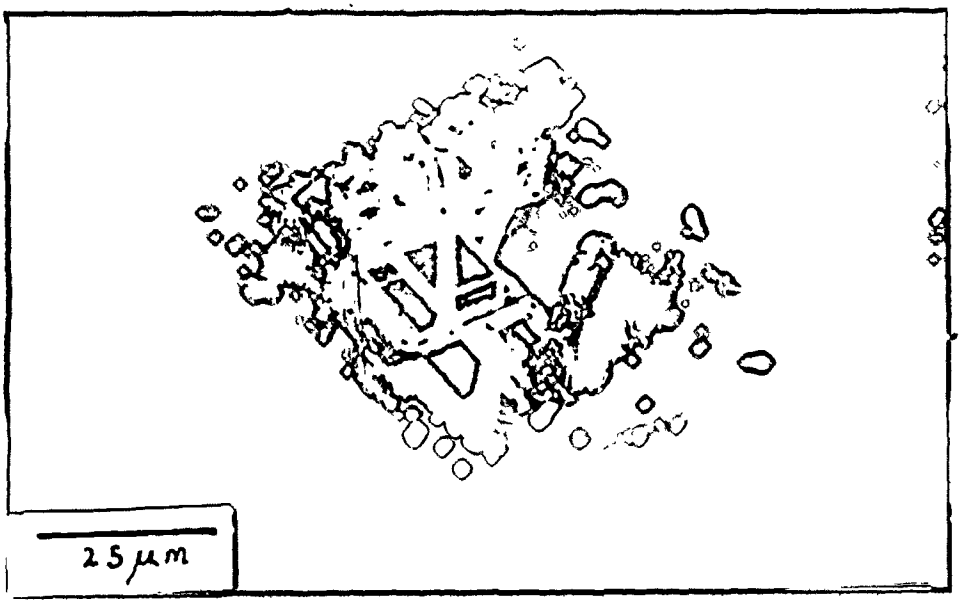

WCS1 This section was taken from near the base.

The hand specimen exhibits a homogeneous texture with amber translucent colouring but no discernible growth bands.

The section shows a homogeneous texture of large equant or tabular anhedral interlocking grains. A few of the crystals show twin-gliding which may be an artefact of the preparation of the section. It is possible that the whole stalagmite was recrystallised.

All the crystals show a fine uniform mottling which is probably associated with the amber colour. It was not possable to say what the mottling is due to.

Growth surfaces cannot be identified. There are a few large ($\approx$1 mm long) fluid inclusions, but detrital material, quartz and opaque grains are absent.

SJLS The section was taken from near the base.

The base region is marked by clear columnar anhedral crystals having a coarse brush extinction. The boundaries are wavy or curved and contain large holes or fluid inclusions. As one scans towards the sides of the stalagmite succeeding crystals change orientation in jumps so as to intersect the lateral growth layers at angles at or just less than 90°.

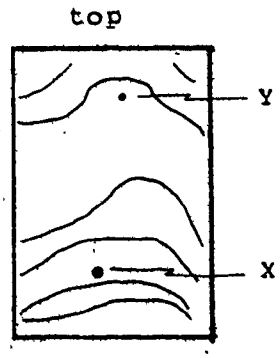

The clear zone ends with the onset of growth horizons marked by fine muck, quartz, opaque grains and by lines of fine thorn-shaped fluid inclusions. Drusy cavities are not uncommon. The quartz grains are few and are angular to subangular. Some appear cemented to one another.

The calcite texture described above together with the marked growth layers is more or less repeated throughout the rest of the section.

The Opaque Grains

A few large (≈1 mm) tabular grains appear deep red. They are rounded and in reflected light give a shiny mottled appearance. The mottling or etching occurs in striations or lines in some cases. A few have been altered from square or hexagonal shapes. One grain is a transparent deep amber colour and appears glassy.

More easily recognisable opaque grains occur along growth horizons with muck and are very common. Their sizes may vary up to 1 mm. They are mostly rounded, subrounded and subangular. Tabular and hexagonal shapes are occasionally seen.

Grain X (plate III.8) is a good example of an oxidised titanomagnetite. The overall shape is a subangular rhomb showing etch-like pits and reentrant cavities. The polished surface shows the lighter coloured broad ilmenite lamellae. The titanomagnetite host contains abundant darker coloured spinel rods. A second grain Y shows hexagonal section and some interior etch effects have taken place along preferred planes.

Plate III.9

Stalagmite SJHS

In transmitted light; the inner core is to the right, and the black layers of the dirt rind are in the centre and left. Cleavage planes are prominent in the crystals at right.

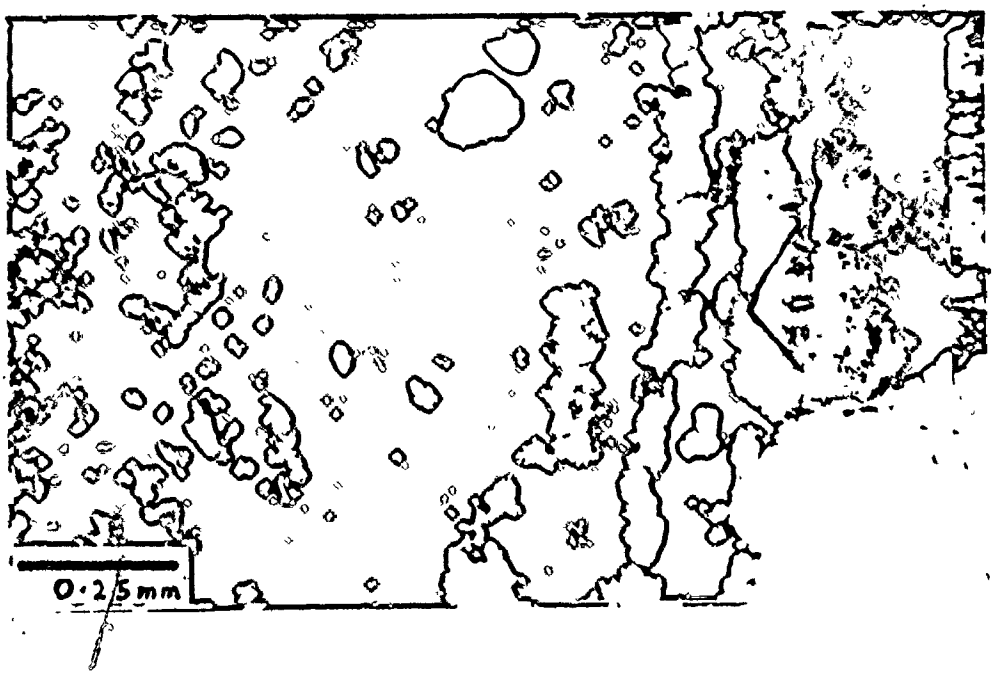

SJHS The tnin section cuts a region of hiatuses*, bcth central cap and lateral growth areas, and the outer dirt rind of this sample.

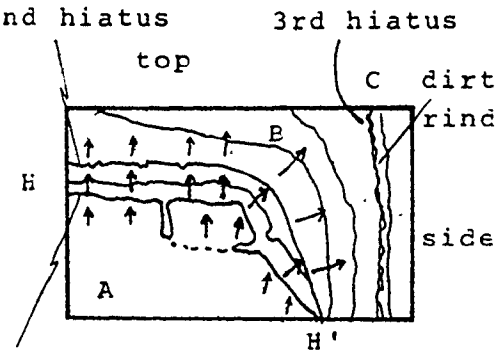

Area A generally consists of length-fast palisade crystals oriented perpendicularly to the growth horizons. Fluid inclusions are common and have angular rod shapes. Tney occur between and within grains. Sets of smaller fluid inclusions help to define growth layers. The larger fluid inclusions grade in size up to drusy cavities wholly or partly lined with microcrystalline calcite, ill-defined muck and small opaque grains.

The hand specimen is marked by a region of several closely spaced hiatuses. Part of this region is designated H - H' in the diagram and is defined by several features, as follows:

1) In the clearer calcite below H - H' occur a few deep holes (≈0.5 mm or greater) connected to a former surface. Dissolution has occurred mostly down boundaries and later precipitation has partly refilled the holes.
2) Post-hiatus growth layers are marked by closely spaced bands of fine fluid inclusions and perhaps fine muck. These bands descend and reascend the holes as successive linings and show to what extent the holes

have been refilled.

3) The fluid inclusion/dirt bands did not nucleate micro-crystals nor has the hiatus prevented crystals from growing across it in optical continuity where the orientation was favourable. Thus in the cap area length-fast columnar crystals grew perpendicularly to the growth horizons before and after the hiatus. They are optically continuous. But in the curved side region the crystal extinctions, under the analyzer, are significantly more vertical before the hiatus than after it, as shown by the arrows in the diagram. One large crystal in the corner of the curve, for example, is inclined 45° to the side bands (of fluid inclusions etc) whereas the crystals on the opposite side are perpendicular to these bands. The discontinuity in c-axis orientation of crystals near H' gives the impression that the stalagmite was considerably wider before its partial dissolution. It is remarkable that even here some smaller crystals still cross the hiatus with optical continuity.

4) Near H - H' the lower inclusion bands have themselves been truncated at a wedge angle by a second solutional event. The overlying horizon is marked by a wide band of much longer fluid inclusions and may be traced back to the cap.

Area B consists of length-fast columnar crystals showing prominent cleavage traces. The area has many cavities partly lined with muck and small opaque grains. One set of such cavities marks a dissolution horizon and corresponds to the second hiatus referred to above.

Area C is the dirt rind of the stalagmite and

consists of two regions. The inner region is marked by a prominent black band. It is an aggregate of fine clumpy opaque material which in some places shows a dendritic structure. The width varies from <0.1 mm up to 0.3 mm. Under high-power lens the edges of the clumps are tinged red-yellow. A thinner layer of the same material occurs about 0.3 mm further out. Neither of these opaque bands show any reflectivity.

Some of the calcite crystals between these two bands show brush extinction in 'fans', and strain interference colours. The yellow coloured sets of crystals are ill-defined due to the muck.

The outer region is a banded fluid inclusion and muck rich layer with crystals showing some optical continuity. Towards the edge some calcite bands become clear and free of inclusions of any kind.

The Opaque Grains

Only very small opaque grains are found in area A and are mostly angular; they occur in drusy cavities.

In area B the opaque grains are often larger than in A and are associated with muck, quartz grains and a few small grains showing a red or amber colour to transmitted light. The opaque grains show etch effects in reflected light.

The rind contains several opaque grains, not necessarily associated with the opaque bands. They are equant - a few showing hexagonal shapes. Two of these showed dark and light gray colours in reflected light and are probably composite titanomagnetite grains.

Plate III.10

Stalagmite DAS2

In reflected light and in oil; a typical opaque grain showing etch effects.

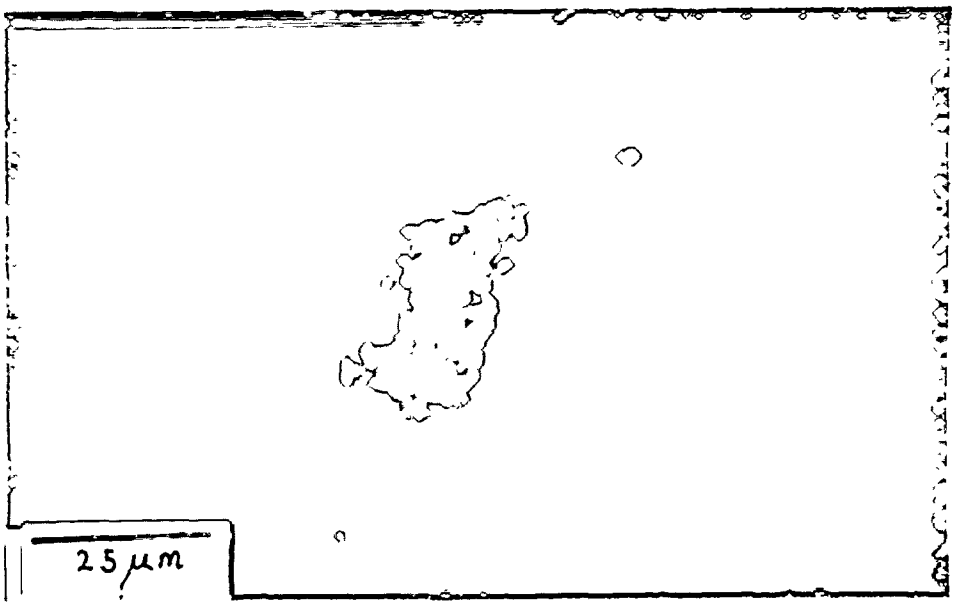

DAS2 The section includes some of the lateral growth layering.

Columnar anhedral crystals with curved or wavy interlocking boundaries are common. Some crystals are fairly convoluted in shape.

The chief crystalline difference in this stalagmite is that many grains are length-fast parallel or subparallel to the growth surfaces. Otherwise there is little textural difference in the calcite when compared with that from other samples.

Growth surfaces occur in wavy lines and are marked by dirt which truncates former crystals and causes the next set to start as microcrystals. Thorn-shaped or globular fluid inclusions are common and are mostly parallel to cleavage traces. One part of the section included the central amber coloured layers but microscopic examination of this area does not indicate what the colour is due to.

The 'wash-off' effect (section 4.6.1) appears as a faint gray-brown translucent colouring but is otherwise undiscernible.

There are only a few opaque grains and these are small and seem to have been solutionally attacked before being incorporated into the calcite fabric.

Note on Hiatuses.

Three types of hiatus may be distinguished in speleothems. The first - the canonical type- is simply due to a cessation in growth. It may or may not be marked by dust layers or by ease of parting between pre- and post-hiatus growth layers. Conversely dust and dirt layers or easily parted layers may not necessarily indicate a hiatus. It is a simple observation that many 'dead' speleothems have dust coatings on them at the present time. However it may not be easy to recognise such layers in speleothems which have restarted growth. Regular dirt layering may have arisen for other reasons , eg from impurities in the feed water, as has been shown repeatedly in this study. An hiatus is certainly identified if the growth rate curve shows a discontinuity across some horizon.

If the feedwater, instead of ceasing, becomes chemically aggressive temporarily, then some of the speleothem will become dissolved away. It may continue to grow as the water changes back to a supersaturated state. The result for the speleothem is what might be termed a 'dissolution-hiatus', and is recognised by the kind of features displayed by the cap of TS (section 4.7.1), and by SJHS as discussed above. (Complete recrystallization of speleothems has been invoked to explain anomalous Th/U ratios (Harmon, 1975; Gascoyne, 1979) in which the uranium has been transported out of the fabric. The exact mechanisms and the environment for recrystallization to occur without a change of speleothem morphology, are not known.)

A third type of hiatus is known from two or three

speleothems in the McMaster collection. This is when a stalagmite of flowstone has become broken for some reason (eg, due to tectonism or cavern collapse) and was followed by later growth. It is recognisable by the unconformity of layers at the break.

APPENDIX IV

The following graphs relate to sample DAS2, except figure 36 which relates to specimen RCB B8Q.

Total magnetization is x 10^{-7} G, unless otherwise stated.

Where there is uncertainty the probable trend is shown by - - - . Greater uncertainty is shown by a ?

The 1 KOe end point mean and error bar is shown by a + .

Figures 1 - 12.

Graphs of NRM versus ARM

Figure 1a

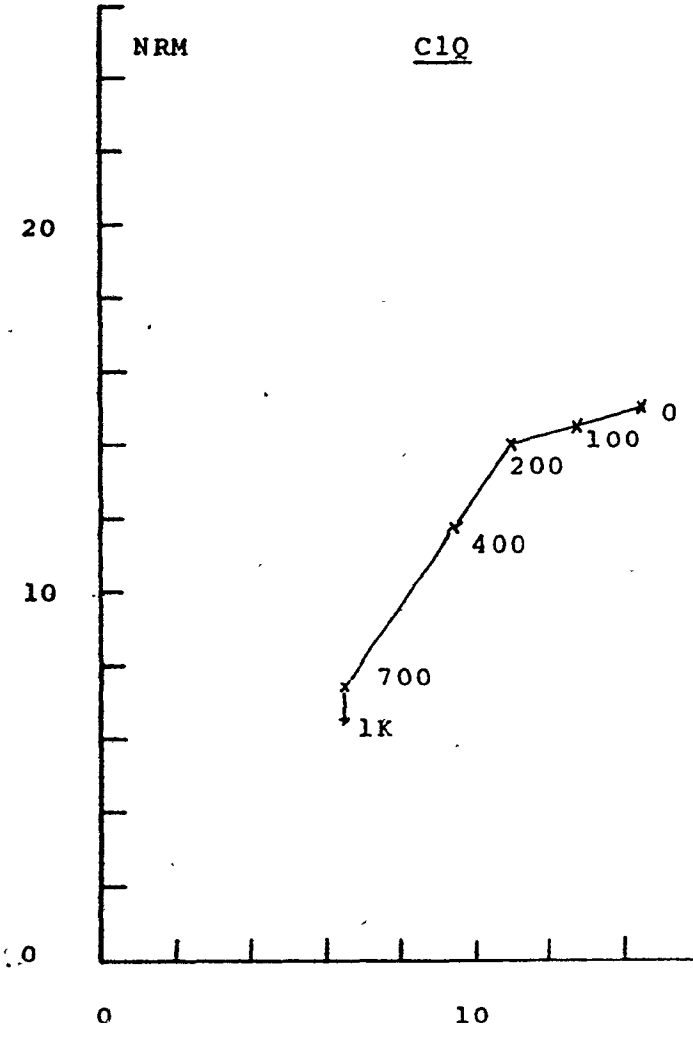

Figure 1b

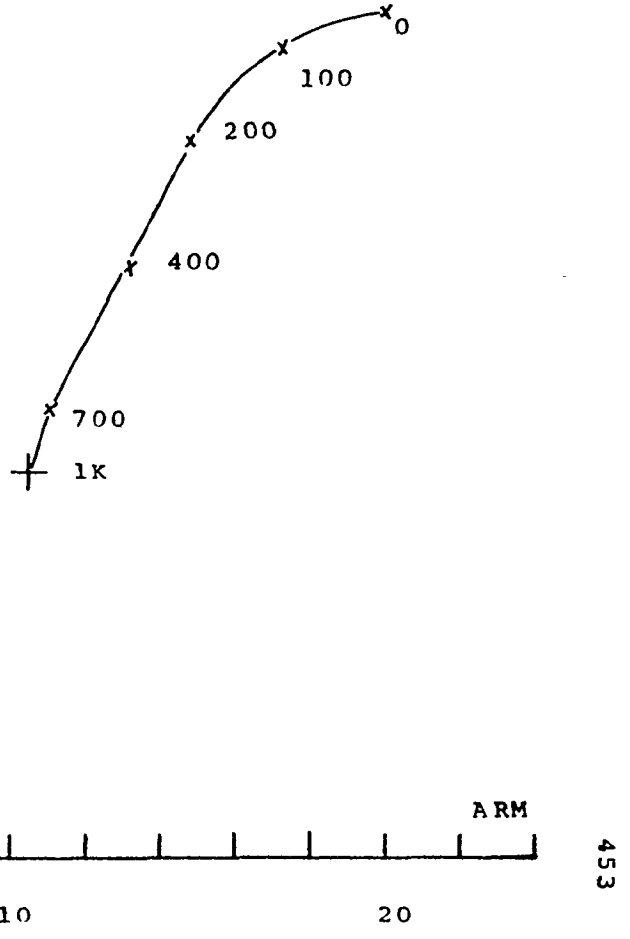

Figure 2

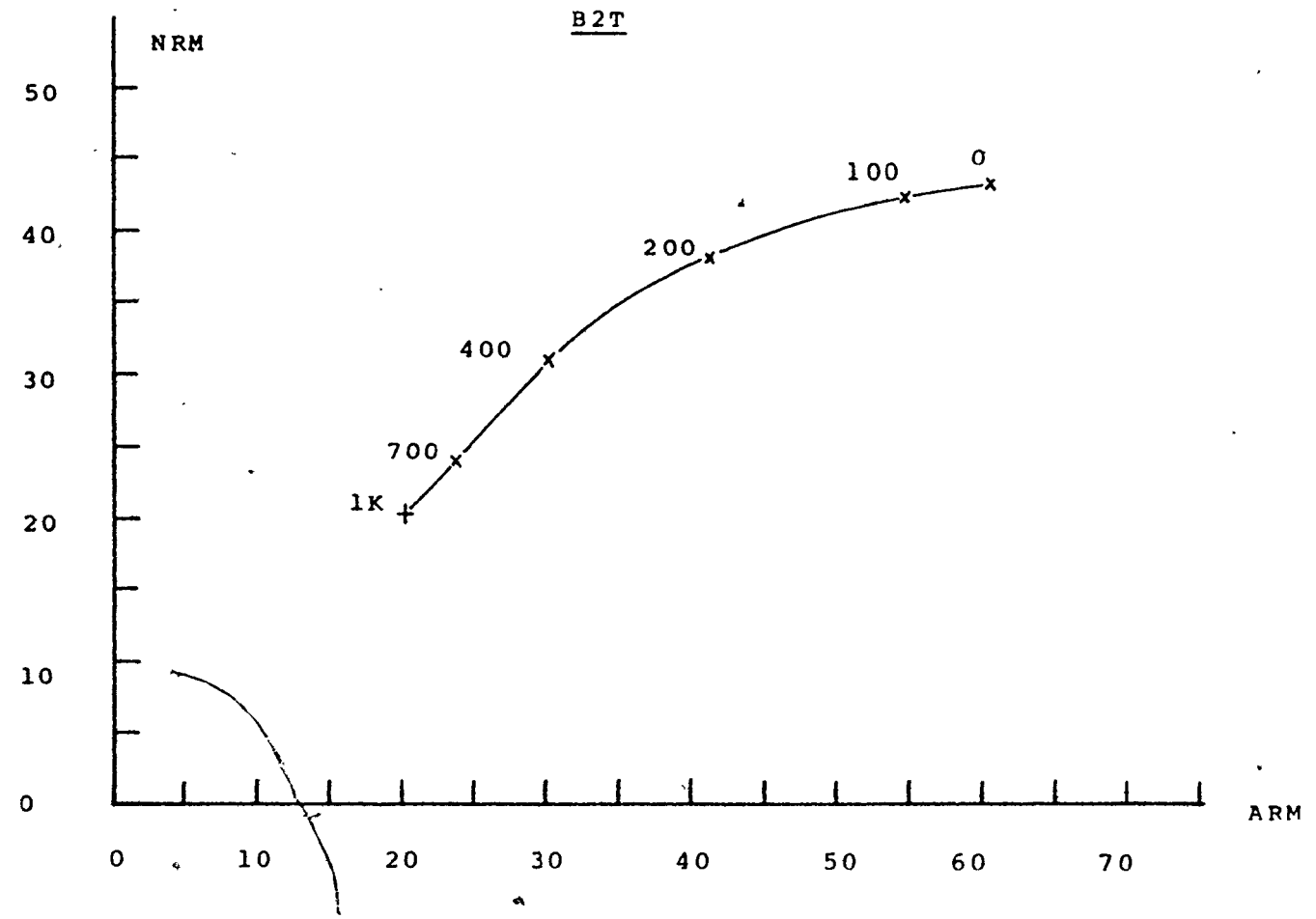
B2T
NRM
50
40
30
20
10
0
0
100
200
400
700
1K
0
10
20
30
40
50
60
70
ARM

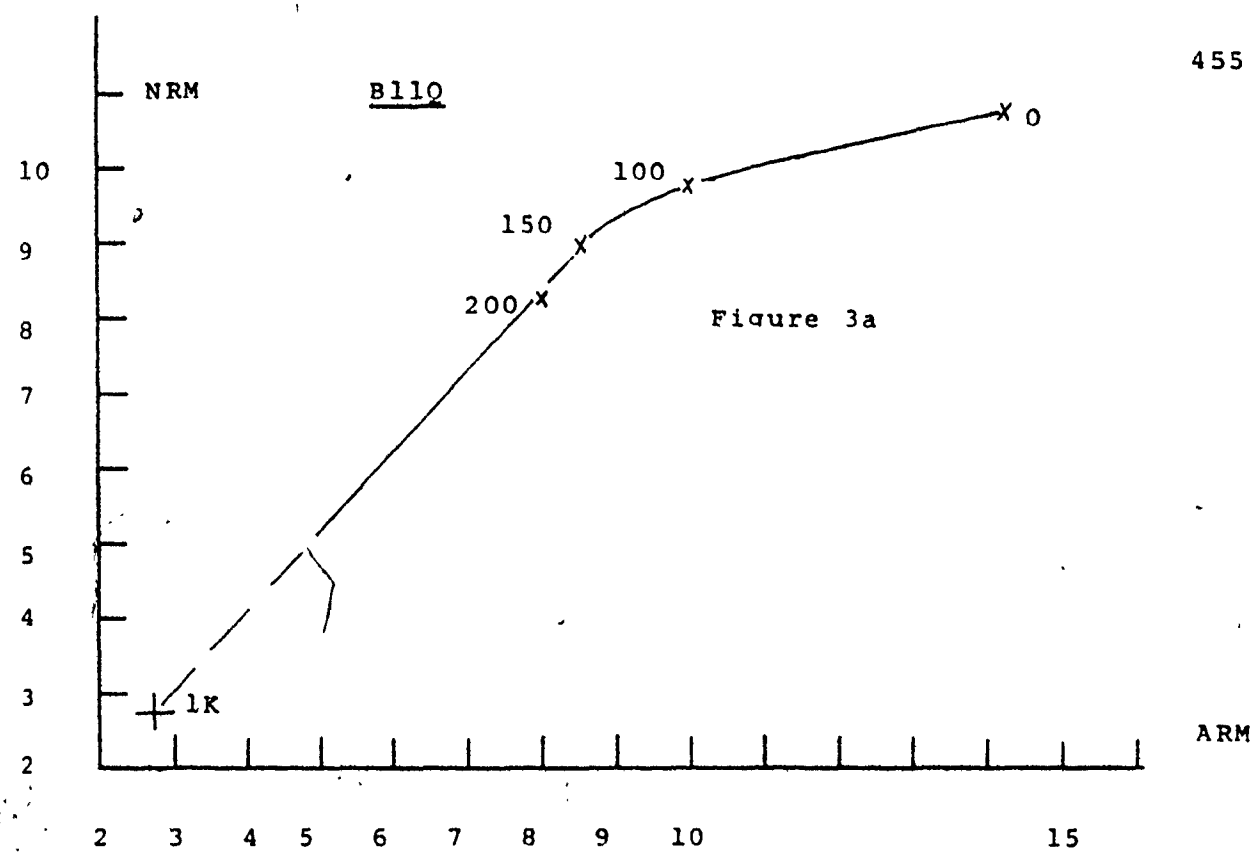

Figure 3a

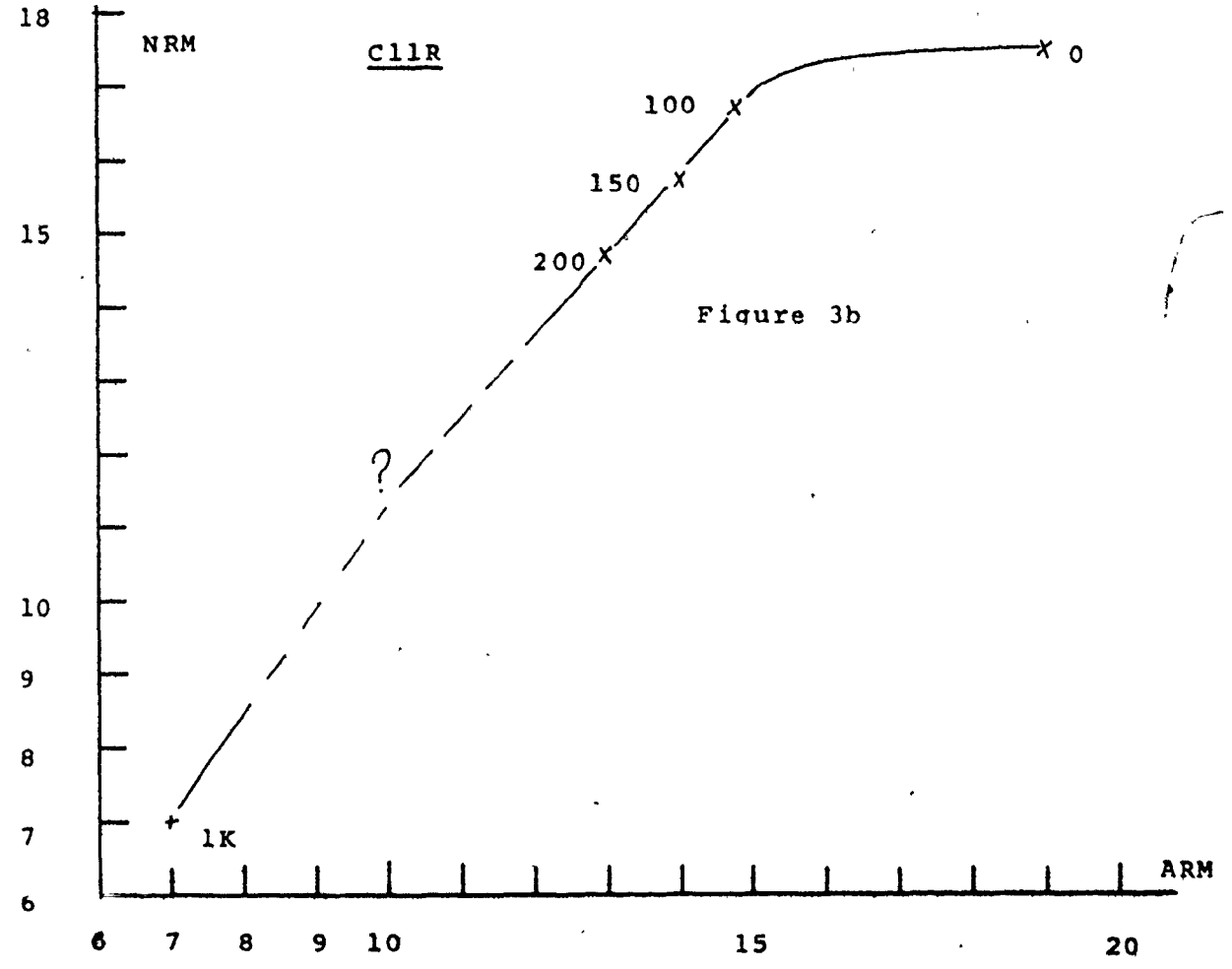

Figure 3b

Figure 4

B120

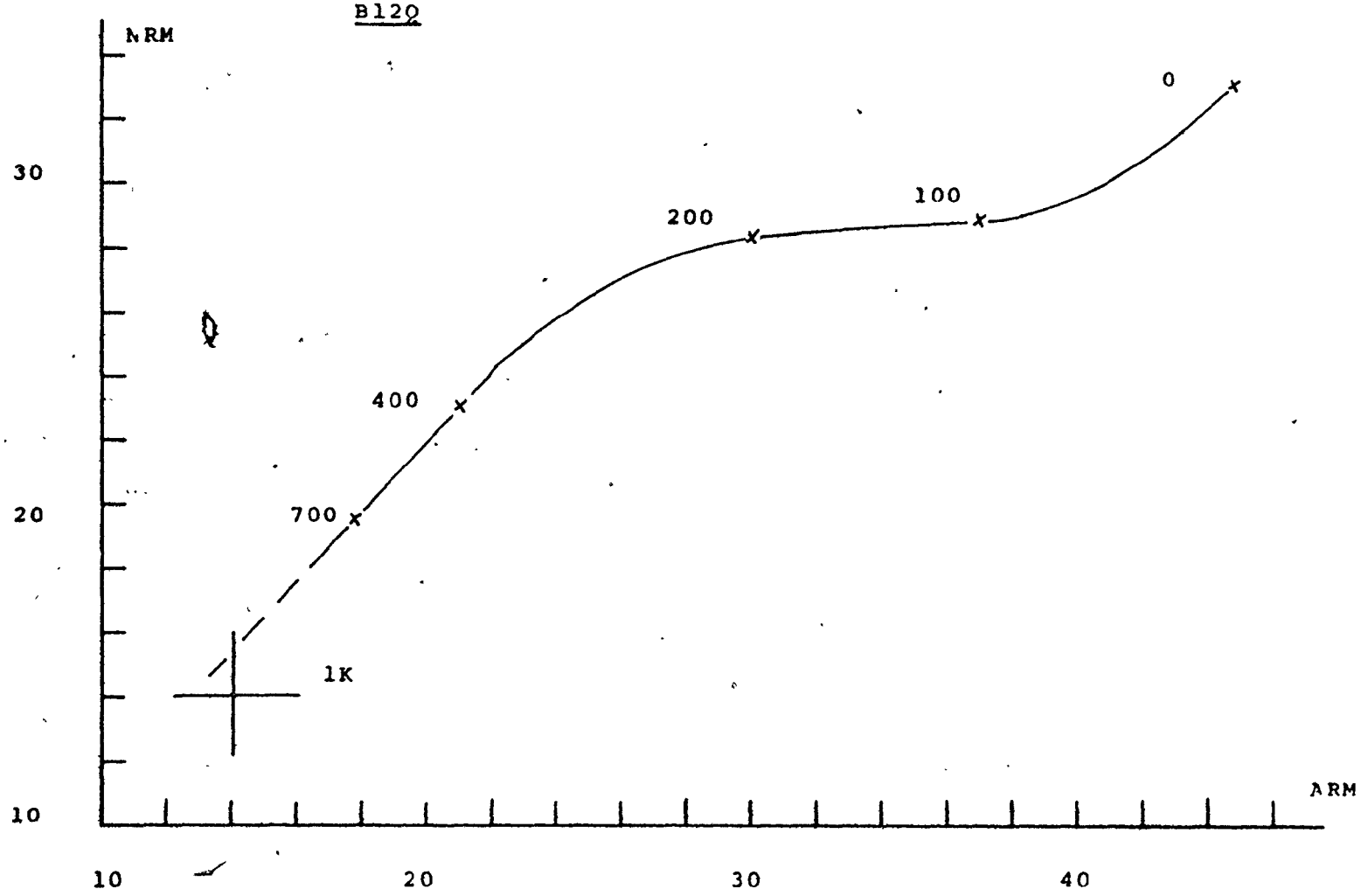

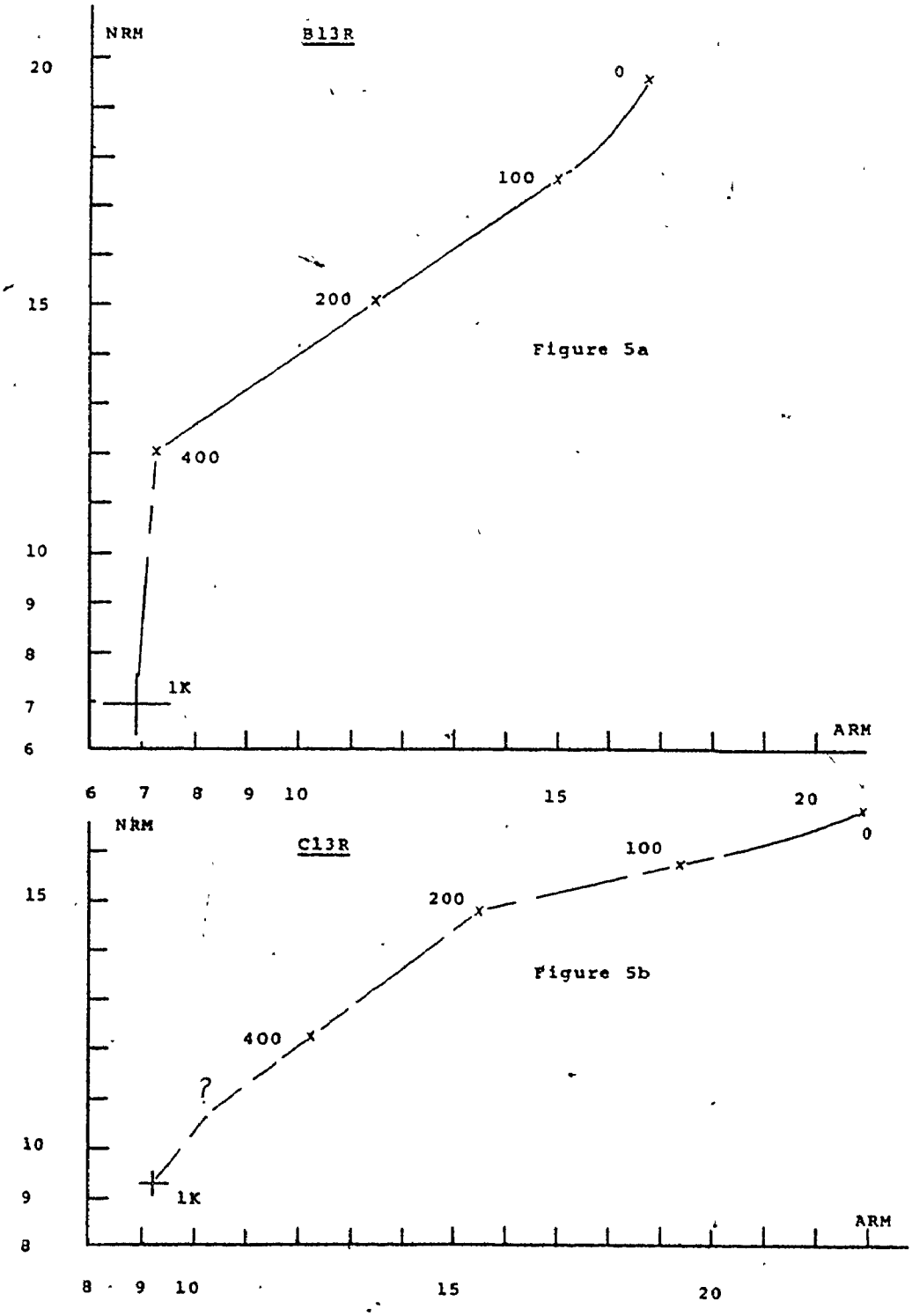

Figure 5a

Figure 5b

Figure 6

B13S

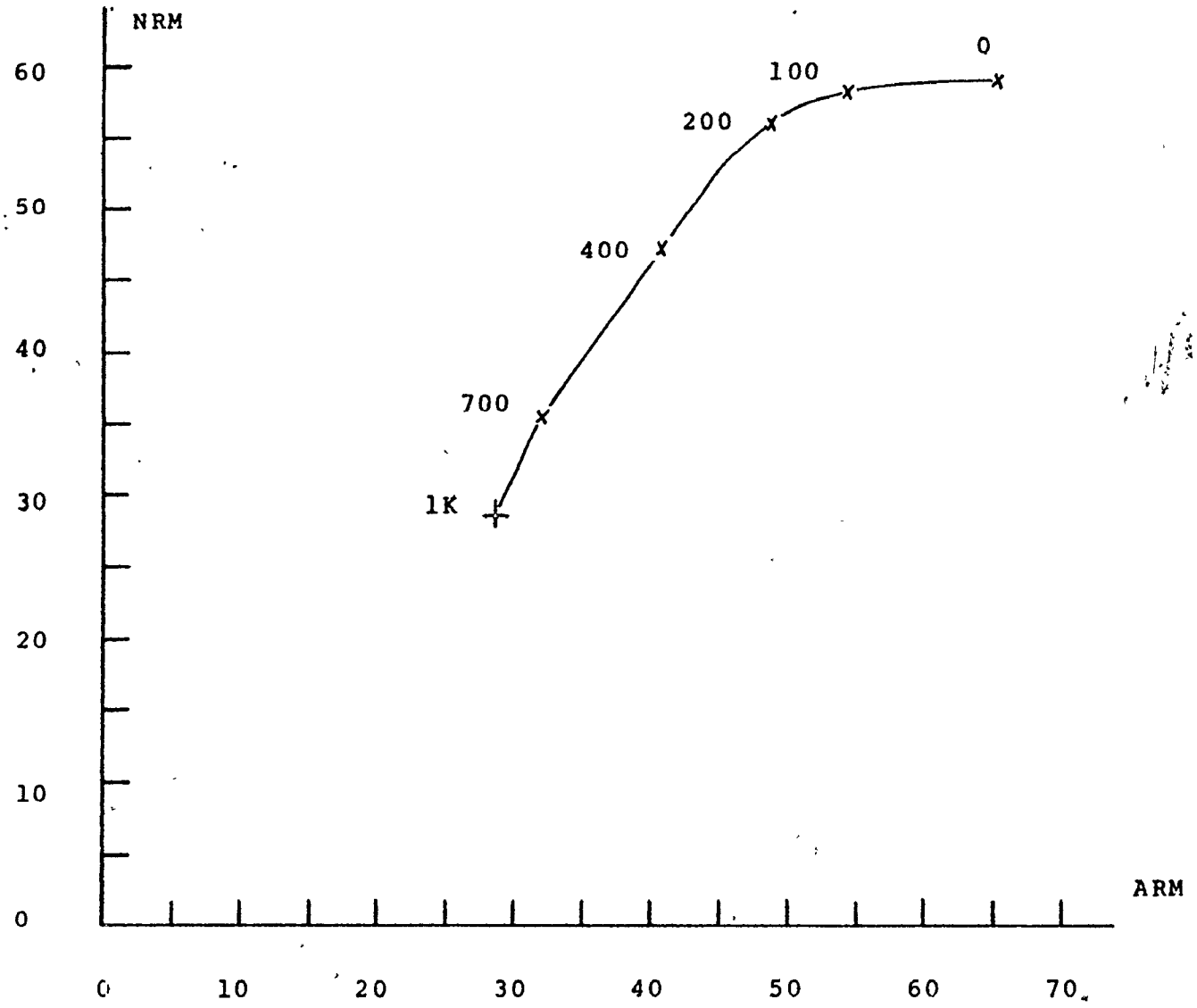

459

Figure 7

C130

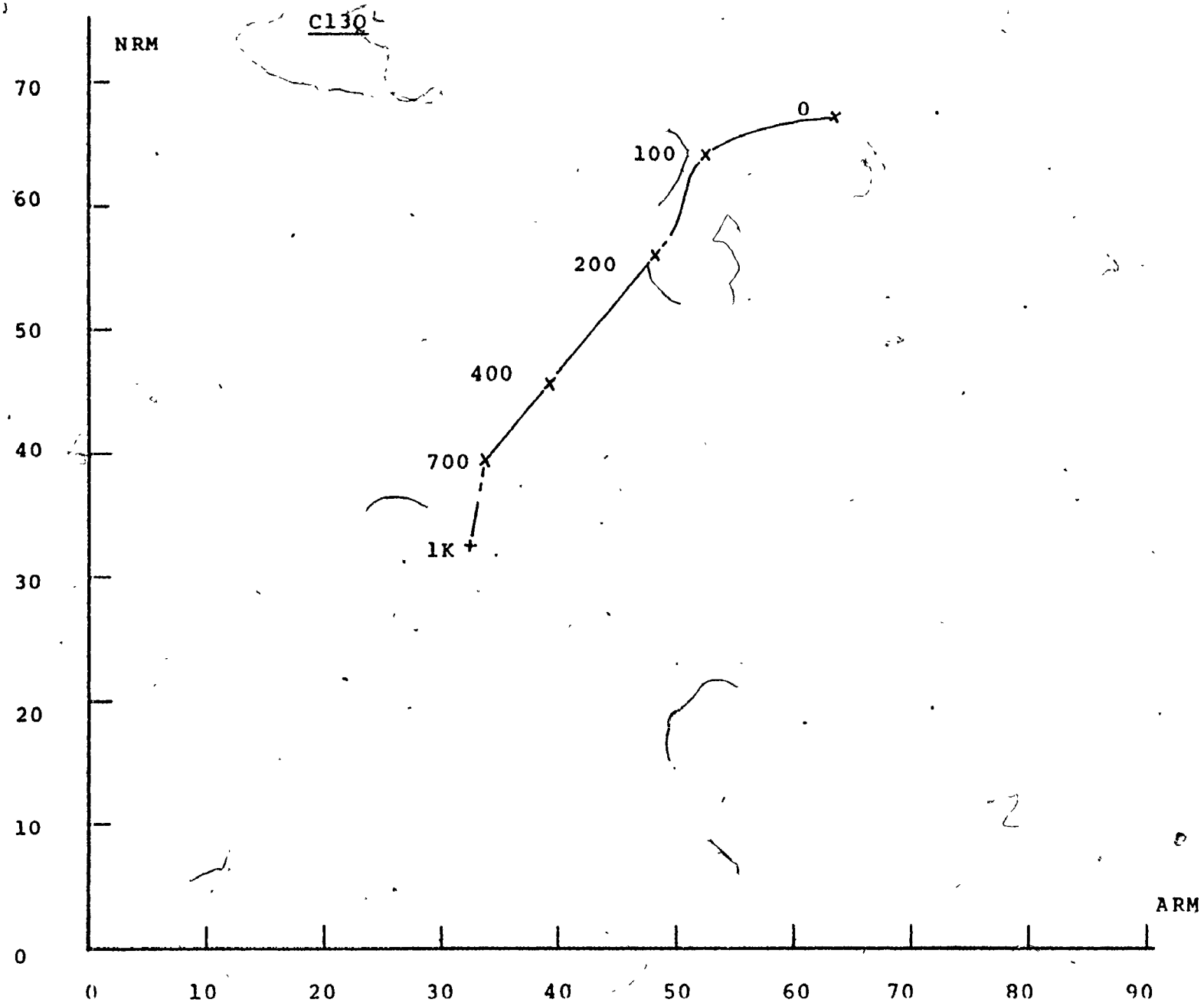

459

B190/R

Figure 8

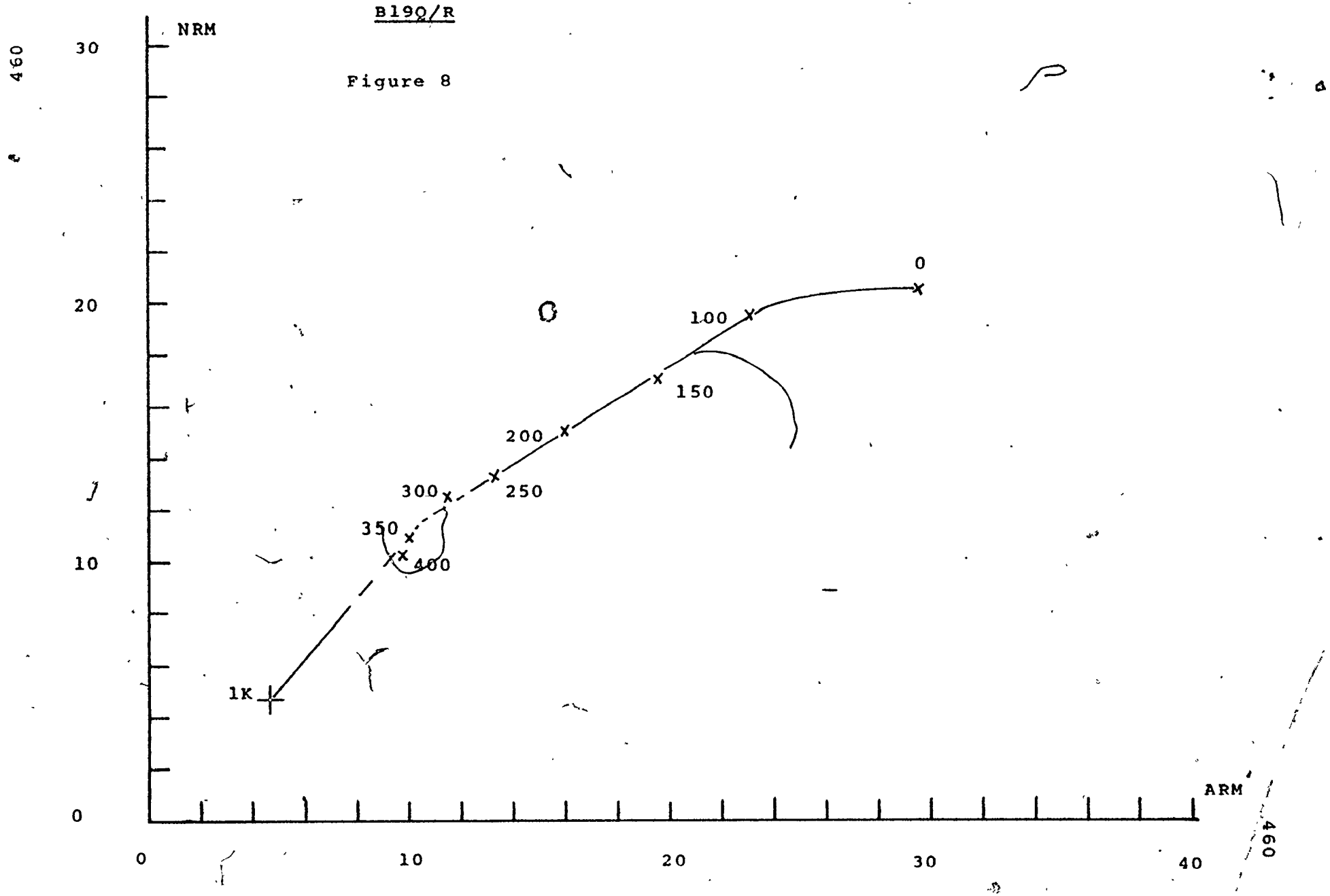

461

B340

Figure 9

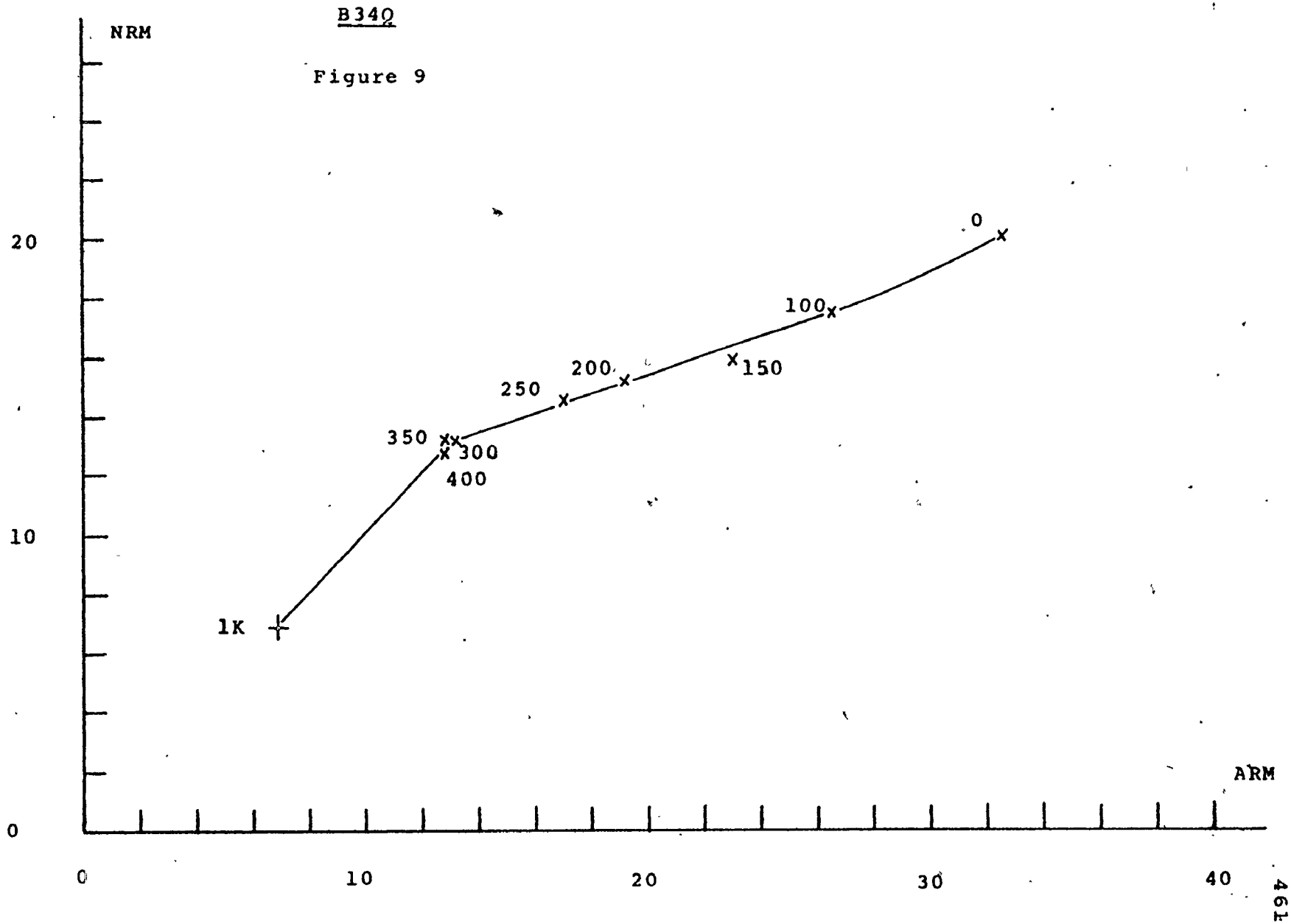

461

Figure 10

C340

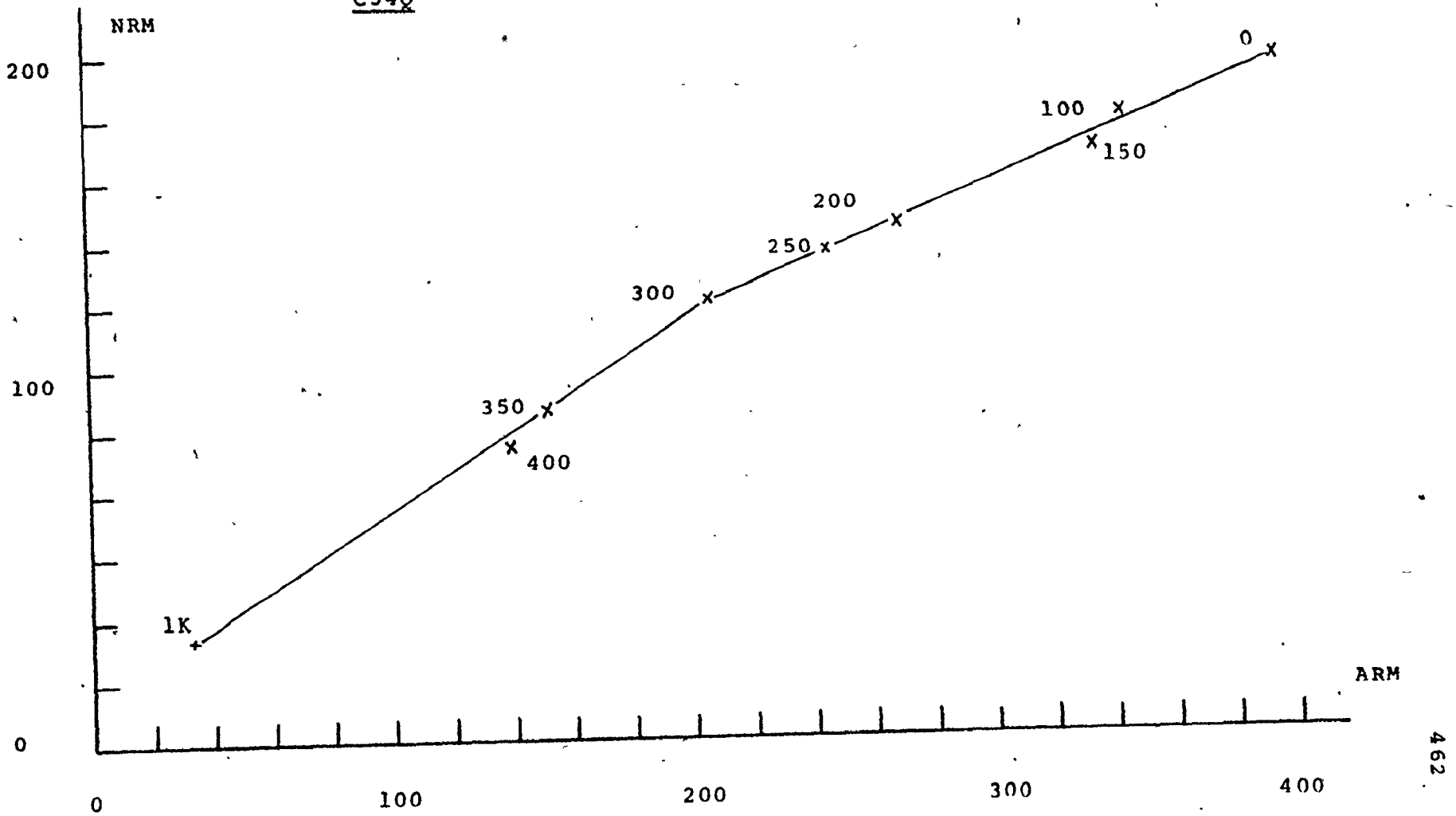

Figure 11

B34R

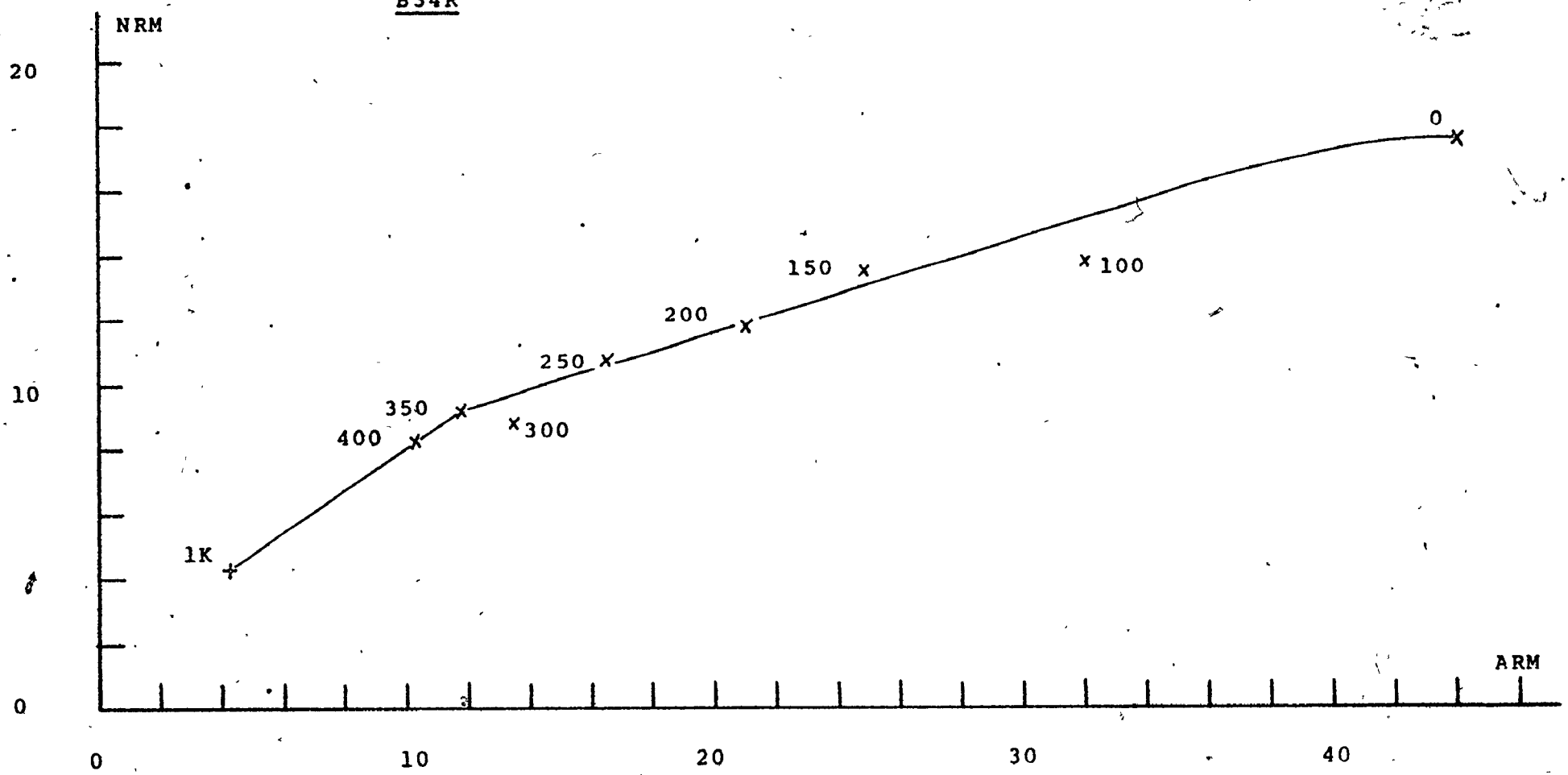

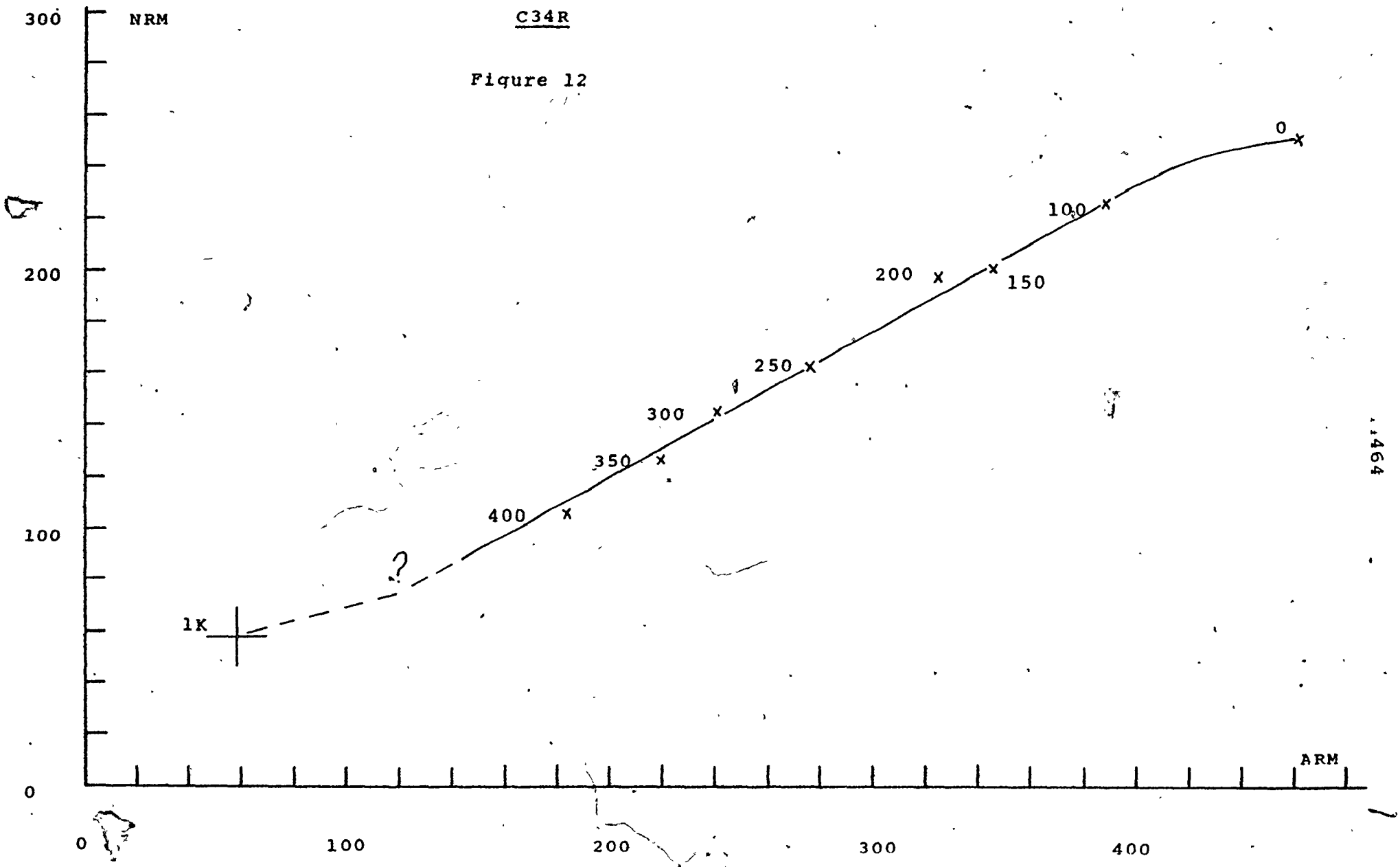

Figure 12

.464

APPENDIX IV

Figures 13 to 16

Graphs of ARM, demagnetized to 100 Oe, against Hd

ARM is x 10^{-7} G, (total moment).

The H_d = 0 end point is the mean of all 1 KOe demagnetizations.

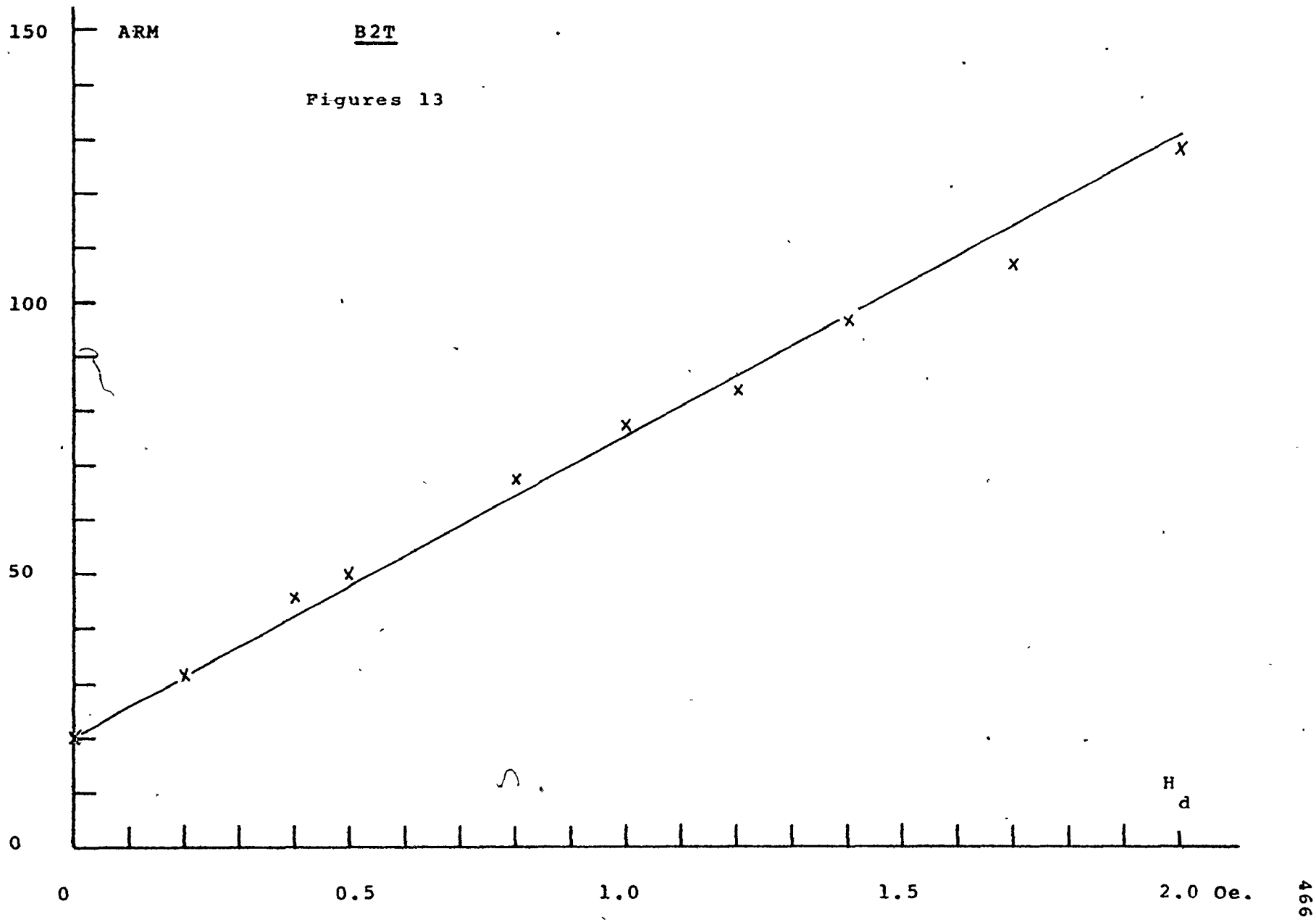

Figures 13

B12Q

Figure 14

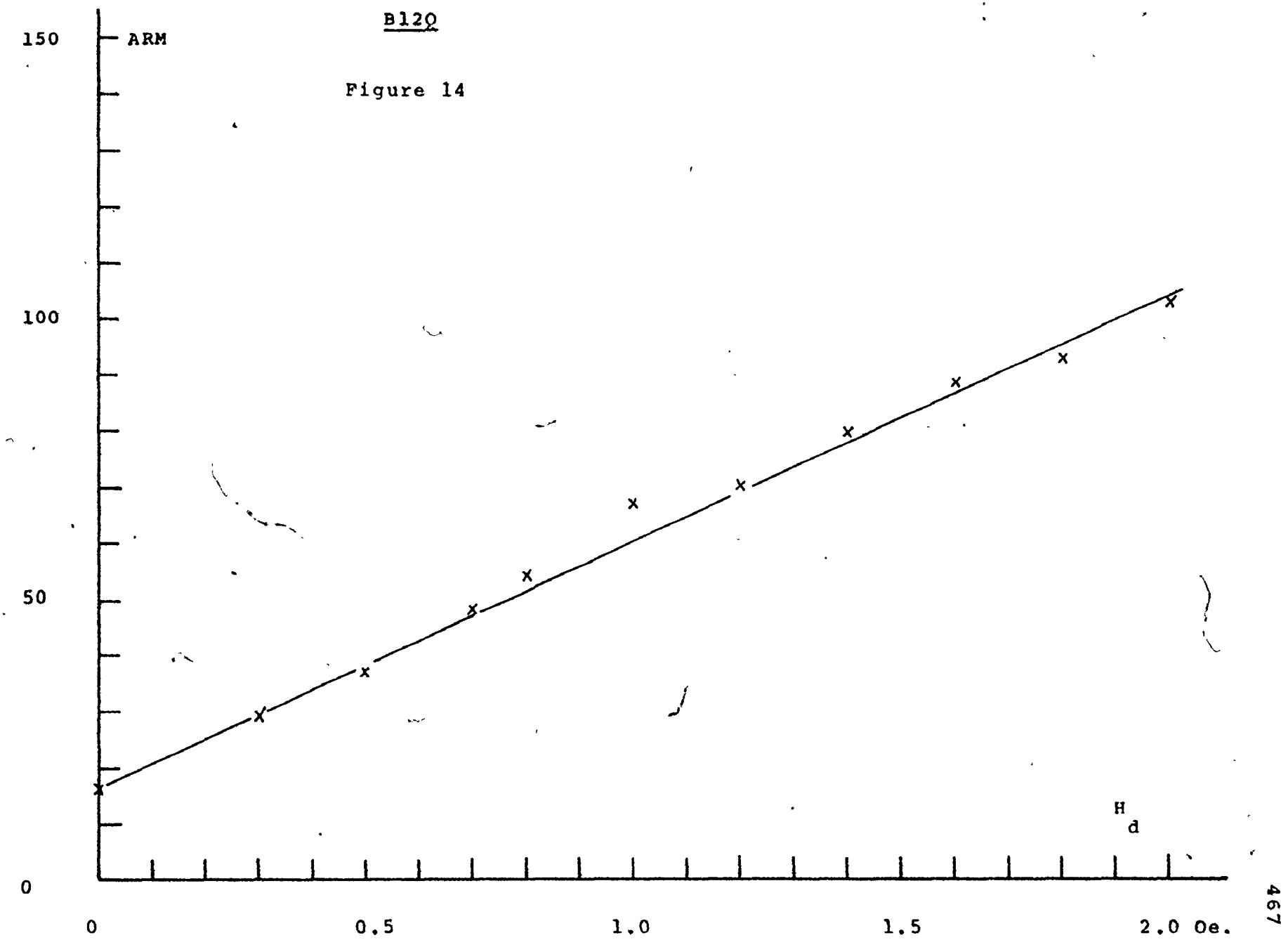

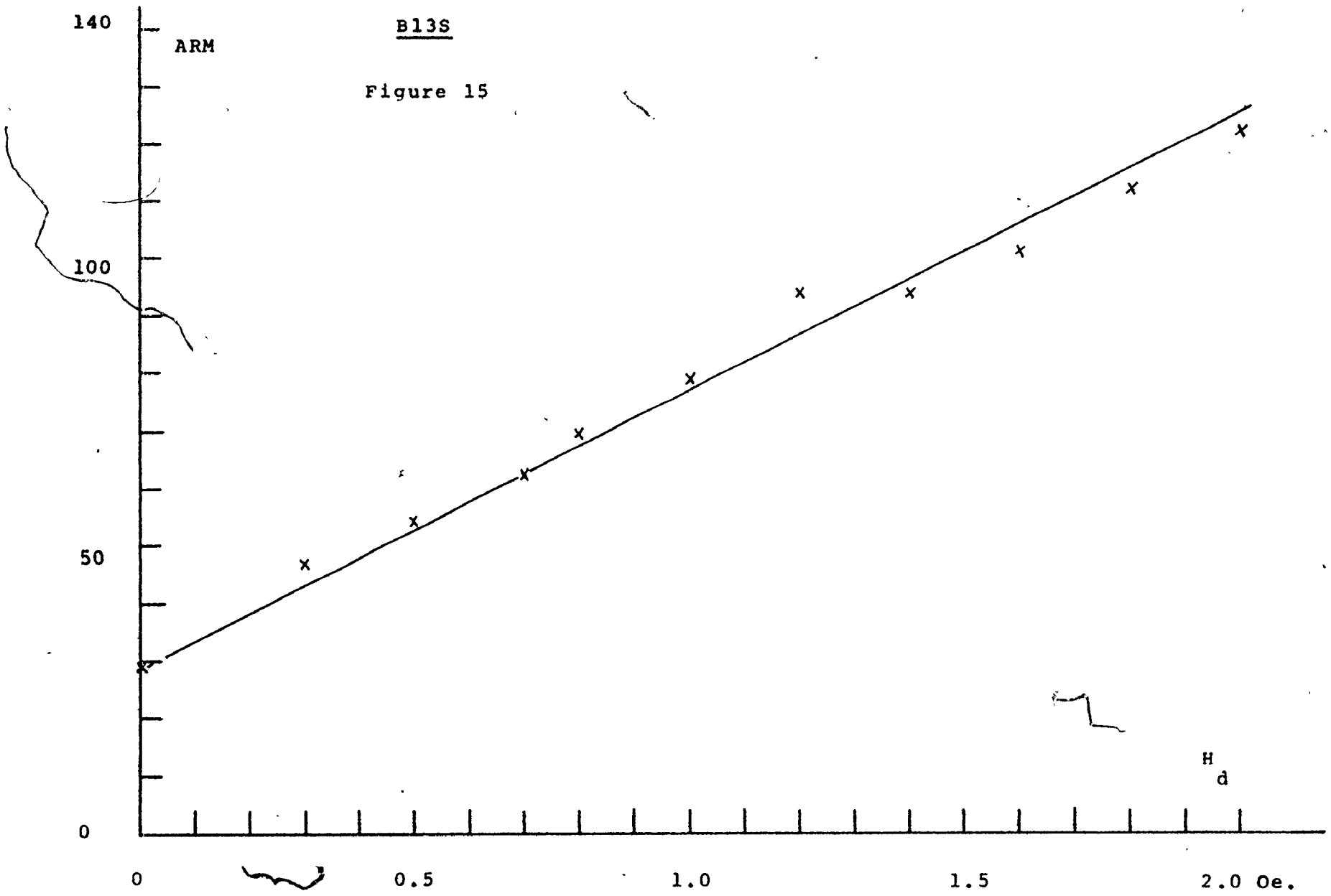

Figure 15

C130

Figure 16.

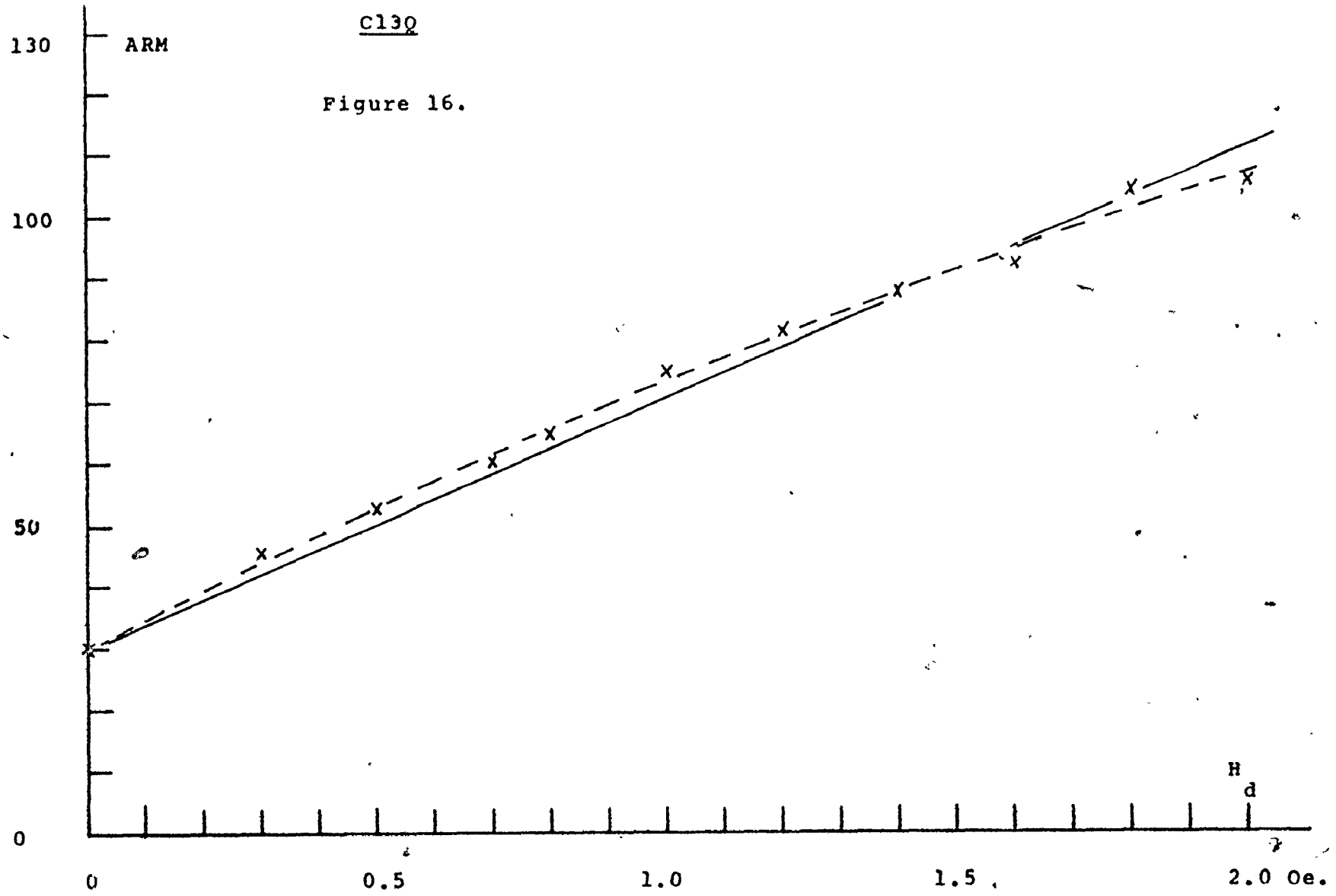

APPENDIX IV

Figures 17a and b

NRM and ARM(0.5) against SIRM for C12Q

The NRM and ARM are in units x 10^{-7} G, total moment.

The SIRM - x 10^{-5} G.

C120

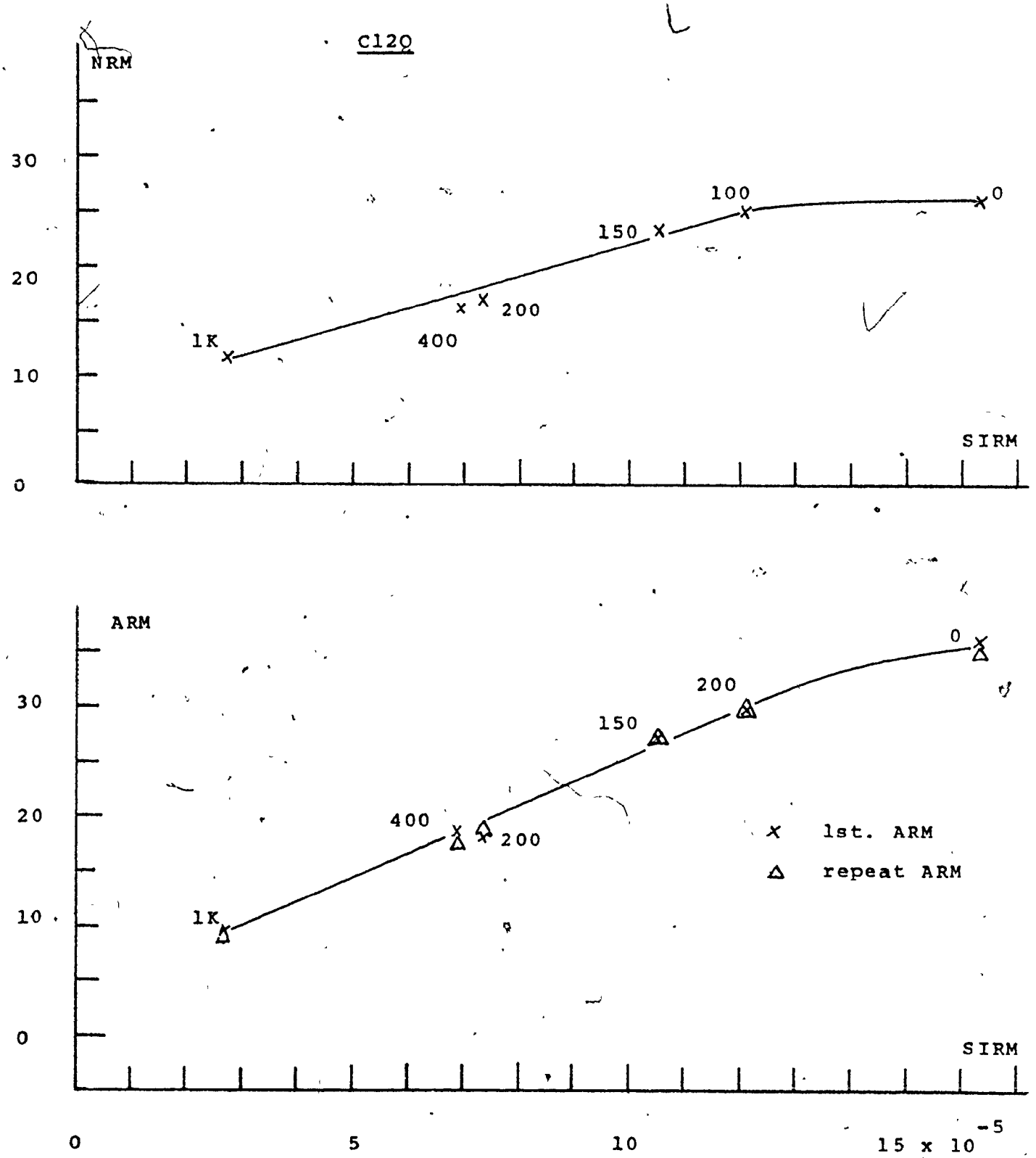
NRM
30
20
10
0
1K
400
200
150
100
0
SIRM
ARM
30
20
10
0
1K
400
200
150
200
0
x 1st. ARM
Δ repeat ARM
SIRM
0
5
10
15 x 10⁻⁵

APPENDIX IV

Figures 18 to 35.

Graphs of NRM versus ARM. These are used in the production of the H_{a-a} values.

ARMs were produced in a field of 0.50 Oe, and magnetizations are x 10^{-7} G (total moment).

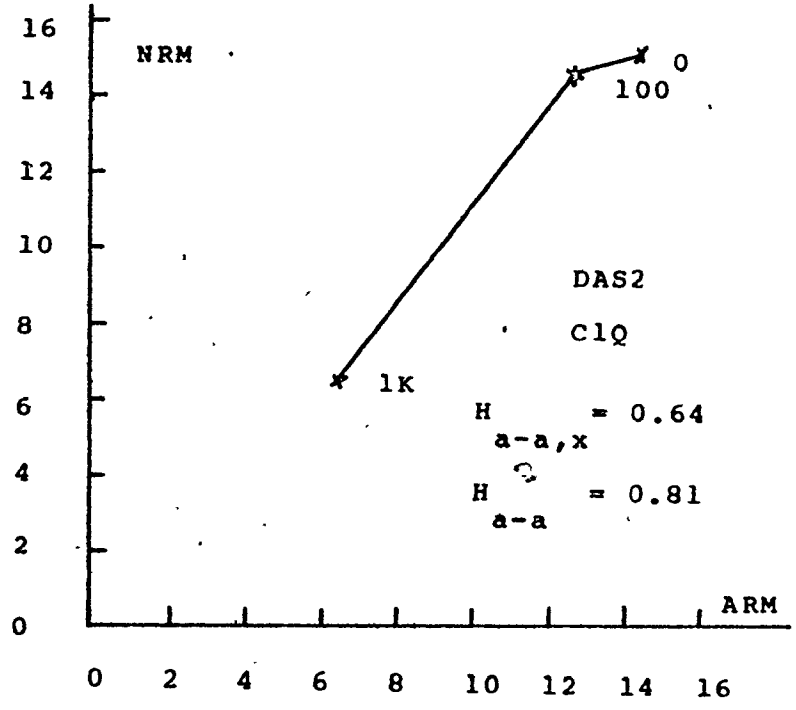
NRM
ARM
0
100
1K
DAS2
C1Q
H a-a,x = 0.64
H a-a = 0.81
0 2 4 6 8 10 12 14 16

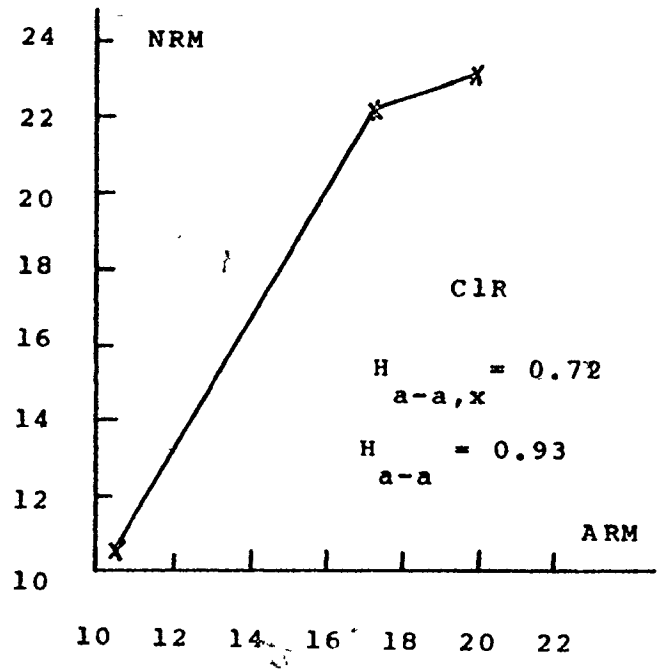
NRM
ARM
C1R
H a-a,x = 0.72
H a-a = 0.93
10 12 14 16 18 20 22

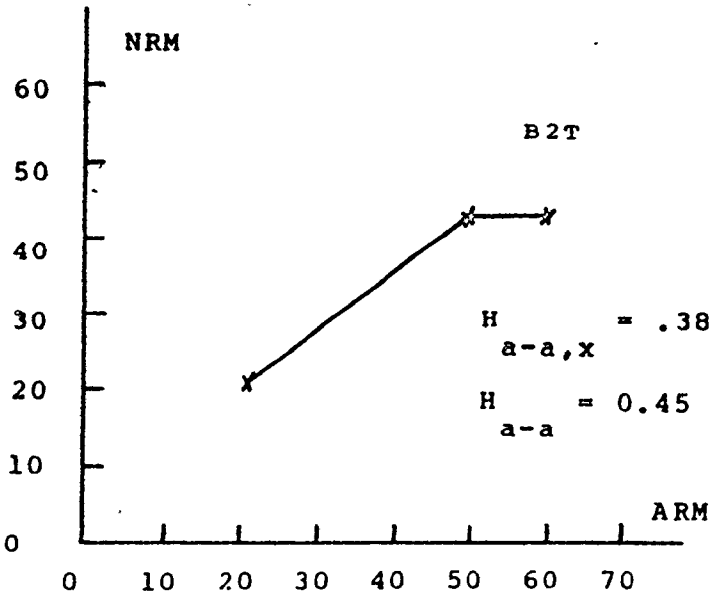
NRM
ARM
B2T
H a-a,x = .38
H a-a = 0.45
0 10 20 30 40 50 60 70

Figure 18

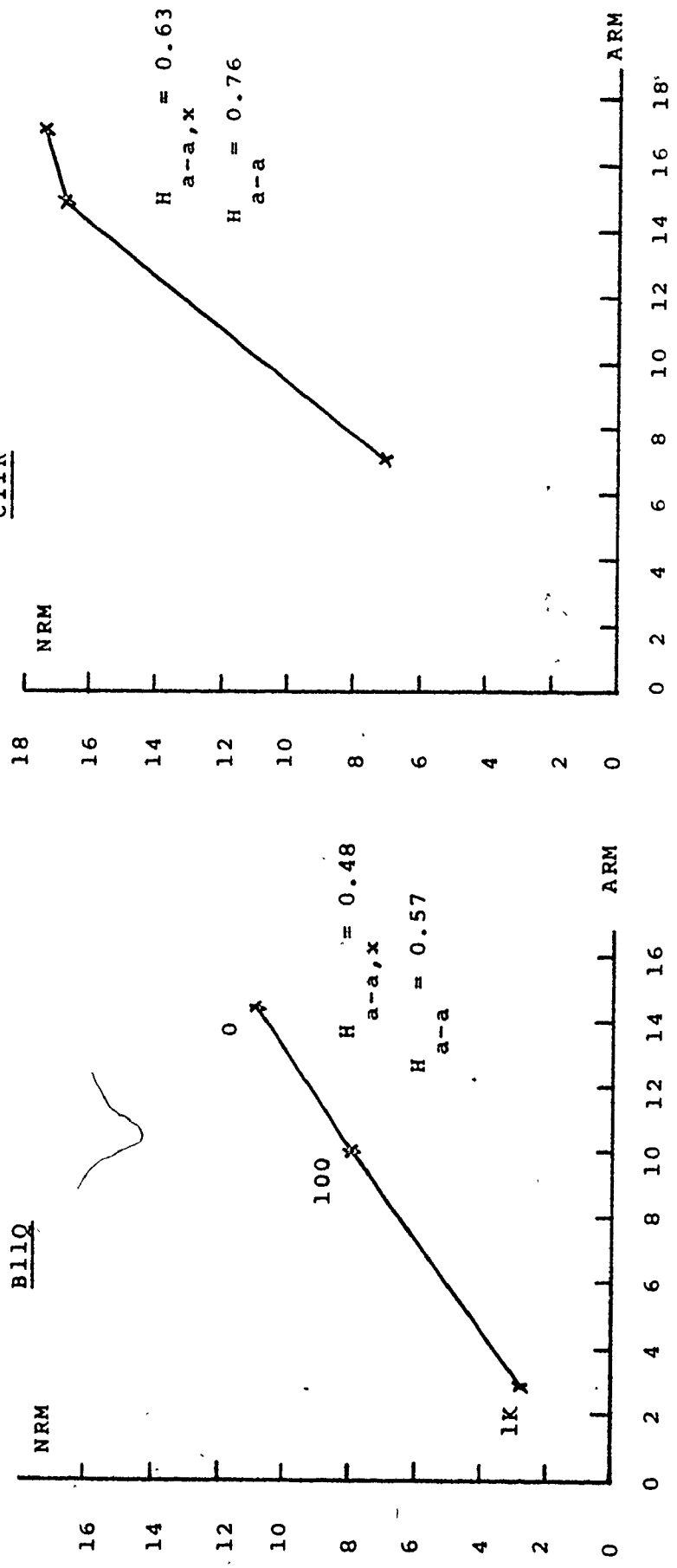
B11Q
NRM
ARM
0
100
1K
$H_{a-a,x}$ = 0.48
H_{a-a} = 0.57
C11R
NRM
ARM
$H_{a-a,x}$ = 0.63
H_{a-a} = 0.76

Figure 19

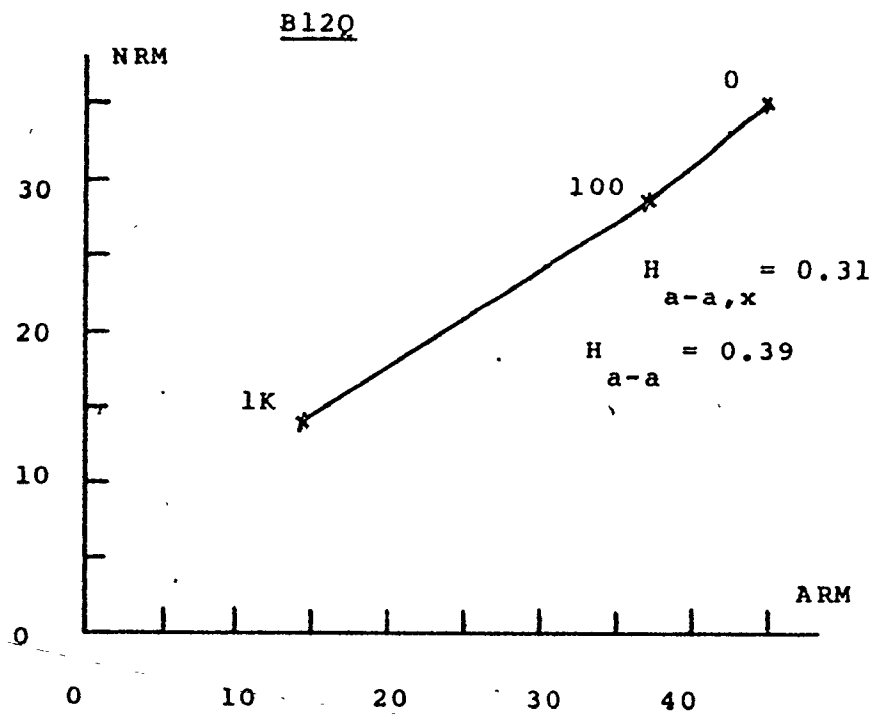
B12O
NRM
0
100
1K
H = 0.31
a-a,x
H = 0.39
a-a
ARM
0
10
20
30
40

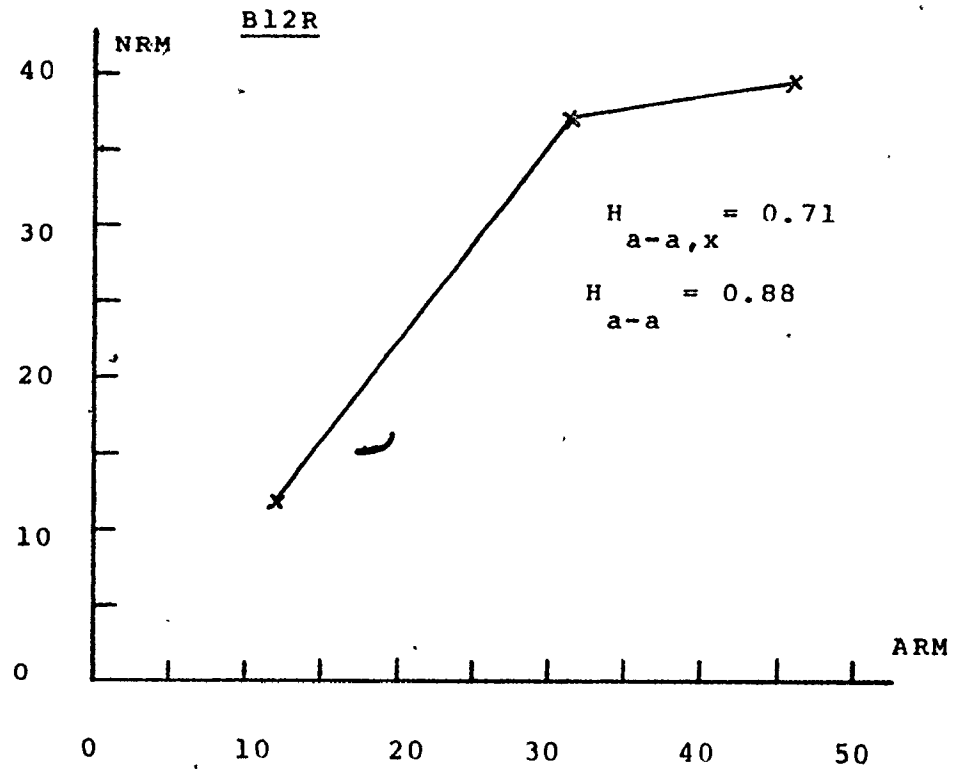
B12R
NRM
H = 0.71
a-a,x
H = 0.88
a-a
ARM
0
10
20
30
40
50

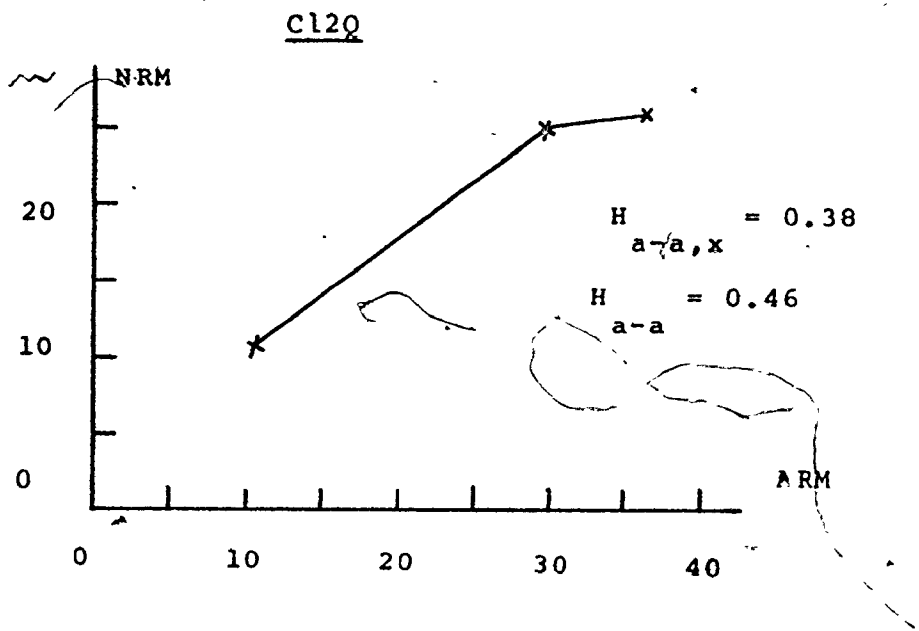
C12O
NRM
H = 0.38
a-a,x
H = 0.46
a-a
ARM
0
10
20
30
40

Figure 20

Figure 21

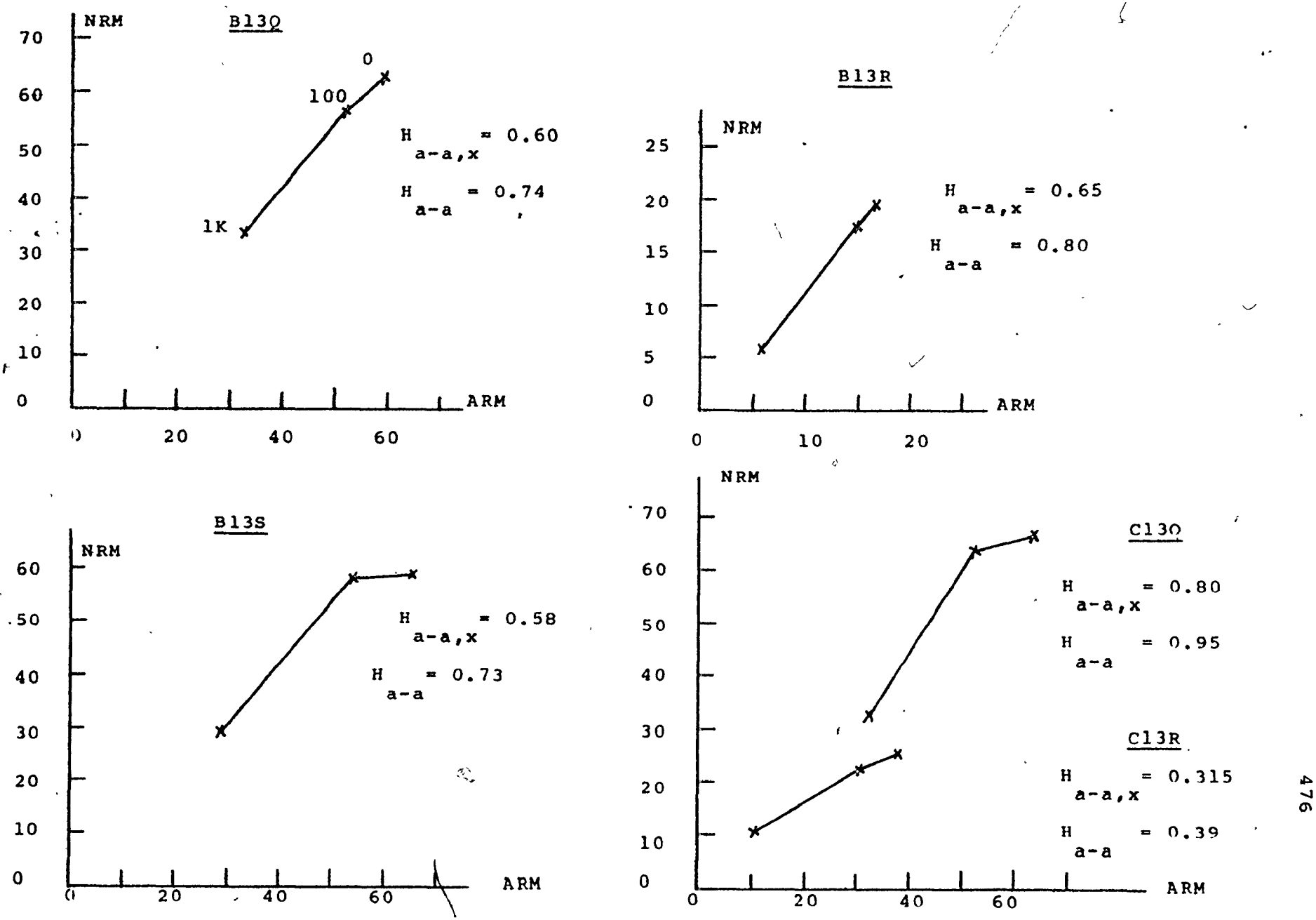
B13Q
NRM
ARM
0
100
1K
H a-a,x = 0.60
H a-a = 0.74
B13R
H a-a,x = 0.65
H a-a = 0.80
B13S
H a-a,x = 0.58
H a-a = 0.73
C13Q
H a-a,x = 0.80
H a-a = 0.95
C13R
H a-a,x = 0.315
H a-a = 0.39

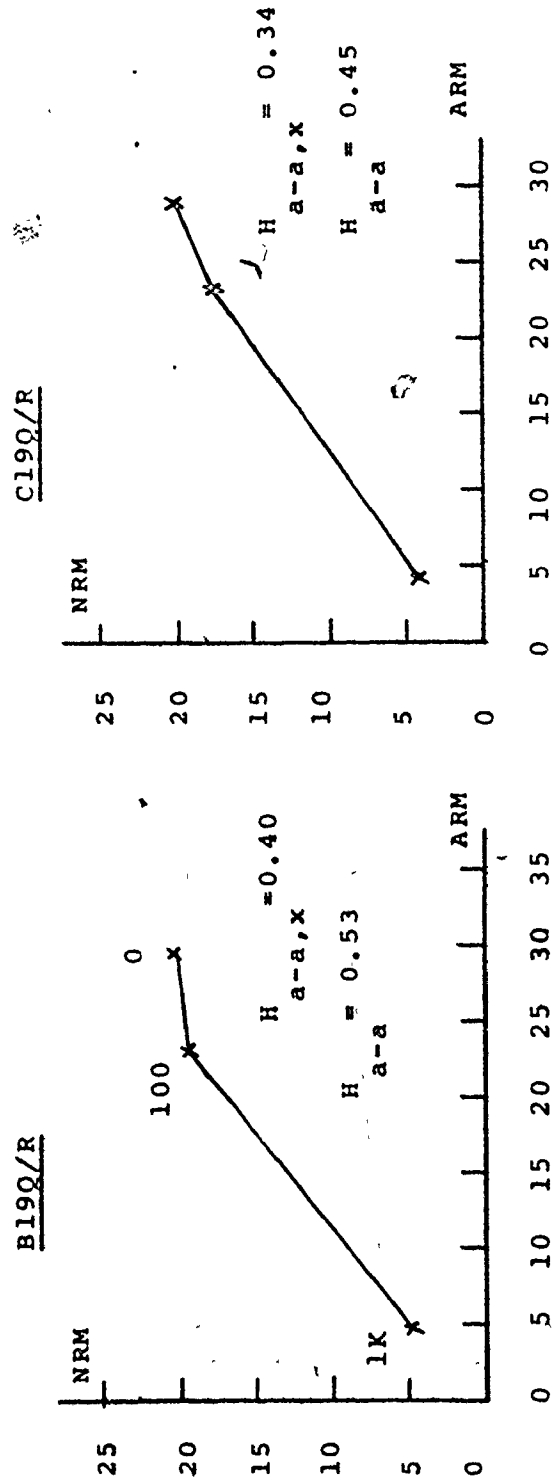
B19Q/R
NRM
ARM
1K
100
0
H a-a,x =0.40
H a-a = 0.53
C19Q/R
NRM
ARM
H a-a,x = 0.34
H a-a = 0.45

Figure 22

Figure 23

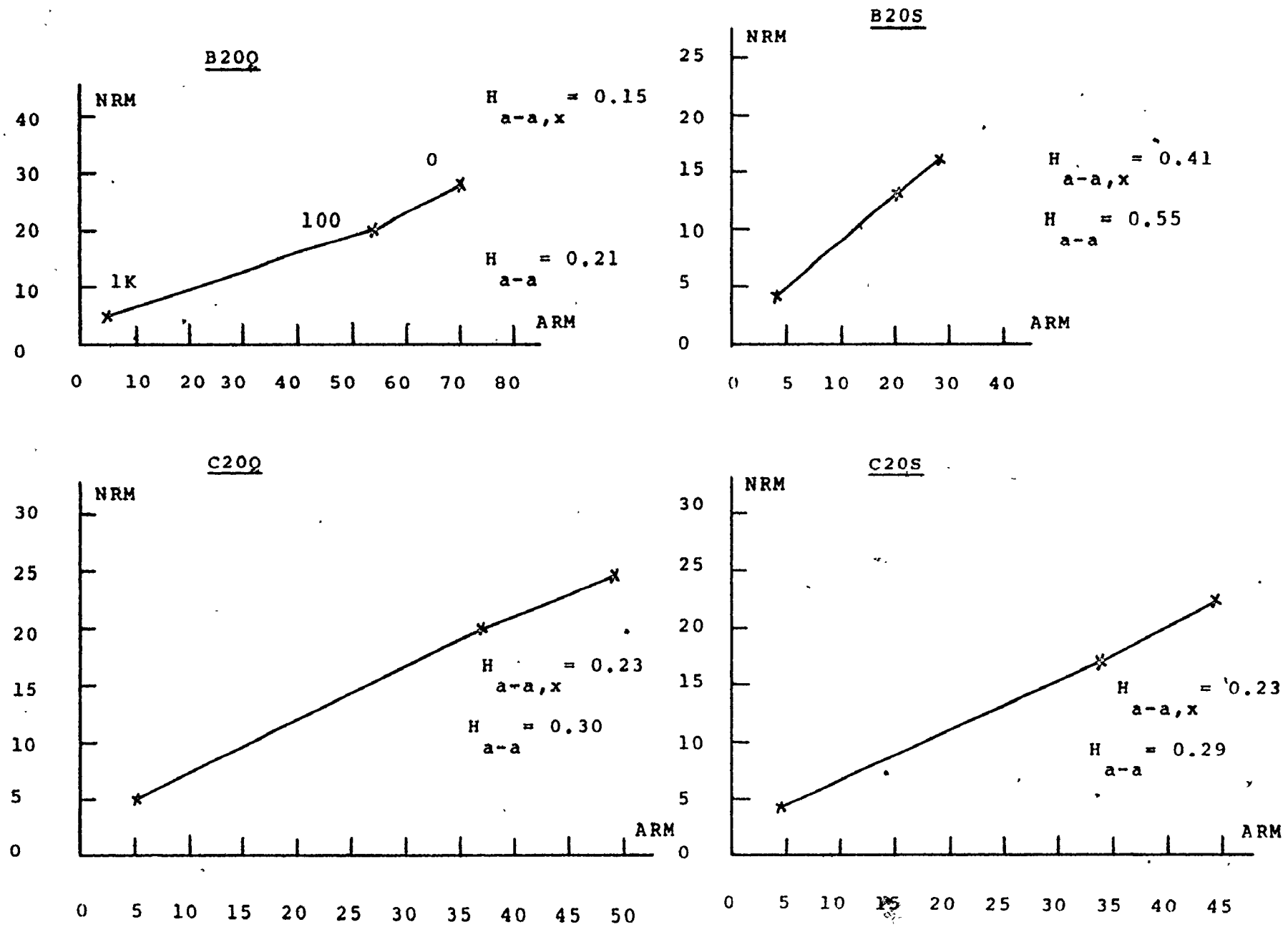
B20Q
NRM
ARM
H = 0.15
a-a,x
H = 0.21
a-a
0
100
1K
B20S
H = 0.41
a-a,x
H = 0.55
a-a
C20Q
H = 0.23
a-a,x
H = 0.30
a-a
C20S
H = 0.23
a-a,x
H = 0.29
a-a

Figure 24

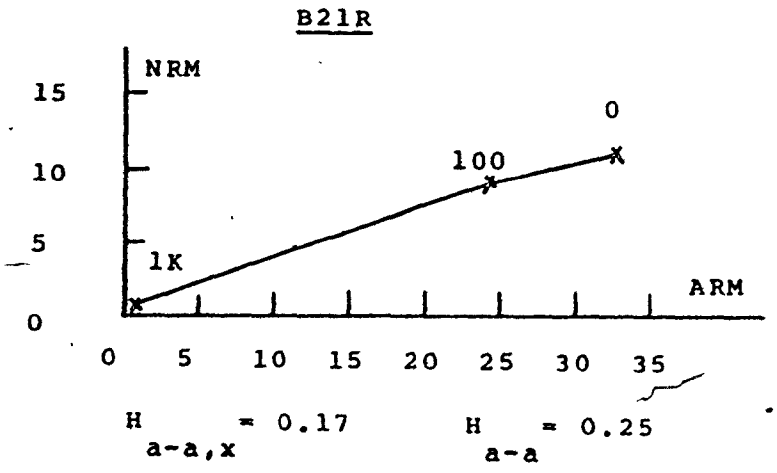
B21R
NRM
15
10
5
0
0
100
1K
ARM
0 5 10 15 20 25 30 35
H a-a,x = 0.17
H a-a = 0.25

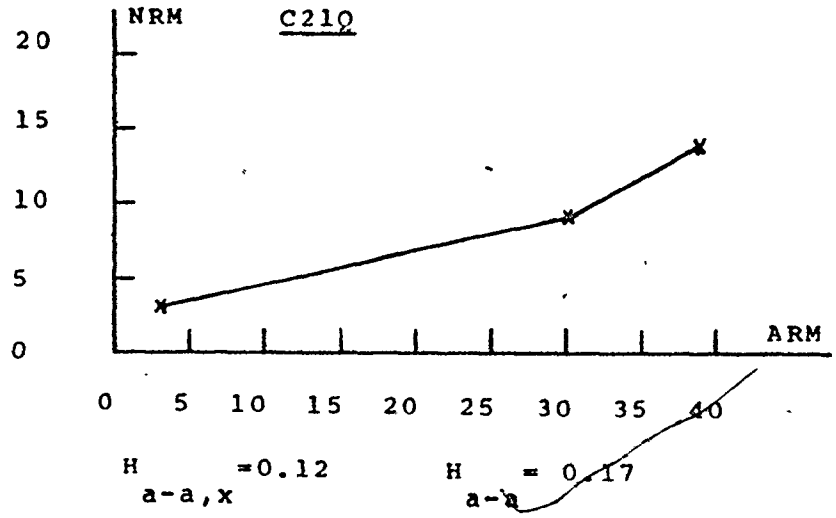
NRM
C210
20
15
10
5
0
ARM
0 5 10 15 20 25 30 35 40
H a-a,x =0.12
H a-a = 0.17

Figure 25

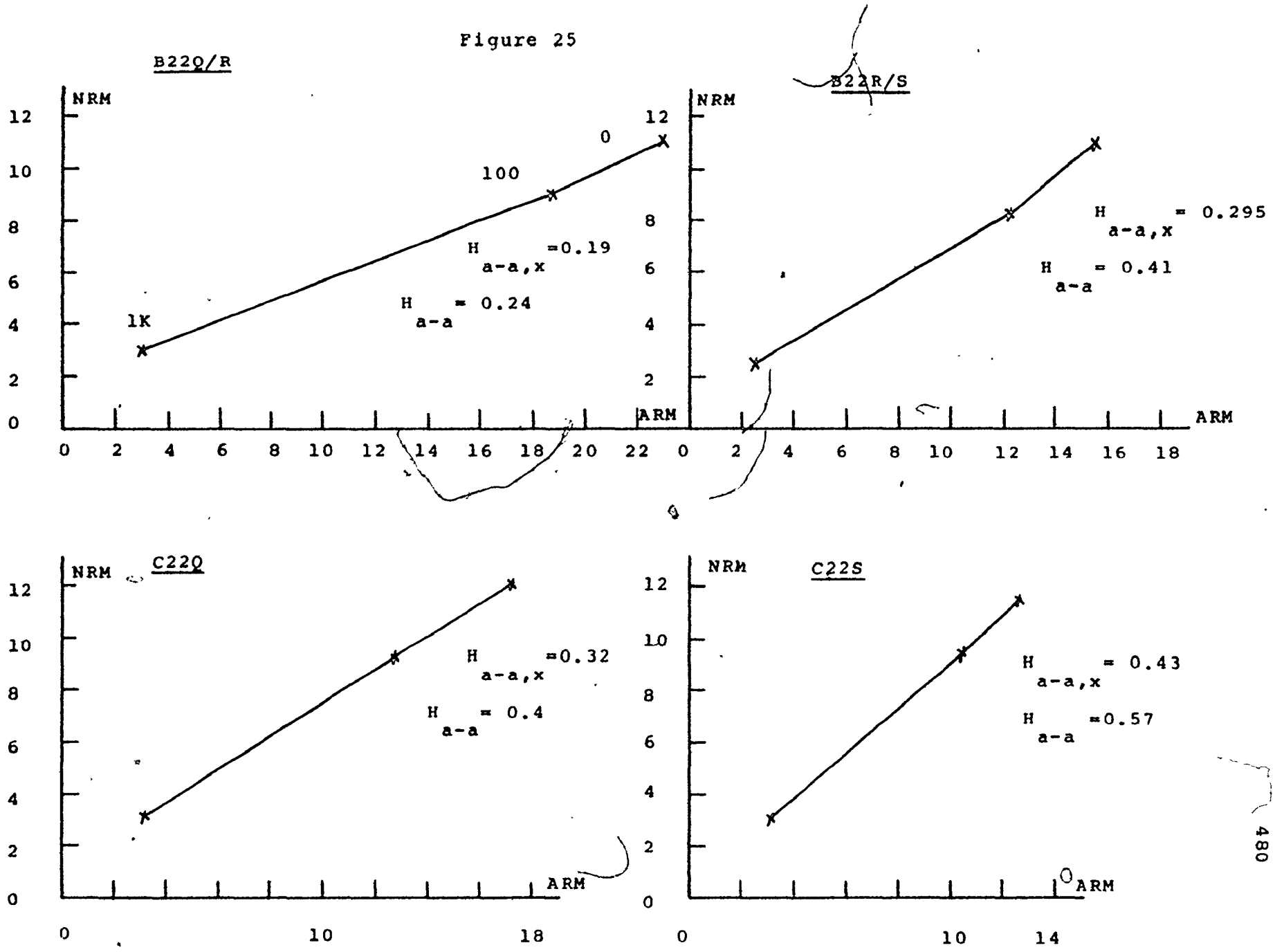
B22Q/R
NRM
ARM
0
100
1K
H a-a,x =0.19
H a-a = 0.24
B22R/S
H a-a,x = 0.295
H a-a = 0.41
C22Q
H a-a,x =0.32
H a-a = 0.4
C22S
H a-a,x = 0.43
H a-a =0.57

Figure 26

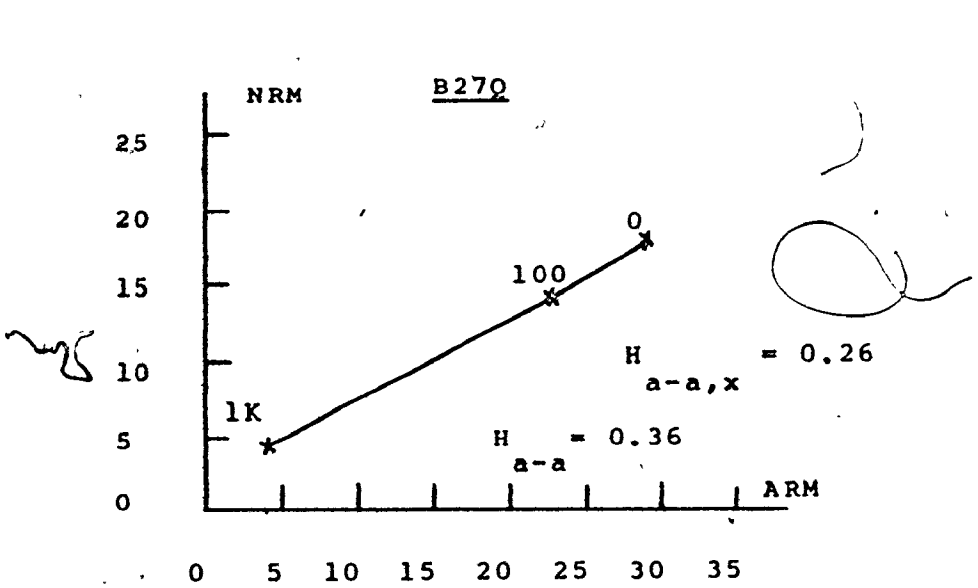
NRM
B27O
25
20
15
10
5
0
0
100
1K
H a-a,x = 0.26
H a-a = 0.36
ARM
0 5 10 15 20 25 30 35

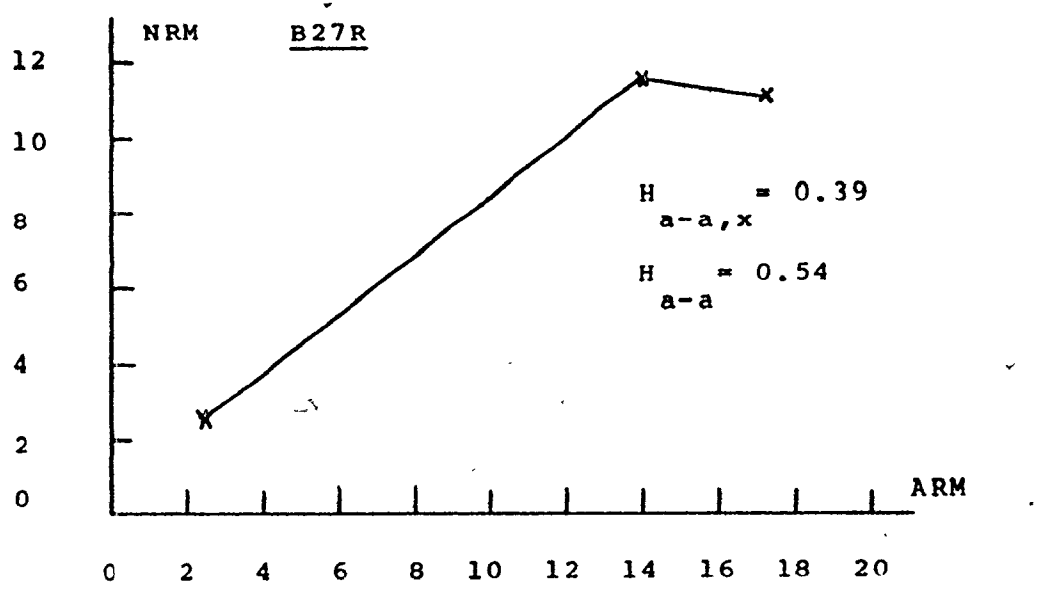
NRM
B27R
12
10
8
6
4
2
0
H a-a,x = 0.39
H a-a = 0.54
ARM
0 2 4 6 8 10 12 14 16 18 20

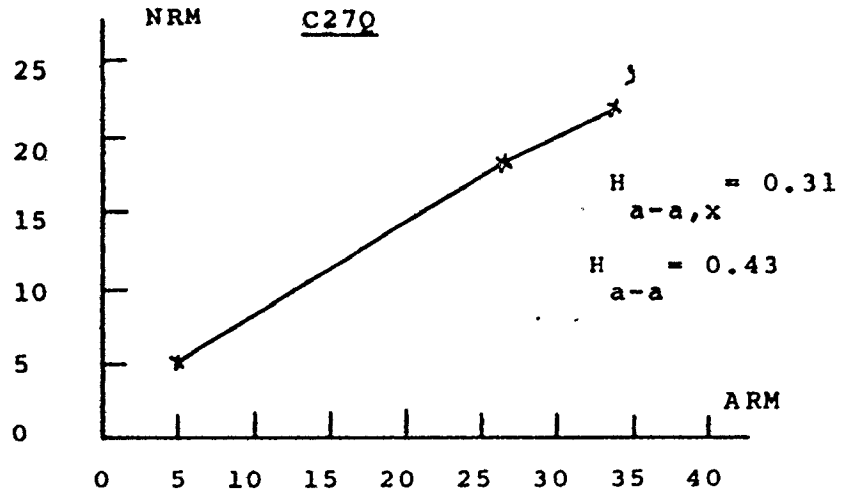
NRM
C27O
25
20
15
10
5
0
H a-a,x = 0.31
H a-a = 0.43
ARM
0 5 10 15 20 25 30 35 40

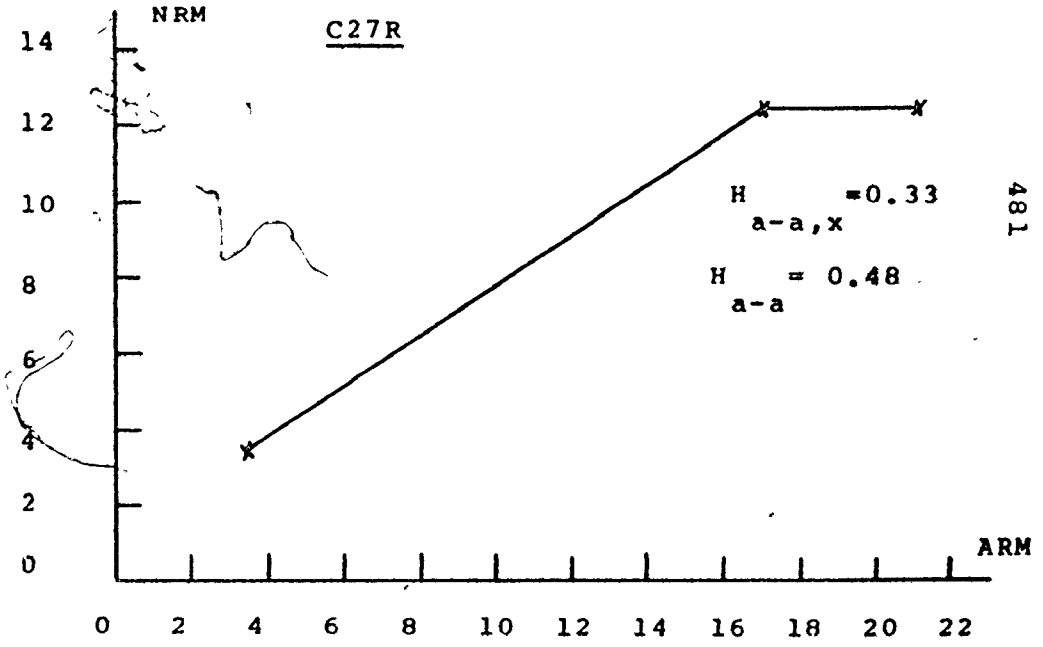
NRM
C27R
14
12
10
8
6
4
2
0
H a-a,x =0.33
H a-a = 0.48
ARM
0 2 4 6 8 10 12 14 16 18 20 22

Figure 27

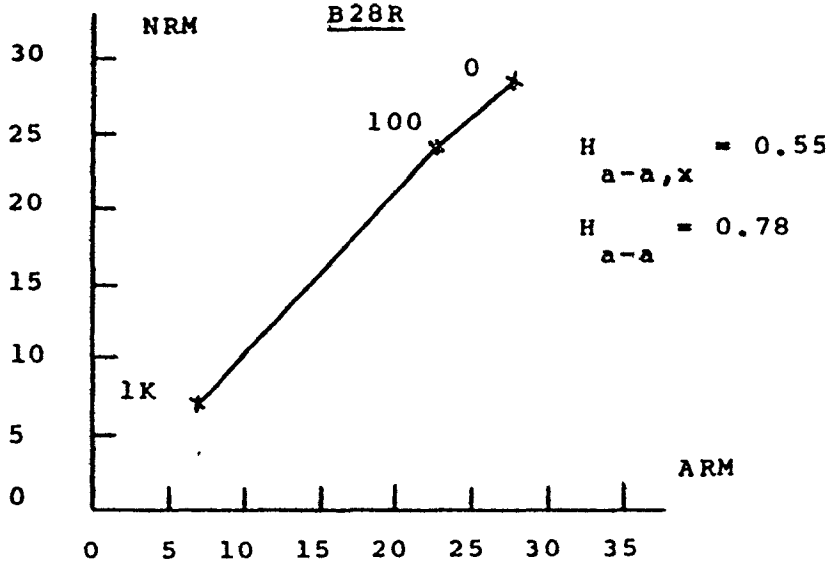
B28R
NRM
ARM
0
100
1K
$H_{a-a,x}$ = 0.55
H_{a-a} = 0.78

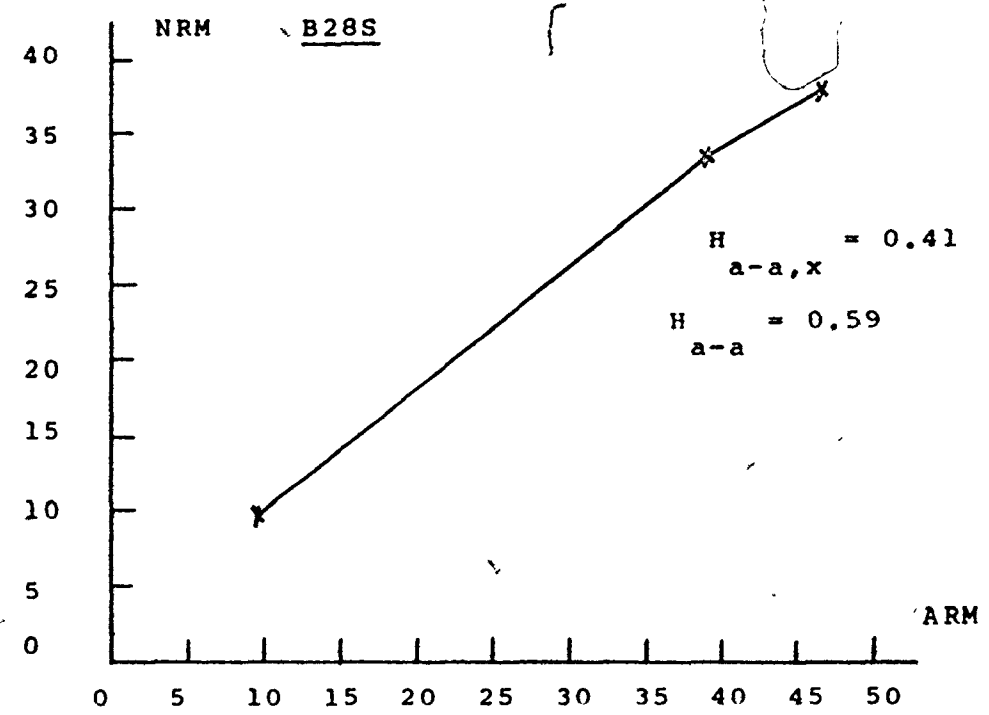
B28S
NRM
ARM
$H_{a-a,x}$ = 0.41
H_{a-a} = 0.59

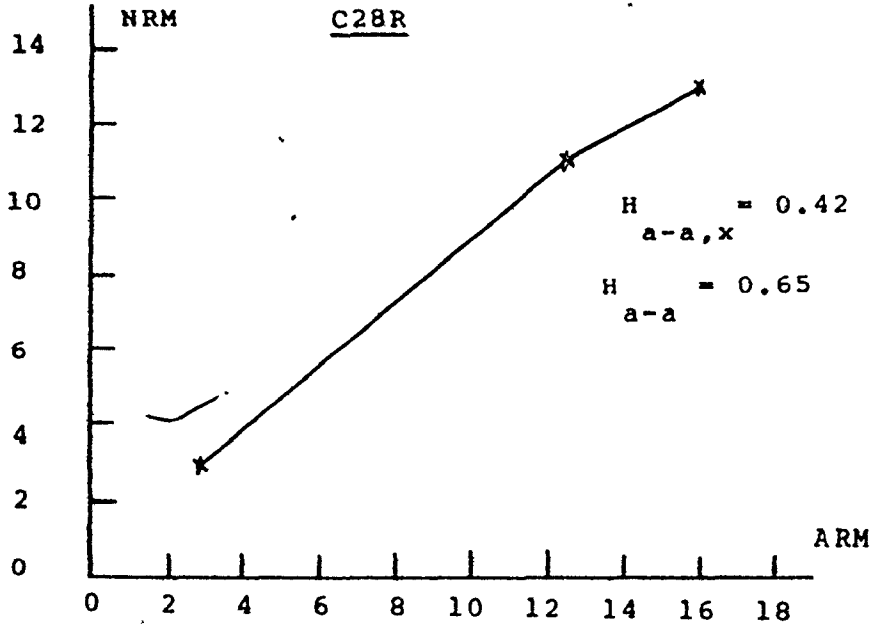
C28R
NRM
ARM
$H_{a-a,x}$ = 0.42
H_{a-a} = 0.65

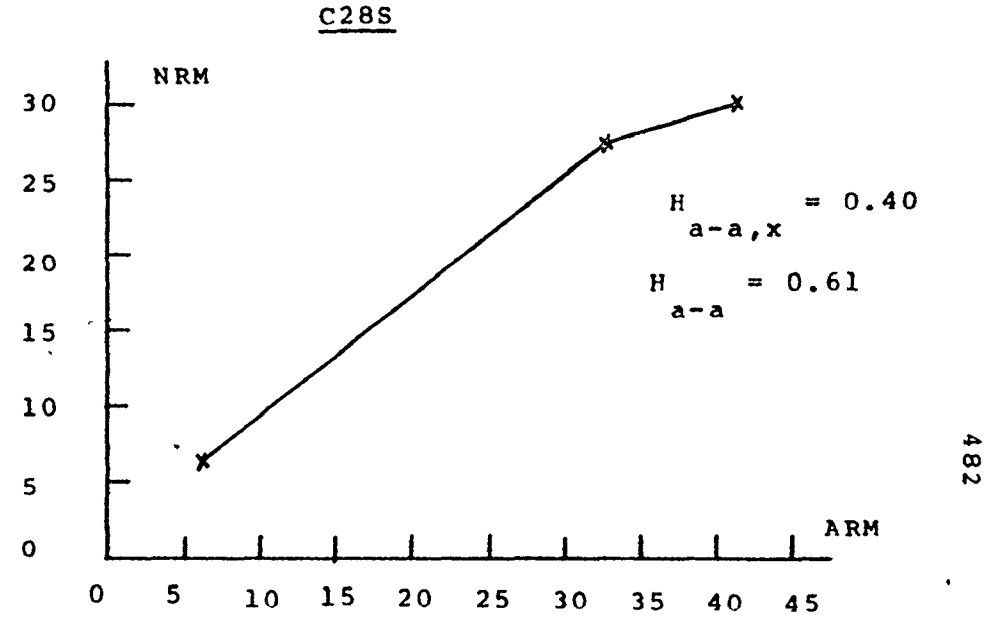
C28S
NRM
ARM
$H_{a-a,x}$ = 0.40
H_{a-a} = 0.61

Figure 28

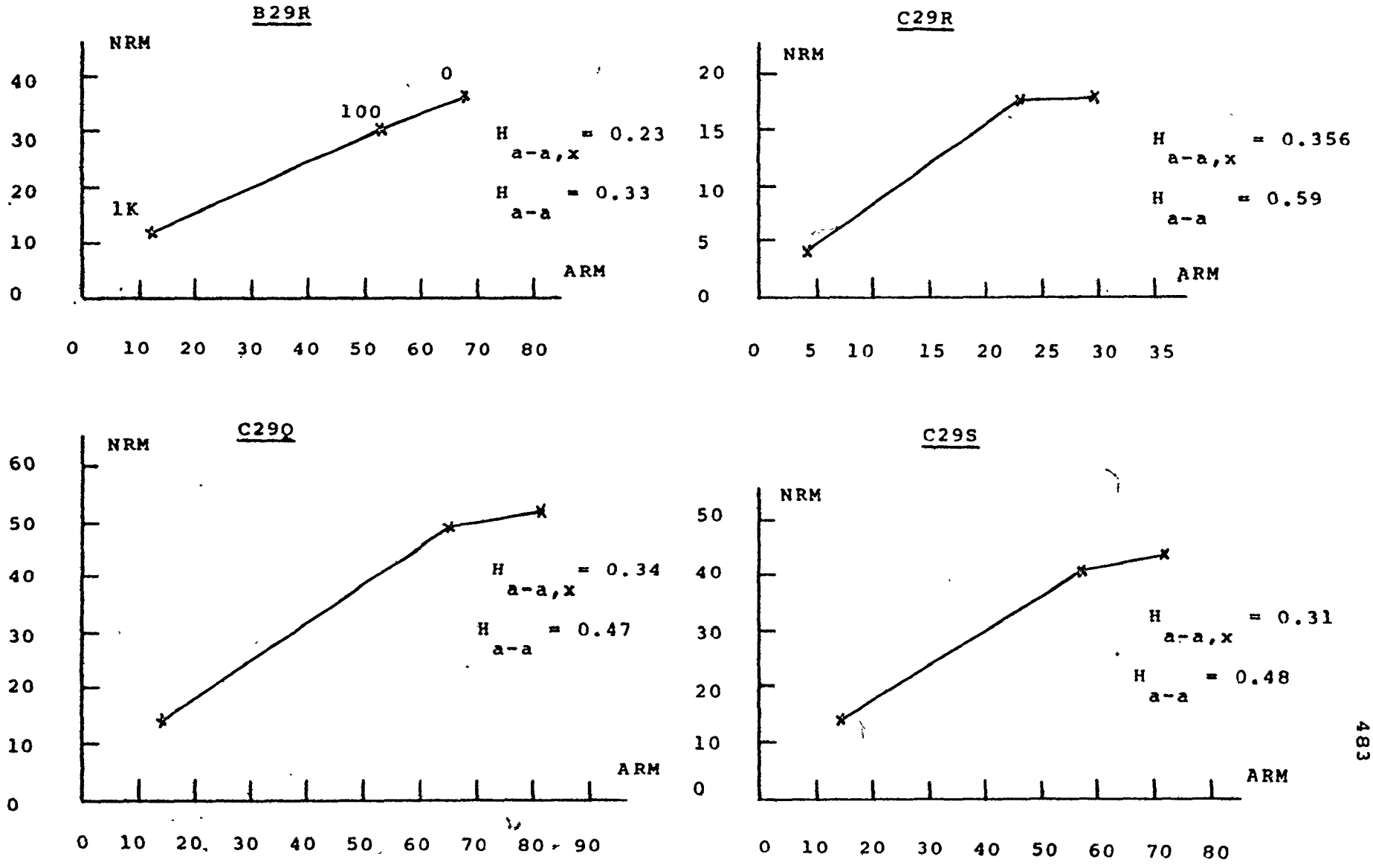
B29R
NRM
ARM
0
100
1K
H a-a,x = 0.23
H a-a = 0.33
C29R
H a-a,x = 0.356
H a-a = 0.59
C29O
H a-a,x = 0.34
H a-a = 0.47
C29S
H a-a,x = 0.31
H a-a = 0.48

Figure 29

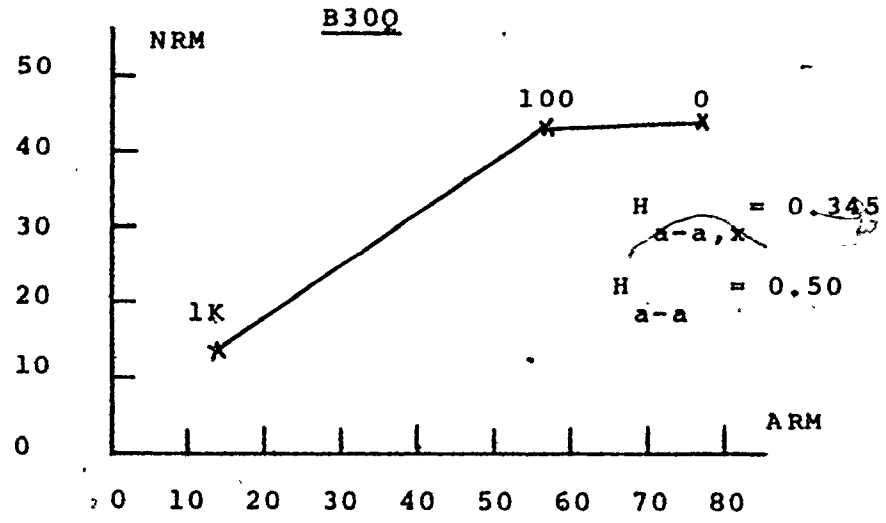
B30Q
NRM
50
40
30
20
10
0
100
0
1K
H a-a,x = 0.345
H a-a = 0.50
ARM
0 10 20 30 40 50 60 70 80

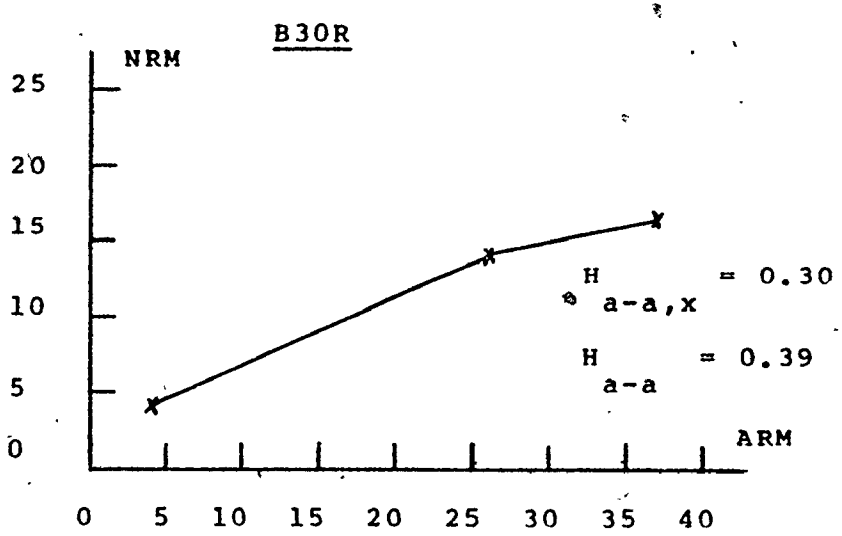
B30R
NRM
25
20
15
10
5
0
H a-a,x = 0.30
H a-a = 0.39
ARM
0 5 10 15 20 25 30 35 40

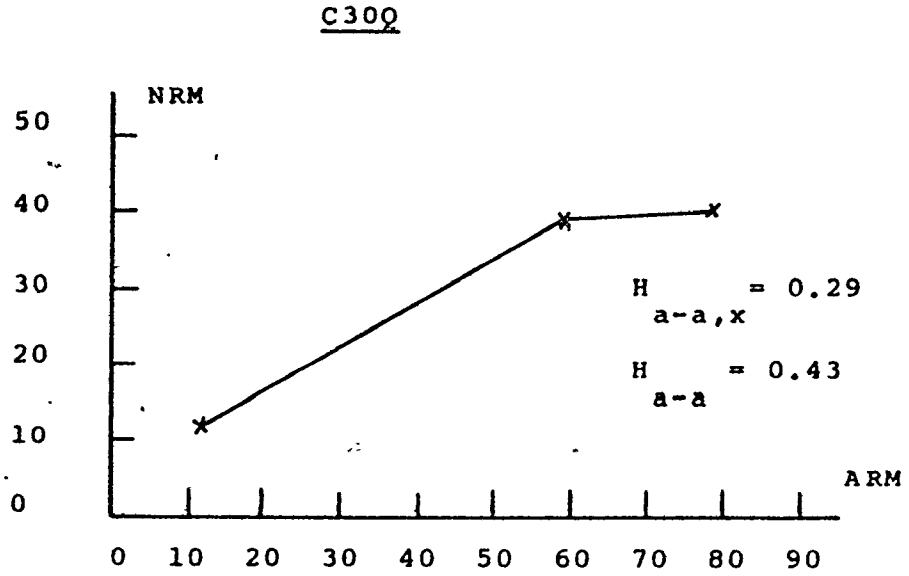
C30Q
NRM
50
40
30
20
10
0
H a-a,x = 0.29
H a-a = 0.43
ARM
0 10 20 30 40 50 60 70 80 90

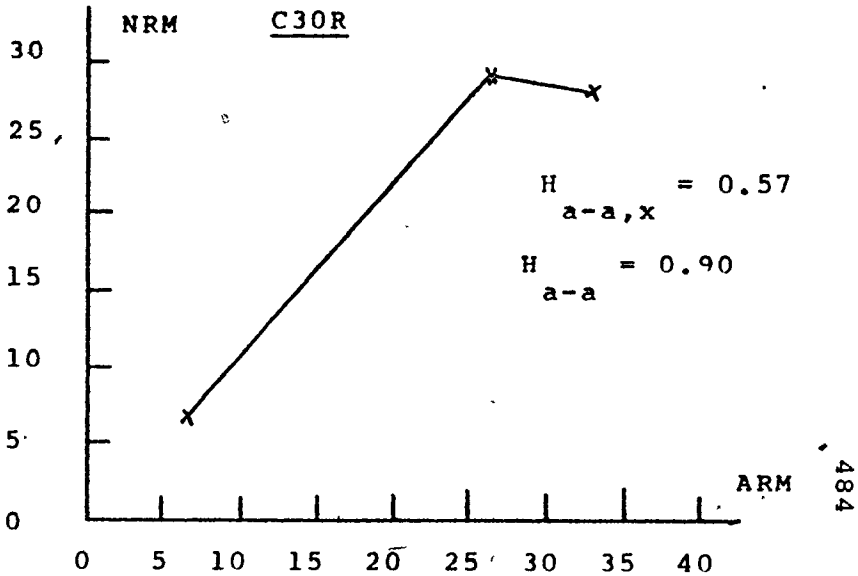
NRM
C30R
30
25
20
15
10
5
0
H a-a,x = 0.57
H a-a = 0.90
ARM
0 5 10 15 20 25 30 35 40

Figure 30

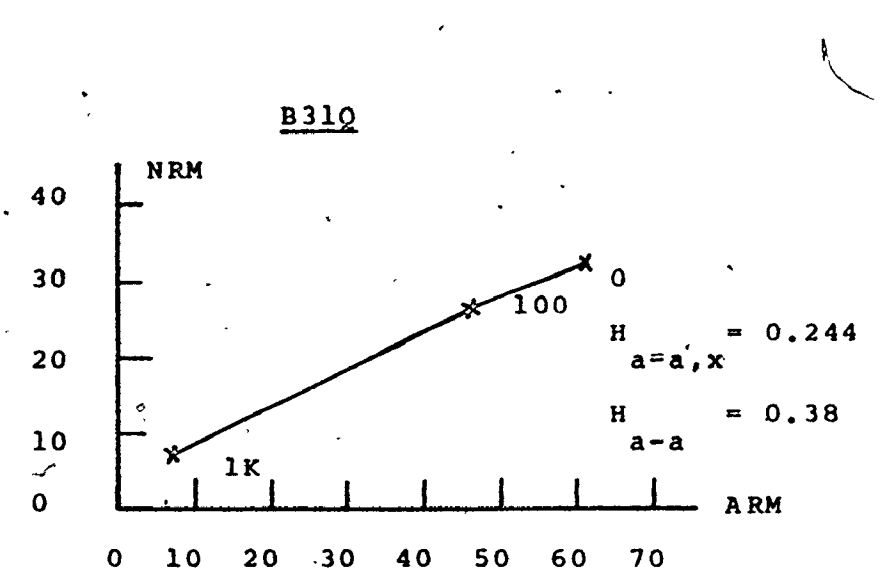
B310
NRM
40
30
20
10
0
0
100
1K
H a=a,x = 0.244
H a-a = 0.38
ARM
0 10 20 30 40 50 60 70

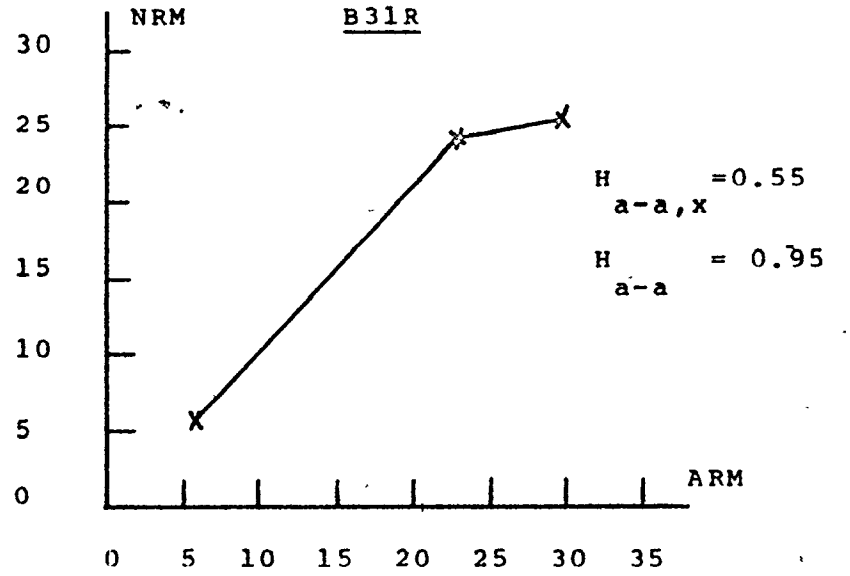
B31R
NRM
30
25
20
15
10
5
0
H a-a,x =0.55
H a-a = 0.95
ARM
0 5 10 15 20 25 30 35

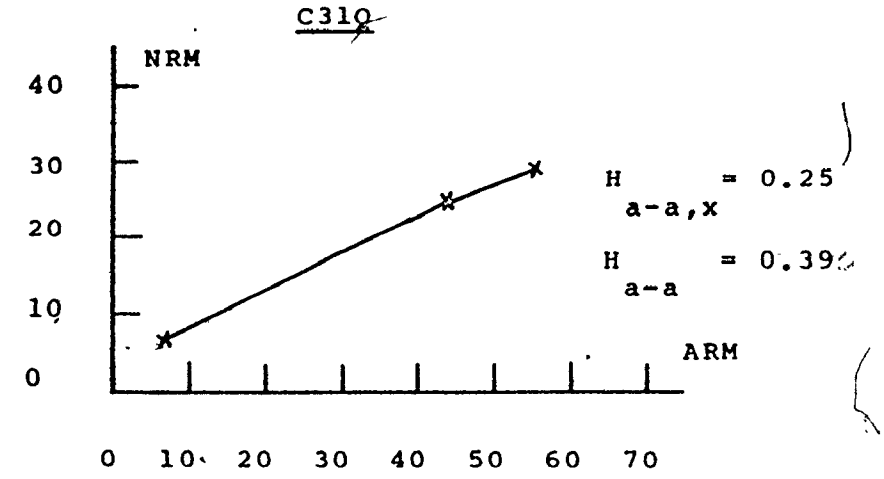
C310
NRM
40
30
20
10
0
H a-a,x = 0.25
H a-a = 0.39
ARM
0 10 20 30 40 50 60 70

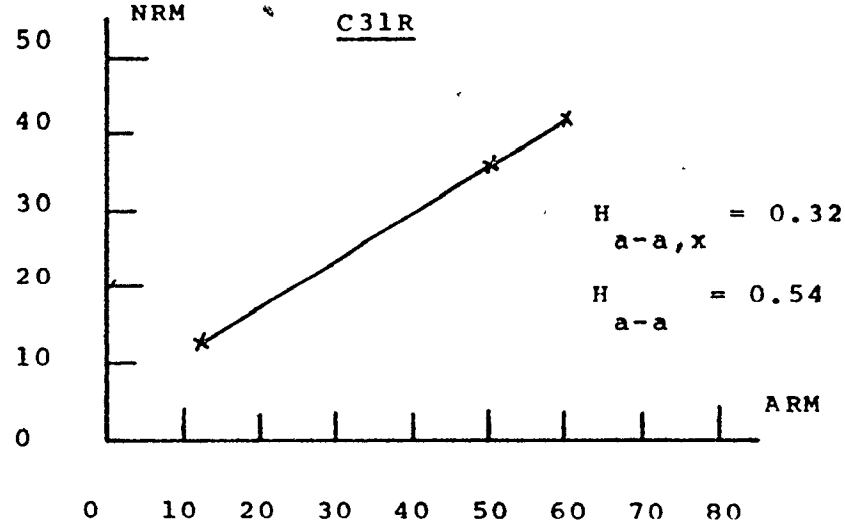
C31R
NRM
50
40
30
20
10
0
H a-a,x = 0.32
H a-a = 0.54
ARM
0 10 20 30 40 50 60 70 80

Figure 31

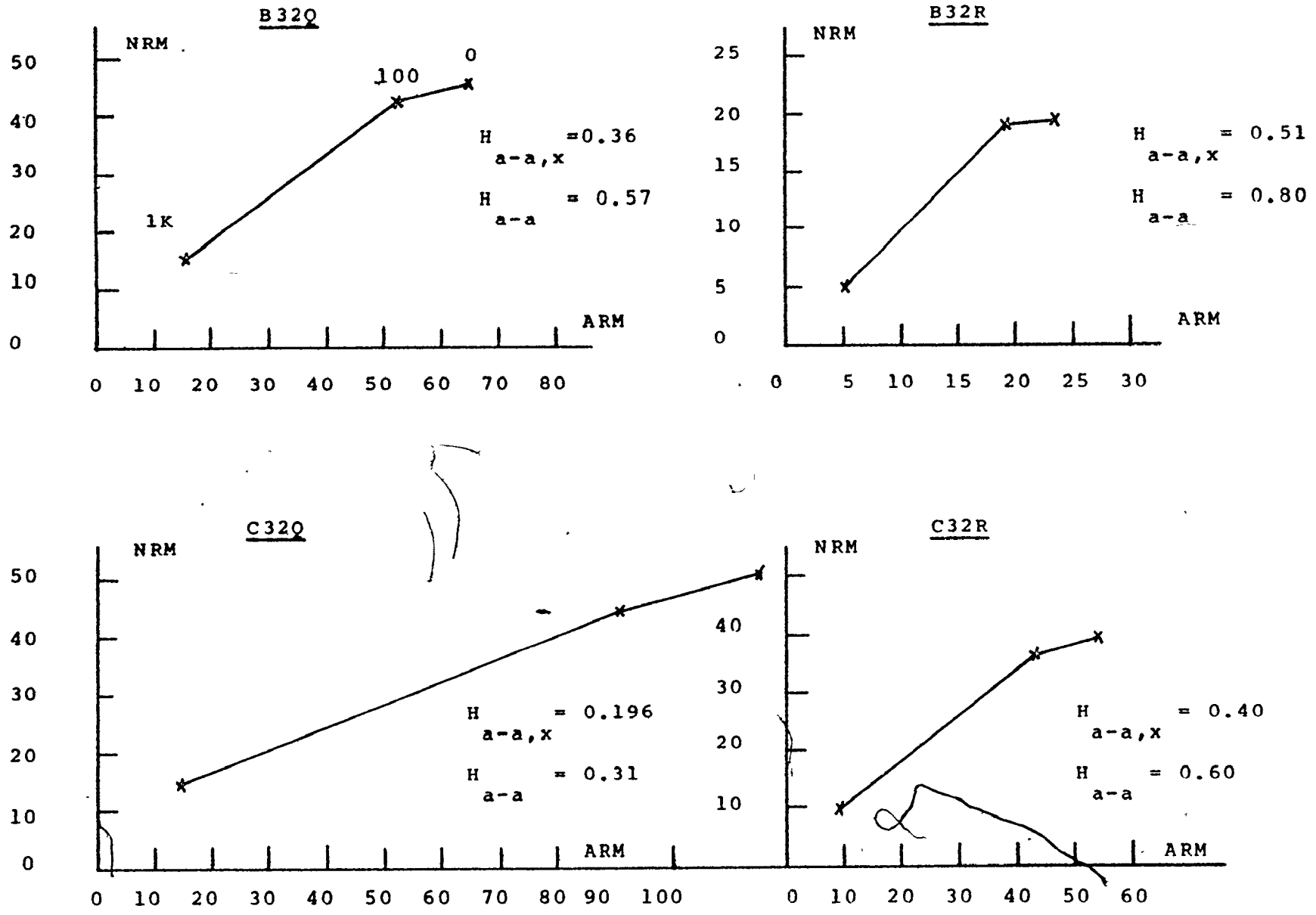
B32Q
NRM
50
40
30
20
10
0
0
100
1K
H a-a,x =0.36
H a-a = 0.57
ARM
0 10 20 30 40 50 60 70 80
B32R
NRM
25
20
15
10
5
0
H a-a,x = 0.51
H a-a = 0.80
ARM
0 5 10 15 20 25 30
C32Q
NRM
50
40
30
20
10
0
H a-a,x = 0.196
H a-a = 0.31
ARM
0 10 20 30 40 50 60 70 80 90 100
C32R
NRM
40
30
20
10
H a-a,x = 0.40
H a-a = 0.60
ARM
0 10 20 30 40 50 60

Figure 32

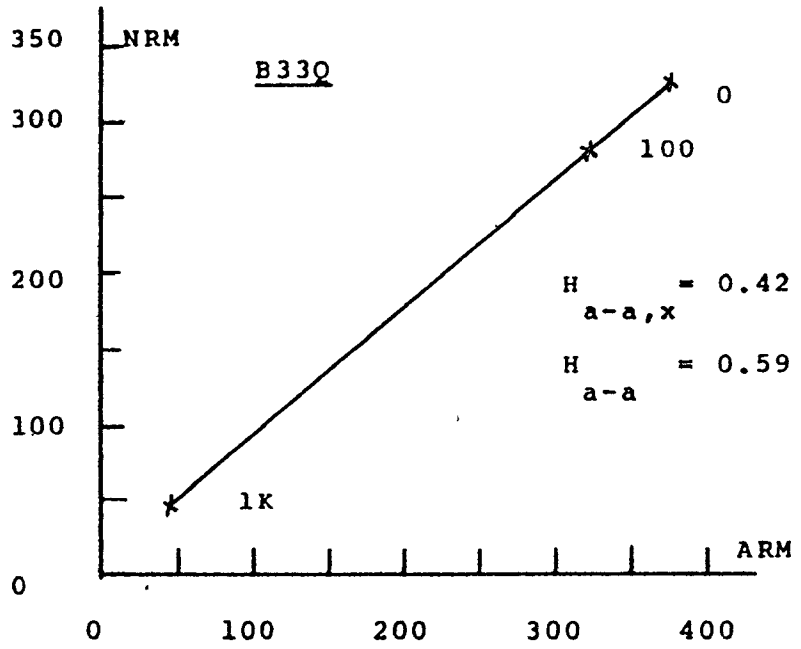
B33Q
NRM
ARM
0
100
1K
H a-a,x = 0.42
H a-a = 0.59
0
100
200
300
350
400

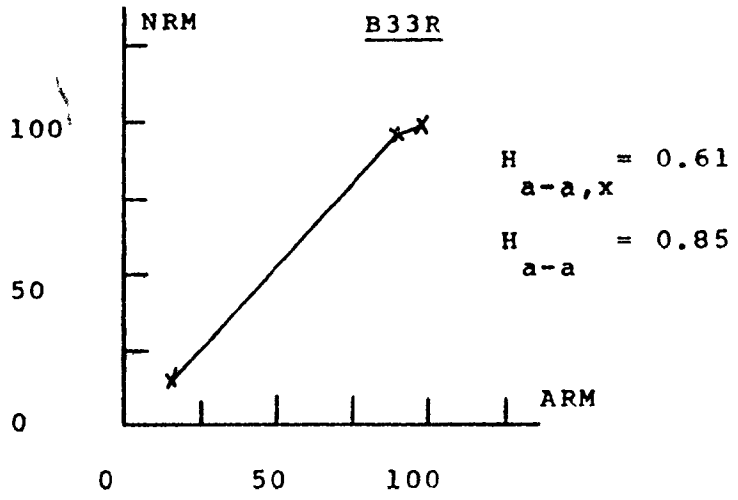
B33R
NRM
ARM
H a-a,x = 0.61
H a-a = 0.85
0
50
100

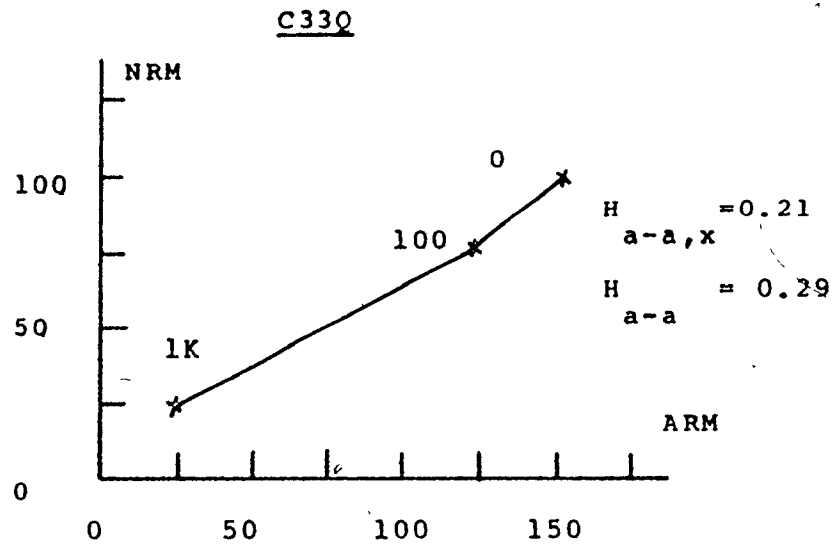
C33Q
NRM
ARM
0
100
1K
H a-a,x =0.21
H a-a = 0.29
0
50
100
150

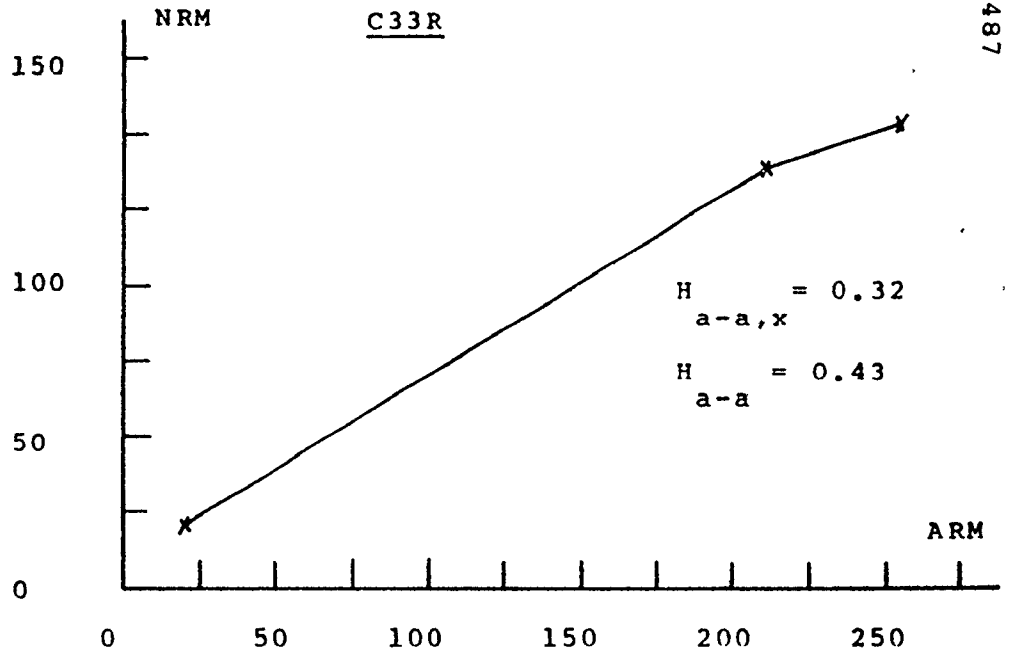
C33R
NRM
ARM
H a-a,x = 0.32
H a-a = 0.43
0
50
100
150
200
250

Figure 33

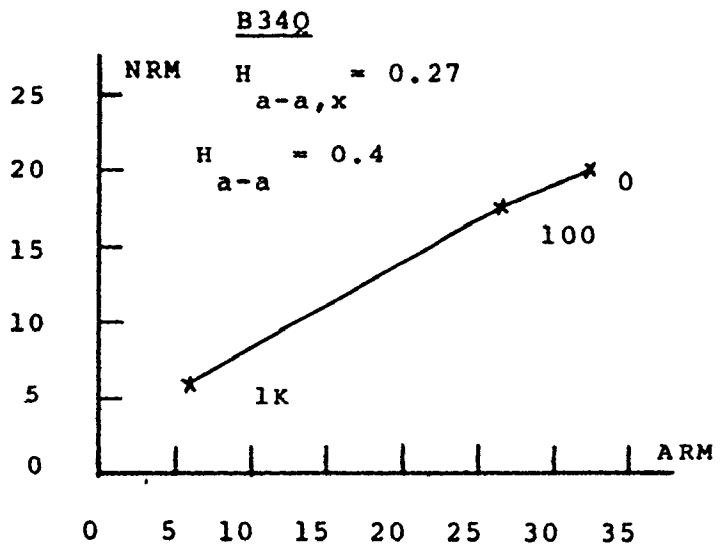
B34Q
NRM
H a-a,x = 0.27
H a-a = 0.4
0
100
1K
ARM
25
20
15
10
5
0
0 5 10 15 20 25 30 35

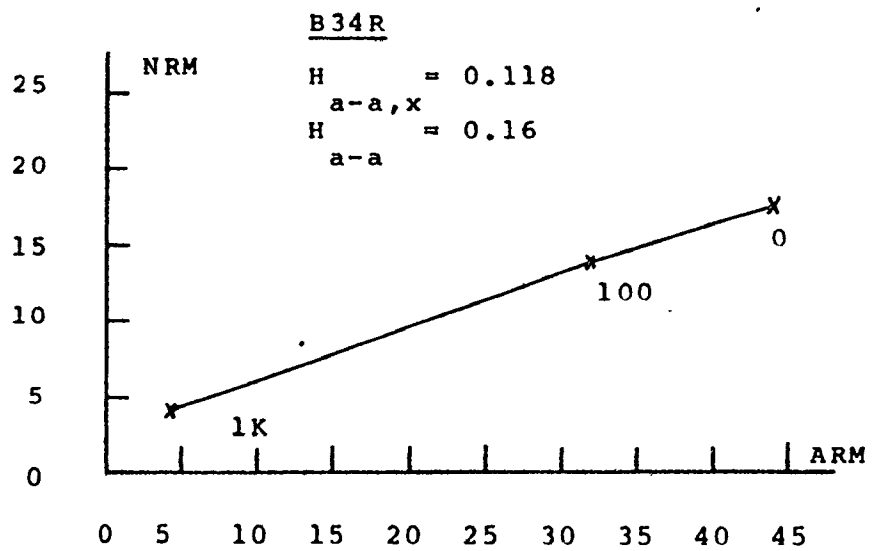
B34R
NRM
H a-a,x = 0.118
H a-a = 0.16
0
100
1K
ARM
25
20
15
10
5
0
0 5 10 15 20 25 30 35 40 45

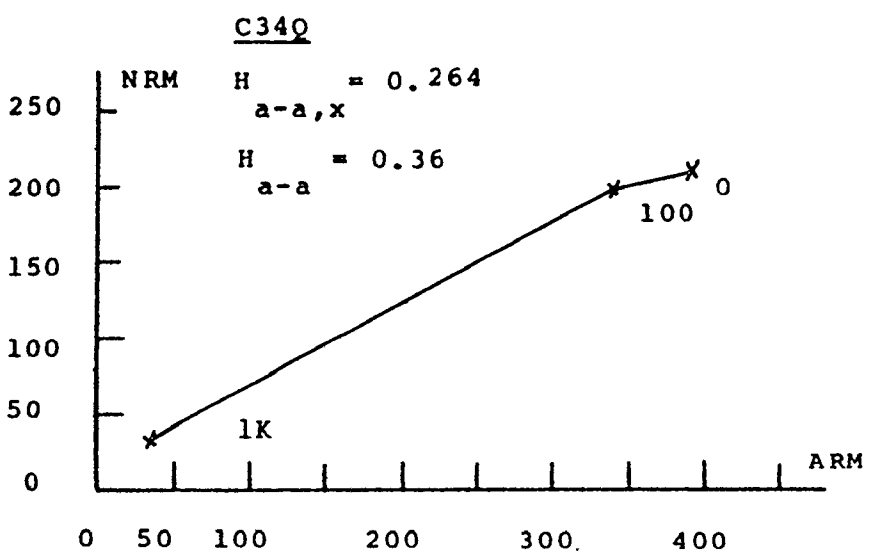
C34Q
NRM
H a-a,x = 0.264
H a-a = 0.36
0
100
1K
ARM
250
200
150
100
50
0
0 50 100 200 300 400

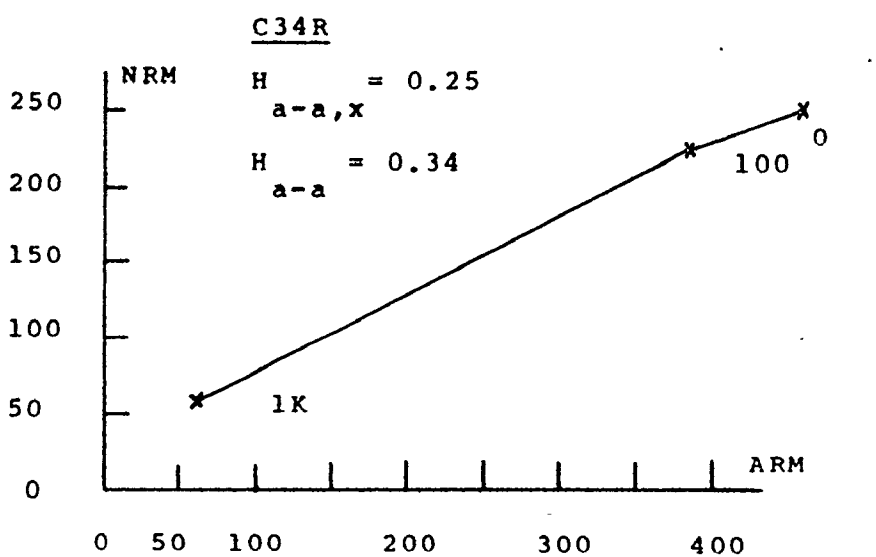
C34R
NRM
H a-a,x = 0.25
H a-a = 0.34
0
100
1K
ARM
250
200
150
100
50
0
0 50 100 200 300 400

Figure 34

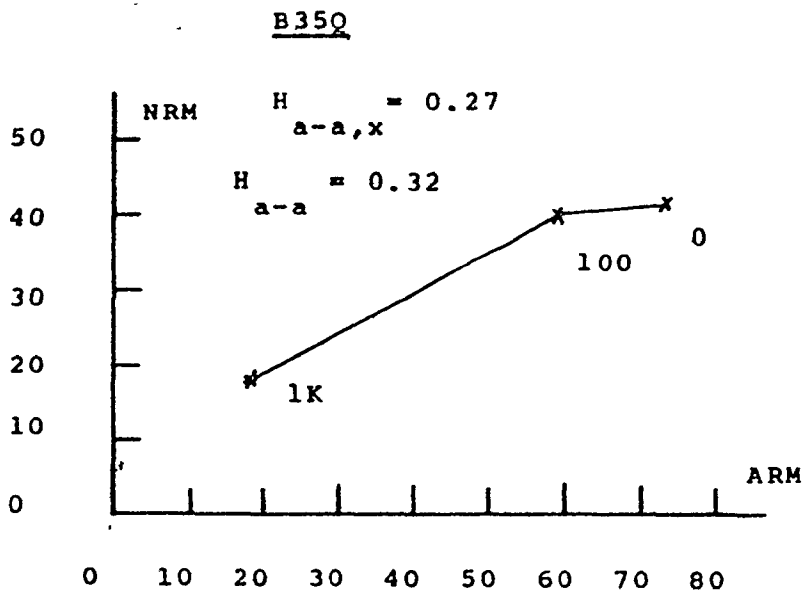
B350
NRM
H a-a,x = 0.27
H a-a = 0.32
1K
100
0
ARM
0 10 20 30 40 50 60 70 80
0 10 20 30 40 50

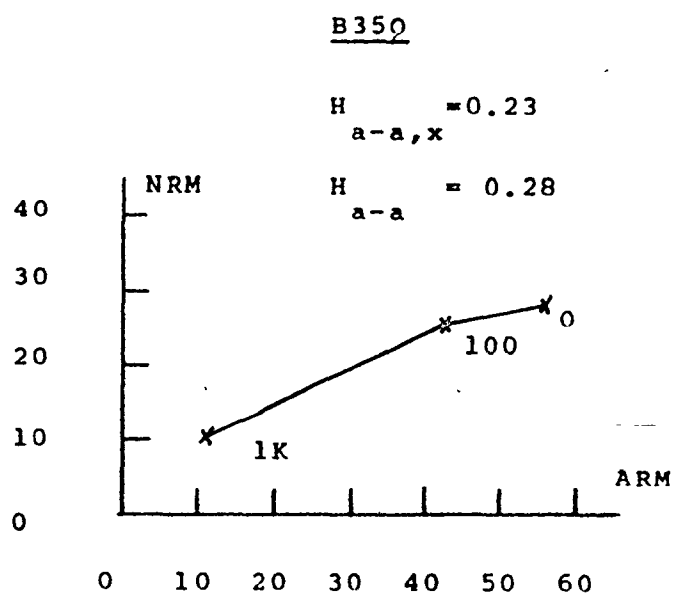
B350
NRM
H a-a,x =0.23
H a-a = 0.28
1K
100
0
ARM
0 10 20 30 40 50 60
0 10 20 30 40

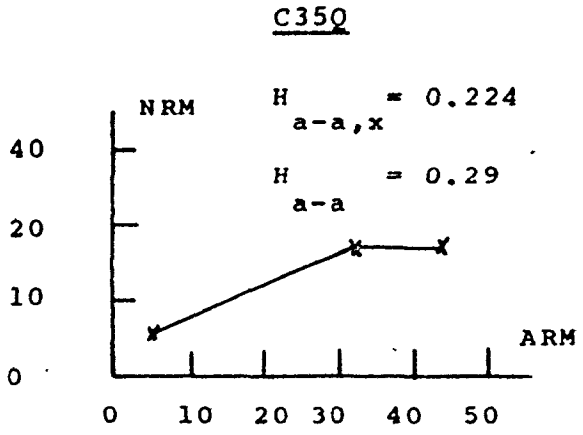
C350
NRM
H a-a,x = 0.224
H a-a = 0.29
ARM
0 10 20 30 40 50
0 10 20 30 40

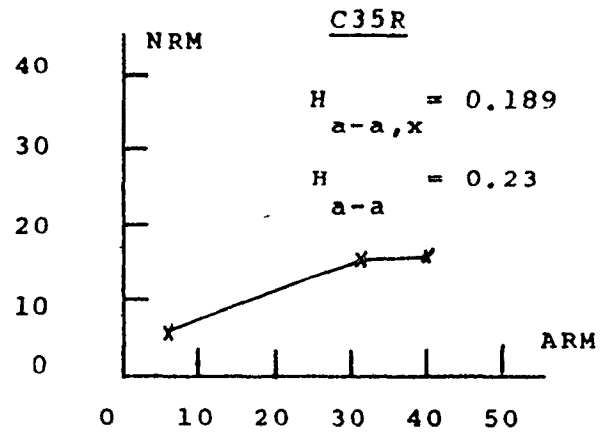
C35R
NRM
H a-a,x = 0.189
H a-a = 0.23
ARM
0 10 20 30 40 50
0 10 20 30 40

Figure 35.

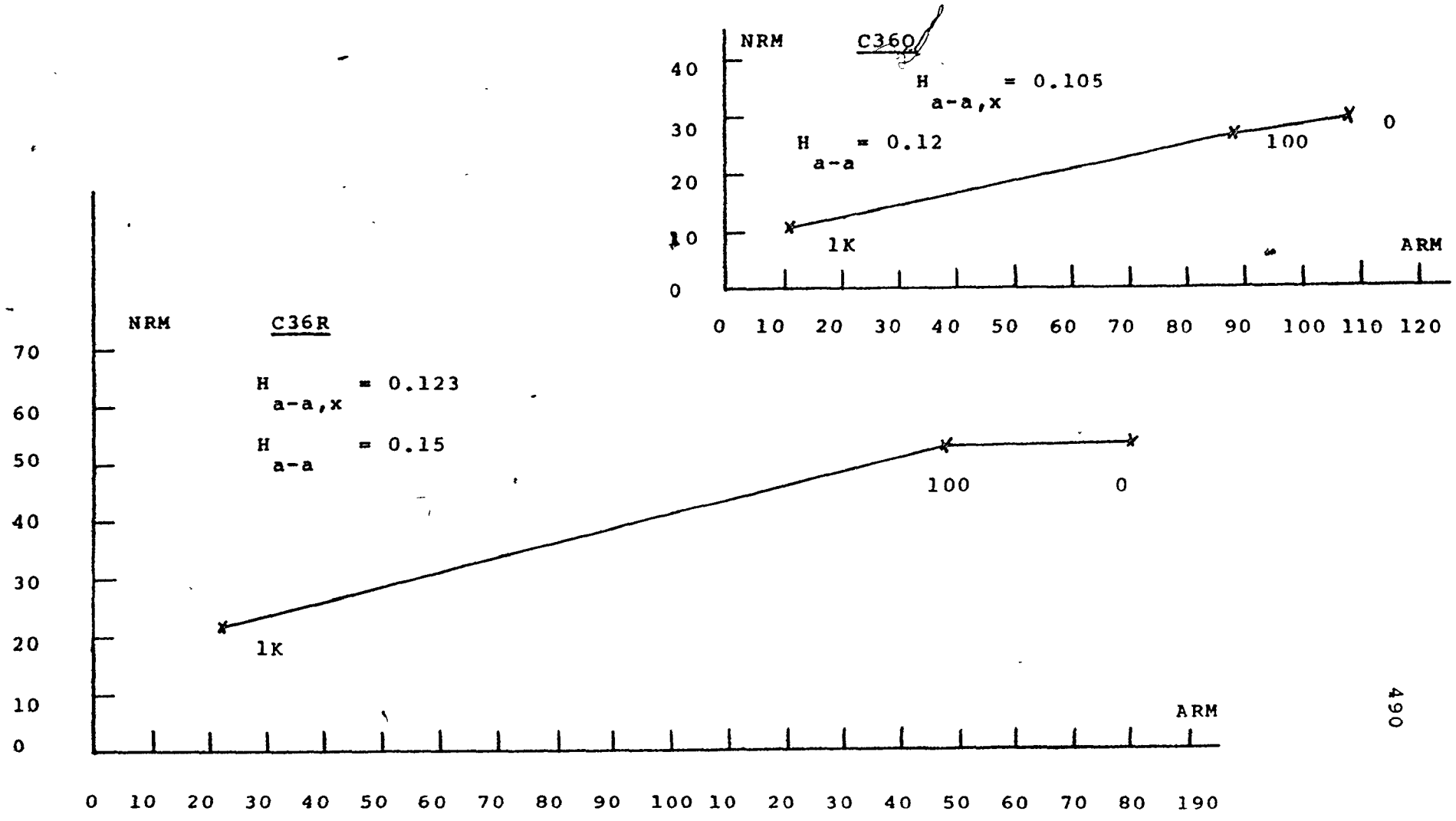
NRM
C360
H a-a,x = 0.105
H a-a = 0.12
0
100
1K
ARM
0 10 20 30 40 50 60 70 80 90 100 110 120
NRM
C36R
H a-a,x = 0.123
H a-a = 0.15
100
0
1K
ARM
0 10 20 30 40 50 60 70 80 90 100 10 20 30 40 50 60 70 80 190

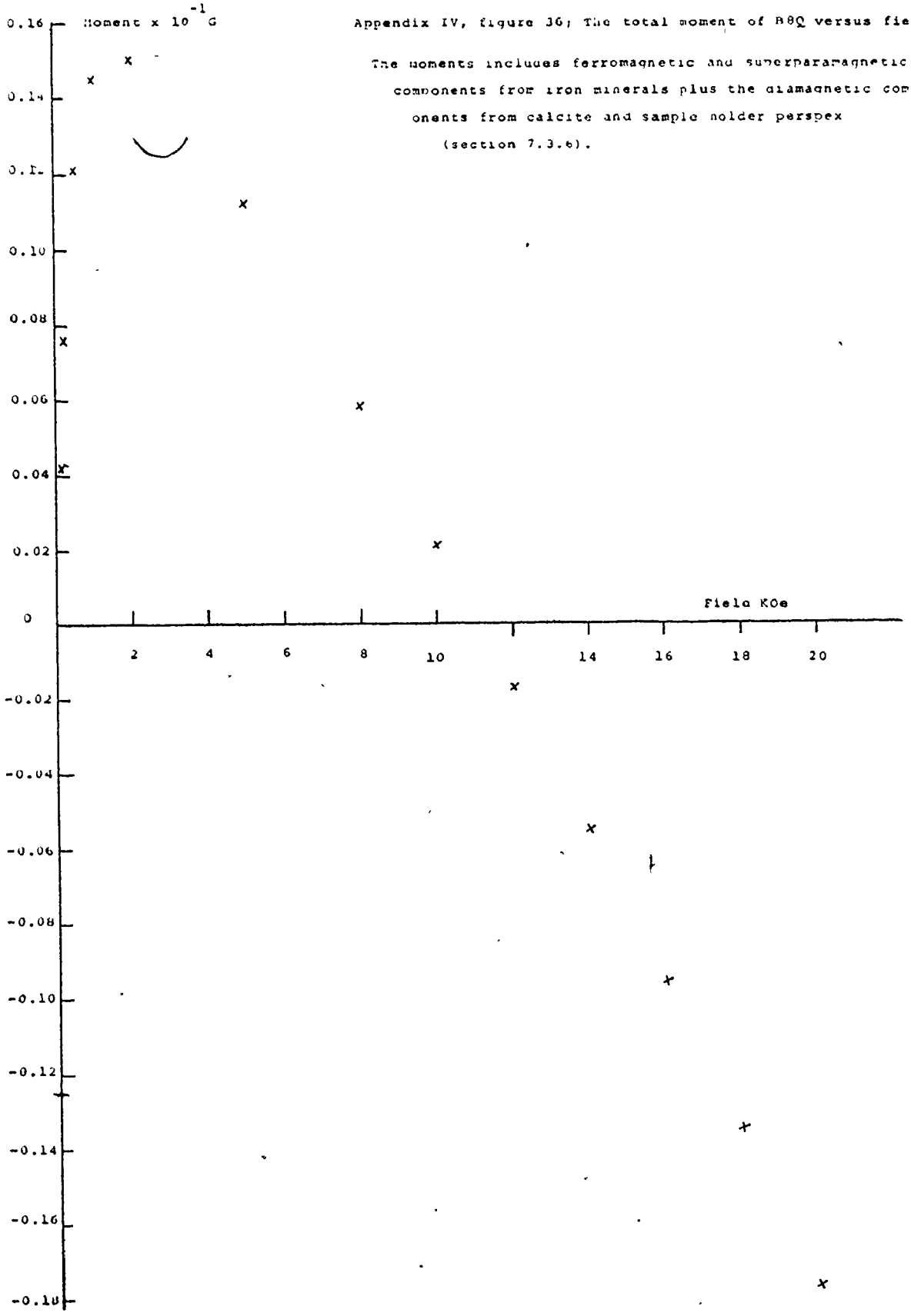

Appendix IV, figure 36; The total moment of B8Q versus field.

The moments includes ferromagnetic and superparamagnetic components from iron minerals plus the diamagnetic components from calcite and sample holder perspex (section 7.3.6).

APPENDIX V

Mössbauer Spectra and Parameters

for:

1) RCB (figures 1-3) - the target was prepared from the soil above the flowstone (section 5.1)

2) OULF (figures 4-6) - the target was prepared from clay blobs which had become included and cemented into the calcite (section 5.5).

3) GYS1 (figures 7-9) - a gray soil associated with the speleothems GYS1 and GYS2 from the Graveyard, Lancaster Hole, England (Appendix II)

4) SJL5 (= SJLS; figures 10 & 11) - the target was prepared from the magnetic extract from speleothem SJLS, and set in a BN_3 matrix (section 6.2)

The samples were prepared by the author. The analyses, site-fitting and interpretation are by Prof. T. Birchall of the Chemistry Dept. of McMaster University.

SOIL SAMPLES (A. LATHAM)

All three soil samples at 298°K have ^{57}Fe Mössbauer spectra which are composed of a main central doublet. These doublets arise from FeIII components. In addition G.Y.S.I. clearly shows the presence of an FeII doublet while O.U.L.F. at room temperature shows that a similar FeII doublet may be present. Attempts to fit these spectra to a single FeIII site, and an FeIII and an FeII in the case of G.Y.S.I. do not give satisfactory fits (see Figs. 1, 4 & 7). In all cases it was necessary to introduce a second FeIII component when the X^2 values dropped significantly and the visual fits (Figs. 2, 5, 8) are clearly much better. The spectra analyzed in this way are summarised in the Table1. The isomer shifts for the FeIII doublets are very similar but one site has a much greater quadrupole splitting than the other site. These data are similar to those reported for species such as α-, β-, γ-FeOOH as well as αFe_2O_3 in their paramagnetic forms (Goodman and Barrow, J. Physique C6-849, 1976. In G.Y.S.I. the FeII doublet has similar parameters to chlorite. The realtive %'s of each component are probably not more accurate than ±5% due to the overlapping nature of the spectra.

In order to check that two FeIII doublets are indeed present, low temperature spectra were recorded. All three spectra at 77K showed a magnetic component from one of the FeIII sites, the second FeIII component remained paramagnetic, and the FeII doublet was visible in O.U.L.F. as well as in the G.Y.S.I. soils. It would appear that it is the FeIII component with the higher quadrupole splitting which was ordered magnetically to give a magnetic field in the range 490-460 KOe, with a negative quadrupole splitting (2ϵ = --0.2). These data could appear to rule out the possibility that the magnetic component is pure αFeOOH (H = 504 KOe), but βFeOOH or α-Fe_2O_3 (fine particles) are more likely. The large line widths for the magnetic components (see Figs. 3, 6, 9) indicates that these magnetic components are not well ordered and

probably consist of a variety of slightly different sites arising from replacement of FeIII by other ions (Al III for example).

The S.J.L. 5 sample is magnetically ordered at room temperature with a maximum field of about 470 KOe: there appear to be three separate hyperfine fields present similar to those found in magnetite though the magnitude of the fields appear smaller - perhaps due to partial substitution by non-magnetic ions.

SOIL SAMPLES (A. LATHAM)

Appendix V; table 1

Sample	Temp °K	δ	Δ	Γ	H		X^2/D
		mm s^{-1}			kOe		
R.C.B. Soil	298	0.37	0.50	0.33	---	54.1	0.87
		0.35	0.80	0.50	---	45.9	
	77	0.45	0.62	0.62	---	26.5	1.12
		0.50	(-0.20)	----	492	73.5	
O.U.L.F. Soil	298	0.37	0.44	0.28	---	38.5	1.04
		0.36	0.70	0.52	---	61.5	
	77	0.45	0.64	0.87	---	23.3	1.00
		1.17	2.07	0.46	---	13.5	
		0.37	(-0.25)	----	463	63.2	
G.Y.S.I. Soil	298	0.37	0.48	0.28	---	31.5	1.24
		1.21	2.45	0.39	---	20.8	
		0.31	0.96	0.52	---	47.7	
	77	0.44	0.85	0.76	---	24.1	1.21
		1.23	2.76	0.52	---	15.3	
		0.47	(-0.24)	----	461	60.6	

Soil*	289K	δ	Δ	Γ
	1	0.37	0.93	0.94
	2	0.34	0.53	0.50

Two doublet fit for the soil sample at room temperature. At 77 K this becomes a mere complex spectrum due to one site being magnetically ordered: the other

	δ	Δ	Γ	H.
1	0.56	-	-	505 KOe
2	0.44	0.64	0.83	-

doublet remains, though slightly broadened. I do not have any plots for you yet as the plotter has been down.

The SJL5 sample which is magnetic at room temperature I have not been able to get to converge and the fit is not very good. The revised parameters for the three-site fit are as follows.

δ	H.
0.135mn s^{-1}	475KOe
0.267	435
0.56	422

Georges Dénès in my group will try and get you some plots when the plotter is fixed.

Tom Birchall,
Professor of Chemistry

Note * This soil is associated with the Petralona samples, section 5.6, and awaits further work.

Appendix V; figure 1

RCB soil, (1 site fit)

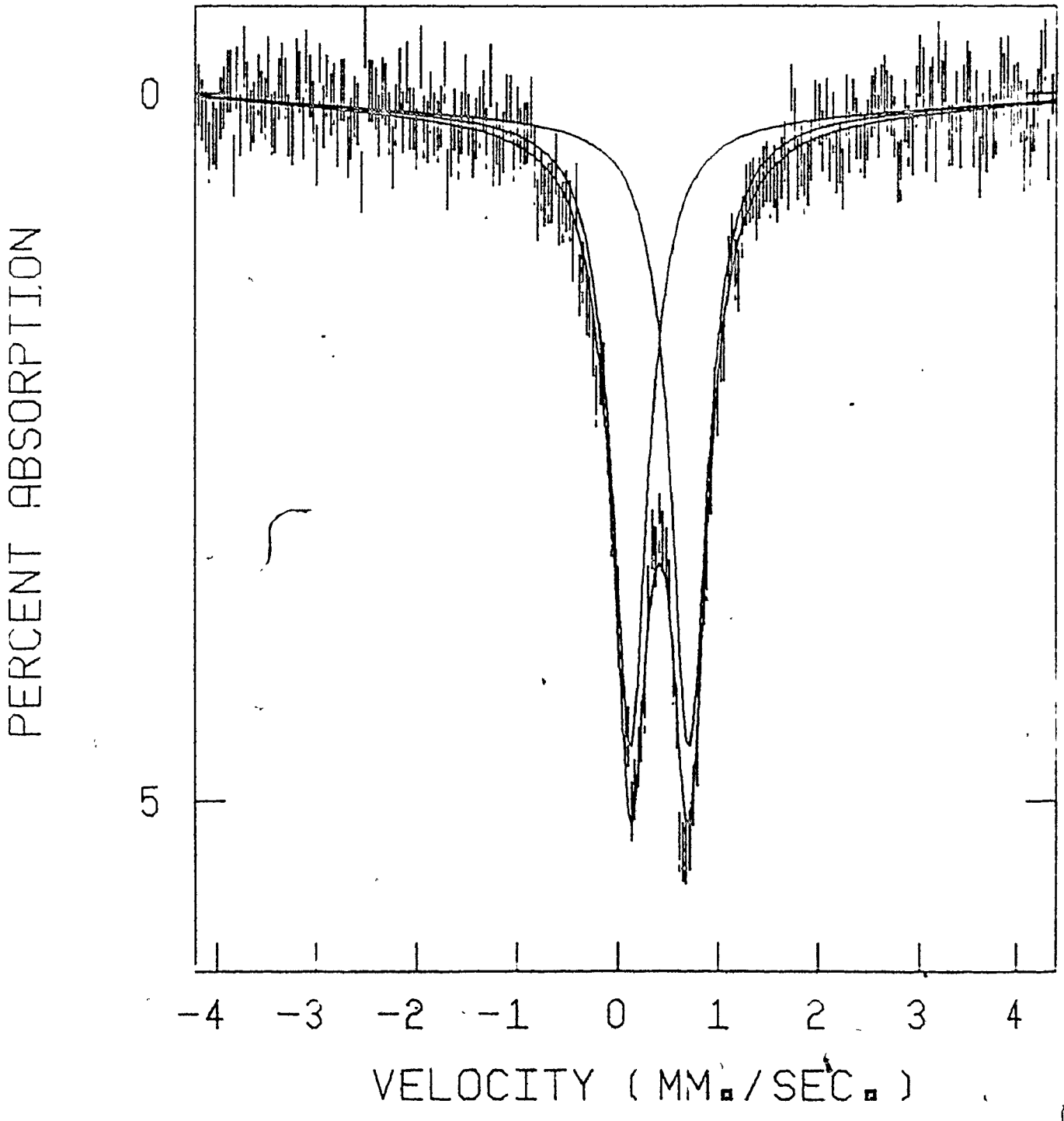

Appendix V; figure 2

RCB soil, at room temp. 2 nd. fit.

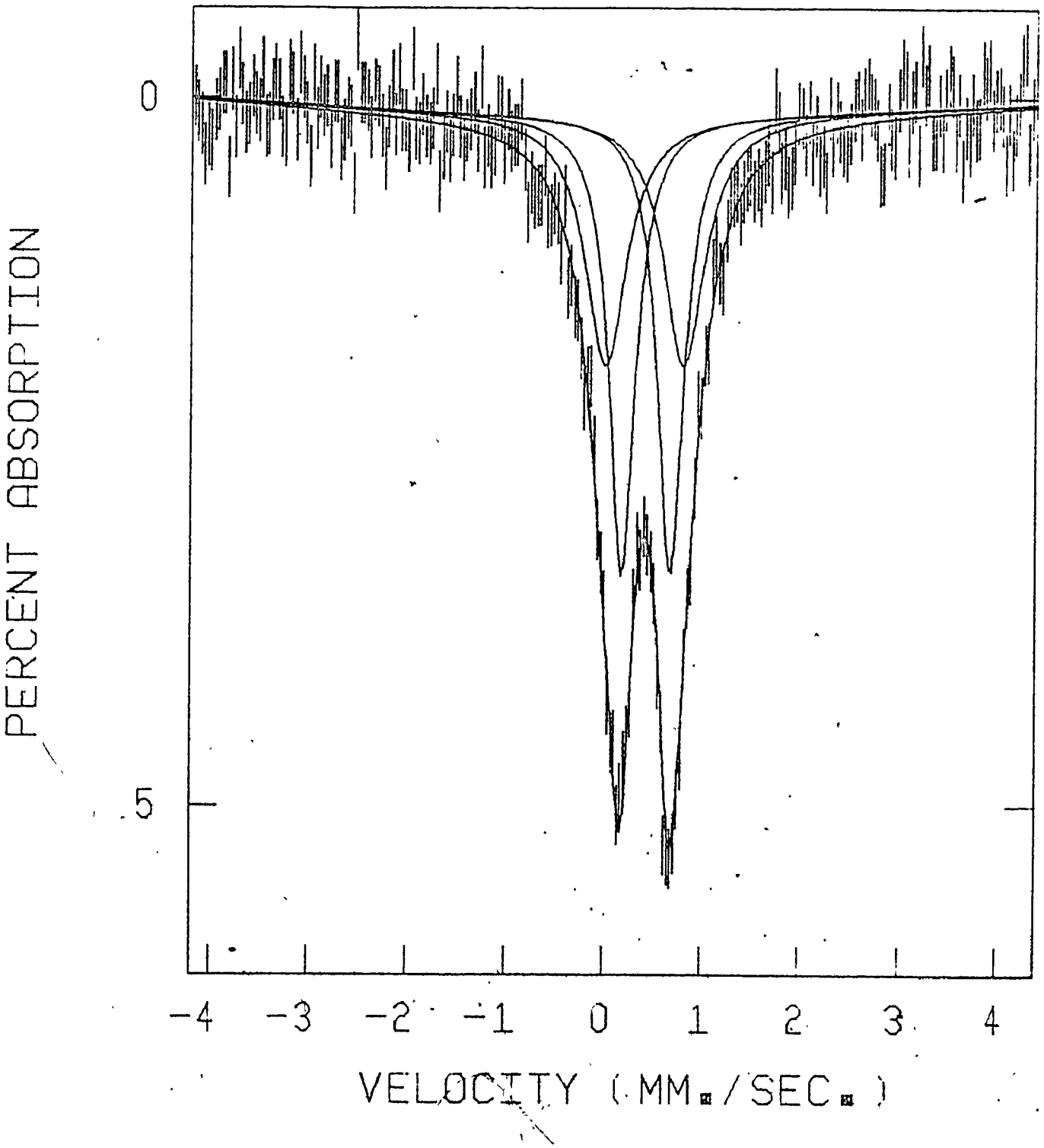

Appendix V; figure 3

RCB soil, at 77 °K

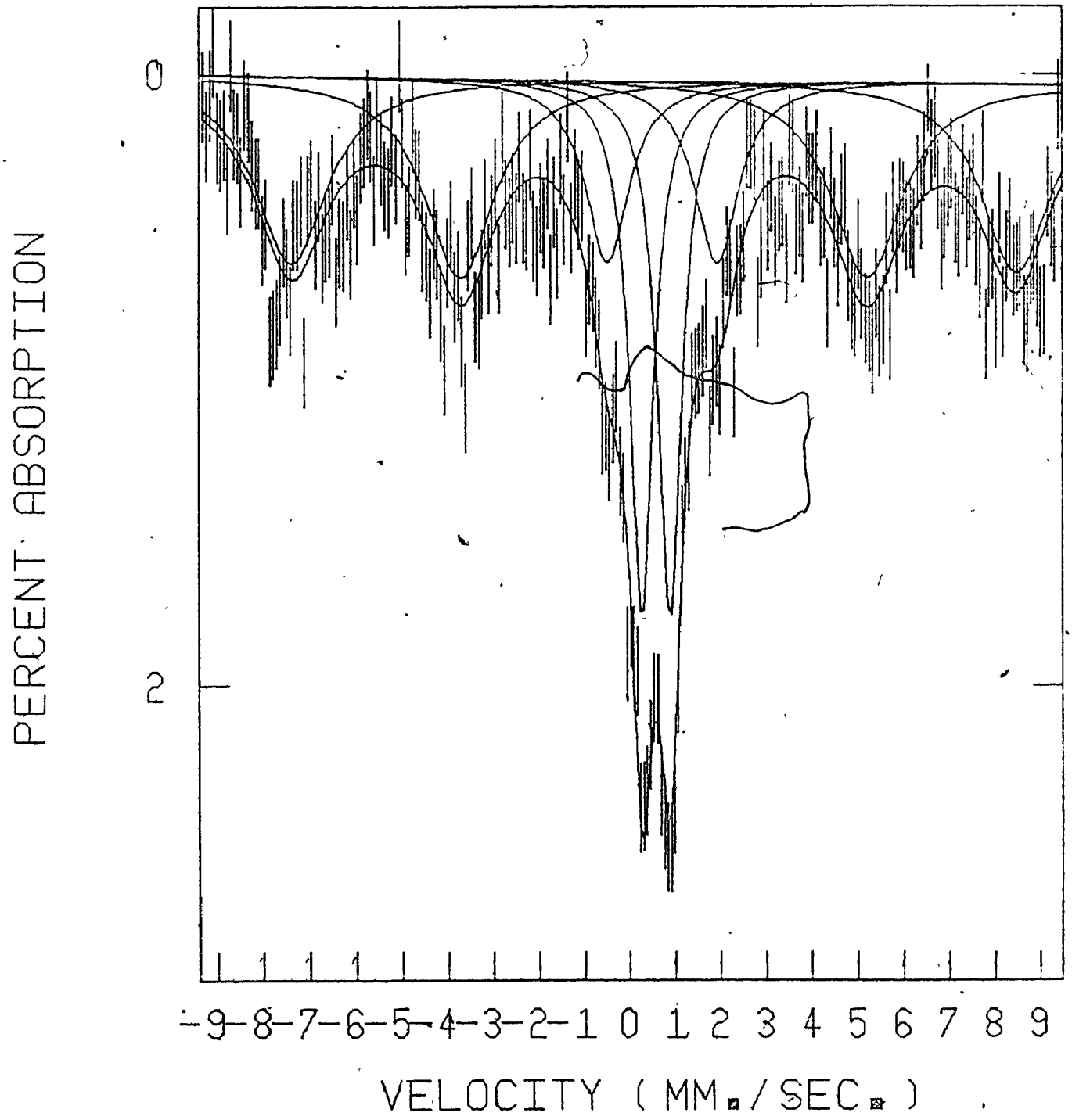

Appendix V; figure 4

GULF clay, room temp, 1 st fit.

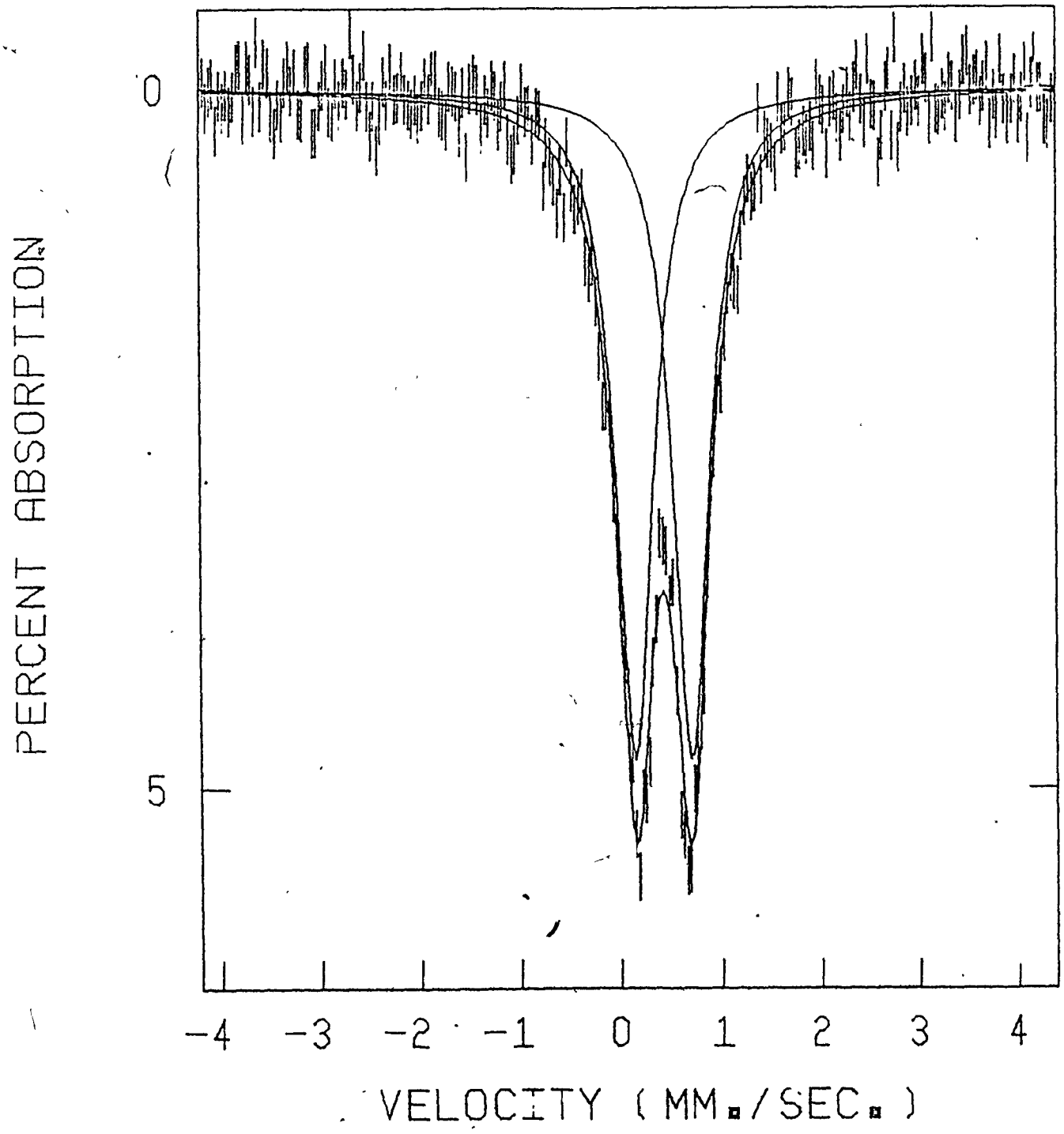

Appendix,V; figure 5

OULF clay, room temp, 2 nd. fit.

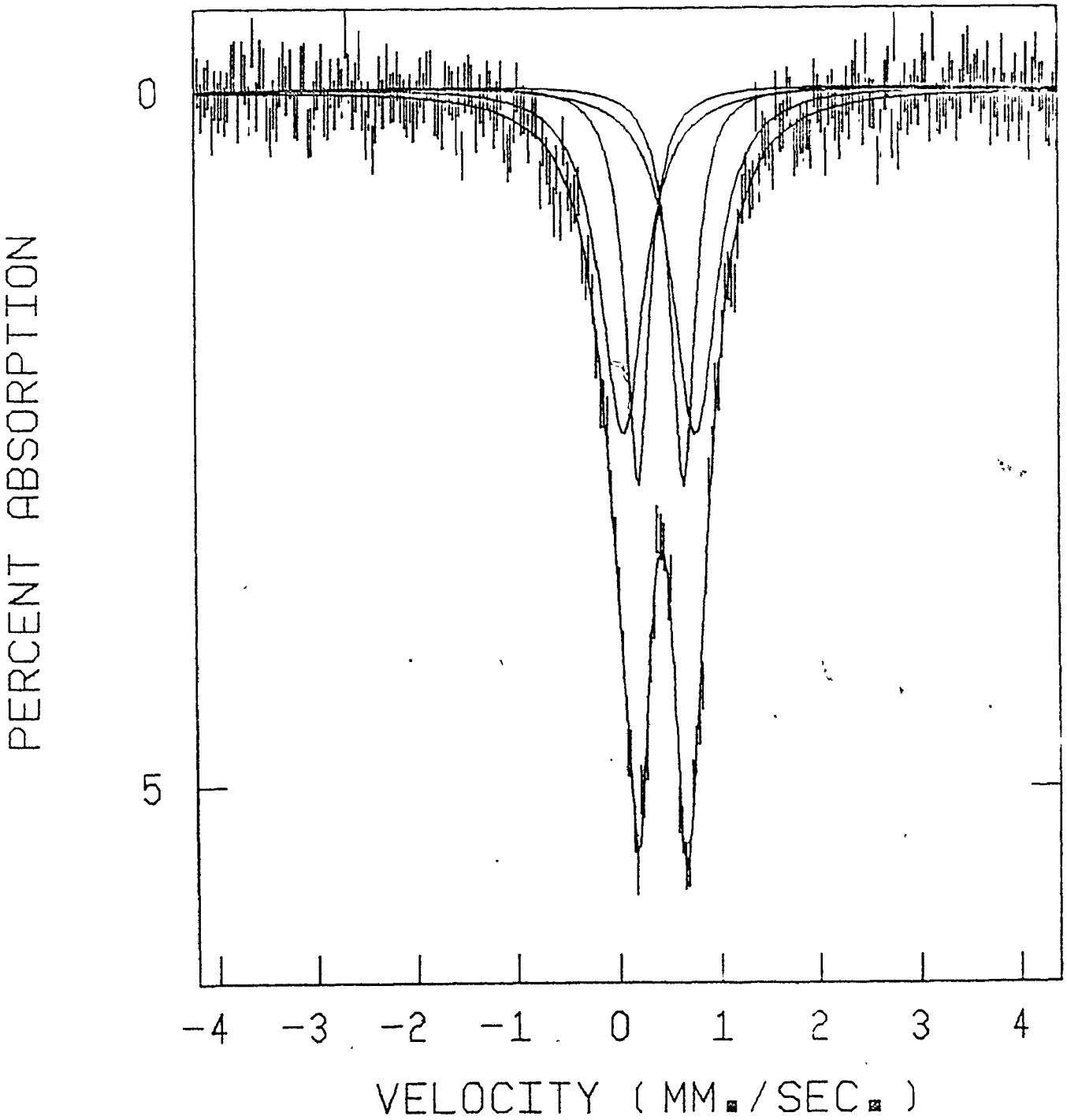

Appendix V; figure 6

GULF clay, 77 °K .

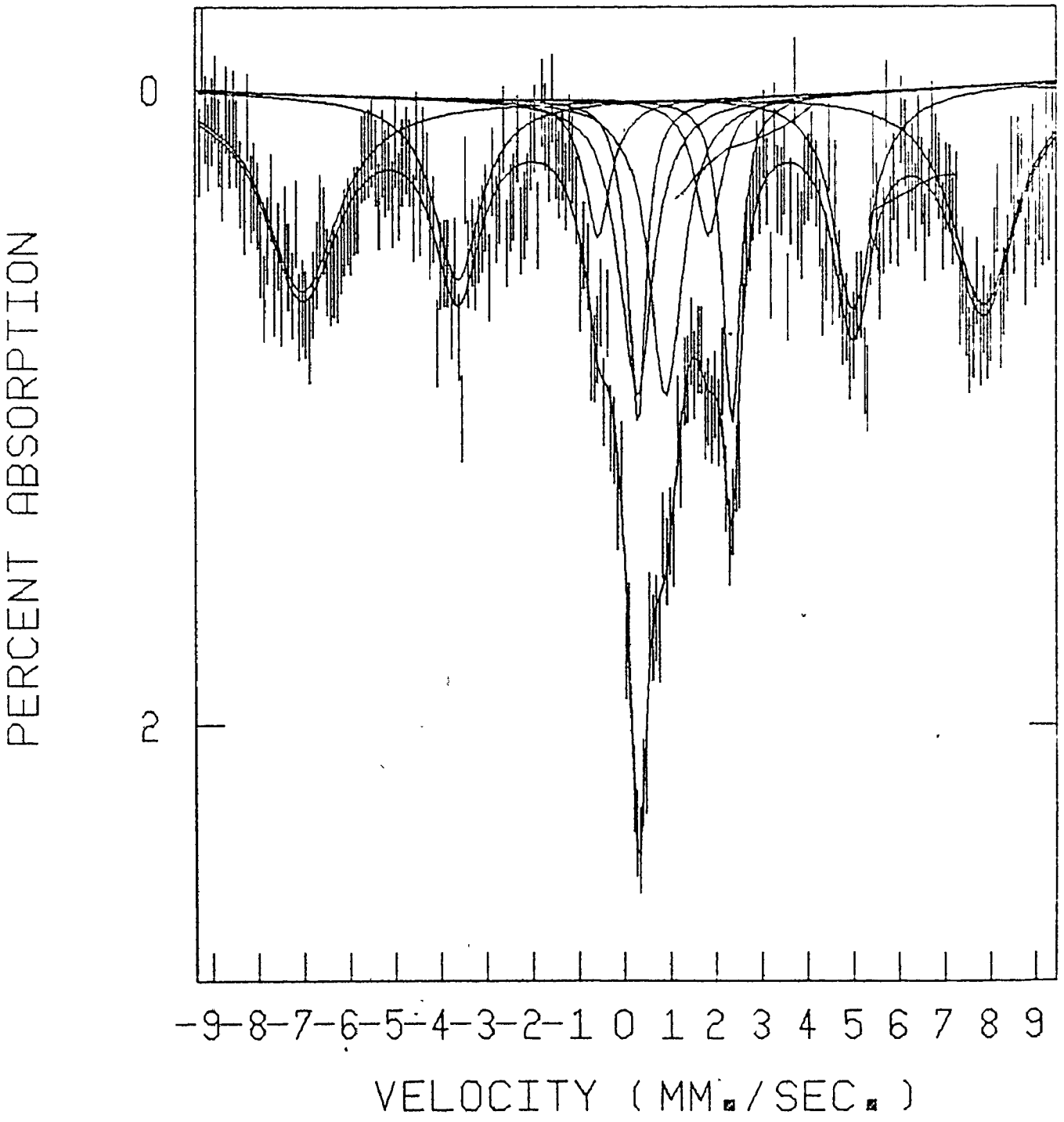

Appendix V; figure 7

GYS1 soil, room temp, 2 site fit.

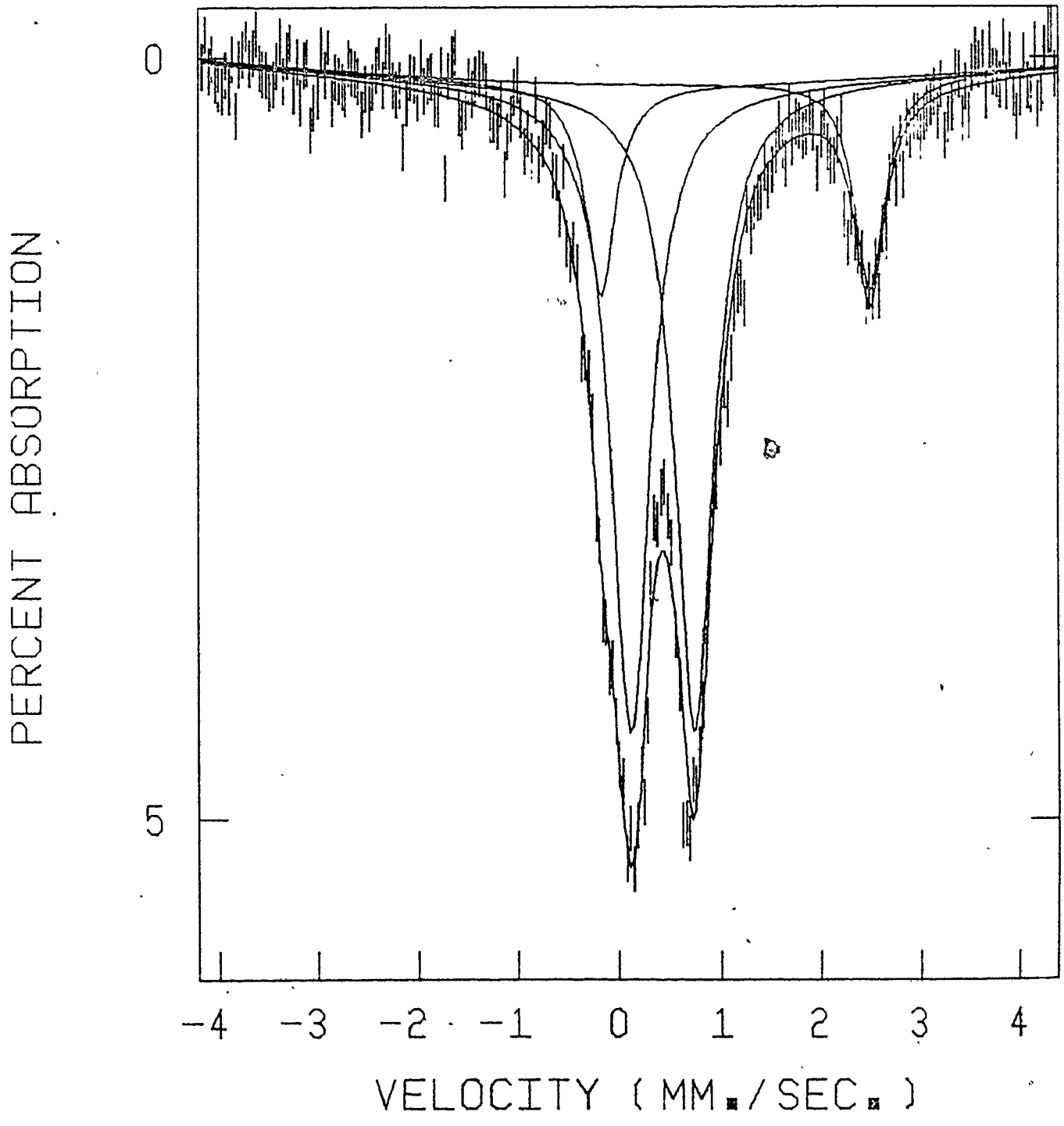

Appendix V; figure 8

GYS1 soil, room temp, 2nd fit.

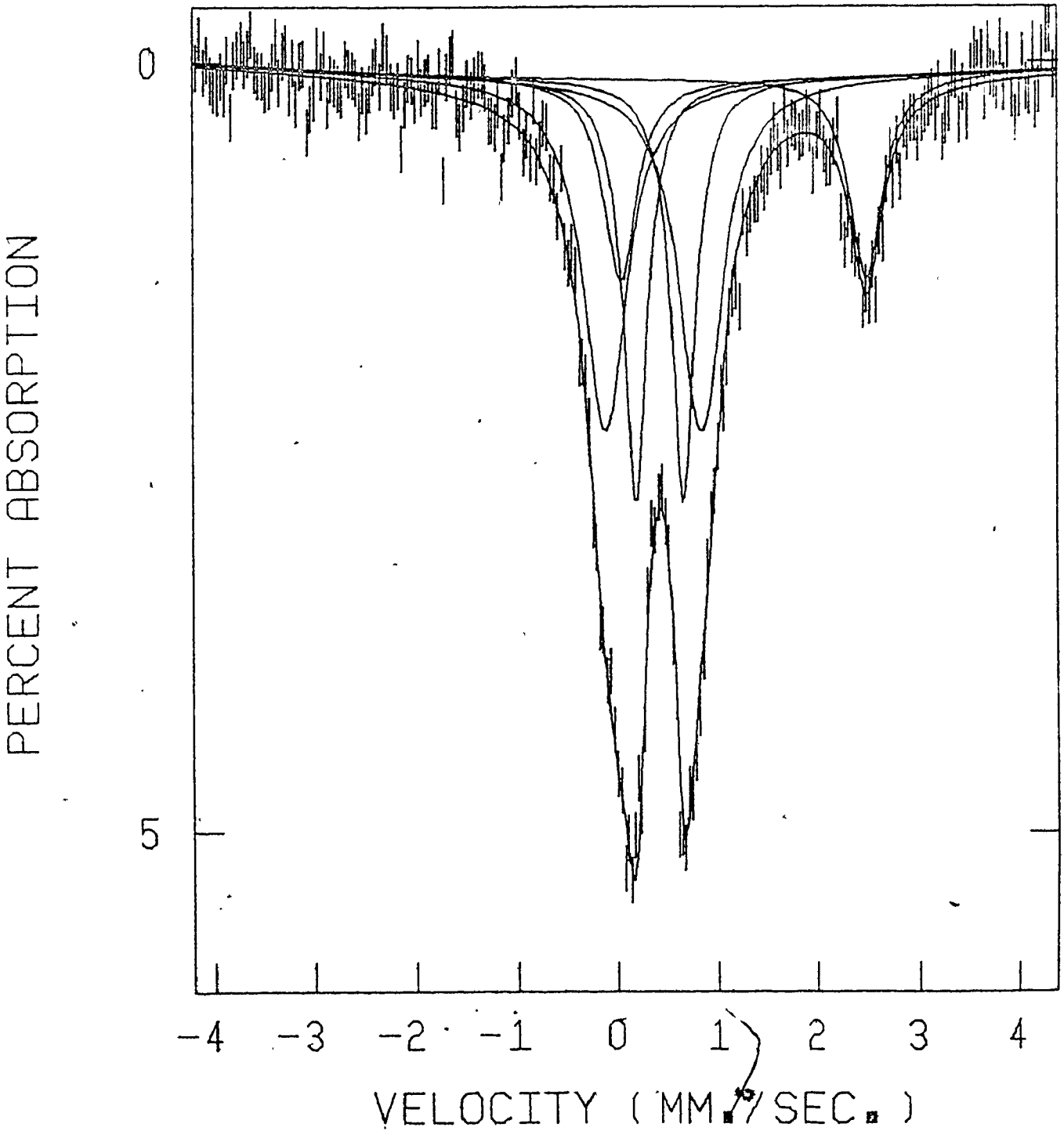

Appendix V; figure 9

GYS1 soil, 77 °K .

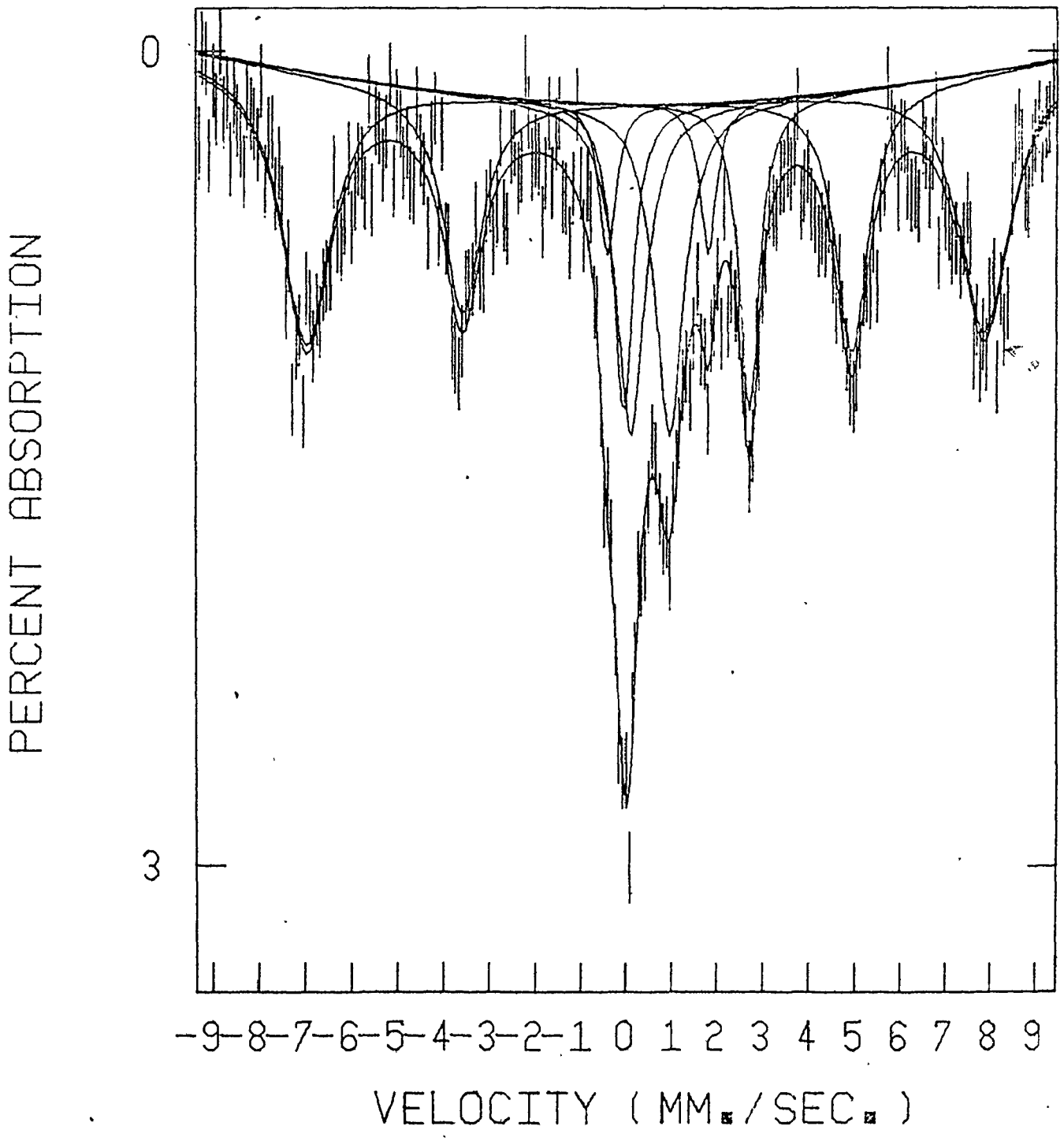

Appendix V; figure 10, SJLS at room temp.

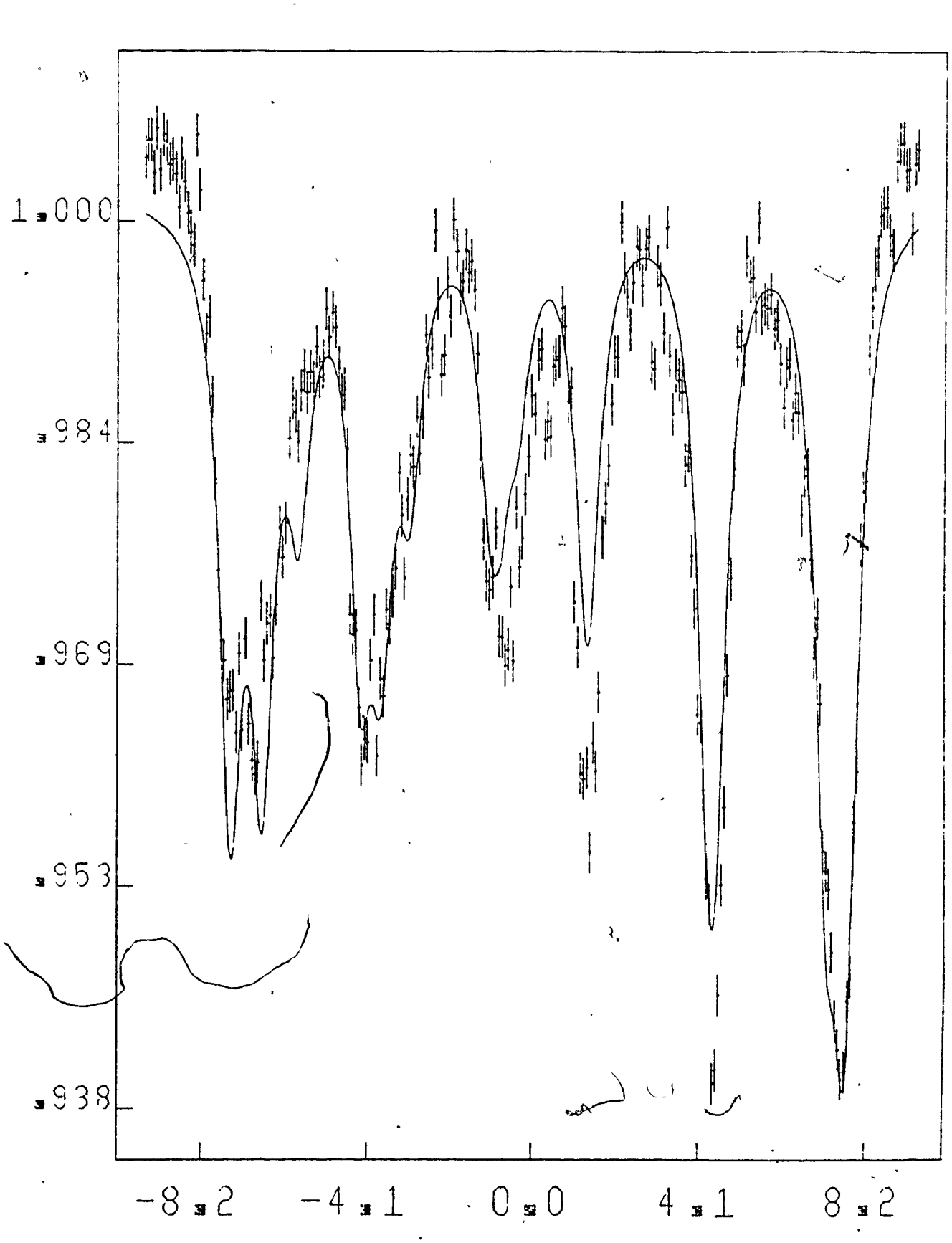

Appendix v; figure 11. SJLS 3-site fit, room temperature. Goodness of fit.